

Drug Eluting Prosthetic Joints through Drug Cluster Morphology Control

by

Vincentius Jeremy Suhardi

S.B. Chemical Engineering

California Institute of Technology, 2012

S.M. Chemistry

California Institute of Technology, 2012

Submitted to the Harvard-MIT Division of Health Sciences and Technology in partial fulfillment of the requirements for the degree of

Doctor of Philosophy in Medical Engineering and Medical Physics

at the

Massachusetts Institute of Technology

June 2017

© Massachusetts Institute of Technology 2017. All rights reserved.

Signature redacted

Signature of Author: _____

Harvard-MIT Division of Health Sciences and Technology

March 29, 2017

Signature redacted

Certified by: _____

Ebru Oral, Ph.D.

Professor of Orthopedic Surgery

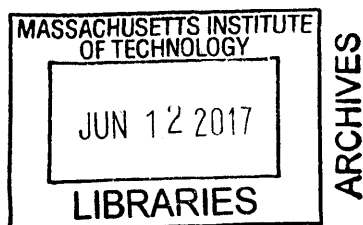
Signature redacted

Accepted by: _____

Emery N. Brown, M.D., Ph.D.

Director, Harvard-MIT Program in Health Sciences and Technology

Professor of Computational Neuroscience & Health Sciences and Technology



Dedication

To my parents Iwan Suhardi and Juliati Prajitno and to my wife, Anastasia Oktarina, for their relentless love and encouragement.

Drug Eluting Prosthetic Joints through Drug Cluster Morphology Control

by

Vincentius Jeremy Suhardi

Submitted to the Harvard-MIT Division of Health Science and Technology

on April 3rd, 2017

in partial fulfillment of the requirements for the degree of

Doctor of Philosophy in Medical Engineering and Medical Physics

More than one million joint replacements are performed in the USA annually. However, around 10 % of patients require revision surgery within 10 years with prosthetic joint infections (PJI) as a common reason. PJI has a recurrence rate of 16 %, a mortality rate of 2.5 %, and end-stage treatments involving arthrodesis and amputation. Most drug eluting polymers that were in development to address this problem failed due to toxic degradation products, insufficient drug release, and insufficient mechanical strength. The gold standard of treatment uses antibiotic eluting bone cement which has a mechanical failure rate of 26-60 % within 49-54 months if used under load bearing conditions. Therefore, despite advances in orthopedic materials, development of drug-eluting devices with effective, sustained delivery with the necessary mechanical strength for a fully load bearing joint implant has been elusive.

Here, we report the synthesis and application of a drug eluting, fully load bearing, and articulating joint prosthesis that has superior mechanical strength and drug elution profile compared to the clinical gold standard, antibiotic eluting bone cement. We modified the eccentricity of drug clusters and percolation threshold in the polymeric matrix of Ultra-High Molecular Weight Polyethylene (UHMWPE), which resulted in maximized drug elution and mechanical strength retention. The optimized antibiotic eluting UHMWPE elutes antibiotic at a higher concentration for a longer period of time than antibiotic eluting bone cement while retaining the mechanical and wear properties of clinically used UHMWPE joint prosthesis. After drug elution, the empty drug clusters in the polymer were filled with biological lubricants during articulation, which through a combination of weeping and elastohydrodynamic lubrication, reduced the overall wear rate of the UHMWPE. Treatment of *Staphylococcus aureus* infected lapine knee with the antibiotic eluting UHMWPE showed complete bacterial eradication without any detectable systemic side effect. Taken together, our study showed that the drug-eluting UHMWPE joint implants in this study are promising candidates for further clinical trial and as the next generation prosthetic joints.

Thesis Supervisor: Ebru Oral, PhD

Title: Assistant Professor of Orthopaedic Surgery

Acknowledgements

I have been very fortunate throughout my graduate studies. First, I am able to achieve the goal that I set myself when I enter the Ph.D. program: working on projects that can someday truly change patients' lives. Second, I have been surrounded by amazing professors, scientists, and physicians that supported me in these projects to achieve a mutual goal of creating better care and treatment for patients. Third, I have interacted with extremely smart and imaginative peers at MGH, MIT, and HMS that are always willing to bounce ideas around and collaborate.

I would like to thank my principal investigator, Ebru Oral, Ph.D., who has always patiently guided me navigating through my projects with invaluable ideas, practical knowledge, and constructive criticism. Thank you for always being available to answer my questions and for always providing fresh perspective when I am at a dead end.

I would like to thank the director of the lab, Orhun Muratoglu, Ph.D., who always provided me with new insights, perspective, and always guided me to put on both my scientific and clinical cap as I am working on my thesis projects.

I would like to thank the team of orthopedic surgeons who has worked with me throughout my thesis projects, Andrew Freiberg, MD, Henrik Malchau, MD, Harry Rubash, MD, and Hani Bedair, MD who always gave insight on what was needed in clinical practice and what would be the best way to use the new innovations.

I would like to thank my thesis committee chair and member, Richard Mitchell, MD, Ph.D., Edward K. Rodriguez, MD, Ph.D., and Jeffrey Karp, Ph.D., who have been very supportive and lend their invaluable time to provide very insightful feedbacks and ideas.

I would like to thank all of Harris Orthopedics Lab members who have helped me running experiments, animal studies, and be extra pairs of the ear to bounce ideas around.

I would like to thank my parents, Iwan Suhardi, JD and Julia Prajitno, JD who gave me unconditional love and support, more than I could ever imagine. Thank you very much for being the one who hears my complaints and gave me encouragement to work smarter and harder. I'm so glad to have two amazing siblings, Angela and Matthew, that are always ready to help me whenever I need it.

I would like to thank my wife, Anastasia Otkarina, MD who provided an enormous amount of love, care, and support. Thank you for always listening to my stories, however boring those stories may be. Love you!

This acknowledgment is certainly incomplete, and to whomever, I accidentally did not mention, please do not hold any grudge against me 😊. I am very grateful to everyone who has helped me throughout my graduate studies.

Contents

Dedication	3
Abstract	5
Acknowledgement	7
Contents	9
List of Figures	14
List of Tables	20
List of Abbreviations	21
Prologue	23
Chapter 1: Background	26
Total Joint Arthroplasty.....	26
Total hip arthroplasty.....	26
Total knee arthroplasty.....	27
Development of UHMWPE technologies to address total joint arthroplasty complications	27
Current complications related to TJA.....	29
Incidence and economic burden of periprosthetic joint infection	31
Pathogenesis of prosthetic joint infection.....	32
Risk factors for Prosthetic joint infection	33
Bacterial strains commonly found in PJI.....	35
Involvement of biofilm in PJI.....	37
Diagnosis of PJI	37
Prophylaxis approaches to reduce incidence of PJI.....	40
Current treatment of patients with PJI.....	41
Recommended antimicrobials for PJI	43
Antibiotic-eluting bone cement (ALBC) as gold standard for local delivery of antibiotics in PJI	45
Problems with the current PJI treatments and proposed solutions.....	48
Polyethylene as weight bearing material	50
Previous works on UHMWPE with additives.....	51
Chapter 2: Drug Percolation in Polymer Matrix and its Effect on Drug Elution	54
Introduction	54
Thermodynamic of drug incorporation into polymer.....	54
Kinetics of drug incorporation into polymer	55
Elution mechanism from drug-incorporated polymer	56
Higuchi equation for release of drug from non-swellable polymeric matrix ..	58
Percolation theory.....	59
Percolation theory on eccentricity of clusters	61
Percolation of previously reported drug eluting polymer	62

Clinical implication of drug cluster morphology.....	63
Methods	64
Results	67
Heat resistance of vancomycin determined by thermogravimetric analysis (TGA).....	67
Spectral analysis of eluted vancomycin from vancomycin-eluting UHMWPE in comparison to pure antibiotics.....	68
Ultraviolet-visible spectroscopy (UV-Vis) of vancomycin eluted from UHMWPE	68
Fourier transform infrared (FTIR) spectroscopy of vancomycin eluted from UHMWPE	69
Nuclear Magnetic Resonance (NMR) of vancomycin eluted from UHMWPE	70
Effect of Drug Cluster Eccentricity on drug elution of vancomycin eluting low density polyethylene (LDPE).....	71
Drug clusters interconnectivity and drug elution from vancomycin eluting UHMWPE	75
Effect of consolidation parameters (compression molding temperature, Compression molding pressure, and vancomycin particle size) on drug elution from vancomycin eluting UHMWPE	78
Computational simulation on effect of drug cluster eccentricity on drug cluster interconnectivity	80
Incorporation of other antibiotics into UHMWPE	81
Heat resistance of antibiotics determined by thermos-gravimetric analysis (TGA).....	81
Ultraviolet-visible spectroscopy (UV-Vis) of antibiotics eluted from UHMWPE	85
FTIR analysis of antibiotics eluted from UHMWPE.....	86
NMR analysis of antibiotics eluted from UHMWPE	88
Scanning electron micrograph of antibiotic eluting UHMWPE	93
Effect of drug hydrophilicity/hydrophobicity on drug elution from drug eluting UHMWPE	95
Discussion.....	98
Most antibiotics can be incorporated into UHMWPE without any sign of thermal degradation	98
Highly eccentric pore morphology in drug-eluting LDPE.....	99
Highly eccentric pore morphology in drug-eluting UHMWPE.....	102
Relation between drug type and elution rate from drug eluting UHMWPE.....	103
Conclusion	105

Chapter 3: Tensile and Impact Properties of Drug Eluting UHMWPE 106

Introduction	106
Contact mechanics of artificial joint in hip and knee.....	106
Theoretical basis of mechanical properties of polymers with fillers	108
Mechanical strength of filled polymer when fillers are weaker than the polymer	109
Characterization of the mechanical strength of UHMWPE for joint implants.....	111
Methods	113

Results	115
The effect of drug cluster eccentricity on mechanical properties of low density polyethylene (LDPE)	115
The effect of pore eccentricity on the mechanical properties of UHMWPE	116
Mechanical properties of vancomycin eluting UHMWPE under various initial drug loading	118
Computational simulation of the effect of drug cluster eccentricity on mechanical strength	119
Effect of manufacturing parameters (compression molding temperature, compression molding pressure, and vancomycin particle size) on the mechanical Properties of vancomycin eluting UHMWPE	123
Effect of gamma irradiation dose on mechanical strength of vancomycin eluting UHMWPE	125
Effect of drug hydrophilicity/hydrophobicity on mechanical strength of drug eluting UHMWPE	127
Discussion	129
Effect of drug amounts and drug cluster eccentricity on mechanical strength of drug eluting polyethylene	129
Effect of drug type and compression molding parameters on mechanical strength of UHMWPE	132
Effect of irradiation dose on mechanical strength of UHMWPE	133
Conclusion	133

Chapter 4: Wear Resistance of Micro Textured Drug Eluting UHMWPE	135
Introduction	135
Wear of polymers	135
Fluid lubrication at mechanical interfaces	136
Wear mechanism of UHMWPE	138
Relation between micro-texture and lubrication film thickness	140
Relation between micro-texture and tribology properties	141
Methods	142
Results	149
Wear resistance of vancomycin eluting UHMWPE	149
Formation of self-assembled micropatterns in drug eluting UHMWPE	151
Investigation of the relationship between self-assembled micropatterns in bupivacaine- eluting UHMWPE and wear resistance	153
Long-term wear testing of bupivacaine-eluting UHMWPE	156
Topographical analysis of self-assembled micropatterns from bupivacaine-eluting UHMWPE (Bupi-PE)	156
Evolution of the surface roughness of Bupi-PE during wear testing	158
Combination of micropatterns with previously developed method to reduce wear rate of UHMWPE	161
Effect of irradiation dose on the wear rate of MPC+Bupi-PE UHMWPE	165
Evolution of surface roughness of combined crosslinked and bupivacaine eluting UHMWPE (Bupi-PE) throughout wear testing	167
Mechanism of wear reduction in microtextured UHMWPE	170
Computational simulation of lubrication film thickness of microtextured and flat UHMWPE	173
Discussion	175
Conclusion	178

Chapter 5: Drug Eluting UHMWPE with Highly Eccentric Drug Cluster Morphology for the Treatment of Prosthetic Joint Infection	179
Introduction	179
Gram-positive bacteria accounts for 80% of all PJI cases	179
Antibiotic penetrates poorly to the infected joints and bone	181
Previously reported antibacterial materials to address orthopaedic-associated infections	182
Two-stage implant exchange as state-of-art treatment of PJI	183
Complications of PMMA bone cement spacer as local antibiotic delivery system	185
Methods	186
Results	192
Optimization of mechanical strength and drug elution of vancomycin eluting UHMWPE as a bearing surface in prosthetic joint implants	192
Vancomycin elution and mechanical properties of optimized vancomycin eluting UHMWPE and comparison against clinically used UHMWPE and antibiotic eluting bone cement	195
Antibacterial activity of VPE, BC1, and BC2	197
Irradiation grafting of vancomycin on surface of VPE prevents bacterial adherence	202
Optimization of combined rifampin-vancomycin eluting UHMWPE (RVPE)	
Activity of RVPE	209
Kinetic of biofilm eradication by RVPE	215
Discussion	217
Conclusion	223
Chapter 6: Pre-Clinical Safety and Efficacy Testing of Drug-Eluting UHMWPE for Treatment of PJI	224
Introduction	224
Both planktonic and biofilm bacteria are involved in prosthetic joint Infection	224
Bacteria adhere to intra-articular components and bone-implant Interface	226
Vancomycin is effective against planktonic bacteria and immature biofilm but not against mature biofilm	227
Gold standard treatment in antibiotic-eluting bone cement spacer	228
Methods	229
Results	235
Murine planktonic bacteria infection model	235
Murine biofilm bacteria infection model	238
Lapine planktonic bacteria prosthetic joint infection model	243
Lapine biofilm bacteria prosthetic joint infection model	250
Discussion	256
Conclusion	259
Chapter 7: Sustained Delivery of Local Anesthetics from UHMWPE with Highly Eccentric Pores	260
Introduction	260
Current postoperative management for total joint arthroplasty	261
Intraarticular delivery of local analgesics	263

Antimicrobial activity of local anesthetics	265
Sustained delivery of local anesthetics using highly eccentric drug clusters- UHMWPE	266
Methods	266
Result.....	272
Elution and mechanical properties of bupivacaine HCl (Bupi HCl) from Bupi HCl eluting UHMWPE	272
Elution of bupivacaine FB eluting UHMWPE	275
Elution and mechanical properties of Bupivacaine HCl (Bupi HCl), Bupivacaine Free Base (Bupi FB) and its combination from Bupi HCl eluting UHMWPE	278
Measurement of minimum inhibitory concentration of bioluminescent <i>S. aureus</i> (Xen29) against Bupivacaine HCl, Bupivacaine FB, and FS	282
In vivo antibacterial activity of Bupi-PE in subcutaneous murine model.....	283
In vivo analgesic activity of Bupi PE in murine model.....	285
Discussion.....	290
Conclusion	295
Epilogue	296
References	299

List of Figures

Figure 2.1. Vancomycin eluting PMMA bone cement with 15 wt % initial vancomycin loading.....	63
Figure 2.2. Thermogravimetric analysis (TGA) of vancomycin HCl powder	68
Figure 2.3. UV-Vis spectra of standard vancomycin and eluted vancomycin HCl	69
Figure 2. 4. FTIR spectra of eluted and standard vancomycin HCl.	70
Figure 2.5. NMR spectra of standard and eluted vancomycin HCl.....	71
Figure 2.6. SEM of Vancomycin eluting LDPE with 2- 10 wt % initial drug content and 2:1, 4:1, 16:1 LDPE granule : vanco particle ratio.	72
Figure 2.7. Vancomycin elution profile from vancomycin eluting LDPE with 2-10 wt % initial drug content and 2:1, 4:1, 16:1 LDPE granule : vanco particle ratio.	73
Figure 2.8. Scanning electron micrograph and μ CT Z-projection of vancomycin eluting UHMWPE at 2 wt %, 4 wt %, 6 wt %, 10 wt %.	75
Figure 2. 9. Overall volumetric porosity and percent accessible pore of vancomycin eluting UHMWPE at different initial vancomycin loading	77
Figure 2.10. Elution profile of vancomycin eluting UHMWPE at different initial vancomycin loading.	77
Figure 2. 11. Elution profile of 4 wt % vancomycin eluting UHMWPE manufactured at different initial vancomycin loading.	79
Figure 2. 12. Computational simulation result of percent accessible cluster	81
Figure 2.13. Thermogravimetric analysis of various antibiotics incorporated into UHMWPE.....	83
Figure 2.14. UV-Vis Spectra of various antibiotics eluted from UHMWPE	85
Figure 2.15. FTIR Spectra of various antibiotics eluted from UHMWPE	88
Figure 2. 16. NMR Spectra of various antibiotics eluted from UHMWPE	88
Figure 2. 17. Scanning electron micrograph of various drug-eluting UHMWPE	93
Figure 2. 18. Elution rate of various drug-eluting UHMWPE	96
Figure 2.19. Elution rate throughout time vs PSA/MV of various drug-eluting UHMWPE.....	97
Figure 2.20. Schematic of solvent casting of Vancomycin eluting LDPE and compression molded vancomycin eluting LDPE.....	101
Figure 2.21. Schematic of drug elution from antibiotic eluting UHMWPE.....	104
Figure 3.1. Mechanical Properties of Vancomycin eluting LDPE.	116
Figure 3.2. Drug cluster morphology and mechanical properties of vancomycin or NaCl eluting UHMWPE.	117

Figure 3.3. Mechanical properties of vancomycin eluting UHMWPE.	118
Figure 3.4. Schematic of the finite element analysis on tensile dogbone samples with single defect and double defect.....	120
Figure 3.5. Percent change in mechanical properties with different eccentricity of the defect.	122
Figure 3.6. Effect of compression molding temperature, compression molding pressure, and vancomycin particle size on UTS, EAB, and IS	124
Figure 3.7. Mechanical properties of vancomycin eluting UHMWPE with and without drug particle size controls.....	125
Figure 3.8. Mechanical properties of irradiated vancomycin eluting UHMWPE.....	126
Figure 3.9. Mechanical strength of other drug eluting UHMWPE.....	127
Figure 4.1 Scanning electron micrograph (SEM) of pre-eluted surface of vancomycin eluting UHMWPE	150
Figure 4.2. Wear resistance of vancomycin-eluting irradiated UHMWPE containing 0-10 wt % Vancomycin	151
Figure 4.3 SEM micrograph of various drug eluting UHMWPE with initial 20% wt drug loading....	152
Figure 4.4 Relation between drug types and wear rate of drug eluting UHMWPE.	153
Figure 4.5 Optical micrograph of surface of bupivacaine eluting UHMWPE post elution at 2-30 wt % initial bupivacaine content	154
Figure 4.6 Relation between initial drug content and wear rate of bupivacaine eluting UHMWPE.	155
Figure 4.7 Wear rate of 20 % Bupivacaine-UHMWPE tested up to 3 million cycles.....	156
Figure 4.8 Surface topography of uneluted and eluted 20 % Bupivacaine-UHMWPE as obtained by stylus profilometry	157
Figure 4.9 Z-Projection of 20 consecutive micro-CT slices (25 μ m slices) of the polymer phase and the pore phase	158
Figure 4.10 Surface texture of 20 wt % Bupivacaine before and after wear testing.....	158
Figure 4.11 Surface roughness contour obtained with AFM of 20 wt % Bupivacaine before and after wear testing	160
Figure 4.12 Progression of surface roughness (Ra) throughout wear testing of 20 wt % Bupivacaine.	161
Figure 4.13 Wear resistance of microtextured UHMWPE with various chemical treatments to reduce wear rate (75 kGy, MPC, and SLIPS)	162
Figure 4.14 Scanning electron micrograph of the surface of the MPC + microtextured UHMWPE and the corresponding EDAX carbon, phosphorous mapping	162

Figure 4.15 Scanning electron micrograph cutting through the thickness of the MPC + microtextured UHMWPE and the corresponding EDAX carbon, phosphorous mapping.....	164
Figure 4.16 Wear rate of Bupi-PE and UHMWPE without bupivacaine irradiated at 0, 25, 50, 75 and 100 kGy.	166
Figure 4.17 Wear rate of 20 % MPC and normal UHMWPE (0% MPC) irradiated at 0, 25, 50, 75 and 100 kGy	166
Figure 4.18 Surface topography of radiation cross-linked Bupi-PE (75 kGy) before and after wear testing	167
Figure 4.19 Surface roughness of radiation crosslinked Bupi-PE (75 kGy) before and after wear testing	169
Figure 4.20 Progression of surface roughness (R_a) throughout wear testing of bupivacaine-eluting UHMWPE.	170
Figure 4.21 Relation between compressive elastic modulus and initial bupivacaine loading concentration in UHMWPE.....	171
Figure 4.22 Representative stress-strain curves of cyclic compression test (100 cycles total) with peak load of 12 MPa.	172
Figure 4.23 Fluorescence microscopy of surface of UHMWPE and Bupi-PE under no compression (0 MPa) and compression (8 MPa).....	172
Figure 4.24 Computational simulation of lubrication film thickness due to elastohydrodynamic lubrication (EHD) and extruded lubricants due to weeping lubrication.	175
Figure 5.1 Optimization field with respect to initial drug loading.....	194
Figure 5.2 Prototype of tibial insert (a) and acetabular liner (b) made from VPE.....	194
Figure 5.3 Elution profile of vancomycin eluting UHMWPE.....	195
Figure 5.4 Mechanical properties of vancomycin eluting UHMWPE and vancomycin eluting bone cement.....	196
Figure 5.5 Representative Kirby-Bauer agar diffusion test of VPE and BC1 after 24 hr incubation	197
Figure 5.6 Area of inhibition throughout time of VPE, BC1, and BC2, against <i>Staphylococcus aureus</i> and <i>Staphylococcus epidermidis</i>	198
Figure 5.7 Gross pictures of VPE or control UHMWPE-Titanium-Bone sandwich.	199
Figure 5.8 Bioluminescent imaging of live Xen29 that adhered to the titanium disc, cortical bone, and polyethylene component in the VPE and control groups.....	200
Figure 5.9 Quantification of the bioluminescent signal from the bacteria adherent to titanium disc and cortical bone disc.	201
Figure 5.10. Plate reculturing of bacteria post sonication of the titanium, bone, and polyethylene components after 48 hr time points.	202

Figure 5.11. Live/Dead stain of bacterial adherent to the surface of irradiated vancomycin eluting UHMWPE	203
Figure 5.12. Sonication and reculturing of bacteria adherent to the surface of irradiated vancomycin eluting UHMWPE	204
Figure 5.13. Immunofluorescence staining of vancomycin grafted to the surface of irradiated vancomycin eluting UHMWPE	205
Figure 5.14. Ratio of eluted rifampin and vancomycin throughout elution time at different initial drugs loading ratio	207
Figure 5.15. Elution rate (a) and total drug eluted (b) of RVPE, VPE and BC2.	207
Figure 5.16. Mechanical properties of RVPE, VPE, and BC2	208
Figure 5.17 Prototype of tibial insert (a) and acetabular liner (b) made from combination of RVPE and non-antibiotic eluting UHMWPE.....	209
Figure 5.18. Schematic of 'sandwich; experiment to treat bacterial biofilm in between bone-titanium often found in patients with chronic PJI.....	210
Figure 5.19. Gross pictures of RVPE or control UHMWPE-Titanium-Bone sandwich	212
Figure 5.20. Bioluminescent imaging of live Xen29 that formed biofilm on the titanium disc, cortical bone, and polyethylene components.....	213
Figure 5.21 Quantification of the bioluminescent signal from the bioluminescent images shown at Figure 5.20.....	214
Figure 5.22. Sonication and reculturing of bacteria adherent on the surface of the titanium, bone, and polyethylene components after 48 hr time points.....	215
Figure 5.23. Two-photon, live-dead imaging of the bacteria that adhered to the surface of titanium at 6 hr and 2 weeks after treatment.	216
Figure 5.24. Percent live dead as function of time of exposure to either control or RVPE.....	217
Figure 6.1. Gross picture of subcutaneously implanted control UHMWPE or VPE discs.	235
Figure 6.2. In vivo bioluminescence color map from Xen 29.....	236
Figure 6.3. Total bioluminescence quantification around the implants	237
Figure 6.4. Post-Mortem sonication of tissues and explants.....	237
Figure 6.5. Gross picture of subcutaneously implanted control RVPE discs and beaded titanium discs.	239
Figure 6.6. In vivo bioluminescence color map from Xen 29.....	239
Figure 6.7. Total bioluminescence quantification around the implants of mice receiving RVPE or control UHMWPE.....	241
Figure 6.8. Two-photon live-dead imaging of explanted UHMWPE and titanium discs.	241

Figure 6.9. Post-Mortem sonication of explanted titanium and polymer (UHMWPE) components.	243
Figure 6.10. Gross picture of UHMWPE and Titanium Rod Implantation in the Lapine Joint Infection Model.	245
Figure 6.11. Survival Curve of Rabbits Receiving Control UHMWPE , BC, or VPE	245
Figure 6.12. Kidney and Liver Function of Rabbits Receiving VPE.	246
Figure 6.13. Necropsy bioluminescent map of rabbit knee infected with Xen 29.	247
Figure 6.14. Total bioluminescence quantification of the rabbit knee receiving control UHMWPE or VPE post necropsy.	248
Figure 6.15. Two-photon live-dead imaging of explanted titanium rods.	248
Figure 6.16. Post-Mortem sonication of tissues and Explants.	249
Figure 6.17. Gross picture of UHMWPE and Titanium Rod Implantation in the Lapine Joint Infection Model.	251
Figure 6.18. Bioluminescence of titanium rods prior to implantation	251
Figure 6.19. Survival Curve of Rabbits Receiving Control UHMWPE , BC, or RVPE.	252
Figure 6.20. Kidney and Liver Function of Rabbits Receiving RVPE.	253
Figure 6.21. Representative gross picture of the dissected knee from control, BC, and RVPE groups.	253
Figure 6.22. Necropsy bioluminescent map of rabbit knee in control, BC, and RVPE infected with Xen 29 bioluminescent on titanium rod.	254
Figure 6.23. Two-photon live-dead imaging of explanted titanium rods from control, BC and RVPE groups.	255
Figure 6.24. Post-Mortem sonication of tissues and Explants.	256
Figure 7.1. Scanning electron micrograph of bupivacaine HCl eluting UHMWPE at different initial loading of bupivacaine HCl.	272
Figure 7.2. Elution Profile of Bupivacaine HCl eluting UHMWPE.	274
Figure 7.3. Mechanical and Wear Properties of Bupivacaine HCl Eluting UHMWPE.	275
Figure 7.4. Ionization state of bupivacaine determines its form in UHMWPE.	277
Figure 7.5. Elution Profile of Bupivacaine FB eluting UHMWPE.	278
Figure 7.6. Elution Profile of Combined Bupivacaine FB and Bupivacaine HCl eluting UHMWPE.	279
Figure 7.7. Mechanical and Wear Properties of Combined Bupivacaine FB and Bupivacaine HCl eluting UHMWPE.	281
Figure 7.8. Antibacterial activity of bupivacaine eluted from UHMWPE and standard bupivacaine solution	282

Figure 7.9. In vivo antibacterial activity of bupi-PE.284

Figure 7.10. Schematic of in vivo testing of analgesic efficacy of bupi-PE286

Figure 7.11. Stance and gait activity of the hind limbs post-implantation of bupi-PE or control UHMWPE287

Figure 7.12. Representative histology of the synovium capsule and the bone-implant interface of the rats receiving control UHMWPE or Bupi-PE288

Figure 7.13. Equilibrium between Bupivacaine HCl and Bupivacaine FB in aqueous solution. ...288

Figure 7.14. Comparison of bupivacaine release rate and total released bupivacaine from single injection, Exparel™, infusion pump, and bupivacaine eluting UHMWPE291

Figure E.1. Current and Proposed New Treatment Protocol for Prosthetic Joint Infections297

List of Tables

Table 1.1 Cumulative incidence of PJI in THA based on number of year since implantation with conventional UHMWPE and HXLPE	30
Table 1.2 Cumulative incidence of PJI in TKA based on number of year since implantation with conventional UHMWPE and HXLPE	30
Table 1.3. Common bacteria causing PJI and the recommended antimicrobial treatment.	44
Table 2.1. PSA/MV of rifampin, gentamicin sulfate, tetracycline HCl, fusidic acid, teicoplanin, ceftriaxone, ciprofloxacin HCl, and tobramycin.	97
Table 3.1. Defect eccentricity and average eccentricity tested for simulation with double defect. .	121
Table 5.1. Type of Bacteria found in PJI patients reported from previous literature.....	180
Table 5.2. Calculation of RV-PE to Clinically Relevant Vancomycin to Rifampin Ratio.	206
Table 5.3. Calculation of RV-PE to Titanium-Bone interface Ratio.....	211
Table 5.4. Implant Design Based on VPE and RVPE and Comparison of Their Mechanical and Wear Rate to Conventional UHMWPE, Highly-Crosslinked UHMWPE (HXLPE), and ASTM F648	221

List of Abbreviations

AFM	Atomic force microscopy
ALBC	Antibiotic-eluting bone cement
BC	Vancomycin-eluting bone cement
Bupi FB	Bupivacaine freebase
Bupi HCl	Bupivacaine hydrochloride
Bupi-PE	Bupivacaine eluting UHMWPE (Layered 20 % Bupivacaine HCl in UHMWPE on 20 % Bupivacaine FB in UHMWPE)
CoCr	Cobalt-chromium alloy
CRP	C-reactive protein
DAIR	Debridement, antibiotics, irrigation, and retention
EAB	Elongation to break
EDAX	Energy dispersive x-ray spectroscopy
EHD	Elastohydrodynamic lubrication
ESR	Erythrocyte sedimentation rate
FTIR	Fourier transform infrared spectroscopy
HXLPE	Highly-crosslinked UHMWPE
ICM-PJI	International consensus meeting on periprosthetic joint infection
IDSA	Infectious diseases society of America
IS	Impact strength
LDPE	Low-density polyethylene
MPC	2-Methacryloyloxyethyl phosphorylcholine

MV	Molecular volume
NMR	Nuclear magnetic resonance
PJI	Prosthetic joint infection
PMMA	Poly(methyl methacrylate)
PROSTALAC	Prosthesis with antibiotic-loaded acrylic cement
PSA	Polar surface area
Ra	Surface roughness
RVPE	6.7 % Vancomycin + 3.3 % Rifampin in UHMWPE
SEM	Scanning electron microscopy
SLIPS	Slippery liquid-infused porous surfaces
TGA	Thermogravimetric analysis
THA	Total hip arthroplasty
TJA	Total joint arthroplasty
TKA	Total knee arthroplasty
UHMWPE	Ultra-high molecular weight polyethylene
UTS	Ultimate tensile strength
UV-Vis	Ultraviolet and visible spectroscopy
VPE	6.5 % Vancomycin in UHMWPE
VRE	Vancomycin-resistant Enterococcus
VTBC	8.3 % Tobramycin and 23 % Vancomycin HCl in PMMA bone cement

Prologue

More than one million joint replacement are performed in USA annually[1]. However, around 10 % of patients suffer complications and need to undergo revision surgery within 10 years [2]. One of the most common reasons for revision surgery is prosthetic joint infection (PJI) [2]. PJI is an increasing healthcare burden [3] with a recurrence rate of 16 % [4] and a mortality rate of 2.5 % [5]. End-stage treatments are severely morbid, including multiple revisions, resection arthroplasty, arthrodesis and amputation [6]. While attempts at developing drug eluting polymers have been made to address peri-prosthetic infection, they have been largely impeded due to toxic degradation products [7], insufficient drug release [8], insufficient mechanical strength [9], and difficulty in consistent large scale manufacturing [10]. To date, the only clinically available drug-eluting polymers for joint surgery are antibiotic-loaded bone cements (polymethyl methacrylate). Bone cements are used primarily for achieving early fixation of the bone-implant interface, providing stability and reducing the risk of loosening-related complications. They were not intended to be weight bearing and have a large incidence of *in vivo* fracture if used under bearing conditions [9]. Therefore, a drug-eluting polymeric surface designed specifically for weight bearing in joint arthroplasty revisions is urgently needed primarily for the prevention and treatment of peri-prosthetic joint infection but also for other conditions which may benefit from sustained delivery of therapeutic agents from the bearing surface such as pain or inflammation.

While bone cements were not developed primarily for weight-bearing and articulation, the incorporation of antibiotics in bone cements have further compromised their mechanical strength. Similarly, incorporation of drugs in polymers designed for weight bearing and articulation is expected to affect the mechanical strength and also the wear resistance, a crucial property of articulating surfaces. Wear particles from the articulating surface are associated with osteolysis and implant loosening, compromising the longevity of these functional devices. The

state-of-the art bearing surfaces in joint replacement comprise a cross-linked ultrahigh molecular weight polyethylene (UHMWPE) 'soft' component articulating against a metal or ceramic 'hard' surface to minimize wear. The total knee prosthesis consists of three components: the femoral and tibial component are usually made of metal, while the plastic spacer is usually made of UHMWPE [12]. The total hip prosthesis consists of four components: The acetabular component, femoral head, and femoral stem are usually made of metal, while the plastic liner is usually made of UHMWPE [12]. Lubrication is disrupted by asperity contacts and the wear of the surfaces are largely governed by the plasticity and large-strain deformation of the polymeric component [11]. There is no literature on the wear behavior of drug-incorporated UHMWPE.

The most important problems to be solved in the design of a drug-eluting bearing surface are i) to minimize the effects of the incorporated drug on the mechanical properties of the polymeric matrix, ii) to obtain sustained elution of the appropriate drugs specific to the application; iii) to maximize lubrication and wear resistance. Understanding the effects of the physical and chemical interactions of an incorporated drug with the polymer matrix can lay the foundation by which processes can be developed to control the structure-property relationships of the polymer based on these interactions. Understanding these interactions will also enable the design of a controlled release profile of drugs most appropriate to the application. Finally, we can also use our new understanding with other chemical and physical methods to manipulate the morphology of the polymeric matrix to synergistic effect.

In this work, drug-incorporated polyethylene networks with modified morphologies were developed. Appropriate therapeutic agents for the treatment of peri-prosthetic infection and post-operative pain management were incorporated and the effects of drug chemistry on drug elution are described. Medical device designs specific for joint replacement implants are proposed for maximized mechanical strength of polyethylene matrices containing drugs and the

efficacy of these drug-eluting polyethylenes are demonstrated *in vitro* and *in vivo*. A new understanding of the effects of drug-incorporated UHMWPE on wear and lubrication is proposed. This work presents the first thorough description of a load-bearing surface with drugs designed to elute for therapeutic effect.

Chapter 1

Background

Total Joint Arthroplasty (TJA)

Arthritis (osteoarthritis and inflammatory arthritis) affects 52.5 million people in the United States annually [13] and it is expected to affect 78 million people by 2040 because of the aging population [14]. Joint arthroplasty, surgical procedure of replacing native joints with prosthetic joints, is the most effective treatment, especially for hip and knee arthritis, with more than one million arthroplasties performed in the USA annually[1]. To restore the joint function back to its normal function, prosthetic joints mimic the anatomical shape and function of the natural healthy joints, which will be detailed further in the sections below.

Total Hip Arthroplasty

The current design of total hip arthroplasty draws large similarity to the first metal on polymer prosthetic joints created by Professor Sir John Charnley in 1958 using Teflon for acetabular component and metal femoral component[15]. Because of its high wear rate, the material needed to be replaced after a couple of years[16]. As a result, in 1962, Charnley started using ultra high molecular weight polyethylene (UHMWPE) instead of Teflon for the acetabular component while continuing to use stainless steel as the femoral component[17]. Long-term follow-up (4-7 years) of 379 patients receiving Charnley prosthesis with UHMWPE acetabular component showed that 100 of patients were relieved of pain and were able to walk again[18].

There are four main components of total hip prosthesis (**Figure P.1.**): Acetabular cup, acetabular liner, femoral head, and femoral stem. The acetabular cup and femoral stem are

usually made of metal, while the acetabular liner and femoral head can be made of metal, UHMWPE, or ceramic. The acetabular cup and acetabular liner mimics the acetabulum of the pelvis, while the femoral head and femoral stem mimic the head and diaphysis of femur[19]. Metallic or ceramic femoral head articulating against UHMWPE acetabular liner are the most preferred choice of bearing surfaces, being used in more than 65 % of all primary joint replacement[20]. Because of the widespread use of UHMWPE in the hip joint prosthesis, in this thesis we focused on creating drug eluting UHMWPE that will be detailed later in this chapter.

Total Knee Arthroplasty

The current design of bicondylar knee implants were first designed in 1971 in Mayo Clinic, and named “Geometric” knee design[21]. The Geometric knee design was composed of two components: A metallic femoral bicondylar component and a UHMWPE tibial plateau, both of which were fixed in place using bone cement. The implants suffered from poor long-term fixation of the UHMWPE component[22], with overall 10-year survival rate of 69%[22]. Since then many modifications in the TKA implants design have been developed, including adding UHMWPE plugs as the patellar component[23], UHMWPE with metal backing[24], and mobile bearing TKA where the UHMWPE articulates against both the metal backing and the femoral component[25].

Modern TKA implants was usually comprised of three components: the femoral component, the tibial backing, and the tibial liner. The femoral component and tibial backing are made of metal, while the tibial liner is made of UHMWPE[12]. All the TKA implants currently used utilize metal femoral component articulating against UHMWPE tibial liner[12].

Development of UHMWPE Technologies to Address Total Joint Arthroplasty Complications

While the Charnley prosthesis in the hip and both Polycentric and Geometric prostheses in the knee significantly improved pain and walking function of patients receiving it, significant portions of the patients suffered complications related to the joint replacement. Among 106 UHMWPE components implanted by Charnley between November 1962 to December 1963 and followed up for 9-10 years, 4-6 % were infected, 1-2 % underwent aseptic loosening and 2 % underwent dislocation[26]. In TJA, most revision surgeries are performed due to prosthetic joint infection and aseptic loosening (each contributes 25 % to the revision rates for TJA)[27, 28]. To address complications related to aseptic loosening, crosslinking technologies related to UHMWPE were developed to address complications related to TJA[29].

Ever since Charnley introduced low friction arthroplasty and used Teflon as part of the hip prosthesis, wear rate had been a concern. Wear particles promoted osteolysis and aseptic loosening, which ultimately required revision surgery[30]. Review of 11,543 revisions in hip arthroplasty in Sweden from 1979 to 1998 showed that 75.7 % of hip revisions occurred due to aseptic loosening[31]. To address the problem with insufficient wear resistance of UHMWPE, highly crosslinked UHMWPE was developed[32].

Highly crosslinked UHMWPE (HXLPE) was created by exposing UHMWPE stock material to ionizing radiation (gamma or electron beam) ranging from 50 to 105 kGy[32]. The irradiated material was then exposed to thermal treatment, by way of either annealing or remelting. After that, the material was machined to the final implant shape and then sterilized[32]. While radiation crosslinking of UHMWPE significantly decreased the wear rate, it also resulted in decreased the material ductility, fatigue resistance, and fracture resistance[33]. Because of the tradeoff between reducing wear rate and decreased fatigue and fracture resistance, manufacturers of the implants for total joint arthroplasty must decide on the optimum radiation dose to create an implant with low wear rate but also sufficient fatigue and fracture resistance[32]. Analysis of 1038 total hip replacements performed with highly crosslinked or conventional (irradiated with low dose for sterilization only) UHMWPE showed that highly

crosslinked UHMWPE significantly reduced *in vivo* wear rates and as a result, also reduced the risk for radiological osteolysis (mean risk ratio comparing highly crosslinked to conventional UHMWPE was 0.40)[34]. Usage of highly crosslinked UHMWPE reduced the 10 year cumulative percent revision in hip to 4-5 %, as compared to 6-13 % in conventional UHMWPE[35].

While early clinical results of HXLPE have been excellent, long-term factors such as *in vivo* oxidation, which deteriorates mechanical strength and wear rate of HXLPE, may become the new limiting factor for the longevity of HXLPE *in vivo*[36]. *In vivo* oxidation of UHMWPE occurs through radiation induced free radicals, which may also be initiated *in vivo* by cyclic loading, and/or through reaction of lipids absorbed from the synovial fluid[37-39]. In order to minimize *in vivo* oxidation, highly crosslinked UHMWPEs stabilized with at least 500 ppm of the antioxidant vitamin E(VE-HXLPE) was added[40]. Accelerated *in vitro* oxidation of VE-HXLPE did not show any sign of oxidation nor decrease in mechanical strength compared to unoxidized VE-HXLPE[40, 41]. Unstabilized HXLPE, on the other hand, showed a 500% increase in total oxidation and a 70-80 % decrease in mechanical strength as compared to VE-HXLPE. [40, 41] A randomized clinical trial comparing VE-HXLPE against HXLPE for two years showed similar wear rates with no unexpected outcomes[40-42]. Because VE-HXLPE was only approved by FDA in 2007 for hip and in 2008 for knee, clinical data to compare longevity of VE-HXLPE vs HXLPE are not yet available[43].

Current Complications Related to TJA

Since the introduction of HXLPE in total hip arthroplasty (THA), incidence of aseptic loosening/osteolysis has significantly diminished [44]. Usage of HXLPE reduced the cumulative incidence of aseptic loosening by 60 % (2.3 % vs 0.92% with conventional vs HXLPE respectively) within ten years post implantation.[44] However, while HXLPE reduces the incidence of aseptic loosening, the cumulative incidence of PJI is similar to those of

conventional UHMWPE (**Table 1.1**). Other THA associated complications such as dislocation, fracture, and pain were also similar between conventional UHMWPE and HXLPE[44]. Overall, with HXLPE, PJI is the second most common reason for THA revision, second only to dislocation.

Number of years since implantation	Cumulative Incidence with conventional UHMWPE (%)	Cumulative Incidence with HXLPE (%)
1	0.28	0.4
5	0.59	0.62
10	0.83	0.77

Table 1.1. Cumulative incidence of PJI in THA based on number of year since implantation with conventional UHMWPE and HXLPE[44].

In total knee arthroplasty (TKA), prostheses using HXLPE had a cumulative revision rate of 3.6 % at 10 years, much lower than the 5.7 % in prostheses using conventional UHMWPE[45]. The large decrease in cumulative revision rate was primarily due to reduced incidence of aseptic loosening in HXLPE vs conventional UHMWPE (0.77 % in HXLPE at 10 years vs 1.65 % in conventional UHMWPE at 10 years) [45]. Similar to the case with THA, while there is a large reduction in aseptic loosening with HXLPE in TKA, the cumulative incidence of revision due to other causes such as prosthetic joint infection, pain, and instability are similar to conventional UHMWPE (**Table 1.2**). [45] PJI was the top reason for TKA revision with HXLPE within one, five, and ten years of implantation. [45]

Number of years since implantation	Cumulative Incidence with conventional UHMWPE (%)	Cumulative Incidence with HXLPE (%)
------------------------------------	---	-------------------------------------

1	0.39	0.42
5	0.90	0.76
10	1.0	1.0
Table 1.2. Cumulative incidence of PJI in TKA based on number of year since implantation with conventional UHMWPE and HXLPE[45].		

In summary, because HXLPE is currently used in 96 % of all THA[44] and 54 % of all TKA[45] with expected further increase in usage due to its wear resistance, incidence of aseptic loosening goes down as compared to conventional UHMWPE, while incidence of PJI becomes more prevalent. Therefore, it is important to develop better prophylaxis and treatment alternatives for PJI to reduce the overall incidence of revision arthroplasty.

Incidence and Economic Burden of Periprosthetic Joint Infection

PJI occurs in 2.05-2.18 % of patients who have undergone TKA and in 1.99-2.18 % of those with THA.¹ PJI incidence in shoulder arthroplasty ranges from 0.8-1.1 %[46, 47], while PJI incidence in elbow arthroplasty is higher at 3.3 %[48]. The higher incidence of PJI in the elbow arthroplasty is attributed to the higher percentage of rheumatoid arthritis in patients undergoing elbow replacement and the limited amount of soft tissue surrounding the elbow, exposing it to infectious microorganisms.[49] The current annual incidence of PJI in the US is 7,100-15,000, and is predicted to be 55,000-75,500 by the year 2030. Adjusting for patient demographic factors such as age, sex, race, and census region, the risk of hip infection increased significantly from 2001 to 2012.[50] The risk for PJI was greatest in the first 2 years after implantation, during which time 60-70 % of PJI occurred.[51, 52]

PJI causes a significant morbidity and mortality to the patient, and also a significant burden to the economy. Compared to the average length of hospital stay for primary THA and TKA without PJI occurrence, an average of 10-12 days is added to the hospital stay for PJI.[50]

Patients who had PJI never return to the functionality of patients who did not have PJI.[53] In addition to significant morbidity, PJI leads to a high mortality rate: PJI treated with two-stage revision had up to 26 % all-cause mortality within two years[53]. Mortality rate as high as 45 % was reported for recurrent PJI.[54]

PJI treatment is estimated to cost as high as U\$ 100,000 per case, which is five times higher than the cost of primary arthroplasty.[55] The cost is attributed to revision surgery being more resource-heavy, long rehabilitation time, and long-term usage of antibiotics and analgesics.[55] The cost of revision surgery due to infection is higher than the cost of revision for non-infectious causes[56]. In 2009, the total cost for the management of prosthetic joint infections was ~ 800 million dollars; this number is predicted to be 1.6 billion dollars by 2020.[50] By all measures, PJI is a significant burden to the patient and the healthcare system.

Pathogenesis of Prosthetic Joint Infection

Bacterial seeding into the prosthetic joints is thought to occur through three main pathways: First, direct bacterial seeding during implantation; second, through hematogeneous spread from other body parts, and third, through recurrent infection[57]. Infection around medical implants is especially difficult to treat because of the dampened innate immune system[58] and bacterial biofilm formation on the surface of the implant which reduces the susceptibility to antibiotics of the bacterial population.[57] An animal infection study showed that 100,000 times less bacterial concentration is needed to induce infection in the presence of a foreign body as compared to the absence of a foreign body[59]. In fact, less than 100 colony-forming units of microorganisms were sufficient to cause an infection.[60] The increased susceptibility to infection in the presence of medical implant is partially due to local granulocyte defects in the environment surrounding the medical implant.[58, 60] In the presence of a foreign body such as a medical implant, neutrophils on the foreign surfaces release peptides that deactivate granulocytes[61].

Based on the time of onset, PJI can be acute or chronic. Seventy percent of PJI occurs acutely, and the remaining thirty percent occurs chronically[62]. Acute infections usually occur within three weeks of joint replacement, are confined to the joint space, do not invade the prosthetic-bone interface, and most do not involve the formation of bacterial biofilms. Patients with acute PJI usually present with fever, increased pain locally, around the surgical site, erythema, and poor wound healing.¹⁰ On the other hand, chronic infection usually occurs at least three weeks post-surgery, but can also occur months to years later, and patients present with a joint that is painful and warm, with an effusion. Since the bacteria have been occupying the prosthetic joint surface for weeks to months, most chronic PJIs involve the formation of a biofilm, which allows the bacteria to adhere strongly to the prosthesis, shield themselves from host immune system, and make them 1000 to 1500 times more resistant to antibiotic treatment.

Acute infections usually occur through two main mechanisms: First, direct bacterial inoculation introduced during the surgery, and second, through contiguous spread of infection from superficial surgical site infections[63].

Chronic or late infections are predominantly due to hematogenous spread.[64] The most common source of hematogenous spread is from a skin infection, respiratory tract infection, dental infection, and urinary tract infections.[65] Only 100-1000 CFU/ml bacteria in blood are needed to cause hematogenous infection of the prosthetic joints[60]. Overall, PJI resulting from hematogenous infection is rare: 1.2-6 % of reported PJI cases are due to hematogenous spread[66]. Of patients with confirmed bacteremia, only 6 % were found with hematogenous PJI[63]. However, some bacteria such as *S. aureus* causes a higher risk of hematogenous PJI: Several studies showed that *S. aureus* bacteremia is associated with 30-40 % risk of hematogenous PJI[63, 67, 68]. In the majority of hematogenous PJI, bacteremia and onset of PJI occur almost simultaneously[63].

Risk Factors for Prosthetic Joint Infection

Various comorbidities and demographic factors such as diabetes[69, 70], preoperative anemia, cardiovascular disorders, chronic renal failure, nutritional status[57], body mass index[71], smoking and alcohol consumption status[72-74], rheumatoid arthritis[75], and usage of antibiotic eluting bone cement[76] have been shown to affect the risk for PJI.

Patient with diabetes had seven times higher risk for PJI than non-diabetic patients[69]. A separate study analyzing 1947 patients receiving TJA showed that diabetic patients occupied 22 % of the infected cohort, as opposed to 9 % in the uninfected cohort.[70] Blood glucose of > 200 mg/dL was found to double the risk of PJI as compared to patients with normal blood glucose[70]. The elevated risk for PJI in patients with diabetes is likely due to impaired wound healing[77] and elevated biofilm formation associated with elevated glucose levels[78].

Poor nutritional status has been associated with increased risk for PJI.[79] A patient is considered in the poor nutritional state if one of the following is satisfied: serum albumin < 3.5 g/dL (healthy range 3.4-5.4 g/dL), total lymphocyte count < 1500 cells/mm³, serum transferrin levels < 200 mg/dL, or serum prealbumin < 15 gm/dL.[80, 81] Patients with total lymphocyte count of < 1500 cells/mm³ was found to have 5 times greater risk for PJI, and patients with albumin levels of < 3.5 g/dL was found to have 7 times greater risk for PJI.[82] Separate study showed that patients who underwent PJI revision surgery and satisfied the poor nutritional status mentioned above were found to have 7 times higher infection rate than patients with good nutritional status.[79] The poor nutritional state has been shown to interfere with the synthesis of collagen and proteoglycan that is crucial for wound healing. Disruption of such processes may lead to persistent wound drainage and increased risk of infection.[81]

High body mass index (obesity) has been shown to have increased risk of PJI after THA and TKA (adjusted hazard ratio of 1.72 and 1.22 respectively).[71, 83] The risk of PJI elevated from 3.3 times higher in patients with BMI > 40 kg/m² (as compared to patients with BMI=18.5-25 kg/m²) to 21 times in patients with BMI > 50 kg/m² [71, 84]. A separate study evaluating

7,181 primary TJA reported elevated PJI rate from 0.37 % in patients with normal BMI to 4.66 % in morbidly obese patients.[85]

Smoking has been shown to significantly increase the rate of surgical site infections[72], the rate of deep wound infections[74], and the rate of wound complications than nonsmokers.[73] The elevated risk of infection due to smoking is likely due to reduced blood flow to the healing tissue, impaired delivery of cellular and humoral immunity to the surgical site, disruption of immune cell function, and disruption of neutrophil defense mechanisms against pathogens[86].

Alcohol consumption has been shown to increase the risk of infection in patients underwent major, non-cardiac surgery[87]. The elevated risk of infection is thought to originate from alcohol-induced disruption of the immune system that is crucial to eradicate microorganisms surrounding prosthetic joints.[88]

Patients with rheumatoid arthritis were reported to have elevated risk of PJI than patients without rheumatoid arthritis (hazard ratio = 1.71 for THA and 1.18 for TKA).[75] The PJI rate for patients with rheumatoid arthritis has been reported to be as high as 2.3 % in the first year[89]. While the reasons behind the elevated risk for infection due to rheumatoid arthritis are poorly understood, reports suggest that the disease itself and immunosuppressive therapies to treat it both contribute to increased risk for PJI[63].

Bacterial Strains Commonly Found in PJI

On average, a positive culture is obtained on 68-94 % of all patients with apparent PJI.[90][64, 91] Gram-positive bacteria account for 90-95 % of all culture-positive PJI,[64] with 54-80 % of PJIs due to the gram-positive *S. aureus* and coagulase-negative *Staphylococcus* species such as *S. epidermidis*, or *S. lugdunensis* [64]. The percentage of PJI caused by *S.aureus* and coagulase negative *Staphylococcus* are relatively equal [63]. Gram-positive streptococci and enterococci account for ~10 % of all PJI [63]. Some of the less common

microorganisms are aerobic gram-negative bacilli, including *E Coli*, present in <10% of all PJI cases[63] and anaerobic bacteria such as *Propionibacterium acnes*, present in 4 % of all PJI cases and are more commonly found in shoulder arthroplasty infection than in PJI of any other joints[63, 92, 93]. In cases where *S aureus* is the culprit for PJI, ~54% are caused by methicillin-resistant *S aureus* (MRSA) and ~ 46% are caused by methicillin-sensitive *S aureus* (MSSA) [63].

Different types of bacteria are associated with different time onset of PJI: *S. aureus*, coagulase-negative staphylococci and aerobic gram-negative bacilli contributed to 84 % of early onset PJI (<1-3 months after surgery) (38 % for *Staphylococcus aureus*, 22 % for coagulase-negative *Staphylococcus*, and 24 % for aerobic gram-negative bacilli). Interestingly, 31 % of early-onset PJI was polymicrobial, possibly indicating inoculation with multiple microorganisms at the time of surgery[63]. In PJI with onset 3 month to 1-2 years after implantation, most are caused by less virulent microorganisms such as coagulase-negative staphylococci and enterococci while gram negative bacilli is rarely found[94]. In the late onset PJI (>1 years to 2 years after implantation), hematogeneous seeding from *S. aureus* predominates.[67, 68]

Chronic PJI with onset of >1 to 2 years after implantation, is often caused by hematogeneous infection of *S. aureus* and *Streptococcus* species at the same frequency, accounting for a total of 80 % of all hematogeneous PJI[95]. Other bacterial species that were found in hematogeneous infection include coagulase-negative staphylococci, *Enterococci* species, and aerobic gram-negative bacilli[51, 96-98]. Therefore, addressing PJI caused by *S. aureus*, *Streptococcus* species, and other gram positive bacteria is of the utmost importance.

Commonly used prosthetic joints use metal for the bone-prosthetic joint interface (cobalt-chromium (CoCr) or titanium alloy (TiAl6V4)) and ultra-high molecular weight polyethylene (UHMWPE) for the articulating surfaces. In the US, fixation of the implants to the bone in the primary surgery is largely done using porous metallic surfaces with the potential of enabling bony ingrowth rather than with the aid of bone cements, which are more commonly used in

Europe [99, 100]. Bacterial recovery from prosthetic joint explants of patients with hip joint infections [101] show that the UHMWPE liner contains the highest bacterial load, followed by the metal femoral head and metal acetabular cup; the metal femoral stem has the lowest bacterial count. Bacterial recovery from explants of patients with knee joint infections [102] also shows that the UHMWPE tibial insert contains the highest bacterial load. Therefore, in order to treat infections in the PJI, both bacteria in the articular space and in between bone-implant interface need to be eradicated.

Involvement of Biofilm in PJI

Biofilm related to PJI consist of communities of microbes embedded in an extracellular polymeric matrix that forms on the surface of prosthetic joints [63]. Bacteria in the biofilms develops into organized, complex communities with structural and functional heterogeneity, resembling a multicellular organism [103]. Bacteria in the biofilm communicate with each other through quorum sensing, allowing them to divide into subpopulations with different functions working together to support the whole biofilm[63]. Formation of biofilms consist of four primary stages: attachment to the surface, growth on the surface, maturation of biofilm, and detachment[63].

The extracellular component of the biofilm is composed of polysaccharides, DNA, and proteins[63]. In the biofilm, bacteria are protected from immune responses and antimicrobial agents, resulting in much greater resistance to killing by antimicrobials[104, 105]. The antimicrobial resistance of biofilm is partly attributed due to reduced bacterial growth in the biofilm because of incomplete penetration of metabolites such as glucose or oxygen throughout the thickness of biofilm[106]. In addition, the presence of antimicrobial resistant subpopulations called persisters and the microenvironment in the biofilm can impair antimicrobial activity [107, 108]. All these factors resulted in much higher antibiotics concentrations needed to eradicate the bacteria in biofilm, which can only be achieved through local administration [109]. While

biofilms can be found in both acute and chronic PJI, biofilm in PJI is especially important in chronic PJI, where most bacteria exist on the surface of the prosthesis, limiting the sensitivity of periprosthetic tissue and fluid cultures.[63] Therefore, an ideal treatment for PJI will be a device that can deliver high local doses of antibiotics to eradicate bacterial biofilm inside the joints. The antibiotics delivered need to have high efficiency against both planktonic and biofilm bacteria (e.g. rifampin [110]).

Diagnosis of PJI

The diagnosis of PJI is based on patient presentation, laboratory findings from peripheral blood and synovial fluid, microbiological culture, histological evaluation of periprosthetic tissue, and radiographic imaging [63]. Patients with PJI may present to the hospital with fever, joint pain, joint swelling, erythema, warmth, drainage, or the presence of a sinus tract around the joint.[90] The frequency of symptoms vary with the onset time of the PJI and the type of bacteria in the PJI: Pain is more common in early onset PJI (<3 months) than later onset PJI, with 79-100 % of patients with early onset PJI reporting pain[111, 112] compared to only 42 % of patients with late onset PJI.[90] Presence of a sinus tract, abscess, open wound, and soft tissue damage are more common in patients with direct inoculation of *S. aureus* during surgery than in those with hematogeneously acquired *S. aureus*[112, 113]. On the other hand, fever and chills are significantly more common in patients with hematogeneous PJI than in patients with direct inoculation PJI [63].

The International Consensus Meeting on PJI (ICM-PJI) released the following diagnostic criteria for PJI[114]:

- Major criteria:
 1. Two positive periprosthetic cultures with phenotypically identical organisms
 2. Sinus tract communicating with the joint
- Minor criteria:

1. Elevated C-reactive protein (CRP) or erythrocyte sedimentation rate (ESR)
2. Elevated white blood count (WBC) in synovial fluid
3. Elevated polymorphonuclear neutrophil percentage in synovial fluid
4. Positive histological analysis of periprosthetic tissue
5. Single positive culture.

The peripheral blood tests for PJI, such as WBC, ESR, and CRP rely on the host response to the infecting pathogen.[63] CRP has better sensitivity than ESR and WBC (88 % for CRP, 75 % for ESR, and 45 % for WBC)[115], and hence is better at ruling out the presence of PJI. The combination of a normal CRP and a normal ESR has 96 % sensitivity in ruling out PJI. However, the specificity when either or both tests are positive is low, only at 56 % [116], and could not predict the type of bacteria nor the antibacterial sensitivity of the infecting bacteria.

Measurement of interleukin-6 (IL-6) with a threshold of 10-12 pg/ml in the peripheral blood has both high sensitivity and specificity for PJI (97 % sensitivity and 91 % specificity)[115]. IL-6 is a cytokine produced by activated monocytes and macrophages in response to inflammation and infection[63]. Determination of serum procalcitonin was also shown to have high specificity to rule in PJI (98%), but low sensitivity (33 %)[117].

Nucleated cell count, neutrophil differential, and leukocyte esterase test in synovial fluid is recommended by the International Consensus Meeting (ICM) and Infectious Diseases Society of America (IDSA) as part of PJI diagnosis [118]. Neutrophil percentage analysis in synovial fluid analysis for PJI has sensitivity and specificity of 91-97% and 88-95 %, respectively [119-121]. Nucleated cell count in synovial fluid has sensitivity of 84-91 % and specificity of 93-99 % [122-124]. Measurement of leukocyte esterase in synovial fluid, which is an enzyme produced by neutrophils, has sensitivity of 81-93 % and specificity of 77-100 % [125, 126]. A relatively new method to diagnose PJI by measuring antimicrobial peptides

produced by neutrophils, such as α - and β -defensins in synovial fluid, showed 92-99 % sensitivity and 92-99 % specificity [127].

Microbial culture of synovial fluid is an indispensable method of confirming diagnosis of PJI, identifying the infecting pathogen, and determining the pathogen's antimicrobial susceptibility.[63] This method was shown to have sensitivity of 86-87 % and specificity of 95-100 % for diagnosing PJI[128-130]. Sensitivity of synovial fluid culture is higher for acute PJI than chronic PJI (91 % vs 79 %)[129], presumably due to the larger amount of bacteria in biofilm form in chronic PJI and larger amount of bacteria in planktonic form for acute PJI.[63]

Beside microbial culture of synovial fluid, several different methods are used to identify the pathogen and its antimicrobial susceptibility. Such methods include intraoperative periprosthetic tissue culture[131] (sensitivity of 80 % and specificity of 97 %), sonication of implants/periprosthetic tissue and reculturing (79% sensitivity and 99 % specificity)[132]. Sonication and reculturing was found to have higher sensitivity (62-94 %) than intraoperative periprosthetic tissue culture (54-88%)[132].[92, 133-135].

Therefore, because the identity of the bacteria and their antimicrobial sensitivity causing the PJI is often unknown, empirical antibiotic treatment providing broad coverage, such as gentamicin, is often administered[136].

Prophylaxis Approaches to Reduce Incidence of PJI

Many strategies have been devised and tried to reduce the incidence of PJI, such as nasal and cutaneous decolonization[137], per-operative antiseptic [138, 139], intraoperative systemic antibiotics[140], hair clipping[141], laminar airflow ventilation[142], body exhaust suits[143], betadine lavage[144], and antibiotic eluting bone cement[145, 146].

Among the strategies aforementioned above, the following strategies have been shown to be effective:

1. Nasal and cutaneous decolonization. A randomized, double-blinded trial showed that cutaneous and nasal decolonization with mupirocin effectively reduced the incidence of infection as compared to placebo [137]. In addition, preoperative mupirocin for all patients undergoing total joint arthroplasty was more cost effective than when no treatment was given[137].
2. Usage of chlorhexidine gluconate as antiseptic in lieu of povidone-iodine was shown to significantly reduce incidence of PJI [55, 138, 139].
3. Antibiotic prophylaxis. Antibiotic prophylaxis was shown to reduce the absolute risk of PJI by 8 % [140]. The clinical practice guideline for antimicrobial prophylaxis in surgery recommended cefazolin for patients with TJA [147]. Vancomycin was recommended as prophylaxis in MRSA-colonised patients and in institutions where MRSA surgical site infections are relatively common [57].
4. Intraoperative lavage. A retrospective study showed a six-fold reduction in PJI rates with dilute betadine lavage as compared to saline lavage[144].

The following strategies have been shown to not reduce or even increase the incidence of PJI:

1. Laminar airflow ventilation. Laminar airflow ventilation was thought to minimize particles in the operating room that could contaminate the surgical site [142]. Unfortunately, a registry analysis [148] and a systematic review [149] showed that laminar airflow increases incidence of early PJI relative to conventional operating rooms.
2. Body exhaust suits. Body exhaust suits are commonly used in TJA to minimize the probability of material from surgeons contaminating the surgical site [143]. However, most investigations showed that the usage of body exhaust did not show any difference or actually increased the incidence of PJI [148].

Current Treatment of Patients with PJI

Three main surgical strategies are currently used to treat PJI: debridement with prosthesis retention (DAIR), one-stage revision surgery, and two-stage revision surgery.[63] Successful PJI treatment is defined as the eradication of the microbiological and the clinical infection, the absence of relapsed infection, the absence of subsequent surgical intervention for the same PJI, and the absence of mortality related to PJI.[150]

In a DAIR protocol, the prior surgical incision is reopened followed by irrigation and debridement of the infected and necrotic tissues (as ascertained visually), the removal of any hematoma and purulence surrounding the prosthesis, replacement of any exchangeable component such as the polyethylene liner and the modular femoral head, aggressive irrigation, and then closure of the surgical site, typically over a drain[151, 152]. Broad-spectrum antimicrobial therapy is indicated immediately postoperatively if the culture result is negative. If culture is positive, tailored antimicrobials are used. Intravenous antibiotics are usually administered for 2 to 6 weeks following DAIR surgery [151-156]. The risk of failure of DAIR to eradicate PJI increases by 4-fold after antimicrobials are stopped, with most failure occurring in the following 4 months [152]. To prevent infection relapse, oral suppressive antimicrobials can be used for at least several months after surgery[118]. Oral rifampin combined with other antibiotics such as β -lactam, glycopeptide, or fluoroquinolones increased the success rate of DAIR for *S. aureus* to 62-80 %[157, 158] as compared to 36 % without rifampin[154]. DAIR should only be performed on patients with early onset of PJI (occurring within the first month), short duration of symptoms (< 3 weeks), stable implant, and in the absence of a sinus tract [64, 118, 153, 159-161]. PJI with *Staphylococcus* species including *S. aureus* is associated with high risk of DAIR failure[95][151-153, 156]. Higher rates of DAIR failure were also observed when infection was caused by methicillin-resistant *S. aureus* (MRSA) (success rate of only 18-33 % even with the use of rifampin) (372, 373)[162][163, 164], vancomycin-resistant enterococci (VRE), or fluoroquinolone-resistant gram-negative bacilli[165]. Overall, the average success rate

of DAIR was 33 % for knee PJI and 52 % for hip PJI[160, 166]. The success range of DAIR ranged from 31 % to 82 % [69, 95, 151-153, 156, 162, 167-174].

In one-stage revision surgery, the surgical site is reopened, arthrotomy and debridements are performed, and infected prostheses are then removed. [63] New implants are then implanted during the same surgery and fixed using antibiotic eluting bone cement.[63] Intravenous antibiotic is then administered for 4-6 weeks, followed by oral antibiotics for 3-12 months.[175-177] Oral rifampin is recommended especially for PJI due to Staphylococci species.[118] Indefinite chronic suppressive antibiotics are typically used to minimize PJI recurrence.[63] One stage revision surgery is usually used for hip joint PJI [175-177], but seldom used for knee PJI.[63] One stage revision surgery is indicated for patients with adequate bone stock, a positive culture that is susceptible to antibiotics that can be incorporated into antibiotic eluting bone cement (ALBC), good surrounding soft tissue, and no sinus tract [64, 118, 159]. The overall success rate for one stage revision surgery ranged from 77-100 % [169, 175, 176, 178-184]. A meta-analysis comparing the success rate of one-stage to two-stage revision surgery found 87 % success rate for one-stage and 90 % success rate for two-stage surgery.[185]

The two stage revision surgery consists of two separate surgeries: In the first surgery, the infected prostheses (both acetabular and femoral components for hip joint and femoral and tibial component for knee joint) are excised, necrotic tissue (bone, muscle, synovial capsule) are debrided, and an antibiotic spacer made from antibiotic-eluting bone cement (ALBC) is implanted for local antibiotic delivery to eliminate bacteria in the joint space and to maintain limb length. In addition to this spacer, systemic antibiotics are administered for four to six weeks following the resection. After that, systemic antibiotics are stopped for 2-6 weeks to evaluate for any sign of ongoing infection through CRP, ESR, and synovial fluid aspiration[91, 186]. If there is still evidence of ongoing infection, repeat debridement might be performed and more systemic antibiotics will be administered[91, 186]. When no sign of ongoing infection is found, the second

surgery is performed, where a new prosthesis is implanted and fixed using ALBC [91, 186]. During the second stage surgery, biopsy of joint tissues is also performed to test if there is still any local infection[91, 186]. Patients are then treated again with intravenous antibiotics until the final analysis of the biopsied tissue shows no sign of infection[91, 186]. Indefinite chronic suppressive antibiotics are sometimes used to minimize PJI recurrence.[63] The overall success rate of two-stage revision surgery was 87-100 % for hip [169, 175, 187-190] and 72-95 % for knee [191-196].

Recommended antimicrobials for PJI

Systemic antimicrobials for 4-6 weeks are recommended for DAIR, one-stage revision, and two-stage revision surgeries for treatment of PJI[151-156][175-177] [91, 186]. In general, antimicrobial therapy administered for PJI patients must be directed by the result of antimicrobial susceptibility testing from the culture of the patient's synovial fluid or tissue biopsy.[63] When the infecting microbes are susceptible to multiple antibiotics, priority should be given to the least toxic, highest efficacy, and narrow-spectrum antimicrobials.[63] When intravenous antimicrobials are administered in an outpatient setting, laboratory monitoring such as complete blood count, metabolic panel, creatinine, blood urea nitrogen, alanine aminotransferase, and aspartate aminotransferase are performed weekly[197].

The following antibiotics are recommended by the Infectious Diseases Society of America (IDSA) for PJI treatment[63, 118]:

Microorganism	Preferred Treatment	Alternative Treatment	Combination therapy
Methicillin-susceptible Staphylococci	Cefazolin or nafcillin	Vancomycin, daptomycin, or linezolid	Rifampin
Methicillin-resistant Staphylococci	Vancomycin	Daptomycin or linezolid	Rifampin
Penicillin-susceptible	Penicillin or ampicillin	Vancomycin,	Aminoglycosides

Enterococci		daptomycin, or linezolid	(gentamycin, tobramycin)
Penicillin-resistant enterococci	Vancomycin	Daptomycin or linezolid	Aminoglycosides (gentamycin, tobramycin)
<i>Pseudomonas aeruginosa</i>	Cefepime or meropenem	Ciprofloxacin or ceftazidime	Aminoglycosides (gentamycin, tobramycin) or fluoroquinolones (ciprofloxacin)
Enterobacter species	Cefepime or ertapenem	Ciprofloxacin	-
<i>Enterobacteriaceae</i>	Beta-lactam or ciprofloxacin	-	-
Beta-hemolytic streptococci	Penicillin or ceftriaxone	-	-
<i>Propionibacterium acnes</i>	Penicillin or ceftriaxone	-	-
Table 1.3. Common bacteria causing PJI and the recommended antimicrobial treatment.			

Antibiotic-Eluting Bone Cement (ALBC) is the Current Gold Standard for Local Delivery of Antibiotics in PJI

ALBC, is the gold standard for clinically used materials for local delivery of antibiotics into the joint, most importantly to the area that could not be reached by intravenous antibiotic administration[198]. To create ALBC, PMMA powder is first either industrially premixed or premixed in situ in the operating room with powdered antibiotics[199]. Liquid monomer is then added slowly, and the mixture is stirred thoroughly to start the polymerization process.[199]

When the resulting solution is viscous enough to be molded into shapes, ALBC is formed into a temporary spacer, or inserted into the interface between bone and the metal stem. During polymerization, the exothermic nature of the reaction causes the temperature of the ALBC to reach 60-80°C. Therefore, only thermally and chemically stable antibiotics can be incorporated into ALBC[200]. Antibiotics in ALBC is released from the surface, cracks, and voids within the cement.[201]

In addition to thermal and chemical stability, antibiotics incorporated into ALBC must also satisfy the following criteria: (1) antibiotics must be above the minimum inhibitory (MIC) and minimum bactericidal concentration (MBC) sufficiently long enough to eradicate the infecting bacteria. (2) antibiotics must be able to overcome the break point sensitivity limit of bacteria, defined as the antibiotic concentration that causes bacteria to transition from sensitive to resistant within 3-4 weeks. (3) Antibiotics must not be present at levels that cause toxicity to the tissues or bone [198]. Several antibiotics that have been shown to satisfy the above criteria include gentamicin[202] and tobramycin[200] (aminoglycosides active against both gram positive and gram negative bacteria), vancomycin (glycopeptide active against gram-positive bacteria)[203], amphotericin B[204], amikacin[204], amoxicillin[204], ampicillin[204], cefazolin[204], cefotaxime[205], cefuroxime[204], ciprofloxacin[204], clindamycin[204], colistin[206], daptomycin[207], erythromycin,[206] fluconazole[208, 209], levofloxacin[204], linezolid[204], meropenem[210], piperacillin/tazobactam[211], or teicoplanin.[208, 209] Rifampin, an antimicrobial that is important for the treatment of *Staphylococcus* PJI with high efficacy against bacterial biofilm, cannot be incorporated into bone cement because it impedes the polymerization of bone cement [212].

The incorporation of multiple different types of antibiotics with different mechanisms of action have been shown to be synergistic in bacterial eradication: ALBC spacers containing gentamicin and vancomycin were more effective in eradicating *S. aureus*, *S. epidermidis*, *E. coli*, and *P. aeruginosa* , as compared to spacers that only contained gentamicin.[213]

Furthermore, the dual vancomycin-gentamicin eluting PMMA spacers are more effectively protected from bacterial colonization than PMMA spacers eluting only gentamicin.[214] ALBC spacers containing vancomycin and tobramycin showed increased release of both antibiotics when compared to the ALBC containing either tobramycin or vancomycin alone.[215, 216] Furthermore, the combination of vancomycin and tobramycin or gentamicin was shown to be synergistic and has a prolonged bactericidal activity relative to spacers loaded with single antibiotics[217].

Several factors affect the mechanical strength and antibiotic elution of ALBC: (1) Increasing the percentage by weight of antibiotic in the bone cement allows a higher amount of antibiotic to be released, but there is a tradeoff between the amount of antibiotic eluted and the mechanical strength of the bone cement[202]. It was generally agreed that for the treatment of PJI, more than 2 gram of antibiotics should be added for each 40 gram of PMMA powder[218-220]. Usually for the treatment of PJI, a total of 6 to 8 gram of antibiotics are added per 40 gram of bone cement[218-220]. When bone cement is used prophylactically to fix the implant, less than 2 gram antibiotics should be added per 40 gram of bone cement to minimize risk of fixation failure[218-220]. (2) Whether the antibiotics are industrially premixed or mixed in situ by surgeons. In situ preparation of ALBC was shown to have lower mechanical strength than industrially prepared ALBC at the same drug content[221]. However, the improvement of mechanical properties in premixed ALBC came with a decrease in antibiotic elution rate [202]; (3) the composition and viscosity of ALBC, also varies based on the ALBC manufacturer. A study showed that gentamicin release from Palacos was higher for a longer period of time than gentamicin release from Simplex.[222] The vancomycin release from CMW1 cement was higher than that from Palacos-R or Simplex-P[203]. A study comparing antibiotic release prepared using the same procedure showed that Palamed released the highest total amount of antibiotics over time (17 % of initial loading), as compared to Palacos (8.4 %) and CMW (4-5.3 %). (4) Surface roughness is another variable, with higher roughness correlating to higher release due

to higher surface area[213, 218]. (5) Porosity, with increased interconnected porosity resulting in increased release, especially continuous release after several days. [213, 218]

As a temporary spacer, there are two types of ALBC: (1) Static spacer, which is a non-articulating spacer and does not allow the infected joint to move when the spacer is implanted. (2) Articulating spacer, which allows joint movement after the first stage surgery.[63] ALBC spacer has two primary functions: for articulation and mechanical support between the first and second surgery, and for local delivery of antibiotics to the infected joint. Better functional outcome is achieved with articulating spacers than with static spacers[223, 224]. ALBC spacers can deliver much higher antibiotic concentrations to the site of the infection without significant toxicity when compared to systemic antimicrobial administration[225, 226]. Vancomycin in combination with gentamicin or tobramycin is the most commonly used antibiotic in the ALBC spacer[187, 227-229], with an initial vancomycin loading of 1-3 grams and 1.2-4.8 grams of gentamicin or tobramycin[188, 189, 224, 225, 229].

Despite its effectiveness for local delivery of antibiotics for PJI, ALBC has several drawbacks. i) After the antimicrobial agent has eluted from the surface of PMMA, bacteria can start adhering to the surface and forming a biofilm; as these bacteria adhere to and grow on the ALBC, they are exposed to low doses of the incorporated antibiotic, and eventually can become resistant to them [231, 232]. Usage of gentamicin eluting bone cement for primary arthroplasty was associated with development of gentamicin-resistant coagulase negative staphylococci [230]. Furthermore, gentamicin-resistant bacteria were found in 88 % of PJI with primary arthroplasty using gentamicin-eluting bone cement, as compared to 16 % of PJI with primary arthroplasty using non-antibiotic eluting bone cement[231, 232]. ii) The antibiotic-eluting spacer has to be removed surgically, and a new, permanent implant added. The second surgery has its own risk for introducing bacteria, which might cause PJI again. iii) If ALBC is only used for the interface between bone and the metal stem, it does not sufficiently eliminate bacteria in the synovial fluid; thus only bacteria at bone-metal interface are killed, not those in the articulating

space [231, 232]. iv) because antibiotics in most cases are added to bone cement by surgeons, and are mixed manually, the efficacy of the ALBC varies, depending on how well the two are mixed [231, 232].

Problems with the Current PJI Treatments and Proposed Solution

While two-stage revision surgery has the highest success rate compared to one-stage and DAIR, there are several drawbacks with the two stage procedure: (1) Increased patient morbidity due to the double surgery [229], (2) the dependence on adequate bone stock to fix the new prosthetic joint [91, 186], and (3) the limited mobility of the patient between the first and second surgeries, due to removal of the prosthetic joint [91, 186]. An ideal solution to the management of both acute and chronic PJI would be the creation of an antibiotic-eluting polymer that acts not only as a device for local delivery of antibiotics, but also as an articulating surface that can bear the weight of the patient. The antibiotic-eluting polymer also needs to be able to incorporate various antibiotics, including rifampin, which cannot be incorporated into the ALBC because it inhibits its polymerization [212]. In order for the antibiotic-eluting polymer to be used as a fully weight bearing articulating surface, it needs to have the mechanical strength and wear resistance that satisfies the biomechanical requirements.

To achieve the goals mentioned above, in this thesis, we specifically focused on creating drug-eluting ultra-high molecular weight polyethylene (UHMWPE) for fully articulating and weight bearing joint prostheses. As mentioned above, to achieve a fully weight-bearing and articulating drug-eluting UHMWPE, it needs to be able to deliver drugs sustainably (detailed in chapter 2), good mechanical strength (detailed in chapter 3), and high wear resistance (detailed in chapter 4). The thesis is organized as follows:

- Chapter 2: We explored the possibility of creating a drug-eluting polymeric surface for weight bearing in joint arthroplasty through varying drug clusters morphology in UHMWPE. We studied the particular effect drug cluster shape on drug elution using low-density

polyethylene (LDPE) because LDPE but not UHMWPE can be solvent casted. To ensure that the drug did not degrade or undergo molecular rearrangement during the incorporation process, we explored the chemical structures of the drugs that were eluted from UHMWPE. Because drug elution that allows longest duration of effective concentration is desired, we explored the drug elution parameter space in relation to manufacturing parameters and type of drugs to help identify the optimum conditions that will be detailed in chapter 5.

- Chapter 3: Because the drug eluting UHMWPE needs to be used for weight-bearing in addition to drug delivery, we explored the mechanical strengths of the drug-eluting LDPE or UHMWPE created in chapter 2. To help us finding the optimum mechanical strength (detailed in chapter 5), we explored the relation between mechanical strength with various parameters such as drug cluster morphology, initial drug loading, compression molding temperature, pressure, etc.
- Chapter 4: In addition to drug elution and mechanical strength, because the drug-eluting bearing surface will also undergo articulation, high wear resistance is required for implant longevity. We therefore analyzed the wear resistance of the drug eluting UHMWPE and explored its wear resistance before and after the drugs have been eluted from UHMWPE.
- Chapter 5: Based on the empiric relation among drug elution (chapter 2), mechanical strength (chapter 3), and wear resistance (chapter 4) to various parameters such as drug cluster shape, initial drug loading and other manufacturing parameters, we designed the optimum drug eluting UHMWPE for prosthetic joints. To ensure effective drug elution, we compared the drug elution and antibacterial activity of our optimum antibiotic eluting UHMWPE to antibiotic eluting bone cement. To ensure that the optimum drug eluting UHMWPE will be able to be used as fully weight bearing and articulating implant, we compared its mechanical strength and wear resistance to clinically used UHMWPE.

- Chapter 6: We performed in vivo testing of our optimized material in both murine and lapine models. We divided the test into two main categories: Planktonic-laden animal model and biofilm-laden animal model.
- Chapter 7: To show the potential use of drug eluting UHMWPE for treatment of other arthroplasty-related complications, we designed and optimized local anesthetics-eluting UHMWPE to minimize post-arthroplasty pain. We performed in vivo murine testing of this preparation to elucidate its efficacy in improving mobility post-arthroplasty.

Polyethylene as Weight Bearing Material

Polyethylene is a semi-crystalline polymer, which means that its secondary structure is comprised of highly ordered chain lamellae (crystalline phase) and unordered chains (amorphous phase). Physical properties of polyethylene greatly varies with its molecular weight[233]. For example, low density polyethylene (LDPE), which typically has molecular weight of less than 50,000 g/mol, melts at 105-115°C with melt flow index of 25 g/10 min[233]. On the other hand, UHMWPE, which has molecular weight of $3.5-7.5 \times 10^6$ g/mol, melts at 132-138°C and has melt flow index of 0 g/10 min (i.e. immeasurable flow at melt) [233]. The high chain entanglement in the UHMWPE prevents it from flowing at melt[233].

In general, UHMWPE has a much higher mechanical strength and wear resistance than the lower molecular weight polyethylene. For example, the tensile strength of UHMWPE is 39-48 MPa, while the tensile strength of LDPE is only 10 MPa[233]. Wear resistance of UHMWPE is 10-14 mg/MC[234], while the wear resistance of LDPE is 100-200 mg/MC¹. Because UHMWPE has the highest mechanical strength and wear resistance among all polyethylenes, it is the material of choice for prosthetic joints, which require materials with high mechanical strength and wear resistance for weight bearing and joint articulations. Because of the low melt flow index of UHMWPE, it cannot be processed through traditional polymer processing methods

¹ Unpublished data

such as injection molding like LDPE, and requires compression molding to form the consolidated material[233].

Because LDPE can be dissolved in organic solvents and solvent cast (unlike UHMWPE) [235], we will explore the effect of drug cluster morphology (spherical vs highly eccentric created through compression molding and solvent casting respectively) by using drug eluting LDPE instead of UHMWPE. We will then translate the lessons learned from LDPE regarding the effect of drug cluster morphology on elution and mechanical strength into drug eluting UHMWPE.

Previous Works on UHMWPE with Additives

The incorporation of drugs into UHMWPE as additives built on the knowledge of several additives that have been previously added to UHMWPE to modify its wear resistance, oxidative potential, and mechanical strength [43, 236, 237]. Based on the miscibility of the additives in UHMWPE, these additives can be divided into two categories: (1) Miscible additives such as α -tocopherol[43], and organic peroxides[236]; miscible additives mean upon mixing with UHMWPE, the additives and the UHMPWE are in a single phase. (2) Poorly miscible additives, such as sodium chloride[238, 239], graphene[240], carbon nanofibers[241, 242], and hyaluronic acid[243]; poorly miscible additives mean upon mixing with UHMWPE, the additives and the UHMWPE are in separate phases. Because these additives are intended to modify the mechanical properties and tribological properties of UHMWPE, the elution profile of these additives are not reported.

In the case of miscible additives such as α -tocopherol additives [43] and peroxides[236], additives cannot generally be distinguished from UHMWPE with imaging methods such as optical microscopy, scanning electron microscopy, or transmission electron microscopy. The mechanical strength of UHMWPE is generally unaffected by the presence of additives, even at a very high concentration[244]: for example, the addition of α -tocopherol up to 45 wt %

concentration of UHMWPE did not impact the tensile mechanical properties[244]. Absence of mechanical strength disruption by the addition of miscible additives is presumably because these additives occupy spaces in the amorphous phase of UHMWPE and do not disrupt the crystalline structure and content of UHMWPE.[245] The mechanical strength of UHMWPE was found to depend on its crystalline morphology and content: Higher crystalline percentage was found to correlate with higher elastic modulus, hardness, fatigue strength, and tensile strength.[246]

In the case of immiscible additives such as NaCl[238, 239], graphene[240], carbon nanofibers[241, 242], lignin[247], and hyaluronic acid[243], additives can clearly be distinguished from UHMWPE. For example, in the NaCl-UHMWPE, the NaCl forms cuboid pores within the continuous UHMWPE phase[239]. In the carbon fiber UHMWPE, long carbon fibers can be seen embedded in the UHMWPE matrix[237]. The mechanical properties of UHMWPE with immiscible additives can be positively or negatively affected based on the type of additives: The presence of NaCl or lignin in UHMWPE significantly decreased its mechanical strength, such as ultimate tensile strength and elongation to break[238, 247]. Mechanical strength of the UHMWPE-NaCl and UHMWPE-lignin were inversely proportional to the initial content of NaCl and lignin, respectively[238, 247]. On the other hand, increasing the concentration of carbon nanotubes in UHMWPE resulted in higher tensile strength, Young's modulus, and toughness [248].

In the next chapter, we will detail our findings on the feasibility of incorporating drugs into LDPE and UHMWPE, and the effect of various physical parameters (e.g. drug cluster shape), manufacturing parameters, and chemical parameters (polarity of drug) on drug cluster interconnectivity and drug elution.

Chapter 2

Drug Percolation in Polymer Matrix and its Effect on Drug Elution

Introduction

Thermodynamics of Drug Incorporation into Polymer

When a drug is mixed with a polymer, it may dissolve and homogeneously distribute within the polymer (no phase separation), it may form separate clusters (phase separated), or it may form a combination of those two states [249]. Drug and polymer mixture will form a single phase if the free energy of the single phase is lower than the phase separated phase and the activation energy is sufficiently low to be overcome at the mixing temperature[250]. The process of mixing is a process to minimize the free energy of the end state by minimizing unfavorable enthalpy contacts between the drug-polymer while maximizing the entropy (eq 1) [251]. Based on the Flory-Huggins theory, the Gibbs free energy change of a mixture of drug and polymer can be expressed as[252]:

$$\Delta G_{Drug-Polymer} = \Delta H_{Drug-Polymer} - T\Delta S_{Drug-Polymer} \quad (1)$$

$$\Delta G_{Drug-Polymer} = RT \left(\phi_{drug} * \ln\phi_{drug} + \frac{\phi_{polymer}}{m} \ln\phi_{polymer} + \chi_{drug-polymer}\phi_{drug}\phi_{polymer} \right) \quad (2)$$

Where ϕ_{drug} and $\phi_{polymer}$ is the volume fraction of the drug and polymer respectively, $\chi_{drug-polymer}$ is the Flory-Huggins interaction parameter, R is the molar gas constant, T is temperature of mixing, and m is the ratio of the volume of a polymer chain to drug molecular volume. $\chi_{drug-polymer}$ can be calculated from eq 3 [253]:

$$\chi_{drug-polymer} = \frac{V_{site}}{RT} (\delta_{drug} - \delta_{polymer})^2 \quad (3)$$

Where V_{site} is the volume of the hypothetical lattice and δ_{drug} and $\delta_{polymer}$ are the Hildebrand solubility parameter of the drug and polymer respectively. To minimize the $\Delta G_{Drug-Polymer}$, the value of $\chi_{drug-polymer}$ also needs to be minimized, which could be achieved by minimizing the Hildebrand solubility parameter difference between the drug and polymer. For example, mixing hydrophobic polymer such as polyethylene and hydrophilic substance such as ibuprofen will result in higher $(\delta_{drug}-\delta_{polymer})^2$, and therefore $\chi_{drug-polymer}$ and $\Delta G_{Drug-Polymer}$, than mixing ibuprofen with the more hydrophilic poly methyl methacrylate (PMMA) [254, 255]. As a result, mixture of ibuprofen with PMMA is more likely to form single phase than mixture of ibuprofen and polyethylene[254, 255]. Several factors may also affect the $\Delta G_{Drug-Polymer}$ other than the drug and polymer itself, including presence of solvent, elevated temperature, or chemical reaction between the polymer and drug[252].

Kinetics of Drug Incorporation into Polymer

If the single phase drug-polymer system is more thermodynamically favorable (lower $\Delta G_{Drug-Polymer}$) than the phase separated state, the single state phase might still be unachievable if the activation energy toward the single state phase can't be overcome. Based on the free volume theory, the movement of drug into the polymer is dependent upon the available free volume within the interstitial space polymer matrix and sufficient energy of the drug molecule to overcome forces between the polymer chains[256]. In order for the drug and polymer to form a single phase, the drug molecules need to overcome the interaction between them and diffuse through the interstitial space of the polymer matrix[257, 258]. Therefore, considering the drug-polymer mixing problem as diffusion of drug into the polymer particles allow us to simplify the problem as:

$$\frac{\partial C}{\partial t} = D_{drug} \left(\frac{\partial^2 C}{\partial x^2} + \frac{\partial^2 C}{\partial y^2} + \frac{\partial^2 C}{\partial z^2} \right) \quad (3)$$

Where the diffusivity of the drug into polymer (D_{drug}) can be written as:

$$D_{drug} = D_o \exp\left(\frac{E_D}{R \cdot T}\right) \quad (4)$$

Where D_o is pre-exponential factor, E_D is the activation energy of diffusion. Based on eq (4), higher activation energy or lower temperature resulted in decreased diffusion of drug into polymer and hence increased the likelihood of the drug-polymer to be phase separated [259, 260].

Elution Mechanism from Drug-Incorporated Polymer

Drug elution from drug filled porous polymers can occur through the combination of two major mechanisms: mass transport (of the drug) through the polymer matrix and fluid transport (of the drug dissolved/dispersed in a solvent/carrier) through the pores or cavities between the polymer matrix [261]. For the transport of the drug through the polymer matrix, the diffusion of the solute (drug) and relaxation of the polymer macromolecular chains allow the drug to travel to the surface of the drug-polymer blend, where it then dissolves in the solvent [262]. Mass transport through the polymer matrix can be rate-limiting when the interaction between the solvent and the polymer is strong (for example, where they have similar polarity and/or when the drugs are entangled in the polymeric chain[263].

Assuming an isotropic and homogeneous system, no chemical reaction, dilute drug in eluting media, constant temperature, constant pressure, and single direction of diffusion, mass transport of a drug through the polymer can be expressed by Fick's diffusion equation as[264]:

$$\frac{\partial C}{\partial t} = D_I \frac{\partial^2 C}{\partial x^2} \quad (5)$$

Where c is the concentration of the drug in the solvent, t is time, D_I is the diffusivity of the drug through the polymer.

The transport of the drug through the polymeric pores can be described as follows [4]: First, the drug filled pores near the surface of the polymeric matrix are filled by the solvent, which creates a driving force for the dissolution of the drugs at the polymer/solvent interface. After the drug on the pore surface is dissolved, the drug will diffuse through the solvents to the rest of the bulk solvents outside the pores. The solvent will then penetrate deeper into the drug-filled pores of the polymer, dissolving more drugs inside the pores at the polymer/solvent interface. The drugs, which are dissolved in the polymer/solvent interface towards the surface of the polymeric matrix will diffuse into the bulk of the polymeric matrix carried by the solvent[265]. This type of diffusion can be expressed in terms of diffusion equation as [265]:

$$\frac{\partial C}{\partial t} = D_{II} \frac{\partial^2 C}{\partial x^2} + k(C_s - C) \quad (6)$$

Where c is the concentration of the drug in the solvent, t is time, D_{II} is the diffusivity of the solvent through the pores of the polymer, k is the dissolution constant of the drug in the solvent. D_{II} is proportionally dependent on porosity (volume fraction) in the drug eluting polymer(ϵ), diffusivity in mediate solvent or dissolving medium (D_{DM}) and inversely proportional to the tortuosity of the diffusional paths of the pores (τ) (eq 2) [265].

$$D_{II} = D_{DM} \frac{\epsilon}{\tau} \quad (7)$$

Overall transport of the drug from the drug-incorporated polymer matrix into the surrounding medium can be simplified into the empirical equation [1]:

$$\frac{M_t}{M_\infty} = k' t^n \quad (8)$$

Where M_t is the total amount of drug released at time t , M_∞ is the total amount of drug released after an infinite amount of time has passed, k' is the elution constant, t is time, and n is the diffusional exponent showing the dependency of drug release with time [1]. Lower bound for n is 0, where it indicates zero-order kinetic release, i.e., no dependency of drug release rate with time. For a thin slab of hydrophilic and initially glassy polymer where one dimensional diffusion can be assumed, $n= 0.5$ for a Fickian drug elution through polymer matrix and $n=1$ for a pure drug elution through diffusion of drug and relaxation of polymer macromolecular chain[261]. Both k' and n greatly depend on the geometry of the polymer, molecular characteristic of the polymer, porosity of the polymer, type of eluting media, and the three dimensionality of the elution direction[266]. For example, increasing the polarity mismatch between the polymer (which is usually hydrophobic) and the drug (which is usually hydrophilic) resulted in increased k' [263, 266].

Higuchi Equation for Release of Drug from Non-Swellable Polymeric Matrix

Based on the Fick diffusion equation mentioned above, Higuchi et al, 1961[267] provided an analytical solution for a drug-eluting polymer fulfilling the following assumptions: (1) drug particles must be much smaller in size than the thickness of the drug eluting polymer (drug particle to polymer thickness ratio < 1:1000) ; (2) negligible swelling or dissolution of the polymer in the solvent; (3) diffusivity of the drug through the polymer is constant, (4) initial drug concentrations in the drug-eluting polymer must be much higher than the solubility of the drug in solvent, and (5) perfect sink condition for drug dissolution from the polymer/solvent interface is maintained. If these assumptions are satisfied, Higuchi showed that the drug elution rate can be expressed as[267]:

$$\frac{M_t}{A} = \sqrt{D(2c_o - c_s)c_s t} \quad (9)$$

Where C_o is the initial drug loading concentration in the polymer, C_s is the dissolution limit of the drug in the solvent, and D is the effective diffusion coefficient. Because C_o , C_s , D , and A are constants, then the equation above can be simplified as:

$$M_t = K * \sqrt{t}, \text{ where } K = A\sqrt{D(2c_o - c_s)c_s} \quad (10)$$

While this equation is often not suitable for most drug eluting polymers[268], this system is likely to be suitable for the drug eluting UHMWPE described in this thesis because its hydrophobicity and high chain entanglement resulted in negligible polymer swelling and dissolution. Assumptions 1, 4 and 5 can easily be fulfilled by ensuring good distribution of small size drug particles into UHMWPE powder and ensuring drug dissolution concentration in the dissolution media is far from its dissolution limit. Assumption 3 can be satisfied by creating a homogeneous drug eluting UHMWPE with relatively constant porosity and tortuosity throughout the thickness of the system. However, deviations from the Higuchi equation have been observed even in systems where all assumptions above are satisfied because of the presence of non-negligible edge effects and three dimensionality of the elution direction[268].

Percolation Theory

In order to preserve the mechanical properties and the crystallization behavior of UHMWPE, on which its properties are based, we will use therapeutic agents (drugs) which have no appreciable solubility in the polymer matrix. In addition, the incorporation of the drug itself will be the major mechanism of creating pores in the polymer. In this case, because UHMWPE is hydrophobic and does not undergo any dissolution or swelling in water-based hydrophilic media such as saline (or serum), we can further assume that the drug elution rate will be primarily determined by transport of the solvent through the pores of the polymer formed by clusters of the incorporated drugs in UHMWPE.

While interpreting elution kinetics in drug-incorporated UHMWPE using a non-soluble drug to create pores, we can use percolation theory, which has long been adapted to study fluid flow [269] through rock and also by physicists to study conduction in heterogeneous materials [270]. Percolation is defined as presence of at least one material-spanning conductive (electrical or fluid) pathway throughout the dimension of the materials. An important parameter is called the percolation threshold, the minimum concentration at which percolation is reached. In a box of continuum matrix for example, adding particles into the box will form small clusters of particles[270]. As we continue adding more particles into the box, we will obtain larger cluster of particles. Ultimately, when we keep adding more particles, we will reach a point where we create a large cluster that span the whole material domain. The minimum amount of particles needed in the system to create this large cluster that span the whole material domain is called percolation threshold[270]. In fact, based on percolation threshold, for a particular cluster size, there exists a condition of certain particular size, distribution, and numbers that maximizes production of that particular cluster size[271].

It is important to note that in finite systems like the box mentioned above, the occurrence of percolation threshold is a probabilistic event, i.e., generation of repeated particle arrays from the same distributions of particle shapes, sizes, locations, orientations, and numbers do not necessarily generate percolating systems every single time[272-274]. However, when the box is expanded to infinitely large dimensions, percolation threshold can be precisely defined as the point where there exists an infinitely large cluster size[271].

Percolation threshold of three dimensional objects in continuum media depends on the particle shape, orientation, and aspect ratio[275, 276]. For example, for the same volume of particle, spherical, cuboidal, and cylindrical particles have percolation threshold (expressed as fraction volume of particles) of 0.2895[277], 0.2773[278], and 0.2819[279] respectively. Using cuboidal particle of the same size, randomly oriented cube has percolation threshold of

0.2168[278], while aligned cube has percolation threshold of 0.2773[278]. Increasing the aspect ratio of ellipsoidal particles from 1 (spherical) to 5, decreases the percolation threshold from 0.2895[277] to 0.1757[277].

Percolation Theory on Eccentricity of Clusters

Percolation threshold of particles in a continuum matrix depends on the aspect ratio or eccentricity (assuming an estimated ellipsoid) [2]. Theoretically, the percolation threshold of ellipsoids decreased from a volumetric fraction of 0.2854 to 0.0012 when the aspect ratio increased from 1 (spherical particles) to 500 or when the aspect ratio decreased to 1/500 [277]. In fact, a maximum in percolation threshold is reached when the particle is spherical [277]. Interestingly, percolation threshold does not decrease symmetrically from its maximum spherical point when the aspect ratio of the ellipsoids are increased (prolate) and decreased (oblate): Percolation threshold is lower when the ellipsoids are prolate than oblate, even though the aspect ratios are the reciprocal of each other[280]. This observation implies that a needle type of network (prolate) is easier and more effective for both fluid transport and electrical conduction than a disc type of network (oblate) [280]. This result was confirmed experimentally, where a polymer-carbon nanotube (prolate) composite had a percolation threshold of 0.070 [281], whereas a polymer-graphene (oblate) composite had a percolation threshold of 0.100 [282].

In summary, the probability of reaching percolation is determined by the volumetric fraction of the particle. For a given volumetric fraction, the probability of reaching percolation threshold is also determined by the eccentricity of the particle, with higher eccentricity resulted in lower percolation threshold [271]. Previously reported drug eluting polymer systems with

spherical drug clusters showed that 40-60 % (w/w) drug content in the polymer was required to reach complete interconnection[283-285].

Percolation of Previously Reported Drug Eluting Polymer

Considering polymer-drug mixture with phase separation, previously reported drug eluting polymers synthesized with various methods such as solvent casting[286, 287], electrospinning[288], emulsion[289], spray coating[290], and injection molding[290] produced drug eluting polymers with spherical drug clusters embedded in a polymeric matrix. There are several possible reasons for the formation of spherical drug clusters in the polymer matrix: (1) Spherical drug clusters minimize the surface area to volume ratio, hence minimizing the unfavorable interaction between the drugs and polymer. (2) The drug particles are spherical in the first place, and the polymer encapsulates the drug particles without disrupting much of the drug particle original shape. These two mechanisms are likely working together to result in formation of spherical drug clusters. For example, incorporation of hydrophilic drugs such as gentamicin or vancomycin into the relatively hydrophobic polymethyl methacrylate (PMMA) resulted in spherical gentamicin or vancomycin clusters within the PMMA matrix to minimize the unfavorable interaction between gentamicin or vancomycin with the PMMA matrix[291]. The methyl methacrylate monomer will then preferentially flow around the spherical drug clusters and encapsulate the spherical drug clusters within the polymer[291].

The spherical clusters will likely impact the drug elution from a system where the drug drug-polymer system is below percolation threshold and penetration of the dissolution medium through the polymer is negligible (e.g. hydrophobic polymer in hydrophilic dissolution media). This is because only drugs that can be accessed from the surface can be eluted[292, 293] and fully encapsulated drug clusters will never be exposed to the dissolution medium; and as a

result, these drugs will never be eluted [294, 295]. In this chapter, we will explore the effect of the drug cluster shape on the drug elution using low density polyethylene (LDPE) as polymer and vancomycin as the drug.

Clinical implication of drug cluster morphology

As mentioned in chapter 1, antibiotic eluting bone cement (ALBC) molded into a spacer is part of the gold standard for PJI treatment. Scanning electron micrograph of the ALBC showed presence of spherical drug clusters dispersed on the PMMA matrix ([296], **Figure 2.1**). Because of the spherical drug clusters in antibiotic eluting bone cement, high drug loading (11-15 %) is required for effective antibiotic delivery to the infected joint[297]. However, even at this high concentration, the loaded drug concentration is still under the percolation threshold (**Figure 2.1**). As a result, 90 % of the drug is trapped inside the bone cement and never be eluted out[298]. In addition, drug eluting bone cements have decreased mechanical strength [299] and have high rates of in vivo fracture (10-14 %) [9, 300].

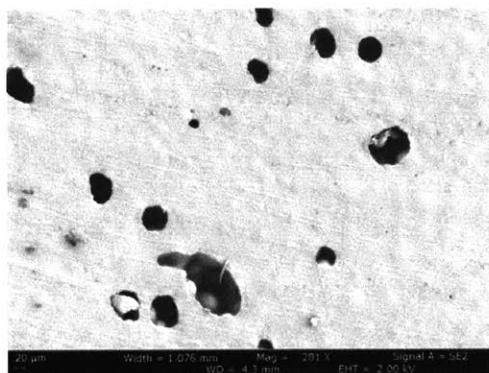


Figure 2.1. Vancomycin Eluting PMMA Bone Cement with 15 wt % initial vancomycin loading

Learning from the weaknesses of the previous system, our new design of drug eluting polymer system needed to have the following characteristics: (1) highly eccentric drug clusters

to minimize drug loading, (2) drug clusters need to be fully interconnected (drug concentration to be above the percolation threshold) to maximize efficacy of drugs being eluted, and (3) maximizing the mechanical strength of the drug-incorporated polymeric matrix.

Methods

General experimental approaches. No samples, or data points are excluded from the analyses. Samples were not randomized to experimental groups unless specified. Lapine experiments and analyses were not performed in a blinded fashion.

Solvent casting of vancomycin eluting LDPE with spherical drug clusters. LDPE was dissolved slowly in boiling xylene (138°C) to reach a concentration of 60 mg/mL. After all LDPE was dissolved in xylene, the resulting solution was cooled to 110°C. Under mechanical stirring, vancomycin crystals with crystal size < 75 µm were added to reach the desired weight percent with respect to the LDPE content (0, 2, 4, 6, 8 and 10 wt %) and kept at 110°C for 30 minutes to further remove the solvent. The resulting viscous solution was then transferred to a stainless steel rectangular mold (50 by 85 mm) and put in a vacuum oven with a vacuum pressure of -0.1 MPa at 90°C to further remove the solvents.

Preparation of vancomycin eluting LDPE with highly eccentric drug clusters. LDPE pellets were cryo-milled and then sieved to the appropriate desired particle size ranges. Vancomycin-HCl was crushed with a mortar and pestle and then passed through a 75 µm sieve. To create a vancomycin-eluting LDPE with 7 wt % drug loading, 0.7 gram of the sieved vancomycin powder was mechanically mixed with the 9.3 gram cryo-milled LDPE powder for 30 minutes at room temperature. The resulting mixture was then transferred to a rectangular mold with dimensions of 50 x 85 mm and compressed at 25°C for 1 minute at 10 MPa. The compressed solid mixture was subsequently heated at 0.1 MPa, 190°C for 30 minutes and then compression molded at 10 MPa for 1 minute, and cooled to 25°C at 10°C/min.

Preparation of optimized vancomycin-eluting UHMWPE with highly eccentric drug clusters (VPE). Vancomycin-HCl (1.75 gram) was crushed with mortar and pestle and then passed through a 75 μ m sieve. Vancomycin powder was then mechanically mixed with GUR1020 UHMWPE powder (Celanese, 23.25 grams) for 30 minutes at room temperature to obtain a 7 wt% vancomycin-blended UHMWPE and poured to circular mold with 10.5 cm inner diameter. Vancomycin-UHMWPE mixture was then consolidated by compression molding at 170°C, 20 MPa, for 5 minutes with a cooling rate of 10°C/min to yield approximately 3 mm-thick and approximately 10.5 cm diameter vancomycin eluting-UHMWPE (VPE).

Preparation of optimized rifampin-vancomycin eluting UHMWPE with highly eccentric drug clusters (RVPE). Rifampin (Sigma-Aldrich, 0.4 gram) was crushed with mortar and pestle and then passed through a 75 μ m sieve. Similarly, vancomycin-HCl (0.8 gram) was crushed with mortar and pestle and then passed through a 75 μ m sieve. Rifampin powder and vancomycin-HCl powders were then mechanically mixed for 30 minutes at room temperature. UHMWPE GUR 1020 (12 gram) was added to the Rifampin and Vancomycin-HCl mixture and mechanically mixed/blended for 30 minutes at room temperature, obtaining a 3.3 wt% rifampin and 6.7 wt% vancomycin-blended UHMWPE. 10 grams of the resulting rifampin and vancomycin-blended UHMWPE were transferred and spread evenly onto a circular stainless steel mold with inner diameter of 11 cm. 25 grams of GUR 1020 UHMWPE without additives was then added and spread evenly on top of the rifampin and vancomycin-blended UHMWPE. The resulting construct was then consolidated by compression molding at 170°C, 20 MPa, for 5 minutes and then cooled at a rate of 10°C/min to room temperature to yield a 3 mm-thick rifampin and vancomycin-eluting UHMWPE (RVPE).

Preparation of vancomycin-eluting PMMA bone cement. Vancomycin-HCl powder that had been crushed with mortar and pestle and passed through a 75 μm sieve was mechanically mixed with PMMA powder (Simplex P, Stryker) for 30 minutes at room temperature. After thorough mixing, the cement's liquid monomer was added and then mixed thoroughly with a spatula. The vancomycin-cement dough was then poured into a stainless steel mold to form its final shape. After about 15 minutes, the hardened vancomycin eluting PMMA bone cement was removed from the mold.

In-vitro drug release from drug eluting UHMWPE and drug eluting PMMA bone cement.

For drug eluting UHMWPE, blocks with dimension of 5 mm x 5 mm x 20 mm (n=6) were cut from the consolidated samples. For drug eluting PMMA bone cement, vancomycin-cement dough was poured into a stainless steel mold to form into blocks with dimensions of 5 mm x 5 mm x 20 mm. Each block was immersed in 1 ml of phosphate-buffered saline at 37°C for a pre-determined time (6 hr, 24 hr, every 24 hr until 1wk, and then once every week up to a total period of 12 months). After each time-point was reached, the specimens were washed with phosphate-buffered saline and placed in a new 1 ml of phosphate-buffered saline. Concentrations of vancomycin and rifampin were determined using Ultraviolet-Visible spectroscopy (UV-Vis) at 280 nm (Vancomycin) and 450 nm (Rifampin). The rate of drug elution was calculated by dividing the measured concentration at the given time-point by the duration the sample was exposed to phosphate-buffered saline.

Scanning Electron Microscopy. All LDPE, UHMWPE, and PMMA bone cement were sputter coated with a thin layer of gold/palladium and imaged on a Zeiss Supra55VP scanning electron microscope (Zeiss, Oberkochen, Germany). Everhart-Thronley and Inlens detectors were simultaneously used to acquire the image.

Structural analysis of drug eluting UHMWPE with highly eccentric drug clusters using Micro-CT. Tomograms of cylindrical pins (9 mm diameter and 5 mm long) were acquired and

reconstructed using a cone-beam X-ray scanner (μ CT 40, Scanco Medical) for 3D reconstruction with voxel resolution of ~ 10 μm . Porosity analysis and pore accessibility were analyzed using iMorph software package (www.imorph.fr; [1]). The resulting image was then thresholded to partition between the pores and the polymeric matrix. Porosity was calculated by dividing the volume belonging to the pore to the total volume of the sample. The accessible porosity module implanted in iMorph allowed quantification of the pore volume accessible from each side of the sample by a particle depending on its size.

Spectral Analysis. Infrared (IR) spectra were recorded on a Fourier transform infrared spectrophotometer between 400cm^{-1} to 4000cm^{-1} at room temperature (Varian 600 series, Varian, Palo Alto, CA). Nuclear magnetic resonance (NMR) was recorded with 400 MHz Spectrometer (Bruker, Billerica, MA). Chemical shifts in CDCl_3 and D_2O were reported downfield from TMS ($=0$ ppm) for ^1H NMR. Ultraviolet-Visible (UV-Vis) spectra were recorded between 200 to 800 nm at room temperature (Cary 600, Agilent, Santa Clara, CA).

Statistical analysis. All statistical tests were performed by Student's two-tailed t-test for comparison of two groups and analysis of variance (ANOVA) for comparisons of multiple groups implemented through software package GraphPad Prism version 4.0. All error bars used in this report are mean \pm s.d. of at least three independent experiments except the lapine study (single experiment). Survival analyses were performed by using a log-rank test, using a statistical software package GraphPad Prism version 4.0. All data are expressed as $t_{\text{mean}} \pm$ s.d., combined from three independent experiments.

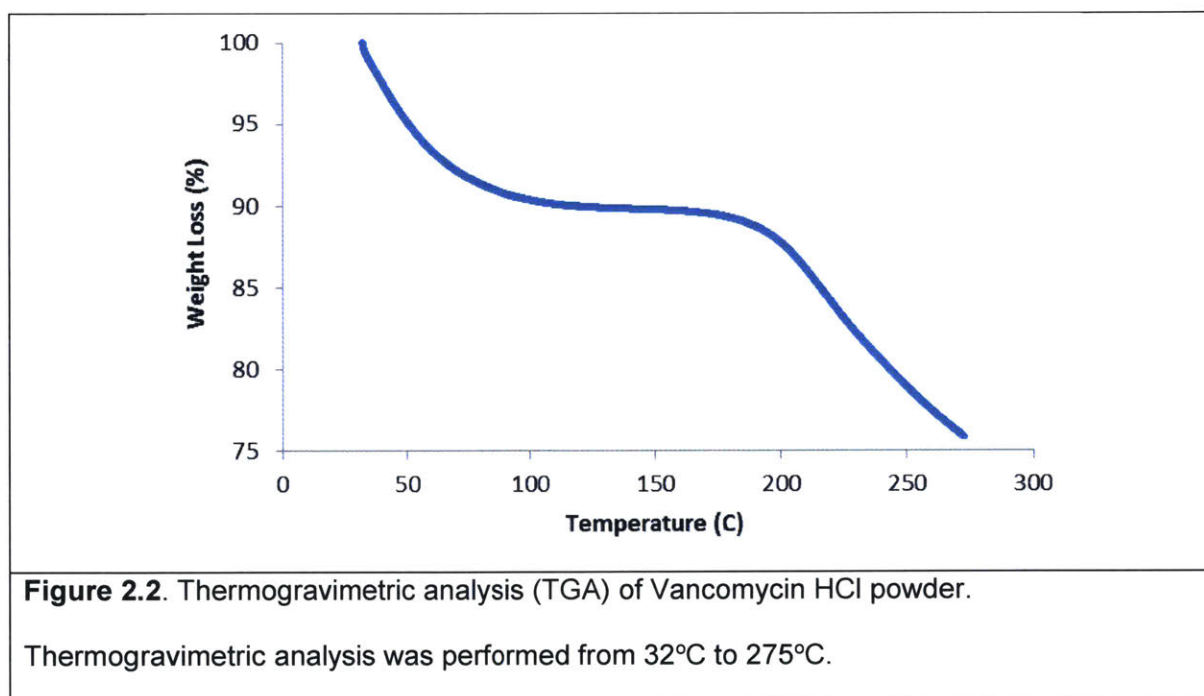
Results

Heat Resistance of Vancomycin determined by Thermogravimetric Analysis (TGA)

Because incorporation of antibiotics to LDPE and UHMWPE involved compression molding of the antibiotics premixed LDPE or UHMWPE at high temperature (130 - 180°C), it was

necessary to determine the extent to which antibiotics might thermally decompose or react with air under these conditions. For an initial test of thermal stability of antibiotics, we conducted TGA. TGA would show the total mass change of sample vs. temperature. If a sample underwent thermal degradation that involved release of gas, total mass of the sample would decrease.

TGA analysis of vancomycin HCl showed a mass decrease between 50°C-110°C, which was likely due to release of adsorbed H₂O from vancomycin crystals. Mass plateau was observed between 110°C to 180°C, followed by complete thermal degradation as indicated by abrupt mass losses (**Figure 2.2**).



Spectral analysis of eluted vancomycin from vancomycin-eluting UHMWPE in comparison to pure antibiotics

To ensure that vancomycin-HCl molecules did not undergo molecular structure change after being consolidated with either UHMWPE or LDPE, we compared the molecular spectra of antibiotics eluted from antibiotic eluting UHMWPE (consolidated at 170°C) to antibiotic control as received from the manufacturer. We performed three types of spectroscopy: Ultraviolet-

Visible Spectroscopy (UV-Vis), Nuclear magnetic resonance (NMR), and Infrared Spectroscopy (IR).

Ultraviolet-Visible Spectroscopy (UV-Vis) of Vancomycin Eluted From UHMWPE

To elucidate the molecular structure of vancomycin after incorporation into UHMWPE, we compared the UV-Vis spectra of antibiotics eluted from the UHMWPE to the vancomycin as obtained from the manufacturer (**Figure 2.3**). No meaningful difference was observed between UV-Vis spectra of eluted vancomycin in the first 24 hr compared to standard vancomycin.

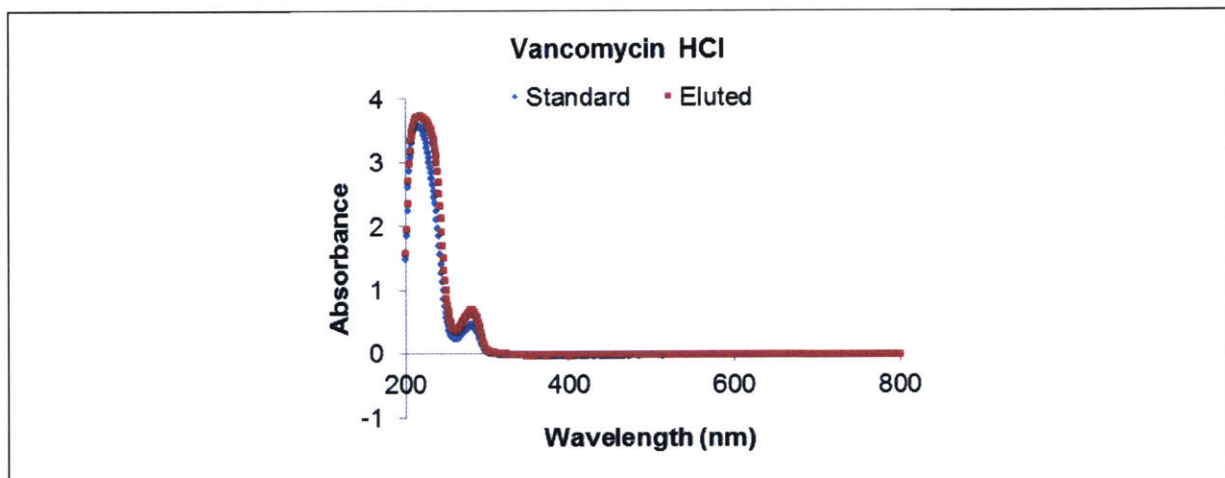


Figure 2.3. UV-Vis Spectra of Standard Vancomycin and Eluted Vancomycin HCl.

Eluted vancomycin was obtained from the first 24 hr elution at 37°C. Standard solution was made by dissolving vancomycin powder into phosphate buffered saline immediately before UV-Vis measurement.

Fourier Transform Infrared (FTIR) Spectroscopy of Vancomycin Eluted From UHMWPE

Because UV-Vis can only detect molecular changes that are UV-Vis active (chromophores), a more sophisticated method is needed to detect potential molecular changes that are not UV-Vis active, such as carbonyl groups, amine, amide, carboxylic groups, ether, etc. FTIR, which is based on measuring the molecular vibration, is very sensitive to changes in the

groups mentioned above. Therefore, we compared the FTIR spectra of eluted vs standard vancomycin (**Figure 2.4**).

No difference in FTIR was observed between eluted and standard vancomycin, further indicating absence of any molecular change in vancomycin after incorporation into UHMWPE.

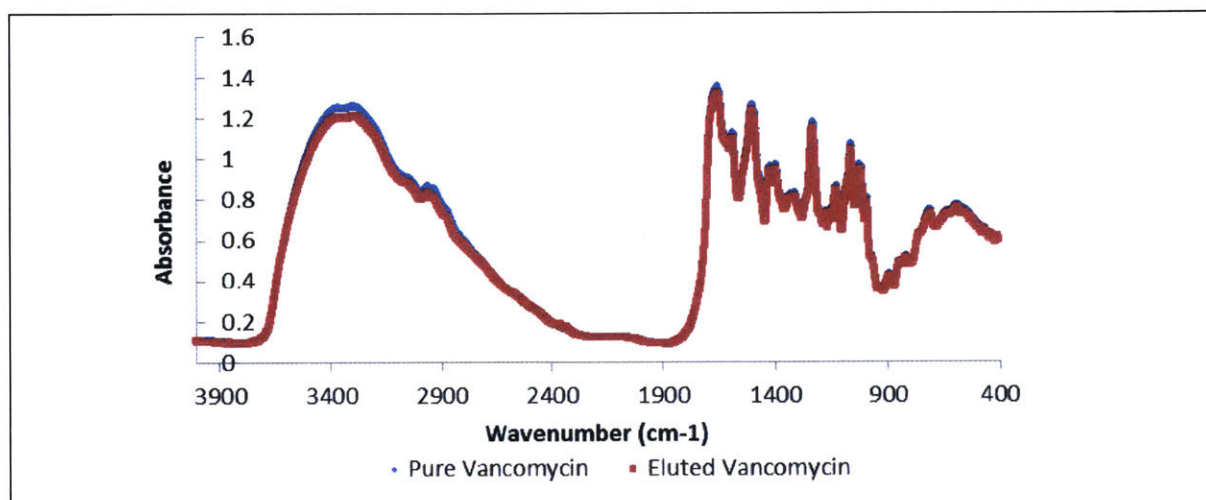


Figure 2. 4. FTIR Spectra of eluted and standard vancomycin HCl. Elution was performed at 37°C in PBS for 24 hr. Standard solution was made immediately before IR spectra measurement.

Nuclear Magnetic Resonance (NMR) of Vancomycin Eluted From UHMWPE

To further ensure that vancomycin eluted from vancomycin eluting UHMWPE did not undergo molecular rearrangement, nuclear magnetic resonance (NMR) spectroscopy of eluted vancomycin was compared to standard vancomycin (standard vancomycin) as manufactured (**Figure 2.5**). No meaningful change in NMR spectra was observed between the eluted vancomycin and pure vancomycin, indicating the absence of any change in molecular structure of vancomycin after incorporation into UHMWPE.

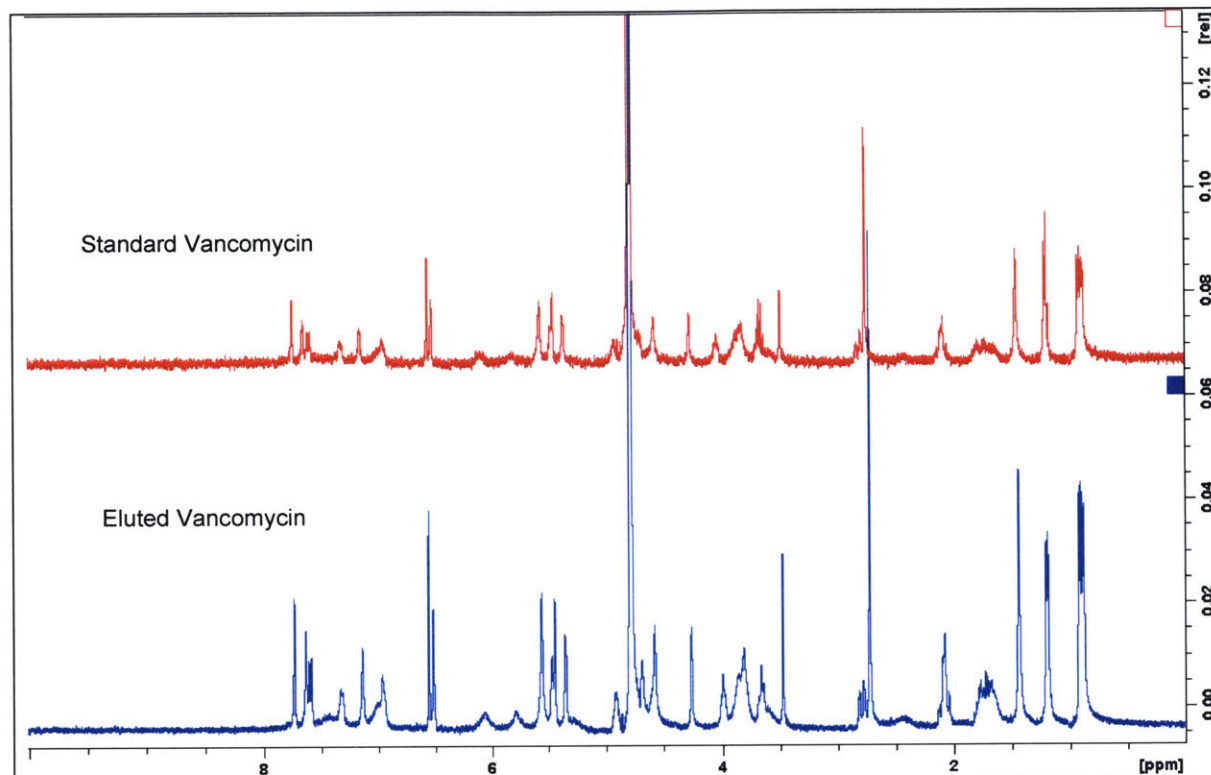


Figure 2.5. NMR Spectra of Standard and Eluted Vancomycin HCl. Elution was performed at 37°C in PBS for 1 week. Standard solution was made immediately before IR spectra measurement. Top (red) spectra were obtained from standard samples and bottom (blue) spectra were obtained from eluted samples.

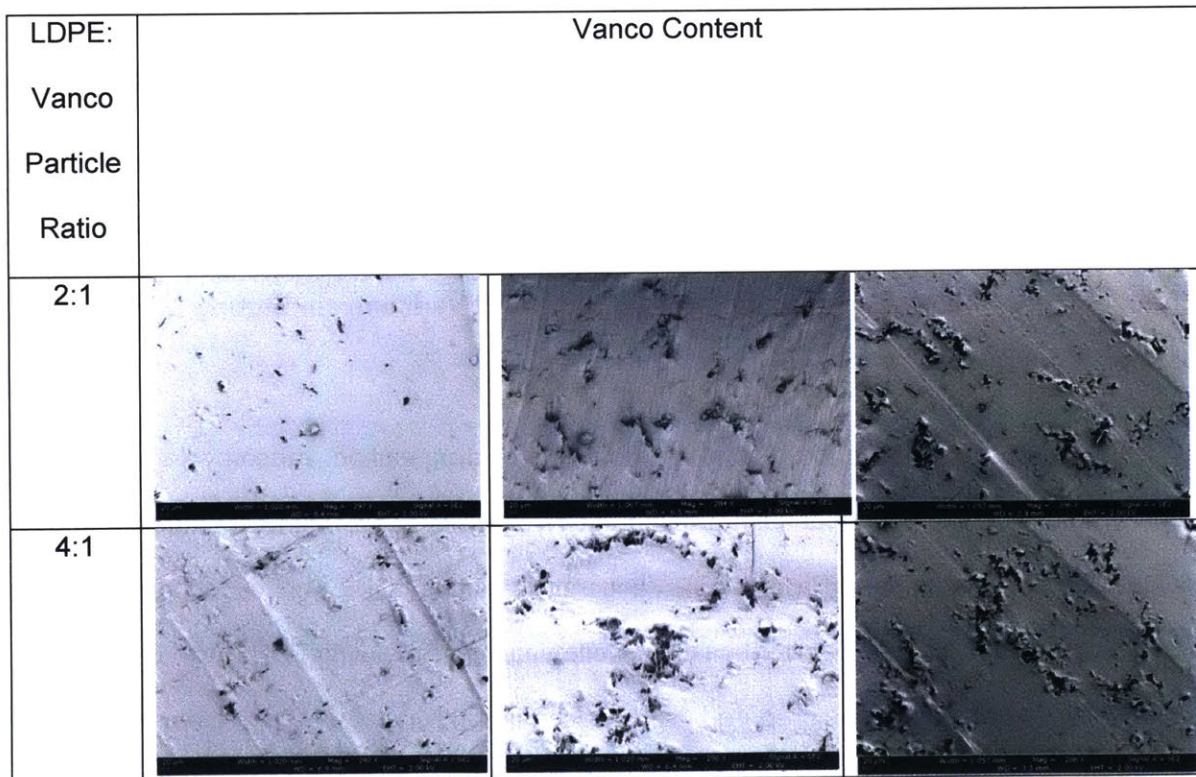
Effect of Drug Cluster Eccentricity on Drug Elution of Vancomycin Eluting Low Density Polyethylene (LDPE)

To study the effect of drug cluster eccentricity on drug elution, vancomycin-eluting low density polyethylene with spherical (low eccentricity) and elongated (high eccentricity) drug clusters were manufactured (**Figure 2.6**). Vancomycin-eluting LDPE with low eccentricity drug clusters was prepared using solvent casting, while vancomycin eluting LDPE with high eccentricity drug clusters was prepared using mechanical mixing of drug particles with UHMWPE granules followed by compression molding. Various initial drug loading (2 wt %, 6

wt %, and 10 wt %) and LDPE granules/drug particle size ratio (6:1, 16:1, and 40:1) were tested to look at the effect of various initial LDPE loading and LDPE granules/drug particle size ratio on drug clusters shape, drug clusters interconnectivity, and drug elution.

Both high eccentricity and low eccentricity drug clusters can be achieved at all initial vancomycin loading (2 wt %, 6 wt %, and 10 wt %) and all LDPE granules/drug particle size ratio (6:1, 16:1, and 40:1). For the same LDPE granules/drug particle size ratio, higher drug cluster interconnectivity was observed as initial vancomycin loading was increased. For the same initial vancomycin drug loading, higher drug cluster interconnectivity was observed as LDPE granules/drug particle size ratio was increased (**Figure 2.6**).

The vancomycin elution from the vancomycin eluting LDPE followed similar patterns as the drug cluster interconnectivity, with higher drug elution observed as initial vancomycin was increased and as the LDPE granules/drug particle size ratio was increased (**Figure 2.7**).



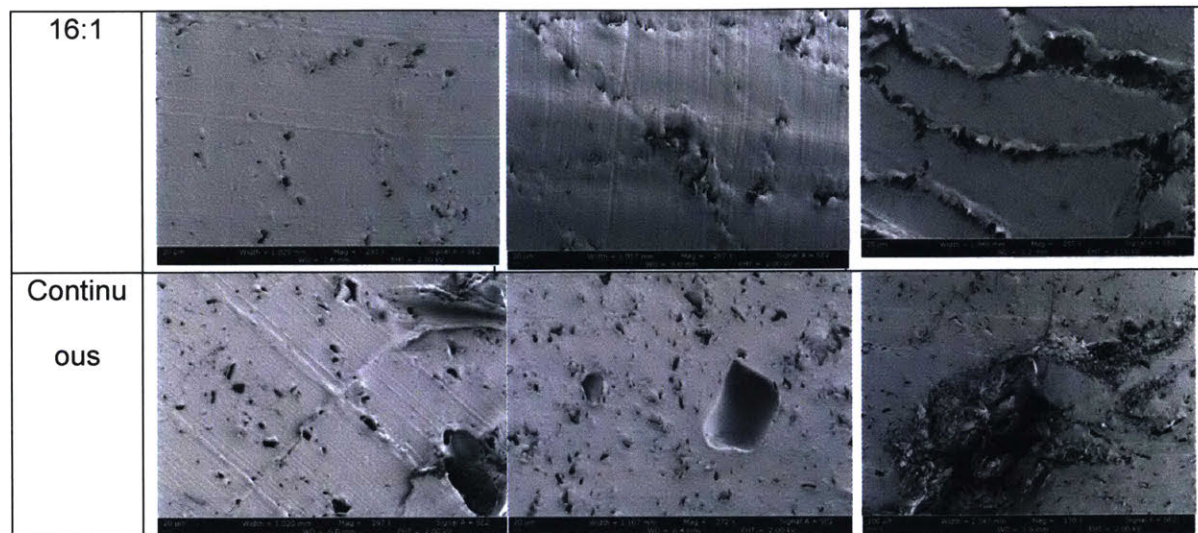
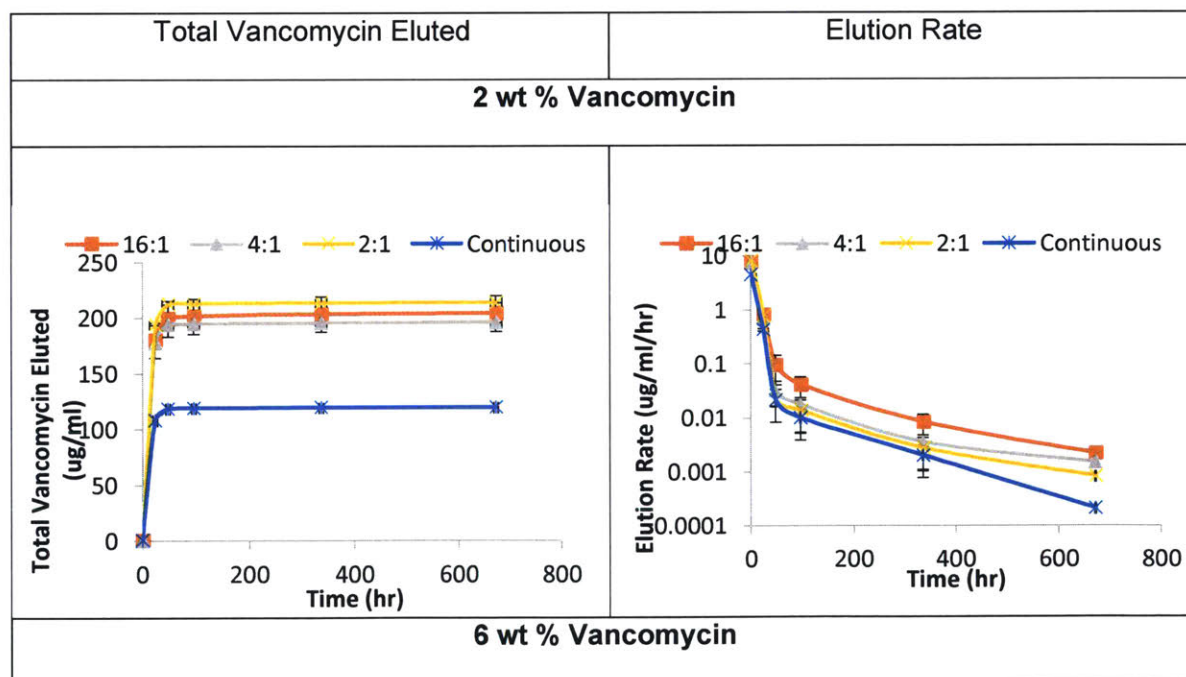
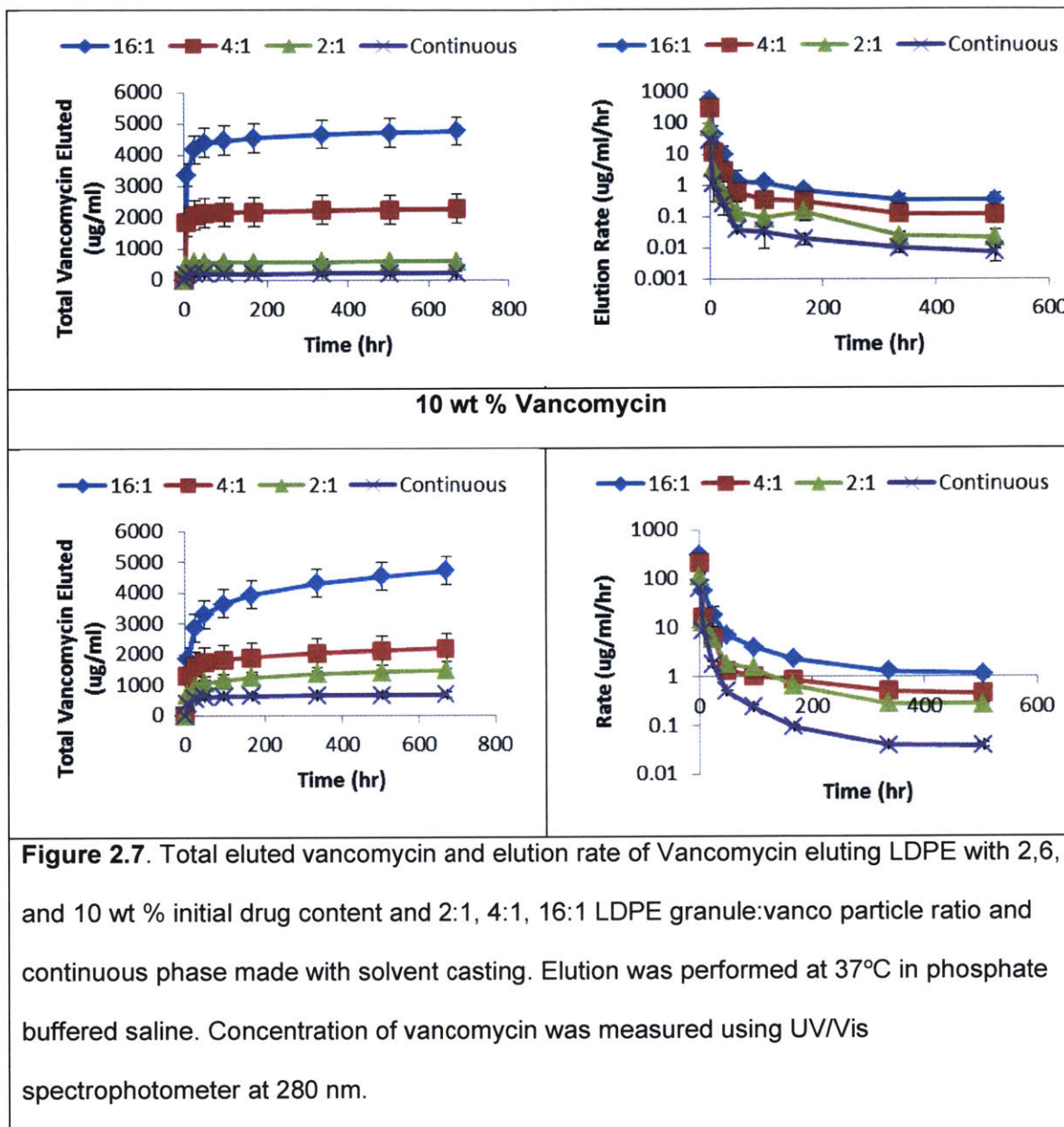


Figure 2.6. SEM of Vancomycin eluting LDPE with 2,6, and 10 wt % initial drug content and 2:1, 4:1, 16:1 LDPE granule : vanco particle ratio and continuous phase made with solvent casting. The darker region indicates the pore previously occupied by the vancomycin.





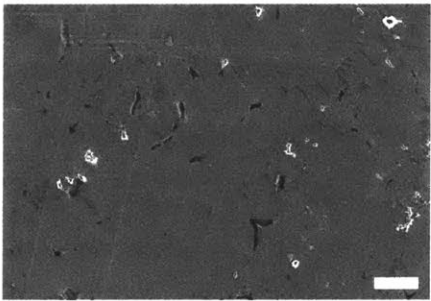
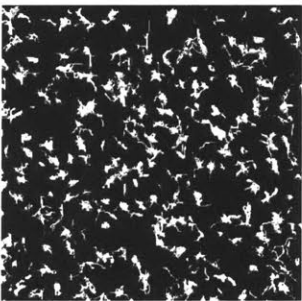
Drug Clusters Interconnectivity and Drug Elution from Vancomycin Eluting UHMWPE

Vancomycin-eluting UHMWPE with various initial drug loading (2%, 4 %, 6%, 8%, and 10 %) were manufactured at a temperature of 170°C, and 20 MPa of pressure. All samples showed highly eccentric drug clusters (**Figure 2.8**), with significant drug clusters interconnectivity began to be observed at initial drug loading of 6 wt %. To further study the drug

clusters interconnectivity in UHMWPE, micro computed tomography (μ -CT) was performed. Volume of the drug clusters and their interconnectivity were then quantified as specified in the method section above.

In general, porosity increased linearly with increasing initial drug loading (**Figure 2.9a**). However, while increasing initial drug content also resulted in increasing drug clusters interconnectivity, a sharp increase in interconnectivity was observed between 4 to 6 wt % (**Figure 2.9b**). Z-Projection of μ -CT pictures also showed increased drug cluster interconnectivity from 2 to 6 wt %, and increased drug cluster thickness from 6 to 10 wt % (**Figure 2.8**).

Change in drug elution rate with respect to initial drug loading followed similar patterns as the change in drug clusters interconnectivity with respect to initial drug loading: Drug elution rate increased as initial drug loading was increased, with sharp increases observed around drug loading of 6 wt % (**Figure 2.10**).

	SEM (Lighter colour= polymer, darker colour =drug cluster)	Z-Projection μ-CT (Black= polymer, white =drug cluster)
2 wt %		

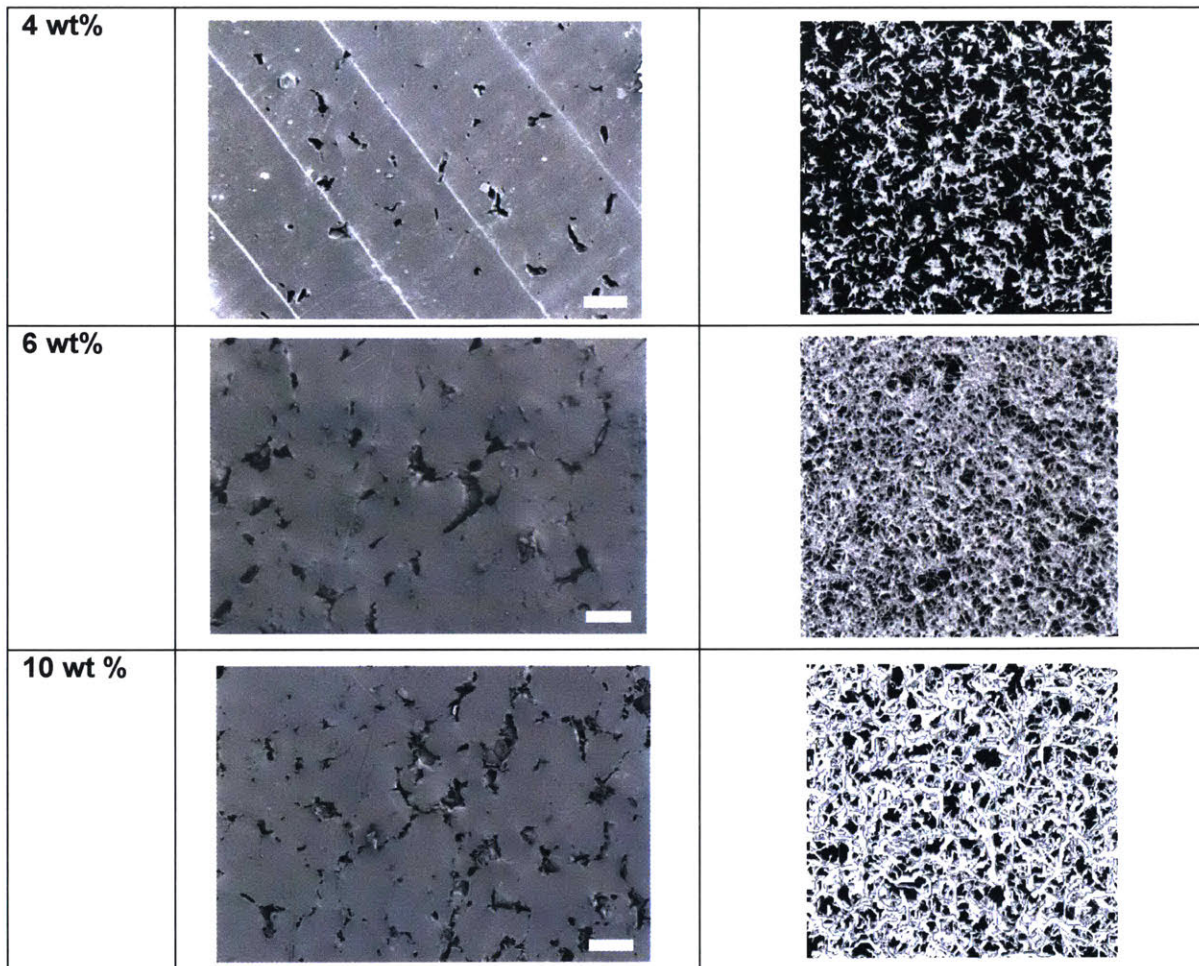


Figure 2.8. Scanning electron micrograph and μ CT Z-projection of vancomycin eluting UHMWPE at 2 wt %, 4 wt %, 6 wt %, 10 wt %. In the scanning electron micrograph, the darker area indicates the pores occupied by the vancomycin, while the lighter area indicates UHMWPE. In the μ CT, white indicates the pores occupied by the vancomycin, while the darker area indicates UHMWPE. Scale bar=100 μ m.

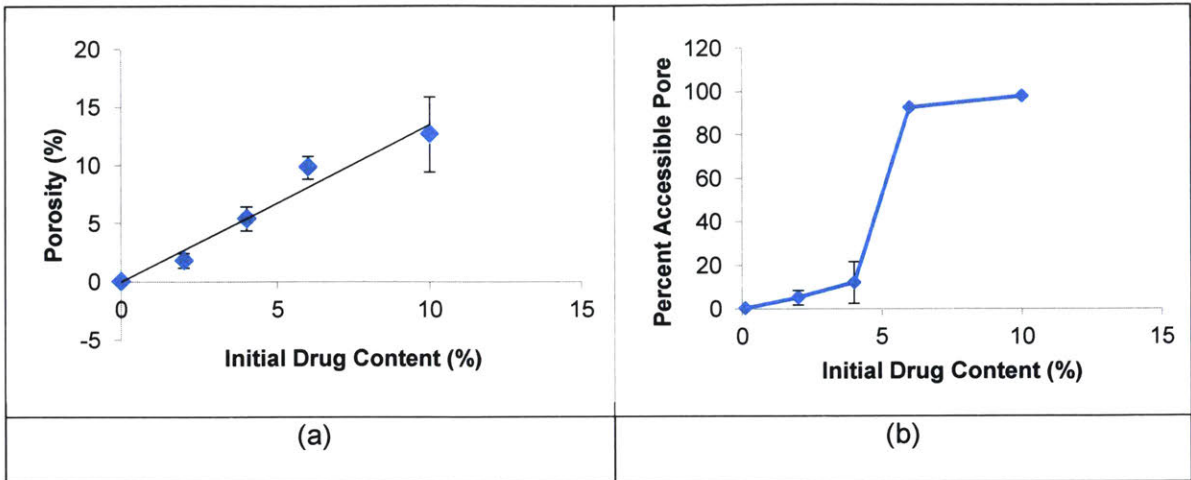
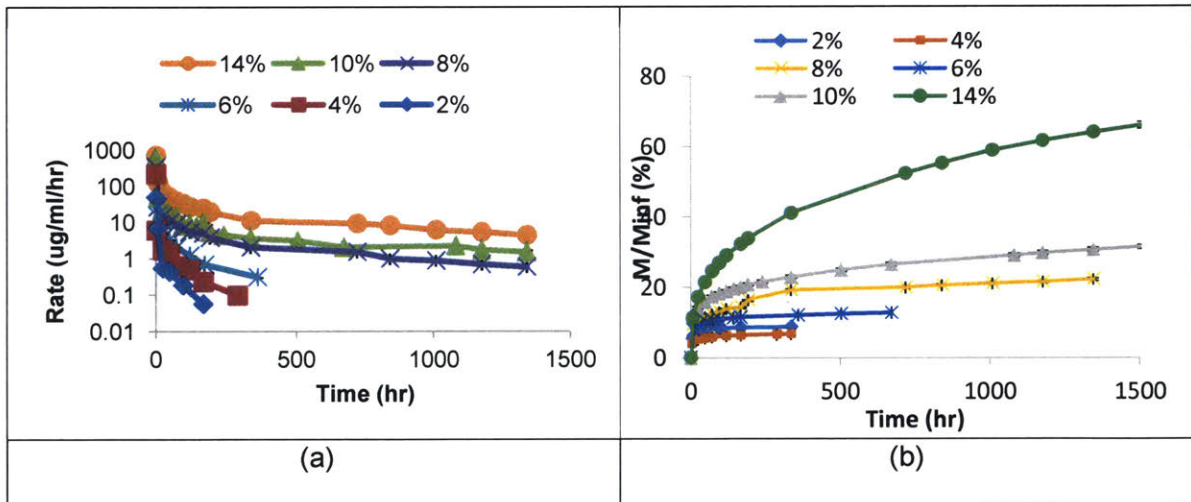
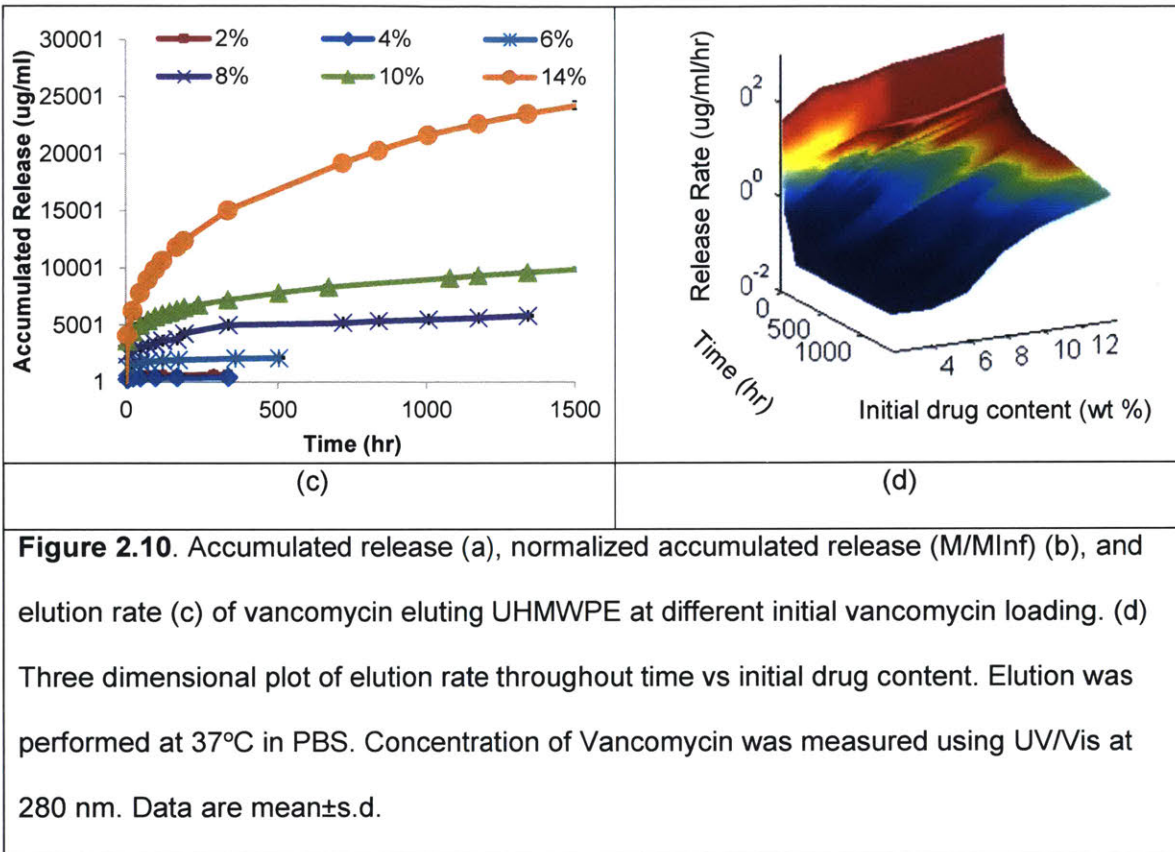


Figure 2. 9. Overall volumetric porosity (a) and percent accessible pore (b) of vancomycin eluting UHMWPE at different initial vancomycin loading. Porosity and percent Accessible pore is calculated using imoprph software using 3D reconstruction of the micro-computed tomography of samples.





Effect of Consolidation Parameters (Compression Molding Temperature, Compression Molding Pressure, and Vancomycin Particle Size) on Drug Elution from Vancomycin Eluting UHMWPE

The effects of manufacturing parameters (temperature during compression molding, pressure during compression molding, and vancomycin particle size) on vancomycin elution were tested by varying each parameter independently. Because TGA of vancomycin showed that vancomycin is stable up to 180°C while UHMWPE melts above 145°C, the effect of compression molding temperatures was tested between 160-180°C (160°C, 165°C, 170°C, 180°C). Pressure of compression molding was tested between 18 MPa-25 MPa (15 MPa, 18 MPa, 19 MPa, 20.5 MPa, 25 MPa). Given constant mean particle size of UHMWPE granule (150

μm), variation in polymer to drug particle size ratio on elution is tested by varying mean vancomycin crystal size between 1.1 μm -145 μm (1.1 μm , 27 μm , 58.44 μm , 145 μm).

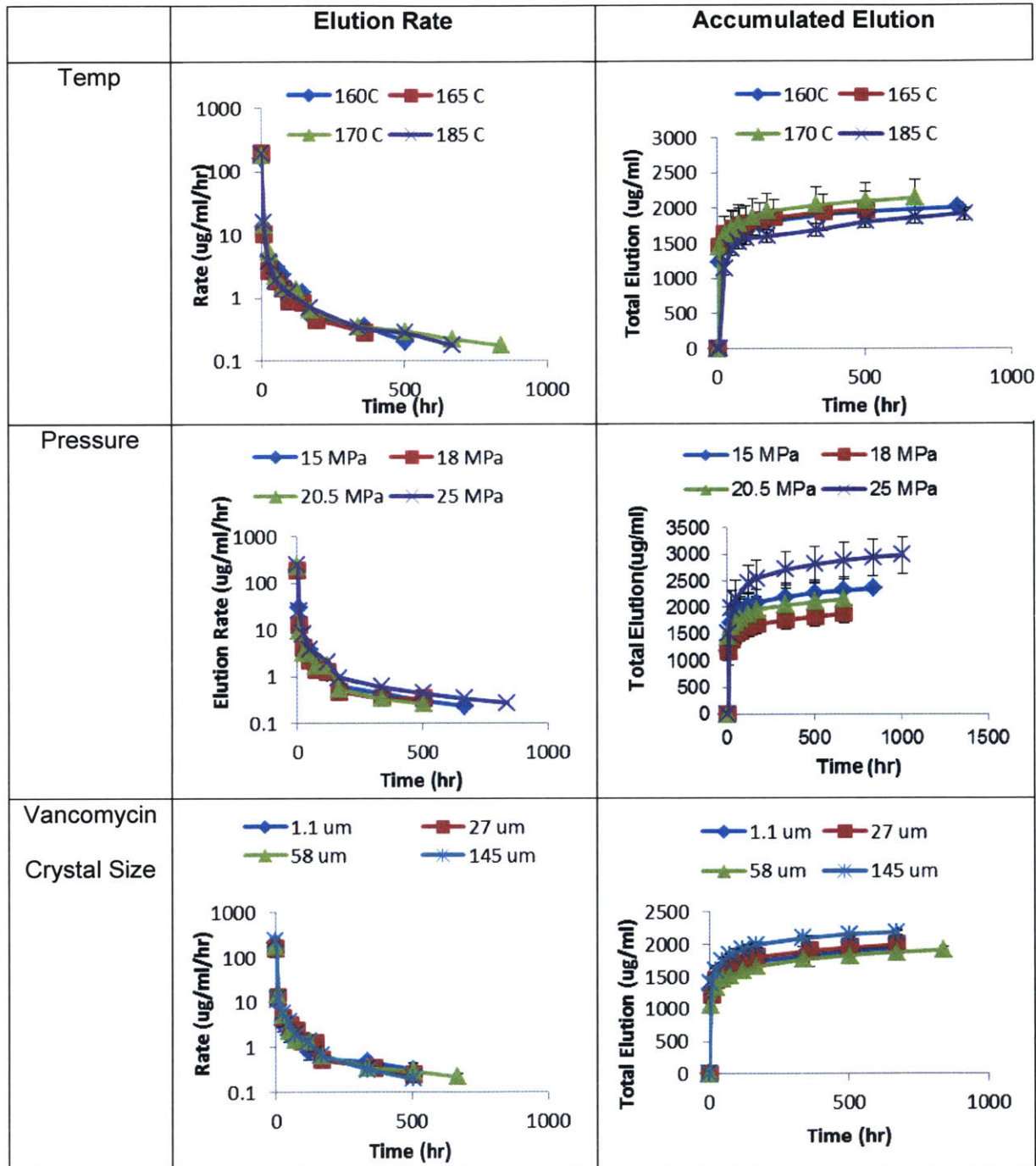


Figure 2. 11. Accumulated release (a) and elution rate (c) of 4 wt % vancomycin eluting UHMWPE manufactured at various temperature, pressure, and vancomycin crystal size. Elution was performed at 37°C in PBS. Concentration of Vancomycin was measured using UV/Vis at 280 nm. Data are mean \pm s.d.

Computational Simulation on Effect of Drug Cluster Eccentricity on Drug Cluster

Interconnectivity

Computational simulation based on monte-carlo algorithm was conducted to examine the effect of drug cluster shape on drug cluster interconnectivity. The relation between computational drug cluster volume fraction vs drug cluster interconnectivity was then compared to the experimental result obtained from μ -CT of vancomycin eluting UHMWPE.

For both high and low eccentricity drug clusters, percent accessible drug clusters from the surface increased as the volumetric pore fraction is increased. For all cluster volume fraction tested, percent accessible drug clusters in highly eccentric drug clusters increased faster than low eccentricity (**Figure 2.12a**). The difference in percent accessible pores was accentuated at higher pore fraction (>0.05 % volume) because the low eccentricity pores reaches a plateau in percent accessible pores, while the percent accessible drug clusters of highly eccentric drug clusters still increased linearly with drug clusters fraction. When compared to the experimental result (**Figure 2.12b**), the rapid increase in accessible cluster was shifted to the right, i.e. instead of direct rapid increase from cluster volume fraction of 0 (simulation), the experimental rapid increase is observed at a later cluster volume fraction, beginning at a cluster volume fraction of 0.02.

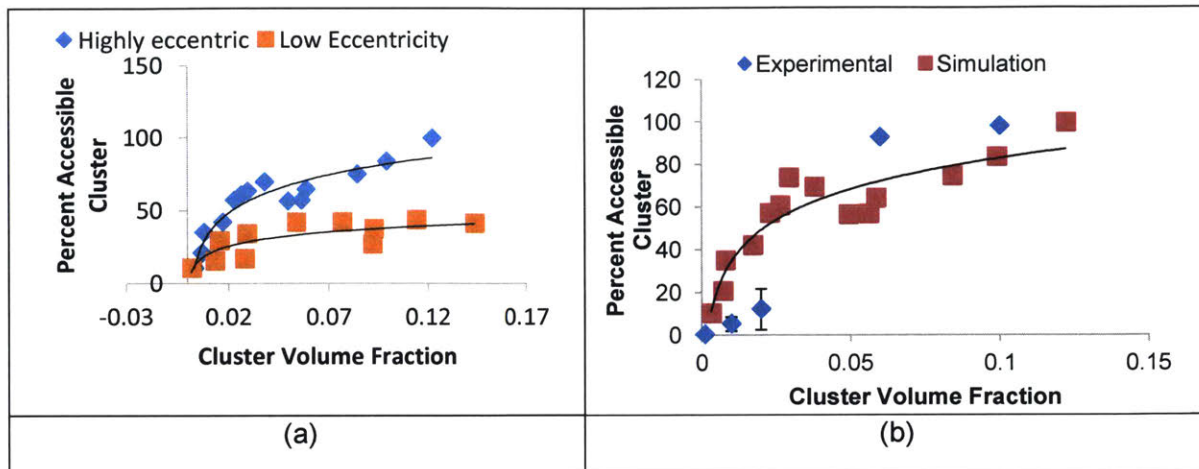


Figure 2. 12. Computational simulation result of percent accessible cluster. (a) Percent accessible cluster of highly eccentric and low eccentric drug cluster in polymeric matrix. (b) Comparison of percent accessible cluster between experimental (micro CT) and computational simulation of highly eccentric vancomycin-UHMWPE.

Incorporation of Other Antibiotics into UHMWPE

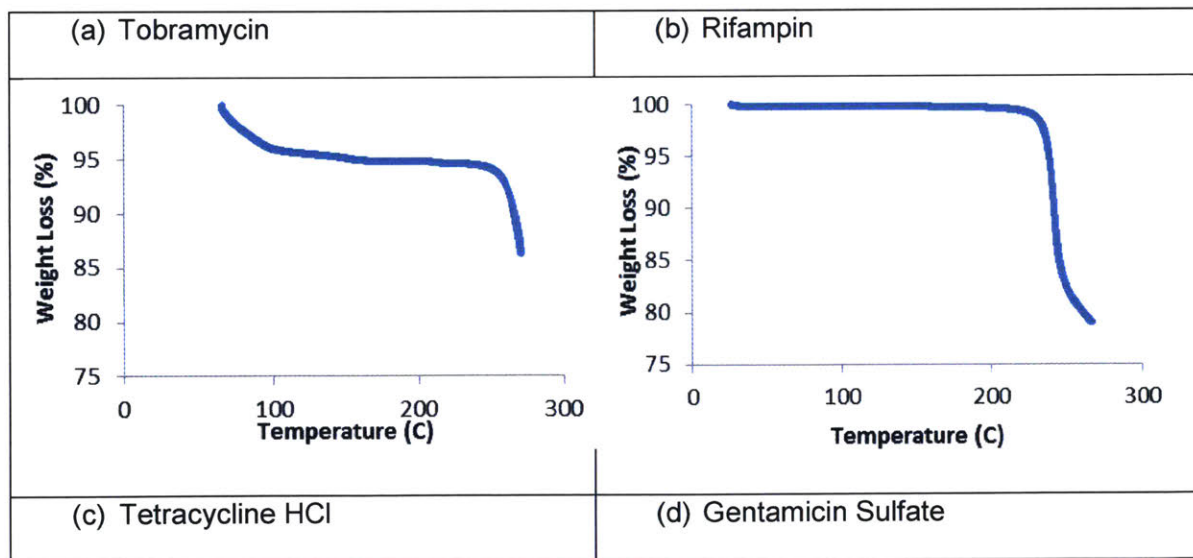
To test the generality of our consolidation method and to determine if drug cluster eccentricity is dependent upon the type of drug, we incorporated other antibiotics into UHMWPE and examined their drug cluster structure, drug elution behavior, and the mechanical properties in comparison to the vancomycin eluting UHMWPE. The optimum temperature, pressure, and crystal size as observed with vancomycin-UHMWPE were used. Therefore, all the other antibiotics eluting UHMWPE were synthesized at $T=170^{\circ}\text{C}$, $P=20.5\text{ MPa}$, and mean crystal size of 25 μm .

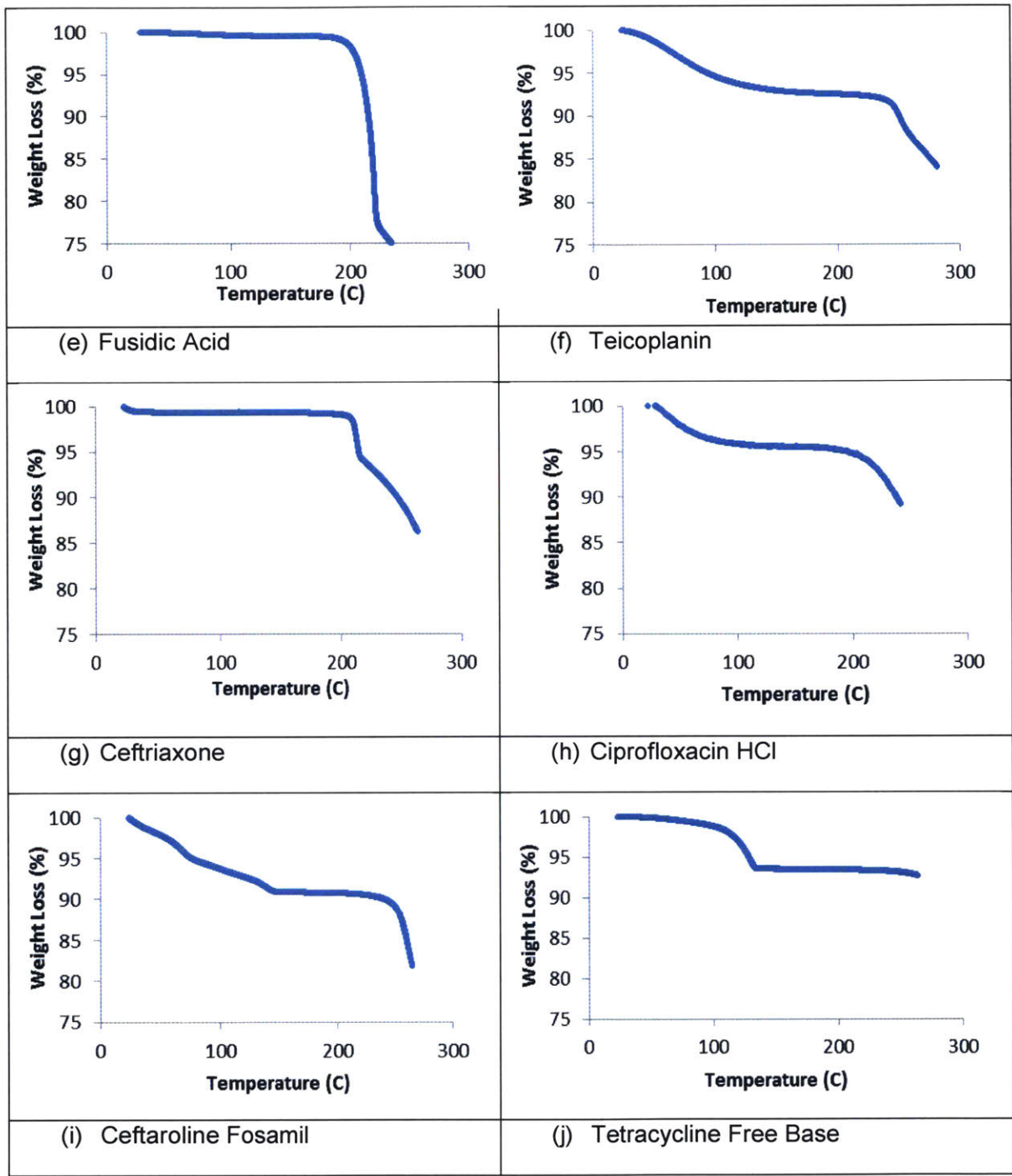
Heat Resistance of Antibiotics Determined by Thermo Gravimetric Analysis (TGA)

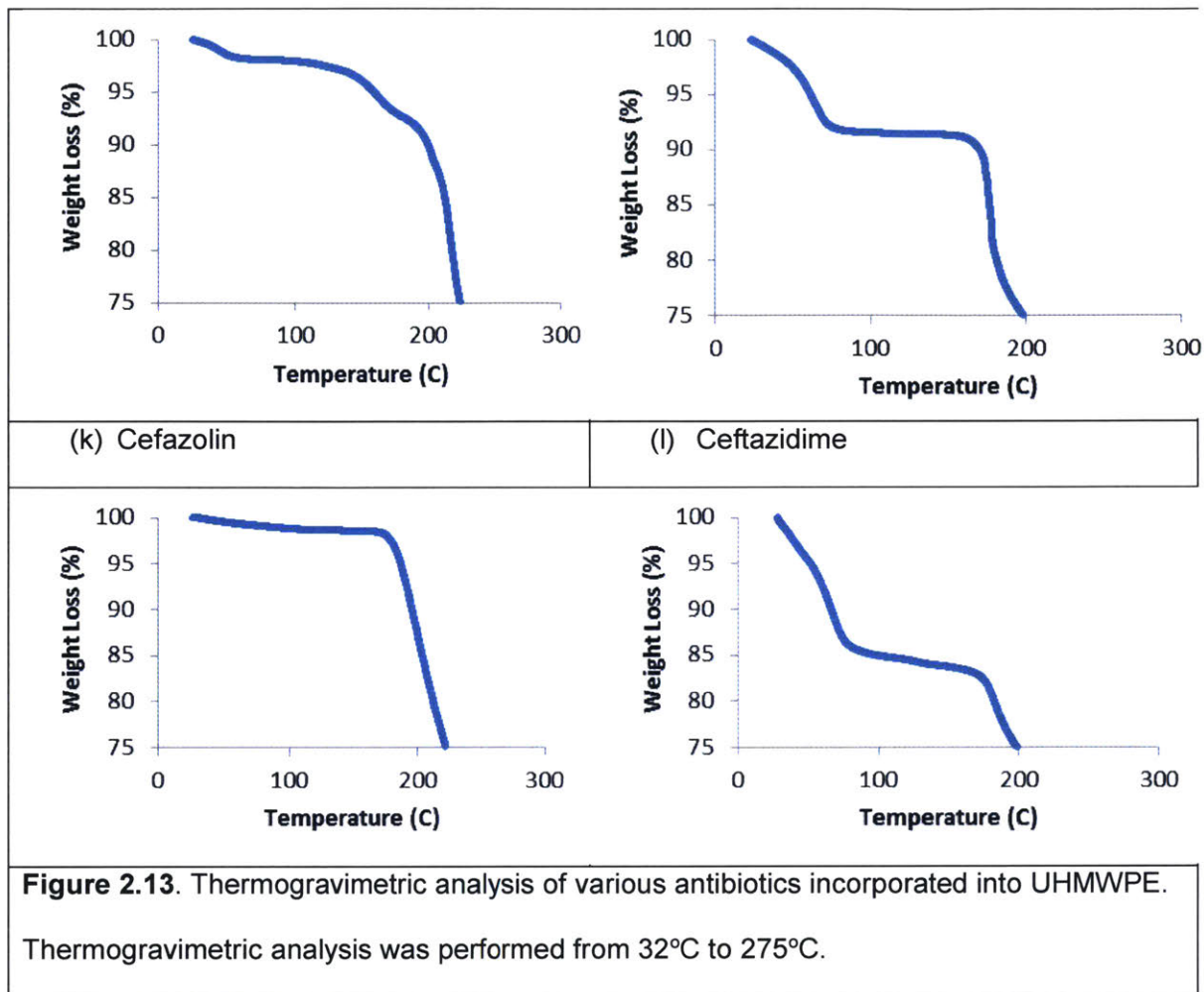
To test the heat resistance of other antibiotics that would be incorporated into UHMWPE, TGA of each antibiotics candidate was performed. Included in the antibiotics candidate lists

were tobramycin, rifampin, tetracycline HCl, gentamicin sulfate, fusidic acid, teicoplanin, ciprofloxacin HCl, cefazolin, ceftriaxone, ceftaroline fosamil, and ceftazidime.

In general, for all samples tested, there was an initial decline in mass between 50°-100°C. The mass then stayed constant for a certain temperature period and then started to decline again when thermal degradation temperature was reached. Antibiotics such as tobramycin, rifampin, tetracycline HCl, gentamicin sulfate, fusidic acid, teicoplanin, ceftriaxone and ciprofloxacin were heat stable up to 200°C (**Figure 2.13a-h**), while antibiotics such as ceftaroline fosamil, tetracycline, and ceftazidime starts to undergo heat degradation at $T < 170^{\circ}\text{C}$ (**Figure 2.13i-l**). Most antibiotics that belongs to the group cephalosporin (cefazolin, ceftaroline fosamil, and ceftazidime) degrades when exposed to $T > 150^{\circ}\text{C}$ except ceftriaxone, which did not show any sign of degradation up to 200°C.





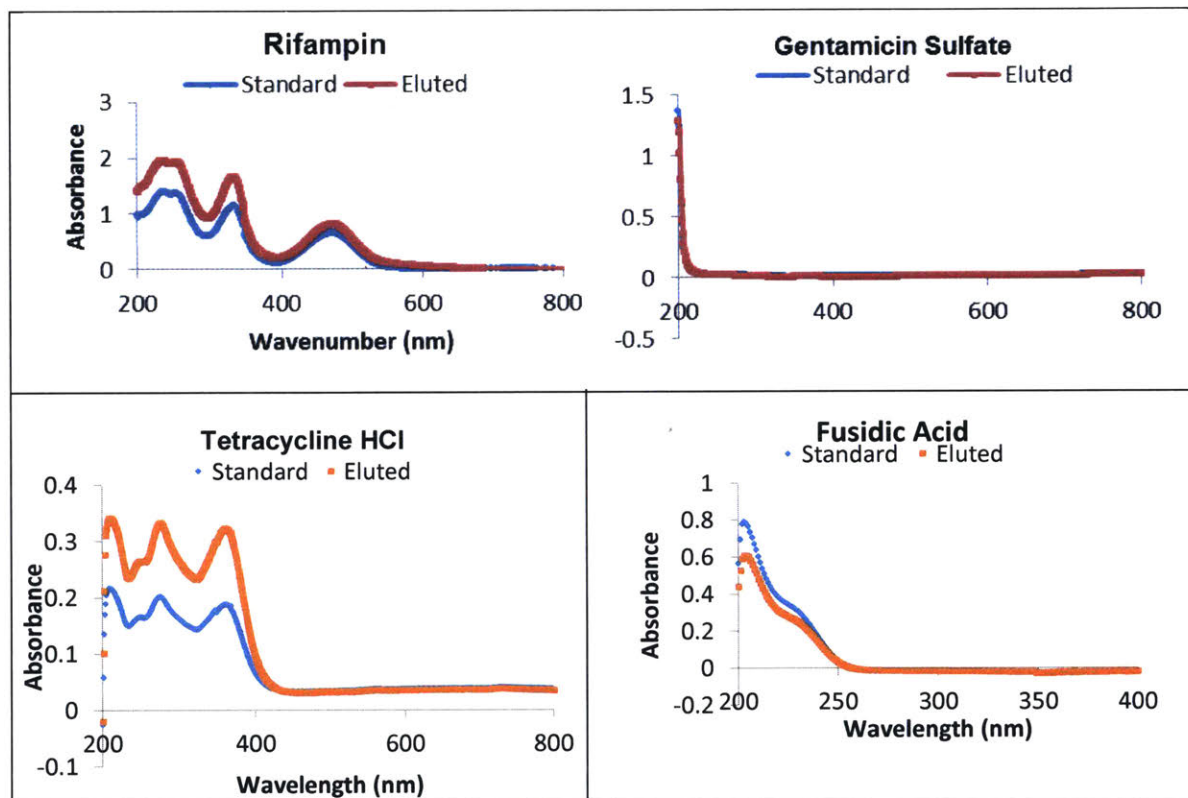


Spectral analysis of eluted antibiotics from antibiotic-eluting UHMWPE in comparison to pure antibiotics

Based on the TGA analysis, eight antimicrobials (ciprofloxacin HCl, tobramycin, tetracycline HCl, gentamicin, rifampin, teicoplanin, ceftriaxone, and fusidic acid) did not show significant degradation and weight loss close to UHMWPE consolidation temperature. We then incorporated these antibiotics into UHMWPE and performed spectral analysis (NMR, IR, and UV-Vis) on the first 24 hr eluted antibiotics and compare it to the standard solution of antibiotics.

Ultraviolet-Visible Spectroscopy (UV-Vis) of Antibiotics Eluted From UHMWPE

UV-Vis spectroscopy analyses were performed on the eight antimicrobials eluted from the antibiotic eluting UHMWPE (Figure 2.14). No meaningful difference was observed between UV-Vis spectra of eluted and standard antibiotics for all eight antibiotics tested. These results showed that there was no change in the UV-Vis active molecular constituents after being incorporated into UHMWPE.



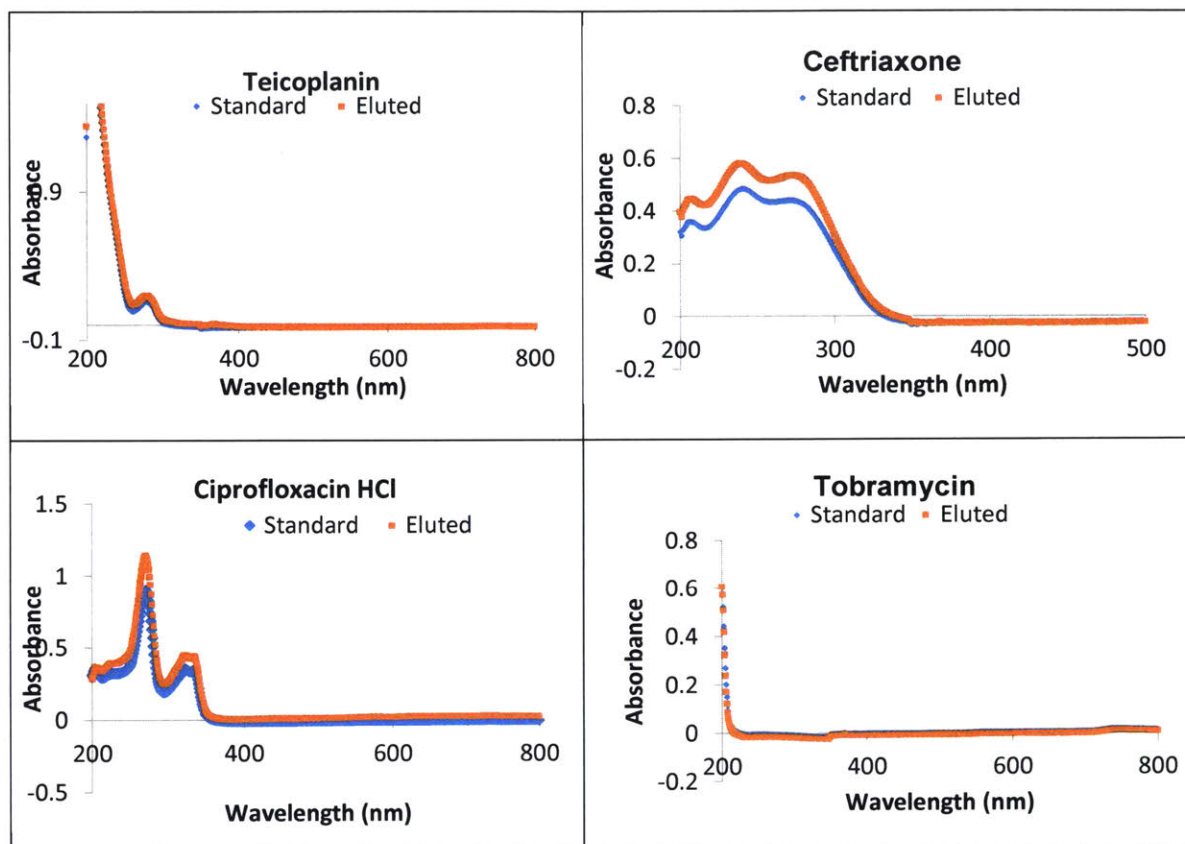
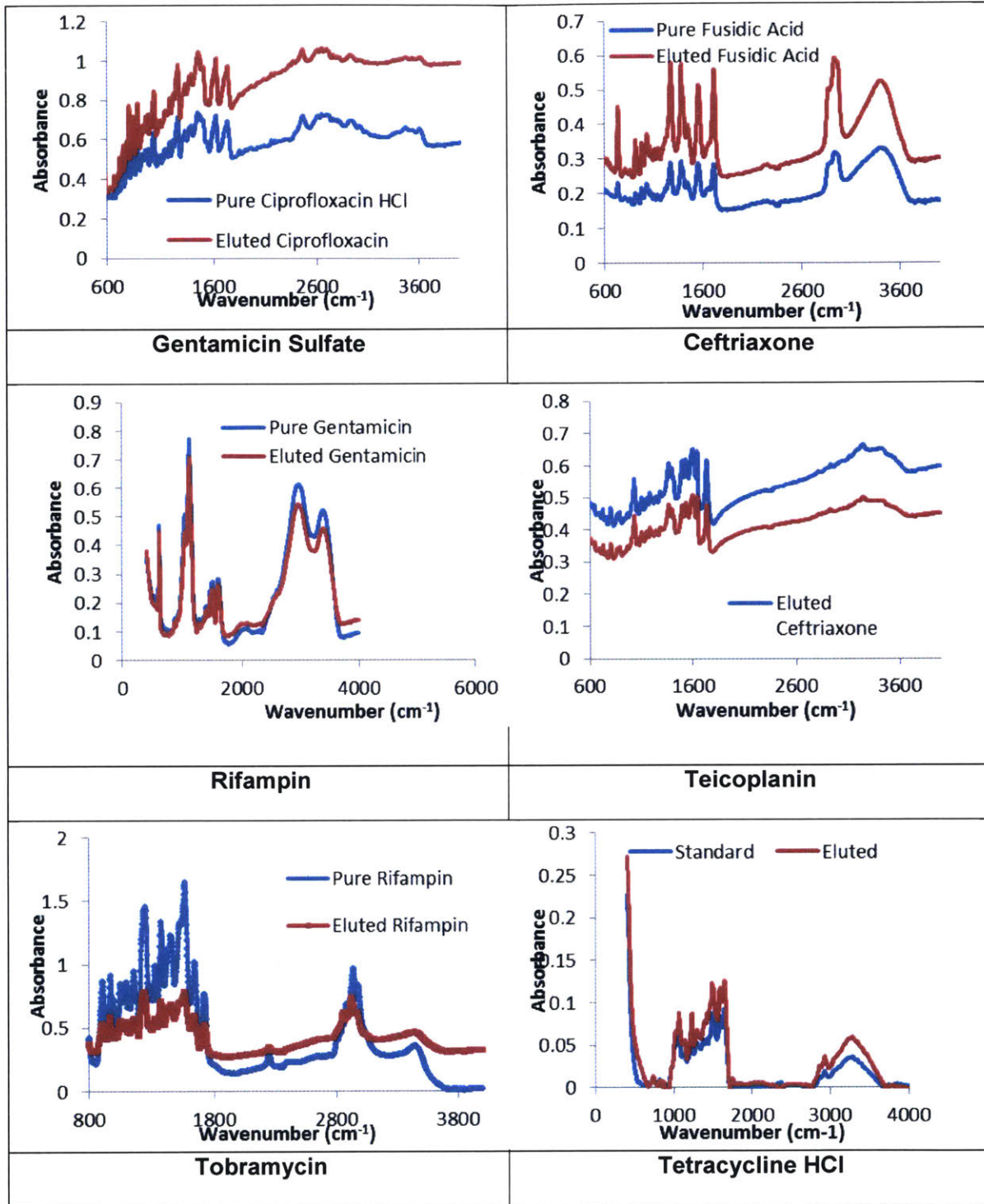


Figure 2.14. UV-Vis Spectra of eluted and standard rifampin, gentamicin sulfate, tetracycline HCl, fusidic acid, teicoplanin, ceftriaxone, ciprofloxacin HCl, and tobramycin. Elution was performed at 37°C in PBS for 24 hr. Standard solution was made immediately before UV/Vis spectra measurement.

FTIR Analysis of Antibiotics Eluted From UHMWPE

FTIR spectroscopies were performed on the eight antimicrobials eluted from the antibiotic eluting UHMWPE (**Figure 2.15**). No meaningful difference was observed between FTIR spectra of eluted and standard antibiotics for all eight antibiotics tested. These results further showed that there was no change in the molecular constituents after being incorporated into UHMWPE.

Ciprofloxacin HCl	Fusidic Acid
--------------------------	---------------------



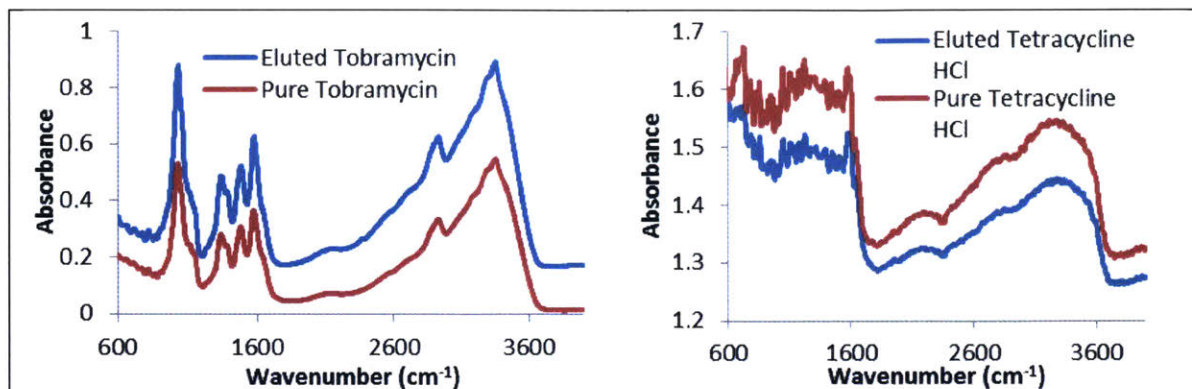
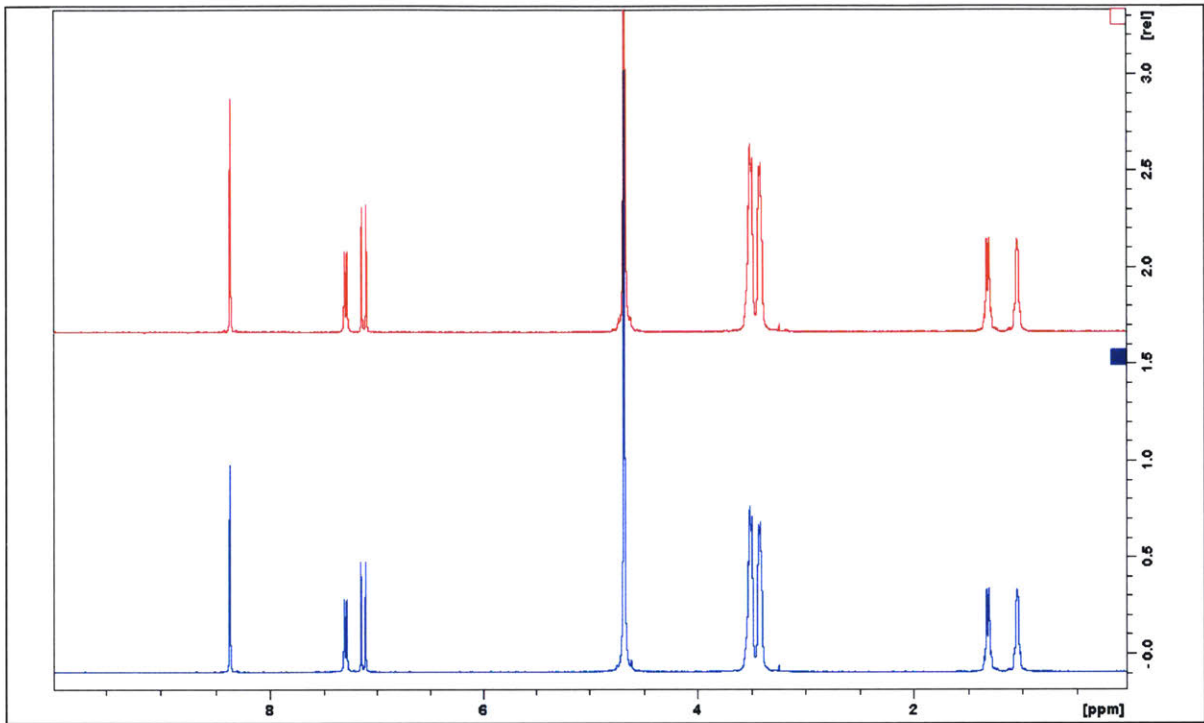


Figure 2. 15. FTIR Spectra of eluted and standard rifampin, gentamicin sulfate, tetracycline HCl, fusidic acid, teicoplanin, ceftriaxone, ciprofloxacin HCl, and tobramycin. Elution was performed at 37°C in PBS for 24 hr. Standard solution was made immediately before IR spectra measurement.

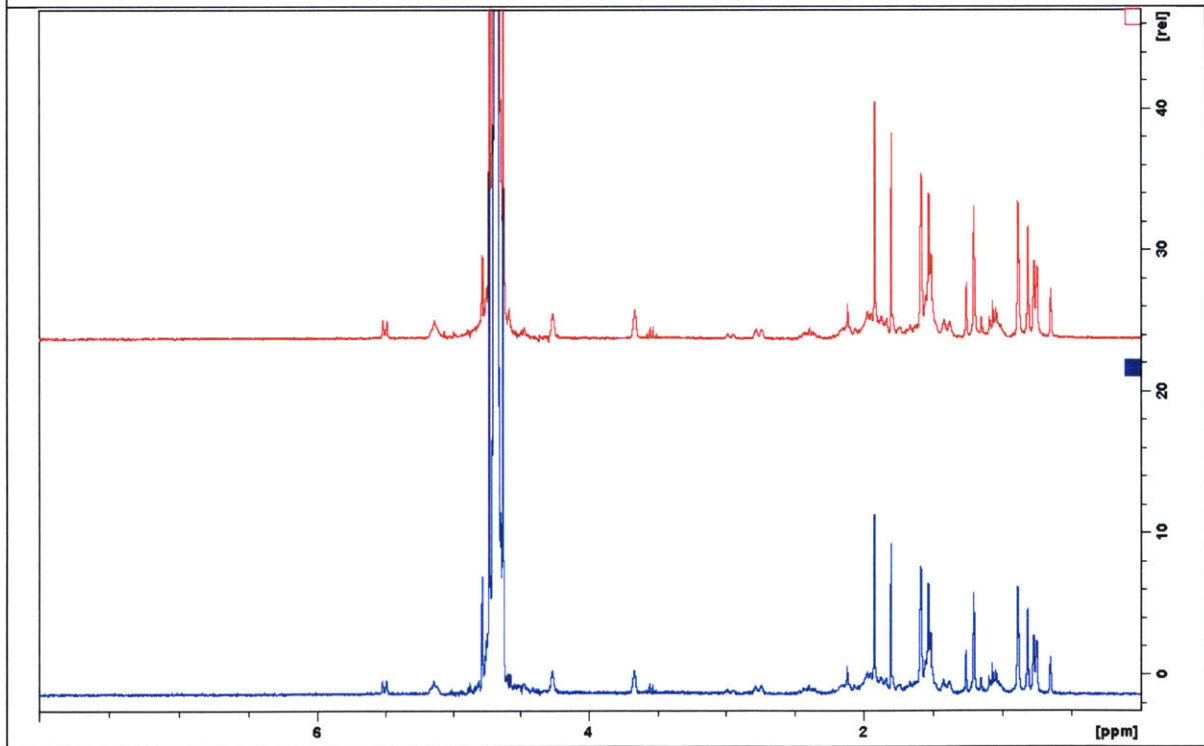
NMR Analysis of Antibiotics Eluted From UHMWPE

For a final characterization of the eluted antibiotics, NMR analyses were performed on the eight antimicrobials eluted from the antibiotic eluting UHMWPE (**Figure 2.16**). As with the UV-Vis spectra and FTIR, no meaningful difference was observed between NMR spectra of eluted and standard antibiotics for all eight antibiotics tested. Together with the UV-Vis and FTIR, it can be concluded that there was no detectable change in the molecular constituents after being incorporated into UHMWPE.

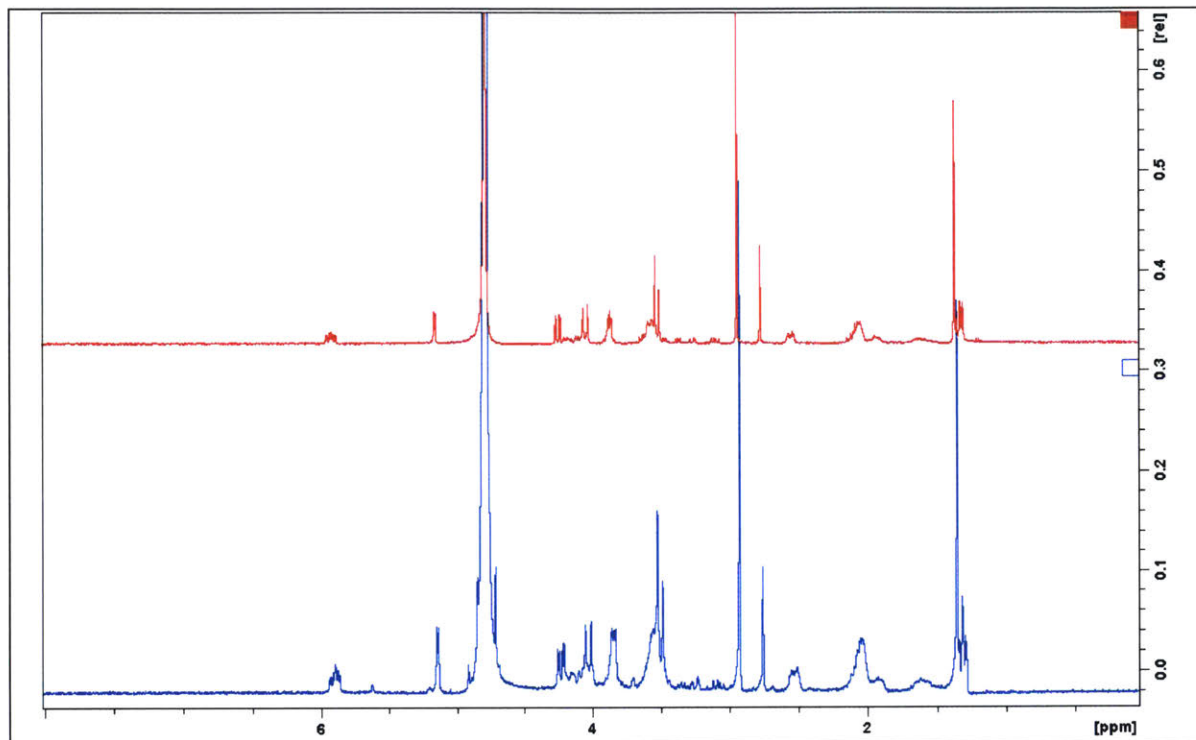
Ciprofloxacin HCl



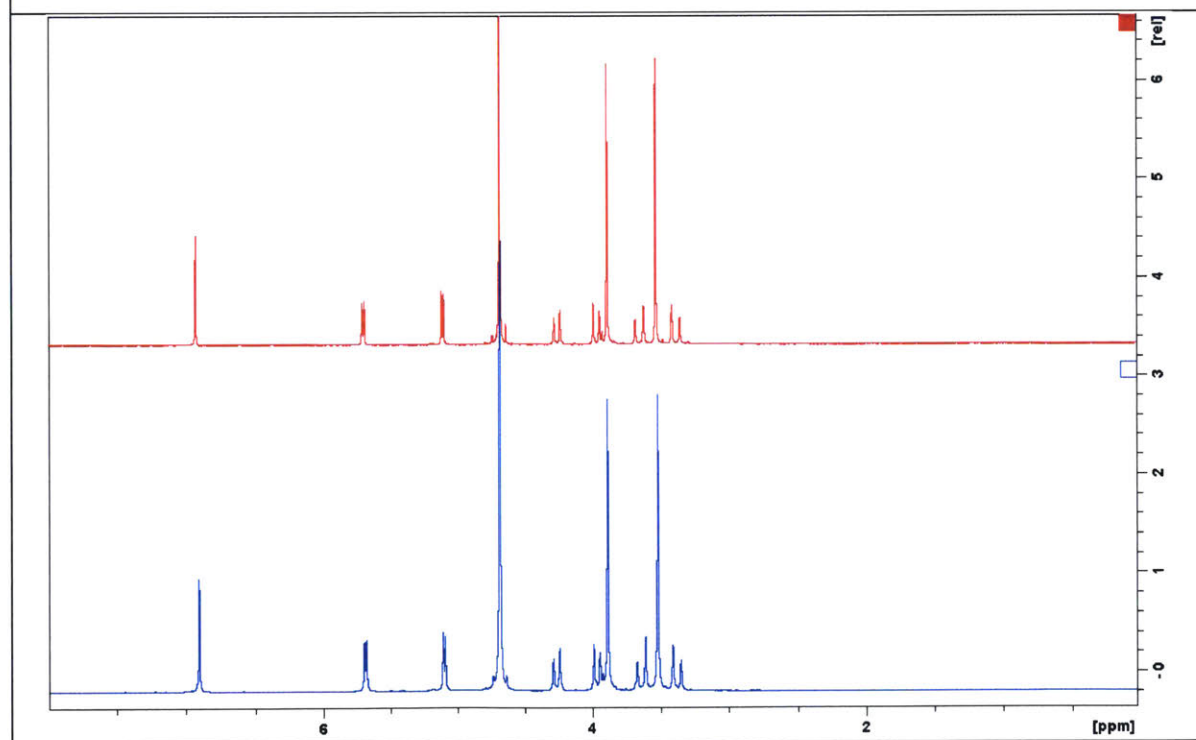
Fusidic Acid



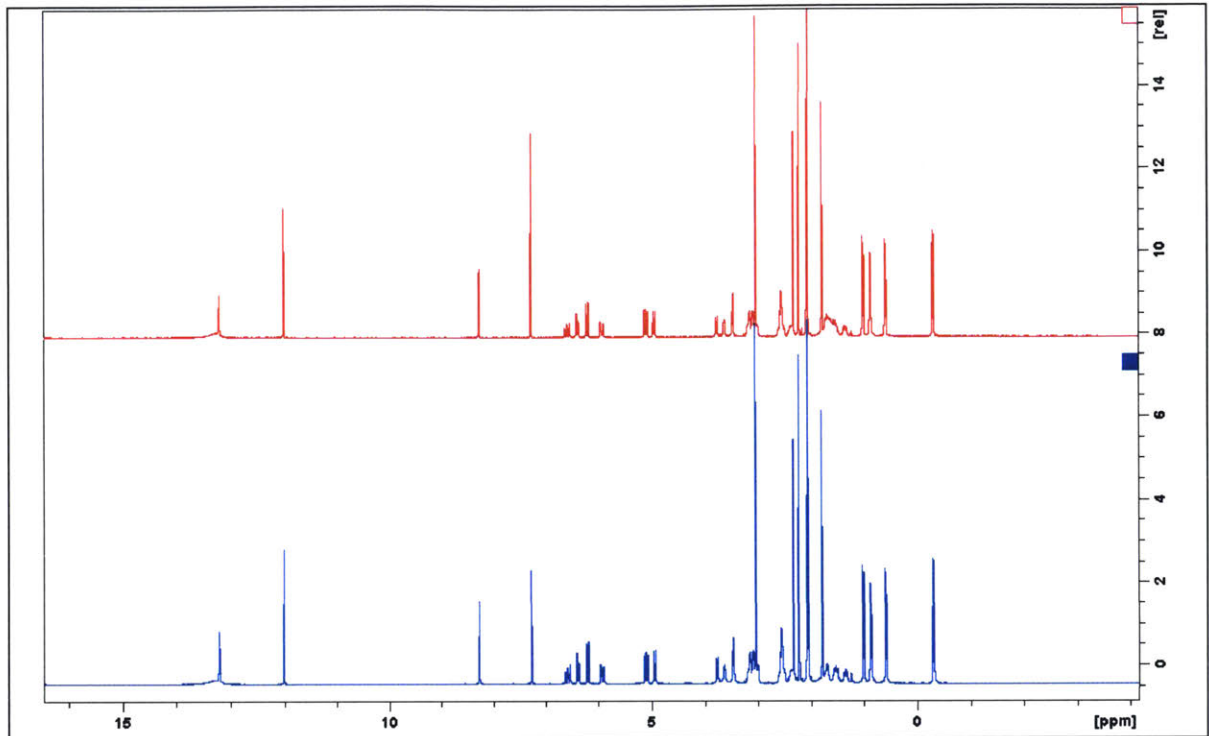
Gentamicin Sulfate



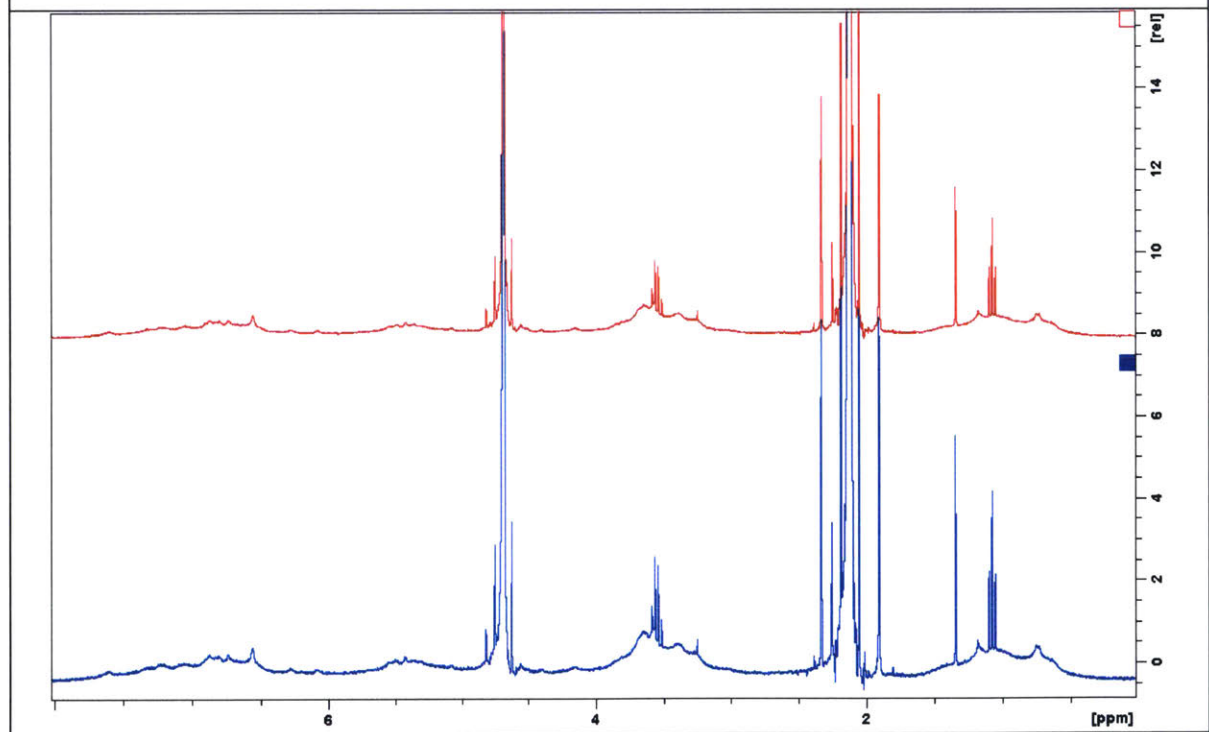
Ceftriaxone



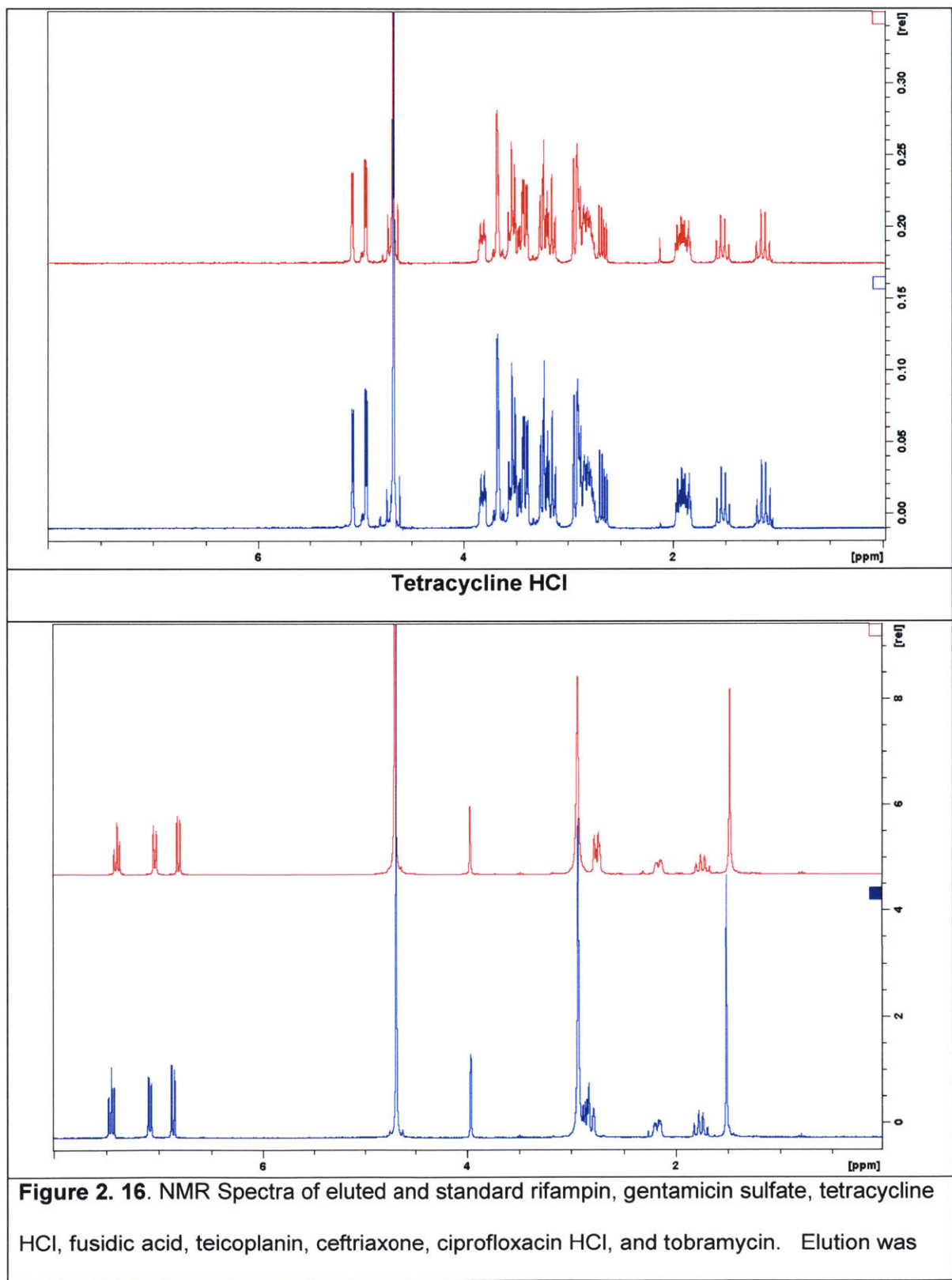
Rifampin



Teicoplanin



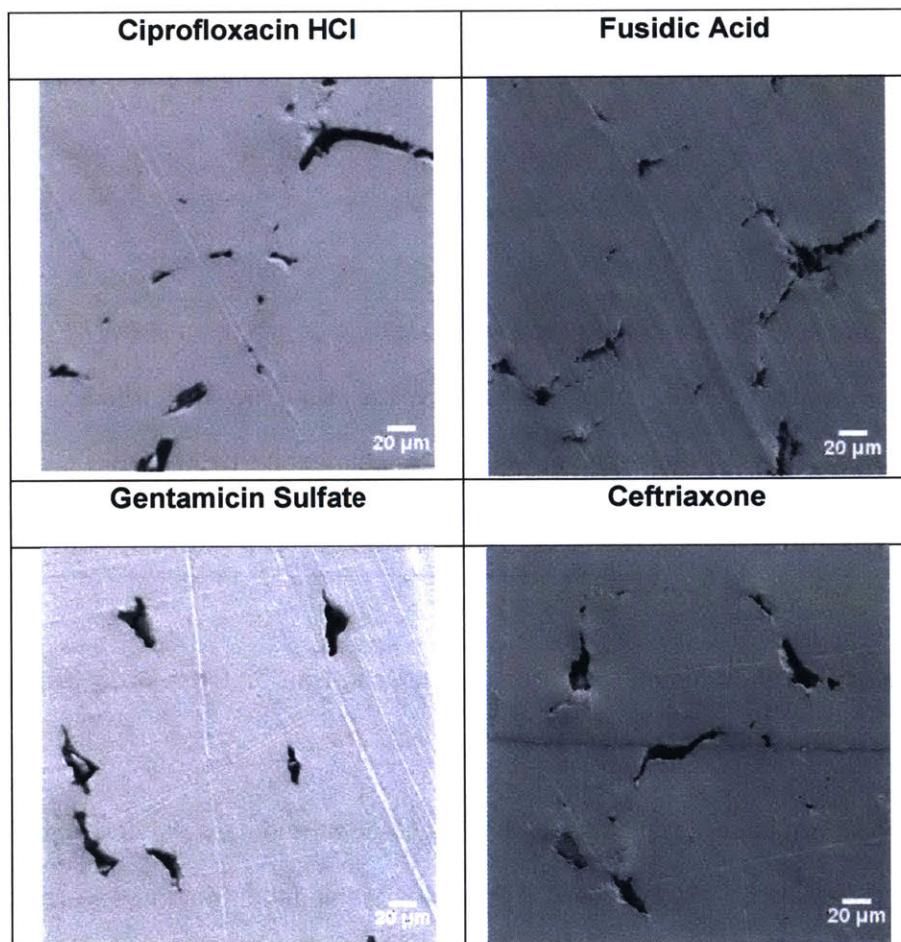
Tobramycin

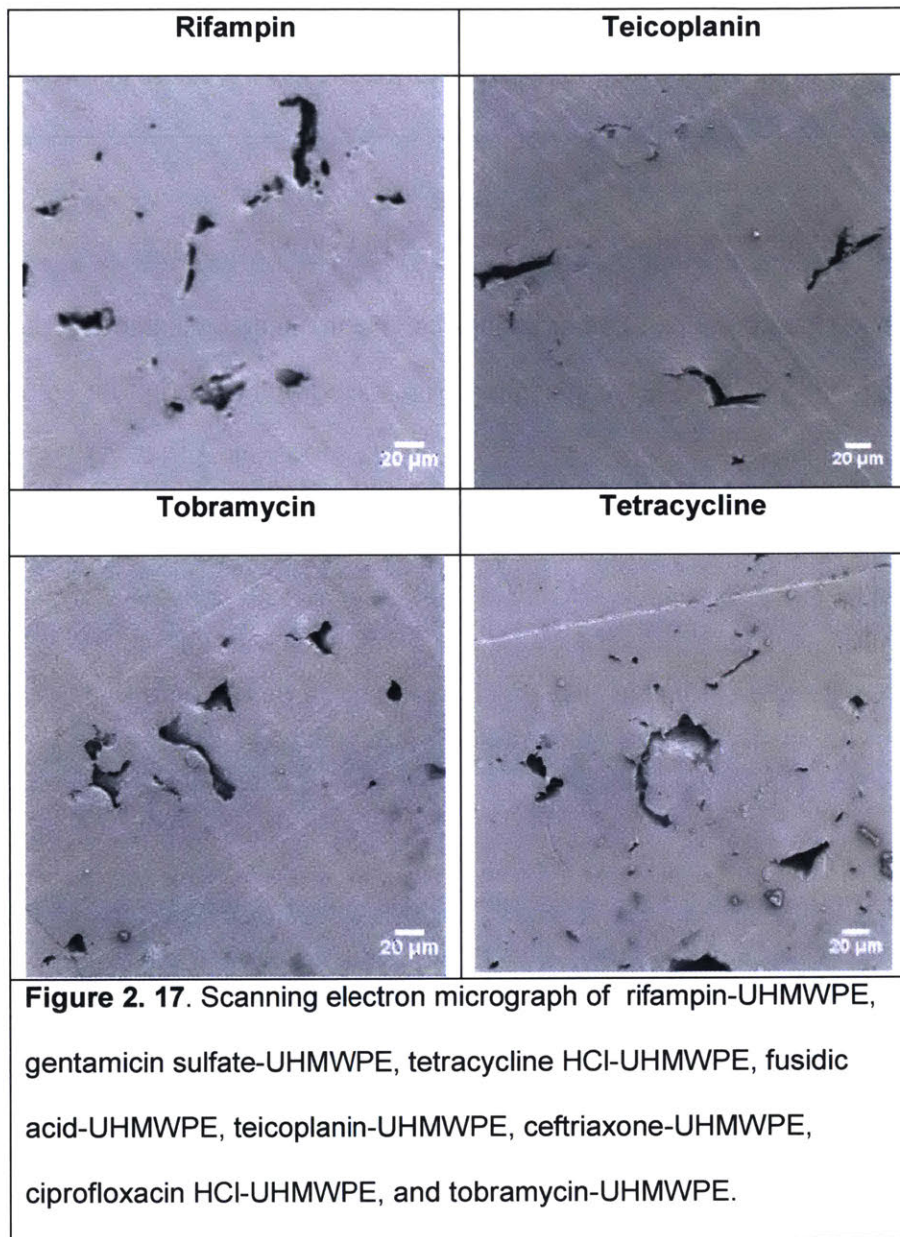


performed at 37°C in PBS for 1 week. Standard solution was made immediately before IR spectra measurement.

Scanning Electron Micrograph of Antibiotic Eluting UHMWPE

To check if incorporation of other antibiotics affects the drug cluster eccentricity of the other antibiotic eluting UHMWPE, scanning electron micrograph were performed on the eight antibiotic eluting UHMWPE (**Figure 2.17**). All eight antibiotics eluting UHMWPE showed highly eccentric drug clusters, similar to vancomycin eluting UHMWPE (**Figure 2.17**).





Effect of Drug Hydrophilicity/Hydrophobicity on Drug Elution from Drug Eluting UHMWPE

After ensuring that drug eluting UHMWPEs blended and consolidated with the eight alternative drugs produced highly eccentric drug clusters and that the drugs were not degraded after being incorporated into UHMWPE, we measured the drug elution from these UHMWPE.

Tobramycin eluted the fastest (**Figure 2.18a**) initially but quickly dropped to the slowest rate of all the eight antibiotics tested. Fusidic acid, on the other hand, had the slowest initial rate of all eight antibiotics, but has the highest ability to sustain the elution rate, resulting in the highest long term elution rate of all eight antibiotics tested. The accumulated elution (**Figure 2.18b**) showed that in the long term, the total elution for all eight-antibiotic eluting UHMWPE converged to the same point, indicating that the total elution was independent of the type of antibiotics.

To further understand the effect of drug type on the drug elution, we plotted the elution rate against the ratio of the antibiotic's molecular polar surface area to its molecular volume (PSA/MV). The PSA/MV was obtained using computational method as mentioned in the method section (**Table 2.1**). The ratio of these values (PSA/MV) was used to normalize polarity by molecular size. We found that more polar compounds (PSA/MV > 0.3, such as tobramycin and ceftriaxone) had a higher elution rate early, but the rate dropped more rapidly over time compared to non-polar compounds (PSA/MV < 0.3, such as fusidic acid, ciprofloxacin, and rifampin) (**Figure 2.19**).

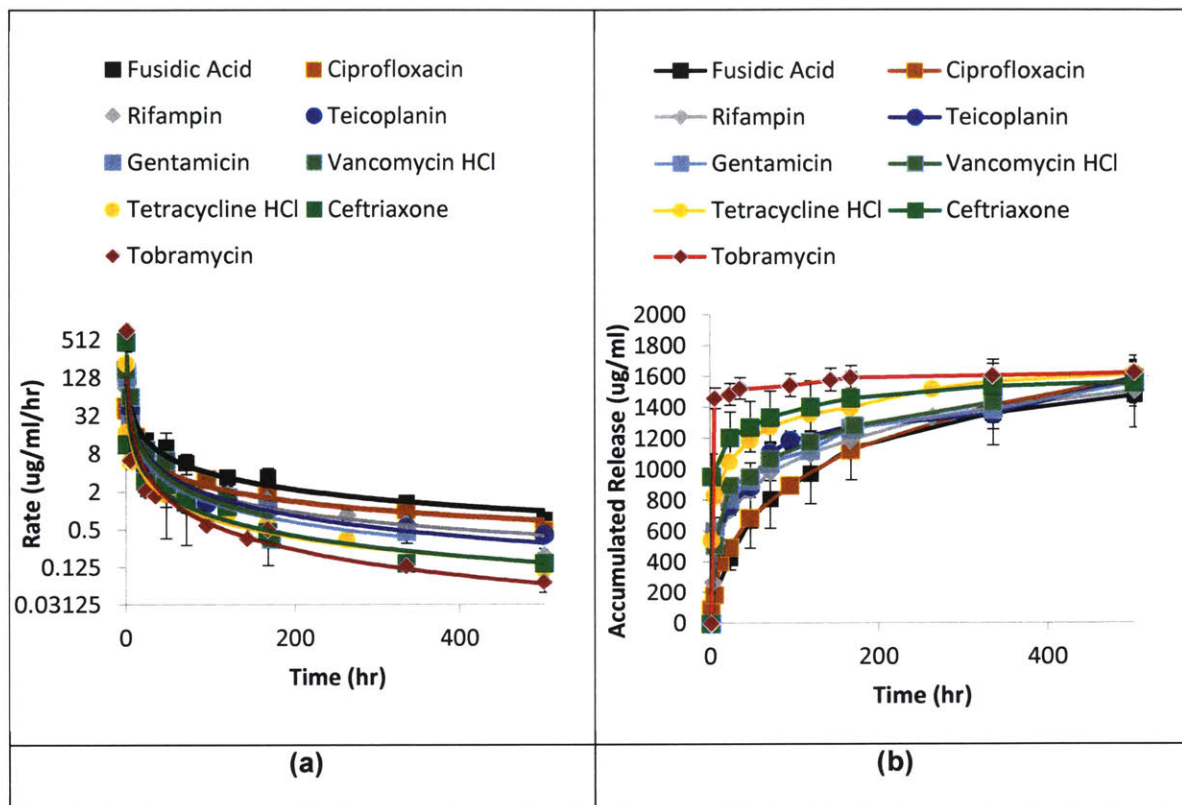


Figure 2. 18. Elution rate (a) and accumulated release (b) of rifampin-UHMWPE, gentamicin sulfate-UHMWPE, tetracycline HCl-UHMWPE, fusidic acid-UHMWPE, teicoplanin-UHMWPE, ceftriaxone-UHMWPE, ciprofloxacin HCl-UHMWPE, and tobramycin-UHMWPE.

Drugs	PSA/MV
Fusidic Acid	0.20
Ciprofloxacin hydrochloride	0.26
Rifampin	0.29

Teicoplanin	0.42
Vancomycin.HCl	0.43
Gentamicin	0.45
Tetracycline.HCl	0.48
Ceftriaxone	0.50
Tobramycin	0.63

Table 2.1. PSA/MV of rifampin, gentamicin sulfate, tetracycline HCl, fusidic acid, teicoplanin, ceftriaxone, ciprofloxacin HCl, and tobramycin.

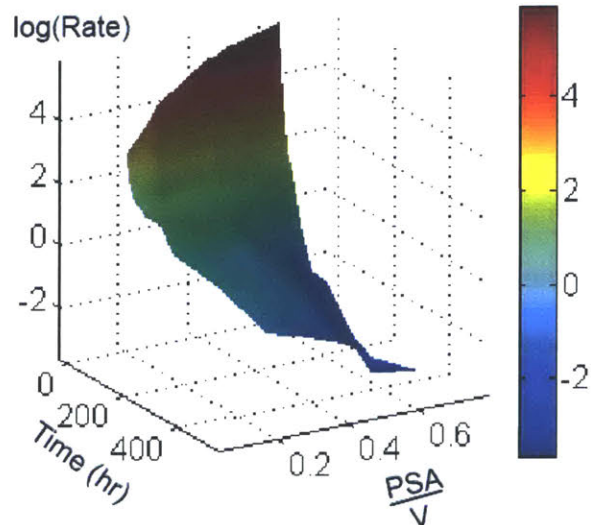


Figure 2.19. Elution rate as a function of time vs PSA/MV (a) and accumulated release (b) of rifampin-UHMWPE, gentamicin sulfate-UHMWPE, tetracycline HCl-UHMWPE, fusidic

acid-UHMWPE, teicoplanin-UHMWPE, ceftriaxone-UHMWPE, ciprofloxacin HCl-UHMWPE, and tobramycin-UHMWPE.

Discussion

Most antibiotics can be incorporated into UHMWPE without any sign of thermal degradation

Thermogravimetric analysis and subsequent comparison of NMR, IR, and UV-Vis showed that vancomycin, rifampin, gentamicin sulfate, tetracycline HCl, fusidic acid, teicoplanin, ceftriaxone, ciprofloxacin HCl, and tobramycin are all heat resistant enough to be incorporated into LDPE and UHMWPE. However, most of the antibiotics in the cephalosporin group, such as cefazolin, ceftaroline fosamil, and ceftazidime started to undergo thermal degradation below 170°C and therefore are unable to be incorporated into LDPE and UHMWPE. The relatively low thermal stability originates from the thermally labile dihydrothiazine cycle at the core of all cephalosporins[301]. The thermal degradation of dihydrothiazine cycle consisted of dehydration process, followed by degradation of the dihydrothiazine ring, and subsequent release of volatile products such as benzene, p-cresol, phenol, azine, N-ethyl-formamide, and carbon disulfide[301].

Some of the thermally stable antibiotics we tested above have also been used in antibiotic eluting bone cements, such as gentamicin, [202] tobramycin[200] (aminoglycosides active against both gram positive and gram negative bacteria), vancomycin (glycopeptide active against gram-positive bacteria)[203], ciprofloxacin[204], and teicoplanin.[208, 209]. However, while there are antibiotics that cannot be incorporated into bone cement because they impede polymerization (e.g. rifampin, an antimicrobial that has high efficacy against bacterial biofilm[212]), such antibiotics can be incorporated into UHMWPE because manufacture of drug-eluting UHMWPE only involves consolidation and reptation between UHMWPE chains (i.e. no

chemical reactions). We have yet to find an antibiotic that is thermally stable but cannot be incorporated into UHMWPE.

Highly Eccentric Pore Morphology in drug-eluting LDPE

We used LDPE to study the effect of drug cluster shape on interconnectivity and elution because LDPE was amenable to both solvent casting, and compression molding due to its lower molecular weight and associated lower viscosity than that of UHMWPE. We hypothesized that the comparison of these two preparation methods could enable us to determine the effect of the drug cluster eccentricity on the structure and properties of the drug-loaded polymeric matrix. While solvent casting of vancomycin LDPE resulted in spherical drug clusters (**Figure 2.6**), mechanical mixing of vancomycin with LDPE and subsequent compression molding while minimizing melt flow resulted in highly eccentric drug clusters (**Figure 2.6**). In both cases phase separation between the drug clusters and LDPE was observed because the single drug-polymer phase is both thermodynamically and kinetically unfavorable: Vancomycin is hydrophilic (partition coefficient in octanol-water = 0.039 [302], while polyethylene is hydrophobic (partition coefficient in octanol-water = $10^{12.2}$ [303]). Assume ideal solutions where the sum of volume fraction of drug (vancomycin) and volume fraction of polymer (polyethylene) = 1, i.e.

$$\phi_{polymer} = 1 - \phi_{drug} \quad (11)$$

Hence eq (2) can be written as:

$$\Delta G_{Drug-Polymer} = RT(\phi_{drug} * \ln\phi_{drug} + (1 - \phi_{drug})) * \ln(1 - \phi_{drug}) + \chi_{drug-polymer} * \phi_{drug}(1 - \phi_{drug}) \quad (12)$$

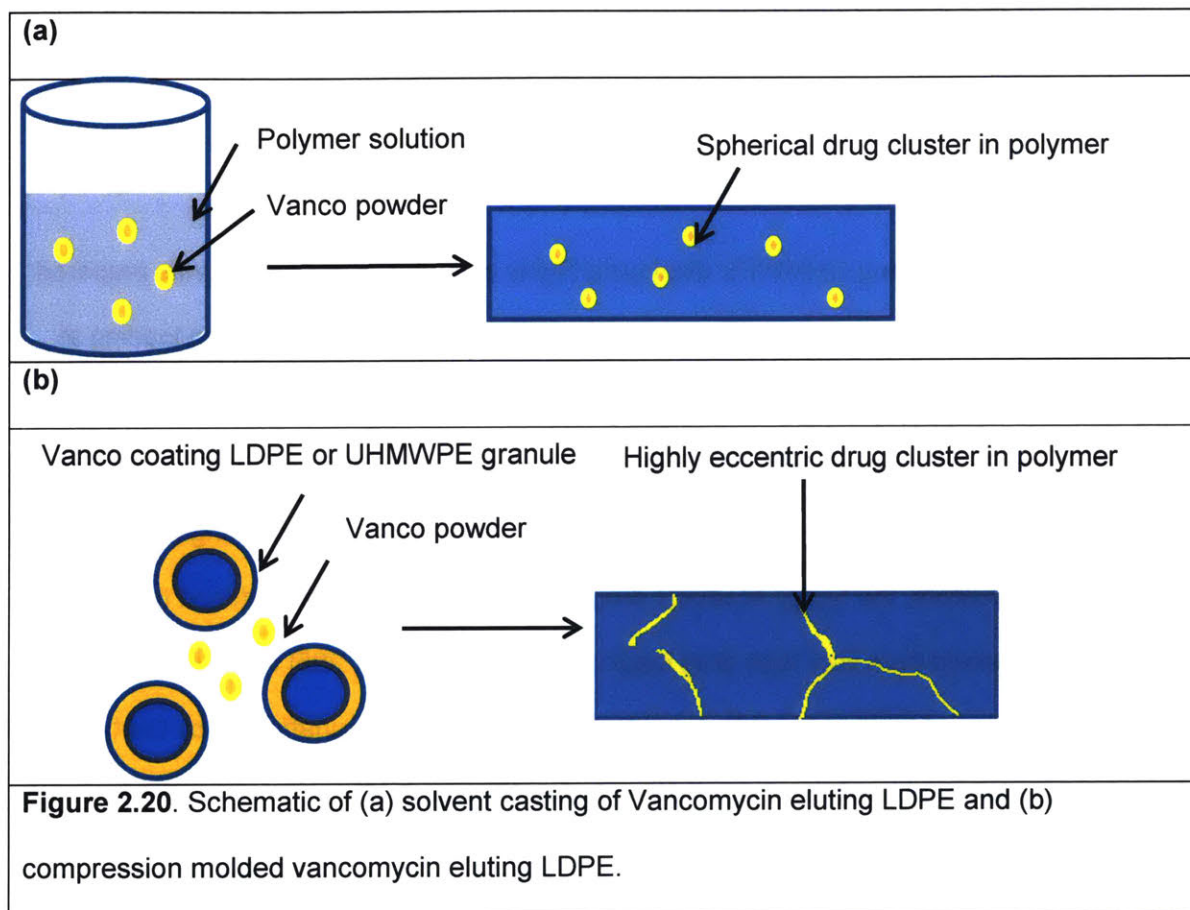
Value of $\chi_{drug-polymer}$ can be calculated from [304]:

$$\chi_{drug-polymer} = \frac{V_m}{RT} ((\delta_{d,drug} - \delta_{d,polymer})^2 + (\delta_{p,drug} - \delta_{p,polymer})^2)$$

Where V_m is the average molar volume of polymer based on the mole fraction. $\delta_{d,drug}$ and $\delta_{d,polymer}$ are the dispersion solubility parameter of drug and polymer respectively. $\delta_{p,drug}$ and $\delta_{p,polymer}$ are dipole force solubility parameters of drug and polymer respectively[304]. For polyethylene, $V_m = 32.8$ cc/mole, $\delta_{d,polymer} = 8.47$, and $\delta_{p,polymer} = 8.61$ [305]. Because of the low octanol-water partition coefficient of vancomycin, the solubility parameters of vancomycin is approximated as short chain alcohol (methanol), which has $\delta_{d,drug} = 7.42$, and $\delta_{p,drug} = 6.0$ [304]. Solving for $\chi_{drug-polymer}$ at compression molding temperature of 170°C gave $\chi_{drug-polymer} = 7.14$. Because the single drug-polymer phase is thermodynamically favorable for $\Delta G_{Drug-Polymer} < 0$, the maximum soluble volume fraction of vancomycin in polyethylene (at $\Delta G_{Drug-Polymer} = 0$) is 0.22 %. This actual dissolved vancomycin in polyethylene is likely even further lower than 0.22 % because the vancomycin exist in solid form during the drug-polymer processing). Hence most of the vancomycin (and other hydrophilic drugs that we used above) will have negligible solvation in the polyethylene.

In the solvent casting method (**Figure 2.20a**), vancomycin, which is hydrophilic, is dispersed in a hydrophobic medium (LDPE dissolved in xylene). As a result, to minimize surface tension, the vancomycin particles tend to agglomerate and form spherical aggregates. Therefore, when the vancomycin-LDPE mixture in xylene is solvent cast and cooled down, the vancomycin clusters stayed in spherical form (**Figure 2.20a**). On the other hand, after mechanical mixing of LDPE granules with vancomycin particles, some of the vancomycin coated the surface of the LDPE granules and some was interspersed in between the LDPE granules (**Figure 2.20b**). When compressed under minimum flow, the LDPE granules and vancomycin were deformed but the vancomycin did not have the configurational and convectional freedom to form aggregates to minimize its surface tension against the unfavorable interaction with hydrophobic LDPE. As a result, highly eccentric vancomycin clusters inside LDPE were obtained (**Figure 2.20b**). These results showed that by using solventless method of

consolidation as well as the application of pressure during consolidation to form these clusters, we can prevent vancomycin clusters from forming the thermodynamically favorable spherical clusters (to minimize surface area to volume ratio, and hence minimizing the unfavorable interaction with polyethylene).



Variation in the content of the antibiotic drug vancomycin (2 wt %, 6 wt %, and 10 wt %) and the LDPE to vancomycin particle size ratio (2:1, 4:1, and 40:1) showed that the polymer with the highly eccentric drug clusters showed higher elution rate than that of the one with spherical drug clusters for 6 and 10 wt% drug loading (**Figures 2.7**). This was because the percolation threshold was reached with this morphology at this loading at a much lower concentration than the conventional spherical cluster system as hypothesized. Because of its

higher drug cluster interconnectivity and lower drug loading, the drug eluting polyethylene with highly eccentric drug clusters had more sustainable drug elution (**Figure 2.7**) than the drug eluting polyethylene with spherical drug clusters. This feature is important because lower initial drug loading also increases the safety margin in adverse scenarios where such a device may structurally fail and incorporated drugs may be unintentionally released in a short period of time.

Highly eccentric pore morphology in drug-eluting UHMWPE.

Vancomycin-eluting UHMWPE displaying highly eccentric drug clusters was prepared using compression molding based on the benefits observed in LDPE. While drug loading at studied levels increased porosity linearly, percolation threshold was reached at a drug loading between 4 and 6 wt% (**Figure 2.9**). The drug elution increased sharply around 6 wt % (**Figure 2.9**), in agreement with porosity analysis. Compared to conventional drug eluting polymers with spherical drug clusters, the highly eccentric drug clusters in polyethylene reduced the drug percolation threshold from very high drug loading (40-60 wt%) [294, 295] to 6-8 wt% (**Figure 2.8**). The formation of highly eccentric drug cluster morphology was unaffected by the type of drugs being used, or at least the drugs that we tested (**Figure 2.16**).

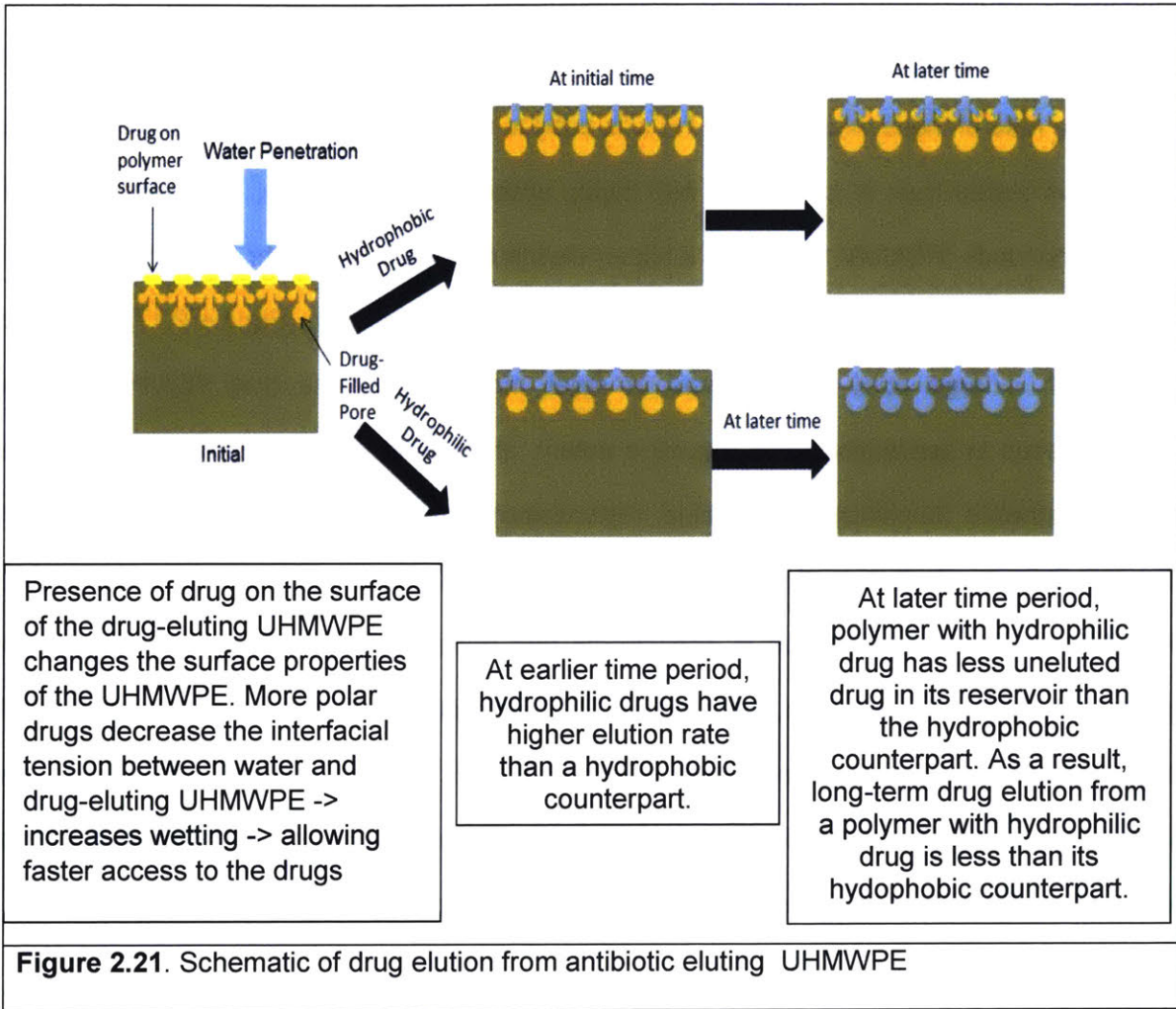
Among the temperatures (160°C-180°C) and pressure being tested (15-25 MPa), no significant difference in elution rate and total elution were observed. In addition, no significant effect of (1) vancomycin crystal size (1-145 μm) was observed on the elution rate or accumulated drug release (**Figure 2.11**). The absence of elution profile dependence with respect to temperature and pressure was presumably due to the absence of drug diffusion (which all exists in the solid form at all time during compression molding). Thus, the primary parameter affecting elution profile and accumulated drug release was initial drug loading.

Relation between drug type and elution rate from drug eluting UHMWPE.

Based on previous work on the effect of drug-polymer interaction on the elution rate from drug-loaded polymeric matrices[306], we hypothesized that the initial release concentration of the incorporated drugs and the overall elution behavior could be controlled by the properties of the drug. We tested nine different antimicrobials (ciprofloxacin HCl, tobramycin, tetracycline HCl, gentamicin, vancomycin HCl, rifampin, teicoplanin, ceftriaxone, and fusidic acid) that spanned different polar surface areas (PSA, (72-663 Å²)) and molecular volumes (MV,(282-1600 Å³)) [307]. The ratio of these values (PSA/MV) was used to normalize polarity by molecular size. Our hypothesis tested true; in UHMWPE with highly eccentric drug clusters, we found that more polar compounds (PSA/MV > 0.3) had a higher elution rate in the first 24 hr, but it dropped more rapidly over time compared to non-polar compounds (PSA/MV < 0.3) (**Figure 2.17**) Therefore, drugs with a large polar surface area or small molecular volume (low PSA/MV) can be advantageous in applications that require a potent, short-term release of medication, such as local anesthetics (bupivacaine, lidocaine, ropivacaine) and anti-fibrinolytics (tranexamic acid). On the other hand, drugs with a smaller polar surface area or larger molecular volume (high PSA/MV) can be advantageous in applications that require a less potent initial release, but sustained elution. For example, pertinent to PJI treatment, rifampin is an antimicrobial that is highly effective in the time-dependent eradication of *S. aureus* biofilm ([308]) but is also hepatotoxic at high concentrations. Therefore, sustained and lower concentration drug release can be beneficial for bacterial eradication while minimizing side effects.

The observed difference in elution rate associated with PSA/MV can be summarized as follows (**Figure 2.21**): Hydrophilic/polar drugs are more easily dissolved in polar media (e.g. water). As a result, these diffuse more quickly out of UHMWPE. However, a larger fraction of the loaded drugs diffuses out of the UHMWPE in the early time period, leaving a smaller fraction for further elution, and as a result the rate of drug elution is decreased. For hydrophobic drugs, which have a higher affinity for UHMWPE, a smaller fraction of the loaded drug diffuses out at

an early time, resulting in a smaller burst release. Since a larger fraction remains in the material, the elution of the drug is sustained for a longer period of time. Therefore, by manipulating the type of drug and initial loading concentration during the formation of the highly eccentric pore morphology with compression molding, release of the desired drugs can be controlled.



Conclusion

In this chapter, we showed that increasing the eccentricity of the drug clusters inside the polymer matrix resulted in a decreased percolation threshold. As a result, for the same drug loading, a higher drug cluster interconnectivity and more sustained elution can be achieved with

higher drug cluster eccentricity. By using solventless and compression molding that minimizes flow during polymer melt, we prevented drug clusters from achieving their most thermodynamically stable phase (spherical clusters) and provided the external force to deform the drug clusters further into highly eccentric shapes. In addition, the effects of drug chemistry and structure have been studied while maintaining the highly eccentric morphology, evaluating the possibility of using this morphology for other drug-polymer combinations to treat various diseases. Due to higher interconnectivity, the highly eccentric drug clusters in polyethylene enabled the reduction of the drug percolation threshold from very high drug loading (40-60 wt%) [295] to 6-8 wt % while maintaining a sustainable drug elution rate. Lower initial drug loading can result in a higher safety margin in adverse scenarios where incorporated drugs may be unintentionally released.

Chapter 3

Tensile and Impact Properties of Drug Eluting UHMWPE

Introduction

Contact Mechanics of Artificial Joint in Hip and Knee

In the hip joint, the acetabular liner made out of UHMWPE, coupled in articulation to the femoral head counterface, undergoes a combination of compressive and tensile stresses [309]: A central area of contact is under compression at all times, while a variable surrounding area is under a combination of compressive and tensile stresses during the articulation cycle [310]. When UHMWPE is used as an acetabular liner, the maximum contact stress was found to be 14-28 MPa with a maximum contact area of 350-400 mm² [309, 311]. The contact stress on the liner was in the equatorial and spherical regions, showing a double peak stress pattern with non-spherical contact area. In addition to compressive and tensile stresses, UHMWPE liners also undergo viscoelastic deformation, which results in creep and material flow away from the contact area [312, 313], eventually increasing the contact area and reducing the peak stress. The contact stress on the acetabular cup depends on the acetabular cup diameter, modulus of elasticity of the UHMWPE, and the thickness of the UHMWPE acetabular liner[311]. A larger acetabular cup diameter and lower modulus of elasticity will decrease the overall contact stress, while decreasing the thickness of the UHMWPE acetabular liner will result in higher contact stress[314]. The range of elastic moduli of the UHMWPE used clinically is from 676 MPa (highly crosslinked UHMWPE) to 873 MPa (conventional UHMWPE)[315]. Experimental measurement of the maximum contact stress using various UHMWPE liner thickness (3-5 mm), various

femoral head diameter-acetabular liner diameter pair (22/39, 28/45, 28/41, 38/51, 48/59 femoral head diameter/acetabular liner diameter), and various types of UHMWPE (conventional or highly crosslinked) showed that the highest maximum contact stress was observed at 28 MPa using conventional UHMWPE liner, a liner thickness of 3 mm, a femoral head diameter of 22 mm and an acetabular liner diameter of 39 mm [315]. The lowest maximum contact stress was observed at 14.1 MPa using highly crosslinked UHMWPE liner, a liner thickness of 5 mm, a femoral head diameter of 48 mm, and an acetabular liner diameter of 59 mm. The most commonly used femoral head-acetabular liner pair involves a 36 mm diameter femoral head and a 52-62 mm diameter acetabular liner[100]. In those cases, the maximum contact stress observed was 17-20 MPa[311].

Similar to the the hip joint, the tibial insert made of UHMWPE in the knee joint also suffers tensile stress in addition to compressive stress [316]. The maximum contact stresses suffered by the tibial insert were found to be 16-28 MPa [317, 318], with a contact area of 200-300 mm²[318] . Maximum contact stress changes throughout the knee flexion, with highest contact stress observed at 15^o and 60^o flexion, and lowest contact stress observed at 45^o flexion [316]. Finite element analysis showed that the maximum contact stress occurs in the lateral and medial condyles and in the mid-contact between the tibial insert and the femoral component [316]. Different from an acetabular liner, the articular area of the tibial insert undergoes cyclic stresses that vary between tension and compression because of shifting contact area during the walking cycle [319]. Because of these cyclic stresses and because of the shifting contact area, the tibial insert is prone to fatigue stress and delamination [320].

Theoretical Basis of Mechanical Properties of Polymers with Fillers

Fillers are usually added to polymer matrix to enhance the properties or the function of the resulting materials. Polymer fillers are usually of two types: particulate or fiber. Particulate fillers have dimensions that are approximately equal in all directions, while fiber fillers usually have length much greater than diameter[321]. Particulate filler morphology can be spherical, platelet-like, or any other regular and irregular geometry [321]. Fillers that are intended to improve the overall strength of the resulting material are usually harder, stronger, and stiffer than the polymer matrix itself [321]. Polymer matrix with fillers can be stronger than the polymer matrix itself provided the polymer has sufficient interaction with the filler to transmit the load from the matrix to the filler[321]. Fillers that are intended for purpose other than mechanical strength (e.g. for delivery of therapeutic agents) reduce the overall strength of the material proportional to the amount of the filler added [322].

In general, the stress of polymer matrix with filler can be expressed as[323]:

$$\sigma_{net} = \sigma_{matrix} + (\sigma_{filler} - \sigma_{matrix}) * \bar{W}_{filler} \frac{\rho_{matrix}}{\rho_{filler}} \quad (1)$$

where σ_{net} , σ_{matrix} , σ_{filler} represent stress on the polymer due to filler, matrix, and filler, respectively. \bar{W}_{filler} is the weight fraction of the filler. ρ_{filler} , ρ_{matrix} are density of the filler and matrix respectively. Assuming the filler and polymeric matrix exhibit linear elastic stress-strain until failure occurs, we can rewrite eq (1) as:

$$\sigma_{net} = E_{matrix}\varepsilon_{matrix} + (E_{filler}\varepsilon_{filler} - E_{matrix}\varepsilon_{matrix}) * \bar{W}_{filler} \frac{\rho_{matrix}}{\rho_{filler}} \quad (2)$$

Where E_{matrix} and E_{filler} are Young's modulus of the matrix and filler respectively. ε_{matrix} and ε_{filler} represent the strain of the matrix and filler, respectively. Assuming non-slip interaction between the filler and matrix (i.e. perfect interfacial bond between filler and matrix with no delamination), then the strain on the polymer with filler is equal to both the strain on the filler and

the strain on the matrix, i.e. $\varepsilon_{net} = \varepsilon_{matrix} = \varepsilon_{filler}$. Thus, we can write the modulus (E_{net}) and ultimate tensile strength (UTS_{net}) of the filled polymer as:

$$E_{net} = E_{matrix} + (E_{filler} - E_{matrix}) * \bar{W}_{filler} \frac{\rho_{matrix}}{\rho_{filler}} \quad (3)$$

$$UTS_{net} = E_{matrix} \varepsilon_{m/f} + (E_{filler} - E_{matrix}) * \varepsilon_{m/f} * \bar{W}_{filler} \frac{\rho_{matrix}}{\rho_{filler}} \quad (4)$$

where $\varepsilon_{m/f}$ is the elongation to break of the matrix or filler. In the case where the elongation to break of filler is greater than the elongation to break of matrix, then eq 4 will use the elongation to break of the filler, and vice versa.

Several fillers have been tried to improve the mechanical properties of UHMWPE, including carbon fiber[324], hydroxyapatite, graphene[325], and UHMWPE fibers[323]. When carbon fiber, which has higher tensile and flexural strength than UHMWPE, is added as filler to UHMWPE, the resulting material has superior tensile strength, flexural strength, and a greater Young's modulus than the unfilled UHMWPE [324]. Graphene, which also has higher tensile and impact strength than UHMWPE, also improved the overall tensile and impact strength of the material when added as filler to UHMWPE[325]. On the other hand, when filler with mechanical strength lower than UHMWPE is added to UHMWPE, the resulting material has inferior mechanical strength compared to unfilled UHMWPE: Hyaluronic acid or NaCl, both of which have weaker tensile strength than UHMWPE, weakened the overall tensile and impact strength of the filled UHMWPE relative to unfilled UHMWPE[326].

Mechanical Strength of Filled Polymer when Fillers are Weaker than the Polymer

In the case where fillers have lower mechanical strength than the polymer matrix, the area occupied by the fillers can be considered as defects [327]. The tensile strength of defect-filled materials depends on the most severe defects that act as initiation point for crack growth

leading to the final failure[328, 329]. Experimental studies showed that the ultimate strength of the material does not correlate with the average defect size but correlates well with the size of the most severe defects[327]. Severity of the defects depends on both the size and orientation of the defects: assuming ellipsoidal defects, larger and more oblate defects weakened the material more than other defect sizes and orientations[327]. Considering an ellipsoidal defect within an infinite polymeric matrix, the three-dimensional problem can be simplified into two-dimensional case by projecting the ellipsoidal defect into the plane that contains the largest cross-sectional area of the defect[327, 330]. The material with such defects will fracture if the stress intensity factor of the material equal or exceeds the fracture toughness of the material[327]. For an elliptical defect exposed to out-of-plane tensile stress, the stress intensity factor can be expressed as[330]:

$$K_I = \frac{\sigma_{\infty} (\pi b)^{0.5}}{E(k)} * \left(\frac{\sin^2 \theta + \frac{b^4}{a^4} \cos^2 \theta}{\sin^2 \theta + \frac{b^2}{a^2} \cos^2 \theta} \right) \quad (5)$$

Where σ_{∞} is the tensile stress applied during testing, where a, b, are the major axis of the ellipsoids, θ is the azimuthal angle of the elliptical defect, and where E(k) is elliptical integral of the defect, which can be written as:

$$E(k) = \int_0^{\pi/2} \left[1 - \left(\frac{a^2 - b^2}{a^2} \right) \sin^2 \varphi \right] d\varphi \quad (6)$$

Based on eq (6), the stress intensity factor (K_I) will increase as the eccentricity of the elliptical defect (b/a) also increases and when the absolute size of the elliptical defect (b) also increases [330].

Because the drug particles added into the UHMWPE are unlikely to have greater mechanical strength than the UHMWPE particles, we hypothesized that addition of drugs into UHMWPE will weaken the material relative to plain UHMWPE. If our hypothesis is correct, we expect that to maximize the strength of the drug eluting UHMWPE, we need to minimize the amount of defects, ensure defect size homogeneity (hence minimizing the probability of creating large critical defects), and adjust orientation of the defects (by making the defects more prolate instead of oblate).

Characterization of the mechanical strength of UHMWPE for Joint Implants

Because the UHMWPE components in the hip and knee are exposed to the significant stress *in vivo* as explained above, suitability of UHMWPE component as part of prosthetic joint will also be determined by its mechanical strength. Mechanical strength of UHMWPE is usually determined by tensile testing, fatigue testing, and impact testing [331].

While the testing of UHMWPE components in pure tension does not exactly replicate the condition *in vivo*, tensile properties of UHMWPE are closely related to and affected by its amorphous and crystalline structure; tensile test has been used as a screening test and therefore is required in evaluating UHMWPE proposed for use in total joint arthroplasty [309, 316]. Two parameters that are of main interest to us can be obtained from the tensile test: The ultimate tensile strength and the elongation to break. Ultimate tensile strength indicates the maximum stress withstood by the material before it completely breaks. For clinically used UHMWPE, the ranges of ultimate strength are 34 MPa (highly crosslinked UHMWPE) to 46.2 MPa (conventional UHMWPE)[332]. Ultimate elongation to break indicates the maximum elongation shown by the material before it completely breaks. For clinically used UHMWPE, the

ranges of elongation to break are 230 % (highly crosslinked UHMWPE) to 414 % (conventional UHMWPE)[332].

The cyclic nature of the loading and articulation in UHMWPE components in the artificial joints (particularly in the knee joint) cause alternating compressive and tensile stresses which can cause the initiation of fatigue cracks that may propagate through the material, causing fracture of the material or fatigue-induced wear [333, 334]. Fatigue testing is used to monitor the fatigue crack propagation by measuring a stress intensity factor range at crack conception and stress intensity factor range when crack growth rate exceeds 10^{-6} mm/cycle [335].

Unfortunately, this test requires a long duration (days even weeks) to test each sample, thus requiring weeks to months to get any statistically meaningful value[331]. Fortunately, previous studies showed that there is linear relation between fatigue crack propagation resistances (obtained from fatigue testing) to the fracture toughness obtained from impact testing[335], which is much faster and therefore suitable for the screening process in evaluating drug-eluting UHMWPE. Impact toughness can be used as surrogate for fatigue crack propagation because based on the stress intensity factor and fracture mechanics theory, a crack will propagate only when a local measure of the singular stress field reaches the fracture toughness of the material[336]. Based on the first law of thermodynamics and Griffith energy criterion, a crack can grow in a body if such a process results in decrease in total energy or remain constant [337], i.e crack will grow if the stress at the tip of the crack (σ) fulfills:

$$\sigma > \sqrt{\frac{G_{IC}E}{\pi*a}} \quad (7)$$

Where G_{IC} is the fracture toughness of the material, E is the elastic modulus, and a is the crack length. Therefore, when the material is exposed to the same stress, assuming the same initial crack length and same elastic modulus, materials with higher fracture toughness will be less

susceptible to crack propagation. For clinically used UHMWPE, the ranges of impact strength are 62 kJ/mm² (highly crosslinked UHMWPE) to 119 kJ/mm² (conventional UHMWPE)[332].

These clinically relevant values for ultimate tensile strength, elongation to break, and impact strength are the ranges that should ideally be satisfied by our drug eluting UHMWPE to minimize the probability of mechanical failure *in vivo*. Therefore, in this chapter, we will use these clinically relevant ranges to guide us in determining the minimum and maximum amount of drugs, irradiation dose, and other compression molding parameters to ensure that the drug-eluting UHMWPE stays within those ranges.

Methods

Tensile strength measurement. Type V samples (n=5 for each group) were stamped out of 3.2 mm thin sections of the materials prepared as described above according to ASTM-D638. These samples were tested in tension (Insight™, Eden Prairie, MN) with a crosshead speed of 10mm/min. The load was recorded at 100Hz and the gauge length was monitored for extension using a laser extensometer. The ultimate tensile strength (UTS), yield strength (YS), elongation at break (EAB), work to failure (WF), and Young's modulus (E) were calculated.

Fracture toughness measurement. Samples with dimensions of 63.5×12.7×6.35 mm³ (n=5) were double notched according to ASTM D256 and were impact fractured with a hammer (CEAST, Instron, Norwood, MA). The energy loss of the pendulum after impacting was recorded as the impact strength of the samples.

Finite Element Analysis Simulation. Finite element analysis was performed on commercial FEA software ABAQUS. Tensile FEA was performed on Type V dogbone sample with hexahedral meshes. During a tensile test, one lower end of the dogbone is constrained to no movement, and tensile load is applied in the direction parallel to the long dimension of the tensile sample on the upper grip of the sample at a strain rate of 10 mm/min. Elasto-plastic analysis was used for the tensile testing. The following parameters were used for the FEA simulation of UHMWPE in the elastic region: ν_{UHMWPE} (Poisson ratio of UHMWPE) = 0.46[338], Young's modulus = 2020 MPa[338], yield strength = 22 MPa[339], density=0.945 g/cm³[338], young's modulus = 830 MPa[338]. For the plastic range, the experimental curve of yield stress and the plastic strain of normal consolidated UHMWPE was manually entered into the material properties. ABAQUS used the elastic material properties until yield stress was achieved, at which point the plastic properties were used. Mesh density analysis was performed to ensure that the result of the tensile test was minimally perturbed by the mesh density. The optimum element size for the tensile sample was determined to be 0.15 mm for the grips and 0.05 mm for the gauge.

The tensile test resulted in a nominal stress-strain curve, which allowed us to obtain ultimate tensile strength and elongation to break. The volumetric change during the plastic deformation was assumed to be negligible, and the relations between true stress (σ_t) and true strain (ϵ_t) and the nominal stress σ_n and nominal strain ϵ_n are as follows[340]:

$$\sigma_t = \sigma_n (1 + \epsilon_n) \quad (5)$$

$$\epsilon_t = \ln(1 + \epsilon_n) \quad (6)$$

Scanning Electron Microscopy. All LDPE, UHMWPE, and PMMA bone cement were sputter coated with a thin layer of gold/palladium and imaged on a Zeiss Supra55VP microscope. Both Everhart-Thronley and Inlens detectors were used to acquire the image.

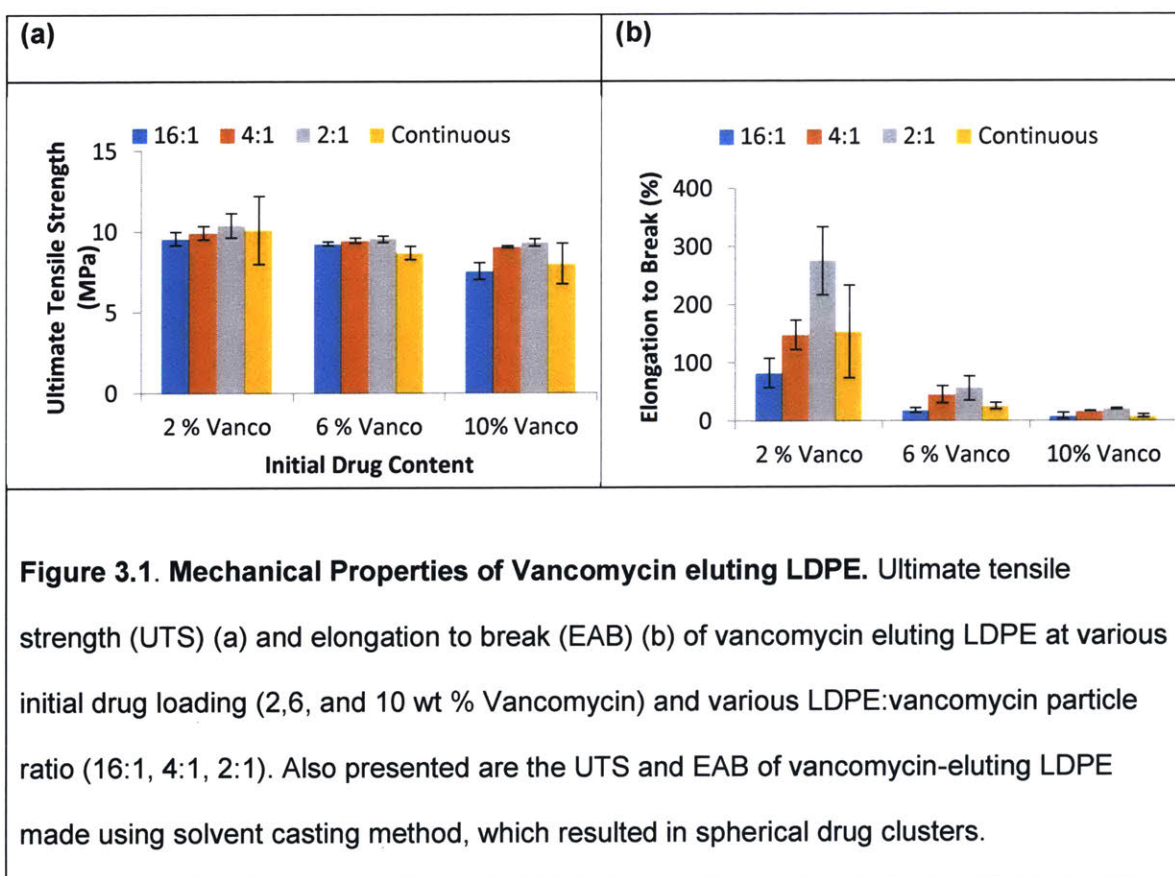
Statistical analysis. All statistical tests were performed by Student's two-tailed t-test for comparison of two groups and analysis of variance (ANOVA) for comparisons of multiple groups implemented through software package GraphPad Prism version 4.0. All error bars used in this report are mean \pm s.d. of at least three independent experiments except the lapine study (single experiment). Survival analyses were performed by using a log-rank test, using a statistical software package GraphPad Prism version 4.0. All data are mean \pm s.d., combined from three independent experiments.

Results

The Effect of Drug Cluster Eccentricity on Mechanical Properties of Low Density Polyethylene (LDPE)

Ultimate tensile strength (UTS) and elongation to break (EAB) were measured for all vancomycin eluting LDPE with various drug loading and LDPE granules/drug particle size ratio as mentioned above. The EAB significantly decreased as initial drug loading was increased regardless of the LDPE granules/drug particle size ratio (**Figure 3.1b**). The UTS significantly decreased between 2 % and 10 % vancomycin loading, but did not reach statistically significant levels when comparing 2 % vs 6 % and 6 % vs 10 % vancomycin loading. At the same initial drug loading, the UTS of samples with highly eccentric pore morphology was higher than samples with spherical drug clusters (designated 'continuous' on the figure legends); statistically significant differences were observed for samples with 6 wt % and 10 wt % initial vancomycin

loading and LDPE granules/drug particle size ratios 4:1 and 16:1 (**Figure 3.1a**). Similarly, for the same initial drug loading, the EAB of samples with highly eccentric pore morphology was higher than samples with spherical drug clusters (**Figure 3.1b**). For the same initial drug loading, LDPE samples with highly eccentric pore morphology with LDPE granules/drug particle size ratio of 4:1 and 16:1 had significantly higher EAB than that of their counterparts with spherical pore morphology.

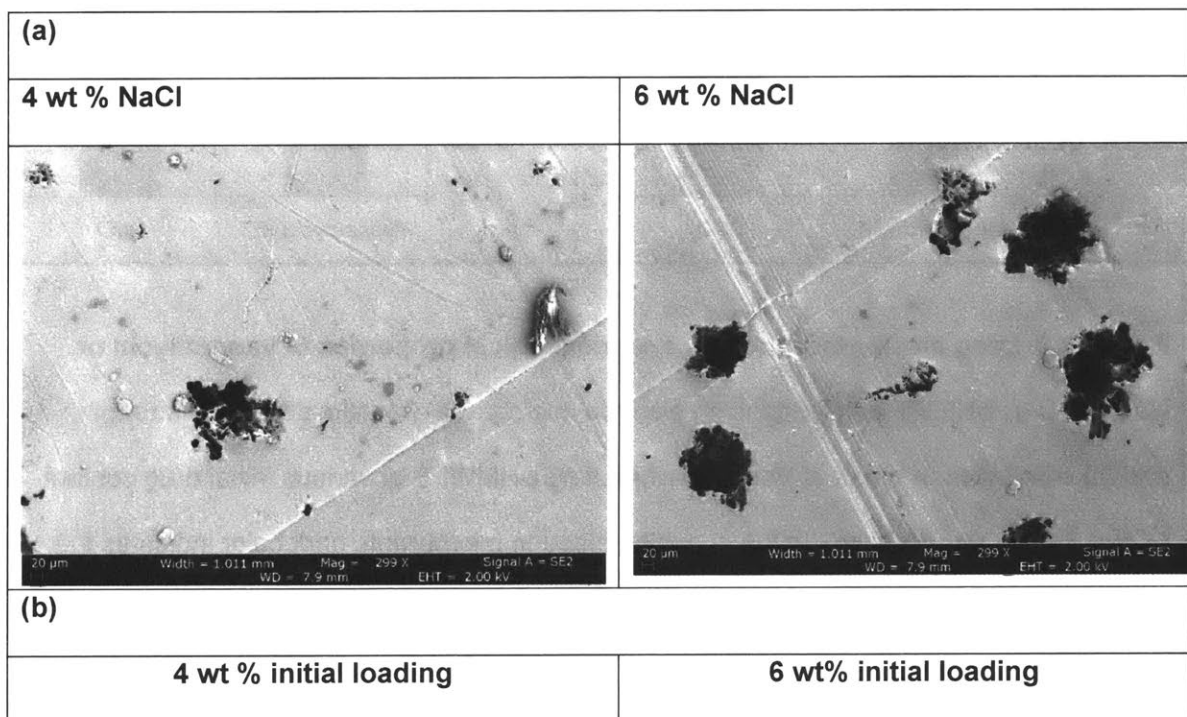


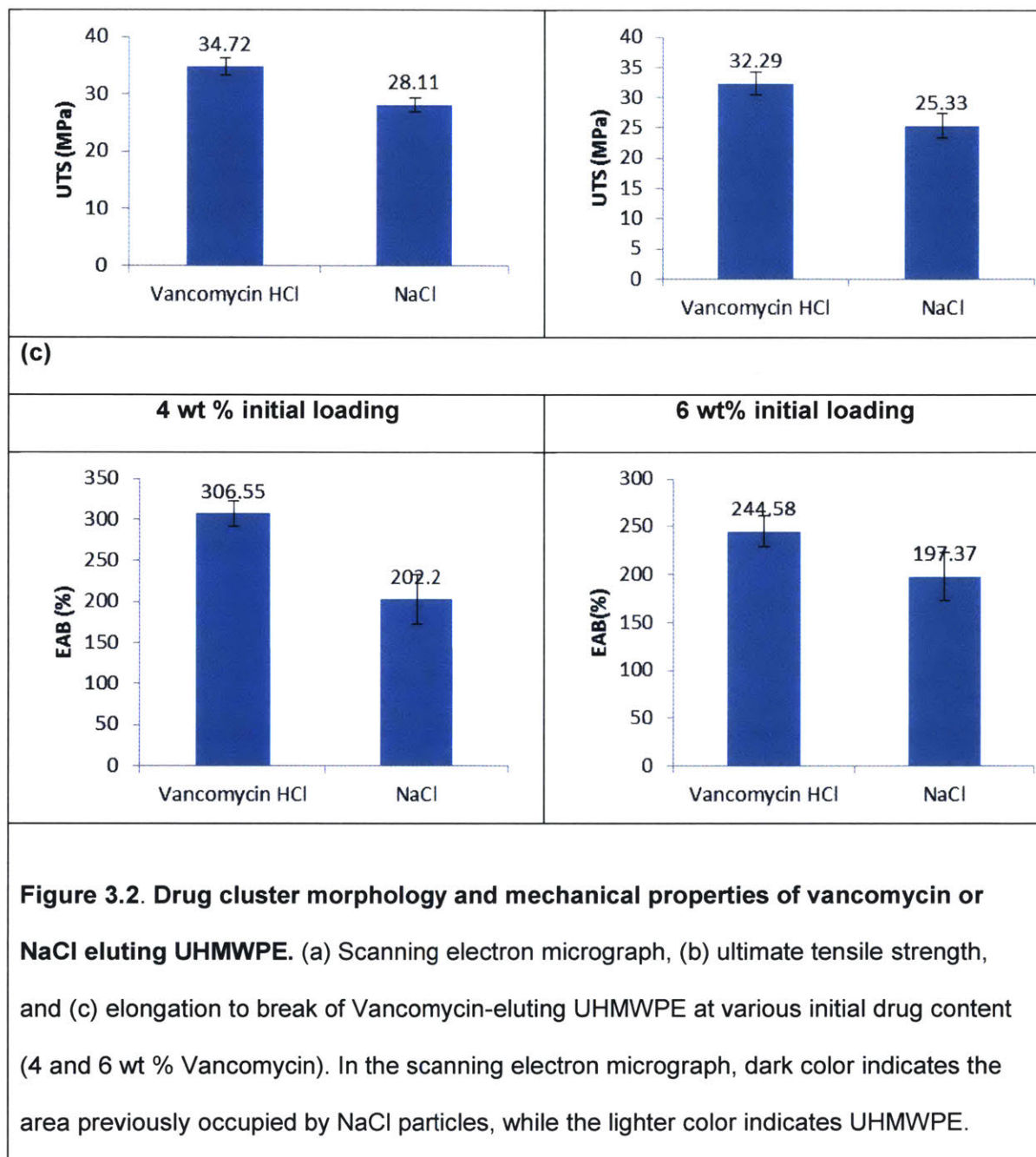
The Effect of Pore Eccentricity on the Mechanical Properties of UHMWPE

To see the effect of drug cluster eccentricity on the mechanical properties of UHMWPE, we incorporated NaCl into UHMWPE to create UHMWPE with spherical pores (**Figure 3.2**), and

compare it against vancomycin-eluting UHMWPE with highly eccentric pores. We compared the effect of low and high eccentricity pores at 4 wt% and 6 wt % initial drug loading.

Unlike the vancomycin-eluting UHMWPE loaded with 6 wt% vancomycin (**Figure 2.7**), the drug clusters of the UHMWPE loaded with 6 wt% NaCl did not show percolation, i.e. each cluster was fully encapsulated within the UHMWPE matrix (**Figure 3.2**). In addition to displaying a morphology inconsistent with percolation, the UHMWPE loaded with NaCl had lower UTS and EAB compared to that of vancomycin-loaded UHMWPE at both 4 wt % and 6 wt % initial drug loading. These results were in agreement with the effect of pore eccentricity on the mechanical properties of drug-loaded LDPE: Loading with highly eccentric drug clusters resulted in higher UTS and EAB than that of the polymeric matrix with spherical (low eccentricity) clusters.

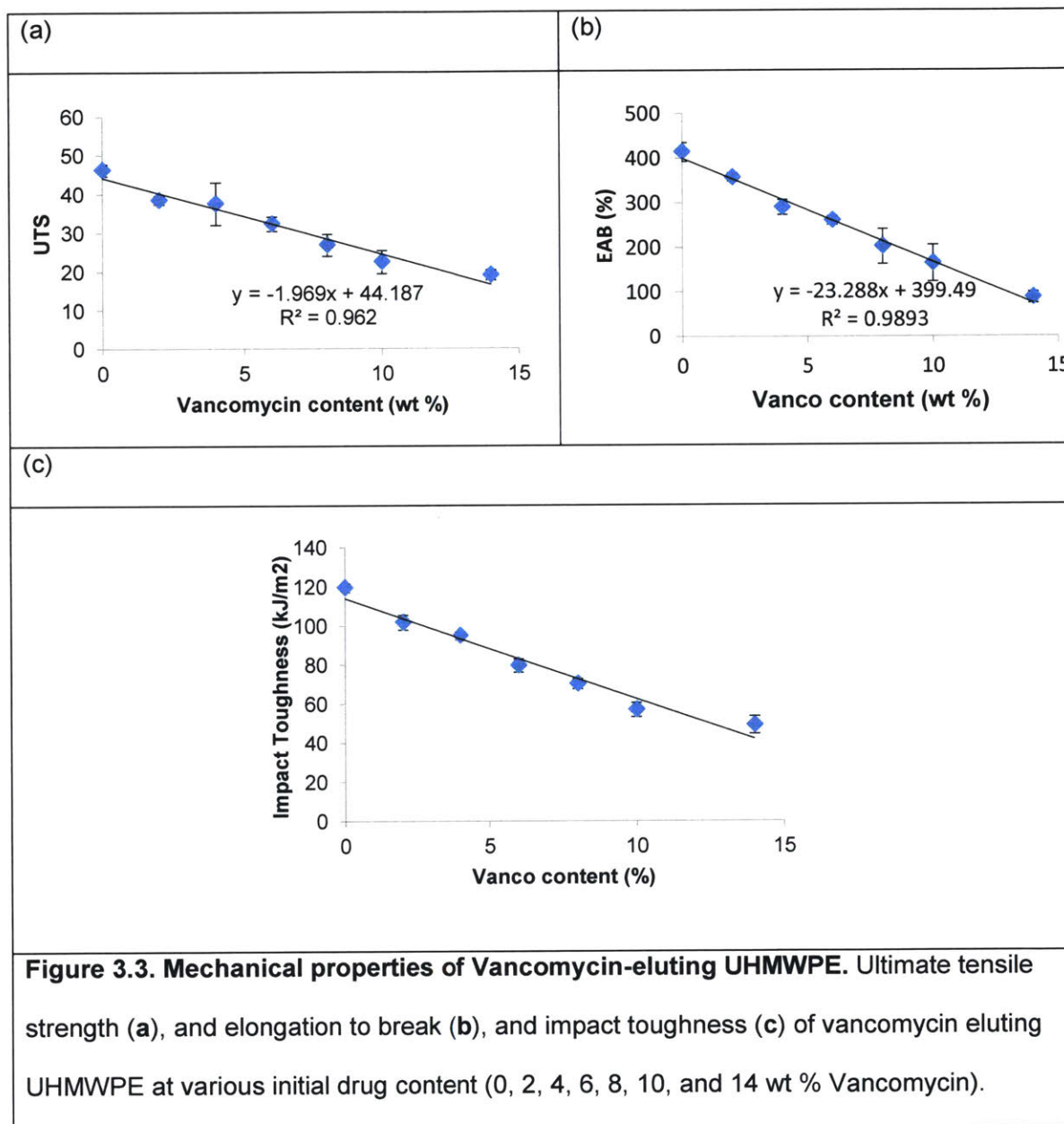




Mechanical Properties of Vancomycin Eluting UHMWPE under Various Initial Drug Loading

The effect of initial drug loading on the mechanical properties of vancomycin-eluting UHMWPE (UTS, EAB, and impact strength) were tested. The UTS, EAB, and impact strength of

vancomycin-eluting UHMWPE decreased linearly with an increase in initial drug loading (**Figure 3.3**). No discontinuity was observed in mechanical properties observed between 6 and 8 wt % initial drug loading (**Figure 2.9**).



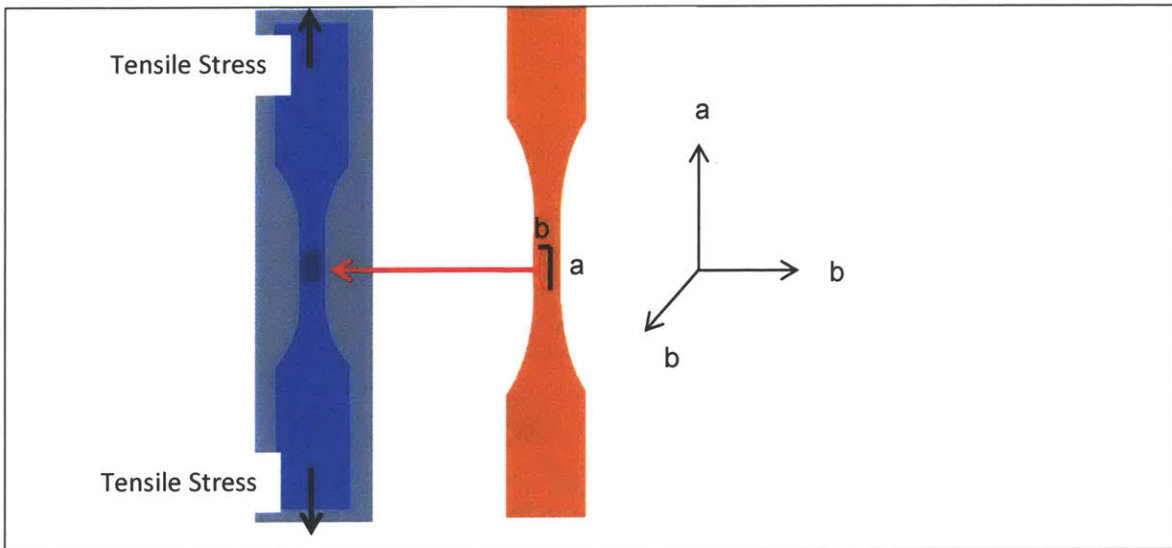
Computational Simulation of the Effect of Drug Cluster Eccentricity on Mechanical Strength

Computational simulation based on finite element analysis was conducted to examine the effect of pore shape formed by drug clusters on the ultimate tensile strength and elongation to break (**Figure 3.4**). Effect of pore eccentricity on the mechanical strength was performed by inserting a single, constant volume defect of different eccentricity in the middle of a tensile dogbone gage. The effect of multiple drug clusters was studied by inserting two same volume defects of different eccentricity in the middle of tensile dogbone gage (**Table 3.1**). For both single and multiple drug clusters, ultimate tensile strength and elongation to break was reported as the percent decrease from samples without any defect. For the single defect, the percent decrease in UTS and EAB was plotted against the eccentricity of the defect, while for the double defect, they were plotted against average eccentricity.

The effect of eccentricity on the mechanical strength (UTS and EAB) was dependent on the orientation of the eccentricity with respect to the loading direction. When the eccentricity increased in the direction parallel to the long axis of the sample (i.e. $a/b > 1$), both the UTS and EAB were increased (**Figure 3.4a-b**). However, when the eccentricity is increased in the direction perpendicular to the long axis of the sample (i.e. $a/b < 1$), both the UTS and EAB were decreased.

With double defects, a similar trend is observed as with the single defect: when average eccentricity is increased in the direction parallel to the long axis of the sample (i.e., $a/b > 1$), both ultimate tensile strength and elongation to break are increased (**Figure 3.4c-d**). However, when the average eccentricity is increased in the direction perpendicular to the long axis of the sample (i.e. $a/b < 1$), both the ultimate tensile strength and elongation to break are decreased.

(a)



(b)

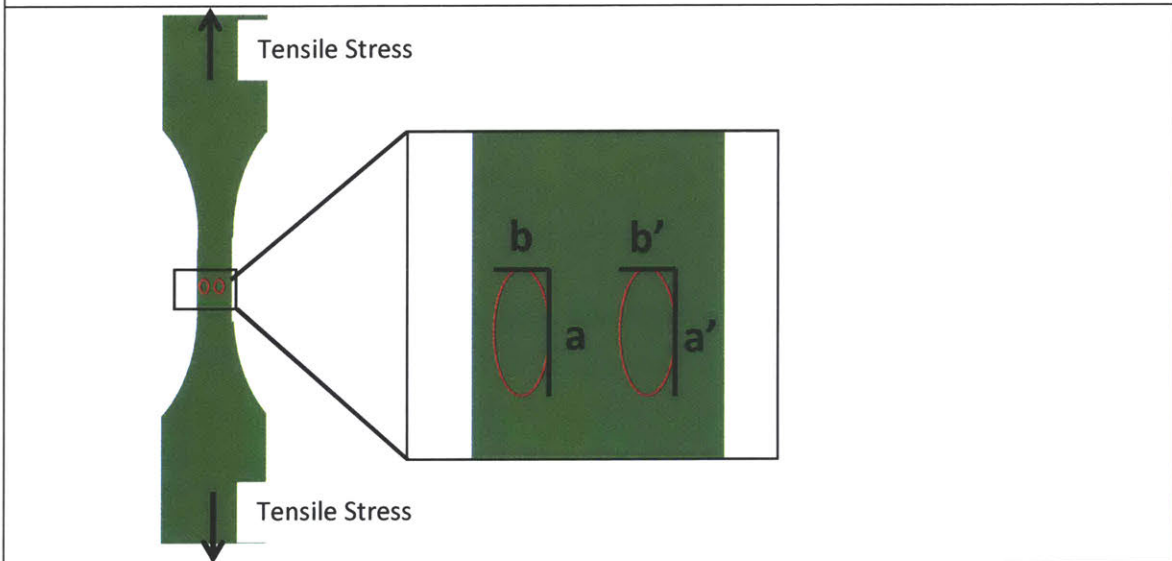
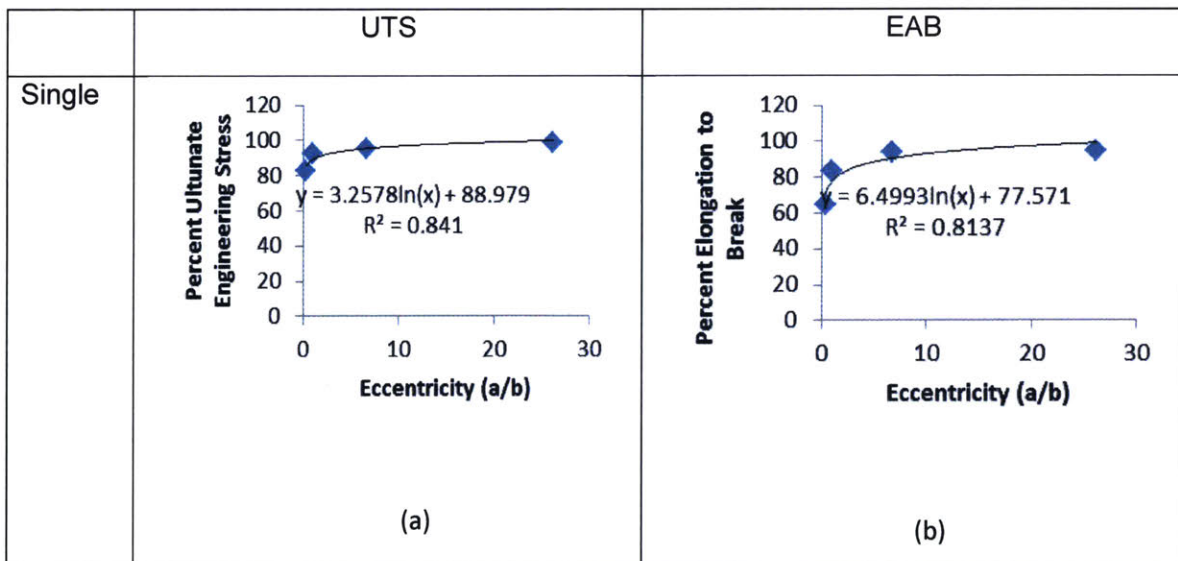


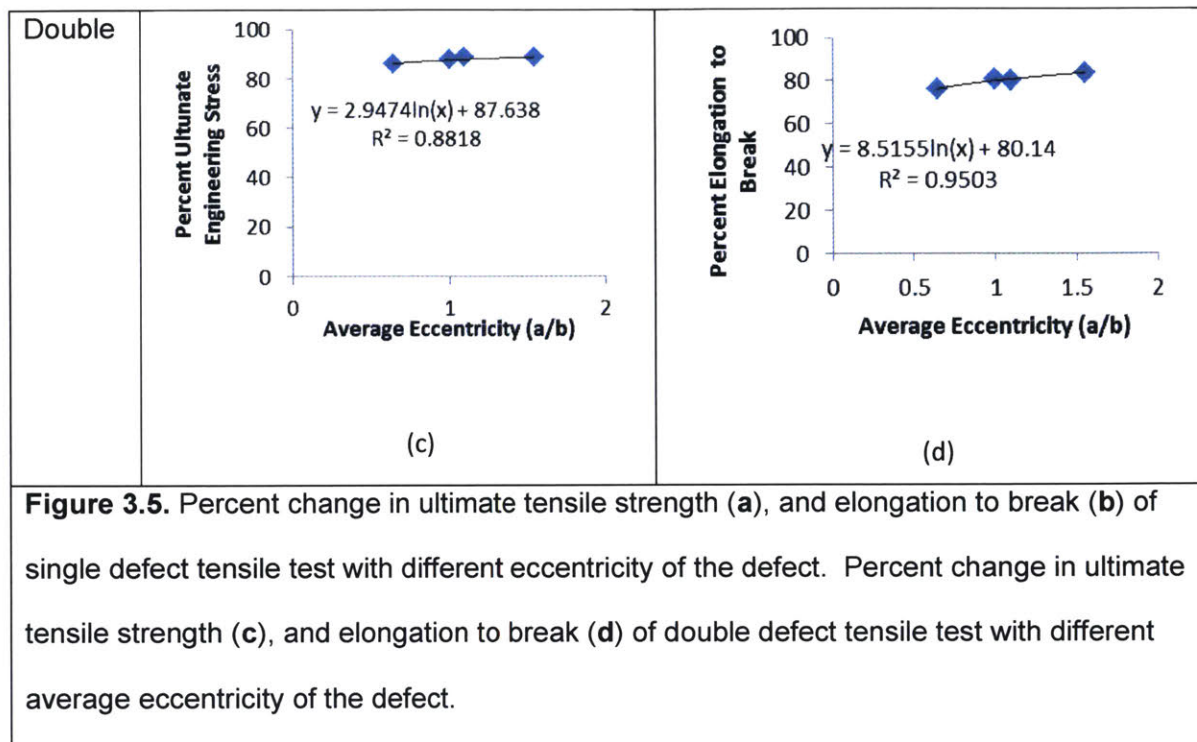
Figure 3.4. Schematic of the finite element analysis on tensile dogbone samples with (a) single defect and (b) double defect. Note that the defect tested in these simulations have the same diameter on the x and y directions (both denoted as b). The arrow indicates direction of the tensile stress.

a/b	a'/b'	Average Ecc
1	1	1

0.64	0.64	0.64
1.55	0.64	1.10
1.55	1.55	1.55

Table 3.1. Defect eccentricity and average eccentricity tested for simulation with double defect.





Effect of Manufacturing Parameters (Compression Molding Temperature, Compression Molding Pressure, and Vancomycin Particle Size) on the Mechanical Properties of Vancomycin-Eluting UHMWPE

Statistically significant decreases in UTS, EAB, and impact strength (IS) were observed between those samples compression-molded at 160°C and those compression-molded between 165 and 180°C. No difference in these mechanical properties was observed between samples molded at 165°C, 170°C, and 180°C (**Figure 3.6a-c**). Statistically significant decreases in UTS, EAB, and IS were observed for samples manufactured at 15 MPa to 18-20.5 MPa and for samples manufactured at 25 MPa to 18-20.5 MPa at 170°C . No statistical significant difference was observed between samples manufactured at 18, 19, and 20.5 MPa (**Figure 3.6d-f**). Despite no difference in mechanical properties between different mean vancomycin particle sizes, failure to control the particle size of the vancomycin at all (i.e. using the vancomycin

powder straight as manufactured) gave significantly lower mechanical strength than samples with controlled particle size (Figure 3.7).

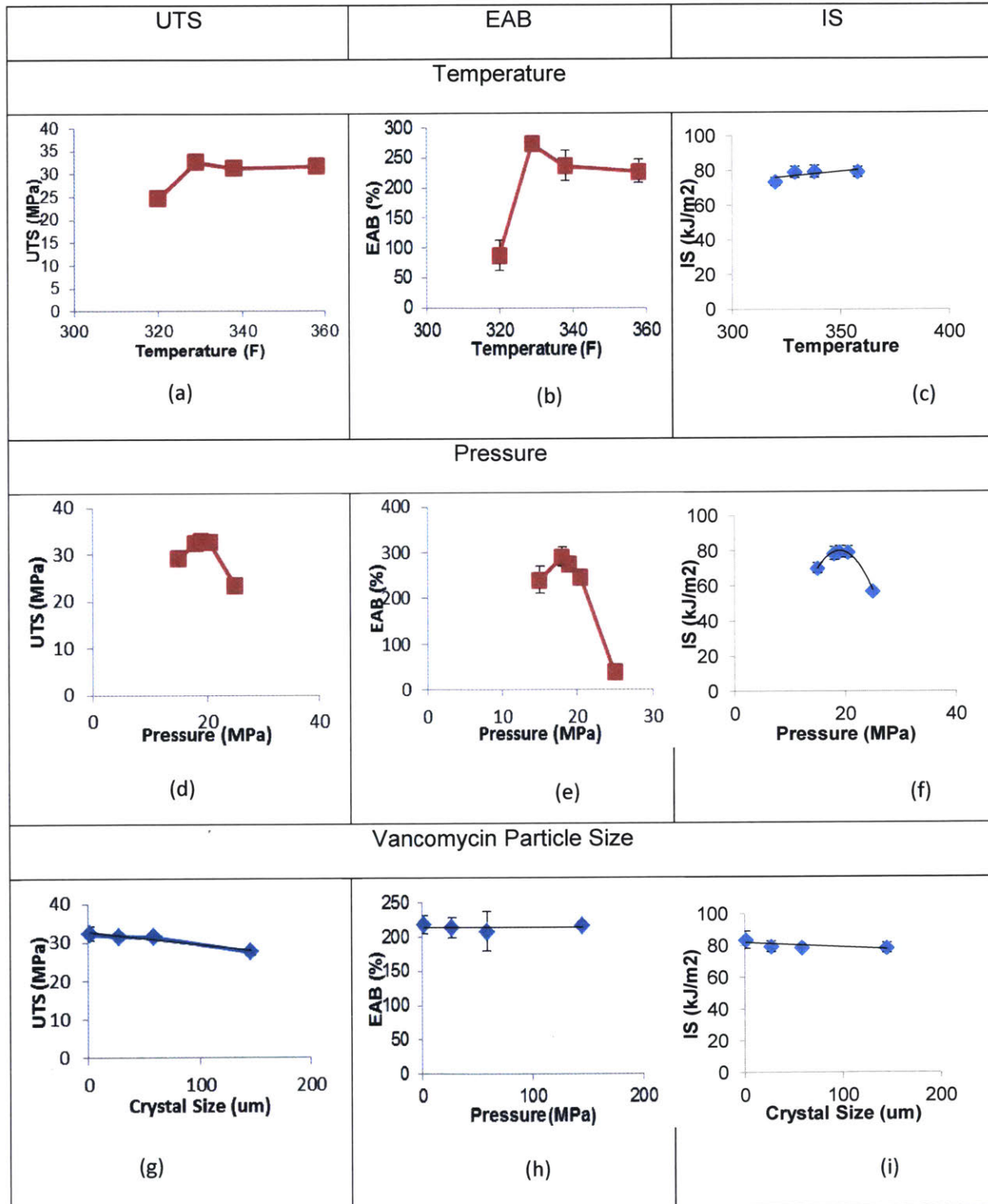


Figure 3.6. Effect of compression molding temperature, comp[ression molding pressure, and vancomycin particle size on UTS, EAB, and IS.

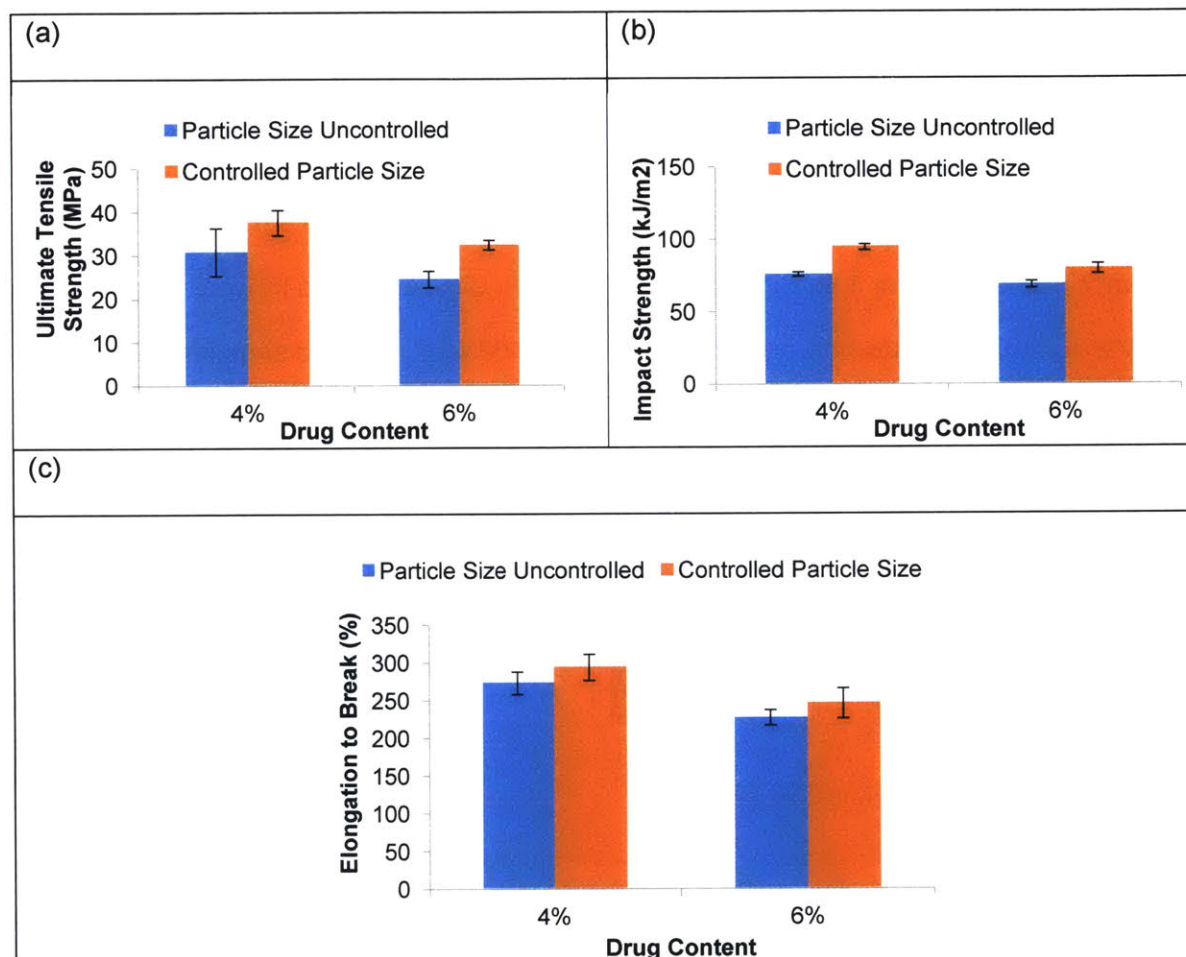
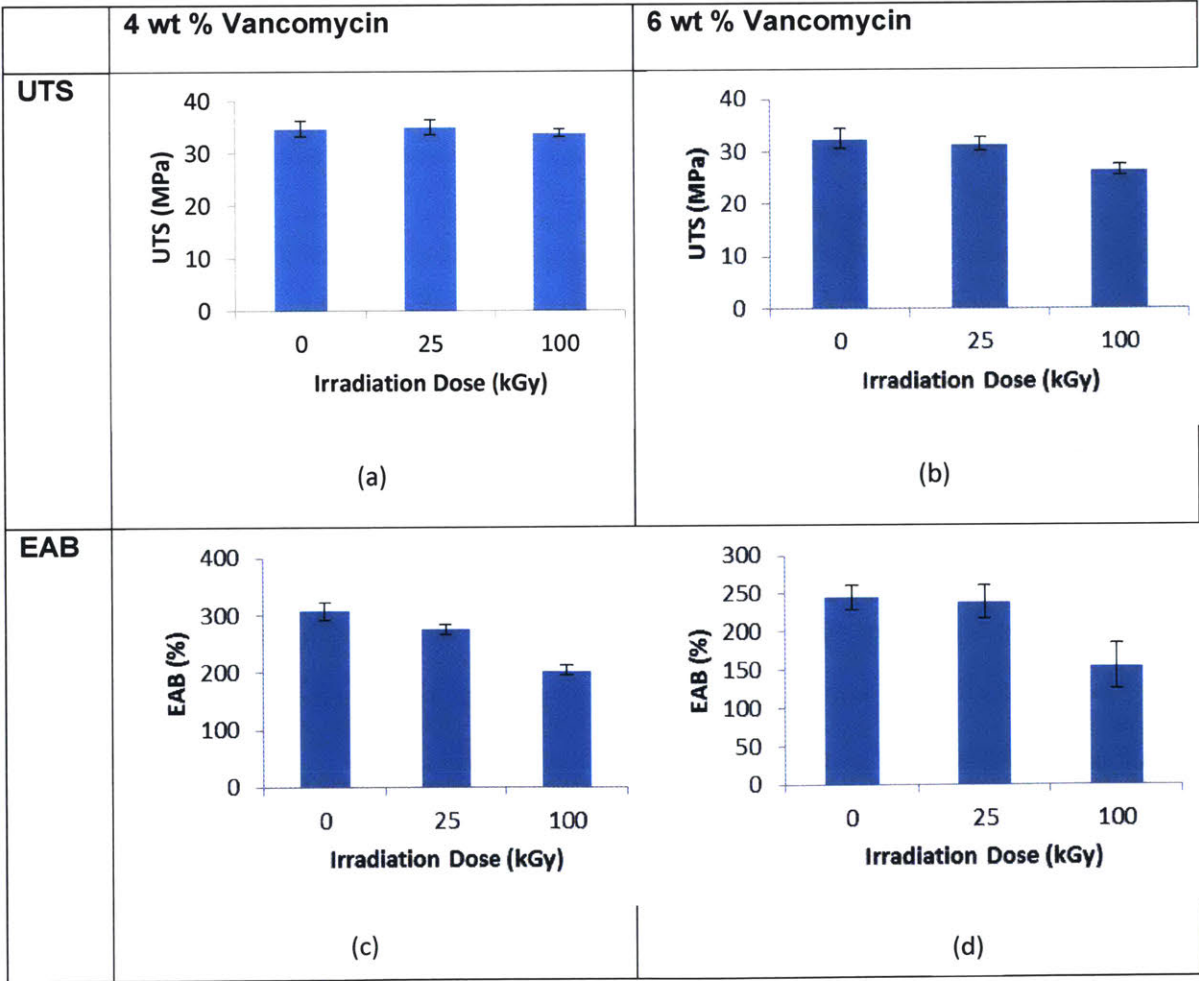


Figure 3.7. Mechanical properties of Vancomycin-eluting UHMWPE with and without drug particle size controls. Comparison of ultimate tensile strength (a), impact strength (b), and elongation to break (c) between particle size-controlled and uncontrolled vancomycin-UHMWPE at 4 wt % and 6 wt % initial drug loading.

Effect of Gamma Irradiation Dose on Mechanical Strength of Vancomycin Eluting UHMWPE

Because most of the UHMWPE implants used today are irradiated either at 25 kGy for sterilization or at 75-125 kGy for highly crosslinked UHMWPE [36], the effect of irradiation dose on the mechanical strength of Vancomycin-eluting UHMWPE were tested. UTS, EAB, and IS of Vancomycin-eluting UHMWPE at 0, 25, and 100 kGy were measured for 4 and 6 wt% vancomycin-loaded UHMWPE.

No statistically significant difference in UTS, EAB, or IS were observed between unirradiated (0 kGy) and 25 kGy-irradiated UHMWPE for both 4 wt % and 6 wt % initial vancomycin loads (**Figure 3.8**). Significant reductions in UTS, EAB, and IS were observed in 6 wt % Vancomycin samples between unirradiated and 100 kGy irradiated samples (**Figure 3.8**).



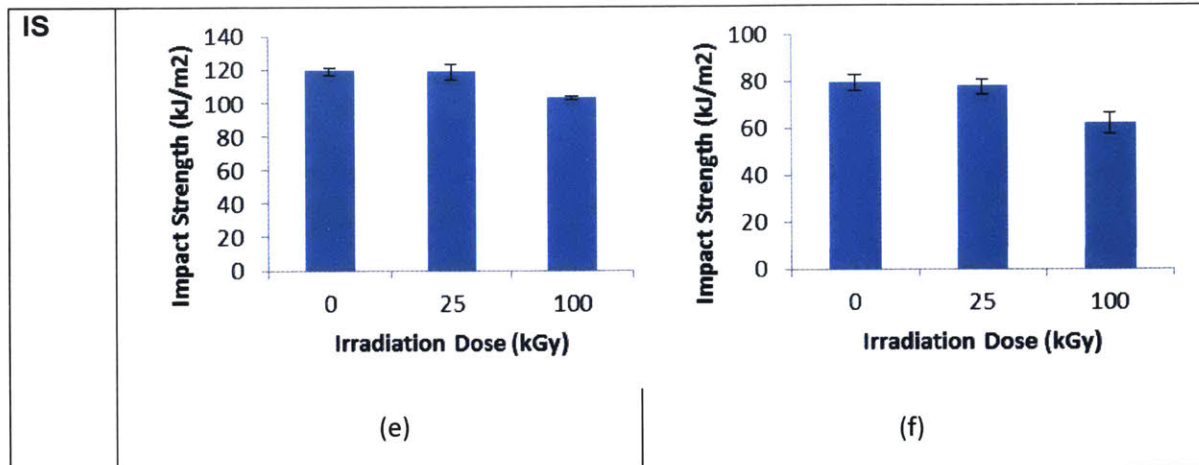
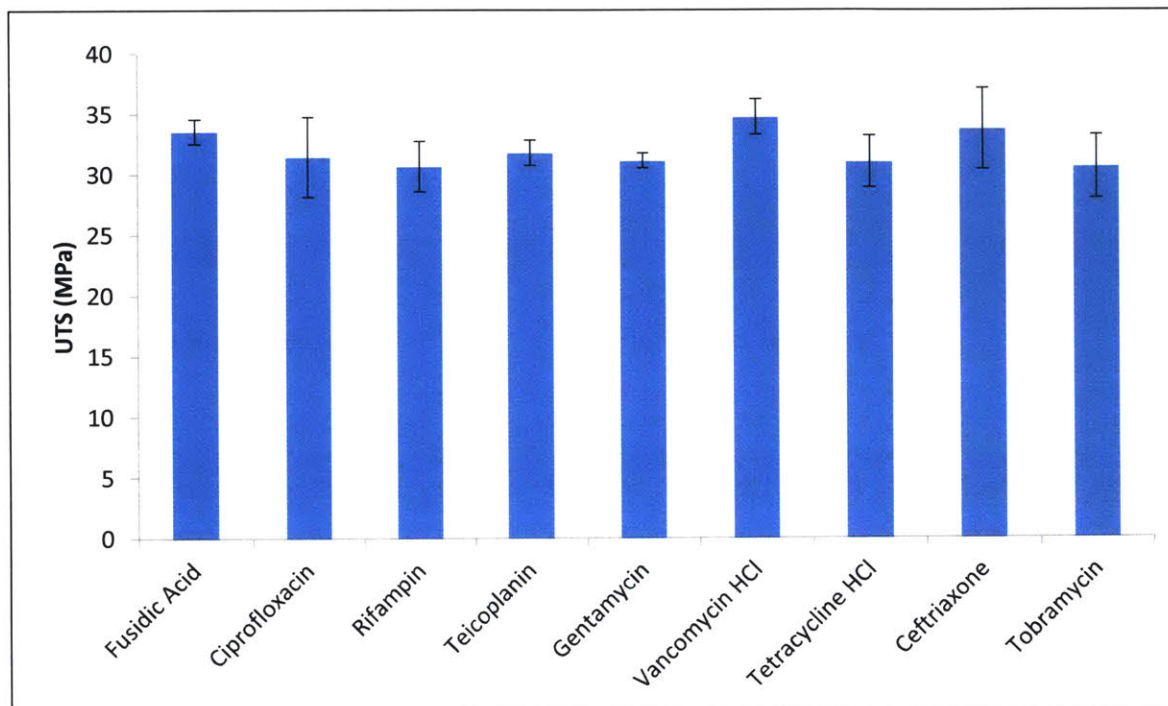


Figure 3.8. Mechanical properties of irradiated vancomycin eluting UHMWPE. Ultimate tensile strength (a-b), impact strength (c-d), and elongation to break (e-f) of vancomycin-UHMWPE irradiated at different irradiation dose (0, 25, and 100 kGy) with 4 wt % and 6 wt % initial vancomycin loading.

Effect of Drug Hydrophilicity/Hydrophobicity on Mechanical Strength of Drug Eluting UHMWPE

To test the effect of drug type on the mechanical strength of drug eluting UHMWPE, we measured both the UTS and EAB of the eight drug-eluting UHMWPE described in chapter 2 (rifampin-UHMWPE, gentamicin sulfate-UHMWPE, tetracycline HCl-UHMWPE, fusidic acid-UHMWPE, teicoplanin-UHMWPE, ceftriaxone-UHMWPE, ciprofloxacin HCl-UHMWPE, and tobramycin-UHMWPE) at an initial drug loading of 4 wt% (**Figure 3.9a-b**). No significant difference in UTS and EAB was observed between all eight drug-eluting UHMWPE mentioned above.

(a)



(b)

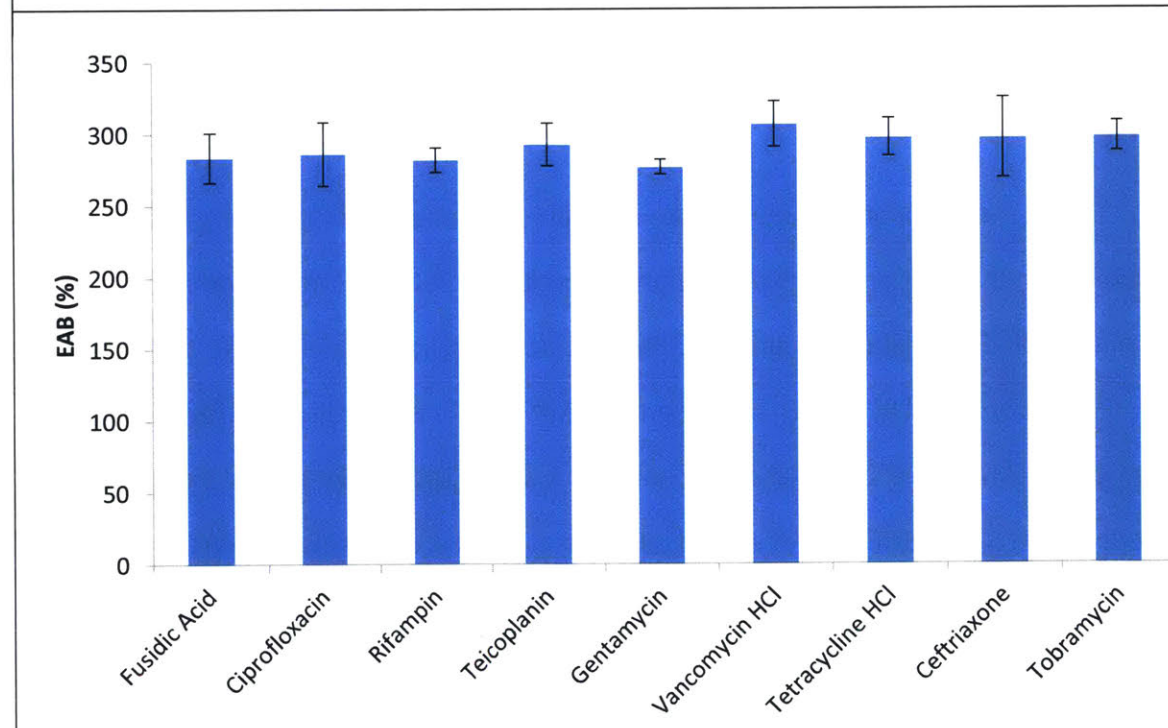


Figure 3.9. Mechanical strength of other drug eluting UHMWPE. Ultimate tensile strength (a) and elongation to break (b) of of rifampin-UHMWPE, gentamicin sulfate-

UHMWPE, tetracycline HCl-UHMWPE, fusidic acid-UHMWPE, teicoplanin-UHMWPE, ceftriaxone-UHMWPE, ciprofloxacin HCl-UHMWPE, and tobramycin-UHMWPE at 4 wt % initial drug content

Discussion

Effect of Drug Amounts and Drug Cluster Eccentricity on Mechanical Strength of Drug Eluting Polyethylene

Previous literature on the mechanical strength of polymers with defects showed that the ultimate strength of the material depends on the largest critical defect within the material [327, 341]. The largest critical defect has the highest tendency to form a defect-initiated crack growth that propagates to cause failure [328, 342]. We performed FEA modelling of drug-filled UHMWPE by assuming the mechanical strength of the drug to be negligible compared to the mechanical strength of the UHMWPE, i.e. from eq (4):

$$UTS_{net} = E_{UHMWPE} \varepsilon_{UHMWPE} - (E_{UHMWPE}) * \varepsilon_{UHMWPE} * \bar{W}_{drug} \frac{\rho_{UHMWPE}}{\rho_{drug}}$$

where the elongation to break is the true elongation to break of the UHMWPE (i.e., the true strain). The assumption that the strength of the drug is negligible compared to UHMWPE was justified because compression of the drug particles only at the compression molding temperature and pressure showed compaction but no structural integrity. Therefore, for the FEA simulation, the drug clusters were simulated as defects inside the UHMWPE matrix (**Figure 3.4**).

Our FEA simulation of UHMWPE with hollow defects showed that the mechanical strength was affected by the eccentricity of the defect, where higher eccentricity resulted (a/b) in higher UTS and EAB (**Figure 3.5**). In this FEA simulation, higher eccentricity (>1) meant that the long axis of the ellipsoid defect was parallel to the direction of tensile loading, while low eccentricity (<1) meant that the long axis of the ellipsoid defect was perpendicular to the

direction of tensile loading. As mentioned in the introduction, based on the stress intensity factor theory, the three dimensional ellipsoidal defect can be simplified into two dimensional problem by projecting the ellipsoids to a two-dimensional plane that contains the largest cross section area of the defect[330, 341]. Larger areas of defect on that two-dimensional plane resulted in larger stress intensity factors, and as a result, weaker ultimate strength [330, 341]. In the case of high eccentricity clusters (large a/b), the projected area of the defect into the 2D plane resulted in a much smaller area than in the case of low eccentricity clusters (small a/b). Therefore, our FEA simulation is consistent with the result obtained from fracture mechanics and stress intensity factor theory. However, it is important to note that the dependency of the ultimate tensile strength and elongation to break on the eccentricity of the defects is much weaker (**Figure 3.5**) compared to their dependency on the initial drug content. Therefore, the most meaningful way to preserve the mechanical strength of the drug filled UHMWPE is to minimize the total drug content.

To test the effect of drug loading and drug cluster eccentricity on the mechanical strength of drug eluting polyethylene, we used low-density polyethylene (LDPE) as a model polymer and vancomycin as a model drug. We chose LDPE instead of UHMWPE for the drug cluster shape experiment because LDPE, but not UHMWPE, can be dissolved in xylene to allow manufacture of solvent casted Vancomycin-eluting LDPE. Furthermore, LDPE is hydrophobic while the mobile phase for elution, phosphate buffered saline, is hydrophilic, therefore minimizing the penetration of the mobile phase through the polymer. We vary the initial vancomycin load in the polymer (2 wt %, 6 wt %, and 10 wt %) and LDPE : vancomycin particle size ratio (6:1, 16:1, and 40:1) and compare it to solvent-casted Vancomycin-eluting LDPE (**Figure 2.5**). SEM micrographs showed highly eccentric drug clusters at all vancomycin initial loading and LDPE : vancomycin particle size ratios (**Figure 2.5**). The solvent-casted Vancomycin-eluting LDPE showed more spherical drug clusters and the presence of large drug

aggregates (**Figure 2.5**). No apparent preferential directionality in the drug clusters eccentricity could be observed in the highly eccentric drug clusters in LDPE. From our FEA simulation, the absence of eccentricity anisotropy would mean that there should not be any significant difference in the mechanical strength between the spherical and highly eccentric drug clusters. However, we observed statistically significant higher ultimate tensile strength in the 2:1 LDPE:Vanco sample than the solvent-casted Vancomycin-eluting LDPE (**Figure 3.1**) at 6 % vancomycin and 10 % vancomycin content. This indicates that the advantage in the ultimate tensile strength is most likely due to the smaller critical size defect in the highly eccentric samples and not necessarily due to the eccentric shape of the drug clusters.

The UTS and EAB of vancomycin-loaded LDPE were inversely related to the LDPE:vancomycin particle size (**Figure 3.1**). When the LDPE:vancomycin ratio was between 4:1 and 16:1, both the UTS and EAB were higher than those of the solvent-cast LDPE with spherical pore morphology. Taking into account both the mechanical properties and the previously shown drug elution behavior, suggests an optimal polymer: drug ratio of 4:1 to 16:1.

Looking at the elution of the vancomycin-loaded LDPE (**Figure 2.7**), the elution from highly eccentric clusters of Vancomycin-LDPE was significantly higher than spherical cluster vancomycin LDPE regardless of the polymer:drug ratio. In combination with the higher ultimate tensile strength and elongation to break with the highly eccentric Vancomycin-LDPE in comparison to the spherical cluster counterpart, we have achieved improvement in both mechanical strength and drug elution by simply changing the eccentricity of drug clusters.

Increasing the initial drug loading in UHMWPE decreased the mechanical strength similar to LDPE (**Figure 3.3**). Furthermore, obtaining highly eccentric drug clusters resulted in higher UTS and EAB than that using low eccentric drug clusters (**Figure 3.2**). Therefore, for maximizing mechanical strength, initial drug loading should be minimized, while the eccentricity of the drug clusters should be maximized.

Effect of Drug Type and Compression Molding Parameters on Mechanical Strength of UHMWPE

Whereas compression molding temperature and pressure did not affect the elution rate and total elution of Vancomycin-eluting UHMWPE (**Figure 2.11**), significant differences in mechanical strength were observed when compression molding temperature was under 329 F (165°C), when pressure was below 18 MPa, or when pressure was above 20.5 MPa. The lower mechanical strength when compression was performed below 165°C was presumably because of incomplete fusion of UHMWPE powder and limited chain reptation, which requires higher temperature to allow for sufficient disentanglement and chain transition[343, 344]. The insignificant difference in mechanical strength when $T > 165^{\circ}\text{C}$ was also previously observed in compression molding of pure UHMWPE[344].

The increased mechanical strength between 15 and 18 MPa, is likely due to better consolidation of the polymer powder and higher crystallinity [345]. Above 20.5 MPa, mechanical strength was decreased presumably because the increased pressure hindered polymer chain movement that is crucial for consolidation of the polymer powder and reduction in the rate of crystallization [345]. Therefore, highest mechanical strength was achieved with compression molding temperature $> 165^{\circ}\text{C}$ and when compression molding pressure between 18 and 20.5 MPa.

Interestingly, the drug particle size and the polarity of drugs did not cause any change in the mechanical strength of drug-eluting UHMWPE (**Figure 3.4g-i** and **3.6a-b**). The lack of a strong correlation between the polarity of the drugs and the mechanical strength is consistent with the assumption that for the purpose of calculating the mechanical strength of the drug-filled UHMWPE, the drug clusters can be considered as empty voids.

Effect of Irradiation Dose on Mechanical Strength of UHMWPE

Because most UHMWPE implants currently used are gamma-irradiated for sterilization (25-40 kGy)[346], we tested the effect of gamma irradiation at the sterilization dose of 25 kGy on the mechanical strength of vancomycin-eluting polyethylene. We found no statistical significant changes in the UTS, EAB, and the IS between unirradiated and gamma sterilized material.

We then explored the effect of high dose of irradiation (as often used to create highly crosslinked UHMWPE implants [347]) on the mechanical strength of vancomycin-eluting UHMWPE. Compared to the unirradiated vancomycin-UHMWPE, the 100 kGy irradiated sample displayed 3-18 % reduction in the UTS, 13-21 % reduction in EAB, and 34-36 % reduction in the IS (**Figure 3.5**). High dose irradiation of UHMWPE without any drug loading (> 50 kGy) is known to reduce its mechanical strength and elongation, presumably due to decreased chain mobility caused by radiation cross-linking [348]. Reduction in the ultimate tensile strength in the drug-eluting UHMWPE after irradiation is presumably due to the same reasons that plain irradiated UHMWPE has less strength than unirradiated UHMWPE: less mobility of the UHMWPE chains to align with the tensile force, allowing the material to break at lower tensile stress[333].

Conclusion

In conclusion, two factors affect the mechanical strength of drug eluting UHMWPE: initial drug loading and eccentricity of the drug clusters. Initial drug loading affects the mechanical strength of UHMWPE to a much greater extent than the eccentricity of the drug clusters. Highly eccentric drug clusters inside the polymeric matrix resulted in higher elution (**Chapter 2**) and higher mechanical strength than with spherical drug cluster samples. The improvement in the

mechanical strength in the highly eccentric drug cluster samples is likely due to smaller critical size defect (more homogeneous drug distribution) than the spherical drug cluster samples.

Gamma irradiation at 25 kGy did not significantly affect the mechanical strength of UHMWPE, while higher doses at 100 kGy significantly deteriorates the mechanical strength of drug-eluting UHMWPE.

Chapter 4

Wear Resistance of Micro-textured Drug Eluting UHMWPE

Introduction

Wear of Polymers

Polymers are widely used in moving mechanical interfaces such as automotive bearings, tires, compressor piston seals [349], and prosthetic joints [234]. Creating highly wear resistant polymers is crucial for these applications, especially in prosthetic joints, where there is multi-directional motion under high contact stress for the lifetime of the devices. Moving mechanical interfaces are composed of polymer and counter face that interact with each other with certain loads, speeds, temperatures, etc. Through mechanical interactions which involve frictional force, impact, contact fatigue, and cavitation forces, regions of the interacting surface may lose mechanical cohesion to the rest of the materials and produce wear debris[349].

Wear of polymer surfaces can be caused by contact-related interactions (adhesions, tribochemical reactions, fretting) and stress-related interactions (surface fatigue, abrasion, delamination wear, fretting) [350] of the surfaces in contact, both of which need to be minimized to minimize wear rate.

Abrasive wear is caused by the presence of hard asperities on the counterface which plough into the softer polymer material. Polymer surfaces undergoing abrasive wear typically exhibit wear grooves, ploughing, tearing, scratching, and surface cracking. The wear debris produced usually is in the form of chips or flecks [351]. Adhesive wear is caused by sticking/pulling of the polymer to the counterface during loading resulting in local plastic

deformation of the polymer. Cyclic motion results in the removal of the adhered polymer from the bulk polymer [352].

Surface fatigue wear is caused by cyclic stress in rolling and reciprocal sliding, which can result in subsurface crack initiation of the polymer. These cracks can propagate parallel to the surface and cause detachment of the areas of the surface from the bulk polymer in the form of wear debris [352]. Delamination wear is similar to surface fatigue wear but the fatigue stress is applied to a larger surface area of the polymer. Similar to fatigue wear, subsurface crack initiation under cyclic loading and subsequent separation of material can occur over large areas of the surface. The wear debris formed through this mechanism looks like flakes with striations over the surface [352].

Fretting wear occurs in mechanical interfaces undergoing continuous small motions (e.g. vibration) under load. The contact at the mechanical interface results in material transfer followed by oxidation of the polymeric material. The wear debris is usually trapped in the mechanical interface and can act as a third-body that accelerates wear process by three-body abrasion [356]. Tribochemical reactions can occur due to the exposure of the mechanical interface to corrosive or deteriorating chemical environments. The process usually occurs in two steps: corrosion or a different deteriorating process will occur on the surface which results in the formation of weaker material on the surface followed by abrasive removal of the corroded surface layer.

Fluid Lubrication at Mechanical Interfaces

Fluid lubrication is commonly used in mechanical interfaces to reduce the adhesion of the polymer to the counterface by coating the contact surfaces and their physical separation. Increasing lubrication film thickness between interacting surfaces was shown to decrease contact pressure [357] and wear rate, particularly abrasive and fatigue wear [358]. In general,

increasing sliding velocity and decreasing normal load resulted in a gradual decrease in the friction coefficient [359]. Lubrication film thickness can be increased through multiple pathways, such as increasing the viscosity of lubricants [358] and reducing contact stress [358].

Based on the film thickness, lubrication can be divided into four main categories (in order of decreasing lubrication film thickness): hydrodynamic lubrication, elastohydrodynamic lubrication, mixed lubrication, and boundary lubrication [360]. In the hydrodynamic lubrication regime, a fully developed fluid film exists between the mechanical interfaces, thus completely (at all times) preventing the two surfaces from directly contacting each other [361]. Under hydrodynamic lubrication, no asperity contact exists, resulting in the lowest coefficient of friction and wear rate of all lubrication regimes [361]. Hydrodynamic pressure and stress on the mechanical interface is proportional to the sliding speed and reciprocal of the film thickness squared [361]. Therefore, to decrease the pressure on the mechanical interface, one can decrease the sliding speed or increase the thickness of the fluid film.

Under elastohydrodynamic lubrication, contacting bodies undergo elastic deformation when they slide or roll against each other, accompanied by changing viscosity of lubricant from compression of contacting surfaces to yield lubrication film that separate the mechanical interfaces [362]. The elastohydrodynamic lubricating film thickness ranges from 1-400 μm thickness and its formation comprises of (1) hydrodynamic film formation, (2) modification of film geometry because of deformation of interacting bodies, and (3) change in lubricant's viscosity and rheology under pressure. The hydrodynamic film is formed when Hertzian contacts are formed on surfaces containing converging and diverging wedges in the presence of lubricants. The deformation of interacting bodies modifies the film geometry by creating a central region of quasi-parallel surfaces between the inlet and outlet wedges. This deformation results in the thickening of lubrication film thickness. When lubricant is exposed to high pressure due to stress from the contacting bodies, it undergoes a phenomena called piezoviscosity, where its

viscosity increases dramatically with pressure. This phenomenon results in an increased ability of the lubricants to separate the two contacting bodies and preventing asperity contact [362].

Under boundary lubrication, asperity contacts occur between the mechanical interfaces and the degree of lubrication depends on the formation of a protective film on the surface of the mechanical interfaces [363]. This protective film can originate from adsorption of lubricants to the surface or chemical reaction between lubricant and the mechanical interface [363]. Computational simulation showed that during boundary lubrication, the adsorbed films remain aligned with the contacting surfaces and helps the mechanical interfaces slide past each other [364]. The lubricating effect of these adsorbed films is the formation of a low shear strength interface between interacting surfaces [365].

Mixed lubrication operates between elastohydrodynamic lubrication and boundary lubrication, where both fluid film and asperity contact are in operation to support the applied load [360]. The micropeaks (asperities) undergo boundary lubrication, while the microvalleys undergo elastohydrodynamic lubrication [366]. Mixed lubrication primarily occurs when the speed of movement is low, there is high load, or there is high enough temperature to significantly reduce the lubricant viscosity [366].

Wear Mechanism of UHMWPE

Most commonly used artificial joints are made of polymer (UHMWPE) articulating against metal (Cobalt Chromium (CoCr) or Titanium Alloy (TiAl6V4)). When implanted, the UHMWPE component (e.g. tibial insert, acetabular liner) and the metal component (e.g. femoral component, femoral head) articulate against each other when the joint moves. This movement is often times multi-directional: in the hip, the primary motion is flexion/extension and the secondary motion is abduction/adduction. In the knee, the primary motion is flexion/extension

and the secondary movement is internal/external rotation [367]. Under ideal conditions, the UHMWPE and metal interface is completely separated by a lubrication film made of synovial fluid [368]. Unfortunately, the minimum lubrication film thickness is only between 0.1-0.25 μm [368], which is less than the typical average surface roughness of UHMWPE which is between 0.1-1 μm [369]. Therefore, the articulation between UHMWPE and metal in human joints is expected to undergo mixed lubrication [368], where both asperity contact and elastohydrodynamic lubrication are in operation.

Because asperity contacts between UHMWPE and metal are present *in vivo*, UHMWPE, which is weaker than its metal counterpart, undergoes more wear, which can cause detrimental secondary effects such as osteolysis [11]. Since an artificial joint operates under sliding and rolling movement [370] as well as cyclic compression, most wear occurs through abrasion, adhesion, and fatigue processes [371]. The UHMWPE wear surface undergoes shear and tensile stress in multiple directions, which results in molecular reorientation, mainly in the direction of primary motion [372]. As a result of the reorientation process, strain softening occurs in the secondary directions of motion and leads to polymer rupture between the oriented molecules. Such rupture initiation on the surface leads to transfer of the load to the subsurface plane and also results in shear rupture and formation of fibrillary wear particles [373].

Most UHMWPE wear debris are fibrillary and elongated [372], with length ranging from 1-20 μm , and submicron fibril diameter. Closer examination of the wear debris shows extensive lamellar orientation perpendicular to the long axis of the wear particle. Since the carbon-carbon chain (C-C chain) of UHMWPE is always perpendicular to the lamellar interface, the C-C chain is therefore in parallel to the long axes of the fibrillary wear particles, in agreement with the molecular reorientation in the direction of primary motion [372].

Tensile testing of pre-stretched UHMWPE showed that increasing the pre-stretching stress in the parallel direction to the tensile testing increases the ultimate tensile strength [372].

However, pre-stretching stress in planes perpendicular to the tensile testing direction resulted in decreasing ultimate tensile strength, showing the susceptibility of reoriented chains to breaking in orthogonal directions relative to the primary direction of motion.

Relation between Micro-Texture and Lubrication Film Thickness

Micro-texturing was shown to improve lubrication film thickness and therefore the tribological performance of mechanical components such as bearings, seals, and piston rings [374-376]. For example, piston rings with two annular bands of circular dimples running on the rings' edges could produce a wedge flow effect and reduced friction by 20-25 % as compared to untextured piston rings [377]. Furthermore, the textured piston rings were also shown to reduce engine fuel consumption by up to 4 % [378].

Both computational and experimental studies showed that micro-texturing increased both the local and average lubrication film thickness, which in turn reduced wear rate and/or friction coefficient [379]. Many shapes of microtexture patterns have been explored and shown to improve lubrication of mechanical interfaces: dimples, radial taper, hydropads, lobes, and grooves[376]. Analysis of lubrication mechanisms and optimization of microtexturing showed that microtexture area density and aspect ratio are the two most important parameters that affect the efficacy of microtexture in improving lubrication [380].

Microtexturing was found to be most helpful in minimizing surface contact at start-up, change of direction, and reversal of motion [375, 381, 382]. Microtexturing could increase the lubrication film thickness by acting as microreservoirs of lubricant, which facilitate lubrication film formation under starving lubricant conditions [383]. As a result, microtexturing expanded the load and speed range of both the hydrodynamic and elastohydrodynamic lubrication regimes,

i.e. presence of microtexturing allowed both hydrodynamic and elastohydrodynamic lubrication to operate at higher load and lower speed than in its absence [376].

Despite improvement in tribological properties through microtexturing, exhaustive searches need to be performed for each set of bearing surface couples to obtain the optimum texture shape, depth, and density [361]. Furthermore, most microtexturing methods are slow and comprise multiple steps such as high energy beam or electric discharge methods (e.g. laser microtexturing [376] and pulsed air arc treatment), etching techniques (e.g. photochemical etching[375], electropolishing, reactive ion etching, maskless electrochemical texturing), and micromachining/forming techniques (e.g. vibrorolling, abrasive jet machining, diamond embossing, shot blasting and photolithography, mechanical indentation, shot peening, and micro-computer numerical control texturing)[384]. The slowness and complexity of machining impede adaptation of micro-texturing into an industrial method for reduction of friction and wear.

Relation between Micro-Texture and Tribology Properties

Ability of microtexturing to reduce both friction and wear rate are mainly due to the prevention of asperity contacts by creating thicker lubrication film and the trapping of wear debris in the grooves of the microtexture, thus reducing the ability of wear particles to act as third body and plow into the bulk material [376].

Reduction of the coefficient of friction occurs when the Hertzian contact dimension is smaller than the size of the pattern [385, 386]; increase in the coefficient of friction is observed when the Hertzian contact dimension is larger than the size of the pattern [359, 387, 388]. When the pattern is smaller than the Hertzian contact dimension, the features of the pattern are too small to function as lubricant reservoirs or increase the thickness of lubricating film[359].

A previous attempt at reducing both friction and wear rate in artificial joints was primarily focused on surface texturing of the metal component (e.g. femoral head) [389]. This study showed that creating circular dimples of 500 μm in diameter and 100 μm deep with 1.2 mm pitch on a CoCr femoral head showed 17% friction reduction and a 36% reduction in the UHMWPE wear rate. The reduction in friction and wear is likely due to enhanced hydrodynamic pressure of the lubricant, the entrapped synovial fluid in the dimples and subsequent extrusion during loading, which ultimately increase the overall thickness of lubrication [389, 390]. No attempt has been made to microtexture UHMWPE to improve friction or wear resistance of UHMWPE against metal.

Methods

Preparation of vancomycin-eluting UHMWPE with highly eccentric drug clusters.

Vancomycin-eluting UHMWPE was prepared at 4 wt %, 6 wt %, 10 wt %, and 20 wt % initial drug content. A representative method to prepare the Vancomycin-eluting UHMWPE with 6 wt % initial drug content is provided below.

Vancomycin-HCl (1.5 gram) was crushed with mortar and pestle and then passed through a 75 μm sieve. Vancomycin powder was then mechanically mixed with GUR1020 UHMWPE powder (Celanese, 23.5 grams) for 30 minutes at room temperature to obtain a 7 wt% vancomycin-blended UHMWPE and poured into a circular mold with 10.5 cm inner diameter. The vancomycin-UHMWPE mixture was then consolidated by compression molding at 170°C, 20 MPa, for 5 minutes with a cooling rate of 10°C/min to yield approximately 3 mm-thick and approximately 10.5 cm diameter Vancomycin-eluting UHMWPE (VPE).

Manufacture of optimized microtextured and porous UHMWPE. Bupivacaine-HCl (2 gram) was crushed with mortar and pestle and then passed through a 75 μm sieve. Bupivacaine powder was then mechanically mixed with GUR1020 UHMWPE powder (Celanese, 8 grams) for 30 minutes at room temperature to obtain a 20 wt% bupivacaine-blended UHMWPE and poured into a circular mold with 10.5 cm inner diameter. 25 grams of GUR 1020 UHMWPE without additives were then added and spread evenly on top of the bupivacaine-blended UHMWPE. Resulting constructs were then consolidated by compression molding at 170°C, 20 MPa, for 5 minutes. The resulting consolidated construct then cooled at rate 10°C/min to room temperature. Bupivacaine was then eluted out from the UHMWPE in deionized (DI) water at 37°C for 2 weeks.

Manufacture of 2-methacryloyloxyethyl phosphorylcholine (MPC)-grafted UHMWPE. Experimental procedure to create MPC-grafted UHMWPE was adapted from [391]. An UHMWPE block was washed with methanol in ultrasonicator for 30 minutes and this procedure was repeated. After the UHMWPE was dried, the block was immersed in a benzophenone solution in acetone (1.0g/dl) for 30 seconds. The block was then dried in the absence of light for 1 hr in a vacuum chamber at room temperature. MPC solution (0.5 M) was prepared by dissolving 5 gram of MPC in 33.9 ml of degassed, double-distilled water. The benzophenone-coated UHMWPE block was placed in a glass vial filled with degassed MPC solution and sealed. Photopolymerization on the polyethylene surface was carried out using an ultraviolet (UV) lamp (Dymax Bluewave 200, Torrington, CT) at 60°C for 90 minutes. The resulting block was then washed with distilled water and hot ethanol (50°C), and then dried in vacuum for 15 hours.

Manufacture of slippery, liquid-infused, porous surface (SLIPS)-treated UHMWPE. The Experimental procedure to create SLIPS-treated UHMWPE was adapted from [392]. An UHMWPE block was exposed to 40 seconds of 250 mTorr radio-frequency (13.56 MHz) oxygen plasma at 100 Watts. The sample was immersed in a liquid silane solution (5% v/v tridecafluoro-1,1,2,2-tetrahydrooctyl trichlorosilane) (Gelest, Morrisville, PA) in anhydrous ethanol (Sigma, St. Louis, MO) for 1 hour at room temperature. It was then rinsed with anhydrous ethanol (Sigma, St. Louis MO), followed by distilled DI water, and then three times with pure ethanol. It was dried gently with nitrogen and then heated in an oven with desiccant at 60°C for 12 hours at atmospheric pressure. The sample was subsequently immersed in liquid perfluorodecalin (PFD) for 1 hour and immediately tested.

Manufacture of radiation-crosslinked UHMWPE. UHMWPE blocks were packaged under vacuum in food packaging. Samples were then gamma-irradiated to 100-kGy.

Manufacture of benzophenone crosslinked UHMWPE. An UHMWPE block was washed twice with methanol in an ultrasonicator for 30 minutes twice. After the UHMWPE was dried, the block was immersed in a benzophenone solution in acetone (1.0g/dl) for 30 seconds. The block was then dried in the absence of light for 1 hour in vacuum at room temperature. The benzophenone-coated UHMWPE block was placed in a glass vial filled with argon and then sealed. Photocrosslinking on the polyethylene surface was carried out using ultraviolet(UV) lamp (Dymax Bluewave 200, Torrington, CT) at 60°C for 90 minutes. The resulting block was then washed with distilled water and hot ethanol (50°C), and dried under vacuum for 15 hours.

Wear testing. Wear testing of UHMWPE was adapted from [234]. Cylindrical pin shaped samples (9 mm in diameter and 11 mm in length) were used under bidirectional pin-on-disk testing at 2 Hz using a 10 mm x 5 mm rectangular pattern. The loading cycle was adapted from [393] and the human gait cycle was adapted from [234]. The UHMWPE pins were articulated against polished CoCr discs ($R_a=0.38\pm 0.005$ μm). Undiluted bovine serum was used as lubricant with 33ml penicillin-streptomycin solution per 500 ml as antibacterial agent and 1mM EDTA as a chelating agent. Weight of the pin was measured every 0.1 million cycles. The wear rate values reported here are the cumulative weight values normalized with the total number of cycles and are averages of six pins.

Friction testing. Cylindrical pin shaped samples (6mm in diameter and 20 mm in length) were used for friction testing. Polished CoCr discs were used as the countersurface against UHMWPE pins. Bovine calf serum with a protein concentration of 30g/L at 37°C was used as lubricant. A pre-determined dead weight was applied to the UHMWPE pins to achieve a total stress of 5 MPa and the metal disc was rotated at 20mm/s. As the disk was rotated, both the axial load pressing the pin against the metal disk and the tangential force generated by the disk rotation were measured and the friction coefficient was calculated by averaging the friction coefficient at steady state, measured after 10 min.

Scanning Electron Microscopy. Samples (except those used for EDAX) were sputter coated with a thin layer of gold/palladium and imaged on a Zeiss Supra55VP microscope. Both Everhart-Thronley and Inlens detector were used to acquire the image.

Energy Dispersive X-Ray Spectroscopy. UHMWPE samples were imaged under variable pressure in the Zeiss Supra55VP system. The chamber pressure was set at 25 Pa and Variable Pressure Secondary Electron (VPSE) detection was used to obtain the scanning electron micrograph. Elemental maps were created by creating spatial maps based on P-K (phosphorus), C-K (carbon), O-K (oxygen), and N-K (nitrogen) lines obtained from the EDAX detector.

Structural analysis using micro-computed tomography (micro-CT). Tomograms of cylindrical pins (9 mm diameter and 5 mm long) were acquired and images were reconstructed using a cone-beam X-ray scanner (μ CT 40, Scanco Medical) for 3D reconstruction with voxel resolution of ~ 10 μ m. Porosity analysis and pore accessibility were analyzed using the iMorph software package (www.imorph.fr, [1]). The resulting tomogram was then thresholded to separate the pores and the polymeric matrix. Porosity was calculated by dividing the volume belonging to pores by the total volume of the sample. The accessible porosity module implanted in iMorph allowed the quantification of the pore volume accessible from one side of the sample by a particle depending on its size.

Compression testing. Cylindrical pins (2 mm diameter and 3 mm long) were stamped out of 3.2 mm thin sections of the materials discussed above. For static compression, these samples were tested with a crosshead speed of 0.25 mm/s using dynamic mechanical analyzer (RSA G2, TA Instruments, New Castle, DE). The stress and strain were recorded at 100 Hz. The engineering stress-strain curves were calculated by using the crosshead displacement. For cyclic compression, these samples were exposed to compressive strain at a crosshead speed of 0.25 mm/s for 0.5 seconds followed by recovery strain at a crosshead speed of 0.25 mm/s for 0.5 seconds. Each sample was tested for 100 cycles.

Analysis of surface topology. Surface topology was analyzed using stylus profilometry (P16 Stylus Profiler, KLA Tencor) and atomic force microscopy (MFP-3D, Asylum). All stylus profilometry measurements were performed at room temperature in contact mode using scan speed of 10 $\mu\text{m/s}$, sampling rate of 20 Hz, stylus radius of 0.5 μm , and scan area of 1000 μm x 1000 μm .

All AFM measurements were performed at room temperature in tapping mode using AC240TS probe (Olympus), captured with a scan rate of 0.35 Hz, and a scan size of 40.0 μm x 40.0 μm in air. Spring constants of the AFM probe were individually calibrated using the thermal noise method with a MFP-3D Asylum AFM. Surface roughness (R_a) of each scanned area was calculated from average deviation of the area. Surface roughness of each sample was calculated from average surface area of three random areas of a sample. Surface roughness of each sample category was calculated from average of surface roughness of three independent samples.

Computational simulation of total lubrication film thickness.

Total lubrication film thickness was approximated by summing the lubrication film thickness due to elastohydrodynamic lubrication and that due to weeping (extrusion) lubrication. The film thickness due to elastohydrodynamic lubrication was calculated from the minimum film thickness using the isoviscous-elastic equation [394]. The weeping (extrusion) lubrication film thickness was calculated from the simulation using the contact mechanics of a ball on flat surface with the assumption of incompressible lubricants [362], and we assume the deformation volume of the ball to be equal to the volume of the extruded lubricants.

The following parameters were used for solving the isoviscous-elastic equations: U (the speed of the wear test) = 1.5 m/s, η_0 (viscosity of lubricant, bovine serum, 25°C) = 0.000089 Pa.s [395], compression modulus of microtextured+porous UHMWPE = 199.8 MPa, compression modulus of flat surface UHMWPE = 499 MPa, compression modulus of TiAl6V4 = 1.14×10^{11} Pa [396], ν_{UHMWPE} (Poisson ratio of UHMWPE) = 0.46, $\nu_{TiAl6V4}$ (Poisson ratio of TiAl6V4) = 0.32 [397], α (water) = 3.6×10^{-10} , k (ellipticity parameter) = 1, P (normal pressure) = 8 MPa, r_{pin} (UHMWPE pin radius) = 0.0045 mm, f (area fraction of microtextured UHMWPE occupied by UHMWPE granule) = 0.785 (from micro-CT analysis). R' is the radius of curvature.

For elastohydrodynamic lubrication:

$$H_{EHL} = 8.70 \left(\frac{W^{\frac{8}{3}}}{U^2 \eta_0^2 E'^{\frac{2}{3}} R'^{\frac{2}{3}}} \right)^{0.67} (1 - 0.85 e^{-0.31 * k}) \quad (1)$$

Where

$$\frac{1}{E'} = \frac{1}{2} \left[\frac{1 - \nu_{TiAl6V4}^2}{E_{TiAl6V4}} + \frac{1 - \nu_{UHMWPE}^2}{E_{UHMWPE}} \right]$$

$$W = P * \pi * (2R')^2 * f$$

For weeping (extrusion) lubrication:

$$H_{ext} = \frac{\pi * \delta \sqrt{\delta(2R' - \delta)}}{R'^2}, \delta = 1.0397 \left(\frac{W^2}{E' R'} \right)^{\frac{1}{3}}$$

Total lubrication film thickness:

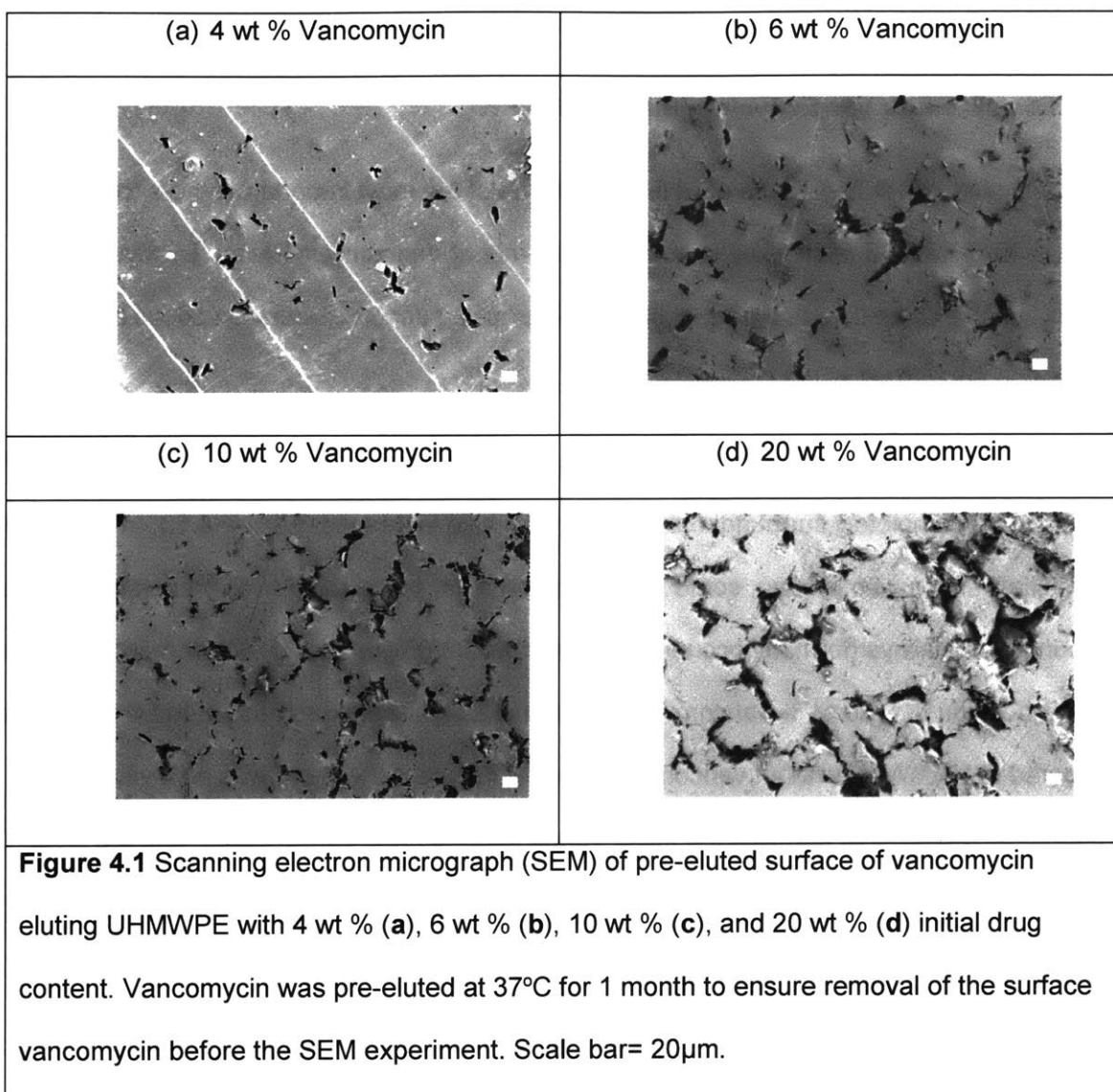
$$H_{Total} = H_{EHL} + H_{ext}$$

Results

Wear Resistance of Vancomycin-Eluting UHMWPE

Because wear resistance of UHMWPE is one of the most important factors for the longevity of UHMWPE *in vivo*, we tested the wear rate of Vancomycin-eluting UHMWPE at various initial drug loading and after being irradiated using various irradiation doses for sterilization and cross-linking.

As the concentration of vancomycin was increased, the probability of a single UHMWPE granule to be completely surrounded by vancomycin also increased (**Figure 4.1.**). In fact, at 20 wt % initial vancomycin loading, some areas showed a flat peak (UHMWPE granule) completely surrounded by valleys (formerly occupied by vancomycin) (**Figure 4.1 d**). Wear testing showed that the addition of 4-20 wt % vancomycin resulted in a significant decrease in the wear rate as compared to UHMWPE without vancomycin (0 wt%; **Figure 4.2**). There was an inversely proportional relationship between the initial Vancomycin-loading concentration and the wear rate of vancomycin-eluting UHMWPE. After gamma irradiation at 25 kGy, the wear rate of all vancomycin eluting UHMWPEs were reduced compared to that of their non-irradiated counterparts; however, there was no significant effect of increasing initial vancomycin loading concentration. After gamma irradiation at 100kGy, the overall wear rate of all the vancomycin eluting UHMWPEs were further lowered compared to that of samples irradiated at 25 kGy. However, the wear rate was increased with increasing initial vancomycin loading concentration.



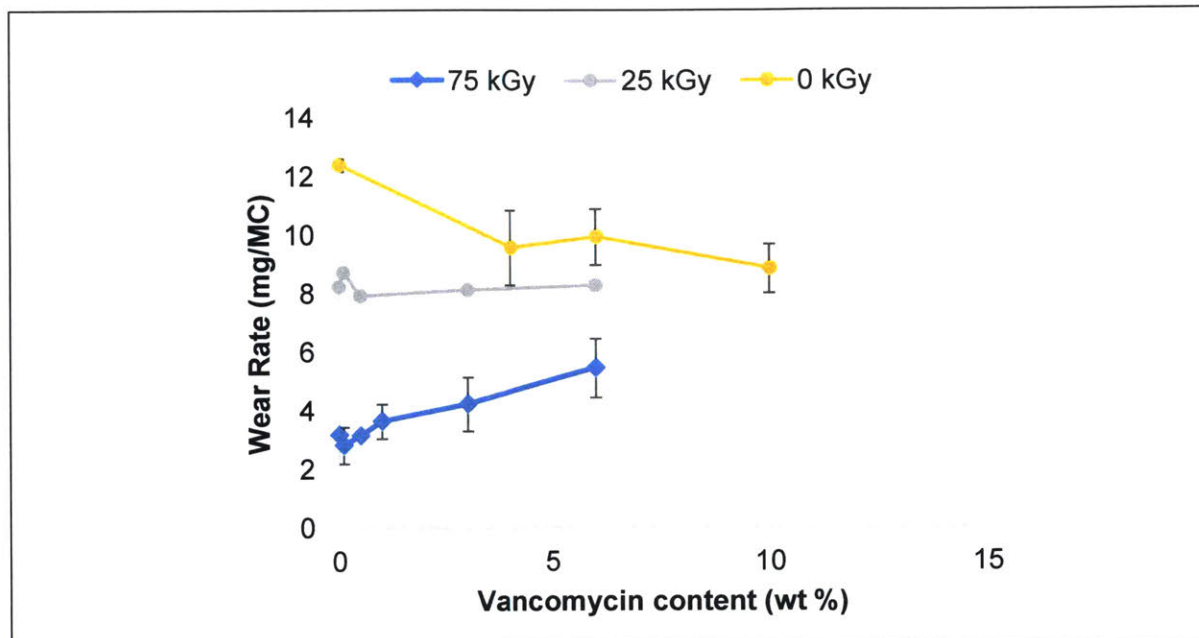


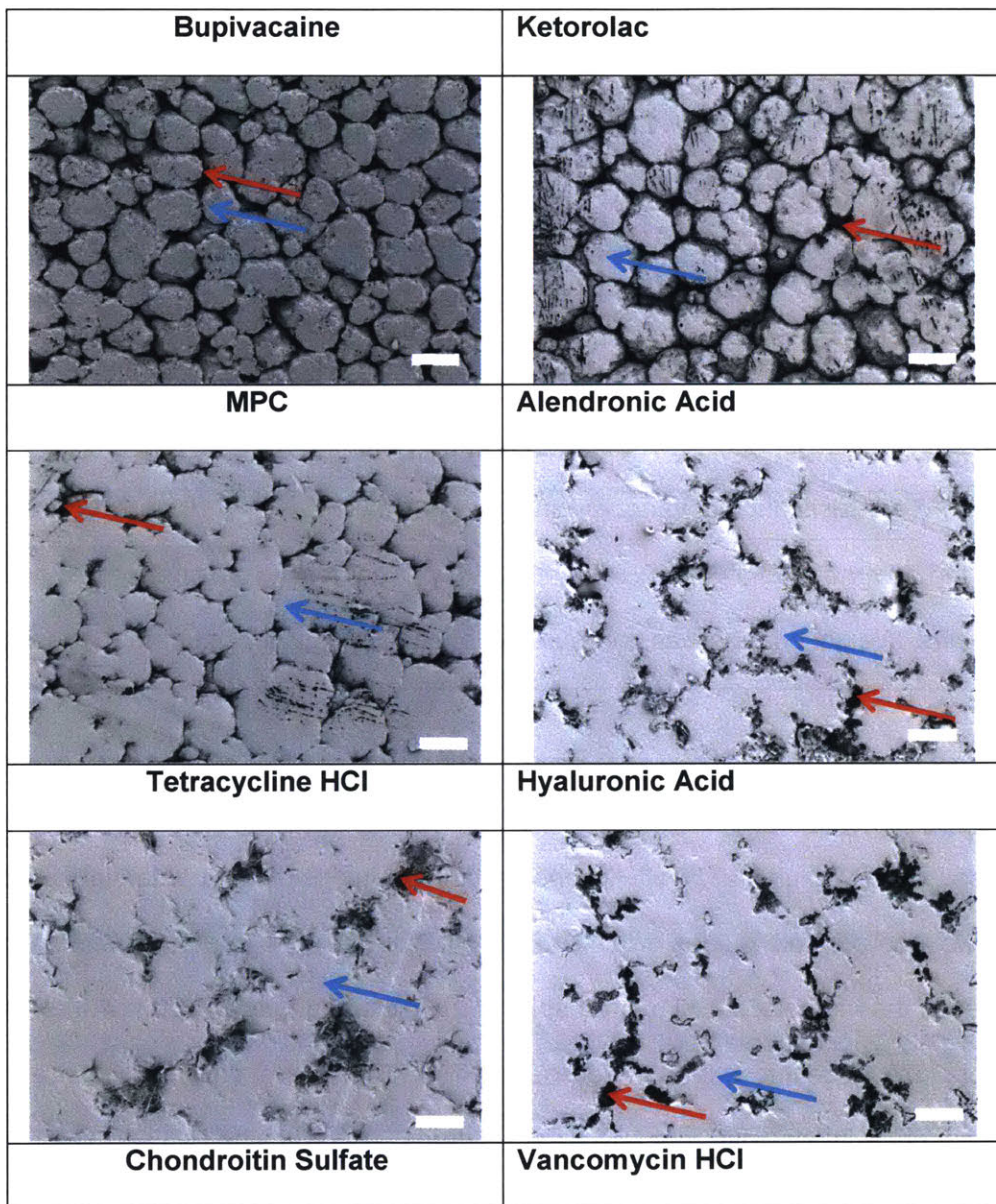
Figure 4.2. Wear resistance of vancomycin-eluting UHMWPE with 0-10 wt % Vancomycin Loading and gamma irradiated at 0, 25, and 75 kGy. Wear testing was performed up to 1 million cycles. Weight change was measured every 100,000 cycle. Data are means±s.d.

Formation of self-assembled micropatterns in drug eluting UHMWPE

Based on the result that 20 wt % vancomycin-UHMWPE showed potential to reduce wear rate, we incorporated various drugs into UHMWPE at 20 wt % and compression molded it as described in the methods. SEM micrographs of the eluted surfaces (**Figure 4.3**) all showed formation of highly eccentric valleys in between UHMWPE granules. However, the degree of valley interconnectivity was different with different drugs: Bupivacaine HCl and ketorolac > MPC > alendronic acid > tetracycline HCl > hyaluronic acid ~ chondroitin sulfate.

Among the drug eluting UHMWPEs mentioned above, bupivacaine HCl and ketorolac showed the lowest wear rate, followed by alendronic acid, MPC, tetracycline HCl, chondroitin sulfate, and hyaluronic acid (**Figure 4.4**). Decreasing wear rate was in the same order as what

was observed qualitatively as the increasing degree of micropattern valley interconnectivity (Figure 4.3).



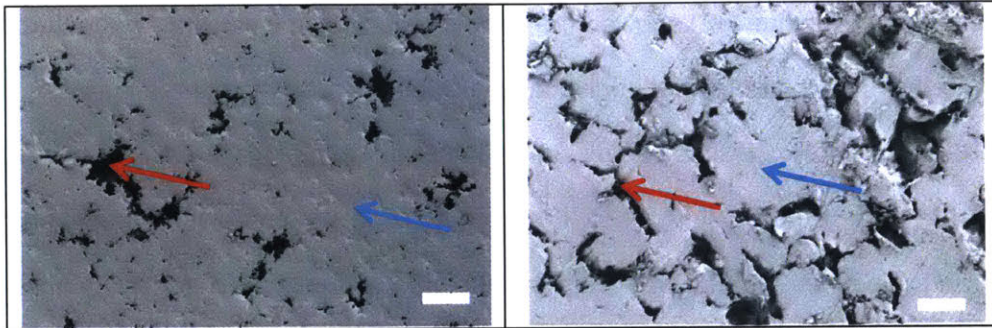


Figure 4.3 SEM micrograph of various drug eluting UHMWPE with initial 20% wt drug loading. Blue arrow = peak of microtexture, red arrow = valley of microtexture. Scale bar = 100 μ m. Drugs were pre-eluted at 37°C for 1 month to ensure removal of the surface drugs before SEM experiment.

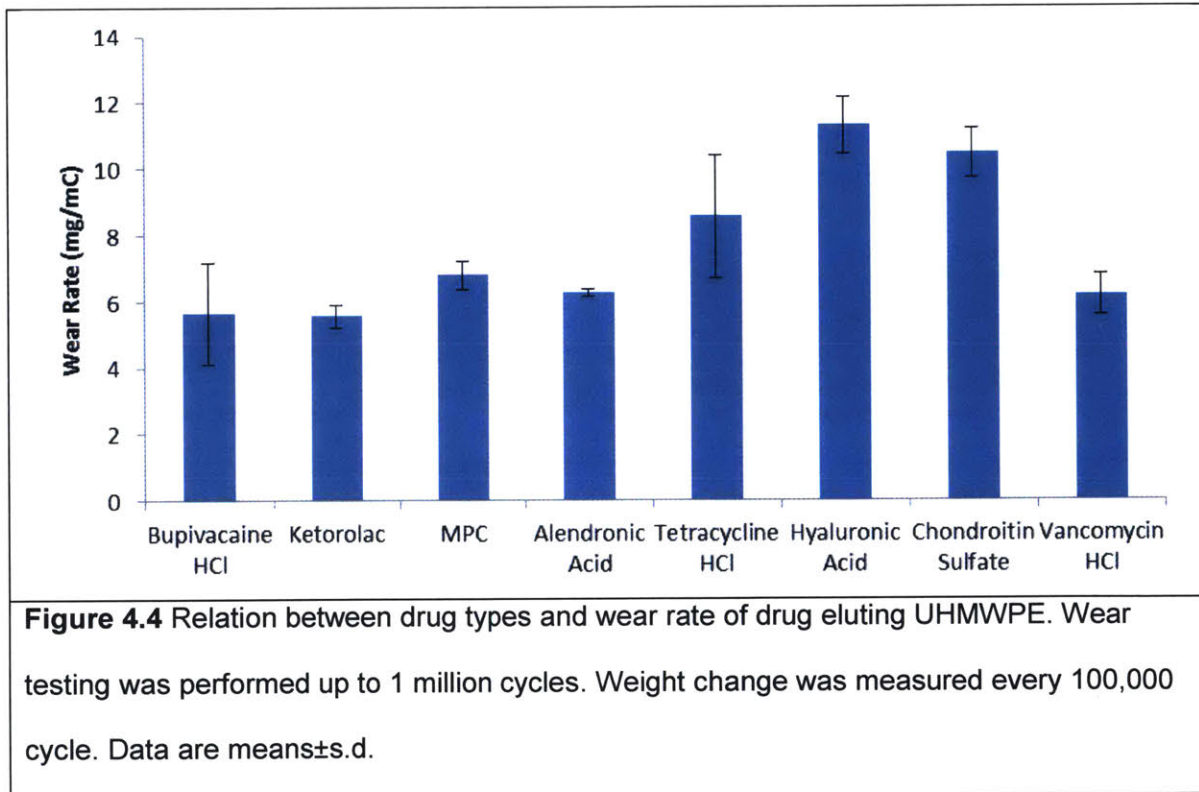
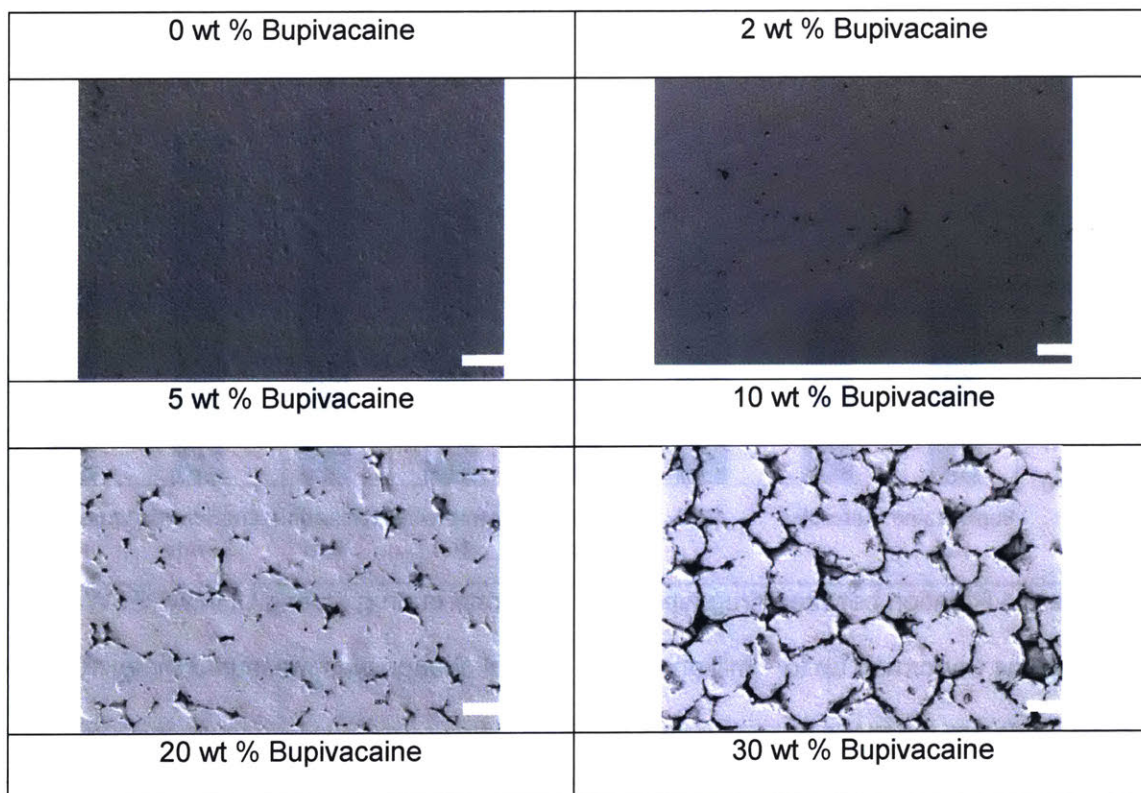


Figure 4.4 Relation between drug types and wear rate of drug eluting UHMWPE. Wear testing was performed up to 1 million cycles. Weight change was measured every 100,000 cycle. Data are means \pm s.d.

Investigation of the relationship between self-assembled micropatterns in bupivacaine-eluting UHMWPE and wear resistance

Because bupivacaine HCl showed the largest reduction in wear rate, we tested the effect of different loading concentrations of bupivacaine HCl on the formation of the surface micropattern (**Figure 4.5**). Bupivacaine dissolved in saline upon elution, leaving valleys (darker) and peaks of UHMWPE granules (lighter) (**Figure 4.5**). High interconnectivity between the valleys began to be observed at 5 wt % bupivacaine HCl, and full interconnectivity between the valleys was achieved at 10 wt %. Upon increasing the bupivacaine loading concentration from 10 wt % to 20 wt %, the valley cross-sections became wider.

The wear rate of bupivacaine-eluting UHMWPE decreased as the initial bupivacaine HCl loading concentration was increased (**Figure 4.6**) until what appeared to be saturation was reached at 20 wt%.



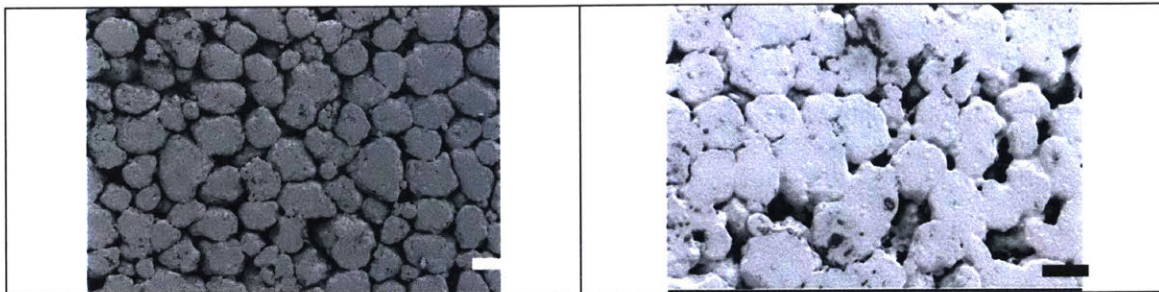


Figure 4.5 Optical micrograph of surface of bupivacaine eluting UHMWPE post elution at 2, 5, 10, 20, and 30 wt % initial bupivacaine content. Drugs were pre-eluted at 37°C for 1 month to ensure removal of the surface drugs before SEM experiment.

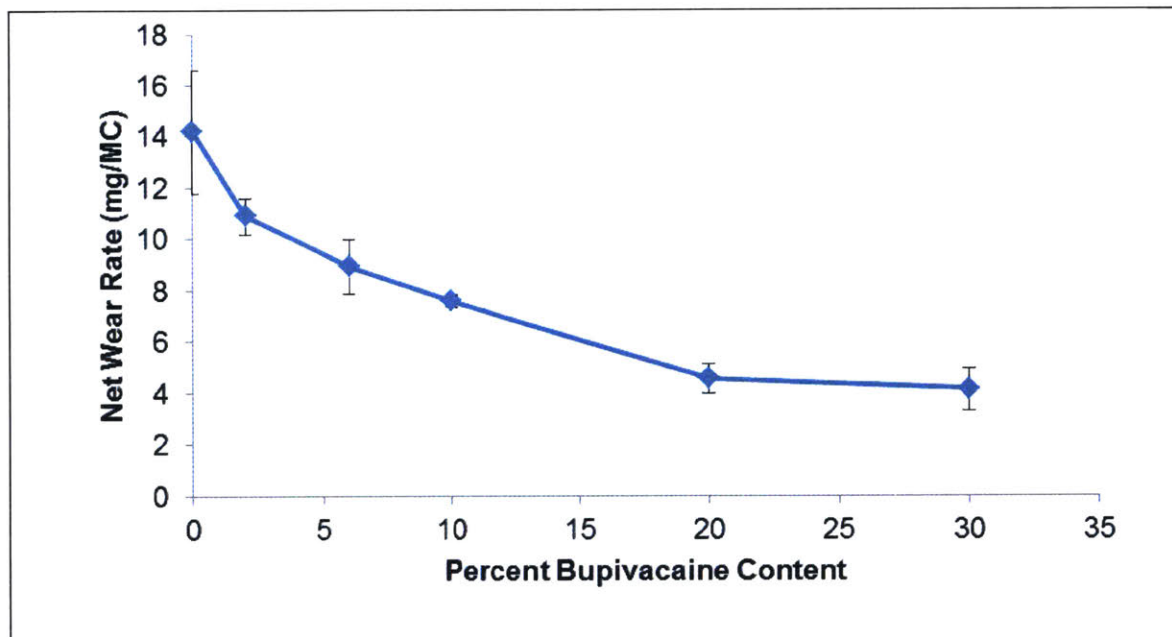


Figure 4.6 Relation between initial drug content and wear rate of bupivacaine eluting UHMWPE. Wear testing was performed up to 1 million cycles. Weight change was measured every 100,000 cycle. Data are means±s.d.

Long-term wear testing of bupivacaine-eluting UHMWPE

To look at the ability of the 20% bupivacaine-UHMWPE to reduce the wear rate for a longer period of time, we performed wear testing on the material up to 3 million cycles. The wear rate of bupivacaine-eluting UHMWPE at 20 wt% initial loading was linear throughout the wear testing, with an average wear rate of 5 mg/MC (Figure 4.7).

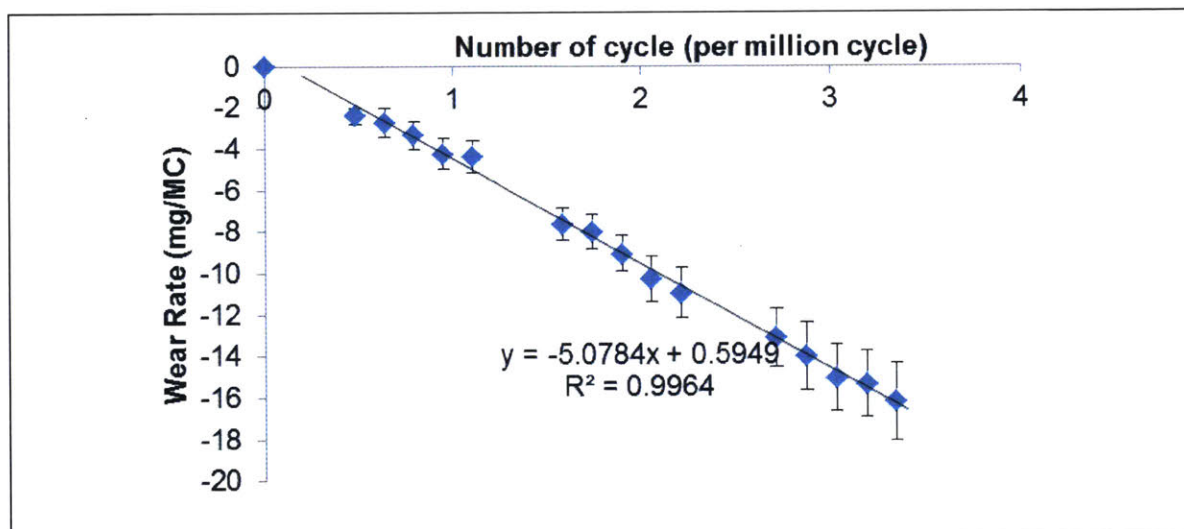
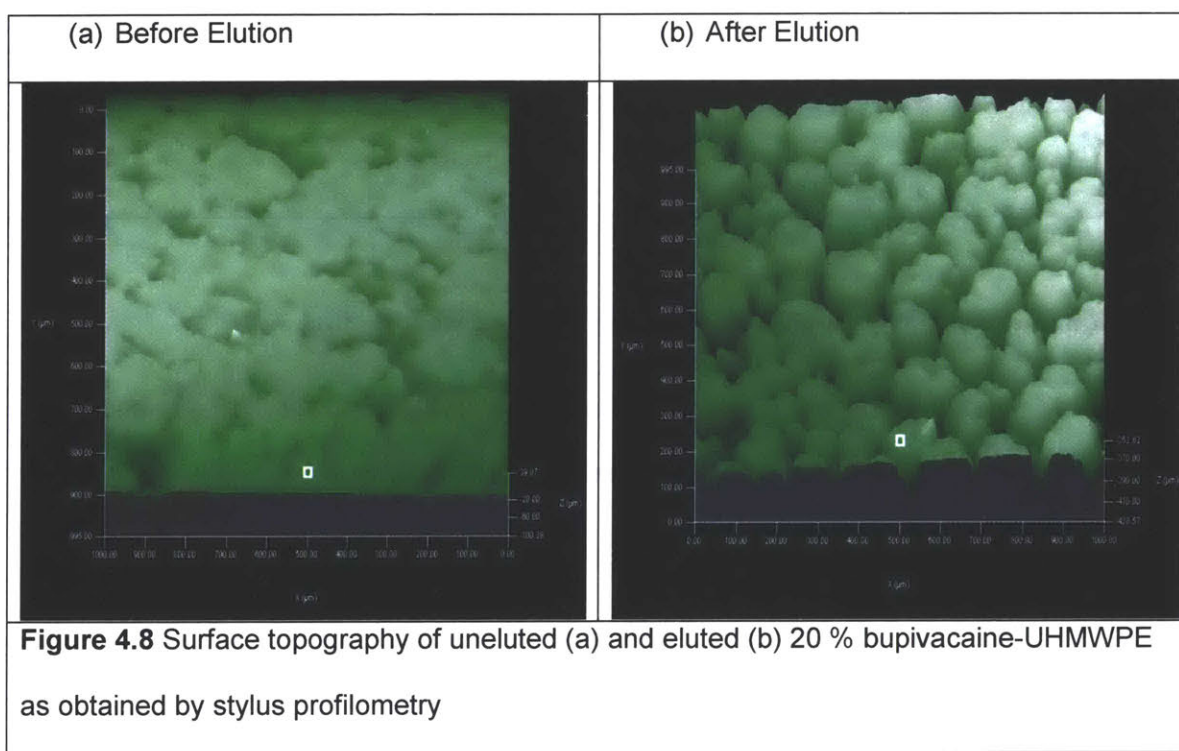


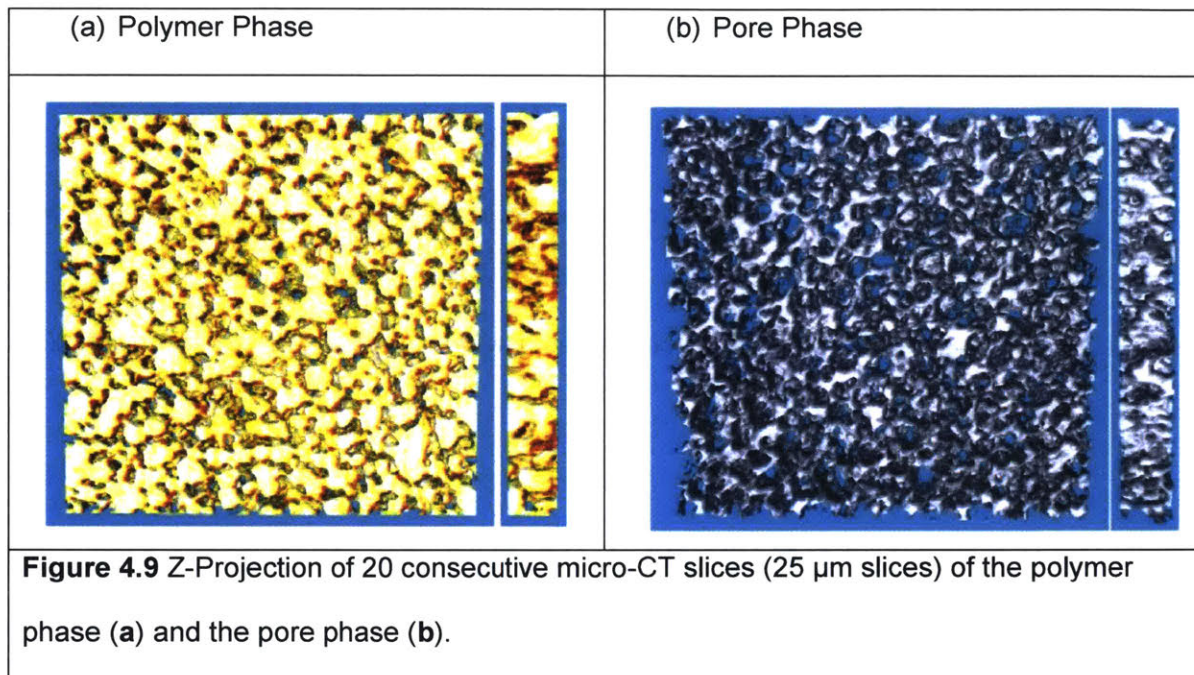
Figure 4.7 Wear rate of 20 % bupivacaine-UHMWPE tested up to 3 million cycles. Wear testing was performed up to 1 million cycle. Weight change was measured every 100,000 cycle. Data are means \pm s.d.

Topographical analysis of self-assembled micropatterns from bupivacaine-eluting UHMWPE (Bupi-PE)

We performed topographical analysis of the micropatterns of bupivacaine-eluting UHMWPE at 20wt% initial loading (Bupi-PE) before and after bupivacaine elution. Before elution (Figure 4.8a), the overall surface was relatively flat with shallow elongated valleys,

formerly occupied by bupivacaine HCl (the bupivacaine could be removed from the surface during cutting of the sample or wiping). After bupivacaine elution for 1 week, we could clearly observe a honeycomb pattern (**Figure 4.8b**), where the frame of the honeycomb was the valley of the micro texture surrounding UHMWPE granules. The mean polymer granule diameter was $105 \pm 5 \mu\text{m}$ and mean valley width was $50 \pm 4 \mu\text{m}$. Micro-computed tomography of the underlying porous polymeric system showed 3D-interconnected networks of pores (**Figure 4.9**), with 30 % porosity.



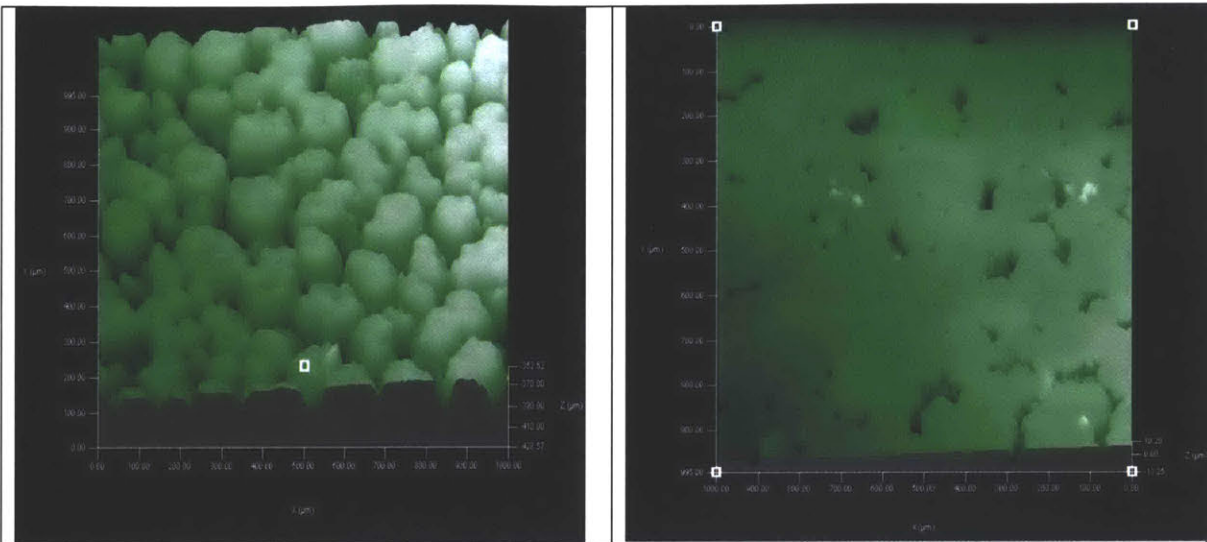


Evolution of the surface roughness of Bupi-PE during wear testing

We analyzed the surface topology of wear-tested pins by stylus profilometry and atomic force microscopy (AFM) throughout the progress of wear testing.

After 100,000 cycles, peaks of the Bupi-PE surface became significantly flatter and smoother (**Figure 4.10 a-b**), while the valleys became significantly narrower. No further flattening or smoothing was observed on further wear testing (500k cycles-1 million cycles, **Figure 4.10 c-d**). Deeper analysis of the surface roughness using AFM also showed that the surface roughness rapidly declined within the first 100k cycle, and stayed relatively constant throughout the test, staying at 23.8 ± 2.2 nm (**Figure 4.11, Figure 4.12**).

Before Wear Testing	100 k cycle



500 k cycle

1 M cycle

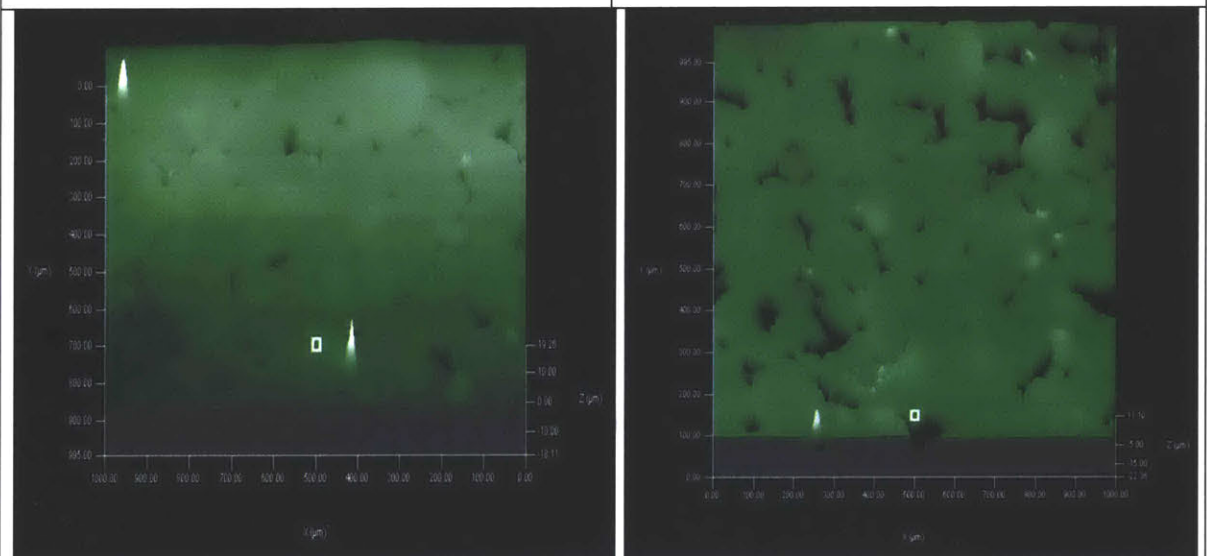
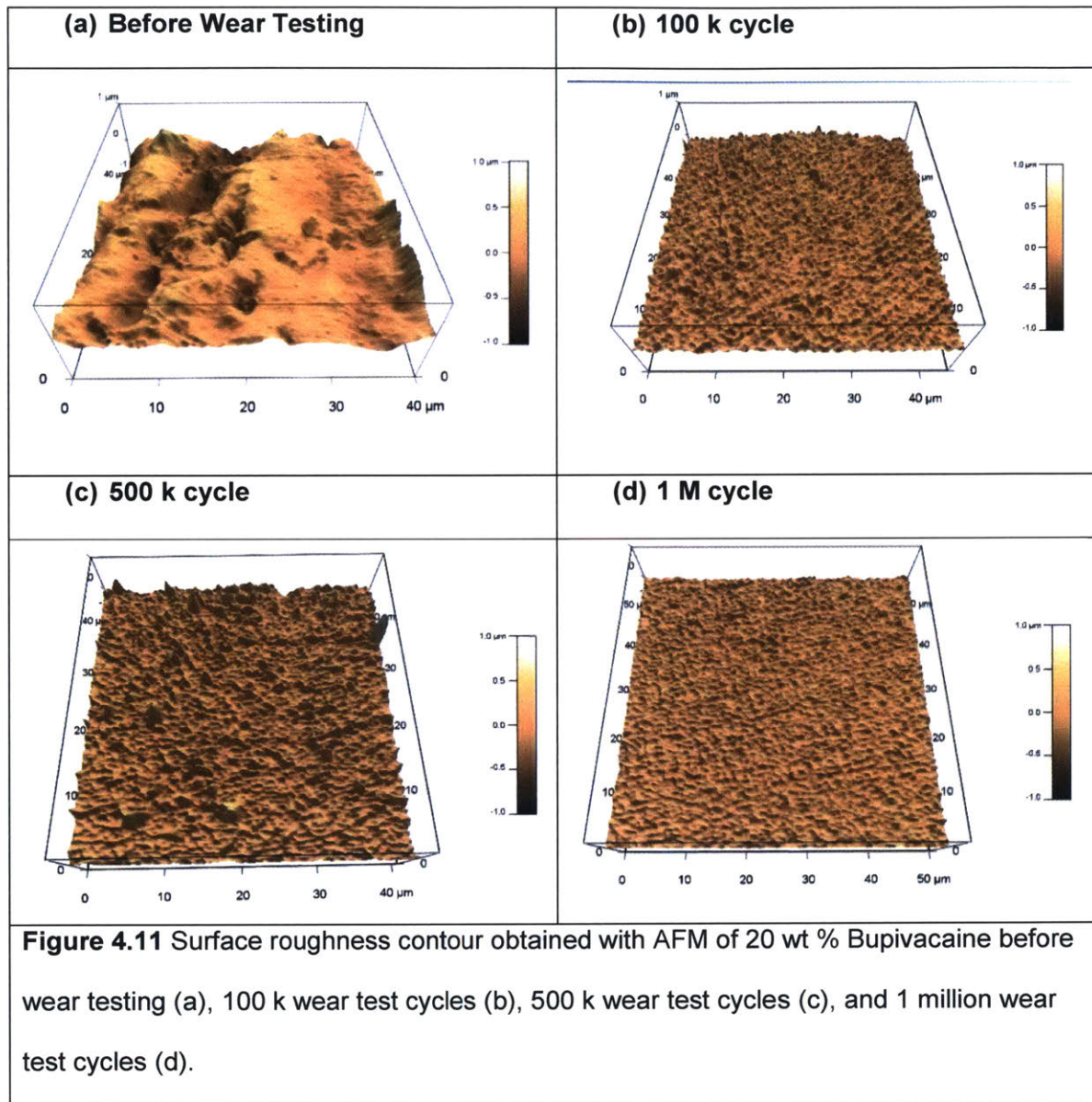
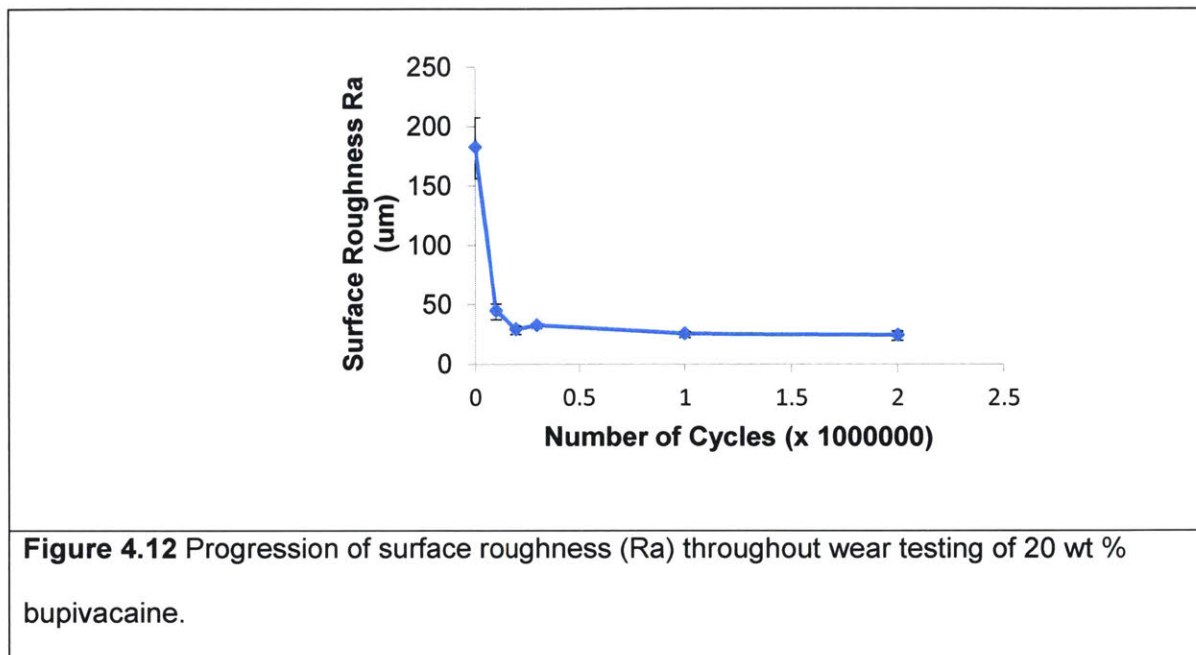


Figure 4.10 Surface texture of 20 wt % Bupivacaine before wear testing (a), 100 k wear test cycles (b), 500 k wear test cycles (c), and 1 million wear test cycles (d). Surface texture was measured using stylus profilometry for area of 1 mm x 1 mm.





Combination of Micropatterns with Previously Developed Method to Reduce Wear Rate of UHMWPE

To test whether combination of micropatterns can be combined with other methods to reduce the wear rate of UHMWPE synergistically, we combined four previously reported methods to reduce friction and/or wear (SLIPS, radiation crosslinking, MPC, and benzophenone crosslinking) with Bupi-PE. Combination of the micro-texture with chemical methods of wear rate reduction, showed significantly lower wear rates than the corresponding chemical method alone (**Figure 4.13**).

The percent wear rate reduction of UHMWPE due to the combination of MPC grafting and micropatterning are the highest compared to other combined methods (83 % for MPC vs MPC+Micropattern, 69% for Flat vs micropattern, 56 % for 75 kGy vs 75 kGy+Micropattern, and 44 % for SLIPS vs SLIPS+Micropattern). Further surface analysis of the MPC+Microtexture

surface using Energy dispersive X-ray spectroscopy (EDAX) (Figure 4.14, Figure 4.15) showed higher concentration of both phosphorous and nitrogen in the pores, indicating the presence of polymerized MPC imbibed into the valley of the microtextures and into the pores in between the UHMWPE granules.

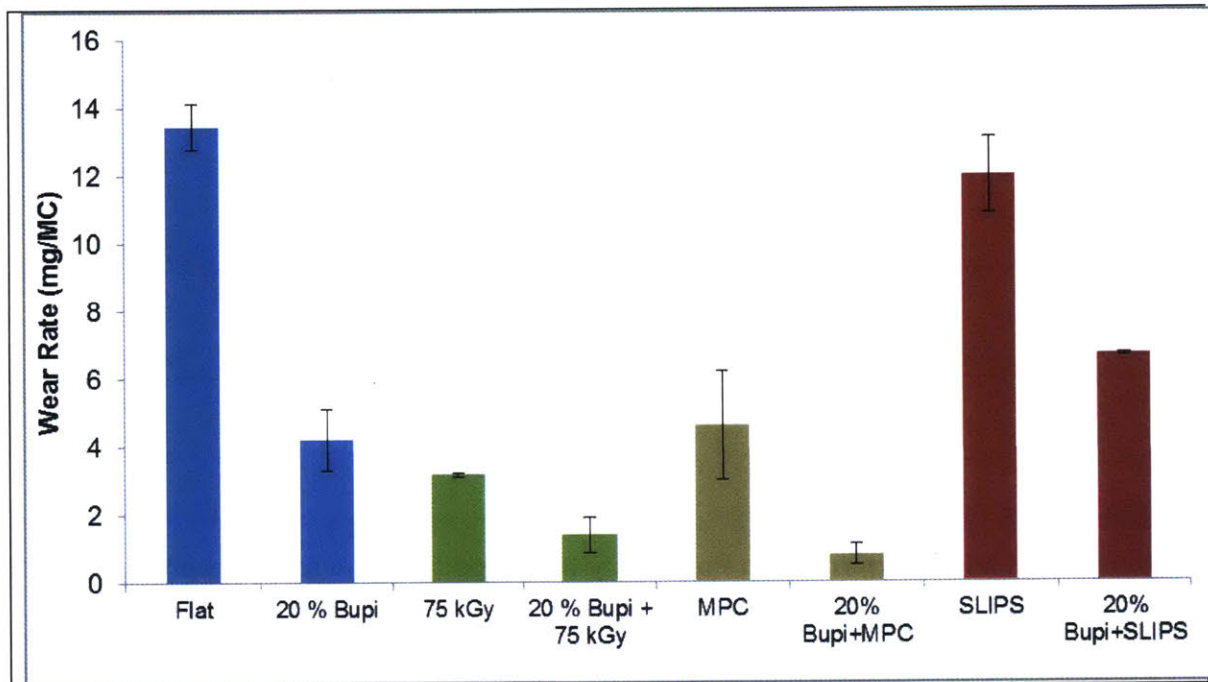
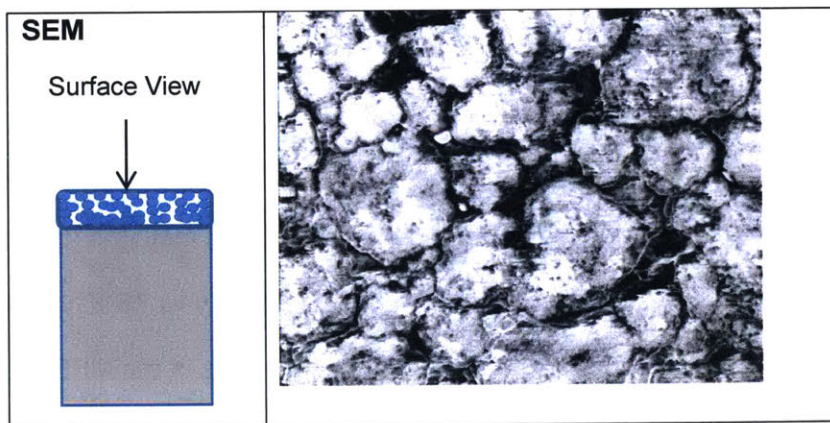


Figure 4.13 Wear resistance of flat UHMWPE with various chemical treatments to reduce wear rate (75 kGy, MPC, and SLIPS) alone, and combined with microtextured UHMWPE obtained from pre-eluted Bupi-PE.



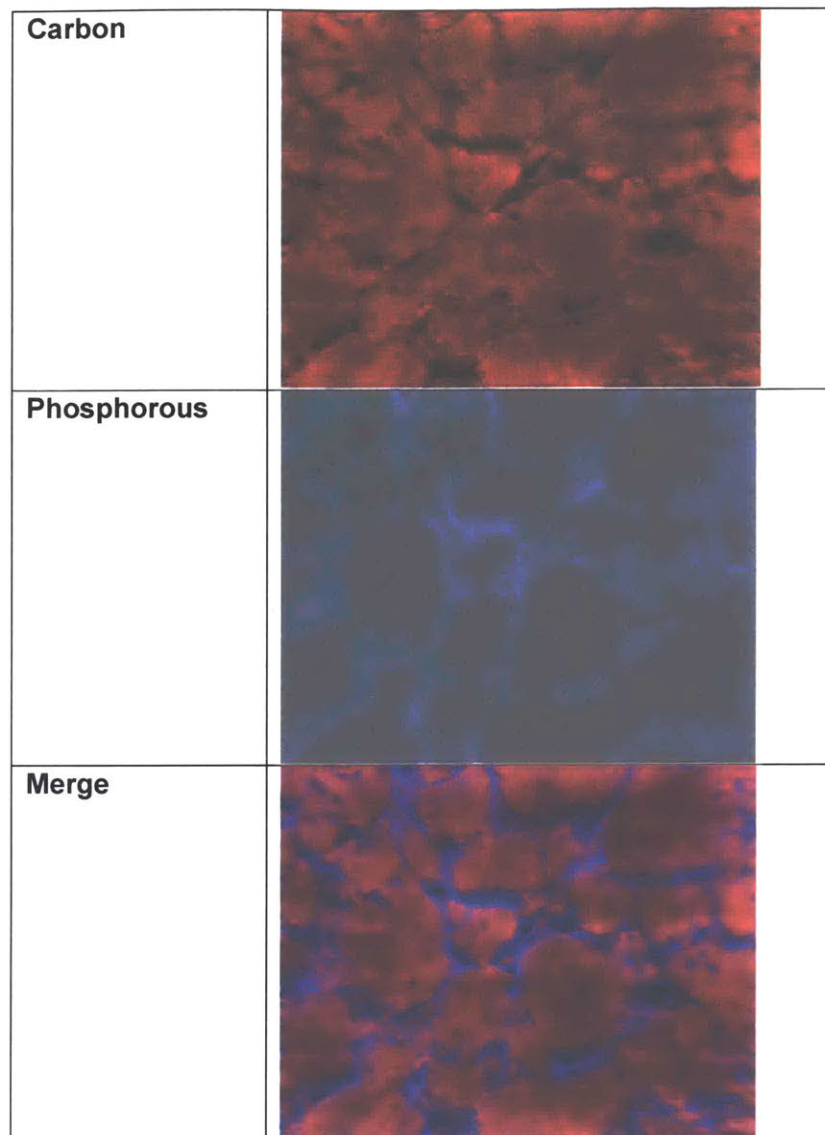
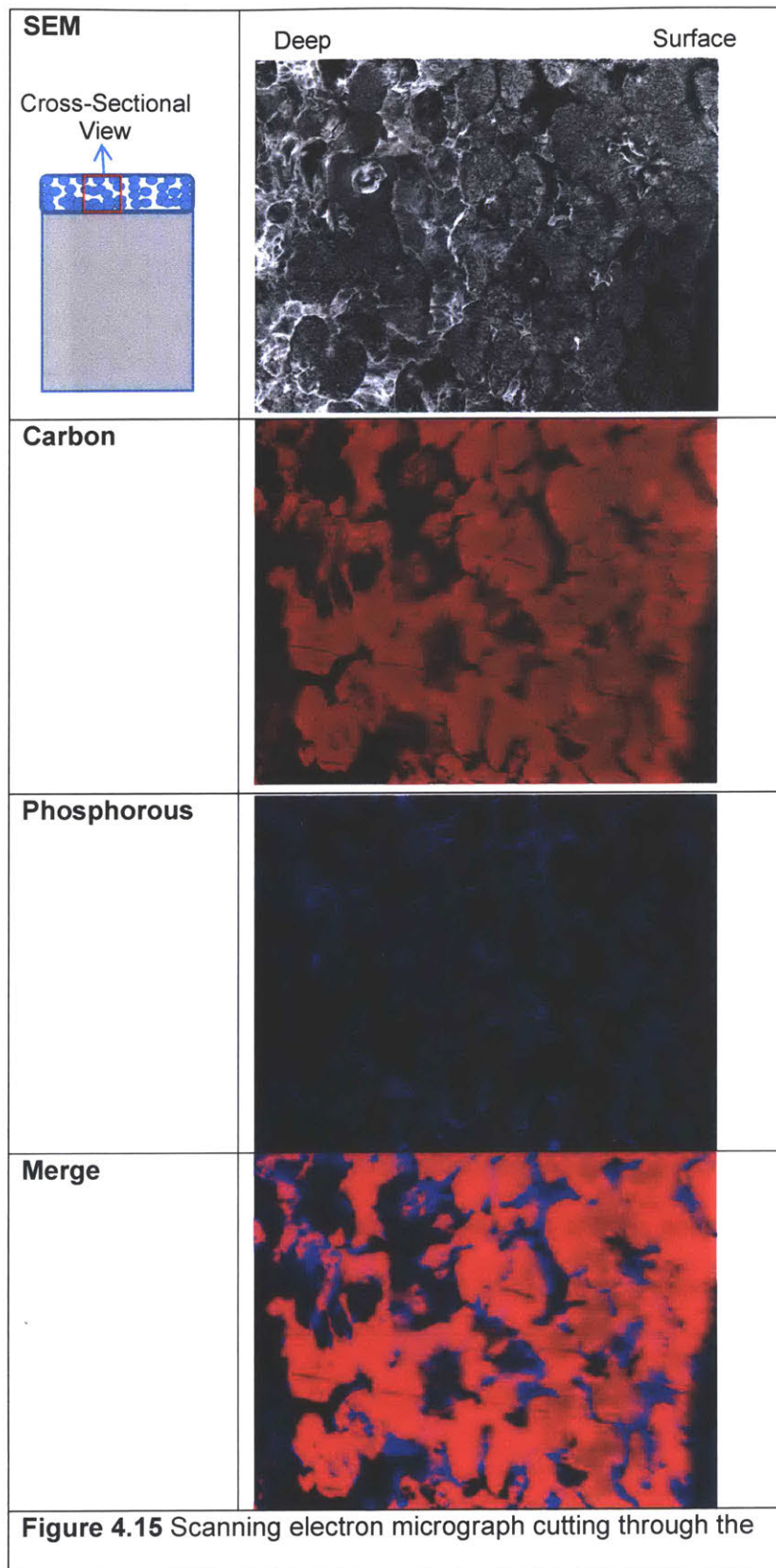


Figure 4.14 Scanning electron micrograph of the surface of the sample and the corresponding EDAX carbon, phosphorous mapping and the carbon-phosphorous merge of the surface of MPC+20 % bupivacaine UHMWPE.



thickness of the sample and the corresponding carbon and phosphorous mapping, and the carbon-phosphorous merge of the surface of MPC + 20 % bupivacaine UHMWPE .

Effect of Irradiation Dose on the Wear Rate of MPC+Bupi-PE UHMWPE

To test the efficacy of wear rate reduction of combined microtexture with irradiation, microtextured-UHMWPE made by loading 20 wt% bupivacaine HCl or 20 wt % MPC oligomer were exposed to various doses of irradiation. Bupivacaine was chosen because it does not possess any functional groups such as alkene, allene, amine, or hydroxyl groups that can make it prone to free radical-initiated grafting onto the UHMWPE chain. On the other hand, MPC oligomers contains an acrylate group which is prone to form free radicals and be grafted onto UHMWPE ([398]).

In general, irradiated bupivacaine-eluting or MPC containing UHMWPE displayed lower wear rate than the corresponding irradiated UHMWPE without the treatment (0% bupivacaine or 0 % MPC) (**Figure 4.16 and 4.17**). This benefit decreased as irradiation dose increased (**Figure 4.18**). Comparing bupivacaine and MPC-containing UHMWPE at the same irradiation dose, larger wear rate reduction was observed with the bupivacaine-UHMWPE. At 75 kGy irradiation dose, significant wear reduction was observed in bupivacaine-UHMWPE as compared to the untextured UHMWPE, but the wear difference in the MPC-UHMWPE was insignificant (**Figure 4.16 and 4.17**).

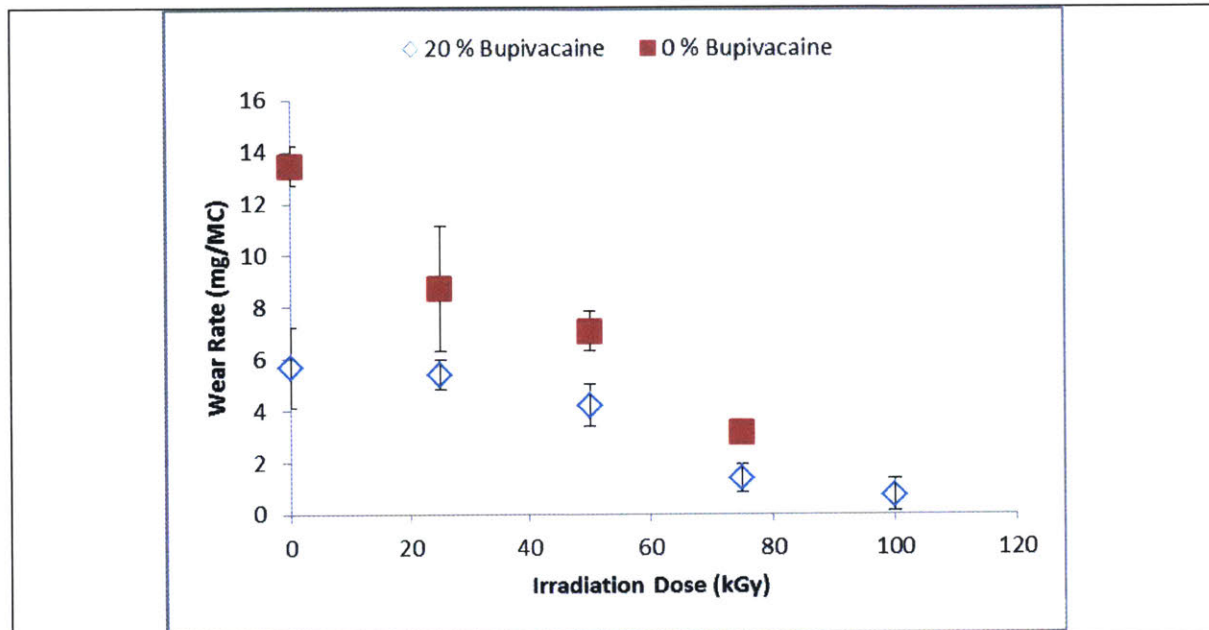


Figure 4.16 Wear rate of Bupi-PE and UHMWPE without bupivacaine irradiated at 0, 25, 50, 75 and 100 kGy .

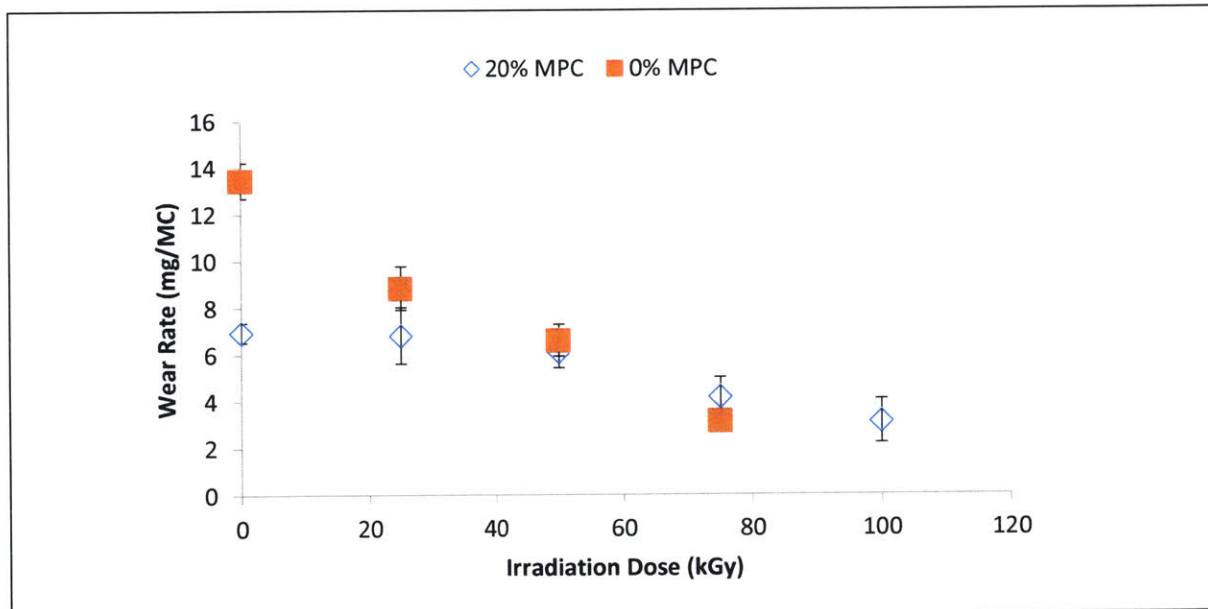
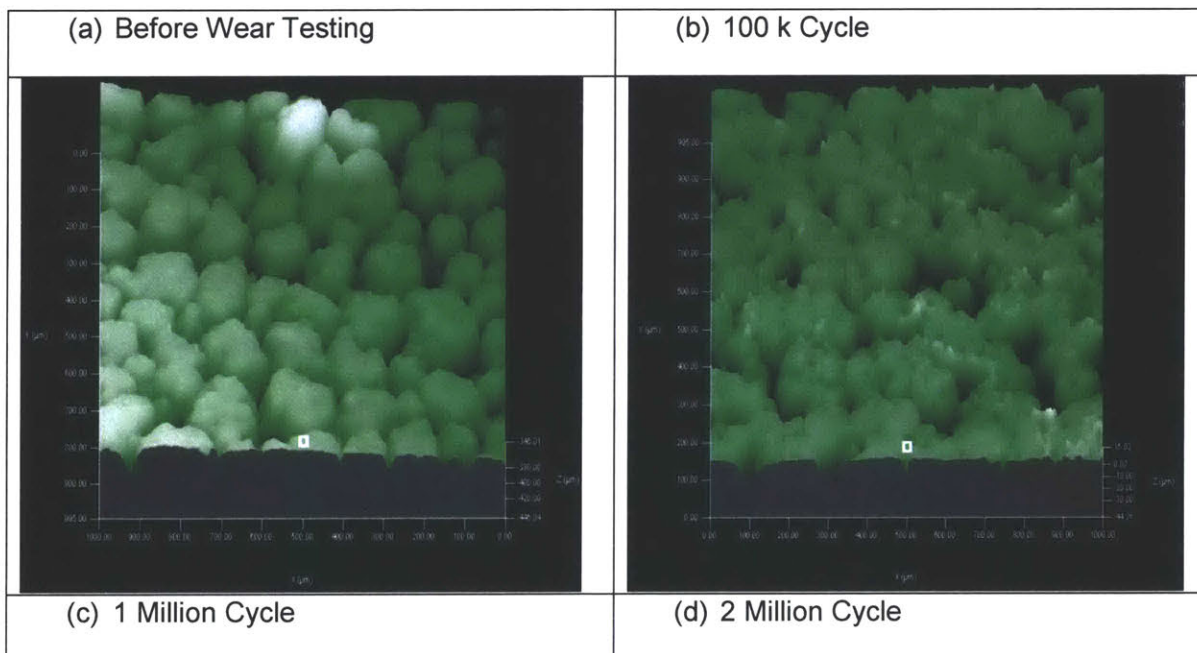


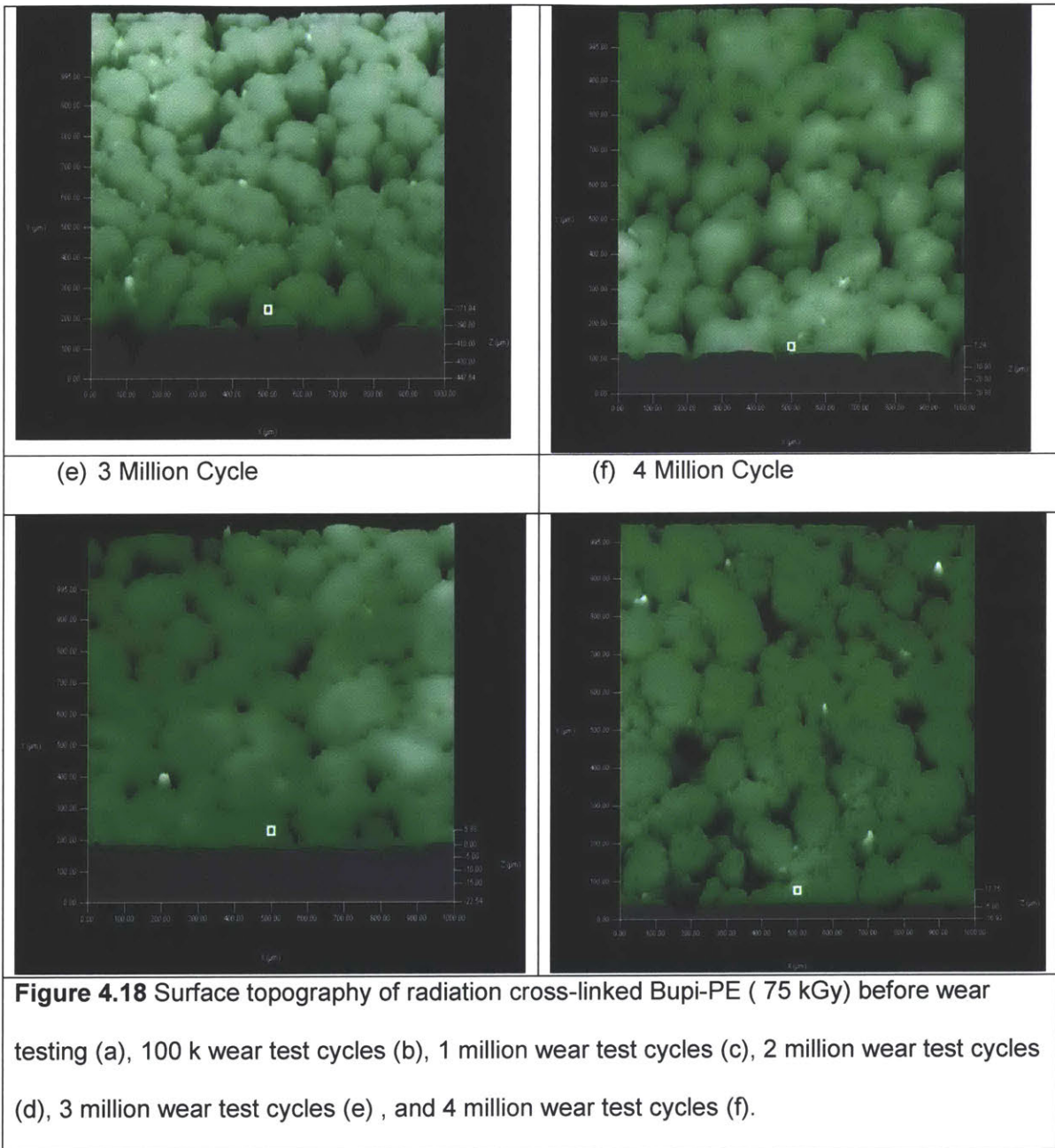
Figure 4.17 Wear rate of 20 % MPC and normal UHMWPE (0% MPC) irradiated at 0, 25, 50, 75 and 100 kGy .

Evolution of Surface Roughness of Combined Crosslinked and Bupivacaine Eluting UHMWPE (Bupi-PE) Throughout Wear Testing

In order to study the surface topology evolution of 75 kGy crosslinked bupivacaine-eluting UHMWPE throughout wear testing, we analyzed the surface topography and roughness with stylus profilometry and AFM respectively.

After 100,000 cycles, peaks of the microtextured surface become flatter and smoother (**Figure 4.18 a-b**). The valleys, while becoming slightly narrower, were still clearly defined and were not covered by the UHMWPE granules. No further flattening or smoothing was observed on further wear testing (1 million-4 million cycle, **Figure 4.18c-f**). Deeper analysis of the surface roughness using AFM also showed that the surface roughness rapidly declined within the first 100k cycle, and stayed relatively constant throughout the test, staying at 36.6 ± 2.1 nm (**Figure 4.19, Figure 4.20**).





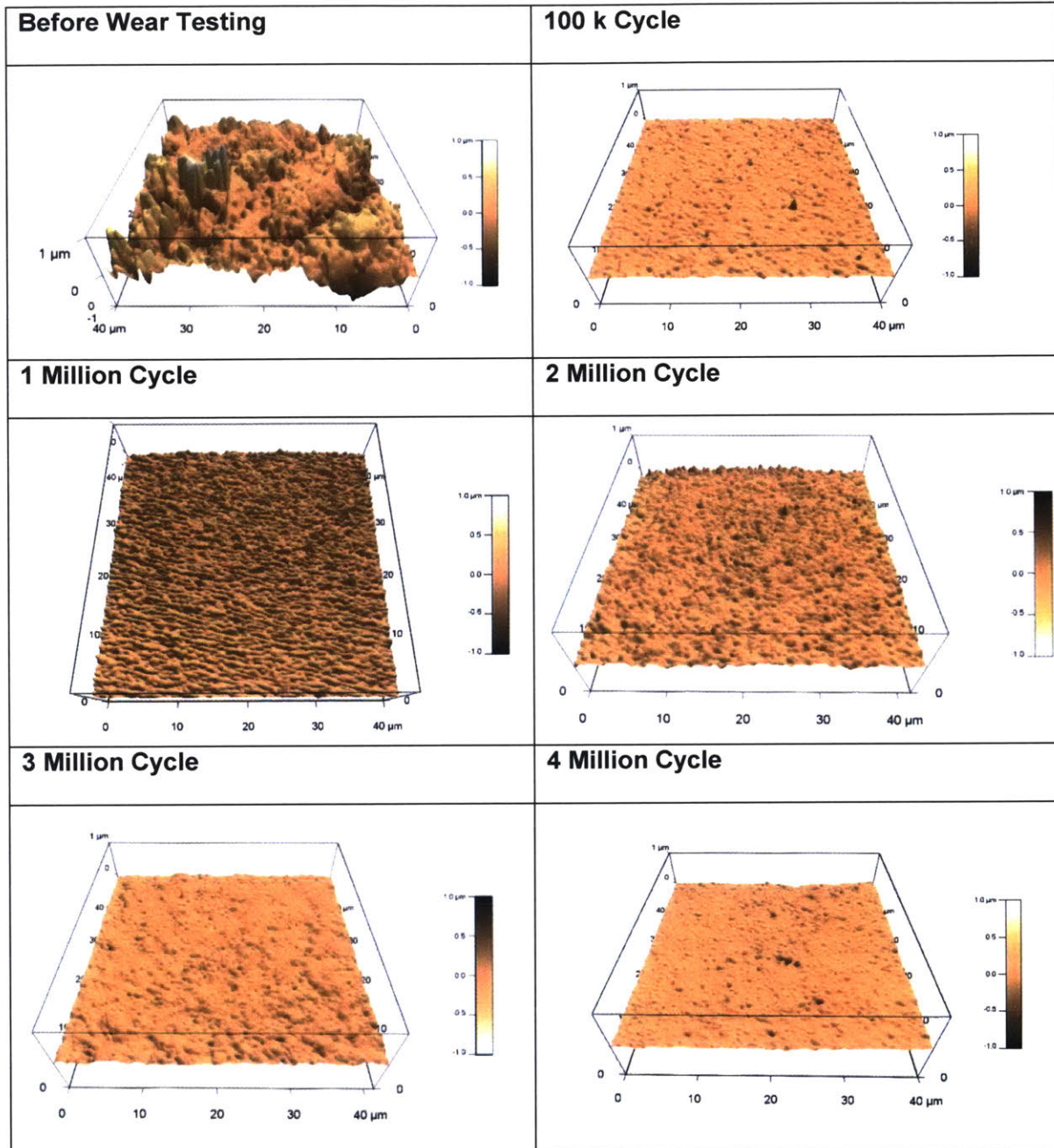
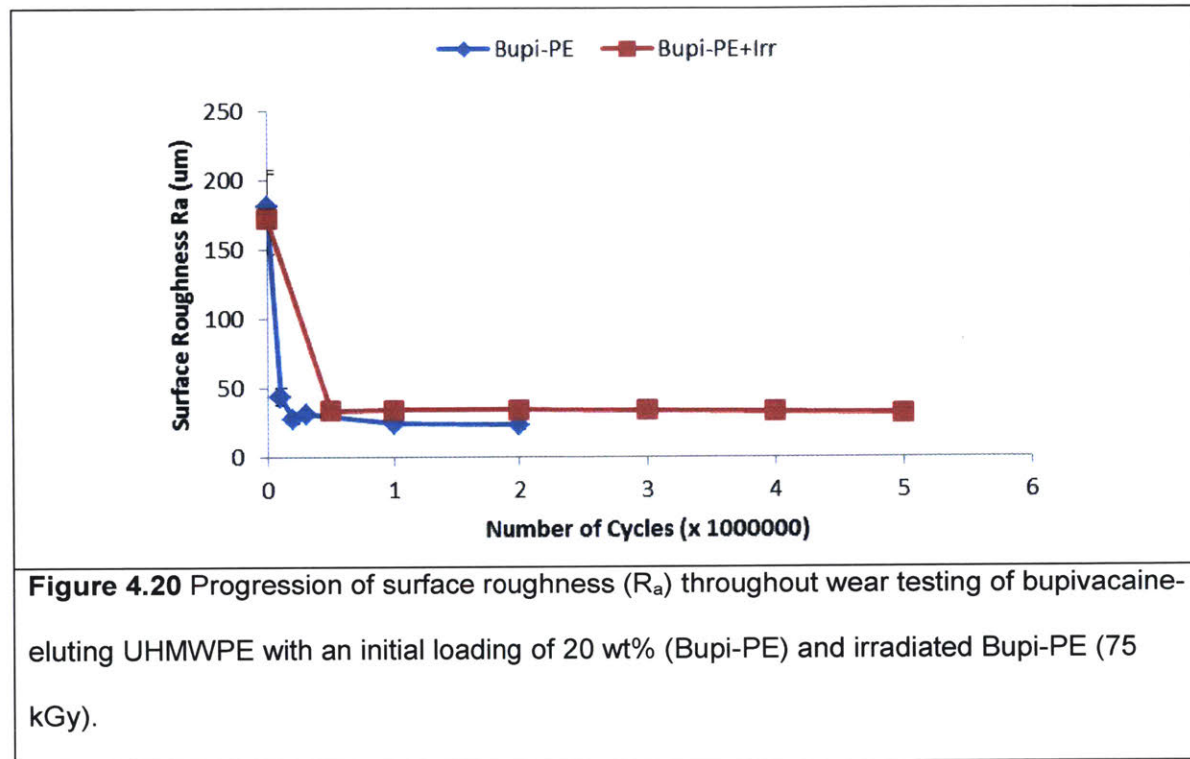


Figure 4.19 Surface roughness of radiation crosslinked Bupi-PE (75 kGy) before wear testing (a), 100 k wear test cycles (b), 1 million wear test cycles (c), 2 million wear test cycles (d), 3 million wear test cycles (e), and 4 million wear test cycles (f).

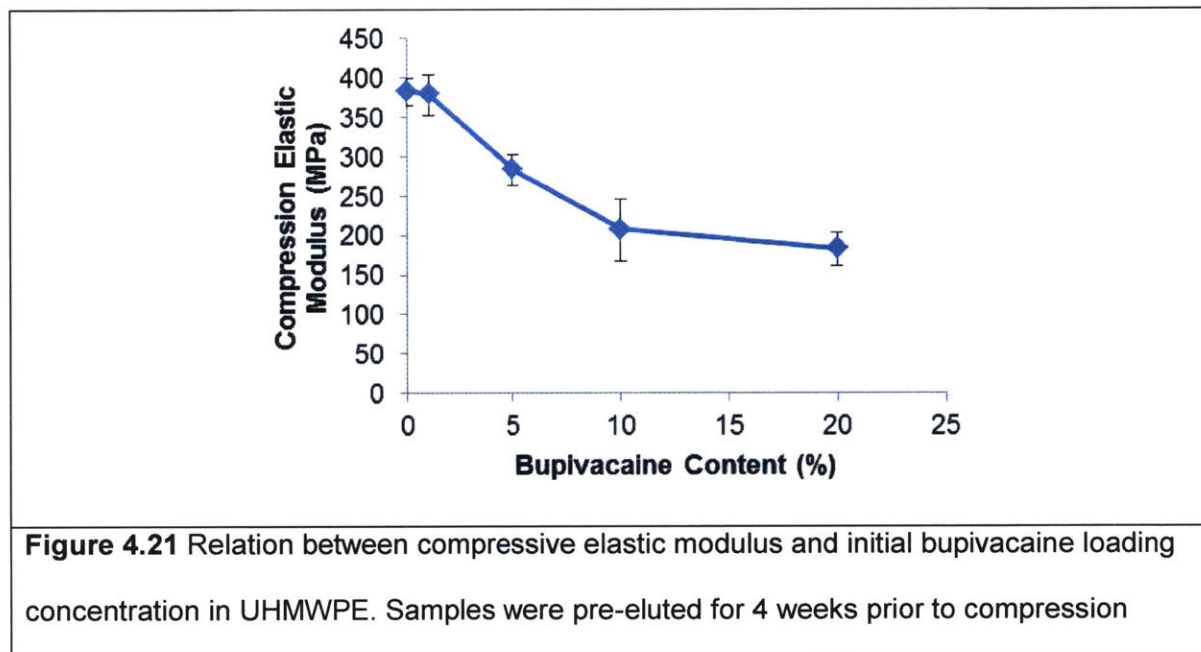


Mechanism of Wear Reduction in Microtextured UHMWPE

We performed three types of mechanical testing under static compression, cyclic compression, and under compression in lubricants combined with fluorescence imaging to understand the mechanism of wear reduction by the micro-textured and porous surface. The static compression test was conducted to determine the modulus of elasticity between bupivacaine-eluting UHMWPE as a function of initial drug loading. The cyclic compression test was conducted to examine the cyclic or dynamic behavior of Bupi-PE in comparison to UHMWPE without bupivacaine loading. Finally, compression in lubricants combined with fluorescent imaging was conducted to examine the surface extrusion of lubricants during loading and unloading cycles.

Both the cyclic and the static (**Figure 4.21** and **4.22**) compression of Bupi-PE showed significantly and consistently lower stiffness than that of flat material without bupivacaine loading.

Dipping of Bupi-PE in fluorescent dye containing lubricant showed positive fluorescence in the valleys of the microtexture, indicating entrained lubricant (**Figure 4.23**, 0 MPa Bupi-PE). Subsequent compression of the material showed an increased area of positive fluorescence, particularly originating from the valleys, indicating extrusion of lubricant from the compressed pores below the micro-textured surface (**Figure 4.23**, 8 MPa Bupi-PE). On the other hand, dipping of the flat material in fluorescent dye with or without compression showed minimum fluorescence, indicating absence of entrained lubricant. These observations strongly suggest that under compression, microtextured UHMWPE extrudes lubricant (weeping lubrication) and contributes to increasing the lubrication film thickness, further decreasing the likelihood of asperity contact and associated wear (**Figure 4.23**).



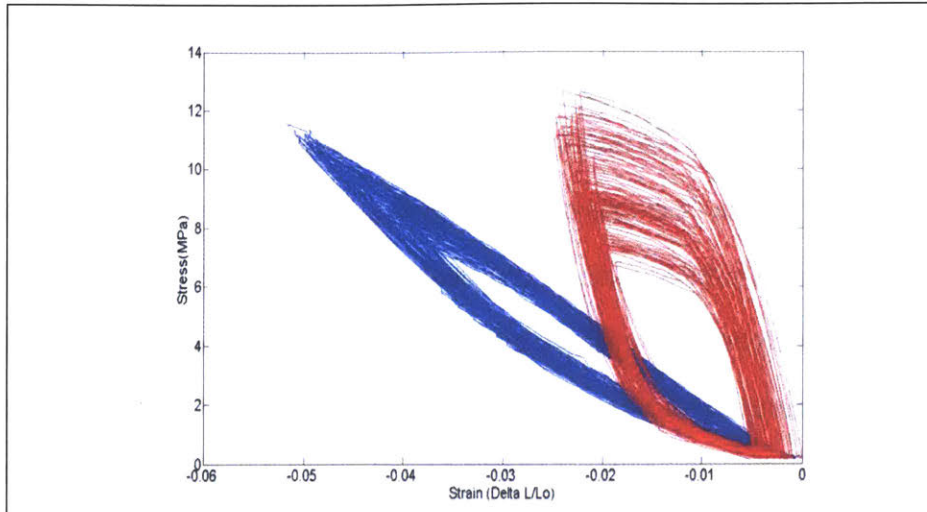

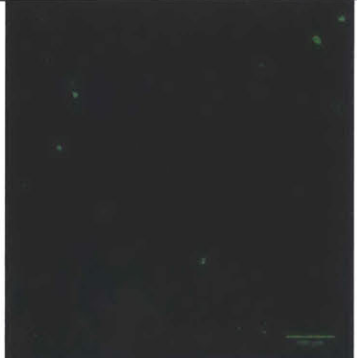


Figure 4.22 Representative stress-strain curves of cyclic compression test (100 cycles total) with peak load of 12 MPa. Red = Bupi-PE, and Blue = UHMWPE.

UHMWPE-0 MPa	UHMWPE-8 MPa
	
Bupi-PE-0 MPa	Bupi-PE-8 MPa

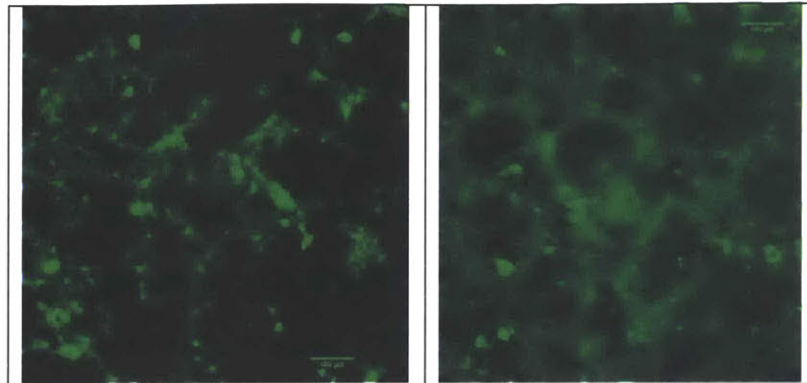


Figure 4.23 Fluorescence microscopy of surface of UHMWPE and Bupi-PE under no compression (0 MPa) and compression (8 MPa). Black indicates area with no fluorescent lubricants (polymer area), green indicates area containing fluorescent lubricants.

Computational Simulation of Lubrication Film Thickness of Microtextured and Flat UHMWPE

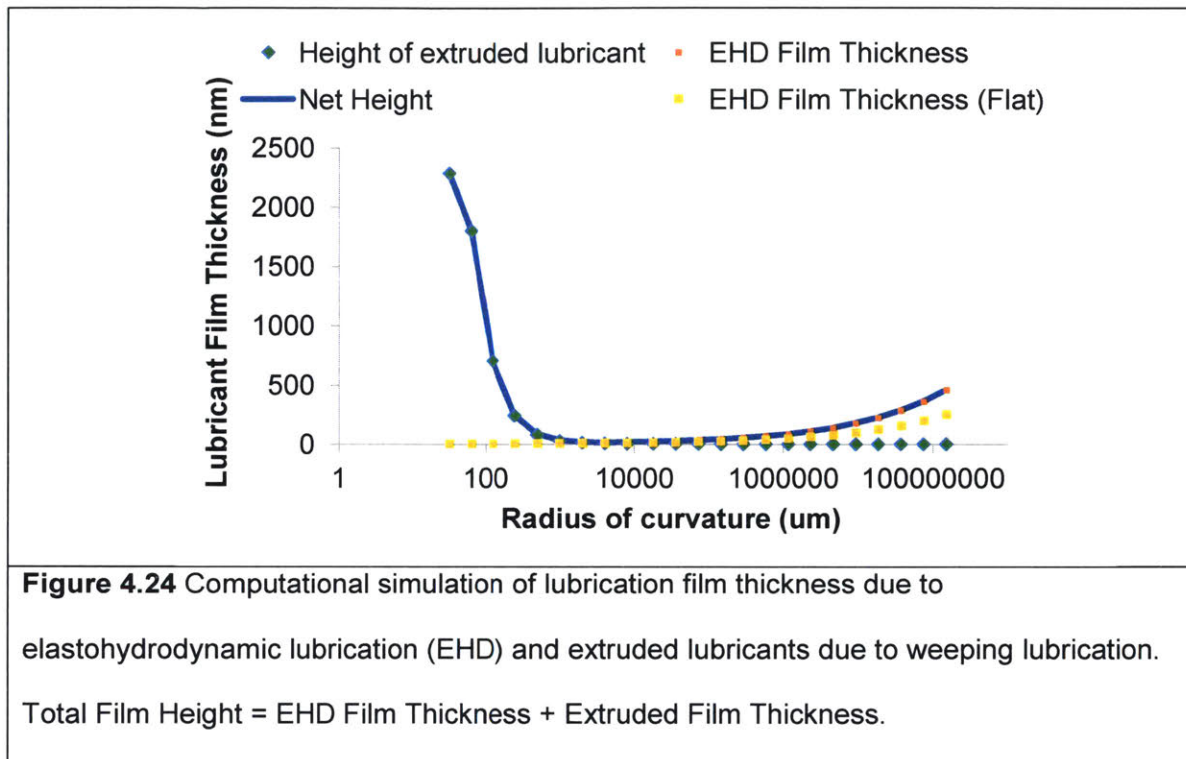
We also performed computational simulations to assess the contribution of elastohydrodynamic lubrication and weeping lubrication mechanisms to the overall lubrication film thickness. For simulation of elastohydrodynamic lubrication, we used isoviscous-elastic equation [394] (**eq 1**), where H_{EHL} is the minimum film thickness, W is contact load (N), U is the entraining surface velocity (m/s), η_0 is the viscosity at atmospheric pressure of the lubricant (Pas), E' is the reduced Young's modulus, R' is the reduced radius of curvature, and k is the eccentricity. For simulation of weeping lubrication, we used the contact mechanics of a ball on a flat surface with the assumption of incompressible lubricants (**eq 2**), where H_{ext} is the height of lubrication film due to extruded lubricants and δ is maximum deflection of the ball. We

approximated the overall lubrication film thickness as the sum of lubrication film due to elastohydrodynamic lubrication and due to extruded lubricants ($H_{min} + H_{ext}$).

$$H_{EHL} = 8.70 \left(\frac{W^{\frac{8}{3}}}{U^2 \eta_0^2 E'^{\frac{2}{3}} R'^{\frac{2}{3}}} \right)^{0.67} (1 - 0.85 e^{-0.31 * k}) \quad (1)$$

$$H_{ext} = \frac{\pi * \delta \sqrt{\delta(2R' - \delta)}}{R'^2}, \delta = 1.0397 \left(\frac{W^2}{E'^2 R'} \right)^{\frac{1}{3}} \quad (2)$$

Our computational simulation showed that the decrease in the radius of curvature of the polymer spheres increased the contribution of the extruded lubricant to lubrication film thickness while decreasing the contribution of the elastohydrodynamic lubrication (**Figure 4.24**). When compared to the flat surface, the microtextured surface had a thicker total lubrication film thickness, especially at regions where polymer granules had a higher radius of curvature (**Figure 4.24**). This is presumably due to the deformed polymer granules having a lower radius of curvature, under which conditions there is an increased amount of extruded lubricants (**Figure 4.24**). Decreased stiffness (E') on MTPS also resulted in a thicker lubrication film due to elastohydrodynamic lubrication, which can reduce asperity contact. Overall, our computational simulation showed that the decreased stiffness and extruded lubricant due to deformation of the pores of MTPS resulted in overall increased lubrication film thickness compared to the flat surface. The increased lubrication film thickness, in turn, would decrease the likelihood of asperity contact and decrease contact stress[399].



Discussion

Elution of the loaded drugs out of UHMWPE resulted in microtextures consisting of valleys surrounding the UHMWPE granules. Increasing the concentration of drugs increased the interconnectivity between the drug clusters until reaching complete interconnectivity (**Figure 4.1** and **Figure 4.6**). When the empty valleys are fully interconnected, they form a honeycomb frame that completely surrounds UHMWPE (**Figure 4.6**). We hypothesized that in the presence of lubricants, these valleys will be filled with lubricants that can be extruded out when the surface is exposed to mechanical stress and therefore are expected to have lower wear than flat untextured UHMWPE. This hypothesis was proven by showing that the wear rate of these microtextured UHMWPE has 50-60% less wear than the untextured flat UHMWPE (**Figure 4.5**). Furthermore, mechanical testing and fluorescent microscopy showed that under compression, Bupi-PE extrudes lubricant (weeping lubrication) and contributes to increasing the lubrication

film thickness, further decreasing the likelihood of asperity contact and, in turn, wear (**Figure 4.22-4.24**). Our computational simulations showed that the decreased stiffness and extruded lubricant due to the deformation of the pores in the Bupi-PE under stress, resulted in overall increased lubrication film thickness.

Wear reduction through lubrication extrusion as observed in this study has some similarity to how cartilage achieves low wear rates [400, 401]. It is generally agreed that the pressurization and flow of interstitial fluid throughout cartilage pores significantly contributes to low wear (13, 14). When cartilage is exposed to compression and shear forces, it deforms anisotropically, with lateral pores deforming to a larger extent than the axial pores (7). As a result, cartilage extrudes interstitial fluid preferentially to the interface, a process known as weeping lubrication, to keep the sliding surfaces apart and protect cartilage from wear (15, 16).

Common chemical methods of radiation or chemical crosslinking of UHMWPE decrease wear due to a decrease in the ability of the polymer to orient [402]. We hypothesized that the wear rate reduction due to the physical microtexturing of the surface with loading bupivacaine could be combined with a chemical method for an enhanced effect. This hypothesis was confirmed for radiation crosslinking, benzophenone crosslinking, SLIPS or 2-methacryloyloxyethyl phosphorylcholine (MPC) grafting (**Figure 4.14**). While radiation and benzophenone cross-linking can reduce wear through decreased orientation, SLIPS and MPC modification of UHMWPE were expected to enhance lubrication and decrease contact between the two articulating surfaces[392, 403]. Especially for MPC-grafting, preliminary results in long-term hip simulator wear testing have shown wear reduction compared to untreated UHMWPE[403]. Energy dispersive X-ray spectroscopy (EDAX) of the MPC grafted microtextured UHMWPE (**Figure 4.15-4.16**) showed high concentration of both phosphorous and nitrogen inside the pores, indicating the presence of polymerized MPC inside the pores. Therefore, the wear rate reduction due to MPC grafting on microtextured surface as compared

to MPC grafting on flat surface (**Figure 4.14**) was potentially due to imbibition of the polymerized MPC into the pores. Imbibition and coating with hydrophilic polymer such as MPC into pores and surface respectively allow better water retention within the polymer, which is crucial in boosting lubrication film thickness and in acting as better boundary lubricants[404]. Using hydrophilic polymer to trap water for better boundary lubricants was also observed in the cartilage where collagen fibrils trap the hydrophilic hyaluronic acid and aggrecan complexes [404]. In the worst case scenario where hydrodynamic, elastohydrodynamic, and weeping lubrication fail, cartilage relies on boundary lubrication that uses a combination of hyaluronic acid, surface active phospholipids, and superficial zone proteins to bind water to act as a boundary lubricant [404].

Interestingly, while irradiation of vancomycin-eluting UHMWPE, Bupi-PE, and MPC-UHMWPE resulted in further decrease in wear rate, the efficacy of irradiation to decrease wear rate decreased as drug content was increased (**Figure 4.3**). The irradiation efficacy decreased to a larger extent in vancomycin-eluting UHMWPE and MPC-grafted UHMWPE than in bupivacaine-eluting UHMWPE (**Figure 4.3, 4.17, 4.18**). This could be due to MPC and Vancomycin-containing molecular moieties that, when irradiated, can form free radicals that may attack UHMWPE chains [398, 405] (MPC has an acrylate group, and vancomycin has a phenolic-OH group). Therefore, the irradiation efficacy was greatly decreased when the drugs contain molecular moiety that can react with free radicals on UHMWPE chains and prevent the UHMWPE from crosslinking to each other.

Surface topology analysis showed that after one hundred thousand cycles of articulation during wear testing, the peaks of the microtexture showed deformation as indicated by significantly flatter and smoother features (**Figure 4.11 and 4.19**). The deformation of the microtexture resulted in the increased radius of curvature of the UHMWPE granule, which, based on our computational analysis (**Figure 4.25**), resulted in lower overall lubrication film

thickness through changes in the radius of curvature of the surface, despite still showing microtexture features and a significant reduction in wear rate.

When the micro-textured material was irradiated for cross-linking, the crosslink between UHMWPE chains resulted in UHMWPE granules being to be less prone to plastic deformation under stress as indicated by much smaller changes in valley width and peak flatness with wear testing (**Figure 4.19**). Based on our computational analysis, surfaces with better preservation of the original polymer granule radius of curvature, as found in these samples, resulted in thicker lubrication film thicknesses and therefore smaller changes in surface roughness. AFM analysis of the surface roughness of Bupi-PE and crosslinked Bupi-PE materials during wear testing confirmed this observation (**Figure 4.21**). Therefore, micro-textured UHMWPE is more likely to preserve the shape and size of the microtexture, and thicker lubrication film can therefore be obtained throughout wear testing (as compared to uncrosslinked microtextured samples) , resulting in reduced asperity contact and overall lower wear rate.

Conclusion

In conclusion, we have showed that the microtextures achieved by mixing of ultra-high molecular weight polyethylene (UHMWPE) powder with model porogens such as bupivacaine reduces wear rate through lubricants extrusion and increased elastohydrodynamic lubrication. In addition, the microtextures provided orthogonal and synergistic methods to augment chemical processes (such as crosslinking and polymer grafting) to reduce UHMWPE wear rate. We anticipate that this method is generalizable to other polymer systems because it is based on a physical change to the surface that is independent of polymer structure.

Chapter 5

Drug Eluting UHMWPE with Highly Eccentric Drug Cluster Morphology for the Treatment of Prosthetic Joint Infection

Introduction

In this chapter we will use our knowledge regarding drug elution, mechanical strength, and wear resistance of highly eccentric drug eluting UHMWPE to create the optimum material for fully functional prosthetic joints. We will analyze the in vitro antibacterial activity, mechanical strength, and wear resistance of our optimized material and compare it against the goldstandard antibiotic-eluting bone cement.

Gram-positive bacteria accounts for 80% of all PJI cases

More than half of periprosthetic joint infections are caused by *S aureus* and coagulase-negative staphylococci ([406, 407], **Table 5.1**). In addition, gram-positive bacteria (including *Staphylococcus*, *Enterococcus*, *Streptococcus*) cause close to 80 % of all prosthetic joint infection, while gram-negative bacteria (including *Pseudomonas*, *Escherichia coli*, *Enterobacter* spp, *Proteus* spp) cause close to 20 % of prosthetic joint infection [407]. Infection by methicillin-resistant *S. aureus* (MRSA) and methicillin-resistant *S. epidermidis* result in the least successful outcomes with 24-40 % reinfection rate [408, 409]. Infection with MRSA decreases the success rate of prosthetic joint infection treatment by about 5 times (89% in methicillin sensitive *Staphylococcus* vs 18 % in methicillin resistant *Staphylococcus*)[410].

In explanted components of prosthetic joints, the highest bacterial loads were found in the UHMWPE components (tibial insert of the knee and acetabular liner of hip), followed by the metal components (tibial tray and femoral component for knee, acetabular cup, femoral head and femoral stem for hip) [101, 102]. In patients with prosthetic joint infections, bacteria can be found in the intraarticular space and at the bone-prosthesis interface ([411]. Therefore, successful treatment of prosthetic joint infection requires eradication of bacteria in both the intraarticular space as well as at the bone-prosthesis interface.

<u>Source</u>	<u>State/Country</u>	<u>MSSA (%)</u>	<u>MRSA (%)</u>	<u>Coag neg Staph (%)</u>
New York Hospital Acquired Infection Report 2011[412]	New York, USA	24.8	24.5	15.8
Salgado et al. 2007. Clin Orthop Relat Res, 461:48-53[406]	Charleston, USA	24	9	N/A
Peel, Trisha. 2012. Antimicrobial Agents and Chem. 56:2386[413]	Melbourne, Australia	26	30	24
Lora, J et al. 2013. Clinical Infectious Disease, 56: 182-194[414]	Spain	76.5 % (of all S. Aureus)	23.4 % (out of all S. Aureus)	N/A
Lindeque, B et al. 2014. Orthopedic, 37:257-265[415]	Meta Analysis (2001-2011)	32	20	20
Kaminski, A et al. 2014. Orthop Traumatol Rehabil. 16:11-16[416]	Bochum and Sande, Germany	49	19	N/A

Post, V et al. 2014. Int. J. Medical. Microb. 14:24[417].	France and Switzerland	83 % of all S. Aureus	17 % (out of all S. Aureus)	N/A
Mashfiqul, M et al. 2013. J of Arthroplasty, 28:44-46[418].	Singapore	N/A	44	N/A
Giulliana et al. 2008. Le Infezioni in Medicina, 204-208[419]	Italy	20	17	36
Moran, E et al. 2007. J Infect, 55:1-7[420]	Oxford, UK	44	8	47
Trampuj, A et al. 2005. Swiss Med Wkly; 135: 243-251[421]	Basel and Liestal, Switzerland	12-23 (MRSA +MSSA)		30-43
Table 5.1. Type of Bacteria found in PJI patients reported from previous literature				

Antibiotic Penetrates Poorly to the Infected Joints and Bone

Antibiotic penetration into the synovial fluid and joint space from intravenously or intramuscularly administered antibiotics are primarily determined by the serum antibiotic concentrations and serum-to-bone antibiotic ratio [422]. Most antibiotics have a bone to serum concentration ratio of 0.05-0.2 except a few antibiotics such as rifampin, doxycycline, levofloxacin, and cefepime which have a ratio close to 1:1 [423]. In addition to the poor bone penetration, some antibiotics such as gentamicin penetrate even less in infected joints than in normal ones [422]. Because of the poor penetration of most antibiotics into bone and the joint space, their local concentrations are not sufficient to eradicate bacteria, as shown by the relatively low cure rate of joint/bone infections in patients treated solely with systemic antibiotics (mean = 78 %, range:54-94 %) [423] Debridement, implant retention, and systemic antibiotic

treatment of 91 PJI patients resulted in treatment failure in 53 patients (58 %) within a follow up period of 700 days [424]. In another study of 33 PJI patients treated with debridement, implant retention, and systemic antibiotics, there were 1-year and 2-year cumulative probabilities of treatment failure of 54 % and 69 %, respectively [425].

In a study focusing on the efficacy of intravenous vancomycin [426] for treatment of 81 patients with hardware-associated osteomyelitis infections were successfully eliminated in only 44 patients (54 % success rate). As a comparison in the same study, treatment of patient with bloodstream infections, pneumonia, and endocarditis achieved 84-88 % success rates. Because of the low antibiotic penetration into the infected bone and joints, local and sustainable delivery on antibiotics into the infected area is likely a limiting parameter for eradication of infection. These studies also suggest that using the current treatment algorithms place the patients at a considerable risk for persistent infection.

Previously Reported Antibacterial Materials to Address Orthopaedic-Associated Infections

One of the primary strategies to overcome low systemic antibiotic penetration is to deliver antibiotics locally by incorporating therapeutic agents into the orthopaedic implants [427-429]. Considering clinically available materials and materials in development for prophylaxis or treatment of orthopaedic associated infections, two general strategies are most commonly used: antibacterial coating on orthopedic implant and drug eluting antibacterial implant.

In the antibacterial coating strategy, drug eluting polymer, antibiotics, or other antibacterial agents are chemically or physically bonded to the surface of the existing implant to cover the entirety of the material with the antibacterial coatings[430]. In order for coating to be successful, it needs to be effective in eradicating bacteria, be biocompatible, to not inhibit any

healing process, and be able to withstand the mechanical stress during implantation process and *in vivo* without unintentionally debonded from the surface of the implant[430]. However, most of the strategies developed so far fail in one of those parameters and therefore prevent it from being used clinically. For example, gentamicin-eluting poly-lactic acid acid was introduced as a coating for intramedullary nails as prophylaxis against deep surgical infections involving intramedullary nails[431]. However, the antibiotic concentration eluted is not sufficiently high for treatment of orthopaedic infections [432]. Furthermore, the press fitting procedure during implantation of joint prosthesis will likely remove the coating due to shear force[432]. In another example, vancomycin grafted on metal surface of orthopedic implants has been shown to be effective in preventing bacterial colonization both *in vitro* and *in vivo*[433]. However, this method is unsuitable as treatment of infection because it is only effective in eradicating bacteria that are in contact with the surface of the implant, while most infections usually involve also involve bacteria that are not in direct contact with the implants[64].

Several non-coating implant materials have also been previously reported for orthopaedic-associated infections, including poly methyl-methacrylate as antimicrobial eluting beads or spacer [9, 294, 429], resorbable ceramics as antimicrobial eluting beads [434], and resorbable polymeric beads (composed of poly(DL-lactide):co-glycolide) as antimicrobial eluting beads [435]. However, their usage in clinical situations have been largely impeded by toxic degradation products [7], insufficient drug release [8], insufficient mechanical strength [9], and difficulty in consistent large scale manufacturing [10].

Two-Stage Implant Exchange as State-of-Art Treatment of PJI

Partly due to the low success rate of alternatives such as debridement/lavage and single stage exchange, the current gold standard for prosthetic joint infection management is the

lengthy 2-stage implant exchange. In the 1st surgery the infected hardware is removed, the joint undergoes a debridement and lavage protocol to remove infected tissues and fluids to the best of the surgeon's ability, and antibiotic-eluting polymethylmethacrylate (PMMA) spacers are placed. Antibiotic-eluting bone cement and intravenous antibiotics are used for at least 6 weeks [136], after which the administration of antibiotics are eliminated for at least 2 weeks to confirm that no re-infection has occurred. After the confirmation of infection cure by cultures, a 2nd surgery is performed where new components are implanted in the patient. For *Staphylococcal* PJI, in addition to the 6 weeks of intravenous antibiotics during the treatment period, oral 350-450 mg rifampin is recommended twice daily followed by rifampin plus a companion oral drug (e.g. ciprofloxacin, levofloxacin) for a total of 3 months for total hip arthroplasty infection and 6 months for a total knee arthroplasty infections [136]. In some cases, where patients are unsuitable for further exchange revision, exchange arthroplasty or amputation, indefinite chronic oral antibiotic suppression consisting of cephalexin, dicloxacillin, co-trimoxazole, minocycline, or rifampin are used [136].

Despite the elaborate treatment protocol involved in the 2-stage implant exchange, 8.8 % (CI: 7.2-10.6 %) of knee PJI patients (comprising of 5,552 participants with 667 reinfection) have recurrent PJI [436]. Reinfection rate of 2-stage hip implant exchange ranges from 8.3 % to 17 % [437, 438]. While the number of patients with PJI are small (~1%) compared to the very large cohort of patients undergoing total joint arthroplasty each year, re-infections account for a fraction of these (~30%), the cure rate of PJI decreases with each re-infection [4], and the consequences can become very dire. In the end, 20-60 % of patients with recurrent PJI had to undergo arthrodesis and 17-20% had to undergo amputation [6, 439-441], with overall mortality rate of 2.5 %. A treatment with more sustained local delivery of antibiotics would be expected to not only improve cure rates of PJI in 2-stage treatment, but may reduce the incidence of recurrent infection in less cumbersome single-stage surgery with improved overall outcomes.

Complications of PMMA Bone Cement Spacer as Local Antibiotic Delivery System

Existing solutions fall short of addressing both the requirement of mechanical strength for prosthetic joints and effective drug elution to address the infection. Antibiotic eluting PMMA spacers (antibiotic eluting bone cement, BC), the only drug eluting polymer clinically available for partial load bearing and part of the two stage treatment have complication rates of 26-60 % within 49-54 months [9, 300], mainly due to dislocation (11-17 %) and PMMA fracture (10-14 %). Firstly, PMMA spacers are only indicated for short term use during treatment without normal weight bearing and articulation; PMMA is brittle and has low initial tensile and impact strength [442, 443], and is therefore unsuitable for prosthetic joints [311, 444-446]. In the cases where there were high incidences of fracture, the PMMA spacers were left in the patient for several months to years (> 180 days) because the 2nd stage surgery could not be performed [9, 447, 448]. High incidence of antibiotic eluting bone cement (BC) fracture is also likely due to its significantly sacrificed mechanical strength due to the high initial drug content required to elute antibiotic effectively [449, 450].

Drug content in BC has to be high because the incorporated drugs have limited accessibility from the implant surface [451] [452]. Even at 15 wt% drug content (which is the highest drug content possible due to mechanical strength limitations), the drug cluster interconnectivity is poor [294, 295]. Comparing BC with other previously reported drug-eluting polymer systems with similar drug cluster shape (spherical, low eccentricity) [294, 295], 40-60 % (w/w) drug content in the polymer is required to reach complete interconnectivity. As a result of this interconnectivity, only a fraction of drugs incorporated into the polymer can be released; multiple in vitro studies [453-456] and in vivo studies [457, 458] showed that only 5-8 % of the antibiotics incorporated into the bone cement are eventually released. Antibiotic elution from

bone cement was shown to drop to sub-effective levels within 48-96 hours post-implantation [459, 460]. This period may not be sufficiently long to completely eradicate bacteria in the joint space. In addition to the poor sustainability of antibiotic elution, bacteria adhered to the bone cement surface form biofilm when antibiotic elutions fell below effective levels [460]. Exposure of adherent bacteria to sub-effective dose of antibiotics is one factor leading to the development of antibiotic-resistant bacteria and creating additional risks for chronic infection [461, 462].

There is a need for antibiotic-eluting prosthetic joints in the treatment of prosthetic joint infections where the joint implant can sustain effective antibiotic elution but also possesses the mechanical strength requirements for load bearing and articulation.

Methods

Manufacture of optimized vancomycin eluting UHMWPE with highly eccentric drug clusters (VPE).

Vancomycin-HCl (1.75 gram) was crushed with mortar and pestle and then passed through a 75 μ m sieve. Vancomycin powder was then mechanically mixed with GUR1020 UHMWPE powder (Celanese, 23.25 grams) for 30 minutes at room temperature to obtain a 7 wt% vancomycin-blended UHMWPE and poured into a circular mold with 10.5 cm inner diameter. Vancomycin-UHMWPE mixture was then consolidated by compression molding at 170°C, 20 MPa, for 5 minutes. Resulting consolidated VPE was then cooled at a rate of 10°C/min to room temperature to yield approximately 3 mm-thick and approximately 10.5 cm diameter vancomycin blended-UHMWPE.

Manufacture of optimized rifampin-vancomycin eluting UHMWPE with highly eccentric drug clusters (RVPE).

Rifampin (0.4 gram) was crushed with mortar and pestle and then passed through a 75 um sieve. Vancomycin-HCl (0.8 gram) was crushed with mortar and pestle and then passed through a 75 um sieve. Rifampin powder and vancomycin-HCl powders were then mechanically mixed for 30 minutes at room temperature. UHMWPE GUR 1020 (12 gram) was added to the rifampin and vancomycin-HCl mixture and mechanically mixed/blended for 30 minutes at room temperature, obtaining a 3.3 wt% rifampin and 6.7 wt% vancomycin-blended UHMWPE. 10 grams of the resulting rifampin and vancomycin-blended UHMWPE were transferred and spread evenly onto a circular stainless steel mold with inner diameter of 11 cm. 25 grams of GUR 1020 UHMWPE without additives were then added and spread evenly on top of the rifampin and vancomycin-blended UHMWPE. Resulting constructs were then consolidated by compression molding at 170°C, 20 MPa, for 5 minutes and then cooled at rate of 10°C/min until reaching room temperature.

Manufacture of Vancomycin-eluting PMMA bone cement.

Vancomycin-HCl powder that had been crushed with mortar and pestle and passed through a 75 um sieve was then mechanically mixed with PMMA powder (Simplex P, Stryker) for 30 minutes at room temperature. After thorough mixing, the cement's liquid monomer was added and mixed manually. The vancomycin-cement dough was then poured into a stainless steel mold to form its final shape. After about 15 minutes, the hardened Vancomycin-eluting PMMA bone cement was removed from the mold.

In-vitro drug release from drug-eluting UHMWPE and drug-eluting PMMA bone cement.

Blocks with dimension of 5 mm x 5 mm x 20 mm (n=6) were cut from the consolidated UHMWPE. In the case of PMMA bone cement, vancomycin-cement dough was poured into a stainless steel mold to form 5 mm x 5 mm x 20 mm blocks. Each block (both UHMWPE and BC) was immersed in 1 ml of phosphate-buffered saline at 37°C for a pre-determined time points (6 hr, 24 hr, every 24 hr until 1wk, and then once every week up to a total period of 12 months. After each time-point was reached, the specimens were washed with phosphate-buffered saline and placed in a new 1 ml of phosphate-buffered saline. Concentrations of vancomycin and rifampin were determined using Ultraviolet-Visible spectroscopy (UV-Vis) at 280 nm (vancomycin) and 450 nm (rifampin). Rates of drug release were calculated by dividing the measured concentration with the duration the sample was contacted with phosphate-buffered saline at the time of sample collection.

Determination of wear rate by bi-directional pin-on-disc (POD) test.

Cylindrical pins (9-mm diameter and 13-mm long, n=3 each) were machined using a CNC mill (ShopBot) from the materials prepared above. The pins were wear tested with a rectangular pattern (5 × 10 mm) against polished CoCr discs at 2Hz in undiluted, preserved bovine serum as a lubricant. The pins were cleaned and weighed before testing and at each 0.16 million cycles (MC) after the first 0.5 MC until a total of 1.2 MC. The wear rate was determined by a linear regression of the weight loss as a function of number of cycles from 0.5 to 1.2 MC.

Antibacterial activity of VPE and vancomycin eluting PMMA bone cement.

Antibacterial activity was assayed using a protocol modified from one previously reported [2]. Cylindrical discs (5-diameter and 3 mm thick) of VPE and Vancomycin-eluting PMMA bone

cement were sterilized using ethylene oxide. Test organisms (*Staphylococcus aureus* (ATCC 29213) or *Staphylococcus epidermidis* (ATCC 35984)) were cultured in tryptic soy broth at 37°C for 24 hr and subsequently plated on Mueller-Hinton agar at 37°C for 18 hr. Three to five colonies were then selected and suspended in Mueller-Hinton broth and the inoculum concentration was adjusted to 0.5 McFarland turbidity standards. The surface of the new Mueller-Hinton agar plate was then covered uniformly with bacteria suspension using a sterile swab. Samples were then placed on the surface of the Mueller-Hinton agar plates that had been seeded with either the *Staphylococcus aureus* or *Staphylococcus epidermidis* strains and further incubated at 37°C for 24 hr. Pictures of the back of the plates and a ruler were taken in the same frame. Area of inhibition (clear area where there is no sign of bacterial growth) was then measured using Image J software. Samples were then transferred to new Mueller-Hinton agar plates that had been seeded with either *Staphylococcus aureus* or *Staphylococcus epidermidis*. These steps were repeated every 24 hours until three weeks.

Determination of vancomycin grafting on gamma beam irradiated UHMWPE.

Gamma-irradiated VPE and RVPE were pre-eluted for 12 months until no eluted vancomycin and rifampin could be detected by UV-Vis and HPLC. Samples were then washed twice with PBS and blocked for 30 min using 10% fetal bovine serum in distilled, deionized water (blocking buffer). Samples were then incubated with mouse anti-VAN IgM (1:300; U.S. Biologicals, Swampscott, MA) in blocking buffer at 4°C for 12 hr, washed with PBS, and incubated with AlexaFluor 488-coupled goat anti-mouse IgM (A-21042, Thermo Fisher Scientific) diluted 1:300 in blocking buffer at room temperature for 1 hr. Samples were then washed three times in PBS, followed by 2x30 min incubations in PBS. Particles were then visualized using an inverted fluorescence microscope (Nikon Eclipse TE2000).

Antibacterial activity of surface-bonded vancomycin on gamma-irradiated UHMWPE.

Gamma-irradiated VPE and RVPE were pre-eluted for 12 months until no eluted vancomycin and rifampin could be detected. Samples are then washed in PBS and sterilized by ethylene oxide and then incubated in 1 ml of 1 % dextrose/PBS. *S aureus* (ATCC 29213) was cultured in trypticase soy broth for 12 hr. The culture was pelleted by centrifugation at 3200 x g for 5 min, and then resuspended in Mueller-Hinton broth to create 1.5×10^8 cfu/ml using 0.5 McFarland standard. Two microliter of the bacterial suspension was added to each well and the cultures were incubated at 37°C for 12 hr. Samples were then washed twice with PBS to remove planktonic bacteria. Samples were then stained using Live/Dead BacLight Viability kit (Molecular Probes) that contain Syto 9 and propidium iodide. Samples were then imaged using inverted fluorescence microscope (Nikon Eclipse TE2000), where green fluorescence indicates live bacteria, and red fluorescence indicates dead bacteria.

Two-photon fluorescence microscopy.

For quantification of antibacterial activity, a home-built, two-photon fluorescence microscope was employed to image samples stained with Live/Dead BacLight Viability kit (Molecular Probes). The system includes a mode-locked Ti:Sapphire Laser (MaiTai DeepSee eHP, Newport), providing light at ~150fs pulse width at 80 MHz repetition rate. The emitted light was detected by two photomultiplier tubes through appropriate dichroic and bandpass filters for Syto9 and propidium iodide. A 10x, 0.3 NA objective (Leica) was used for visualization of multiple beads in one field-of-view (FOV at 10x~ 600 x 600 μm^2), while a 40x, 0.6 NA objective (Nikon) was used for quantification of live/dead bacteria fluorescence. At least 5 images randomly selected throughout the sample were taken for each sample for data quantification.

Antibacterial activity of RVPE on biofilm in between bone-titanium interface.

RVPE created as described above was machined into discs (5 mm diameter). The following were also used: (1) a 4 mm-thick consolidated UHMWPE without additives (control), prepared using the same molding conditions and (2) titanium discs coated with titanium beads (10 mm diameter, 5 mm thickness, bead diameter 100µm. Manufactured by Orchid Orthopedics, Memphis, TN, USA) and (3) bovine cortical bone discs (10 mm diameter, 3 mm thickness. Bovine cortical bone is machined from bovine tibia obtained from Animal Technology, Texas, USA). All samples were sterilized with ethylene oxide gas. Fresh overnight liquid culture of bioluminescent *S. aureus* (Xen 29) was diluted to 5×10^4 cfu/ml. 50 µL of the liquid culture was added on top of the beaded-surface of the titanium discs to simulate an infection at an orthopaedic implant-bone interface. Cortical bone was added on top of the titanium disc seeded with bacteria and held together with a circular clamp (McMaster-Carr). The constructs were then immersed in 5 ml of fresh Mueller-Hinton II broth and then incubated at 37°C for 48 hr. After 48 hr of incubation, the media was aspirated, clamps were removed, and titanium discs and cortical bone were separated and washed with PBS to remove planktonic bacteria. Biofilm formation was then measured using a bioluminescence camera (IVIS 100, Perkin-Elmer). Cortical bone was placed back on top of the titanium after imaging and either control UHMWPE or RVPE were added underneath the titanium-bone constructs and clamped using sterile clamps. Samples were separately placed in their own wells in a 6-well plate and 5 ml of Mueller-Hinton II broth was added to each well. All samples were then incubated at 37°C. Bioluminescence was measured at 24 hr, 48 hr, 96 hr, 120 hr, 1 wk, and 2 wk after exposure to either control or RVPE. During each bioluminescence measurement, media was aspirated, clamps were removed, titanium discs and cortical bone were separated and washed with PBS to remove planktonic bacteria, and titanium discs and cortical bone were imaged separately. After imaging,

constructs were reassembled, new sterile clamps were placed, and new Mueller-Hinton media was added. Media was replaced every 24 hr. After the samples reached the predetermined time point, samples were stained using Live/Dead BacLight Viability kits (Molecular Probes) containing Syto 9 and propidium iodide. Samples were imaged using two-photon fluorescence microscopy where live bacteria shows exhibit green fluorescence, and dead bacteria shows red fluorescence. Percent red fluorescence, corresponding to percent cell death was calculated using Matlab by dividing the number of detected red pixels by the total number of fluorescent pixels.

Results

Optimization of mechanical strength and drug elution of vancomycin eluting UHMWPE as a bearing surface in prosthetic joint implants

Because there is a tradeoff between drug elution and mechanical strength of vancomycin eluting UHMWPE, we created and utilized an optimization equation to maximize the ultimate tensile strength (UTS), impact strength (IS), and drug elution rates (**Eq. 1-3**). We assumed that initial drug concentration (C), mean drug particle size (R), molding temperature (T), molding pressure (P), and time (t) were independent variables and have zero covariance:

$$\text{Global Optimization Equation: } (0.5 * UTS (C, T, P, t) + 0.5 * IS (C, T, P, t)) + (Rate (C, t)) \quad (1)$$

$$UTS = f_1 (R, t) + f_1 (C, t) + f_1 (T, t) + f_1 (P, t) \quad (2)$$

$$IS = f_2 (R, t) + f_2 (C, t) + f_2 (T, t) + f_2 (P, t) \quad (3)$$

$$\text{Elution Rate} = f_3 (R, t) + f_3 (C, t) + f_3 (T, t) + f_3 (P, t) \quad (4)$$

Because UTS, IS, and elution rates were variable on different scales, their contributions to the optimization were normalized with their respective maximum values (UTS and IS at 0%

drug loading and elution rates by 14 % drug loading). From chapter 3, we found that there was no statistically significant change in UTS and IS as a function of time (**Figure 3.4**). Therefore, the UTS and IS equation could be simplified as (**eq 5,6**):

$$UTS = f_1(C) + f_1(T) + f_1(P) \quad (5)$$

$$IS = f_2(C) + f_2(T) + f_2(P) \quad (6)$$

While controlling mean drug size was important for both UTS and IS (**Figure 3.5**), both tensile and impact strength (**Figure 3.4**) were independent of the drug particles size, R. Mechanical strength was maximized when compression molding temperature and pressure were $T > 160^\circ\text{C}$, and $P \in [18-21]$ MPa (**Figure 3.4**), therefore the optimum temperature (T_{opt}) and pressure (P_{opt}) were $T_{\text{opt}} > 160^\circ\text{C}$, and $P_{\text{opt}} \in [18-21]$ MPa, respectively. From chapter 2, we obtained that the drug elution rate was independent of T, P, and R (**Figure 2.10**), resulting in simplification of elution rates and global optimization equation (**7-8**).

$$\text{Elution Rate} = f_3(C, t) \quad (7)$$

$$\text{Opt Eq: Max } (0.5 * \% \text{ UTS } (C) + 0.5 * \% \text{ IS } (C) + (\text{Rate } (C, t))) \quad (8)$$

From eq 5-8 above, only C simultaneously affects the drug elution rate, IS and UTS (**Figure 2.6 and 3.6**); the drug elution rate was directly proportional to C, while UTS and IS were inversely proportional to C. Plotting % UTS, % IS, and elution rates as obtained from chapter 2 and chapter 3 from vancomycin-eluting UHMWPE resulted in the highest value for the global optimization equation at initial drug loading (C_{opt}) of 6.5 % (**Figure 5.1**). Above this concentration, the additional gain in drug elution rate was offset by the decrease in the mechanical properties, while below this concentration the drug elution rate was not sustained at an effective level for treating PJI. Prototype of tibial insert and acetabular cup has been successfully made from the optimized vancomycin-eluting UHMWPE (**Figure 5.2**).

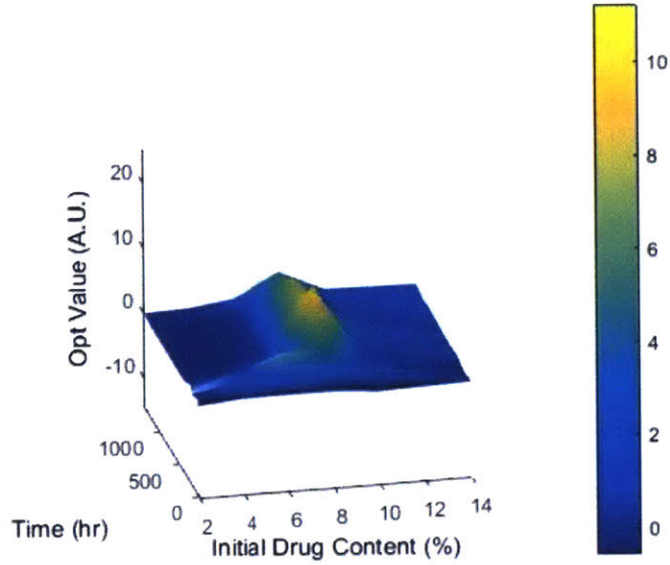


Figure 5.1 Optimization field with respect to initial drug loading. Plot of optimization equation value (Opt value, (eq 8)) against initial drug content (wt%) and elution time (hr). Peak corresponds to the optimum initial drug content.

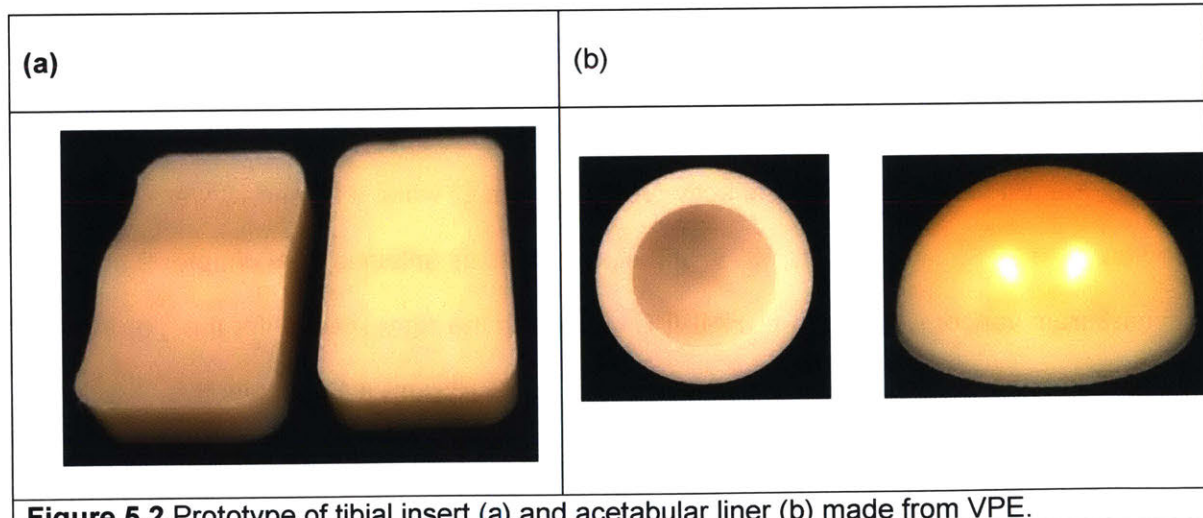


Figure 5.2 Prototype of tibial insert (a) and acetabular liner (b) made from VPE.

Vancomycin Elution and Mechanical Properties of Optimized Vancomycin-Eluting UHMWPE and Comparison Against Clinically Used UHMWPE and Antibiotic-Eluting Bone Cement

To test if our material could provide sufficient drug elution in PJI situation while maintaining the necessary mechanical strength for use as prosthetic joints, we compared the elution and mechanical properties of our optimized vancomycin-eluting UHMWPE (6.5 % initial vancomycin loading, VPE) against clinically-used UHMWPE and antibiotic-eluting bone cement (1.5 % and 11 % initial vancomycin loading (BC1 and BC2 respectively)). We used 1.5 % and 11% vancomycin in bone cement (BC) because these are the lowest drug content used and the highest drug content that can still maintain the industry standard of 70 MPa for compressive strength, respectively [297]. The vancomycin elution rate and antibacterial activity of 7 wt% vancomycin-loaded UHMWPE (VPE) was superior to that of 1.5 % vancomycin in BC and similar to that of 11 % vancomycin in BC (**Figure 5.3**).

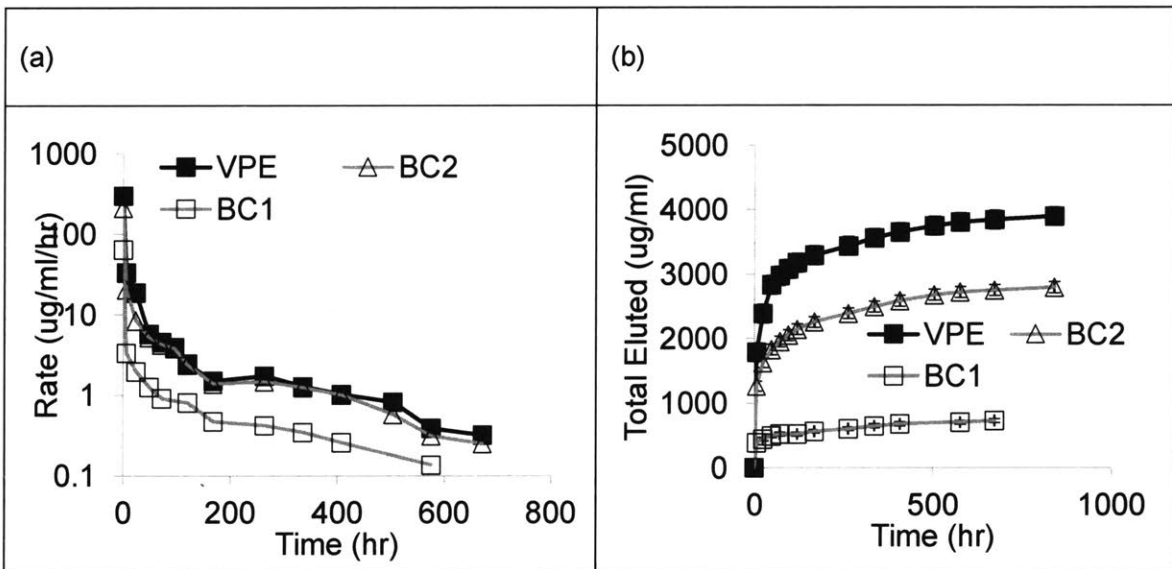


Figure 5.3 Elution profile of vancomycin eluting UHMWPE. Vancomycin elution (a) and total vancomycin eluted (b) from 6.5 % vancomycin eluting UHMWPE (VPE), 1.5 % vancomycin in PMMA bone cement (BC1), and 11 % vancomycin in PMMA bone cement

(BC2).

Compared to the properties of clinically available UHMWPE bearings, VPE was well within acceptable range for UTS (34-59 MPa) [332], IS (56-108 kJ/m²), and wear rate (-9.55±1.27 mg/million cycle for VPE, clinically relevant range: -21 to -0.1 mg/million cycles [463]). Furthermore, the UTS, EAB, and IS were superior to both BC1 and BC2 (**Figure 5.4**).

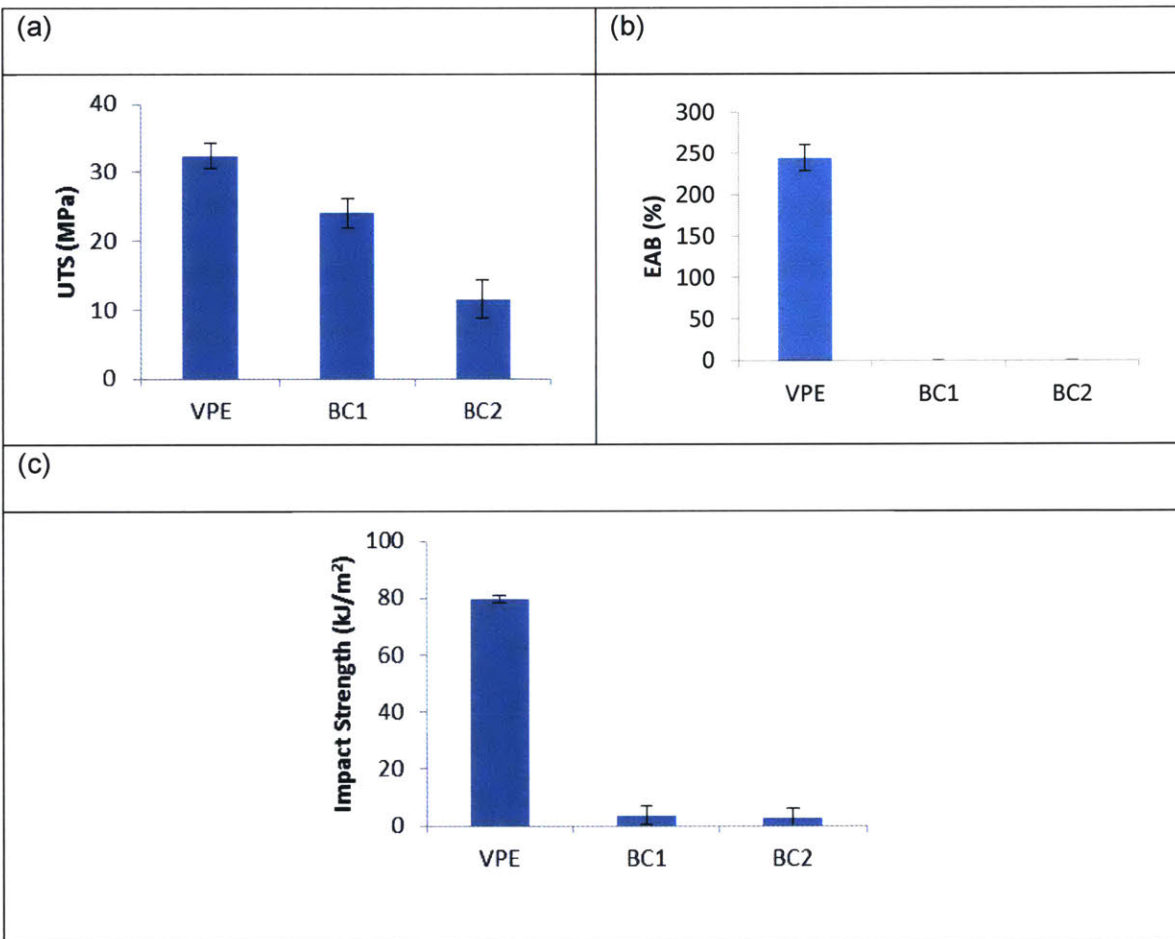
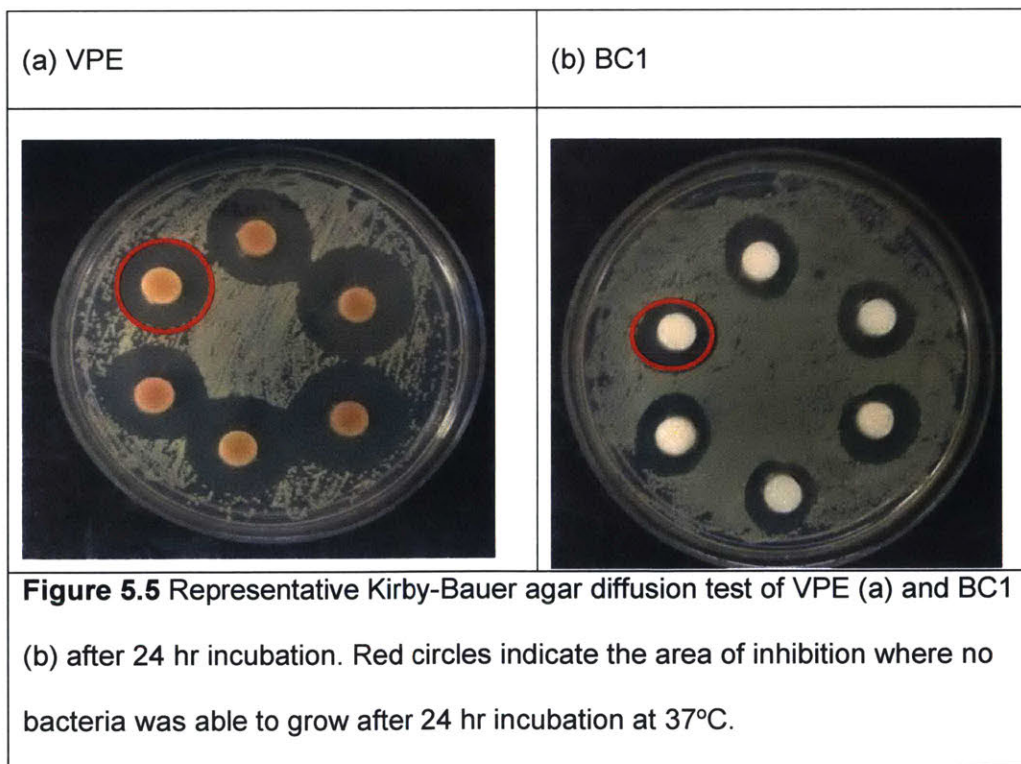


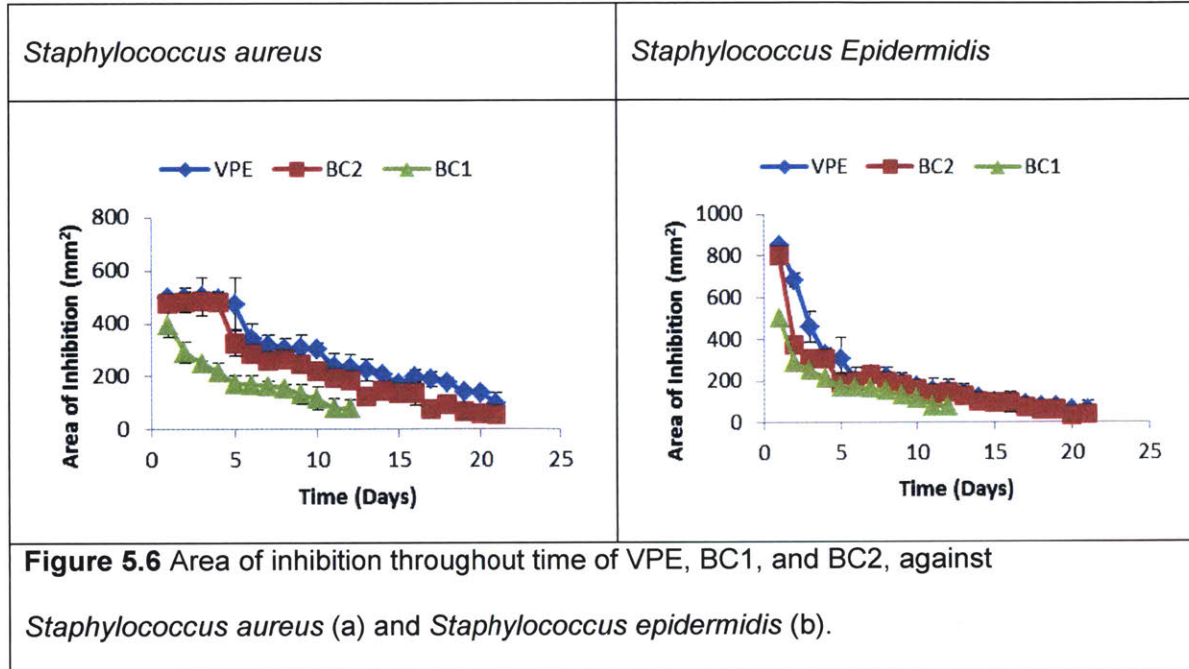
Figure 5.4 Mechanical properties of Vancomycin-eluting UHMWPE and Vancomycin-eluting bone cement. Ultimate tensile strength (a), elongation to break (b), and impact strength (c) from 6.5 % vancomycin-eluting UHMWPE (VPE), 1.5 % vancomycin in PMMA bone cement (BC1), and 11 % vancomycin in PMMA bone cement (BC2).

Antibacterial Activity of VPE, BC1, and BC2

We tested the antibacterial activity of VPE, BC1, and BC2 against the two most common bacteria causing PJI: *Staphylococcus aureus* and *Staphylococcus Epidermidis*. The method of the test was adapted from the Kirby-Bauer agar diffusion test, where the VPE, BC1, and BC2 were placed on the surface of bacteria-covered agar surface.

Ability of VPE to inhibit bacterial growth (as measured by area of inhibition (**Figure 5.5**)) was superior to BC1 and similar to BC2 (**Figure 5.6**) for both *S. epidermidis* and *S. aureus*. These results are in agreement with the elution data which also showed VPE had superior elution than BC1 but similar to BC2. All three materials were more effective in inhibiting growth of *S. epidermidis* than *S. aureus* as shown by the larger area of inhibition for all three materials against *S. epidermidis* than *S. aureus*.

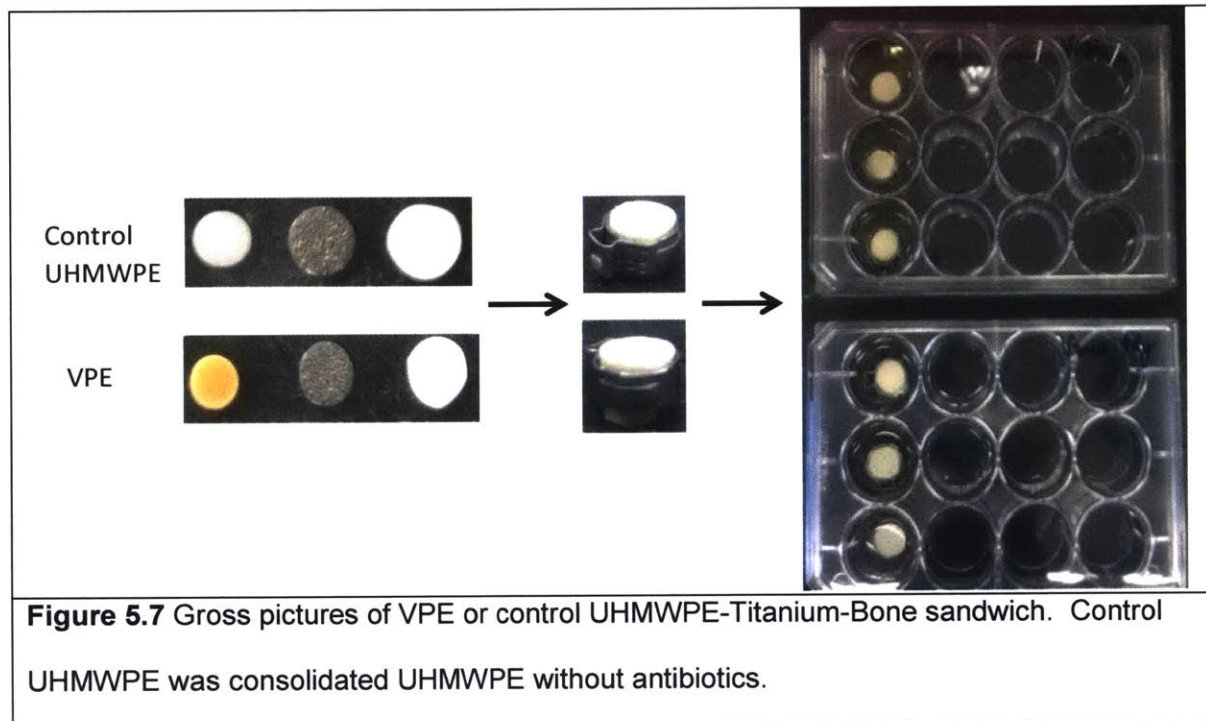


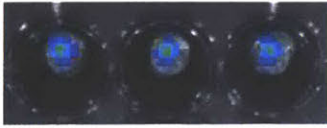
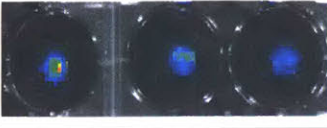
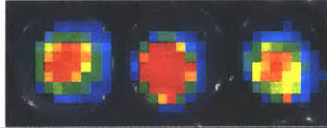
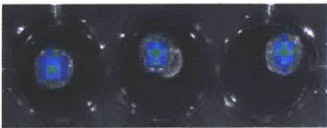
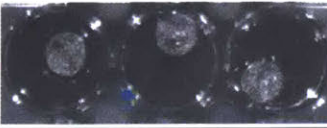
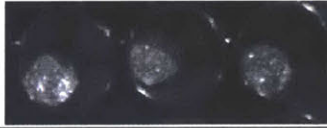
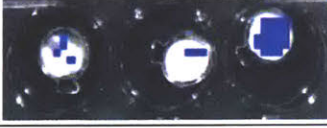
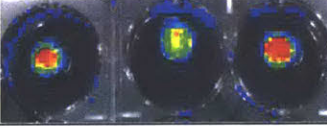
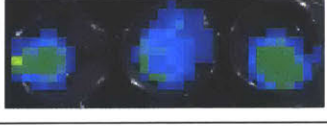
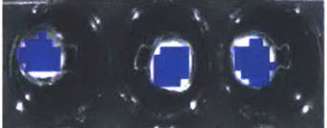
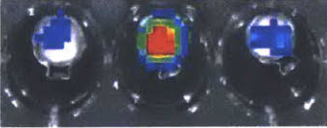
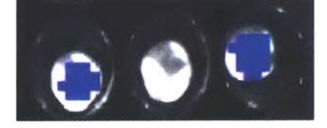
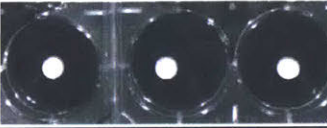

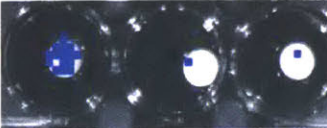



To test whether the vancomycin eluted from the VPE could eradicate bacteria that might be at the bone and titanium interface, we created a VPE-Titanium-Bone sandwich where bioluminescent *S. aureus* (Xen 29) bacterial culture was added to the interface between the titanium and bone (**Figure 5.7**). First, bacterial cultures were added to the textured titanium disc, then the textured surface covered with bovine cortical disc and then clamped. VPE was added below the titanium disc and the whole constructs were incubated in Mueller-Hinton media for 24 hr at 37°C. To image the bone-titanium interface, the bone and titanium were sterically removed from the clamps and then put under bioluminescent imaging camera. After imaging, another dose of fresh bacterial culture was added to the bone-titanium interface and re-clamped and incubated for further 24 hr. After 24 hr, the bone-titanium interface was re-imaged with bioluminescent imaging camera.

After 24 hr incubation, the titanium, bone, and VPE surface had significantly lower bioluminescent signal than the titanium, bone, and polyethylene in the control UHMWPE group

(Figure 5.8 and 5.9). In fact, no bioluminescent signal was observed on the titanium surface of the VPE groups both at 24 and 48 hr. Sonication of the titanium, bone, and UHMWPE components with subsequent re-culturing showed eradication of bacteria on all components in the VPE group (Figure 5.10).



Titanium Plate			
	0 hr	24 hr	48 hr
Control			
VPE			
Bone			
	0 hr	24 hr	48 hr
Control			
VPE			
Polyethylene			
	0 hr	24 hr	48 hr
Control	N / A		
VPE	N/A		

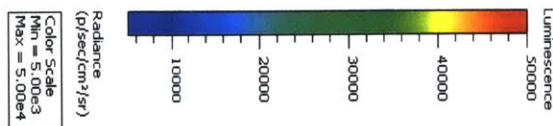


Figure 5.8 Bioluminescent imaging of live Xen29 that adhered to the titanium disc, cortical bone, and polyethylene component in the VPE and control groups.

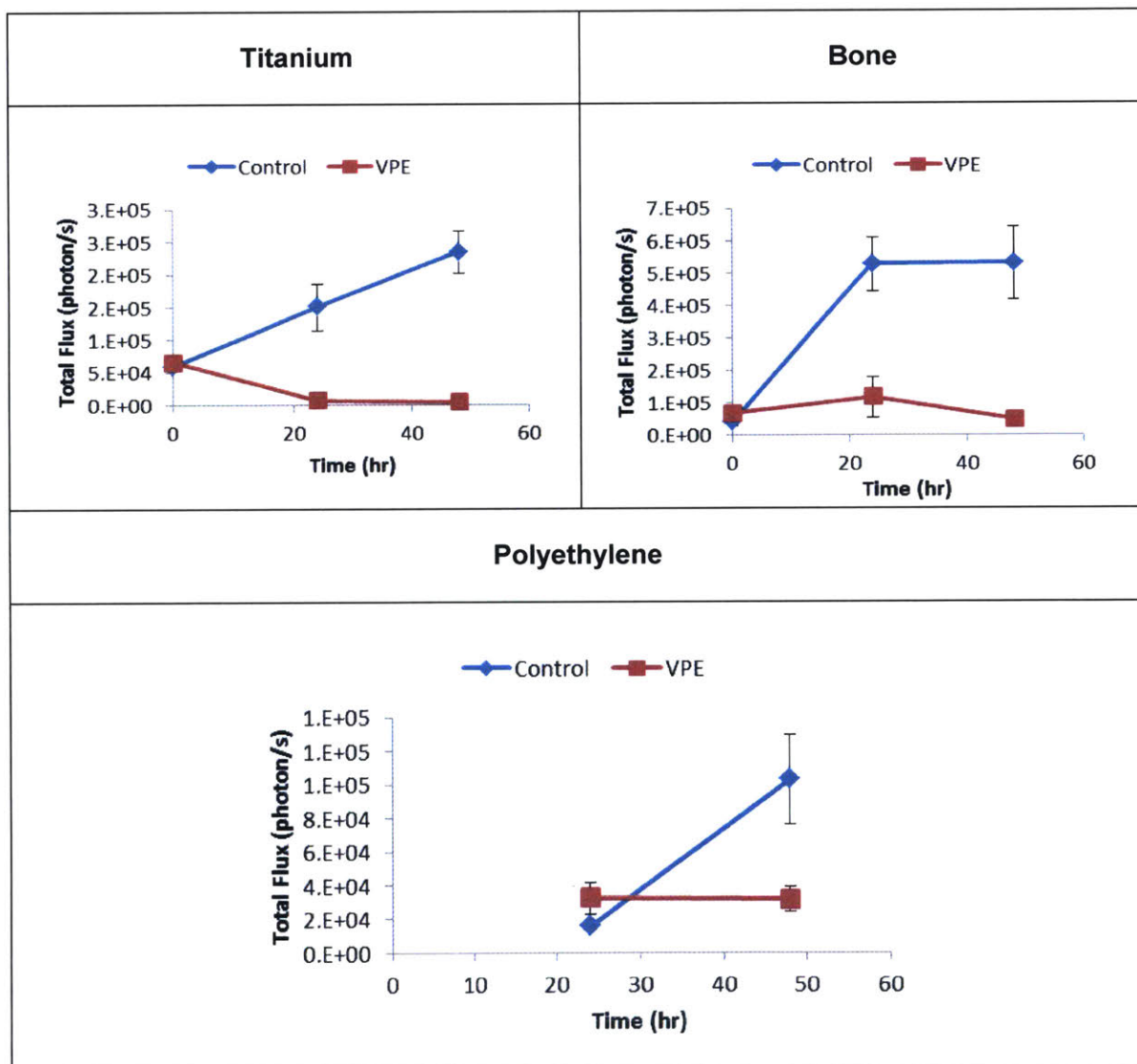


Figure 5.9 Quantification of the bioluminescent signal from the bacteria adherent to titanium disc and cortical bone disc.

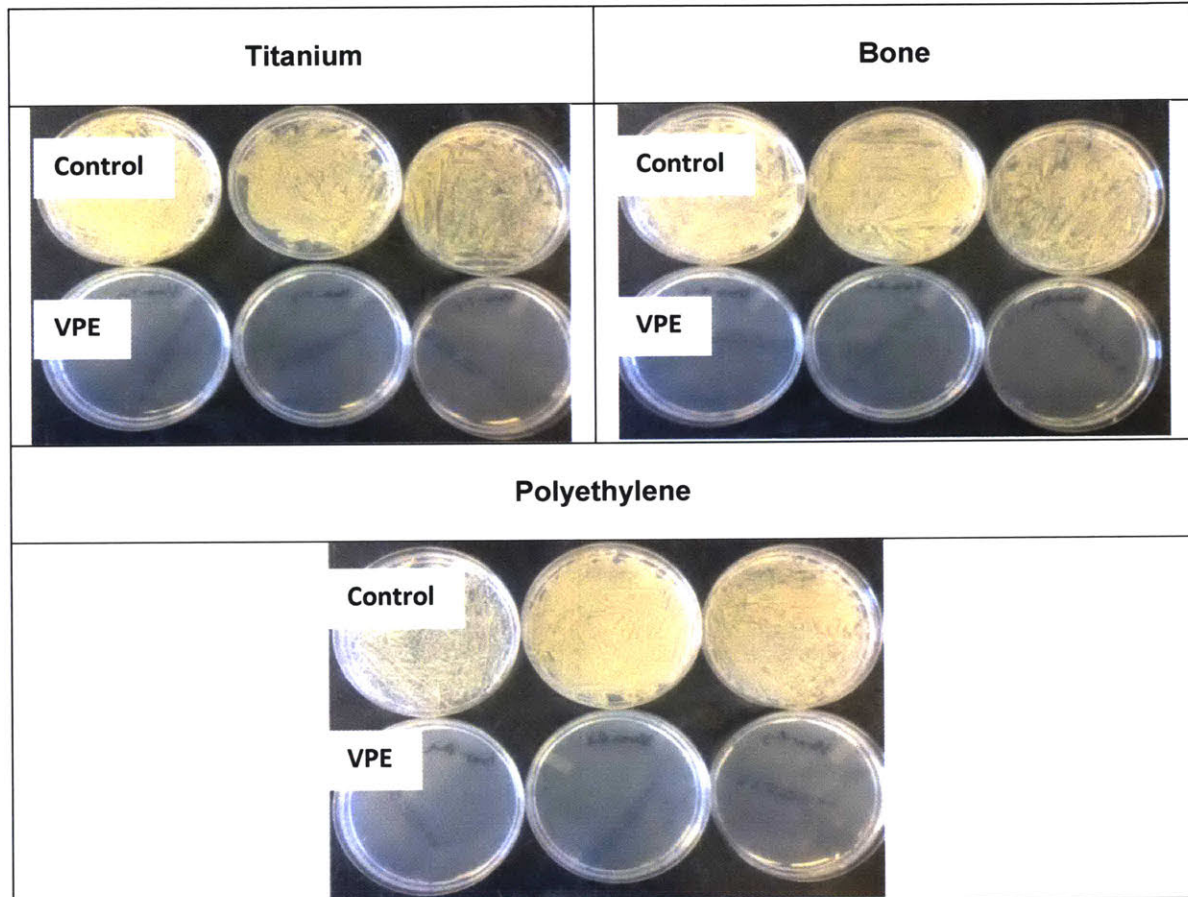


Figure 5.10. Plate reculturing of bacteria after sonication of the titanium, bone, and polyethylene components after 48 hr time points.

Irradiation Grafting of Vancomycin on Surface of VPE Prevents Bacterial Adherence

In this experiment, the goal was to study the potential for bacterial re-colonization of unirradiated and irradiated VPE after vancomycin was eluted for a sufficiently long time such that its concentration in the medium fell below the minimum inhibition concentration of the

organism in question. To do this, we eluted vancomycin from VPE for six months until no further elution of vancomycin could be detected by liquid chromatography (detection limit = 0.1 ug/ml). We then incubated the samples with fresh culture of *S. aureus* for 24 hr at 37°C. We then fluorescently labelled the bacteria to image the adherent bacteria (**Figure 5.11**). On a separate set of samples, after incubation with *S. aureus* for 24 hr, we sonicated and recultured the bacteria (**Figure 5.12**)

Irradiated VPEs both at 25 and 100 kGy showed less bacterial adherence than unirradiated VPE and control UHMWPE (**Figure 5.11**). Sonication and subsequent reculturing corroborated the imaging experiment also showing less live bacteria adhered to the surface of irradiated VPE than both unirradiated VPE and control UHMWPE. There was no statistical significant difference in bacterial concentration between control UHMWPE and unirradiated UHMWPE. There was also no statistical significant difference in bacterial concentration between 25-kGy irradiated and 100-kGy irradiated VPE (**Figure 5.12**).

To further understand the mechanism of the reduction of bacterial adherence on irradiated VPE, we performed immunofluorescence staining of vancomycin on control UHMWPE, unirradiated VPE, and irradiated VPE (**Figure 5.13**). Fluorescence was seen on the surfaces of the irradiated VPEs but not on unirradiated VPE (**Figure 5.13**), indicating the presence of vancomycin bound to the surfaces of the VPE after all elutable drug was released.

Irradiation Dose	
Control UHMWPE	0 kGy

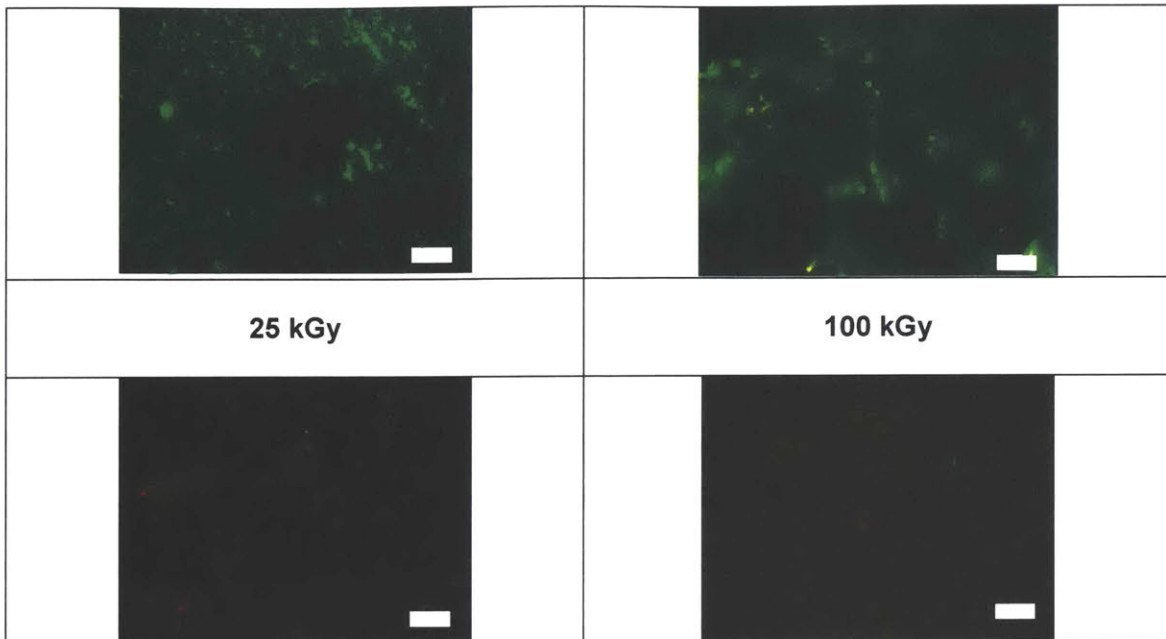


Figure 5.11. Live/Dead stain of bacterial adherent to the surface of control UHMWPE, unirradiated VPE, 25 kGy-irradiated VPE, and 100 kGy-irradiated VPE. Green indicates live bacteria, red indicates dead bacteria. Scale bar = 100 μ m.

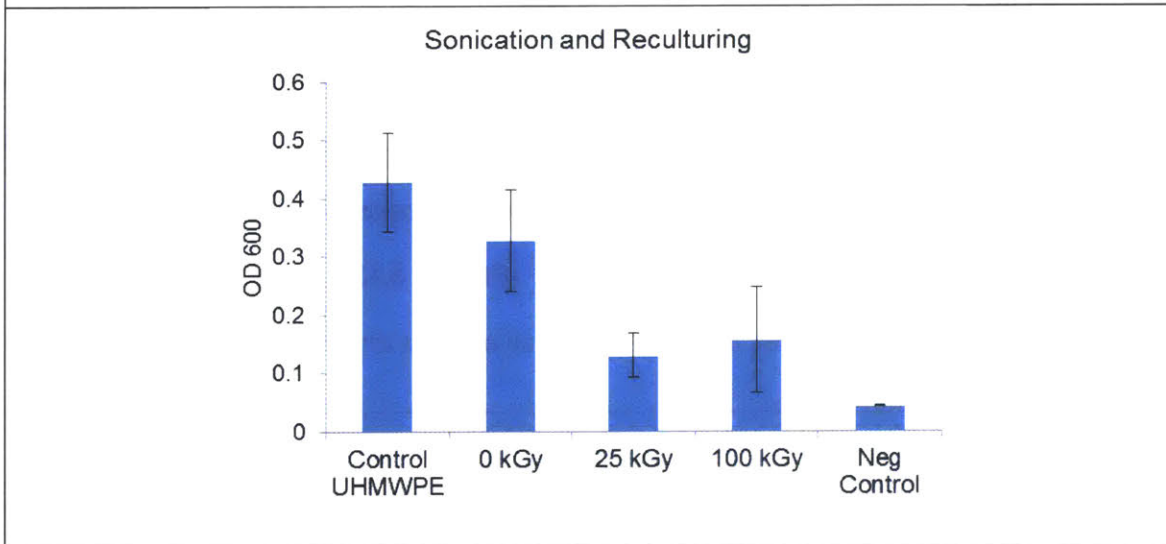


Figure 5.12. Sonication and reculturing of bacteria adherent on the surface of control UHMWPE, unirradiated VPE, 25 kGy-irradiated VPE, and 100 kGy-irradiated VPE. Bacterial count was then conducted by measuring its absorbance at 600 nm (OD 600).

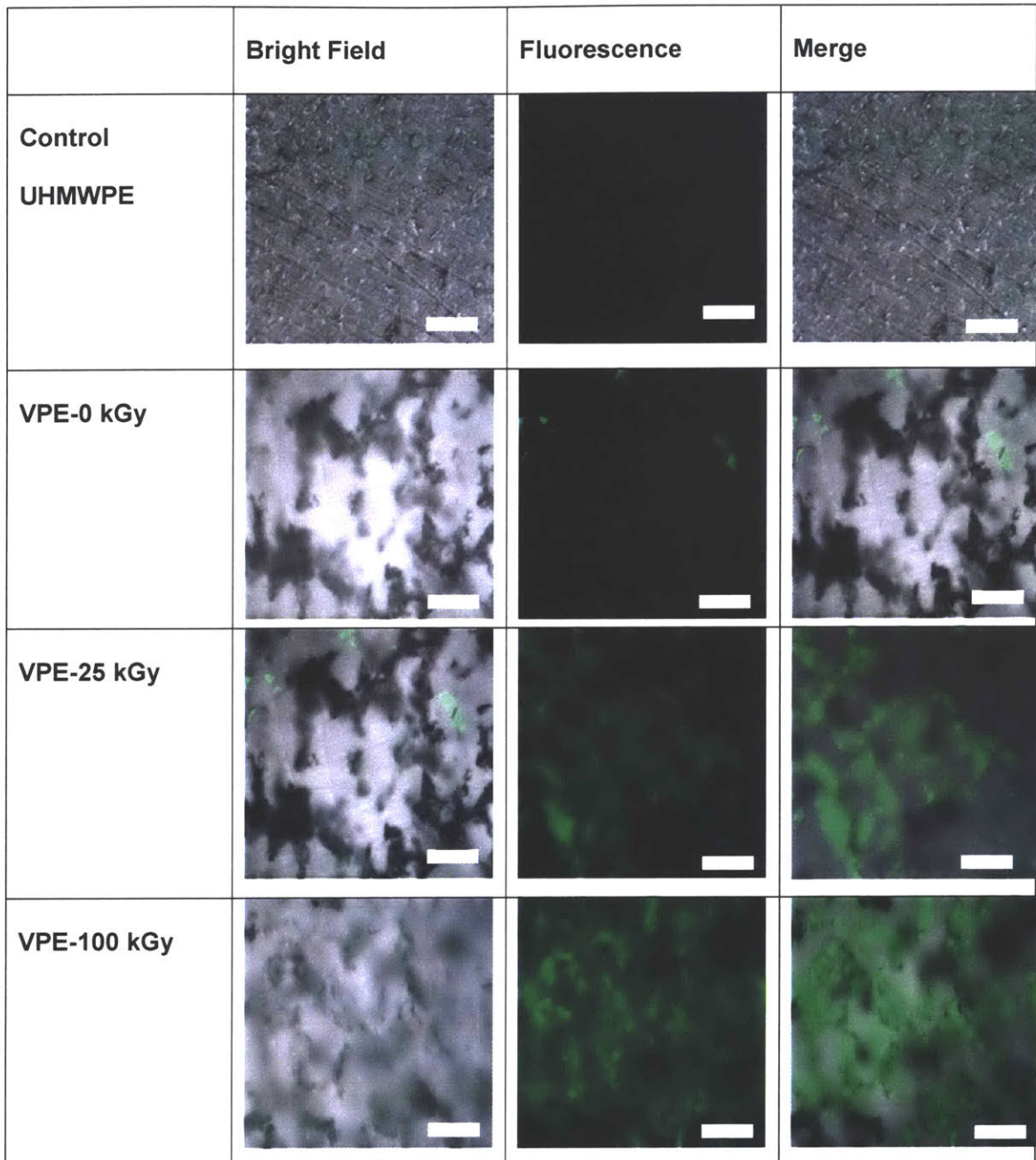
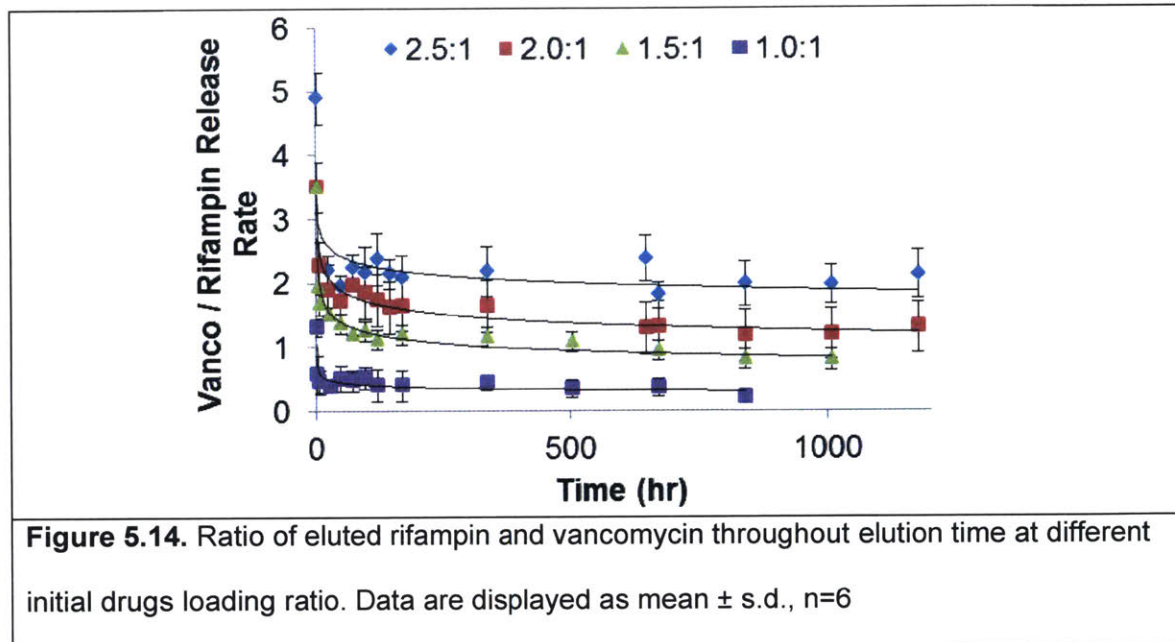


Figure 5.13. Immunofluorescence staining of vancomycin on the surface of control UHMWPE, V-PE that was irradiated 0, 25, and 100 kGy that had been preeluted for 6 months. Scale bar = 200 μ m.

Optimization of Combined Rifampin-Vancomycin-Eluting UHMWPE

Based on clinical guidelines for vancomycin:rifampin concentration for the treatment of PJI (Table 5.2), incorporation of 2.5:1 vancomycin: rifampin allowed long term maintenance of vancomycin:rifampin elution rate ratio closest to the clinically desired trough ratio (Figure 5.14).

Parameter	Magnitude	Unit
Vancomycin Dose (A) ¹	15	mg/kg per 12 hr
Rifampin Dose (B) ¹	450	mg/kg per 12 hr
Serum trough concentration of rifampin (C) ²	1.875	ug/ml
Serum trough concentration of vancomycin (D) ³	20	ug/ml
Rifampin penetration to bone(E) ⁴	100	%
Vancomycin penetration to bone (F) ⁴	21	%
Rifampin concentration in infected bone (G=C*E)	1.875	
Vancomycin Concentration in infected bone (H=D*F)	4.2	
Vancomycin to Rifampin Ratio (H/G)	2.24	
Table 5.2. Calculation of RV-PE to Clinically Relevant Vancomycin to Rifampin Ratio.		



We observed that the vancomycin elution rate was consistently higher than the rifampin elution rate for UHMWPE incorporated with 3 wt% rifampin in addition to 7 wt% vancomycin (RVPE; **Figure 5.15**) and vancomycin elution rate from RVPE was significantly higher than that of VPE and BC2 (**Figure 5.15**). Mechanical strength (ultimate tensile strength and impact strength) and wear rate of RVPE and RVPE+VPE constructs within the limit of clinically used UHMWPE and are both higher than BC (**Figure 5.16**).

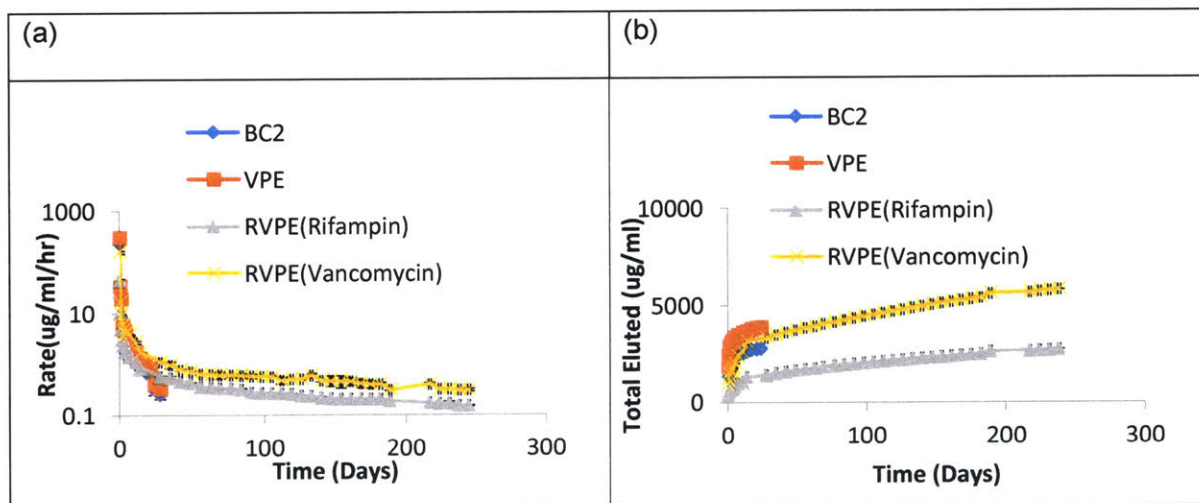
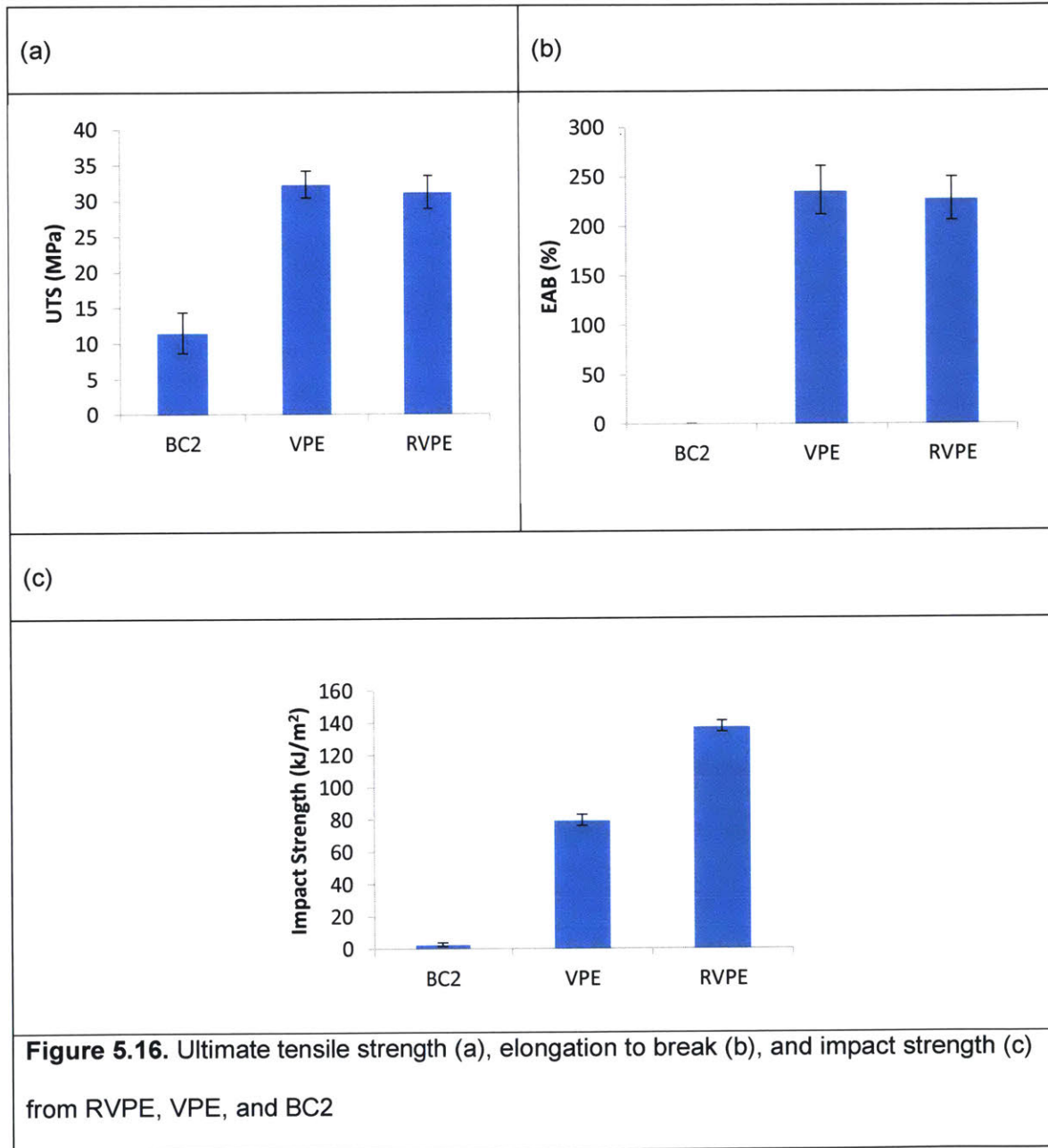


Figure 5.15. Elution rate (a) and total drug eluted (b) of RVPE, VPE and BC2.



Prototype of acetabular liner and tibial insert was successfully manufactured from Rifampin and vancomycin-eluting UHMWPE (RVPE) with a total drug concentration of 10 wt% that was localized on surface non-articulating regions (such as acetabular rim and tibial insert backside) to minimize the effect of the lower mechanical properties of increased drug concentration on the potential implant (**Figure 5.15**).

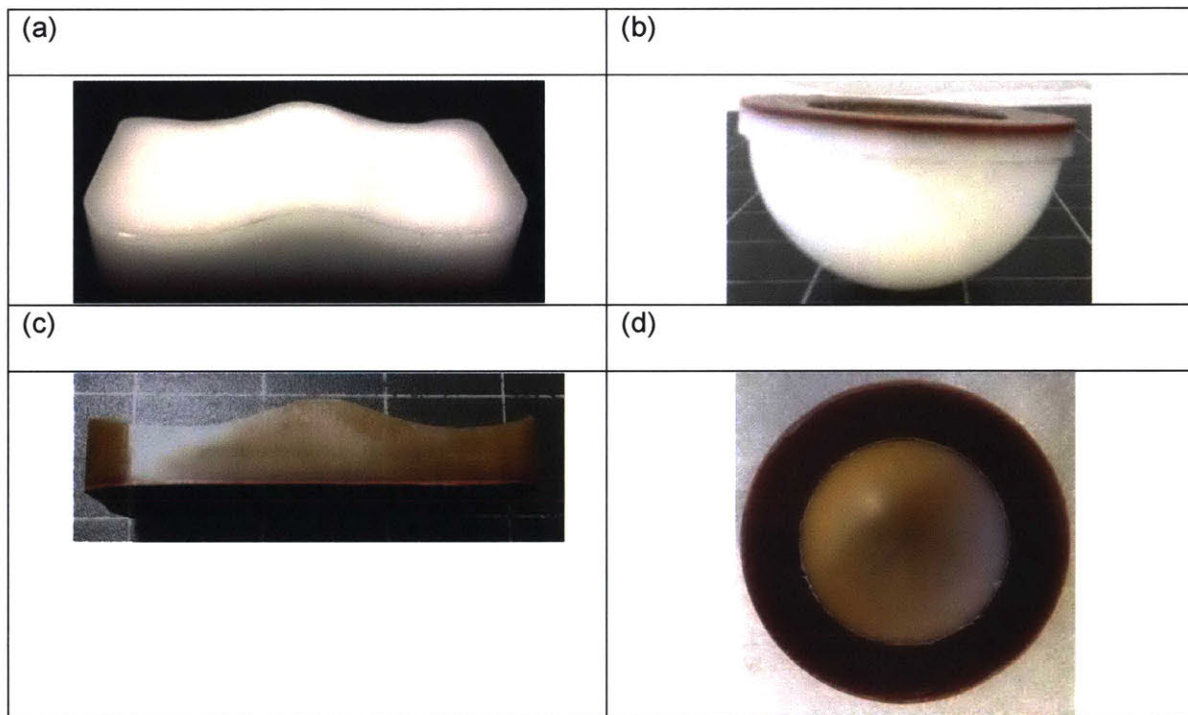


Figure 5.17 Prototype of tibial insert (a) and acetabular liner (b) made from combination of RVPE (red) and non-antibiotic eluting UHMWPE (white). Prototype of tibial insert (c) and acetabular liner (d) made from combination of RVPE (red) and VPE (brown).

Activity of RVPE

An in vitro simulation of biofilm formation at the bone-implant interface of a joint implant was done by sandwiching bone, titanium and UHMWPE (**Figure 5.18**). A bioluminescent *S. aureus* (Xen 29, Perkin Elmer) biofilm was grown on the porous surface of titanium discs for 48 hr. The surfaces were clamped together with the biofilm-laden porous titanium surface in contact with the bone and the non-porous surface in contact with UHMWPE (**Figure 5.19**). The average synovial fluid volume and the size of the femoral component of a knee implant were used to scale down the size of the RVPE, the volume of media, and the bone-titanium interface respectively (**Table 5.3**). The average biofilm thickness as quantified by two-photon microscopy was $25.5 \pm 2.2 \mu\text{m}$, in agreement with previous reports [464].

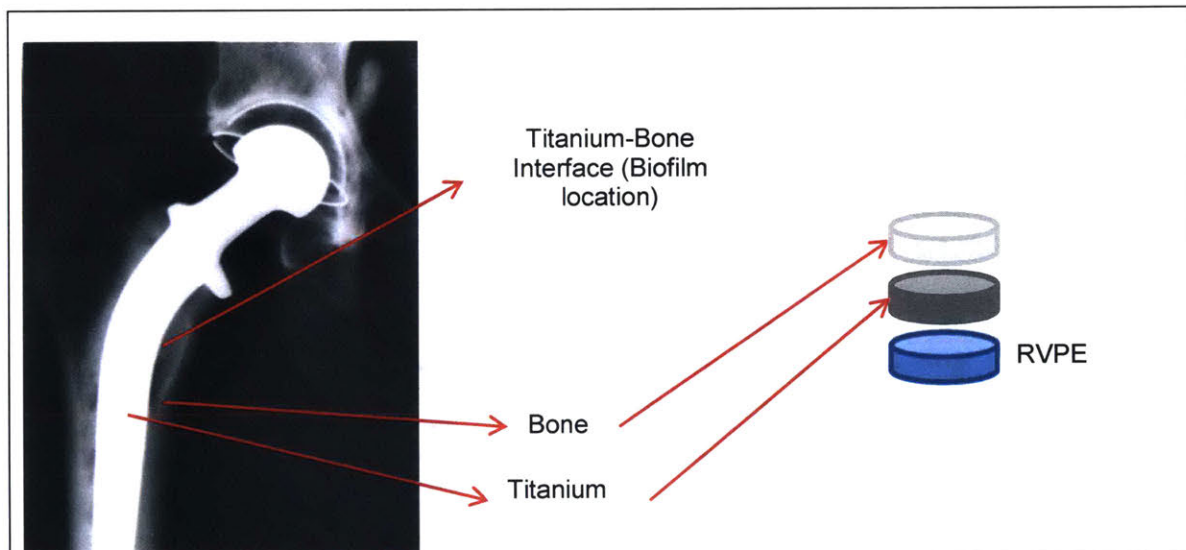


Figure 5.18. Schematic of 'sandwich' experiment to treat bacterial biofilm in between bone-titanium using either non-antibiotic eluting UHMWPE (control) or RVPE. Bacterial biofilm inbetween titanium is often found in patients with chronic PJI.

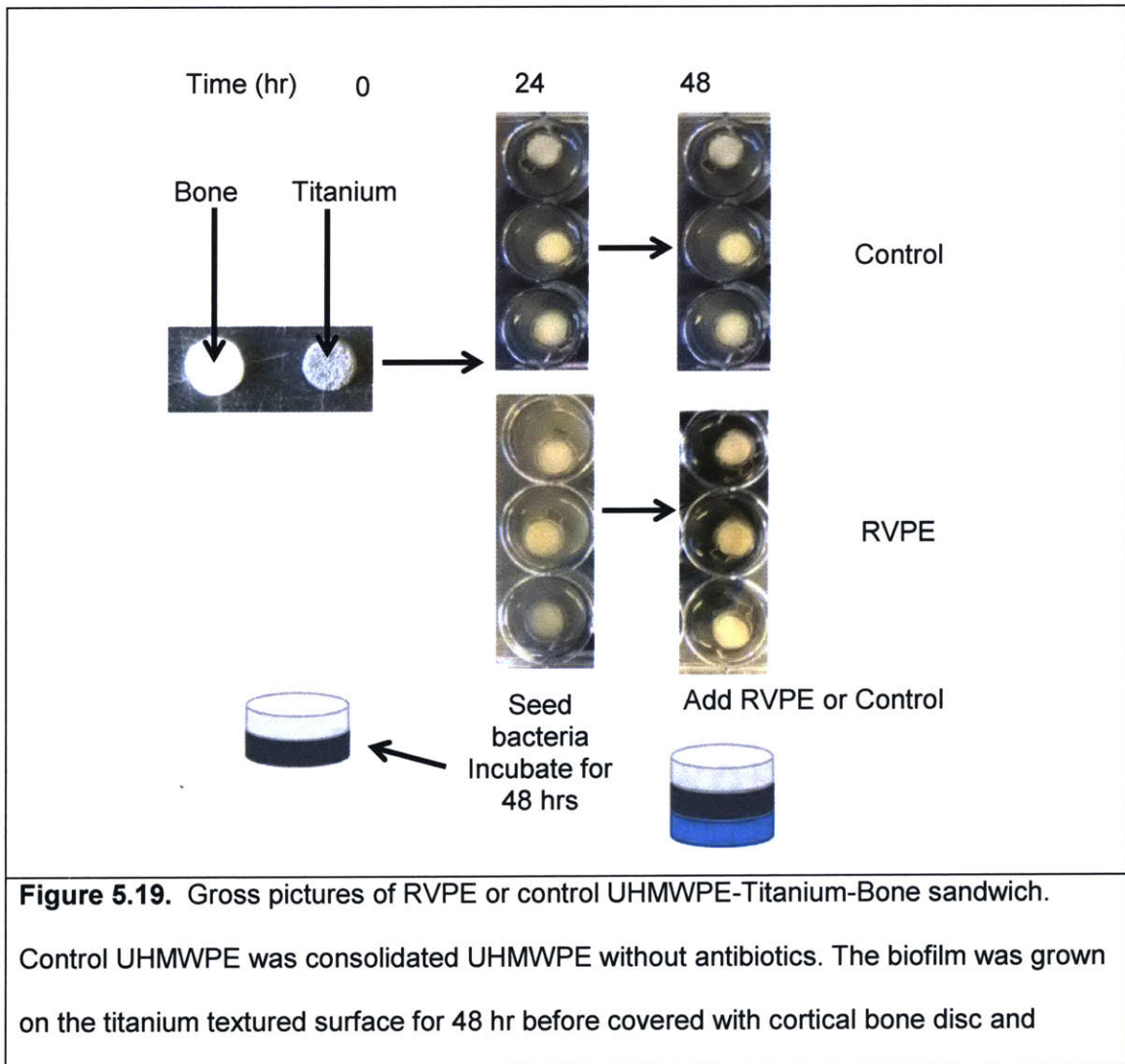
At the beginning of the experiment ($t=0$), titanium with bacterial biofilm on its textured surface was covered with bovine cortical bone, clamped and incubated in fresh media. RVPE or control UHMWPE was added under the titanium disk. After 24 hr of incubation ($t=24$ hr), the

bone-titanium construct treated with control UHMWPE showed increased turbidity in the media, indicating bacterial growth. However, the media of constructs treated with RVPE were still clear, indicating absence of bacterial growth. Replacing the bacterial media with fresh media after 24 hr and incubating them for further 24 hr showed turbid media again in the control branch but clear media in the RVPE branch (**Figure 5.19**). Bioluminescent imaging of the bone-titanium interface showed absence of any bioluminescence in all three components in the RVPE group after 24 hr incubation (**Figure 5.20, 5.21**). Sonication and reculturing of all the components after 48 confirmed the bioluminescent imaging that all bacteria in the RVPE constructs were eradicated (**Figure 5.22**).





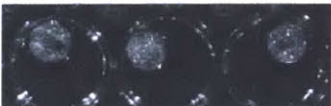
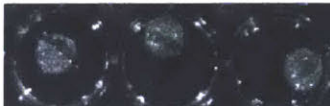
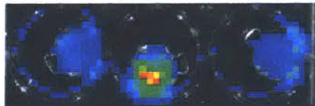
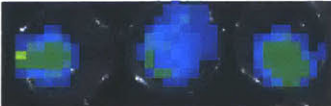
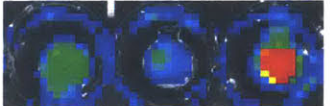
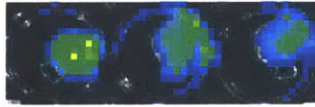
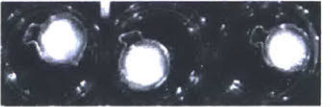
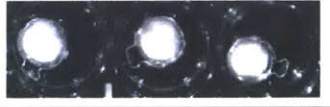
Parameter	Magnitude	Unit
In Vivo		
Synovial fluid volume in the knee (Kraus et al, Osteoarthritis Cartilage, 2007, 15(10):1217-1220).	3.0 ± 1.1	ml
Approximate tibial insert dimension (L x W x H)	40 x 80 x 6	mm
Titanium-Bone interface surface area from tibial tray (approximate using 40 x 80 mm as contact area)	3.2 x 10 ³	mm ²
Titanium-Bone interface surface area from tibial tray (approximated to be twice the surface area from tibial tray)	6.4 x 10 ³	mm ²
Total titanium-bone interface area	9.6 x 10 ³	mm ²
In Vitro		
Titanium-Bone Interface Area	7.1	mm ²


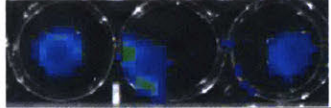


RV-PE surface area	2.4	mm ²
Media (1 ml media was used instead of 2.2 uL to ensure the bone, titanium, and RV-PE were all immersed. Using 1 ml instead of 2.2 uL was a worse case scenario because the eluted antibiotics were diluted by ~450 times).	2.2	uL

Table 5.3. Calculation of RV-PE to Titanium-Bone interface Ratio



clamped. Control or RVPE was then added under titanium disk and incubated in fresh Mueller-Hinton II media for 24 hr. After 24 hr, old media was replaced with fresh media and re-incubated for 24 hr.

Titanium Plate			
	0 hr	24 hr	48 hr
Control			
RVPE			
Bone			
	0 hr	24 hr	48 hr
Control			
RVPE			
Polyethylene			

	0 hr	24 hr	48 hr
Control	N / A		
RVPE	N/A		

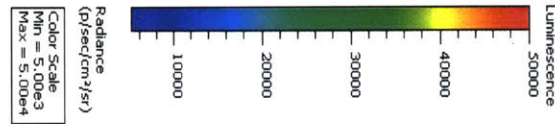
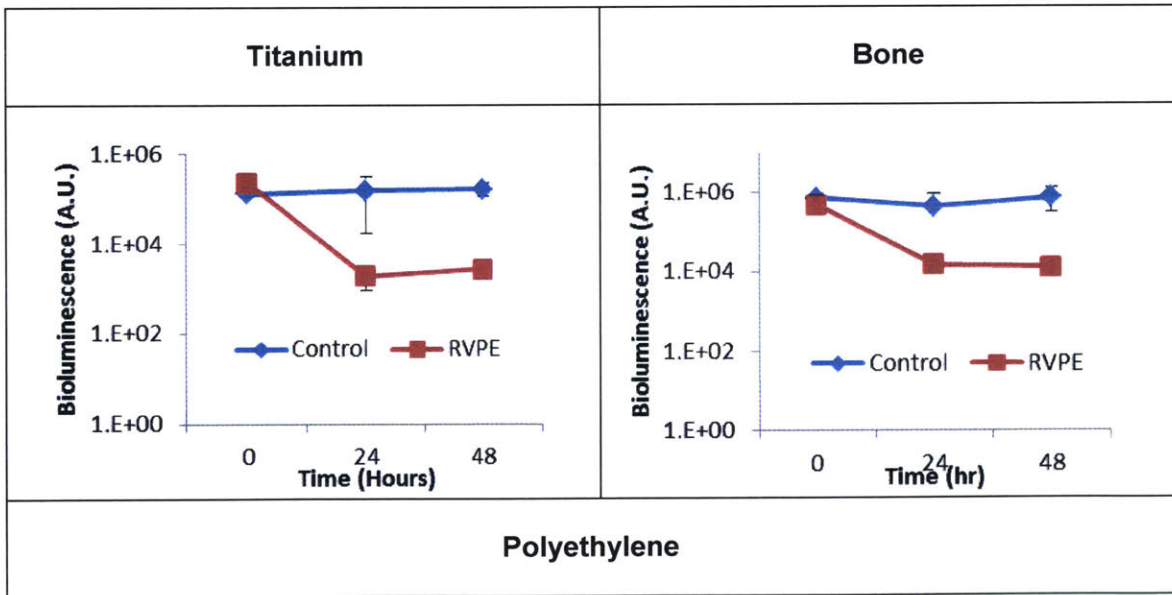


Figure 5.20. Bioluminescent imaging of live Xen29 that formed biofilm on the titanium disc, cortical bone, and polyethylene component in the RVPE and control groups.



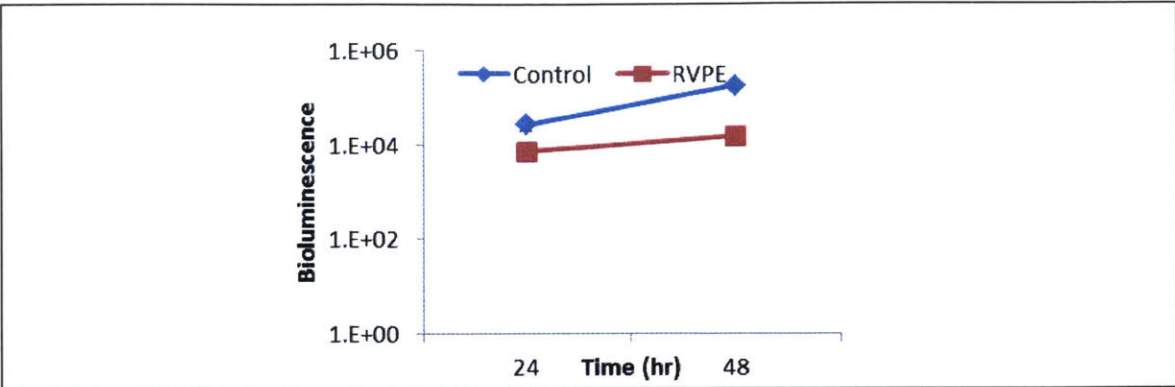


Figure 5.21 Quantification of the bioluminescent signal from the bioluminescent images shown at Figure 5.20.

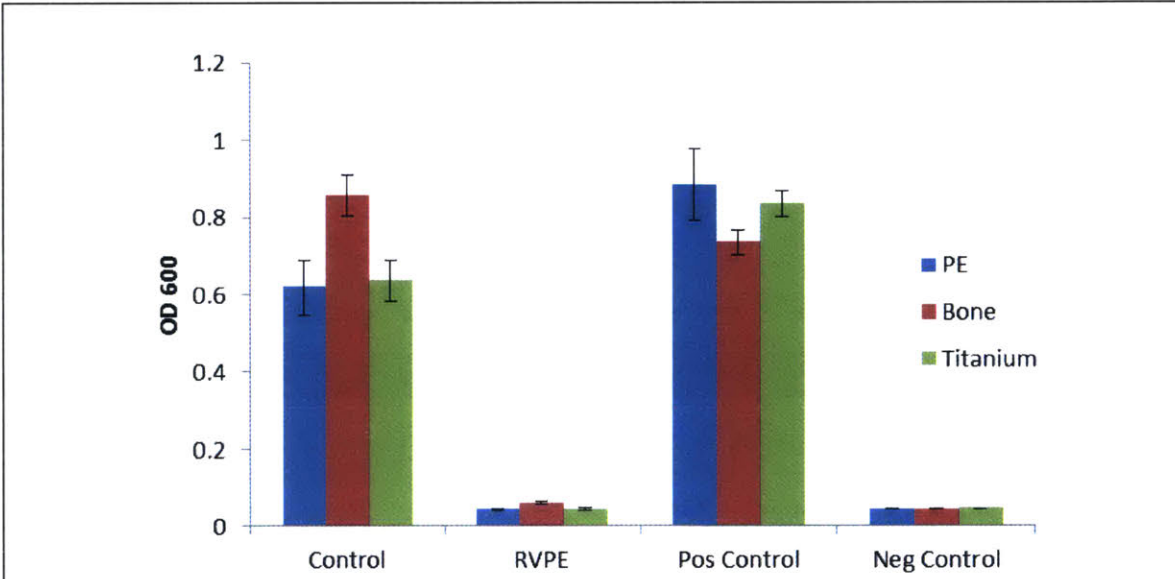


Figure 5.22. Sonication and reculturing of bacteria adherent on the surface of the titanium, bone, and polyethylene components after 48 hr time points.

Kinetic of Biofilm Eradication by RVPE

To study the kinetics of biofilm eradication by RVPE, a similar sandwich experiment as mentioned above was performed with 42 constructs (21 constructs for RVPE and 21 constructs for control). At pre-defined time points (6 hr, 24 hr, 48 hr, 96 hr, 120 hr, 1 wk, 2 wk, n=3 each for

each time point), bone and titanium were stained with live-dead imaging kits and imaged with two-photon fluorescence microscopy.

Two-photon live-dead fluorescence excitation imaging of the Ti beads revealed > 95 % biofilm eradication in the RV-PE group within 96hr, while the bacteria viability in the controls remained constantly elevated for 2 weeks (Figure 5.23, 5.24).

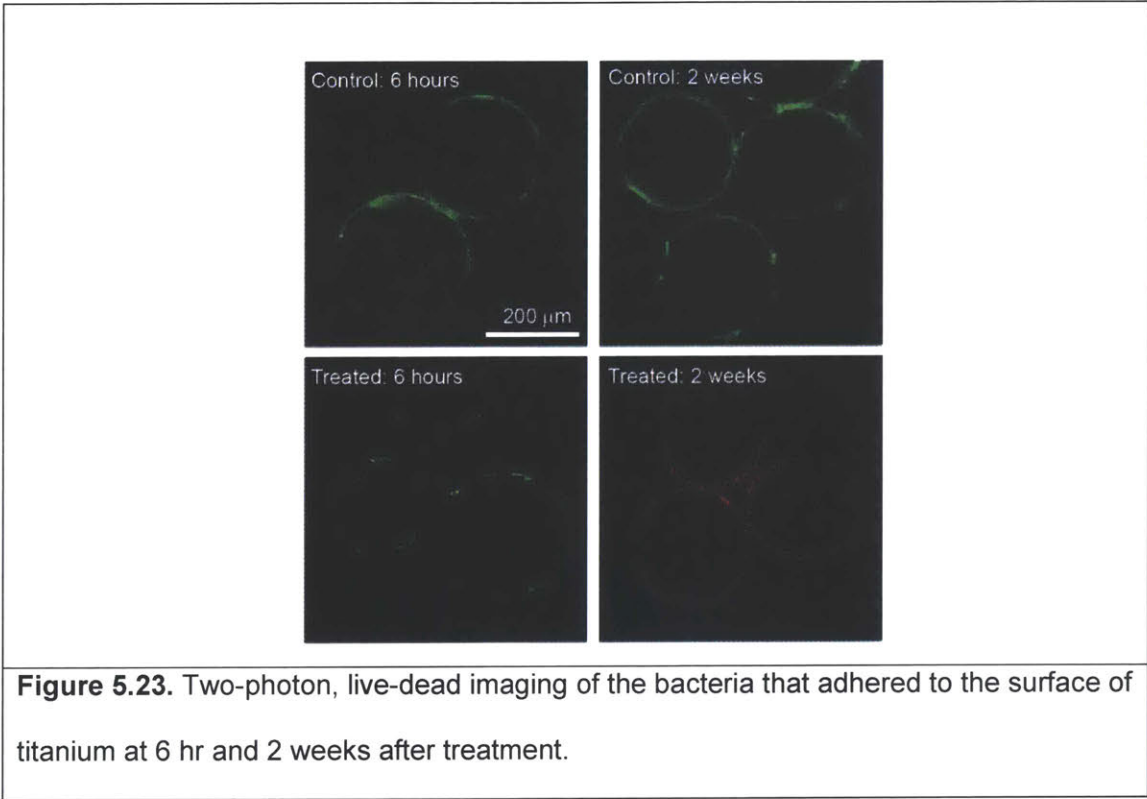
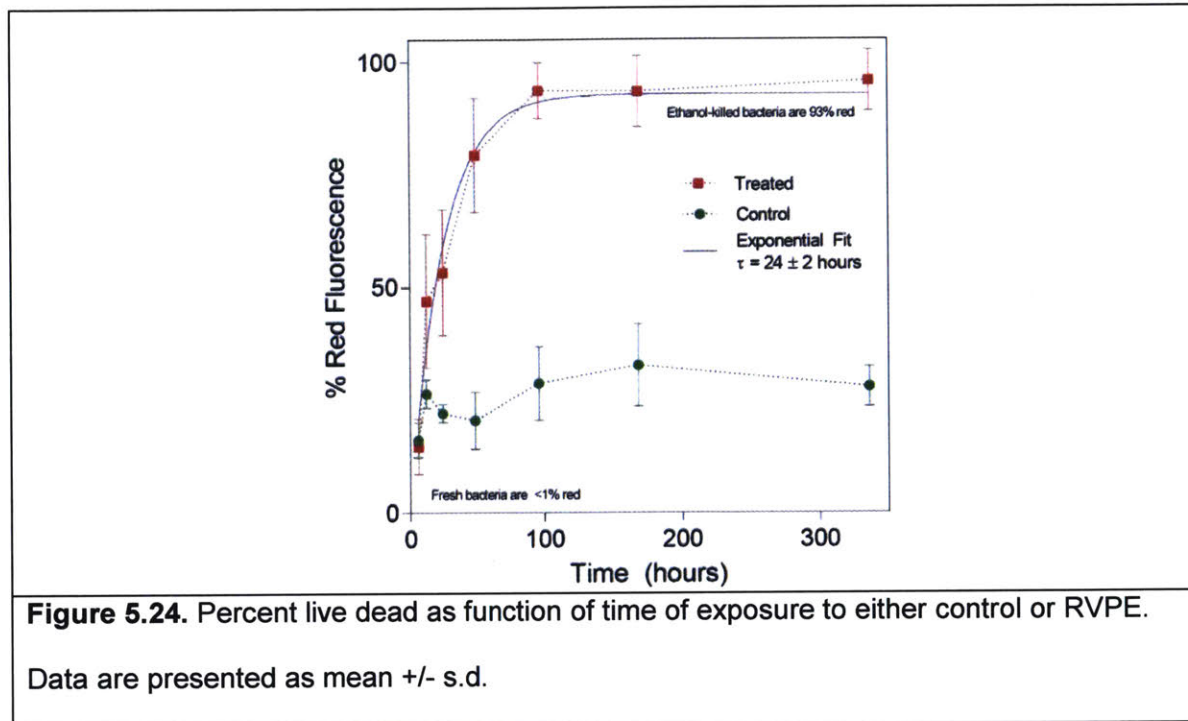


Figure 5.23. Two-photon, live-dead imaging of the bacteria that adhered to the surface of titanium at 6 hr and 2 weeks after treatment.



Discussion

Because of the poor bone and joint penetration of most antibiotics[423], treating PJI solely with systemic antibiotics (intravenous, oral, intramuscular) results in high reinfection rate [424] [12]. To address this problem, polymeric matrices have been used as local antibiotic delivery devices because they enable more effective drug delivery directly to the infected site [465]. Two general strategies are most commonly used for local antibacterial delivery: antibacterial coating on orthopedic implant and drug eluting antibacterial implant. Previously reported approach with an orthopaedic implants suffered from several drawbacks including insufficient antimicrobial release, the coating unintentionally inhibit healing process[7], and coating unintentionally debonded from the surface of the implant during implantation or during patient's movement [430]. Using other polymeric materials for local delivery of antibiotics in the form of beads [434] [435], spacer[9, 294, 429], or bone defect fillers[466] carries several drawbacks such as degradation products that can be toxic [7], drug elution rates that fall below

effective levels [8], and drug releases with low efficacy [8]; none of these have sufficient mechanical strength to be used as fully load bearing and articulating prosthetic joints [9, 300]. The most commonly used polymers to treat PJI are antibiotic-eluting BC made of PMMA [467], which can only be used in limited load-bearing applications such as spacers between the first and second stage replacement surgery [468]. However, antibiotic-eluting bone cements have several major drawbacks such as high dislocation and fracture rate [9, 300], less sustained elution [459, 460], and risk of recolonization by bacteria[460].

To address the need for antibiotic-eluting polymers with high mechanical strength and wear resistance for usage as prosthetic joint, we aim to use the highly eccentric drug-eluting UHMWPE. The mechanical and tribological requirements of UHMWPE as load-bearing prosthetic joints are dictated by the biomechanics of each joint. In the hip, UHMWPE is used as acetabular cup with maximum contact stress of 14-16 MPa.[49] In the knee, UHMWPE is used as tibial insert with higher maximum contact stress of 16-28 MPa [59, 60]. In addition to strength requirements to resist deformation and fracture against contact stresses, wear resistance is required against multi-directional articulating motion between UHMWPE and its counter surface in the joints. Multidirectional, but not unidirectional motion has been shown to induce transverse rupture of elongated UHMWPE fibrils, resulting in the wear of UHMWPE bearing surfaces.[61] Wear resistance is an essential requirement because wear particles have long been associated with peri-prosthetic osteolysis, which leads to loosening and failure of the implants.

Radiation cross-linking is the universally accepted method of increasing wear resistance of UHMWPE bearing surfaces. Increasing radiation dose is used to increase wear resistance but also decreases mechanical strength and toughness. The lowest radiation dose used is for 'conventional' UHMWPE, which receives radiation only for the purpose of sterilization in the (0-40 kGy) range. There are number of highly cross-linked UHMWPEs (>40 kGy irradiated), which have been developed for higher wear resistance [33, 62]. In total hips, where wear resistance

requirements are higher (due to higher frequency of multidirectional motion), about 95% of all joints comprise a highly cross-linked UHMWPE bearing surface[63] in contrast to about 50% of total knee replacements, where wear resistance requirements are less stringent (due to higher frequency of unidirectional motion).

Tensile mechanical testing, impact testing and in vitro pin-on-disc wear testing or simulator testing are the most common methods of evaluating UHMWPE formulations in vitro[63]. Conventional UHMWPE has an ultimate tensile strength (UTS) of 47-50 MPa[64], an elongation to break (EAB) of 373-421 %[64], impact strength (IS) of 90-96 kJ/mm² [65] and wear rate of 6-11 mg/million cycles [66]. Highly-crosslinked UHMWPEs have UTS of 34-47 MPa [29, 67], EAB of 230-330 %[29], IS of 56²-122 kJ/mm² [65], and wear rates of 0.1-2.3 mg/million cycles [66]. Highly cross-linked UHMWPEs (without distinction of dose at this point) have decreased the incidence of peri-prosthetic osteolysis 87% over the last decade [3] compared to conventional UHMWPE in total hips.

Our goal here was to develop methods by which therapeutic agents are incorporated into UHMWPE load-bearing surfaces, without increasing any risk associated with their use, and adding the benefit of antibacterial properties. However, it is also expected that any changes to the structure of the polymer may result in the compromise of one or more properties. There are UHMWPEs with a range of properties that are successfully used in different applications and in different patient populations according to the clinicians' discretion as briefly explained above. Drug-eluting UHMWPE with mechanical and tribological properties within the limits of conventional and highly-crosslinked UHMWPEs are expected to perform well as a part of fully weight-bearing prosthetic joint.

A fully load-bearing permanent implant using UHMWPE can address the shortcomings of other drug-eluting polymers in joint replacement. Our novel method of creating highly


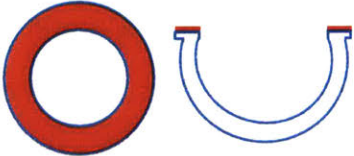

² Unpublished data for E1® Biomet

eccentric drug clusters combined with our spatial controlled consolidation technology can enable the sustained delivery of the state-of-the-art antibiotic combinations without sacrificing the required mechanical properties of the implant. The combination of UHMWPE's long track record of safety and efficacy [29] with well-known antibiotics such as vancomycin and rifampin has the potential of eliminating the use of antibiotic-eluting spacers and reducing the gold standard two-stage treatment surgeries for PJI to a single surgery. Based on the mechanical properties of VPE and RVPE and the contact stresses of the joint[309], we proposed several implant designs (**Table 5.4**). All of the designs have mechanical strengths and wear rate within the range of clinically used UHMWPE (conventional UHMWPE and highly-crosslinked UHMWPE (HXLPE) (**Table 5.4**). Therefore, in addition to their ability in eradicate bacteria, we expect them to have similar lifetime and non-infectious complication rate as conventional UHMWPE or HXLPE.

The VPE and VPE+RVPE designs were intended for temporary (6-8 weeks) usage or patients with low activity because the wear rate was closer to conventional UHMWPE than HXLPE. The VPE design was intended for addressing acute prosthetic joint infection, where minimum amounts of bacterial biofilm are involved. The VPE+RVPE design was intended for addressing chronic prosthetic joint infection, where significant bacterial biofilm was involved. In the case for knee tibial insert, the RVPE layer would be on the backside of the insert (opposite to the articulating surface). The wear rates of VPE and VPE+RVPE were similar to those of conventional UHMWPE (**Table 5.4**), which had > 90% survival rate after 10 years; the cumulative incidence of revision due to aseptic loosening is 1.6 %. However, given that HXLPE's cumulative incidence of revision due to aseptic loosening of <0.5 %[2], material with lower wear rate was ideal.

For long term usage (years), we proposed the RVPE only design (**Table 5.4**, which was intended for implantation during the second stage surgery or during single stage replacement

surgery. Because osteolysis usually occurs after several years[44], minimizing wear rate to the level of state-of-the-art HXLPE was desired. Therefore, in the RVPE only design, the articulating surface was composed of HXLPE which gave the implant a low wear rate. In the case of a knee tibial insert, the RVPE layer would be on the backside of the insert. To our knowledge, this is the first report of an antibiotic-eluting polymer with high enough mechanical strength and favorable wear rate to be used as part of a fully functional prosthetic joint for temporary or long-term use.

Implant	UTS (MPa)	EAB (%)	Impact Strength (kJ/mm ²)	Wear Rate (mg/MC)
VPE (Brown=VPE) 	32.9 ±1.9	245 ±22	79.5 ±3.4	9.6 ±1.3
RVPE (Red=RVPE, White= Highly-Crosslinked UHMWPE) 	31.4±5.3(RVPE) 34.0±3.0(HXLPE)	228±22(RVPE) 230±17(HXLPE)	78.7±3.9 (RVPE) 62.2±1.6 (HXLPE)	9.0±1.0 (RVPE) 0.6±0.0(HXLPE)
VPE+RVPE (Red=RVPE, Brown = VPE) 	31.4 ±5.3 (RVPE) 32.9 ±1.9 (VPE)	228 ±22(RVPE) 245 ±22(VPE)	78.7 ±3.9(RVPE) 79.5 ±3.4(VPE)	9.0 ±1.0 (RVPE) 9.6 ±1.3 (VPE)
Conventional UHMWPE	46.2±1.5	414 ±21	119.3 ±2.3	9.3 ±0.80
Highly-Crosslinked UHMWPE (HXLPE)	34.0±3.0	230 ±17	62.2 ±1.57	0.6 ±0.03

ASTM F648	27	250	25	N/A
Table 5.4. Implant Design Based on VPE and RVPE and Comparison of Their Mechanical and Wear Rate to Conventional UHMWPE, Highly-Crosslinked UHMWPE (HXLPE), and ASTM F648				

In addition to the risk of mechanical failure during weight bearing, antibiotic-eluting PMMA BCs showed bacterial adhesion [469] even during antimicrobial elution [461]. On the other hand, radiation-sterilized VPE prevented bacterial adherence during antibiotic elution and decreased it further up to 6 months through surface-bonded vancomycin (**Figure 5.12 and 5.13**). This is in agreement with previous reports on vancomycin grafting on titanium preventing biofilm formation [433]. Reduction of bacterial adherence and hence biofilm formation was shown to reduce infection rate [470]. Surface-bound vancomycin has been shown to eradicate bacteria by making the peptidoglycan layer less rigid and more permeable. As a result, the osmotic pressure will cause bacterial death[433]. Thus, in addition to sustaining effective concentration of antibiotic elution, grafting of the antibiotic by irradiation may hinder bacterial attachment in antibiotic-eluting UHMWPE providing that biofouling did not completely cover the surface with grafted vancomycin.

Usage of antibiotic intravenously, orally, or in the form of antibiotic eluting bone cement, VPE, and RVPE all come with a risk of developing resistance bacteria. It has been shown that even when bacteria are exposed to 200 times the minimum inhibitory concentration (MIC), they can develop resistance within 10 hr[57]. This suggests that our previous understanding of bacterial resistance [58] may be incomplete. Nevertheless, by matching the vancomycin elution of VPE to clinically-used Vancomycin-eluting bone cement (**Figure 3d**), we expect VPE to pose no extra risk in bacterial resistance development to antibiotic eluting bone cement. In the case of RVPE, by creating elution of vancomycin that exceeds the antibiotic eluting bone cement

(**Figure 3d**), and by ensuring that vancomycin elution is always higher than rifampin to prevent sole exposure of bacteria to rifampin, we also expect that RVPE will not pose any extra risk of bacterial resistance development to antibiotic eluting bone cement.

Conclusion

In conclusion, VPE and RVPE had superior mechanical strength and wear rate than antibiotic eluting bone cement with similar to higher antibiotic elution rate. In vitro antibacterial testing showed that VPE and RVPE can potentially be used in lieu of antibiotic bone cement. Therefore these materials warrant further in vivo testing.

Chapter 6

Pre-Clinical Safety and Efficacy Testing of Drug-Eluting UHMWPE for Treatment of PJI

Introduction

In this chapter we tested safety and efficacy of the optimized antibiotics eluting UHMWPE (VPE and RVPE) in murine and lapine infection models. Because vancomycin is much less effective against biofilm bacteria than rifampin[471, 472], we tested the VPE in the primarily planktonic infection to simulate acute prosthetic joint infection and the RVPE in the primarily biofilm infection to simulate chronic prosthetic joint infection. In our lapine joint infection models, we compared the efficacy of VPE and RVPE against antibiotic eluting bone cement, which is part of the gold standard of current PJI management.

Both Planktonic and Biofilm Bacteria are Involved in Prosthetic Joint Infection

Based on the time onset of infection, prosthetic joint infection is commonly divided into either acute or chronic. Acute infection is defined as one that is clinically manifested within the first three months after surgery [107]. Acute infection is usually caused by a virulent organism (e.g. *S. aureus* and gram-negative bacilli) that was exogenously seeded during prosthetic joint implantation [107]. Chronic infection is defined as one that is clinically manifested after three months postoperatively, and usually is caused by less virulent organisms such as coagulase-negative staphylococci and *P. acnes* [107].

The bacteria in acute forms of PJI originate from either direct contact or aerosolized contamination of the joint prosthesis or surgical site [447]. In the acute prosthetic joint infection, bacteria are often found in free-floating (planktonic) form in synovial fluid [473] and in immature stage biofilm [474] on the prosthesis. The immature stage of biofilm involved in the acute PJI renders it more sensitive to antimicrobial agents (as compared to the mature biofilm) and is more prone to be eliminated by the immune system [109]. The presence of a prosthesis lowered the bacteria inoculation concentration sufficient to cause symptomatic infection: in a hip hemiarthroplasty rabbit model, less than 10^2 cfu of *S. aureus* was sufficient to cause infection, as compared to 10^4 cfu when no implant was placed [475]. Because the bacteria still have high sensitivity toward antimicrobials, relatively good control of infection can be achieved (86 % at three years) for treatment of acute PJI with debridement of necrotic tissues, exchanging the UHMWPE liner, and local application of high dose antibiotics via antibiotic eluting bone cement [476]. In comparison, none of the patients who had a late chronic infection could be successfully treated with debridement, UHMWPE liner exchange when the remaining components of the prosthesis were retained [477].

While some chronic infections originate elsewhere in the body and are hematogeneously seeded into the joint [478], chronic infection can also originate from direct contact or aerosolized contamination of the joint prosthesis or surgical site [478]. However, because the bacteria involved have less virulence, the infection is clinically manifested several months to years post-surgery [479]. Because chronic infection usually involves mature and extensive biofilm formation on the implanted material, two-stage revision surgery is often needed to eradicate infections [136].

Based on the stratification of clinically presented infections and the differences in their susceptibility to treatment with antibiotics, we designed two animal models to simulate a primarily planktonic and a primarily biofilm infection. The primarily planktonic infection model is

intended to mimic acute onset of PJI where abundant planktonic bacteria exist and minimum biofilm is formed. The primarily biofilm infection model is intended to mimic chronic onset of PJI where abundant biofilm is formed on the implant material.

Bacteria Adhere to Intra-articular Components and Bone-Implant Interface

Bacterial isolation from retrieved total knee prosthesis revised due to prosthetic joint infection showed the presence of adherent bacteria on all knee components (femoral component, tibial tray, tibial insert and patellar component)[102]. The highest amount of bacteria was found in the tibial insert which was made of UHMWPE, followed by the tibial tray, femoral component, and the patellar component, all of which were made of metal [102]. Bacterial isolation from retrieved total hip prostheses due to prosthetic joint infection showed that bacteria adhered to all four components of the total hip prosthesis: femoral stem, femoral modular head, acetabular liner, and acetabular-cup/shell[101]. Highest bacterial adherence was found on the acetabular liner, which was made of UHMWPE, followed by the femoral head, the acetabular cup, and the femoral stem, all of which were made of titanium or titanium alloy (Ti6Al7Nb) [101].

These results showed three important points regarding bacterial adherence to infected hip prosthesis: First, bacteria are more adherent to UHMWPE than to metals such as titanium and titanium alloy. Second, bacteria adhered to a higher extent to intra-articular components such as the acetabular liner and the femoral head than to intraosseous components such as the acetabular cup and the femoral stem. Third, bacteria could be found both in the intra-articular space and the bone-implant interface.

Therefore, to effectively mimic prosthetic joint infection, bacteria must be present both in the intraarticular space and in the bone-implant interface. In that respect, an effective treatment

for PJI must effectively eradicate bacteria in the intraarticular space and in the bone-implant interface.

Vancomycin is Effective against Planktonic bacteria and Immature Biofilm but not against Mature Biofilm

Intravenous vancomycin is part of the gold standard treatment of prosthetic joint infection [136]. Local delivery of vancomycin as part of multi-pathway antibiotic administration [480] either through vancomycin-eluting bone cement [481] or direct infusion to the infected joint was also shown to be effective treatment for prosthetic joint infection.

While vancomycin was able to significantly reduce bacterial load in young biofilm (6 hr old biofilm), it is ineffective against mature biofilm (48 hr old biofilm)[471, 472]. The inability of vancomycin alone to eradicate mature bacterial biofilm even when its concentration exceeds the minimum inhibitory concentration (MIC) and the minimum bactericidal concentration (MBC) of the microorganism [482, 483] is not due to the inability of vancomycin to penetrate the biofilm [482]. In fact, vancomycin concentration in the biofilm often exceeds the MIC and MBC [483]. On the other hand, the reduced vancomycin susceptibility observed in biofilm bacteria is more likely due to a phenotypical change of the bacteria themselves [484].

To effectively eradicate bacteria in the biofilm, a combination of antibiotics, which can be effective against the various stages of bacterial growth is required, with one of the agents ideally acting on adherent-stationary phase bacteria [485]. Among combination antibiotics, rifampin has been shown both in vitro and in vivo to be one of the most powerful co-agents in biofilm bacteria eradication [486], with excellent biofilm penetration and excellent bactericidal activity in biofilm shown for rifampin+daptomycin [487], rifampin+vancomycin [482, 488], and rifampin+linezolid [482, 488] .

In summary, vancomycin alone is effective against planktonic *S. aureus* but is much less effective against *S. aureus* in the biofilm [471, 472]. Therefore, to eradicate the bacteria in the biofilm, addition of agents that are active against adherent-stationary phase bacteria, such as rifampin should be used. A combination of rifampin and vancomycin is currently one of the primary combinations drug of choice for treatment of *S. aureus* associated PJI because of its good ability to eradicate biofilms [136, 482, 488]. Therefore, we chose combination of rifampin-vancomycin-eluting UHMWPE (RVPE) to eradicate biofilm bacteria in our in vivo animal model.

Gold Standard Treatment in Antibiotic-eluting Bone Cement Spacers

As mentioned in the previous chapter, the gold standard treatment for PJI comprising the local delivery of antibiotics involves implantation of an antibiotic eluting bone cement spacer during the first stage of a two-stage revision. One of the gold standard antibiotic eluting bone cement spacers is antibiotic-loaded acrylic cement (PROSTALAC) system because it has several advantages over other antibiotic eluting bone cement spacer: First, the PROSTALAC system allowed functional hip movement and partial weight bearing [489, 490]. Second, various antibiotics were incorporated into the PROSTALAC system, such as vancomycin only[491], tobramycin alone[492], tobramycin-vancomycin[492-494]. In conjunction with systemic antibiotics, the reinfection rate after two stage replacement surgery using PROSTALAC as spacer during the first revision surgery ranges from 9 % [492] to 15 %[493].

A major downside with PROSTALAC is functional and mobility limitation of patients: patients are only allowed to partially weight bear during the first couple of weeks after the first surgery, and then walk with the aid of crutches until the second revision surgery is performed[491]. Major complications after PROSTALAC implantation are dislocation and implant fracture (8 %)[495]. Patients with PROSTALAC reported higher pain and stiffness than

primary arthroplasty patients[495]. Patients with PROSTALAC also reported lower physical function than primary arthroplasty patients [495].

Because PROSTALAC system containing tobramycin and vancomycin is the most widely reported [492-494] of all PROSTALAC system, we used tobramycin-vancomycin eluting PROSTALAC system to compare against VPE and RVPE for our *in vivo* studies.

Methods

Murine Planktonic Bacterial Infection Model

Study approval was granted from Massachusetts General Hospital Institutional Animal Care and Use Committee (protocol 2010N000065).

Studies were conducted to test the efficacy of VPE against bioluminescent *S. aureus* (Xen 29) in the dorsal subcutaneous pockets of BL6/C57 fully immune-competent mice. Minimum inhibitory concentration of Vancomycin against Xen-29 was 1 ug/ml.[496] Ten mice were used in this study, randomly divided into two groups: control group and the VPE group. Anesthesia was achieved using intramuscular ketamine-xylazine (40 mg/kg-5 mg/kg) and inhaled isoflurane (1.5-2.5 %) supplemented with oxygen (1.2 liter/min). Pre-emptive analgesia was administered before the procedure started (buprenorphine 0.02 mg/kg). No pre or postoperative antibiotics were administered. Each mouse in the control group received a disc implant made from conventional UHMWPE (diameter = 6 mm, thickness = 3 mm) in the dorsal subcutaneous pocket, while each mouse in the VPE group received a disc implant made from VPE (diameter= 6 mm, thickness = 3 mm) in the dorsal subcutaneous pocket. After closure of surgical incision using monofilament suture, each mice in both groups received subcutaneous injection of 5×10^7 cfu of Xen 29 in 50 uL 0.9% saline. This concentration of bacteria for inoculation was injected adjacent to the implants. Bioluminescence was measured using an IVIS

100 imaging system 5 minutes after bacterial injection, at 3 hr, 24 hr, and 48 hr. Note that only live bacteria luminesce, and therefore the amount of live bacteria is directly proportional to the total bioluminescence.

At the end of the study (48 hr after bacterial injection), all mice were sacrificed and implants were explanted aseptically and placed into a sterile 15cc Falcon tube containing 2 ml 0.9 % saline. Falcon tubes containing the explants and saline were sonicated to detach the bacteria from the explants, 100 uL were sampled and added to 1900 uL of fresh Mueller-Hinton II broth, and incubated at 37°C for 24 hr. Concentrations of bacteria were then determined by measuring absorbance at 600 nm (OD 600).

Murine Biofilm Bacterial Infection Model

Study approval was granted from Massachusetts General Hospital Institutional Animal Care and Use Committee (protocol 2010N000065).

Studies were conducted to test the efficacy of RVPE against biofilm formed by bioluminescent *S. aureus* (Xen 29) on titanium discs implanted in the dorsal subcutaneous pockets of BL6/C57 fully immune-competent mice. The minimum inhibitory concentration (MIC) of rifampin against Xen-29 was 0.01 ug/ml.[496] Ten mice were used in this study, randomly divided into two groups: control group and a RVPE group. All mice in this study received a titanium disc (10 mm diameter, one surface covered with titanium bead of 100-300 um in diameter) with pre-grown Xen-29 biofilm on the beaded surface. Each mouse in the control group received a disc implant made from conventional UHMWPE (diameter = 6 mm, thickness = 3 mm) in the dorsal subcutaneous pocket, while each mouse in the RVPE group received a disc implant made from RVPE (diameter= 6 mm, thickness = 3 mm (1 mm of RVPE, 2 mm of conventional UHMWPE) in the dorsal subcutaneous pocket. After closure of the surgical incision using monofilament suture, each mouse in both groups received a subcutaneous injection of 5 x

10^7 cfu of Xen 29 in 50 μ L 0.9% saline. This concentration of bacteria for inoculation was injected adjacent to the implants. Bioluminescence was measured using an IVIS 100 imaging system 5 minutes after bacterial injection, at 3 hr, 24 hr, and 48 hr. Note that only live bacteria luminesce, and therefore the amount of live bacteria is directly proportional to the total bioluminescence.

At the end of the study (1 week after bacterial injection), all mice were sacrificed and implants were explanted aseptically and placed into a sterile 15cc Falcon tube containing 2 ml 0.9 % saline. Falcon tubes containing the explants and saline were sonicated to detach the bacteria from the explants, 100 μ L were sampled and added to 1900 μ L of fresh Mueller-Hinton II broth, and incubated at 37°C for 24 hr. Concentration of bacteria were then determined by measuring its absorbance at 600 nm (OD 600).

Lapine Planktonic Bacteria Prosthetic Joint Infection Model

Study approval was granted from Pine Acres Rabbitry Farm Institutional Animal Care and Use Committee (protocol 15-06, Norton, MA). A total of ten fully immune-competent, skeletally mature male New Zealand rabbits aged 12 months were used in this study. Animals were randomly assigned to control (non-antibiotic eluting UHMWPE) or VPE groups (7 wt% vancomycin-blended UHMWPE). Each rabbit in the control group received two UHMWPE-only implants (3 mm diameter x 6 mm in height) in the patellofemoral groove, and one beaded titanium rod in the tibial canal (4 mm diameter x 12 mm length). Each rabbit in the VPE group received two VPE implants (same dimensions as control) in the patellofemoral groove and one beaded titanium rod in the tibial canal (same dimensions as control).

Anesthesia was achieved using intramuscular ketamine-xylazine (40 mg/kg-5 mg/kg) and inhaled isoflurane (1.5-2.5 %) supplemented with oxygen (1.2 liter/min). Pre-emptive analgesia was administered before the procedure started (buprenorphine 0.02 mg/kg). No pre or postoperative antibiotics were administered. The rabbits were placed in the supine position and the right or left leg was prepped and draped in a sterile fashion (randomization of operated leg established using random.org). A parapatellar incision was performed, the joint capsule was incised, the patella was displaced, and two osteochondral defects were created in the trochlear groove (2.9 mm diameter x 6 mm depth). No antibiotics (control branch) or VPE (VPE branches) implants were press-fitted into the defects. For the titanium implant, the tibial plateau was accessed, and a defect was created by drilling distally into the marrow, creating a 3.9 mm diameter and 12 mm depth defect. 5×10^7 cfu of bioluminescent *S. aureus* (Xen 29, Perkin Elmer) in 50 uL 0.9 % saline was injected into the tibial defect, followed by press-fitting the titanium implant, sealing the bacteria *in situ*. The patella was then replaced onto the trochlear groove and tissues were sutured. An additional dose of 5×10^7 cfu of bioluminescent *S. aureus* (Xen 29, Perkin Elmer) in 50 uL 0.9 % saline was injected into the knee. All animals received buprenorphine 0.02-0.05 mg/kg SC or IM q12 h for 5 days following surgery. After recovering from anesthesia, rabbits were housed individually in cages (22"x25"x26"). Load bearing on implants was allowed immediately after surgery, as no postoperative limiting motion device was utilized. Twice a day, rabbits were removed from their cages and placed in an open space to visually inspect the operated joint and gait. All animals were monitored at least twice per day for 3 days following surgery and at least once per day for the remainder of the study. Complete blood count (CBC) and chemistry (Vancomycin, Creatinine, BUN, ALT, and ALP) were assessed before surgery, and on post-operative day 3, day 7, day 14, and day 21.

Post-mortem bioluminescence imaging was performed on all operated knees (a midline incision was performed on the knee and the joint capsule was opened to expose the joint space).

Bioluminescence signal was measured whenever the rabbits expired, or when the study endpoint was reached (day 21). After imaging, the knees were dissected to aseptically isolate the femur, quadriceps tendon (including patella and patellar tendon), tibia, titanium and UHMWPE implants. The titanium rods were stained with BacLight® Bacterial Live-Dead Stain and imaged using two-photon fluorescence microscopy to detect the presence of live bacteria. The femur, quadriceps tendon, tibia, and UHMWPE implants were separately sonicated in sterile saline; saline was then cultured in Mueller-Hinton II broth at 37°C for 24 hr to detect presence of live bacteria.

Lapine biofilm bacteria prosthetic joint infection model

Ten rabbits were randomly assigned to control (non-antibiotic eluting UHMWPE) or RVPE groups (a layered construct of 6.7 wt % vancomycin and 3.3 wt % rifampin in UHMWPE on UHMWPE without any antibiotics; Table 5.X). Each rabbit in the control group received two UHMWPE plugs without additives (each 3 mm in diameter and 6 mm in length) in the patellofemoral groove, and one beaded titanium rod covered with Xen 29 *S. aureus* biofilm in the tibial canal (4 mm diameter and 12 mm in length). Each rabbit in the RVPE group received two RVPE implants (each 3 mm in diameter and 6 mm in length) in the patellofemoral groove and one beaded titanium implant covered with Xen 29 *S. aureus* biofilm in the tibial canal (4 mm diameter and 12 mm in length).

To create the Xen 29 *S. aureus* biofilm covered titanium rod, fresh overnight liquid culture of Bioluminescent *S. aureus* (Xen 29) was diluted to 5×10^4 cfu/ml. 50 uL of the liquid culture was then added to the 2 ml Mueller-Hinton II broth. A sterile titanium rod was then immersed in the bacterial suspension and incubated at 37°C for 48 hr. Titanium rods were then washed with PBS twice and then imaged with bioluminescent imaging to ensure uniform biofilm

formation on all of the samples. One titanium rod was sacrificed for measurement of pre-implantation biofilm thickness. To measure the biofilm thickness, the titanium rod was stained using Live/Dead BacLight Viability kit (Molecular Probes) that contained Cyto 9 and propidium iodide and imaged using two-photon fluorescence microscopy.

Anesthesia was achieved using intramuscular ketamine-xylazine (40 mg/kg-5 mg/kg) and inhaled isoflurane (1.5-2.5 %) supplemented with oxygen (1.2 liter/min). Pre-emptive analgesia was administered before the procedure started (buprenorphine 0.02 mg/kg). No pre or postoperative antibiotics were administered. The rabbits were placed in the supine position and the right or left leg was prepped and draped in a sterile fashion (randomization of operated leg established using random.org). A parapatellar incision was performed, the joint capsule was incised, the patella was displaced, and two osteochondral defects were created in the trochlear groove (2.9 mm diameter x 6 mm depth). Control (for control branches) or VPE (for VPE branches) implants were press-fitted into the defects. For the titanium implant, the tibial plateau was accessed, and a defect was created by drilling distally into the marrow, creating a 3.9 mm diameter and 12 mm depth defect. The biofilm-laden titanium implant was then press-fitted into the tibial canal. Load bearing on implants was allowed immediately after surgery, as no postoperative limiting motion device was utilized. Twice a day, rabbits were removed from their cages and placed in an open space to visually inspect the operated joint and gait. All animals were monitored at least twice per day for 3 days following surgery and at least once per day for the remainder of the study. Complete blood count (CBC) and chemistry (Vancomycin, Creatinine, BUN, ALT, and ALP) were assessed before surgery, post-operative day 3, day 7, day 14, and day 21.

Post-mortem bioluminescence imaging, tissues and implant sonication were performed as described above.

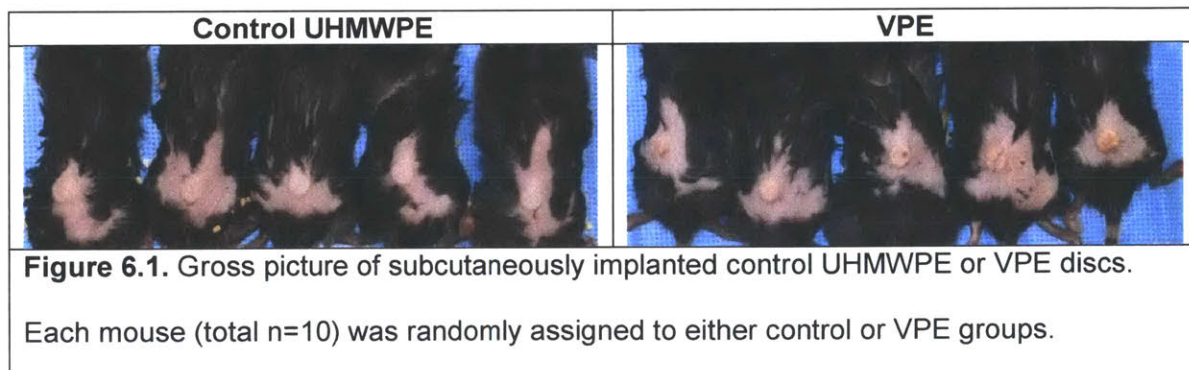
Results

Murine Planktonic Bacteria Infection Model

Ten mice were divided equally and randomly into two groups: The first group of mice received control UHMWPE discs and the second group of mice received VPE discs. Control UHMWPE and VPE discs were implanted subcutaneously on the dorsum of mice under general anesthesia.

Both mice receiving control UHMWPE and VPE fully recovered from anesthesia with no sign of acute allergic reaction (within three hours) around the implant area (**Figure 6.1**). All mice were mobile and eating normally post-anesthesia.

All mice in both control and VPE groups showed similar bioluminescence subcutaneously at the time of injection (**Figure 6.2 and 6.3**). At 3 hr, all mice in the control group showed significantly higher bioluminescence than that of the VPE group ($p < 0.05$; indicating more live bacteria in control than in VPE groups). Minimum bioluminescence was maintained in the VPE group after 48 hr, while the control group still showed high bioluminescence (**Figure 6.2 and 6.3**). Sonication of the bacteria into a sterile Mueller-Hinton II medium and subsequent re-culturing for 12 hr at 37°C showed absence of bacteria in the VPE groups but high amount of bacteria in control groups (**Figure 6.4**).



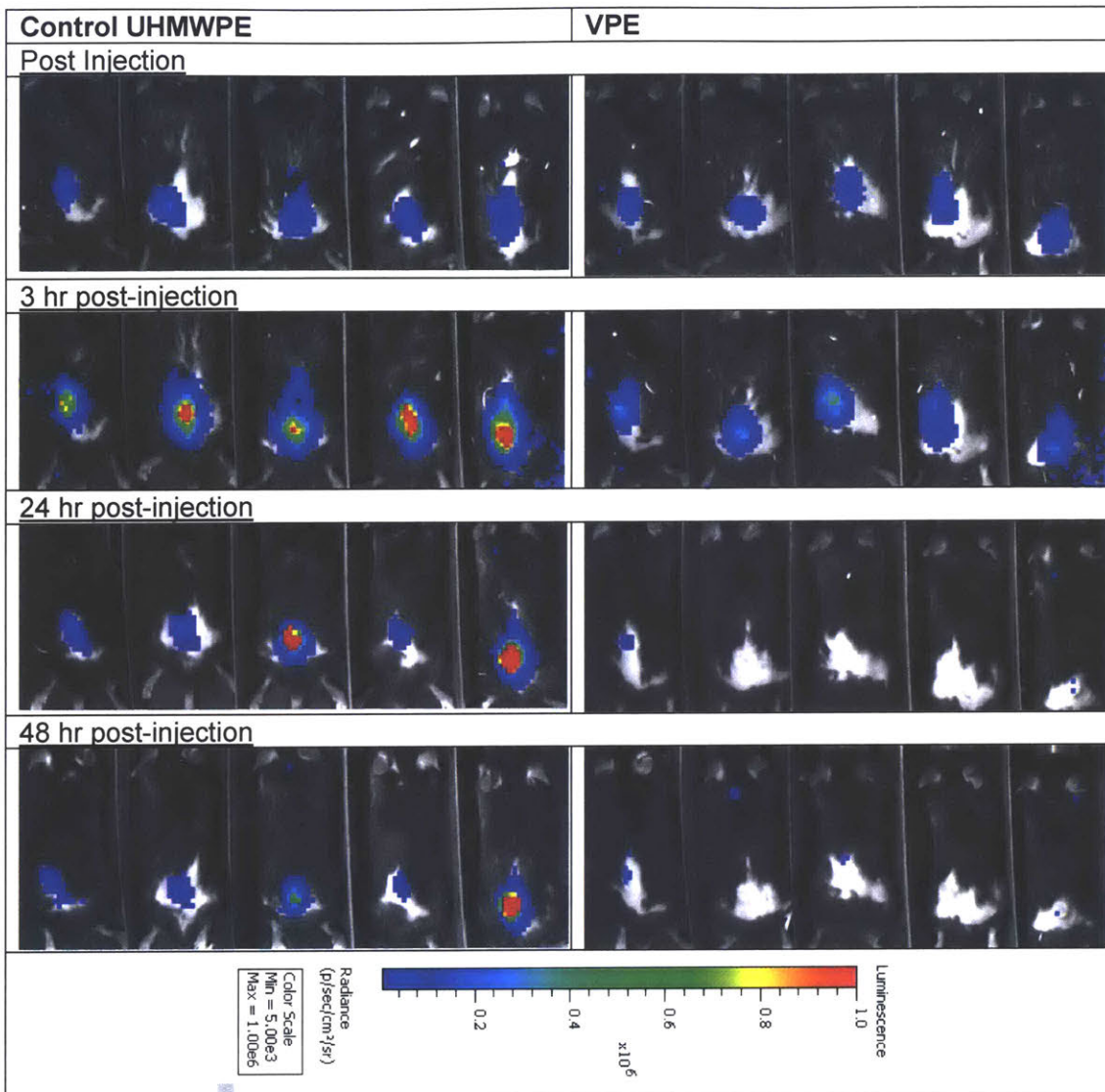


Figure 6.2. In vivo bioluminescence color map from Xen 29. Bioluminescent *S. aureus* Xen 29 was injected subcutaneously on top of the UHMWPE discs and total flux were measured by bioluminescent camera (IVIS 100, Caliper). Total flux bioluminescence map was measured immediately after post-injection, 3 hr, 24 hr, and 48 hr post-injection.

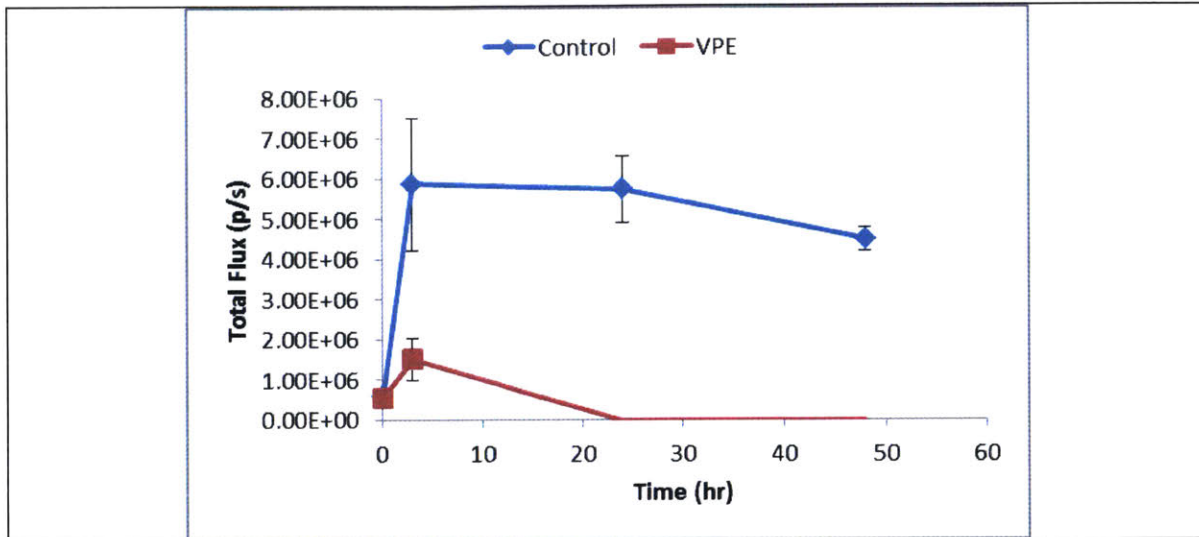


Figure 6.3. Total bioluminescence quantification around the implants. Region of interest was drawn around the implant area for each figure and total bioluminescence was calculated. Data are presented as mean \pm s.d. (n=5 for each group).

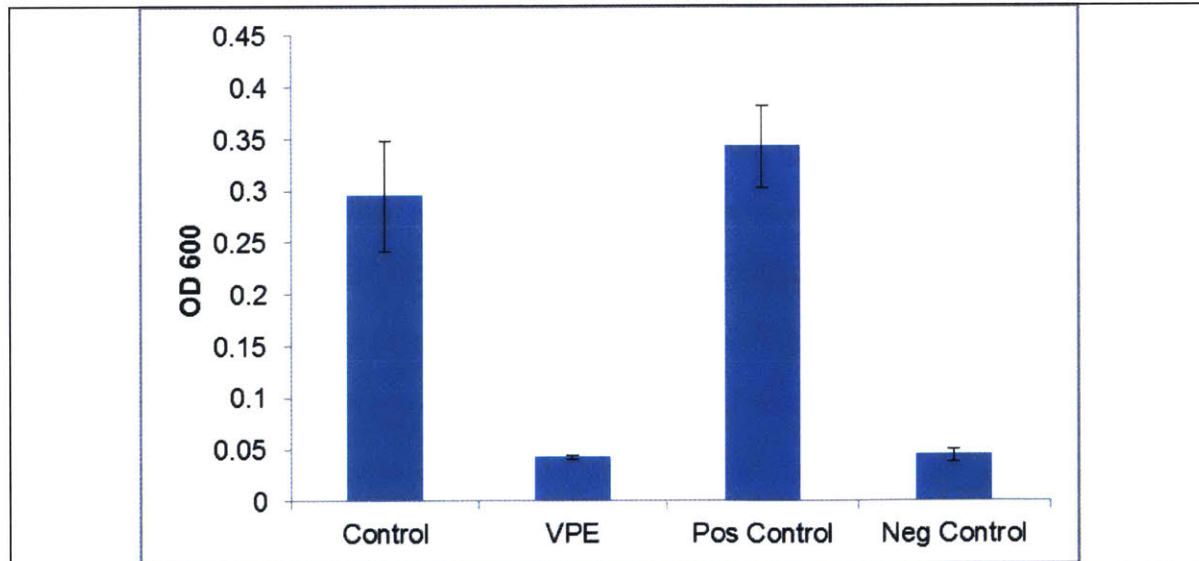


Figure 6.4. Post-Mortem sonication of tissues and explants. Absorbance at 600 nm (OD600) after sonication of control UHMWPE or VPE from the dorsal subcutaneous pocket of mice. After sonication the media was recultured for 12 hr at 37°C. Positive control was 12 hr culture of bacteria in Mueller-Hinton II media. Negative control was media only. Data

are presented as mean \pm s.d. (n=5 for each group).

Murine Biofilm Bacteria Infection Model

Ten mice were divided equally and randomly into two groups: The first group of mice received control UHMWPE discs without antibiotics and the second group of mice received RVPE discs (**Figure 6.5**). In addition to the UHMWPE discs, all mice also received a titanium disc covered with titanium beads (mean diameter of beads = 20 μ m) (**Figure 6.5**). Control UHMWPE, RVPE, and beaded titanium discs were implanted subcutaneously on the dorsum of mice under general anesthesia. Both mice receiving control UHMWPE and RVPE fully recovered from anesthesia with no sign of acute allergic reaction (within three hours) toward either control UHMWPE or RVPE (**Figure 6.5**). All mice were mobile and eating normally post-anesthesia.

All mice in both control and RVPE groups showed similar magnitudes of bioluminescence at 5 minutes after being injected subcutaneously (**Figure 6.6 and 6.7**). After 24 hr, much higher bioluminescence signal was observed in the control UHMWPE while no bioluminescence was observed in three out of four mice in the RVPE group (**Figure 6.6 and 6.7**). After 48 hr, bioluminescence was absent in all RVPE mice. Bioluminescence was consistently high for the control mice until 72 hr where all control mice were euthanized to minimize suffering. No bioluminescence was detected in RVPE groups at six days post injection and therefore euthanized for further bacteria viability analysis (**Figure 6.6 and 6.7**). Live-dead staining of the bacteria on the explanted beaded titanium disc showed significant amount of live bacteria on the control discs and dead bacteria on the RVPE discs (**Figure 6.8**).

Final sonication and culturing of the explants, distal femur, proximal tibia, meniscus, and patellar tendon showed no bacteria in the RVPE group but a high amount of bacteria in the control group (Figure 6.9).

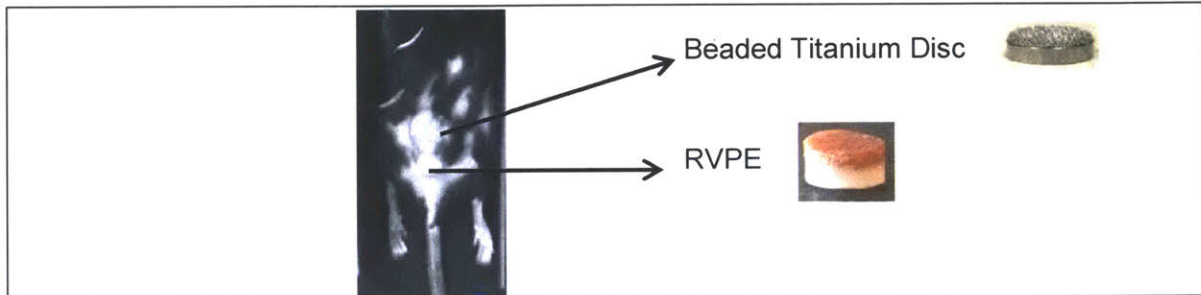


Figure 6.5. Gross picture of subcutaneously implanted control RVPE discs and beaded titanium discs. Xen 29 biofilm was grown in-vitro on the beaded titanium disc (beaded side) for 48 hr prior to implantation. During implantation, the biofilm-covered titanium disc was implanted first followed by either RVPE or control UHMWPE. Each mouse (total n=8) was randomly assigned to either control or RVPE groups.

Control UHMWPE	RVPE
Post Injection	
24 hr post-injection	
48 hr post-injection	
72 hr post-injection	

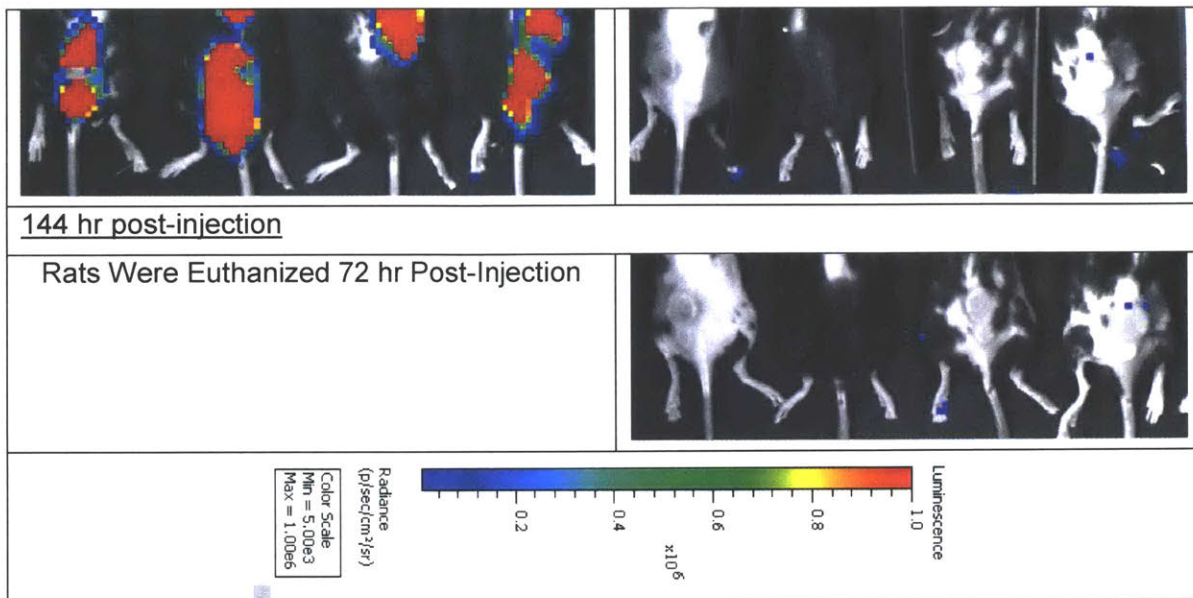


Figure 6.6. In vivo bioluminescence color map from Xen 29. Biofilm of bioluminescent *S. aureus* Xen 29 was grown *in vitro* on the beaded titanium disc for 48 hr and subsequently implanted into dorsal subcutaneous pocket of mice. In addition to the beaded titanium disc, each mice also received either a control UHMWPE or RVPE disc. Total bioluminescence flux was measured by bioluminescent camera (IVIS 100, Caliper). Total flux bioluminescence map was measured immediately after post-injection, 24 hr, 48 hr, 72 hr and 144 hr post-injection.

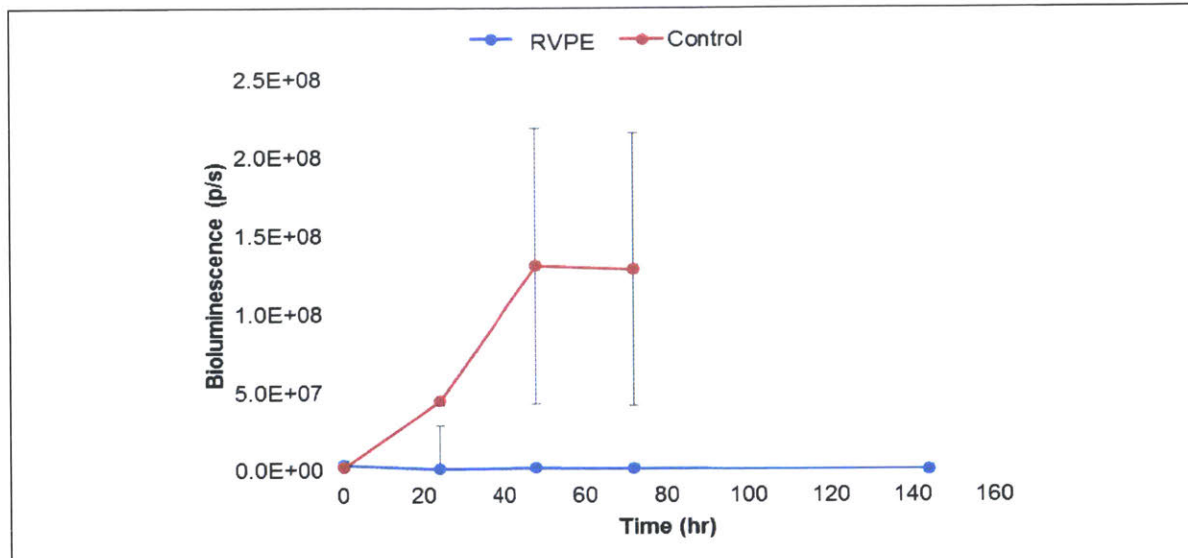
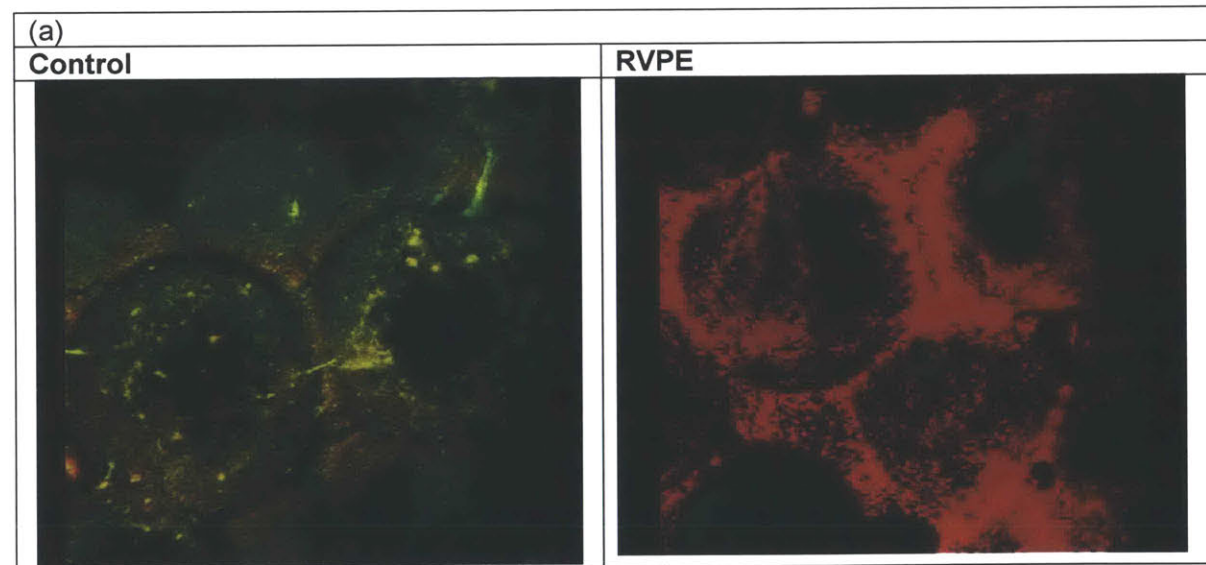


Figure 6.7. Total bioluminescence quantification around the implants of mice receiving RVPE or control UHMWPE. Region of interest was drawn around the implant are for each mice and total bioluminescence was calculated. Data are presented as mean \pm s.d. (n=5 for each group).



(b)

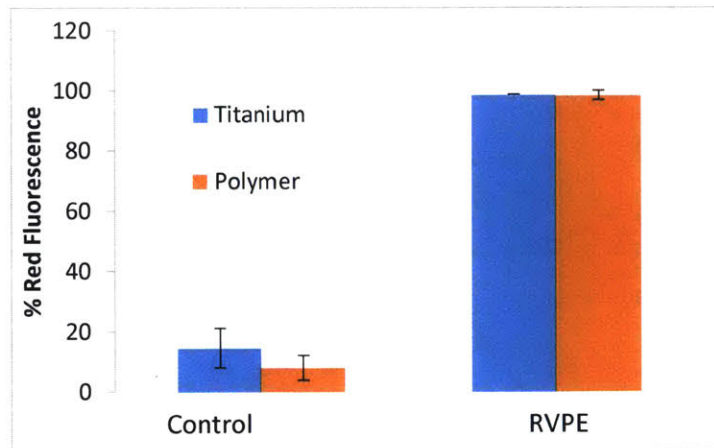


Figure 6.8. Two-photon live-dead imaging of explanted UHMWPE and titanium discs.

(a) Representative two-photon live-dead imaging of the bacteria on the titanium discs after retrieval. Green indicates live bacteria, red indicates dead bacteria. Scale bar = 200 μm . (b)

Mean percent bacterial death of the bacteria adherent to the surface of titanium discs and UHMWPE after retrieval. Mean percent bacterial death is calculated from ten different regions of the two photon figures and quantified as percent of bacteria with dominant red/total number of bacteria. Data are presented as mean \pm s.d. (n=40 for each group).

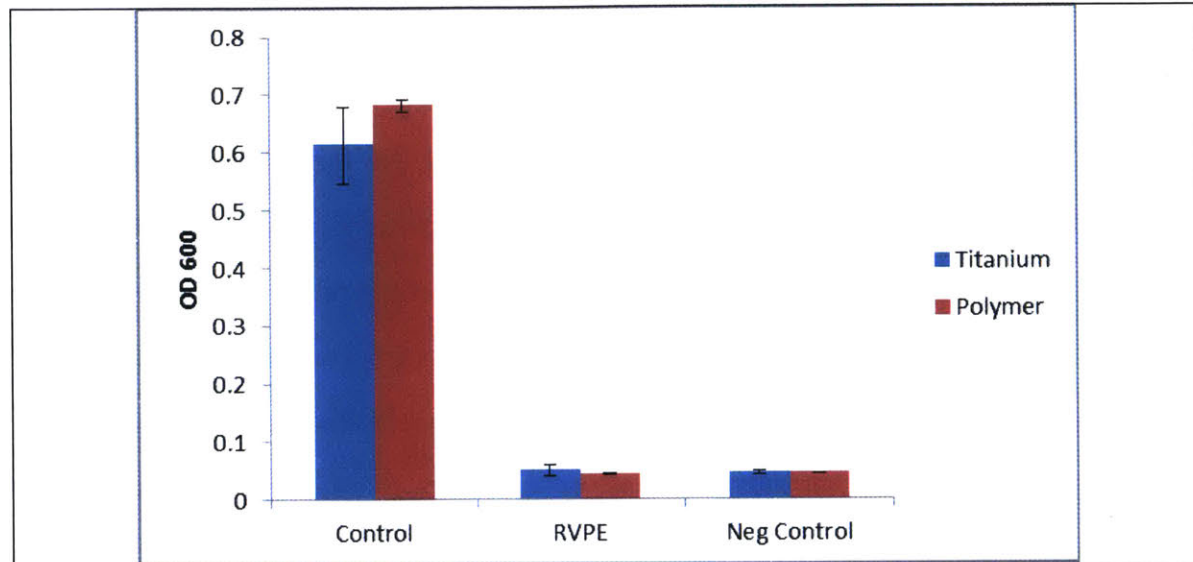


Figure 6.9. Post-Mortem sonication of explanted titanium and polymer (UHMWPE) components. Absorbance at 600 nm (OD₆₀₀) of recultured media after sonication of the polyethylene, and titanium discs explanted from the dorsal subcutaneous pockets of the mice. Negative control is bacterial media only. Data are presented as mean \pm s.d. (n=5 for each group).

Lapine Planktonic Bacteria Prosthetic Joint Infection Model

An intra-articular PJI model was created; osteochondral plugs of VPE, UHMWPE without antibiotics, or commonly used antibiotic-eluting bone cement [497] (8.3 % tobramycin sulfate and 2.3 % vancomycin HCl, S-BC) were implanted in the femoral trochlear groove and a titanium plug with a porous surface was implanted in the tibial plateau of skeletally mature New Zealand white rabbits. All rabbits received one bacterial injection (5×10^7 CFU/ml each) in the distal tibial canal and another in the intra-articular space (**Figure 6.10**). None of the rabbits received any additional antibiotics for the duration of the study (3 weeks).

Overall, 60% of VPE and 40 % of S-BC rabbits survived compared to none of the rabbits which received UHMWPE plugs without any antibiotics (**Figure 6.11**). Immediately post-surgery,

no difference in gait and joint movement was visually observed between control, S-BC and VPE group. However, after several days, the infected knee in control rabbits were more swollen, retracted, and passive than rabbits receiving S-BC or VPE. No mechanical failure including deformation, fracture, delamination or pitting was observed in the retrieved implants. Since vancomycin can be toxic [498], the serum vancomycin concentration was determined. No vancomycin was detected systemically in any of the rabbits at any time point (detection limit 10 ng/ml). Kidney function byproducts (creatinine and body urea nitrogen, or BUN) and liver function enzymes (alanine aminotransferase or ALT and alkaline phosphatase or ALP) remained within normal limits for all rabbits in the VPE group for the duration of the study (**Figure 6.12**).

Bioluminescence imaging of the knee joints at the end-point (**Figure 6.13**), two-photon live dead imaging (**Figure 6.14**), and sonication and culturing of joint tissues and implants (**Figure 6.15**) did not show any bacterial growth on any component for the rabbits implanted with VPE, suggesting complete eradication of bacteria. However, significant amount of live bacteria were found on all rabbits receiving S-BC albeit lesser than that found on rabbits receiving control samples, indicating ongoing infection in the S-BC group (**Figure 6.13-6.15**). These results showed the relative efficacy of vancomycin eluted from radiation sterilized VPE *in vivo*.

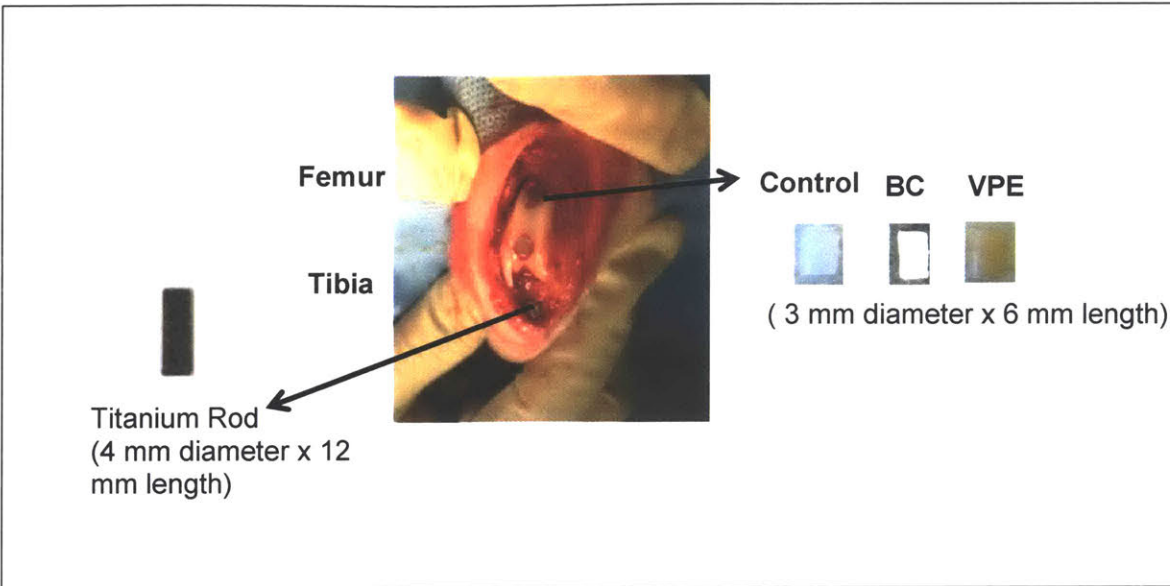


Figure 6.10. Gross picture of UHMWPE and Titanium Rod Implantation in the Lapine Joint Infection Model. Two control, BC, or VPE plugs were implanted in the intercondylar femoral notch. All rabbit also received a sterile titanium rod in between the intercondylar eminence of proximal tibia. Xen 29 bacterial solution was injected into the distal tibial canal before implantation of the titanium rod and into the intraarticular space.

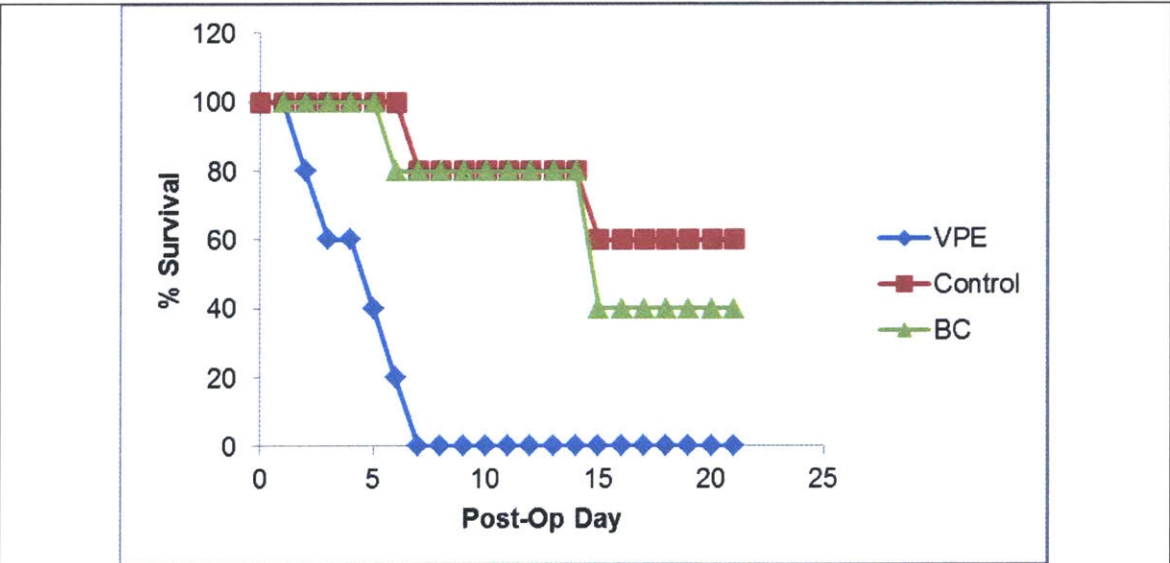
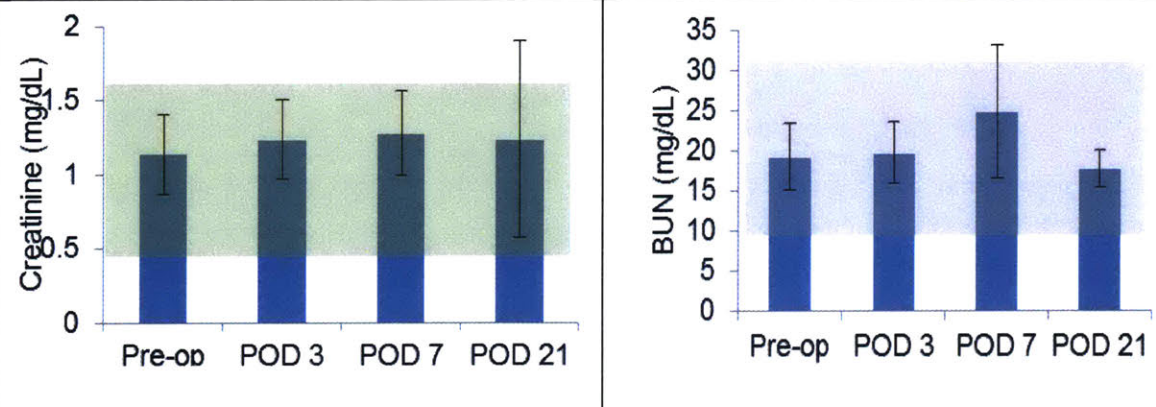


Figure 6.11. Survival Curve of Rabbits Receiving Control UHMWPE, BC, or VPE.

Each group consisted of 5 rabbits, all surviving animals by 21st day (end of study) were euthanized and counted as surviving animals.

Kidney Function



Liver Function

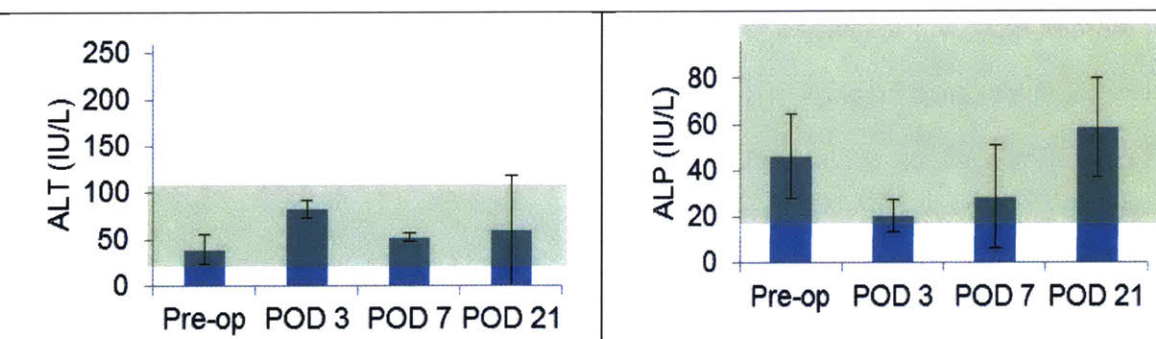


Figure 6.12. Kidney and Liver Function of Rabbits Receiving VPE. Serum creatinine (a), Blood Urea Nitrogen (BUN) (b), serum alanine transaminase (ALT) (c), serum alkaline phosphatase (ALP) (d) of rabbits treated receiving V-PE plugs. Bloods were drawn and analyzed prior to surgery (Pre-op), post operative day 3 (POD 3), post operative day 7 (POD 7), and post-operative day 21 (POD 21). Data are displayed as mean ± s.d., n=5. Normal ranges for rabbits are shown in the shaded regions.

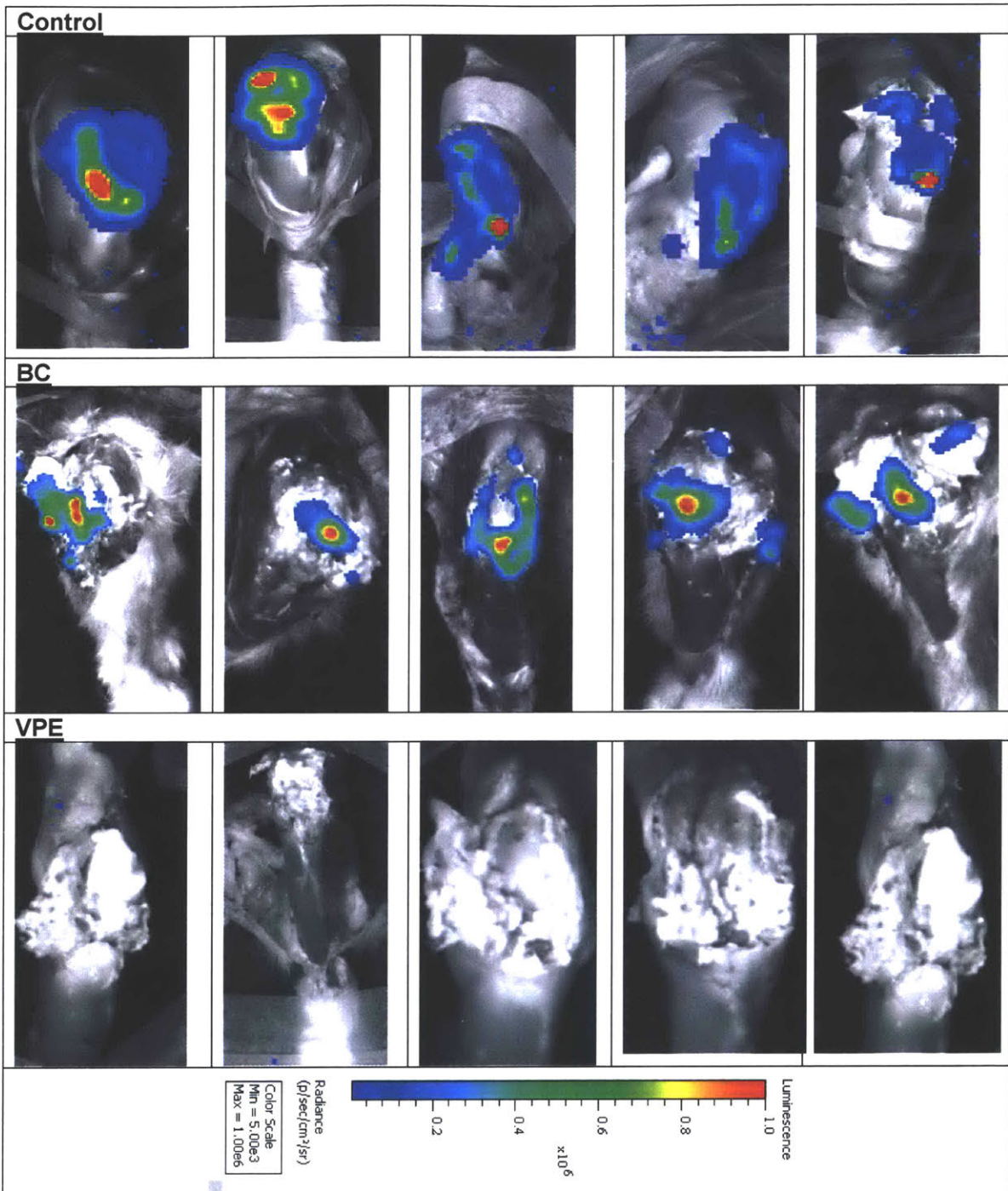


Figure 6.13. Necropsy bioluminescent map of rabbit knee infected with Xen 29.

Bioluminescent imaging was conducted right after each animal was either naturally deceased or euthanized. Imaging was conducted after knee capsule was carefully

dissected to minimize structural disruption.

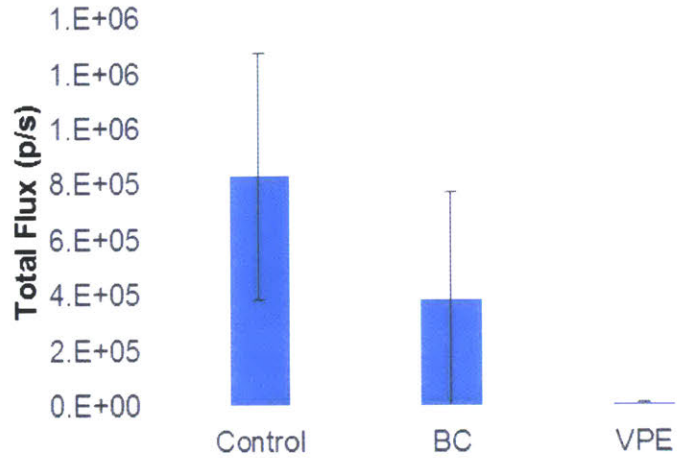
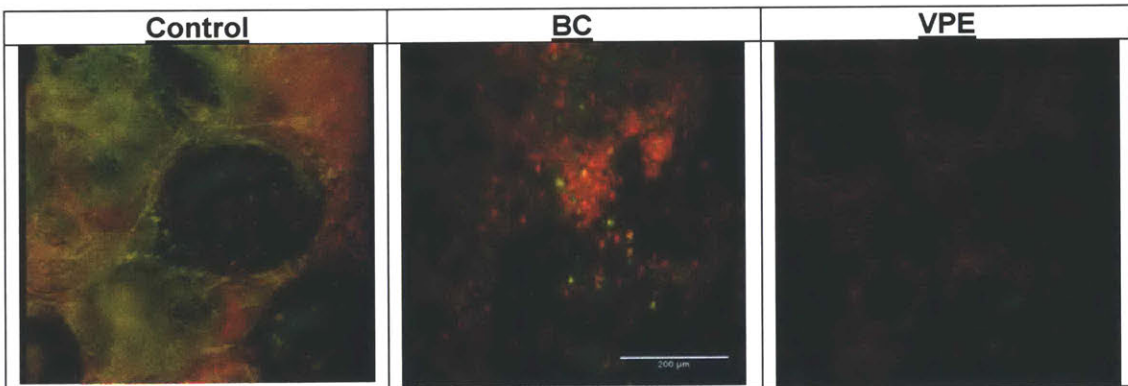


Figure 6.14. Total bioluminescence quantification of the rabbit knee receiving control UHMWPE or VPE post necropsy. Region of interest was drawn around the knee for each figure and total bioluminescence was calculated. Data are presented as mean \pm s.d. (n=5 for each group).



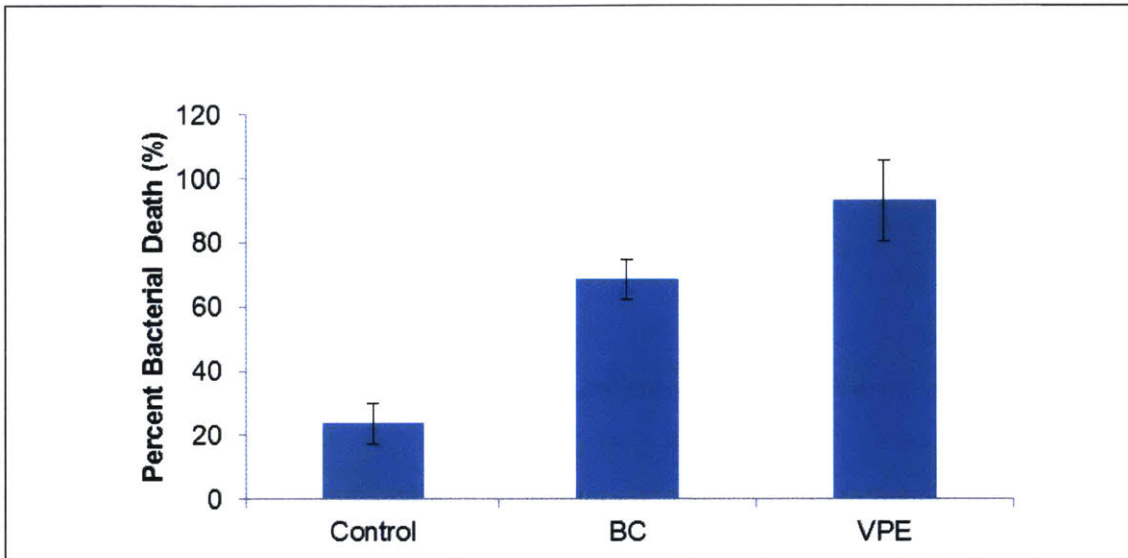


Figure 6.15. Two-photon live-dead imaging of explanted titanium rods. (a)

Representative two-photon live-dead imaging of the bacteria on the titanium rods after retrieval. Green indicates live bacteria, red indicates dead bacteria. Scale bar = 200 μm . (b) Mean percent bacterial death of the bacteria adhered to the surface of titanium rods after retrieval. Mean percent bacterial death is calculated from ten different area of the two photon figures and quantified as percent of bacteria with dominant red/ total number of bacteria. Data are presented as mean \pm s.d. (n=50 for each group).

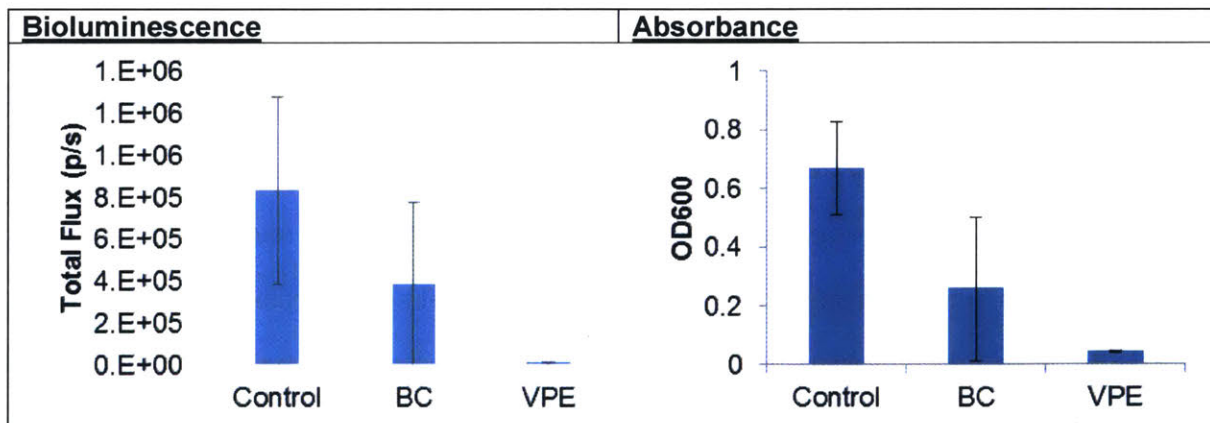


Figure 6.16. Post-Mortem sonication of tissues and Explants. Bioluminescence and absorbance at 600 nm (OD600) of therecultured medium after sonication of the tibia, the

femur, the meniscus, the polyethylene, and the titanium rods explanted from the knee of rabbits in the control, BC, and VPE groups. Data are presented as mean \pm s.d. (n=5 for each group).

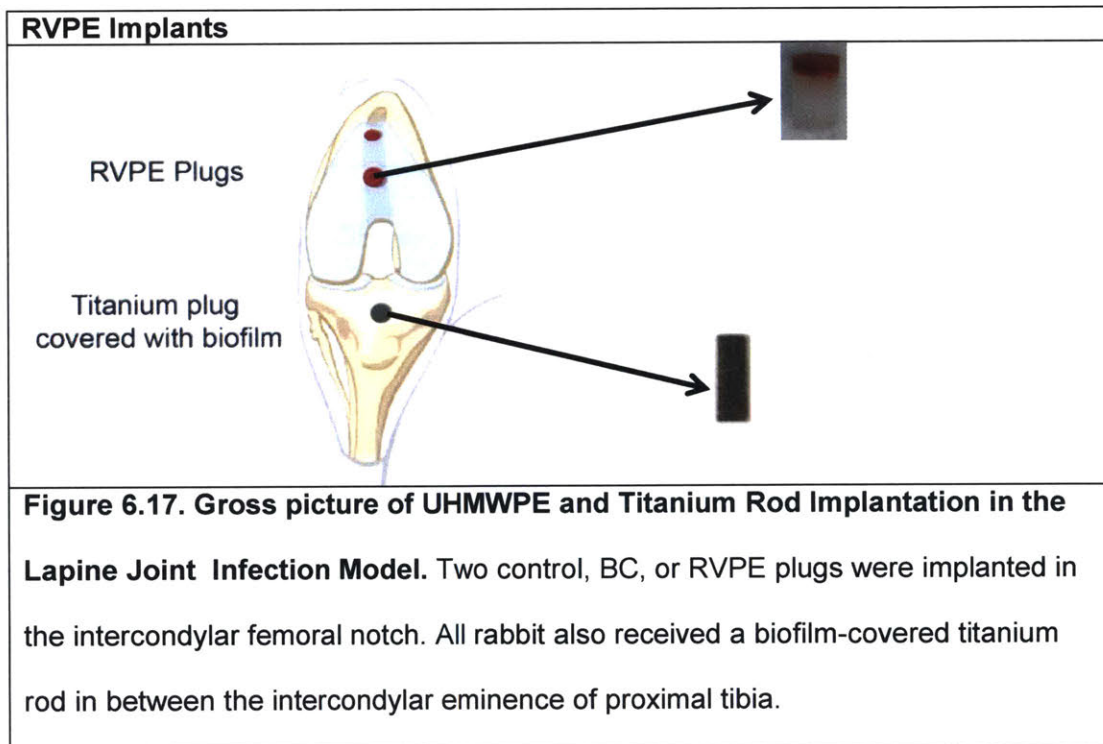
Lapine Biofilm Bacteria Prosthetic Joint Infection Model

In an adaptation of the PJI model for infections with planktonic bacteria above, all rabbits received a titanium rod with fully 48 hr in vitro grown bioluminescent *S. aureus* biofilms in the tibial canal (**Figure 6a**). Bioluminescent imaging was conducted on the bacteria prior to implantation and no statistically significant difference in total flux was observed between control, BC, and RVPE groups (**Figure 6.18**). Average thickness of biofilm of $25.5 \pm 2.2 \mu\text{m}$ was measured using Live-Dead two-photon fluorescence microscopy.

None of the rabbits received any systemic antibiotics for the duration of the study (3 weeks). Overall, 100% of VPE and 20 % of BC rabbits survived compared to none of the rabbits which received UHMWPE plugs without any antibiotics (**Figure 6.19**). Immediately post-surgery, no difference in gait and joint movement was visually observed between control, BC and RVPE group. However, after several days, the infected knee in control and BC rabbits were more swollen, retracted, and passive than rabbits receiving RVPE. No mechanical failure including deformation, fracture, delamination or pitting was observed in the retrieved implants. No vancomycin was detected systemically in any of the rabbits at any time point (detection limit 10 ng/ml). Because vancomycin can be nephrotoxic while rifampin can be hepatotoxic, kidney function byproducts (creatinine and body urea nitrogen, or BUN) and liver function enzymes (alanine aminotransferase or ALT and alkaline phosphatase or ALP) were measured. All values

were within normal limits for all rabbits in the RVPE group for the duration of the study (**Figure 6.20**).

Dissection of the knee post mortem showed significant amount of pus in the BC and control rabbits but not in the RVPE rabbits (**Figure 6.21**). No live bacteria were observed in the RVPE group as tested by bioluminescence (**Figure 6.22**), two-photon live dead imaging (**Figure 6.23**), and reculturing of the medium after sonication of joint tissues and implants (**Figure 6.24**). These results confirmed the efficacy of RVPE against a *S. aureus* biofilm *in vivo*.



Control					
BC					

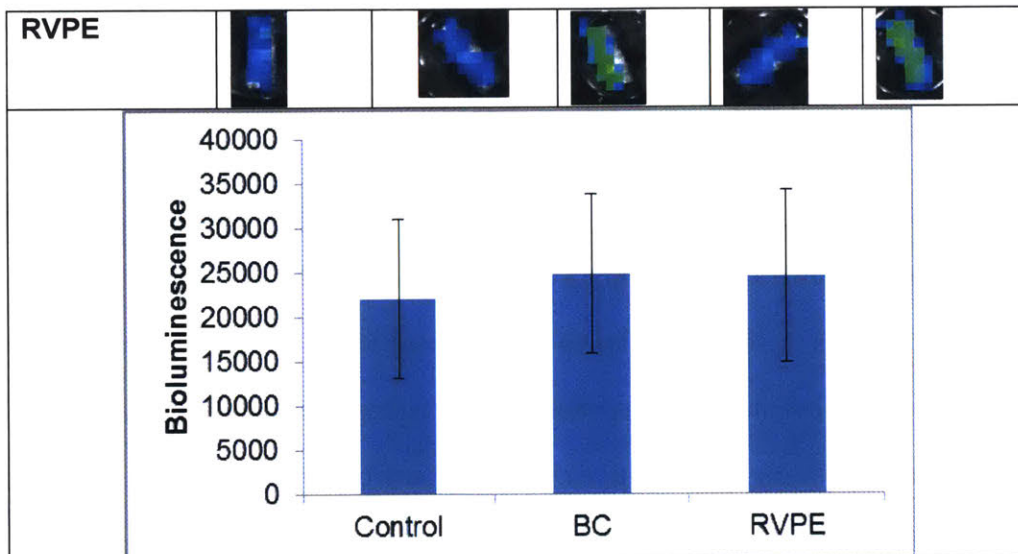


Figure 6.18. Bioluminescence of titanium rods prior to implantation.

Bioluminescence imaging and total flux quantification of the titanium rods for control, BC, and RVPE groups prior to implantation into rabbits.

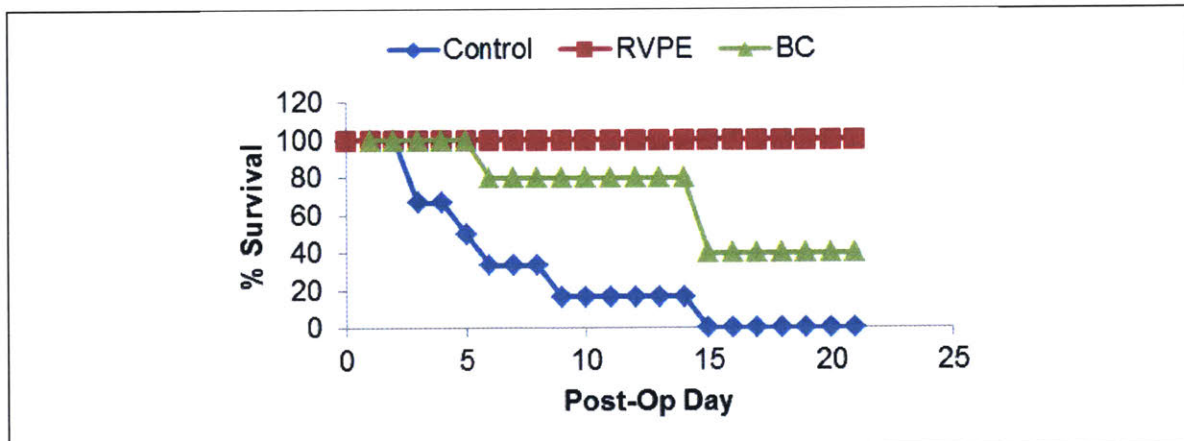
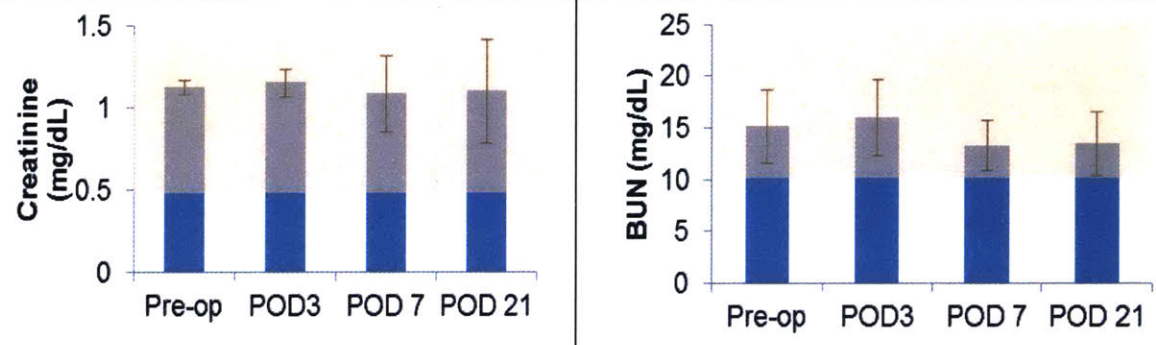


Figure 6.19. Survival Curve of Rabbits Receiving Control UHMWPE, BC, or RVPE.

Each group consisted of 5 rabbits, all surviving animals by 21st day (end of study) were euthanized and counted as surviving animals.

Kidney Function



Liver Function

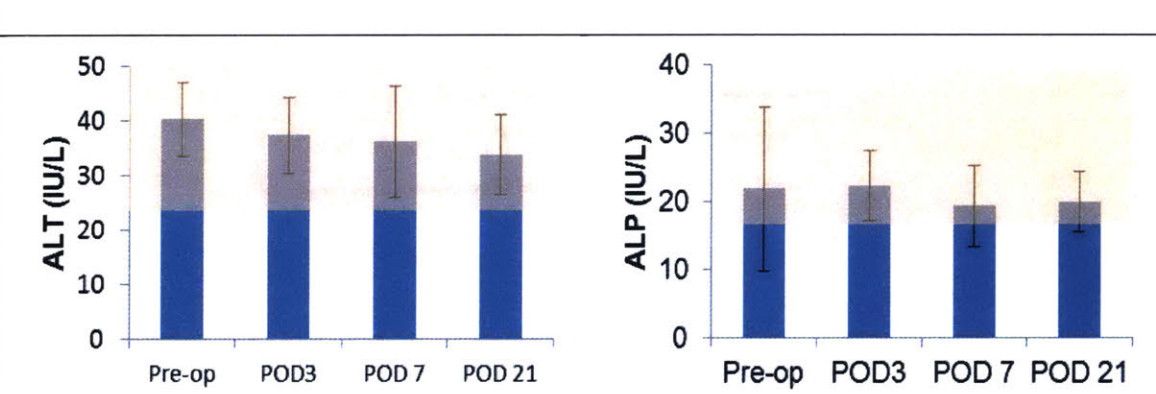
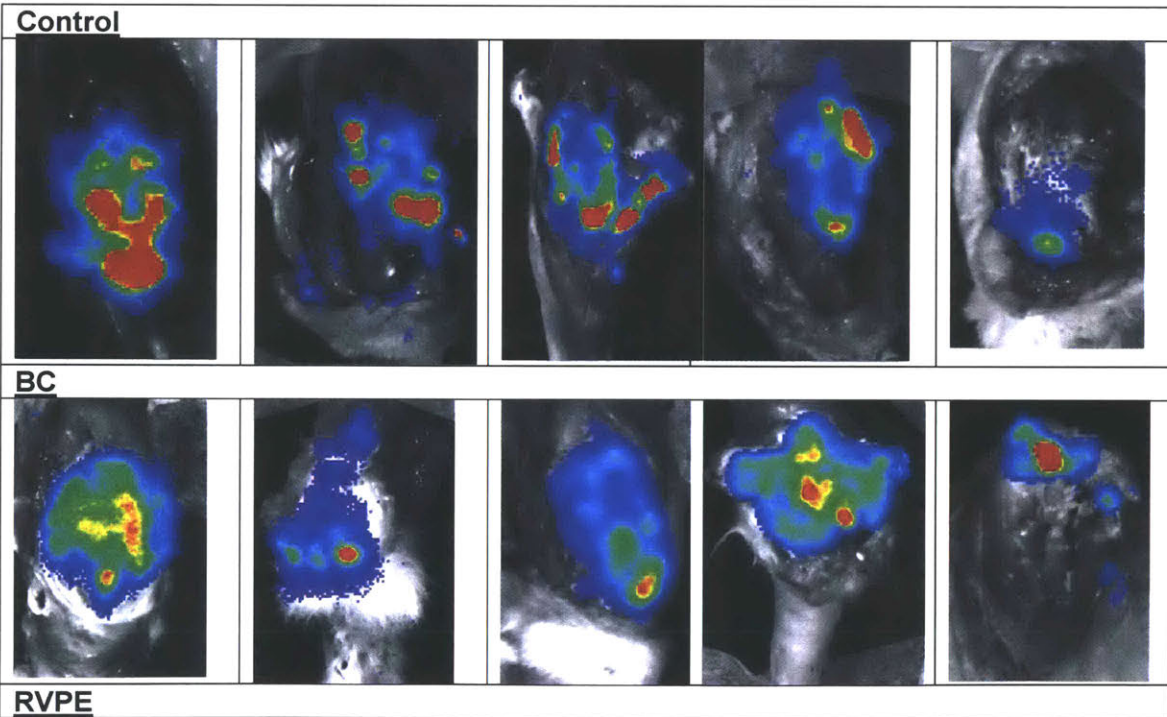


Figure 6.20. Kidney and Liver Function of Rabbits Receiving RVPE. Serum creatinine (a), Blood Urea Nitrogen (BUN) (b), serum alanine transaminase (ALT) (c), serum alkaline phosphatase (ALP) (d) of rabbits treated receiving V-PE plugs. Bloods were drawn and analyzed prior to surgery (Pre-op), post operative day 3 (POD 3), post operative day 7 (POD 7), and post operative day 21 (POD 21). Data are displayed as mean \pm s.d., n=5

Control	BC	RVPE
----------------	-----------	-------------



Figure 6.21. Representative gross picture of the dissected knee from control, BC, and RVPE groups. After animals were euthanized, the operated knee was minimally dissected to expose the articular surface.



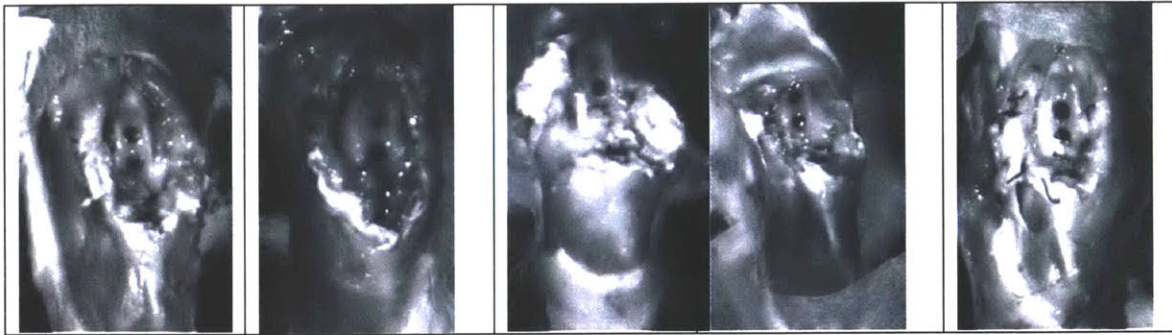


Figure 6.22. Necropsy bioluminescent map of rabbit knee in control, BC, and RVPE infected with Xen 29 bioluminescent on titanium rod. Bioluminescent imaging was conducted right after each animal was either naturally deceased or euthanized. Imaging was conducted after knee capsule was carefully dissected to minimize structural disruption.

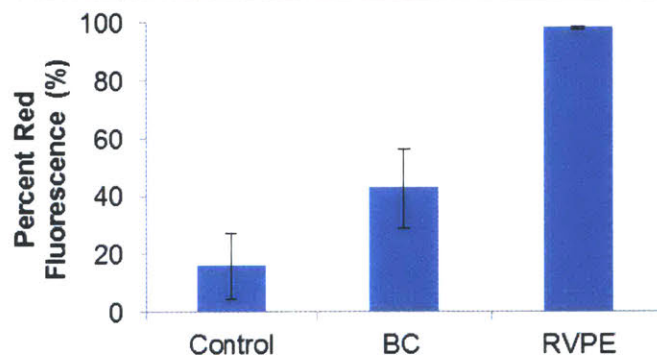
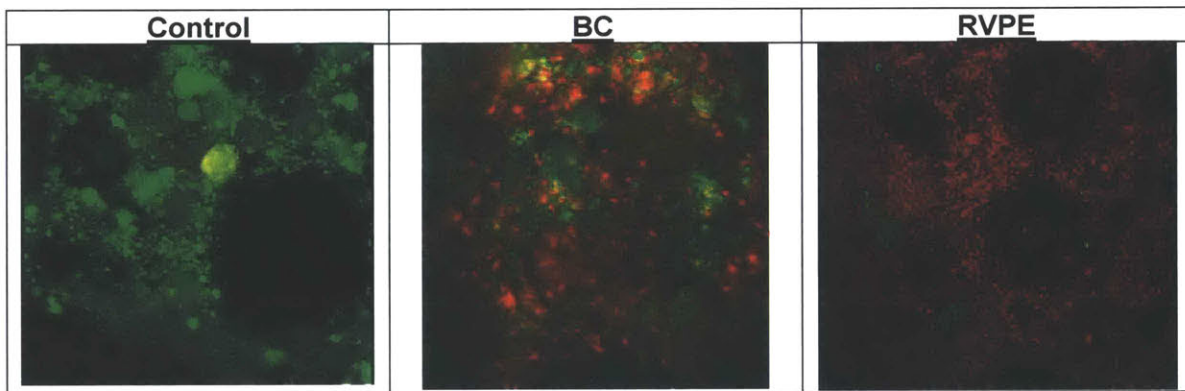


Figure 6.23. Two-photon live-dead imaging of explanted titanium rods from control, BC, and RVPE groups. (a) Representative two-photon live-dead imaging of the bacteria

on the titanium rods after retrieval. Green indicates live bacteria, red indicates dead bacteria. Scale bar = 200 μm . (b) Mean percent bacterial death of the bacteria adhered to the surface of titanium rods after retrieval. Mean percent bacterial death is calculated from ten different area of the two photon figures and quantified as percent of bacteria with dominant red/ total number of bacteria. Data are presented as mean \pm s.d. (n=50 for each group).

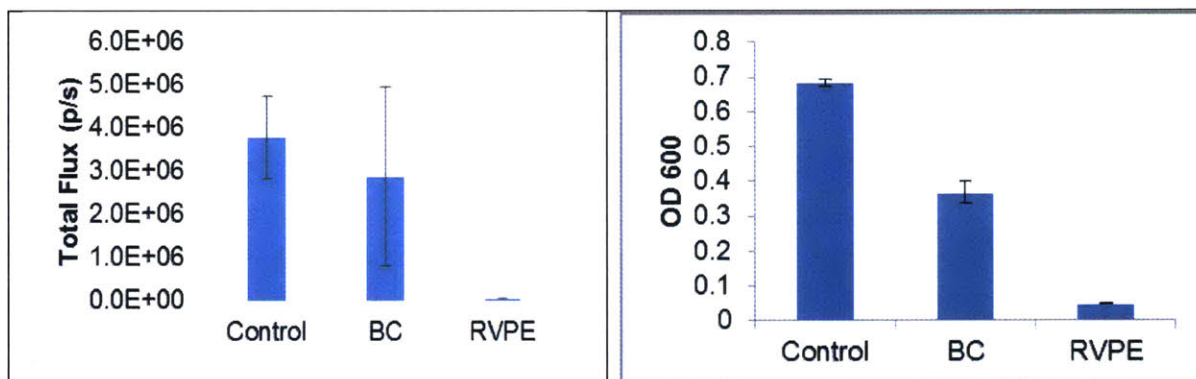


Figure 6.24. Post-Mortem sonication of tissues and Explants. Bioluminescence and Absorbance at 600 nm (OD600) after sonication of tibia, femur, meniscus, polyethylene, and titanium rods explanted from the knee of rabbits in the control, BC, and RVPE groups. Data are presented as mean \pm s.d. (n=5 for each group).

Discussion

Acute prosthetic joint infections were shown to involve significant amounts of planktonic bacteria in the intraarticular space (free floating in synovial fluid) without significant presence of biofilm [473] [474]. On the other hand, chronic infections involved formation of significant amount of biofilm on the implant surfaces [136]. To address the efficacy of the materials we

designed against both types of infection, we created two types of PJI model: a primarily planktonic infection model and a primarily biofilm infection model.

In the primarily planktonic infection model, local antibiotic delivery device was implanted at the same time as the administration of planktonic bacteria in suspension to obtain a short time interval between bacterial inoculation and start of antibiotic treatment. This model simulated the exogenous seeding of bacteria during a primary total joint replacement procedure, resulting in an acute prosthetic joint infection presenting clinically within 3 months post-operatively (**Figure 6.1 and 6.10**). The short time interval is desired to minimize excessive biofilm maturation. In the primarily biofilm infection (**Figure 6.5 and 6.17**), the bacterial biofilm was grown on the surface of an implant prior to implantation. The local antibiotic delivery device was then implanted at the same time as the implantation of biofilm covered device. By implanting the antibiotic delivery device at the same time as implantation of biofilm-covered device, we could mimic antibiotic administration after full formation of biofilm. This situation simulates more closely a chronic prosthetic joint infection where the biofilm is present on surfaces and/or a revision surgery where the implants with biofilm are not sufficiently removed or cleaned. A revision surgery model should ideally involve the inoculation of the biofilm in a separate surgery to accurately mimic the clinical situation (i.e. implanting device on first surgery and allowing biofilm to form *in vivo*, followed by second surgery to implant the antibiotic eluting device). However, the extra morbidity to the test animals exposed to multiple step surgeries necessitated the use of our single-stage infection/treatment strategy in each model. We chose two types of controls for our study: persistent infection control and clinically relevant control. In the persistent infection control, no antibiotic was administered to the infected animals to ensure that the bacterial concentration for inoculation was above that which can be eradicated by the immune system alone. In the clinically relevant control, an antibiotic eluting bone cement spacer (gold standard of infection treatment) was used. The clinically relevant control was used to

compare the efficacy of our new device against the current standard. Bone cement spacers with combined tobramycin and vancomycin (8.3 % tobramycin sulfate and 2.3 % vancomycin HCl) was chosen because it is the most widely reported in literature [492-494] and a commercially available premade spacer was also available with the aforementioned antibiotic content[499].

In both the murine and lapine models, VPE was able to completely eradicate planktonic and adherent bacteria on the metal implants (**Figure 6.2-6.4** for murine, **Figure 6.11-6.16** for lapine). The persistent infection control in both models showed that the complete eradication was unlikely solely due to the immune system, as none of the animals without VPE was able to completely eradicate the bacteria. While similar survival rate was observed for animals treated with VPE and S-BC, only VPE (but not S-BC) completely eradicated all the bacteria in the joint (**Figure 6.11, Figure 6.13-6.16**). This may be partly due to Xen29's higher susceptibility to vancomycin[500] than to tobramycin[501]. The liver and kidney functions stayed within normal limits for all VPE rabbits with negligible systemic level of vancomycin, indicating that VPE was able to eradicate bacteria in the joint without causing systemic toxicity (**Figure 6.12**).

RVPE was able to eradicate biofilm bacteria on the metal implants both in the murine and lapine infection models (**Figure 6.6-6.9** for murine, and **Figure 6.19-6.24** for lapine). The persistent infection control in both models showed that the complete eradication was unlikely solely due to the immune system, as none of the animals without RVPE or S-BC was able to completely eradicate the bacteria. The survival rate and bacterial burden of rabbits treated with S-BC fell between that of rabbits implanted with control UHMWPE and that of rabbits treated with RVPE. The ability of S-BC to control the bacterial concentration in the biofilm model was worse than that in the planktonic model presumably because bacterial susceptibility to vancomycin and tobramycin decrease by at least 1000 fold in biofilm form[502]. The liver and kidney function stayed within normal limits for all RVPE rabbits, indicating that RVPE was able to eradicate bacteria in the joint without causing systemic toxicity (**Figure 6.20**).

One limitation of our models was that the local antibiotics delivery device was implanted at the same time as bacteria administration. In reality, patients with PJI treated with one-stage revision surgery will receive a total of two surgery (one primary and one revision) and three surgeries (one primary and two revisions) for two-stage revision surgery. Because of the time lag between bacteria growth in the joint and symptoms, the bacteria have more time to travel around the joints and adhere to tissues[503]. In addition, in reality, focal bacteria colonies within the bone-titanium interface could exist despite well fixation between the implant and the bone[476]. In such a case, simply implanting VPE or RVPE without supplement of systemic antibiotics might not be sufficient to completely eradicate bacteria in the joint because of limited direct access from the articular space to the focal infected bone-joint interface.

Conclusion

In conclusion, VPE, which contained a uniform concentration of vancomycin while maintaining acceptable clinically relevant properties and RVPE, which contained an optimized concentration of rifampin and vancomycin together and was designed to have superior clinically relevant properties, outperformed clinically-used antibiotic eluting bone cement S-BC in planktonic and biofilm PJI models, respectively. VPE and RVPE improved the survival rates in our pre-clinical infection models and significantly reduced the local bacterial burden on the implants (subcutaneous pocket and joint space). No systemic toxicity was observed in any of the animals receiving VPE or RVPE. Therefore, these materials are candidates for further clinical testing in the multi-stage treatment of patients presenting with PJI.

Chapter 7

Sustained Delivery of Local Anesthetics from UHMWPE with Highly Eccentric Pores

Introduction

More than half of patients undergoing surgery experience higher than tolerable levels of postoperative pain [504-507]. Postoperative pain due to orthopaedic surgery is especially hard to manage [507-511]. Extreme postoperative pain in patients undergoing surgery [512-514] is cited as one of the most common reasons why patients are dissatisfied with the outcome of their total joint replacement (arthroplasty; TJA) [515-517]. Furthermore, postoperative pain is one of the main concerns for patients who are planning to undergo total joint arthroplasty [518] and is often the main reason for delaying or cancelling the surgery [519].

Post-operative pain has also been associated with serious complications such as ischemic cardiac events [520], decreased pulmonary functions[521], gastrointestinal complications such as ileus [522], and thrombus formation. Postoperative pain after TJA also results in delayed recovery, longer hospitalization, and higher economic burden [504, 505, 511-514, 520, 521, 523]. Current standard of treatment includes usage of systemic opioids, which results in various side effects including gastroparesis (37 % of patients), cognitive effects (34 % of patients), urinary retention (16 % of patients), pruritus (15 % of patients) and respiratory depression (2 % of patients) [524].

In addition to having significant side effects, opioid usage leads to a risk of dependence. Almost 50 % of patients who underwent major elective surgery receive a prescription for opioids

[525]. Of those, 3.3-7.7 % continue to use opioids for more than three months [525, 526]. The number of patients who use opioids in the long-term post-surgery is even higher in total joint replacement: 8.2 % of total knee arthroplasty and 4.3 % of total hip arthroplasty patients who were naïve to opioids still consumed opioids at 6 months [527]. 53.3 % of TKA and 34.7 % of THA patients who were using opioids at the day of surgery still used opioids at 6 months [527]. Patients who are taking oral morphine preoperatively have 80 % likelihood of persistent use postoperatively [527]. More concerning, change in the affected joint pain (knee or hip) was not predictive of opioid use, indicating that patients continue opioid use despite the lack of change to their pain [527]. A separate study using national samples of patients undergoing total knee arthroplasty showed that 14 % of patients who had used opioids before TKA and 3 % of patients who were naïve to opioids before surgery still used opioids at 12 months [528]. Long-term usage of opioids has been associated with higher incidence of dependency and hyperalgesia [529]. Prolonged usage of opioid after total joint arthroplasty has also been associated with poorer functional outcome such as higher stiffness, lower physical functioning of joints, and activity [529].

To minimize the opioid consumption, current postoperative pain management in TJA emphasizes two concepts: (1) Preemptive management; initiating pain control before start of surgery and (2) Multimodal management; using two or more categories of pain medications to address the pain [530].

Current Postoperative Management for Total Joint Arthroplasty

Analgesic management of postoperative pain associated with total joint arthroplasty consists of preoperative, intraoperative, and postoperative management [530].

Preoperative analgesics can be administered orally or injected to provide nerve block [530]. Oral drugs such as non-steroidal anti-inflammatory drugs (NSAID) [531, 532], cyclooxygenase [COX]-2 inhibitors [531, 532], opioids [533] or anesthetic injection through regional anesthesia [534, 535] or peripheral nerve block [536] have been shown to be effective in reducing postoperative pain when administered at least an hour before surgery [530]. As a result, consumption of analgesics post-surgery [523, 530, 537] and opioid-related side effects are reduced [523, 531, 538, 539].

Three types of intraoperative analgesia are recommended. (1) Regional analgesia through delivery of anesthetics through catheters to the spinal or epidural space [511-513]. Medications that are delivered to the spinal or epidural space include local anesthetics such as bupivacaine, chloroprocaine, lidocaine, opioids such as fentanyl, sufentanil, morphine, and agent that can modify the rate of absorption of the pain medication such as epinephrine and clonidine [511-513]. Regional anesthesia is contraindicated in patients with high risk of bleeding and may cause epidural hematoma or paraplegia due to hemorrhage [540-543]. (2) Peripheral nerve block through single-injection or catheter to block the femoral nerve [538, 544-546]. Femoral nerve blocking has been reported to be as effective as epidural analgesia but may cause quadriceps femoris weakness, compromised proprioception, and increased risk of falling after total joint arthroplasty [544, 547-549]. (3) Periarticular and intraarticular delivery of analgesics, such as opioids and local anesthetic agents (bupivacaine, lidocaine, ropivacaine). Periarticular and intraarticular analgesics administration have been shown to reduce pain [512, 550-553] without any complications such as infection [512, 550-553]. No statistically significant difference in pain and long term function levels were found between intraarticular and periarticular administration of local anesthesia [554]. However, intraarticularly administered local anesthetics provided better improvement in pain during first time mobilization [555].

Postoperative analgesics can be administered orally or through intravenous patient-controlled analgesics (IV-PCA). Opioid IV-PCA is the most common and most effective postoperative pain management modality [556, 557]. However, as mentioned above, the usage of opioid resulted in opioid-related side effects such as nausea, vomiting, respiratory failure, urinating difficulty, constipation, and pruritus.[511, 558] Oral analgesics such as acetaminophen, COX-2 inhibitors, tramadol, and oxycontin have been shown to produce maximum pain relief and reduce opioid consumptions, thus maximizing patient satisfaction and minimizing complications [511-513, 523].

Intraarticular Delivery of Local Analgesics

Three main methods are currently used for local delivery of analgesics directly into the joint: (1) single injection of local anesthetics, (2) injection of liposomal analgesics, and (3) indwelling catheter in the joint that is connected to a drug infusion pump (e.g. Q-pump™).

Local anesthetics such as bupivacaine and ropivacaine are often injected in combination with epinephrine into the intraarticular space after joint surgery to improve analgesia and decrease the need for postoperative narcotics [559]. Intraarticular injection of 20-30 ml of 0.5 % bupivacaine in saline and 1:200,000 epinephrine in saline resulted in significant decrease in pain, increased range of motion, and reduced time to discharge from hospital as compared to patients receiving an intraarticular saline injection [559]. Intraarticular injection of 60 ml of 0.5 % bupivacaine has also been shown to significantly reduce the first 24 hr opioid consumption as compared to patients receiving saline injections [560]. Intraarticular injection of morphine or bupivacaine significantly decreased postoperative pains compared to patients receiving intraarticular saline injection [561]. However, the pain relief was only short-lived: intraarticular

injection of 60 ml, 0.5 % bupivacaine provided relief for the first 9 hours as compared to an intraarticular injection of saline [562].

Intraarticular administration of liposomal analgesics such as bupivacaine (Exparel™) provides controlled release of bupivacaine, despite being relatively short lived [563]. Exparel™ consists of microscopic, spherical, and lipid based particles encapsulating bupivacaine [563]. Degradation of the lipid based particles exposes the bupivacaine and allows bupivacaine to exert its action [563]. Patients receiving liposomal bupivacaine post total knee arthroplasty consumed less opioid in the first 24 hr as compared to those not receiving liposomal bupivacaine [564] or patients receiving femoral nerve block [565]. A meta-analysis taking into account 16 clinical trials of liposomal bupivacaine for pain management after total joint arthroplasty found a marginally better and more sustained pain control, especially when compared to femoral nerve block as control [566]. Use of liposomal bupivacaine also marginally decreased the length of hospital stay (reduction by 0.17 days) [566]. Administration of liposomal bupivacaine resulted in 139 % relative risk reduction of patients having pain in the postanesthesia care unit (PACU) [564]. Thus, liposomal bupivacaine delivers bupivacaine more sustainably than a direct bupivacaine injection but its effect is still short-lived, only significant for 48-72 hr after administration [8, 567, 568].

Delivery of bupivacaine through an infusion pump (Q-pump™) has been shown to significantly reduce pain at postoperative day one and two compared to patients receiving saline through the same infusion pump [569]. Furthermore, patients receiving the bupivacaine infusion significantly consumed less opioid on post-operative day two and three (33 % and 54 % respectively) [569]. At four week post-surgery, groups receiving the bupivacaine infusion showed lower pain level than the saline infusion group [569]. Beside bupivacaine, infusion of ropivacaine into the knee using Q-pump™ also showed decreased pain intensity and opioid use for the first three days after surgery.[570] Groups receiving the ropivacaine infusion also showed

decreased length of hospital stay and improved immediate functionality and comfort [570]. Ropivacaine infusion was shown to be superior to femoral nerve block in terms of reducing mean hospital stay length [571] and allowed earlier ambulation than both epidural and femoral nerve block [572].

Antimicrobial Activity of Local Anesthetics

Antimicrobial activity of local anesthetics have been previously reported and have shown to reduce the incidence of infection in clinical practice [574]. Retrospective analysis from the American College of Surgeons National Surgical Quality Improvement Database showed that local anesthesia reduces the incidence of surgical site infection by half (0.7 % with local anesthesia vs 1.4 % without local anesthesia) [574].

Minimum inhibitory concentrations of local anesthetics are much higher than those commonly found in antibiotics (0.25-16 mg/ml for local anesthetics vs <2 µg/ml for antibiotics) [575]. Among local anesthetics, bupivacaine hydrochloride has the highest antimicrobial activity (MIC=0.25-2 mg/ml), followed by mepivacaine hydrochloride (MIC=1.1-8.0 mg/ml), lidocaine hydrochloride (2.0-8.0 mg/ml), procaine hydrochloride (MIC=2.0-8.0 mg/ml), butanilicaine hydrochloride (MIC=0.5-16.0 mg/ml), prilocaine hydrochloride (MIC=2.0-16.0 mg/ml), and articaine hydrochloride (MIC=2.5-8.0 mg/ml) [576]. The minimum bactericidal concentration (MBC) of the local anesthetics range from 1-2 times of the corresponding MIC [576]. Considering in particular *Staphylococcus* and *Streptococcus* species, bupivacaine has the lowest MBC (3.8-4.9 mg/ml), followed by butanilicaine hydrochloride (6.8-7.5 mg/ml), articaine hydrochloride (9-10 mg/ml), mepivacaine hydrochloride (13.0-14.0 mg/ml), lidocaine hydrochloride (13-20 mg/ml), prilocaine hydrochloride (16.7-30 mg/ml), and procaine

hydrochloride (>29 mg/ml) [576]. Therefore, bupivacaine hydrochloride has the highest activity against *Staphylococcus* and *Streptococcus* species, which is the most common culprit of PJI.

Bupivacaine hydrochloride has broad spectrum antimicrobial activity: MIC against gram-positive coccus such as *Staphylococcus aureus*, *Streptococcus sanguinis*, *streptococcus pyogenes* ranges from 0.8-2 mg/ml [576]. MIC against gram-positive rods such as *Actinomyces* species and *Eubacterium* species ranges from 0.25-2.0 mg/ml [576]. MIC against gram-negative cocci such as *Neisseria* species, *Kingella indologens*, and *Veillonella parvula* ranges from 0.9-2.0 mg/ml [576]. MIC against gram-negative rods such as *Actinobacilulus* species, *Haemophilus influenza*, *Serratia marcescens*, and *Escherichia coli* of 0.8-2.0 mg/ml [576]. The MIC of these microbes are less than the concentration of bupivacaine HCl commonly injected into the intraarticular space (commonly injected bupivacaine HCl is at 0.5 wt %, which is equivalent to 5mg/ml).

Sustained Delivery of Local Anesthetics using Highly Eccentric Drug Clusters-UHMWPE

Learning from the strengths and caveats of the three methods that are currently used clinically for intraarticular delivery of local anesthetics, we believe that the ideal intraarticular delivery of local anesthetics needs to be at a sufficiently high dose to significantly reduce pain, to be sustainably delivered for at least one week up to several weeks, and to be fully contained in the joint, i.e. without an open connection to the outside world.

The following chapter describes a bupivacaine eluting UHMWPE designed to fulfill these aims.

Methods

Preparation of Bupivacaine Eluting UHMWPE

Bupivacaine-HCl or Bupivacaine free base (2 gram) was crushed with a mortar and pestle and then passed through a 75 μm sieve. Bupivacaine powder was then mechanically mixed with GUR1020 UHMWPE powder (Celanese, 8 grams) for 30 minutes at room temperature to obtain a 20 wt% bupivacaine-blended UHMWPE and poured into a circular mold with 10.5 cm inner diameter. 25 grams of GUR 1020 UHMWPE without additives were then added and spread evenly on top of the bupivacaine-blended UHMWPE. The resulting constructs were then consolidated by compression molding at 170°C, 20 MPa, for 5 minutes. The resulting consolidated construct was then cooled at rate 10°C/min to about room temperature. Bupivacaine was then eluted out from the UHMWPE in deionized (DI) water at 37°C for 2 weeks.

Preparation of Layered Bupivacaine HCl and Bupivacaine Free Base UHMWPE

The bupivacaine free base-blended UHMWPE (20 grams) was prepared as described above and poured into a circular mold with 10.5 cm inner diameter. 10 grams of GUR 1020 UHMWPE blended with bupivacaine-HCl were then added on to of the bupivacaine free base-blended UHMWPE powders and spread evenly. Resulting constructs were then consolidated by compression molding at 170°C, 20 MPa, for 5 minutes. Resulting consolidated construct was then cooled at rate 10°C/min to room temperature. Bupivacaine was then eluted out from the UHMWPE in deionized (DI) water at 37°C for 2 weeks.

In-vitro drug release from drug eluting UHMWPE

For bupivacaine eluting UHMWPE, blocks with dimension of 5 mm x 5 mm x 20 mm (n=6) were cut from the consolidated pucks. Each block was immersed in 1 ml of phosphate-

buffered saline at 37°C for a pre-determined time (6 hr, 24 hr, every 24 hr until 1wk, and then once every week up to a total period of 12 months). After each time-point was reached, the specimens were washed with phosphate-buffered saline and placed in a new 1 ml of phosphate-buffered saline. Concentrations of vancomycin and rifampin were determined using Ultraviolet-Visible spectroscopy (UV-Vis) at 263 nm. The rate of drug elution was calculated by dividing the measured concentration by the duration the sample was exposed to phosphate-buffered saline at a particular time point.

Tensile strength measurement

Type V samples (n=5 for each group) were stamped out of 3.2 mm thin sections of the materials mentioned above according to ASTM-D638. These samples were tested in tension (Insight™, Prairie, MN) with a crosshead speed of 10mm/min. The stress and strain were recorded at 100Hz and the gauge length was monitored using a laser extensometer. The engineering stress-strain curves were calculated by using the crosshead displacement. The ultimate tensile strength (UTS), yield strength (YS), elongation at break (EAB), work to failure (WF), and Young's modulus (E) were calculated.

Fracture toughness measurement

Samples with dimensions of 63.5×12.7×6.35 mm³ (n=5) were double notched according to ASTM D256 and were impact fractured with a hammer (CEAST Instron). The energy loss of the pendulum after impacting was recorded as the impact strength of the samples.

Wear testing

Wear testing of UHMWPE was adapted from [234]. Cylindrical pin shaped samples (9 mm in diameter and 11 mm in length) were used under bidirectional pin-on-disk testing at 2 Hz

using a 10 mm x 5 mm rectangular pattern. The loading cycle was adapted from [393] and the human gait cycle was adapted from [234]. The UHMWPE pins were articulated against polished CoCr discs ($R_a=0.38\pm 0.005$ μm). Undiluted bovine serum was used as lubricant with 33ml penicillin-streptomycin solution per 500 ml as antibacterial agent and 1mM EDTA as chelating agent. Weight of the pin was measured every 0.1 million cycles. The wear rate values reported here are the cumulative weight values normalized with the total number of cycles and are averages of six pins.

In Vivo Antibacterial Efficacy of Bupi-PE

Study approval was granted from Massachusetts General Hospital Institutional Animal Care and Use Committee. Based on the pilot in vivo rat study, the standard deviation in total flux from bioluminescence is 200,000 p/s. Taking type I error of 5 % and 80% power, to detect mean difference of total bioluminescent flux between control and treatment groups of 370,000 p/s, sample size of at least 4.6 is needed per group. A total of ten fully immune-competent, skeletally mature male Sprague-Dawley rats aged 8 weeks were used in this study. Animals were randomly assigned to control (non-antibiotic eluting UHMWPE) or Bupi-PE groups (layered 20 % Bupivacaine HCl-UHMWPE on 20 % Bupivacaine FB-UHMWPE). Each rat in the control group received a UHMWPE disc made from either non-drug eluting UHMWPE (control) or Bupi-PE (diameter = 6 mm, thickness = 3mm).

Anesthesia was achieved using inhaled isoflurane (1.5-2.5 %) supplemented with oxygen (1.2 liter/min). Pre-emptive analgesia was administered before the procedure started (buprenorphine 0.02 mg/kg). Subcutaneous cefazolin was administered (15 mg/kg) as prophylaxis antibiotics 1 hr before surgery. The rats were placed in the prone position and the dorsal area was prepped and draped in a sterile fashion (randomization of operated leg established using random.org). An incision was created at the caudal dorsum (3 cm from

proximal tail), and a subcutaneous tunnel was created on the fascial plane toward the rostral area. UHMWPE discs then inserted from the caudal incision site along the tunnel to the rostral end of the tunnel. After the incision was closed, 5×10^7 cfu of bioluminescent *Staphylococcus aureus* (Xen 29, Perkin Elmer) in 50 μ L 0.9 % saline was injected into the immediate surrounding of the UHMWPE discs. Bioluminescence was measured using an IVIS 100 imaging system 5 minutes after bacterial injection, at 24 hr, 48 hr, 72 hr, and 1 week. Note that only live bacteria luminesce, and therefore the amount of live bacteria is directly proportional to the total bioluminescence.

At the end of study (1 week after bacterial injection), all mice were sacrificed and implants were explanted aseptically and placed into a sterile 15cc Falcon tube containing 2 ml 0.9 % saline. Falcon tubes containing the explants and saline were sonicated to detach the bacteria from the explants, 100 μ L were sampled and added to 1900 μ L of fresh Mueller-Hinton II broth, and incubated at 37°C for 24 hr. Concentration of bacteria were then determined by measuring its absorbance at 600 nm (OD 600).

In Vivo Anesthetic Efficacy of Bupi-PE

Based on the pilot *in vivo* rat study, the standard deviation in bone volume/total volume (BV/TV) is 15 %. Taking type I error of 5 % and 80% power, to detect a mean difference of BV/TV between control and treatment groups of 23 %, a sample size of at least 4 rats was needed per group. Twelve Sprague-Dawley rats aged 8 weeks were randomly assigned into either control (non-antibiotic eluting UHMWPE) or Bupi-PE (layered 20 % Bupivacaine HCl-UHMWPE on 20 % Bupivacaine FB-UHMWPE). Each rat in the received either Bupi-PE or control plugs (each 3 mm in diameter and 4 mm in length) transcondylarly in the medial distal femur.

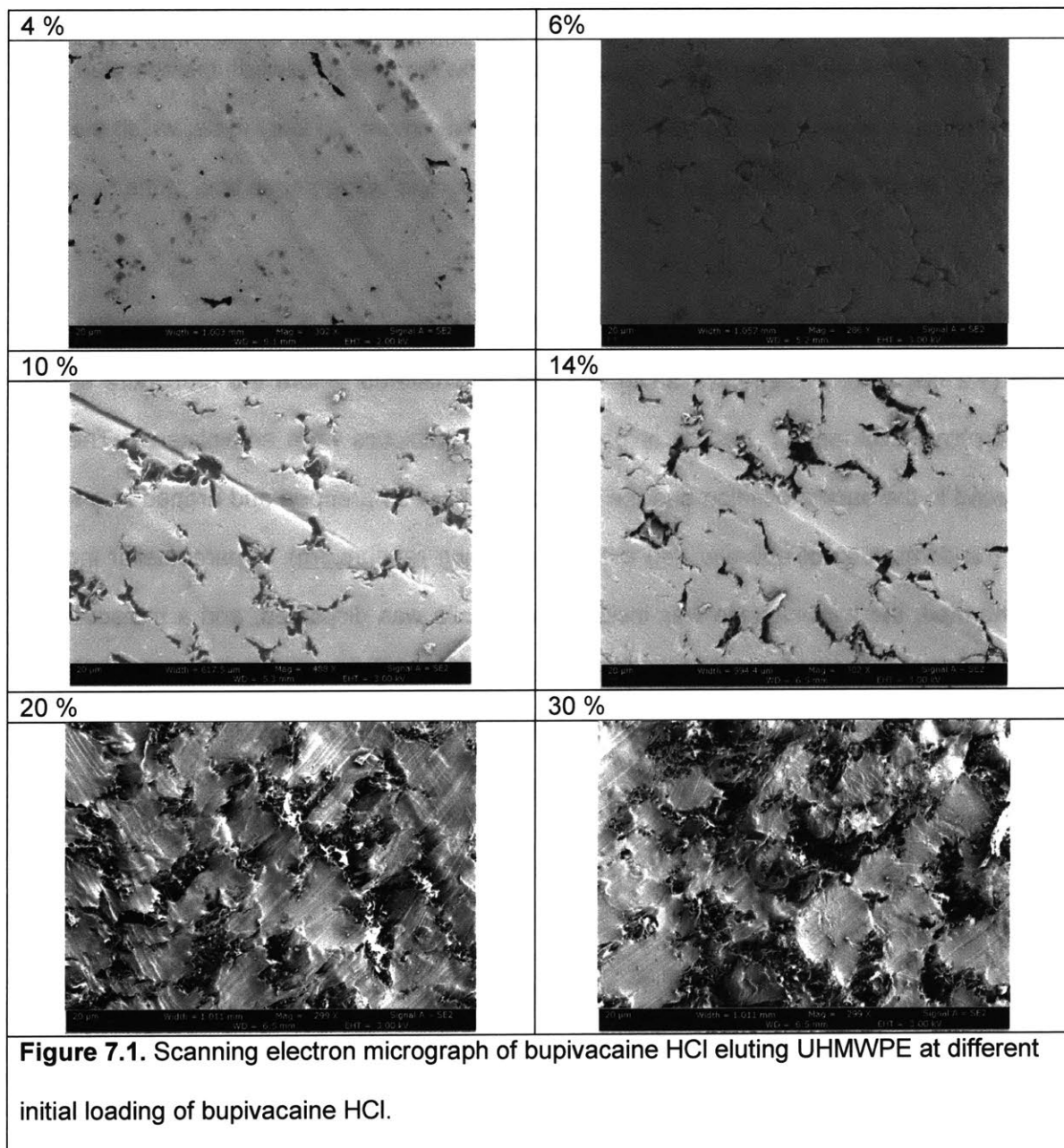
Before surgery, gait and standing pattern of the rats were measured using video recording and pressure sensitive grid pad (Tekscan™) respectively. The Tekscan™ system (Model VH3) is composed of 5,808 sensors distributed equally to an area of 33.5x11.2 cm. The sensor density is 15.5 sensors/cm² with capability of measuring pressure up to 41 kPa. The stance testing was conducted on the pressure sensitive pad (Tekscan®) for 5 x 30 s. The gait testing was conducted by recording the rats during walking for a total of 50 full walking cycle from each rat. Two parameters were measured: (1) F_{Ratio} , which is the force ratio between the operated leg and the contralateral leg as obtained from the stance measurement. (2) Duty cycle, which is the ratio of stance time of the operated leg to the sum of stance and swing phase time of the operated leg.

Anesthesia was achieved using inhaled isoflurane (1.5-2.5 %) supplemented with oxygen (1.2 liter/min). Pre-emptive analgesia was administered before the procedure started (buprenorphine 0.02 mg/kg). No pre or postoperative antibiotics were administered. The rats were placed in the supine position and the right or left leg was prepped and draped in a sterile fashion (randomization of operated leg established using random.org). A parapatellar incision was performed, the joint capsule was incised, the patella was displaced, and a transcondylar defect on the medial distal femoral condyle was created. Control or Bupi-PE implants were press-fitted into the defects. Load bearing on implants was allowed immediately after surgery, as no postoperative limiting motion device was utilized.

After surgery, gait and stance measurement were performed on all rats. Gait and stance testing were again performed 24 hr, 48 hr, 72 hr, 1 week, and 2 week post-surgery. At the end of two weeks, the animals were euthanized using CO₂ asphyxiation. Distal femur of the operated knee and surrounding synovium tissue were isolated. We decalcified the bony tissues and embedded both the decalcified tissues and the soft tissues in paraffin. Subsequently, the embedded tissues were sectioned and stained with hematoxylin and eosin.

Results

Elution and mechanical properties of bupivacaine HCl (Bupi HCl) from Bupi HCl eluting UHMWPE

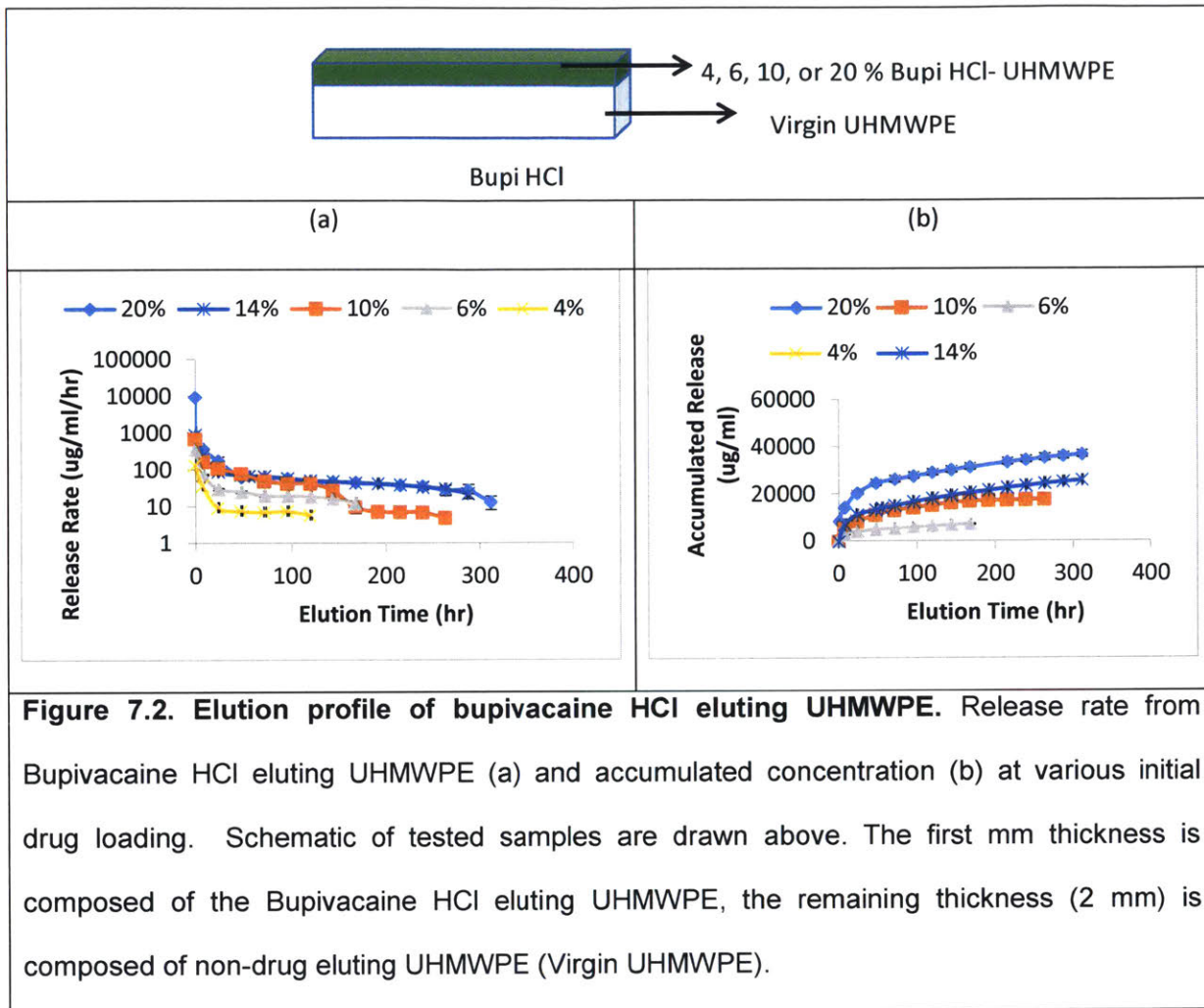


A layered structure consisting of Bupi HCl eluting UHMWPE on top of virgin UHMWPE was synthesized as detailed in methods. The Bupi HCl-UHMWPE layer is 1 mm thick, and the remaining thickness of the sample (2 mm) is composed of only UHMWPE (virgin UHMWPE). Bupi-HCl UHMWPE was fabricated at initial drug loading of 4 wt %, 6 wt %, 10 wt %, 14 wt %, and 20 wt % (**Figure 7.1**).

For all initial Bupi HCl loading, high Bupi HCl elution rate was observed in the first 24 hr, followed by a relatively constant elution rate (**Figure 7.2**). This phenomenon was mirrored in the accumulated release, where an initial steep increase in the total drug released in the first 24 hr, followed with a more gradual and sustained release after 24 hr. The drug release rate increased at all elution time points when the initial drug loading is increased from 4 wt % to 6 wt % to 10 wt %. When comparing the sample with initial drug loading of 10wt %, 14 wt % and 20 wt %, the release rate at < 6hr was increased as the initial drug content was increased, however, the release rate between 6 hr and 144 hr were similar. The release rate after 144 hr was lower for the 10% Bupi HCl. The release rate after 144 hr between 14% and 20% was similar.

The tensile strength and elongation to break decreased when Bupi HCl content was increased from until 10 wt %, after which there was no further change up to 30% (**Figure 7.3**). The wear rate significantly decreased as the Bupi HCl content was increased until 20 wt %, after which there was no statistically significant change (**Figure 7.3**).

Based on the scanning electron micrograph, interconnectivity of Bupi HCl was increased as the initial drug loading was increased. High and fully interconnected Bupi HCl cluster interconnectivity in the UHMWPE was observed at 6 wt % and 10 wt % Bupi HCl respectively (**Figure 7.1**). Upon increasing the drug loading even further (to 14,% 20 %, and 30 wt % BupiHCl content), the width of the drug cluster channels increased.



Elution of Bupivacaine FB eluting UHMWPE

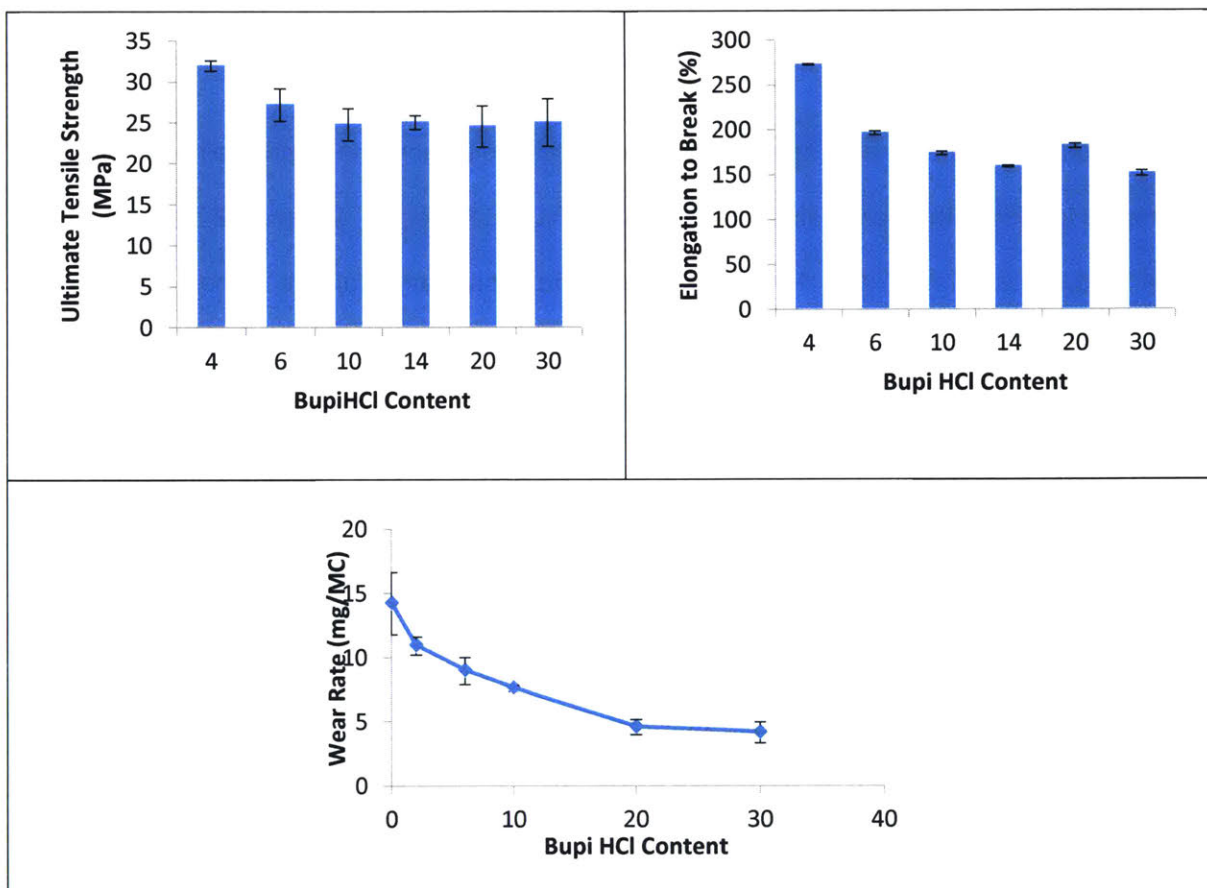


Figure 7.3. Mechanical and wear properties of bupivacaine HCl eluting UHMWPE.

Ultimate tensile strength, elongation to break, and wear rate of Bupivacaine HCl eluting UHMWPE at various initial drug loading. A schematic of tested samples are drawn above. The first mm thickness is composed of the Bupivacaine HCl eluting UHMWPE, the remaining thickness (2 mm for tensile test and 9 mm for the wear test is composed of non-drug eluting UHMWPE (Virgin UHMWPE).

To elucidate the effect of incorporating bupivacaine free base (Bupi FB) on the elution of bupivacaine from UHMWPE, samples composed of homogeneous Bupi FB eluting UHMWPE were prepared. Bupivacaine FB was diffused into pre-consolidated virgin UHMWPE of size 5 mm x 3 mm x 20 mm at either 115°C or 150°C for 24, 48, or 72 hr. Unlike the Bupi HCl eluting

UHMWPE that showed clear phase separation between the Bupi HCl clusters and the UHMWPE granules, no phase separation between Bupi FB and UHMWPE was observed (Figure 7.4)

Based on the gravimetric analysis before and after diffusion, the bupivacaine content in the samples loaded with bupivacaine FB by diffusion at 115 °C for 24, 48, and 72 hr were 5.2 ± 1.4 %, 6.8 ± 0.9 %, and 7.0 ± 1.1 % respectively. The bupivacaine content in the samples diffused at 150°C for 24, 48, and 72 hr were 18.3 ± 1.1 %, 19.7 ± 2.1 %, 20.5 ± 1.4 % respectively. Both the elution rate and the accumulated release from samples loaded with bupivacaine FB by diffusion at 150°C were higher than that of samples diffused at 115°C. The elution rate and accumulated elution of samples loaded by diffusion at 48 and 72 hr at 115°C were higher than that from the samples diffused for 24 hr at the same temperature (Figure 7.5). There was no statistically significant difference in both elution rate of and total elution from samples loaded by bupivacaine FB by diffusion at 115°C for 48 hr and 72 hr.

Similar to the trend observed for samples loaded with bupivacaine by diffusion at 115°C, the elution rate of and the total eluted concentration in the medium of samples loaded by bupivacaine by diffusion at 48 and 72 hr at 150°C were higher than that of samples after 24 hr at the same temperature. There was no statistically significant difference between samples diffused for 48 hr and 72 hr.

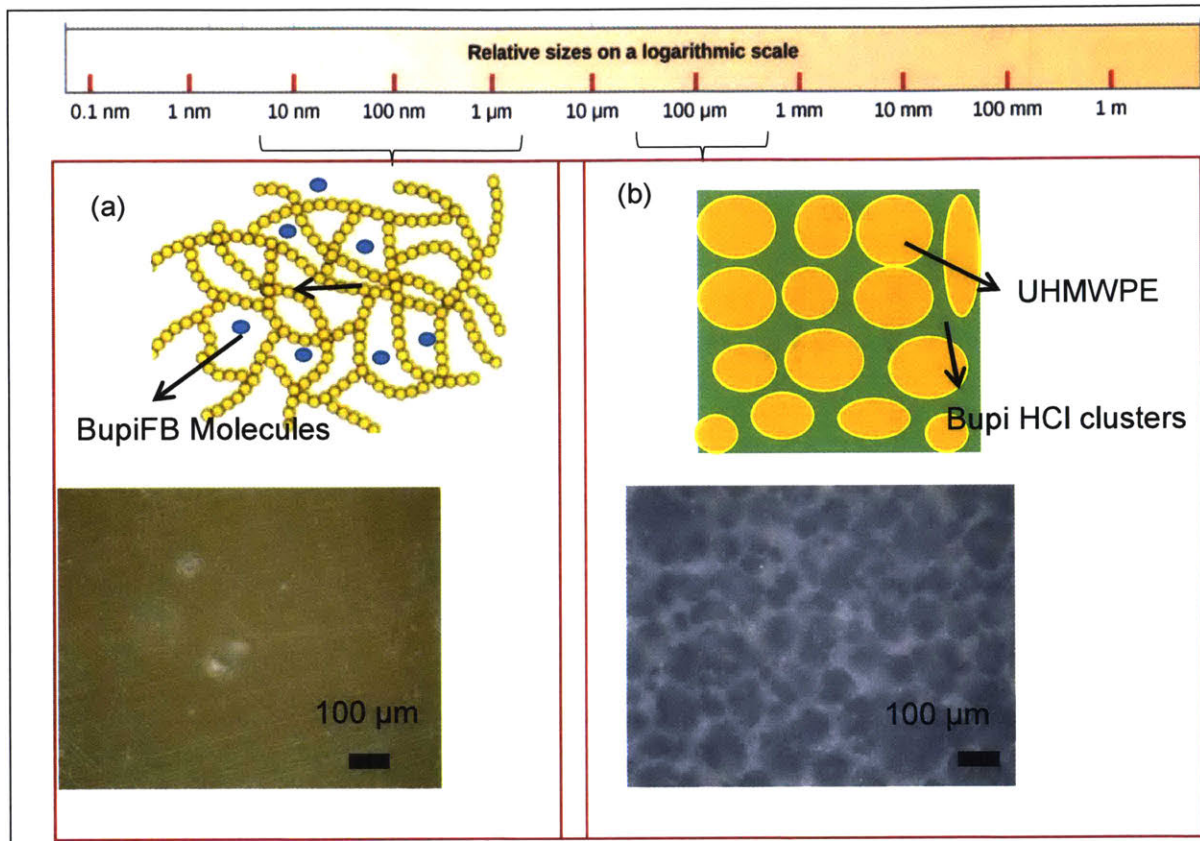
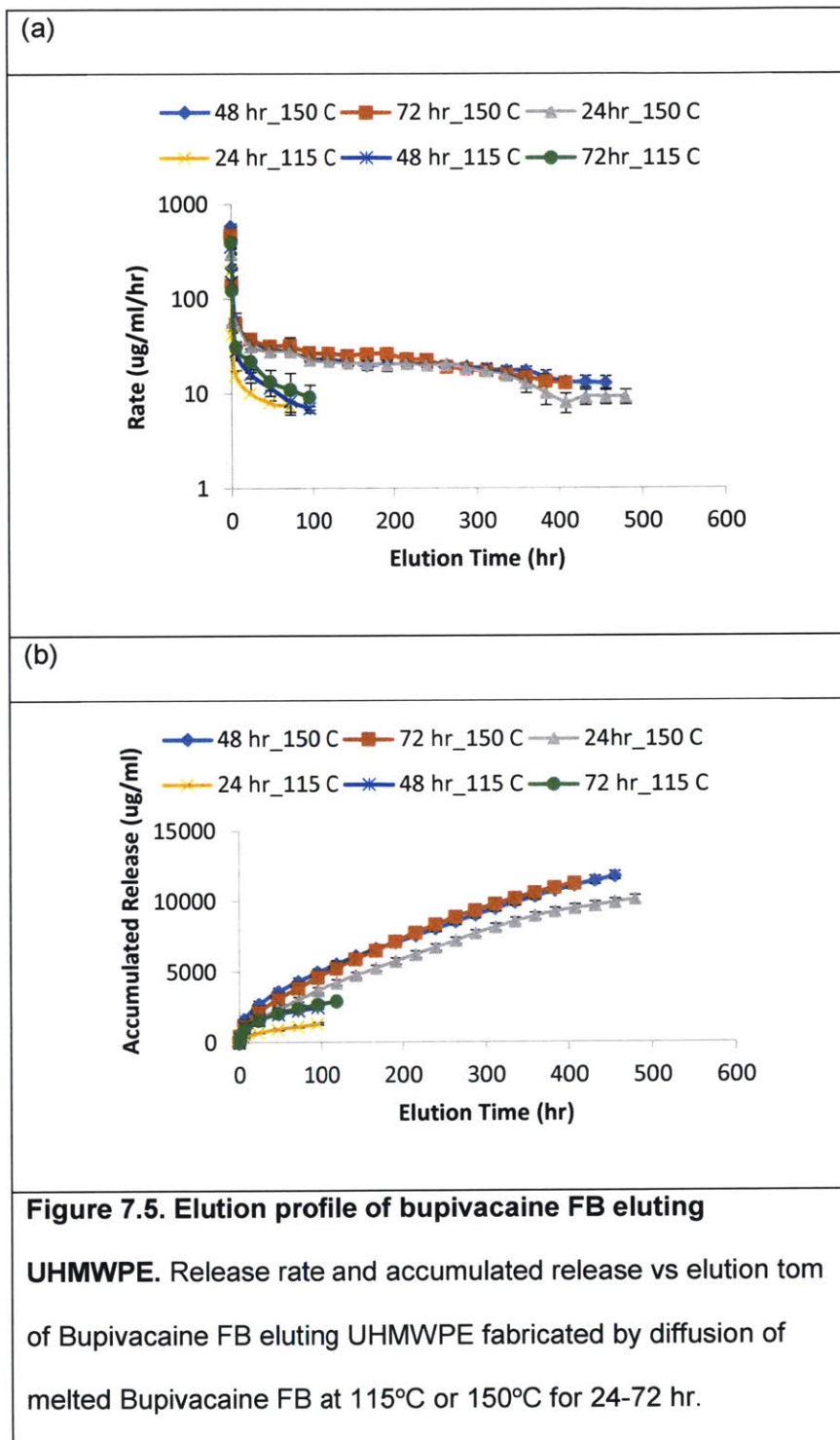


Figure 7.4. Ionization state of bupivacaine determines its form in UHMWPE. (a) Bupivacaine FB, which is much more hydrophobic than its salt form and melts at 103-104°C, did not show any sign of phase separation from UHMWPE based on the optical micrograph, indicating that it is intermingled in between the UHMWPE chains (left). (b) bupivacaine HCl, which is much more hydrophilic and does not melt until > 200°C showed clear phase separation (as shown in the optical micrograph) between the bupivacaine HCl clusters and the UHMWPE granules (right).



Elution and mechanical properties of Bupivacaine HCl (Bupi HCl), Bupivacaine Free Base (Bupi FB) and its combination from Bupi HCl eluting UHMWPE

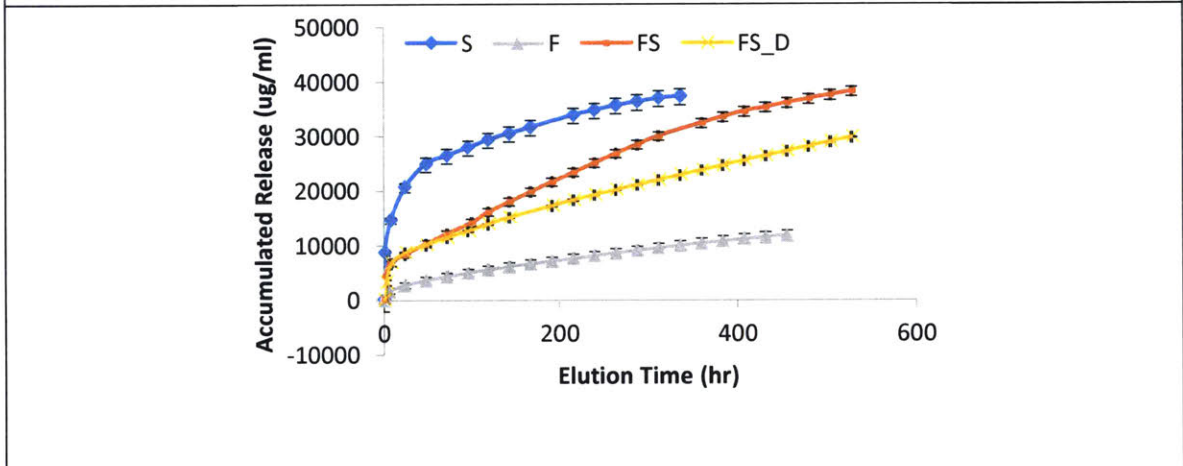
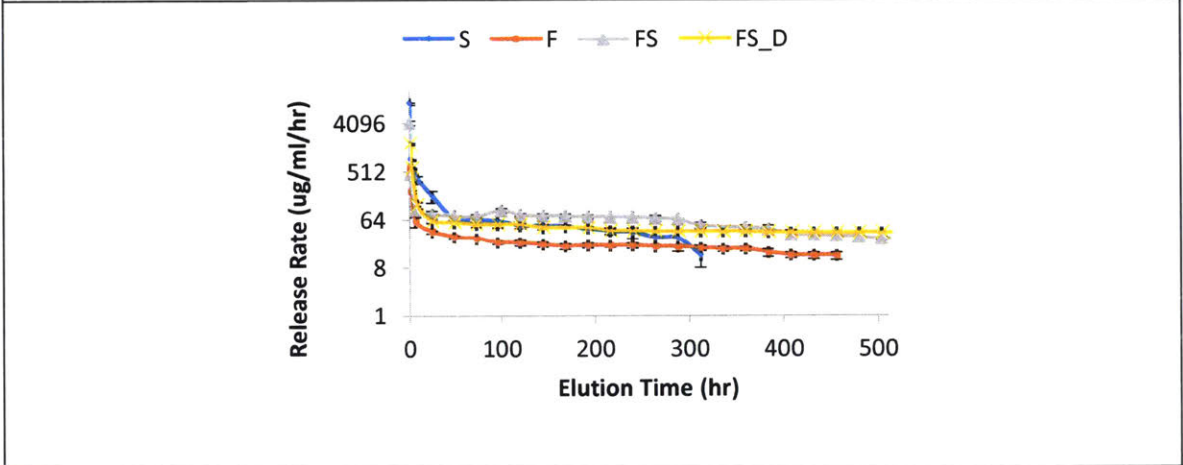
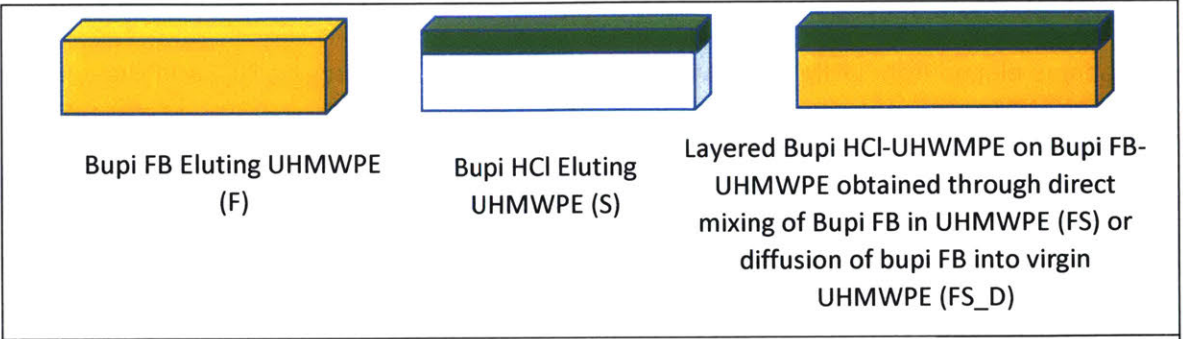


Figure 7.6. Elution profile of combined bupivacaine FB and bupivacaine HCl eluting UHMWPE. Release rate and accumulated release of homogeneous bupivacaine FB eluting UHMWPE loaded by diffusion for 48 hr at 150°C (F), layered 20% bupivacaine HCl eluting UHMWPE on Virgin UHMWPE (S), layered 20 % bupivacaine HCl on 20 % Bupi FB in UHMWPE (FS), and layered 20 % bupivacaine HCl on Virgin UHMWPE subsequently dipped into Bupivacaine FB at 150°C for 48 hr (FS_D).

To elucidate the effect of combining Bupivacaine FB and Bupivacaine HCl on the overall bupivacaine elution from UHMWPE, two combined samples Bupivacaine HCl and Bupivacaine FB eluting UHMWPE were fabricated: (1) A layered construct composed of 20 % Bupi HCl-UHMWPE on top of 20 % Bupi FB in UHMWPE. The Bupi HCl-UHMWPE layer was 1 mm thick, and the remaining thickness of the sample (2 mm) was composed of 20 % Bupi FB-UHMWPE. In this sample, both the Bupivacaine HCl and the Bupivacaine FB was pre-mixed with the UHMWPE before consolidation (FS). (2) A layered construct composed of 20 % Bupi HCl in UHMWPE (1 mm) on top of Virgin UHMWPE (2 mm), then subsequently diffused with bupivacaine FB at 150°C for 48 hr (FS_D). For the remainder of the study, the 20 % Bupi HCl in UHMWPE layered on top Virgin UHMWPE will be referred as S and the homogeneous 20 % Bupi FB in UHMWPE will be referred as F.

Both the FS and FS_D showed significantly lower burst release (release in the first hour) than Bupi HCl sample (Release rate in the first hour were 1750 ± 73 $\mu\text{g/ml/hr}$, 4196 ± 395 $\mu\text{g/ml/hr}$, 9546 ± 534 $\mu\text{g/ml/hr}$ for FS_D, FS, and S respectively). FS and FS_D were able to maintain high release rate longer than S, most notably at elution time of >288 hr where S elution rate decreased sharply while the elution rate of FS and FS_D were relatively constant (**Figure 7.6**). No statistically significant difference in elution rate between FS and FS_D after the first hour until 384th hr. The elution of FS then started to decrease and diverged from the FS_D until the end of the study.

The mechanical and tribological properties (ultimate tensile strength, elongation to break, impact strength, and wear rate) of S, F, FS, and FS_D were measured.

The ultimate tensile strength of F was slightly lower than virgin UHMWPE (40.2 ± 1.4 MPa and 46.2 ± 1.5 MPa, respectively). There was no significant difference in the elongation to break, impact strength, and wear rate (**Figure 7.7**). The ultimate tensile strength, elongation to break, and wear rate of FS, FS_D, and S were similar to each other (**Figure 7.7**) and were

significantly lower than that of virgin UHMWPE and F. There are no statistically significant difference in impact strength between any group of samples.

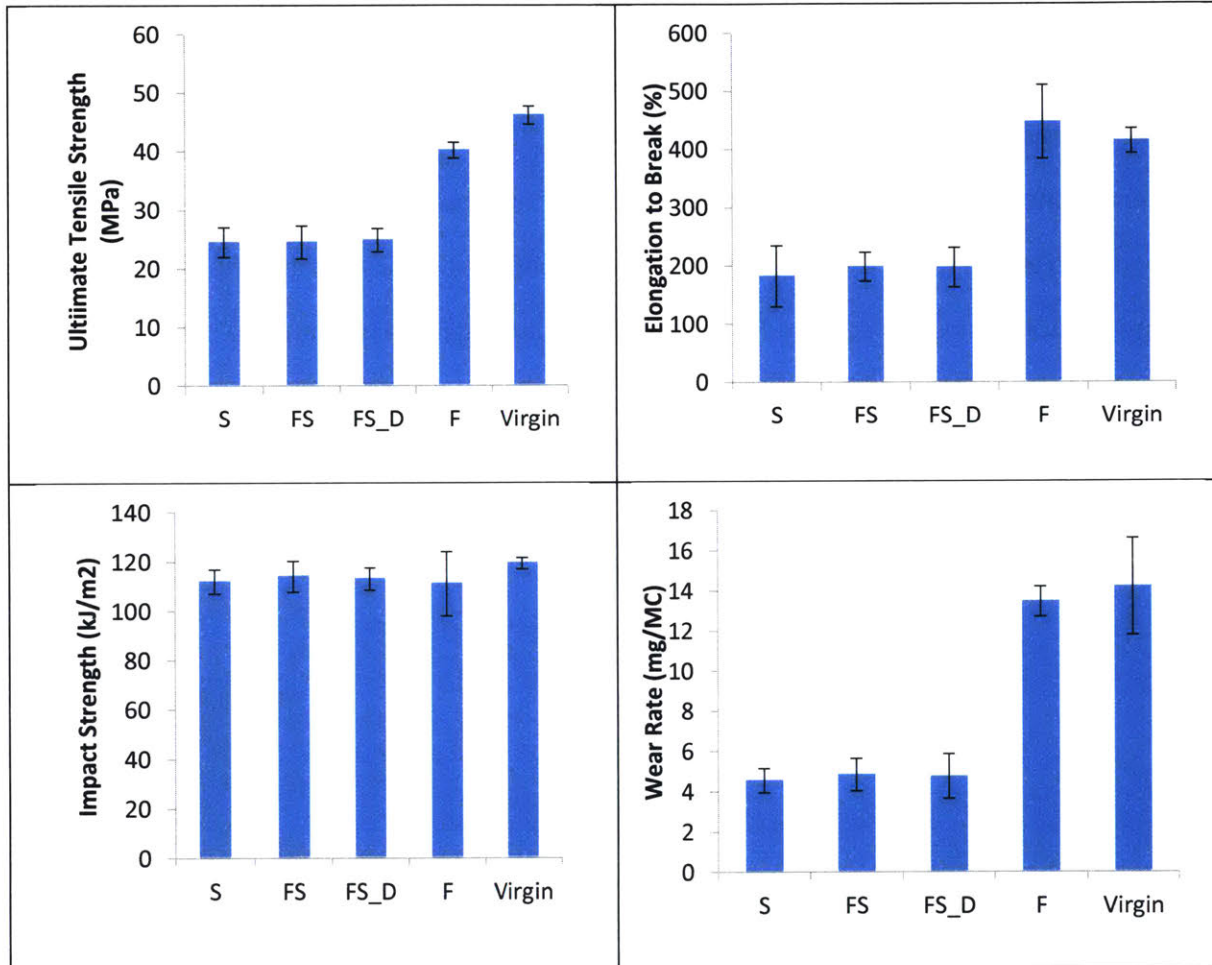


Figure 7.7. Mechanical and wear properties of combined bupivacaine FB and bupivacaine HCl eluting UHMWPE. Ultimate tensile strength, elongation to break, and wear rate of S, FS, FS_D, F, and virgin UHMWPE. For layered constructs such as S, FS, and FS_D, the first mm thickness is composed of the Bupivacaine HCl eluting UHMWPE, the remaining thickness (2.2 mm for tensile samples, 5.4 mm for impact test, and 9 mm for wear test) were made of non-drug eluting UHMWPE (Virgin UHMWPE) or F.

Measurement of minimum inhibitory concentration of bioluminescent *S. aureus* (Xen29) against Bupivacaine HCl, Bupivacaine FB, and FS

Antibacterial activity of Bupivacaine HCl and Bupivacaine FB against the bioluminescent *S. aureus* (Xen 29) were measured as detailed in Methods. The minimum inhibitory concentrations of Bupi HCl and Bupi FB against Xen 29 was 2 mg/ml (**Figure 7.8**). When the concentrations of bupivacaine eluted from the Bupi-PE in the first 24 hr was measured with UV-Vis and then tested for its MIC, 1.8 mg/ml MIC was obtained, indicating that the antibacterial activity of bupivacaine eluted from FS was similar to the bupivacaine standard solution, which was prepared by dissolving as received bupivacaine into the Mueller-Hinton II media.

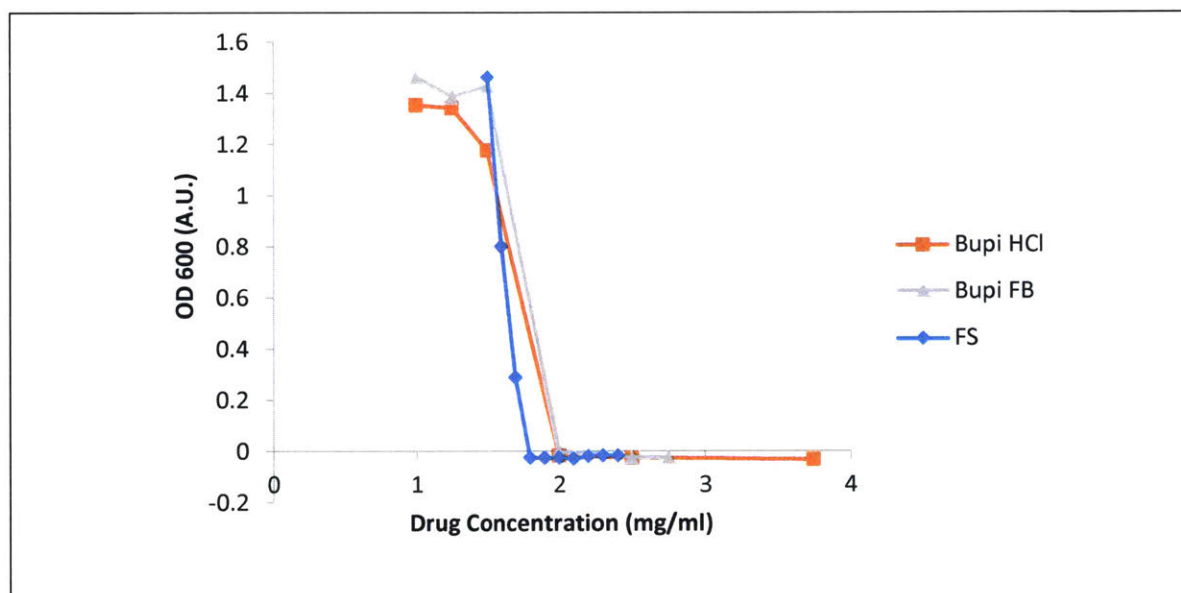


Figure 7.8. Antibacterial activity of bupivacaine eluted from UHMWPE and standard bupivacaine solution. Measurement of minimum inhibitory concentration of standard Bupivacaine HCl solution (Bupi HCl), standard bupivacaine FB solution (Bupi FB), and bupivacaine eluted from Bupi-PE (Bupi-PE). MIC is defined as the minimum concentration where the OD 600 is statistically indifferent to the negative control (media only).

In Vivo Antibacterial Activity of Bupi-PE in Subcutaneous Murine Model

Ten rats were divided equally and randomly into two groups: The first group of rats received UHMWPE disc without any bupivacaine (control) and the second group of rats received Bupi-PE discs. The Bupi-PE disc was made of FS with 1 mm thick 20% Bupi HCl-UHMWPE and 2 mm thick 20% Bupi FB-UHMWPE. Diameter and thickness of control and Bupi-PE discs were 5 mm and 3 mm, respectively. Control UHMWPE and Bupi-PE discs were implanted subcutaneously on the dorsum of rats under general anesthesia. All rats received subcutaneous cefazolin (15 mg/kg).

Both rats receiving control UHMWPE and Bupi-PE fully recovered from anesthesia with no sign of acute allergic reaction (within three hours) around the implant area. All rats were mobile and eating normally post-anesthesia.

All rats in both control and Bupi-PE groups showed similar magnitudes of bioluminescence at 5 minutes after being injected subcutaneously (POD 0, **Figure 7.9**). At 24 hr after injection (POD 1), all rats in both groups showed statistically significant lower magnitude of bioluminescence, indicating that significant amounts of the bacteria were eradicated by the host immune system and by the prophylactic antibiotics administered before surgery. No detectable bioluminescence was observed in the Bupi-PE group at POD1, while bioluminescence was observed in the control group. No bioluminescence was observed in the Bupi-PE group until the end of study, while significant amount of bioluminescence was still observed in the control group at 1 week after surgery. All rats in the Bupi-PE group survived until the end of the study (1 week), while the two out of five (40 %) of the control rats naturally expired, presumably due to sepsis. Sonication of the bacteria into a sterile bacteria medium and subsequent re-culturing of the explants showed no live bacteria in the Bupi-PE group but high amount of bacteria in the control groups (**Figure 7.9**).

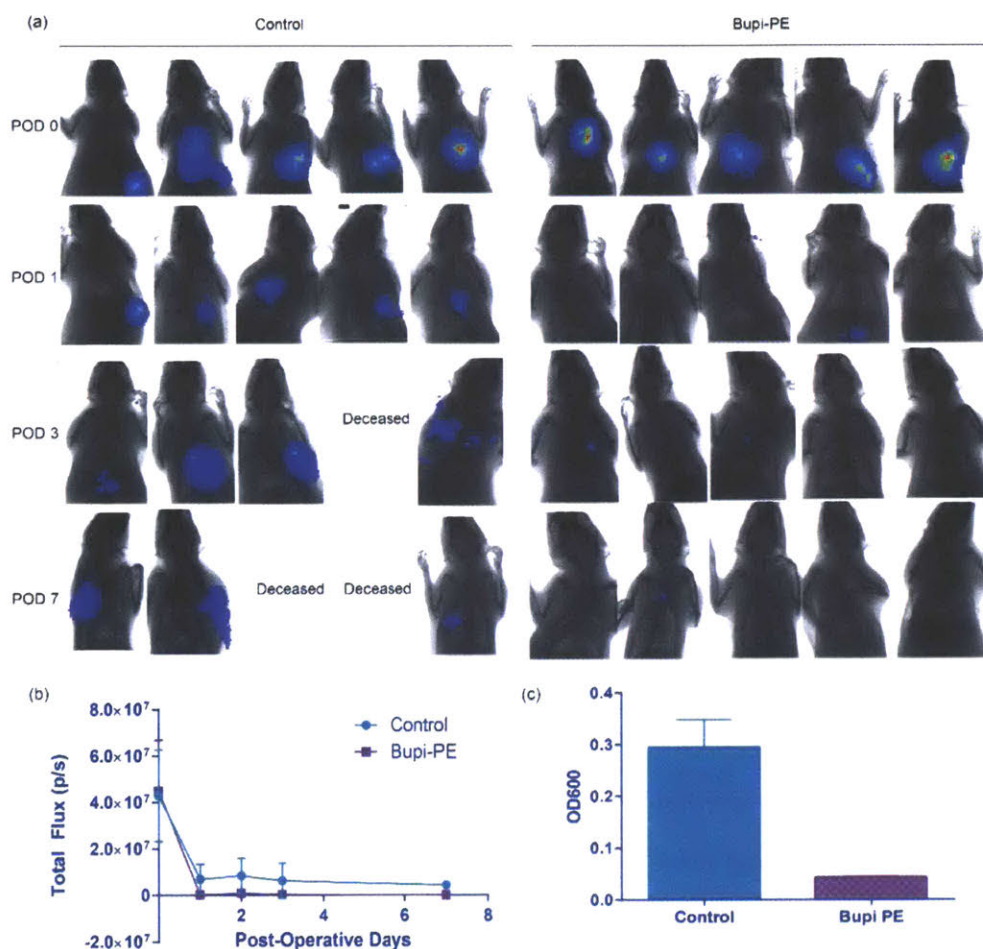


Figure 7.9. In vivo antibacterial activity of bupi-PE. (a) In vivo bioluminescence color map from Xen 29. Bioluminescent *S. aureus* Xen 29 was injected subcutaneously on top of the UHMWPE discs and total flux was measured by a bioluminescent camera (IVIS 100, Caliper). (b) Total bioluminescence quantification. Region of interest was drawn around the implant area for each figure and total bioluminescence was calculated. Data are

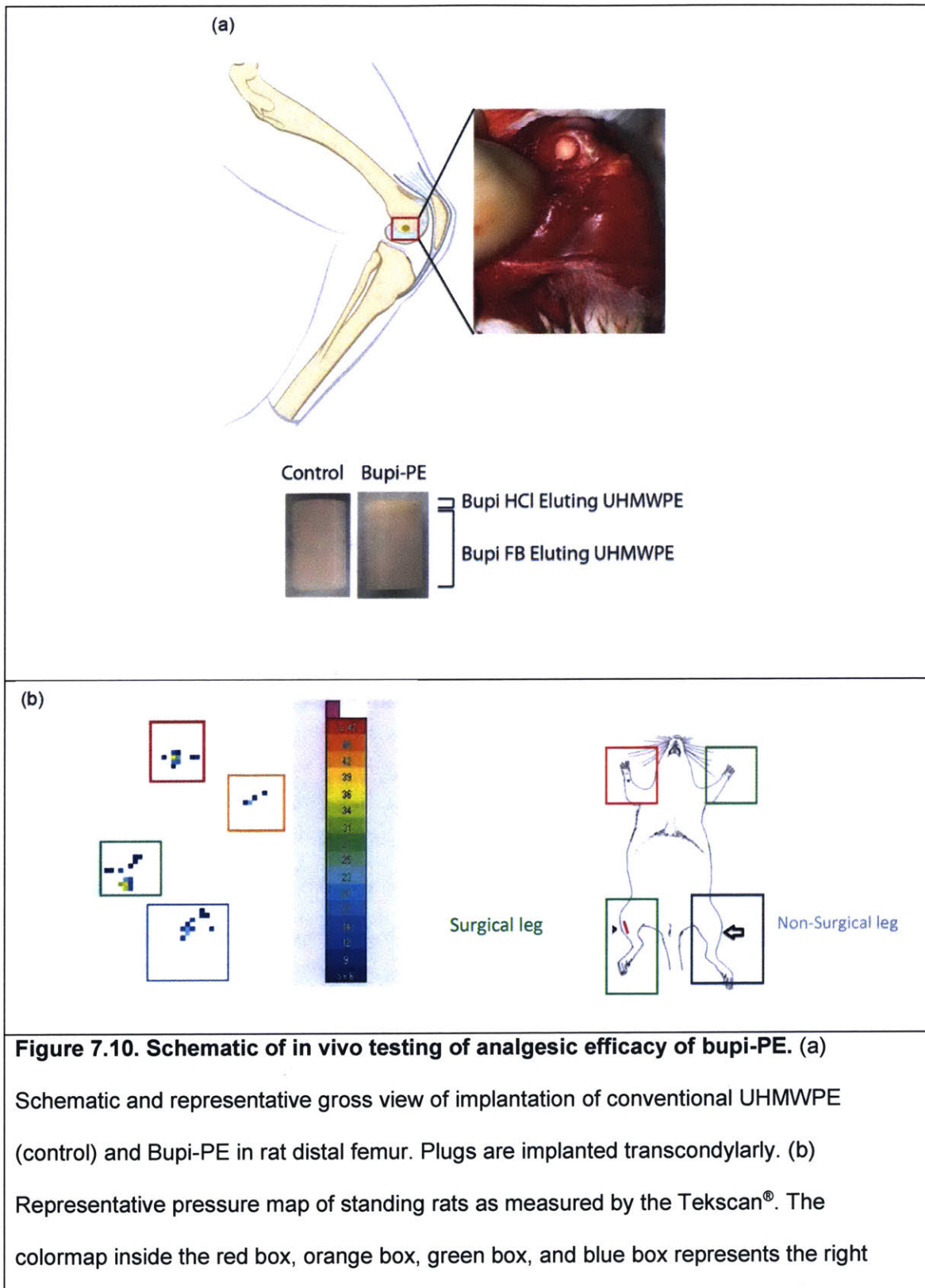
presented as mean \pm s.d. (n=5 for each group). (c) Post-Mortem sonication of tissues and Explants. Absorbance at 600 nm (OD600) after sonication of control UHMWPE or Bupi-PE from the dorsal subcutaneous pocket of mice. Data are presented as mean \pm s.d. (n=5 for each group).

In Vivo Analgesic Activity of Bupi PE in Murine Model

All rats were mobile and eating normally post-anesthesia. Immediately after the rats recovered from the anesthesia, all rats underwent stance and gait testing again. Gait and stance testing were also performed on all rats at post-operative day (POD) 1, 2, 3, 7, and 14.

Prior to surgery, there was no difference in both the F_{Ratio} and the duty cycle between the rats in the control group and the rats in the Bupi-PE group. Immediately after the surgery, significant difference in both the F_{Ratio} and duty cycle were observed between the control and Bupi-PE groups (**Figure 7.11**): F_{Ratio} in the control group fell to a level which was much lower than that prior to surgery and the duty cycle of the operated leg (right leg) significantly decreased, while the duty cycle of the contralateral leg (left leg) was significantly increased. The F_{Ratio} and duty cycles of the rats in the Bupi-PE were similar to that prior to surgery (**Figure 7.11**).

The F_{Ratio} and duty cycles of rats in the Bupi-PE groups remained similar throughout the study, and at no point significantly differed from that measured before the surgery. The F_{ratio} of the rats in the control group remained significantly below the preoperative level until POD 7, with lowest value observed immediately after the surgery. The duty cycles of the rats in the control group significantly deviated from the preoperative value until POD 3, followed by convergence toward baseline preoperative values at POD 7.



forelimb, left forelimb, right hindlimb, and left hindlimb respectively. The UHMWPE plugs were implanted on the distal femur of the right hindlimb.

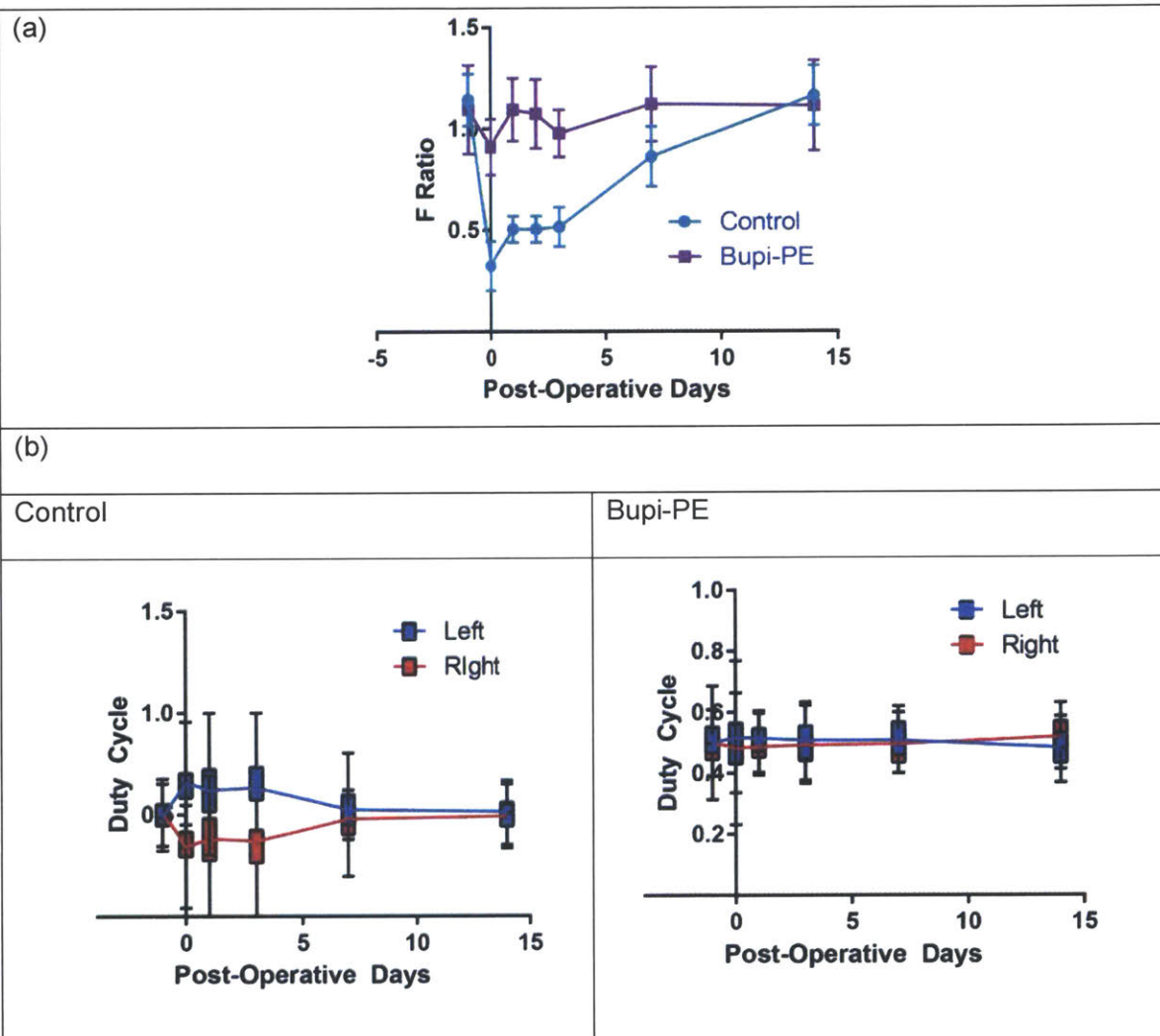
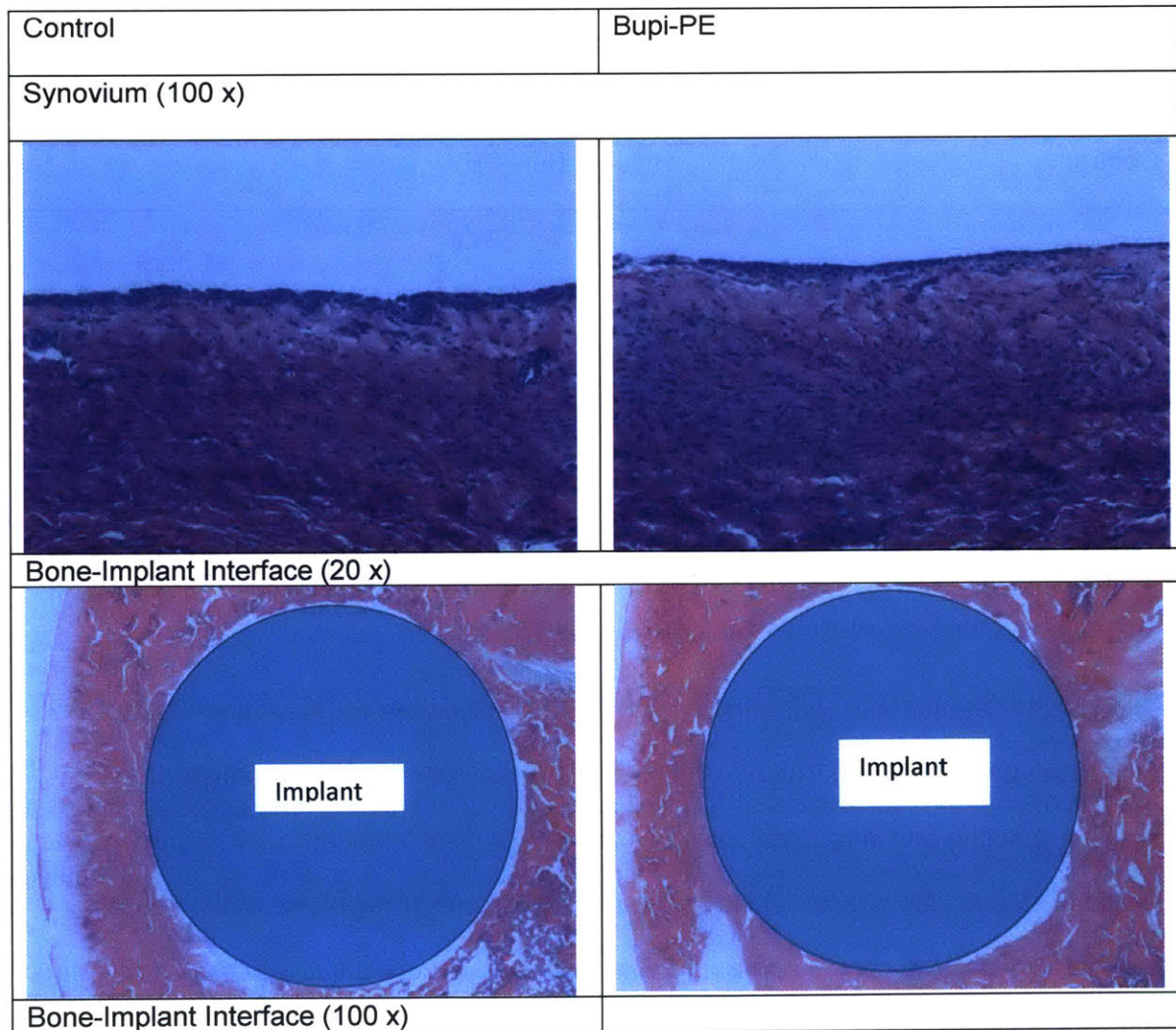


Figure 7.11. Stance and gait activity of the hind limbs post-implantation of bupi-PE or control UHMWPE. (a) Force ratio between the operated leg and contralateral leg as measured during standing. Data are means of 5x30 s measurements \pm SD. (b) Duty cycle (Ratio of stance time of operated leg to sum of stance and swing phase of the operated leg) of the rats in the control and Bupi-PE groups. Data are means of 300 steps (50 from each rat, n= 6 rats in each group) \pm SD.

All rats were euthanized after two weeks and distal femur and synovial tissues of the operated knee were isolated and stained with H&E stain (**Figure 7.12**). No significant difference in the synovium tissue appearance was observed between samples obtained from control rats and Bupi-PE rats. No sign of inflammation (such as neutrophils, macrophages, plasma cells, etc) was observed in the bone tissue surrounding either the control UHMWPE or Bupi-PE. Taken together, Bupi-PE was biocompatible and did not cause extra inflammatory reaction compared to non-drug eluting UHMWPE.



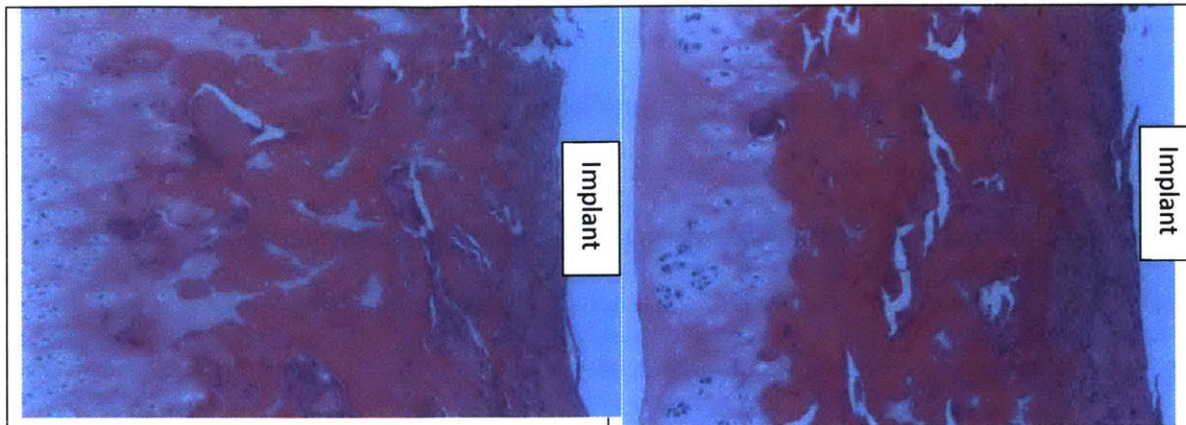
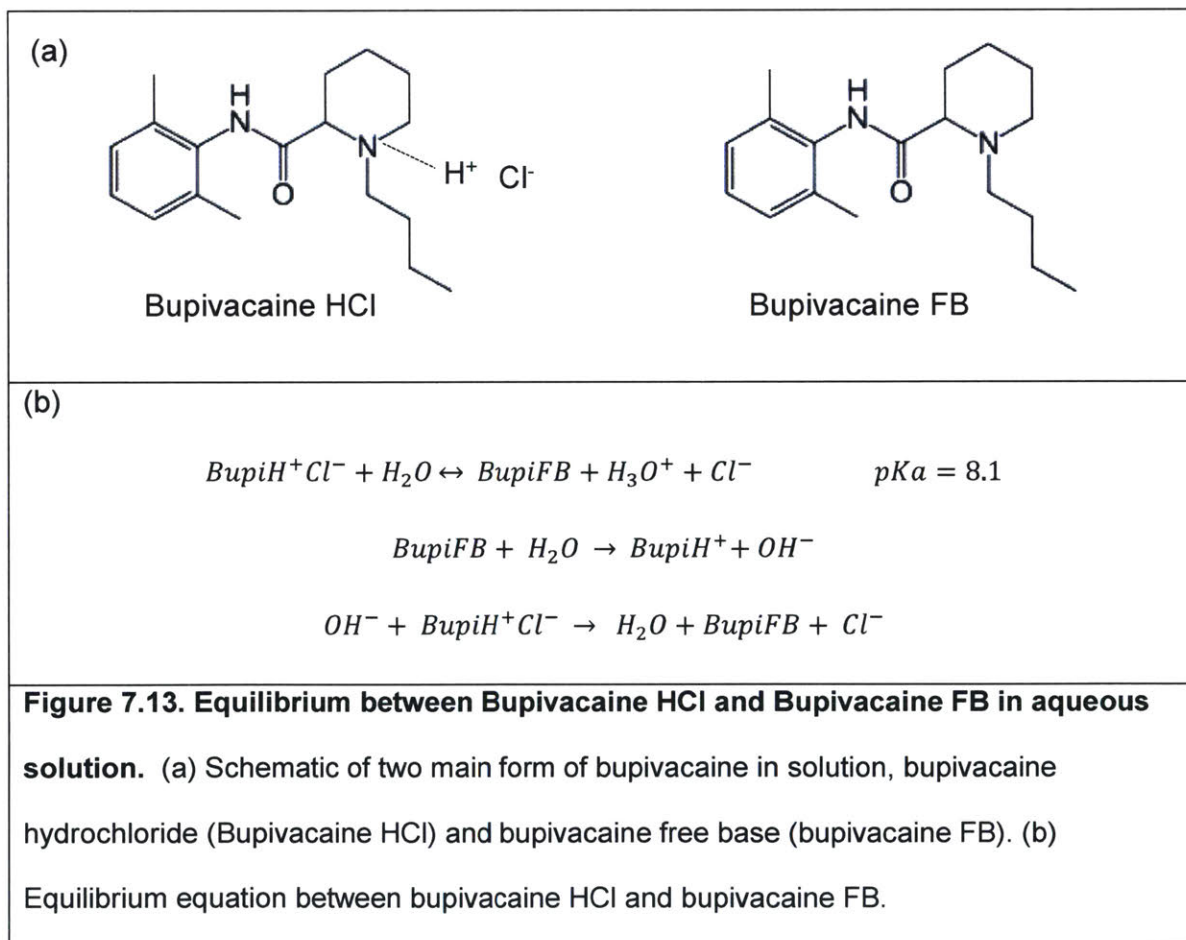


Figure 7.12. Representative histology of the synovium capsule and the bone-implant interface of the rats receiving control UHMWPE or Bupi-PE.

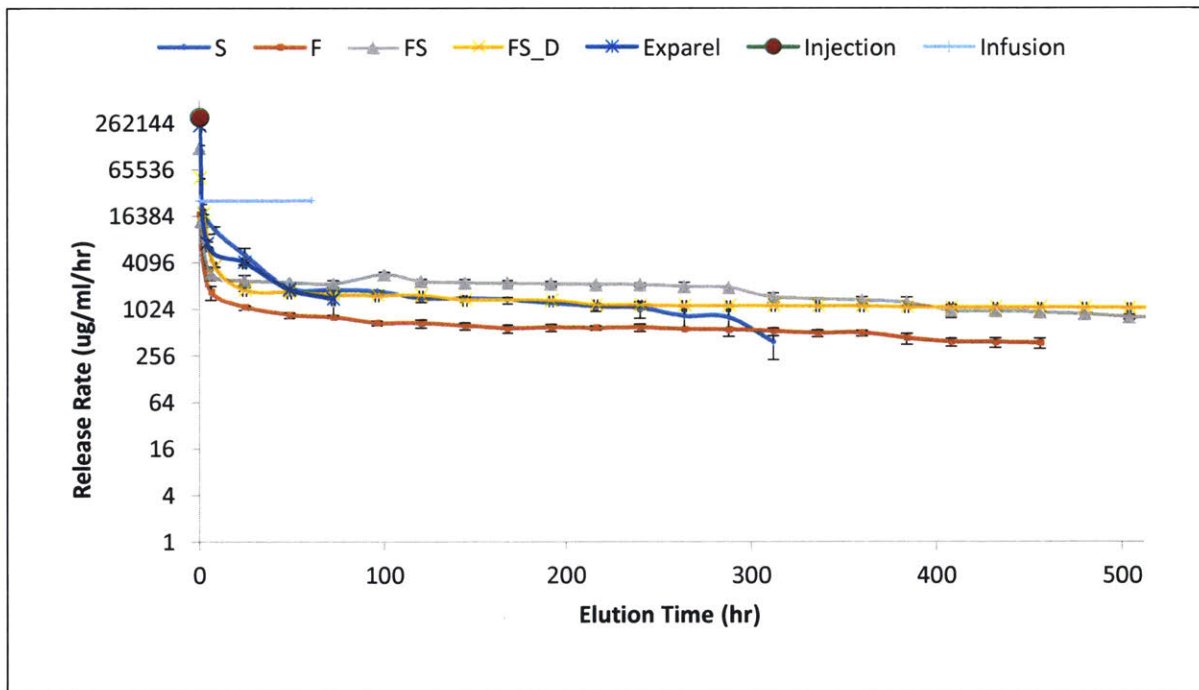


Discussion

In this study, we developed bupivacaine eluting UHMWPE for sustained intraarticular delivery of local anesthetics post-arthroplasty to reduce post-arthroplasty pain. Because post-arthroplastic pain peaked immediately after surgery and decreased linearly to baseline at 3 weeks, we aimed to design local anesthetic eluting UHMWPE that was effective for at least 3 weeks. We incorporated two types of bupivacaine, Bupivacaine HCl and Bupivacaine free base (**Figure 7.13**). The bupivacaine HCl is composed of a positive bupivacaine ion with Cl⁻ as countercharge, while the free base form is non-polar and uncharged. Bupi HCl is highly soluble in water, while Bupi FB is poorly soluble in water (40 mg/ml in water at pH =7 for Bupi HCl and 2.1 mg/ml in water at pH = 7 for Bupi FB) [577-579]. While Bupi FB melts at 107-108°C[580], Bupi HCl melts at 249-251°C [581]. The minimum local analgesic concentration of both bupivacaine hydrochloride and bupivacaine free base are 0.065 mg/ml, which is much lower than other local anesthetics such as lidocaine (0.37 mg/ml)[582], and ropivacaine (0.156 mg/ml)[583]. In addition to its analgesic properties, bupivacaine also possesses antibacterial activity, despite being much weaker than conventional antimicrobials (MIC=0.25-2 mg/ml) [575] (**Figure 7.8**). We found that there was no significant difference in antibacterial activity between bupivacaine HCl and bupivacaine FB against *S. aureus*.

Bupivacaine eluting UHMWPE, in particular S, FS, and FS_D have a more sustained release rate and higher accumulated release of bupivacaine than Exparel™, especially after 72 hr elution (**Figure 7.14**). Compared to 72-96 hours for Exparel, bupivacaine-eluting UHMWPE was able to sustain analgesic/anesthetic elution rate > 1340 mg/ml in the medium for 5, 6, 14 days for FS_D, S, and FS respectively. The release rate of all four types of bupivacaine-eluting UHMWPE remained lower than the rate achieved using a single intraarticular injection for the entire release period (300-500 hours or 15 to 24 days), reducing the probability of increased side effects of bupivacaine elution from bupivacaine-eluting UHMWPE. FS and FS_D could

sustain the bupivacaine elution rate better than S with lower burst release rate (within the first hour) than the S. The lower burst release rate of FS can be explained by the relationship between the bupivacaine HCl-bupivacaine FB equilibria, the pH in the microenvironment and the solubility of these molecules (**Figure 7.13b**, [579]): Shah et al [579] reported that the elution of bupivacaine depends more on the microclimate pH immediately surrounding the bupivacaine eluting device than on the bulk pH. When bupivacaine is dissolved in the dissolution medium, it will alter the pH in the diffusion layer through a self-buffering action. Dissolution of bupivacaine HCl will likely lower the microclimate pH compared to the bulk, therefore maintaining high solubility of bupivacaine HCl at 40 mg/ml [579]. On the other hand, dissolution of bupivacaine FB will likely increase the microclimate pH compared to the bulk, therefore decreasing the solubility of both bupivacaine FB and bupivacaine HCl. As a result, presence of bupivacaine FB in the diffusion layer will decrease the overall solubility of bupivacaine.



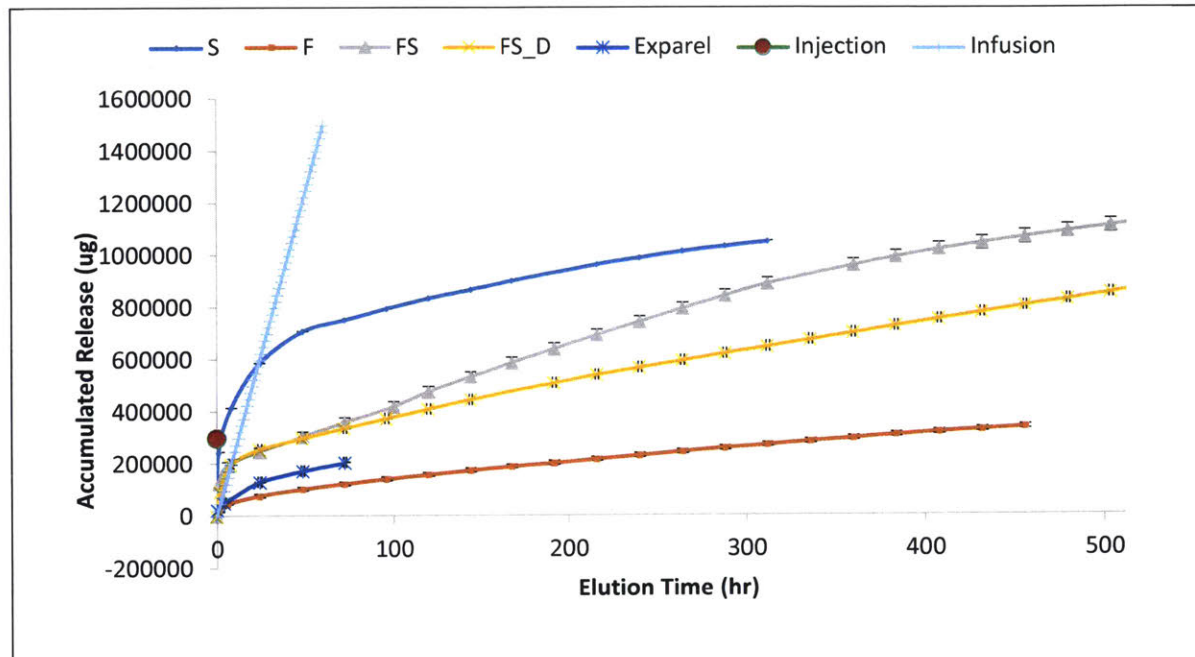


Figure 7.14. Comparison of bupivacaine release rate and total released bupivacaine from single injection, Exparel™, infusion pump, and bupivacaine eluting UHMWPE (S, F, FS, FS_D). For single injection, 60 ml of 0.5 % Bupivacaine was used based on [560]. For Exparel™, dosage of 266 mg of the liposomal bupivacaine was used. Release rate of Exparel™ was obtained from [584]. Infusion is delivery of 5 ml/hr, 0.5 % Bupivacaine for a total of 60 hr based on [585]. Dimension of the bupivacaine eluting UHMWPE: Anterior-Posterior = 50 mm, Medial-lateral = 71 mm, thickness=12 mm. To calculate the surface area, the implant is approximated as a block with dimensions mentioned above. For layered systems such as in S, FS, and FS_D, the thickness of Bupi HCl-UHMWPE is 1 mm and the thickness of virgin UHMWPE or Bupi FB-Diffused is 11 mm.

Complete *S. aureus* eradication by implanted FS disc (Bupi-PE) was observed in murine prophylaxis model, as verified by both bioluminescence and sonication (**Figure 7.9**). In this model, bacteria were injected around the implant to simulate bacterial contamination to the surgical site during hip or knee arthroplasty. To simulate the antibiotic regimen in patients

undergoing primary arthroplasty more closely, prophylactic antibiotics (Cefazolin 15 mg/kg) were administered within one hour before surgery to all rats [586]. A significant portion of the bacteria was killed 24 hr after bacterial injection in both control and Bupi-PE groups, presumably due to combination of the antimicrobial prophylaxis and the host immune system. Larger degree of bacterial eradication was observed in the Bupi-PE groups than in the control groups, likely because the additional antibacterial activity of the bupivacaine eluted from Bupi-PE helped in bacterial eradication. By the end of study (POD 7), bacteria are completely eradicated by POD 7 in the Bupi-PE group, while significant amount of surviving bacteria could be detected in the control group. Therefore, FS, in conjunction with antibiotic prophylaxis, was effective in eradicating bacteria inoculated during surgery.

Pain and arthritis were shown to affect both the load/weight bearing and the dynamic gait pattern in animal models and in humans [587-589]. This finding can enable us to determine a 'functional pain model', where the measured function of the joints in load bearing and the gait patterns can be linked to the efficacy of our devices in eliminating pain. Animal models of monoarthritic hindlimb and patients with unilateral knee osteoarthritis displayed reduced weight bearing ratio on the arthritic and painful limb compared to the contralateral hind limb [587-589]. In addition to the weight bearing, dynamic gait parameters such as velocity, stride length, stance phase duration, swing phase duration, swing speed, and duty cycle were also affected in both animal models and in human[587, 590]. The stance phase and the duty cycle were both decreased in the arthritic/painful limb as compared to the contralateral limb [587, 591, 592]. Both the weight bearing and the dynamic gait parameters converged back to pre-arthritic or before pain values when the animals were treated with analgesics such as indomethacin, morphine, rofecoxib, and celecoxib[592, 593].

In this study, we observed that immediately after surgery, the weight bearing of the rats in the control group was biased toward the contralateral non-operated legs ($F_{ratio} < 1$) (**Figure**

7.11a), which was most severe immediately after surgery and was healed back to normal values ($F_{ratio} = 1$) at POD7. F_{ratio} has been found to be associated with pain level of the ipsilateral limb as compared to the contralateral limb, where lower F_{ratio} is correlated with higher pain of the ipsilateral limb [587-589]. $F_{ratio} = 1$ indicates indifferent pain level between the both hind limbs [587-589]. For the rats in the Bupi-PE group, the F_{ratio} was not significantly different from the F_{ratio} before surgery, suggesting that the rats could load their operated legs as well as their non-operated ones. On the other hand, the weight bearing of the rats in the control group was biased toward the contralateral non-operated leg, presumably because the operated leg was painful. This contrast was likely because of the analgesic effect of the eluted bupivacaine from Bupi-PE, which was the controlled difference between the two groups.

Similar to the load bearing capacity, the duty cycle of the control rats significantly diverged from the pre-operative value immediately after the surgery, with the operated leg (right) had significantly lower duty cycle than the unoperated (left) leg. This was in agreement with the previous study that showed duty cycle were decreased in the painful limb as compared to the contralateral limb [587, 591, 592]. The duty cycle of the operated left remained significantly lower than the unoperated leg until POD 3, after which the values started to converge back to the pre-operative values. Like the F_{ratio} of the Bupi-PE rats, the duty cycles of the Bupi-PE rats also did not significantly differ from the postoperative value, most likely because of the analgesic effect of the eluted bupivacaine from Bupi-PE.

Histological analysis of the bone tissues and synovium surrounding the Bupi-PE implants did not show any sign of inflammation and did not show any significantly different characteristics than those of control UHMWPE. Therefore, Bupi-PE did not incite any extra inflammation than clinically biocompatible UHMWPE, and therefore could be considered biocompatible.

Conclusion

In conclusion, we have created bupivacaine-eluting UHMWPE that had more sustained elution than Exparel and single intraarticular injection. The bupivacaine eluting UHMWPE was biocompatible and effective in preventing joint infection and in reducing post-surgical pain.

Epilogue

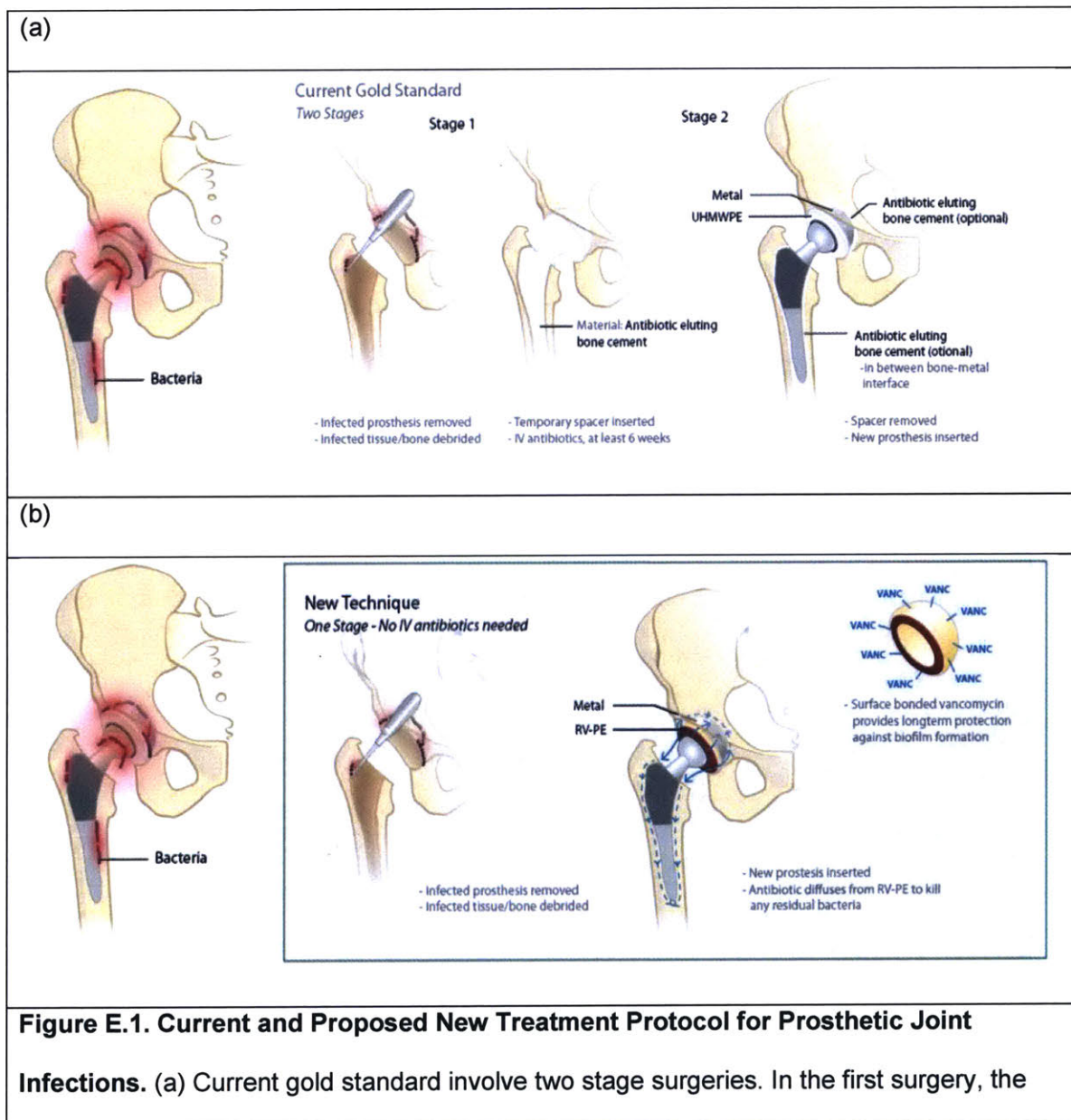
In summary, we found that increasing the eccentricity of drug clusters inside the polymeric matrix of UHMWPE increased the drug cluster interconnectivity, drug elution sustainability, and mechanical strength. The highly eccentric drug clusters achieved advantage in drug elution and mechanical strength than the conventional spherical drug clusters through two pathways: (1) Highly eccentric drug clusters allow better cluster interconnectivity, hence allowing more complete drug elution than spherical clusters. As a result, less total amount of drug is needed in the drug eluting polymer to match the elution from spherical clusters, thus it has higher mechanical strength than the polymer with spherical drug clusters. (2) Compared to the spherical drug clusters, highly eccentric drug clusters allow reduction of critical size defect that initiate crack that leads to the ultimate failure of the material.

We also found that after the drugs eluted out, the empty drug clusters formed on the surface of UHMWPE were able to entrain lubricants and extrude them out during load bearing, hence preventing asperity contacts and reduced wear compared to non-drug eluting UHMWPE.

We found that the optimized vancomycin-eluting UHMWPE (VPE) and rifampin-vancomycin eluting UHMWPE (RVPE) had higher mechanical strength and drug elution than antibiotic eluting bone cement. Furthermore, both the VPE's and RVPE's mechanical strength are within the clinically successful UHMWPE prosthetic joints, hence increasing the probability of VPE's and RVPE's success as long term implants. Because of VPE's and RVPE's capacity to fully load bear, fully articulating, and able to elute drugs sustainably, we believe that these materials are strong candidate for a new way to treat PJI.

Joint prosthesis made of VPE and RVPE will allow significant improvement in treatment protocol of prosthetic joint infection by replacing two-stage surgeries with single stage surgery without concern of incomplete bacteria eradication as with the current single stage surgery

(Figure E.1). Unlike in the current treatment protocol of two stage surgery where the patients need to be immobilized after the first stage (Figure E.1a) to prevent fracture of the spacer, the new treatment protocol incorporating drug eluting UHMWPE will allow direct mobilization right after the surgery while still ensuring more complete bacterial eradication than the current single stage surgery (Figure E.1b).



infected tissues are debrided, infected hardware is removed, and antibiotic-eluting bone cement spacer is implanted. To prevent fracture of the antibiotic eluting bone cement, the patient is immobilized for several weeks to months until second stage surgery is ready to be performed. In the second surgery, the spacer is removed, new hardware is implanted, and intravenous antibiotics are administered for at least 6 weeks. (b) The new treatment will involve infected tissue debridement, removal of the infected prosthesis, and implantation of the drug eluting prosthesis. Patients can be mobilized after surgery and no second surgery is needed.

Lastly, we found that the microtextures and pores left by bupivacaine eluting UHMWPE were able to provide orthogonal and complementary methods to chemical methods (such as crosslinking and polymer grafting) for wear reduction. Furthermore, we also observed that the porogen (e.g. bupivacaine) can be eluted sustainably and have a more favorable profile than the current clinically available method for controlled delivery of bupivacaine (e.g. Exparel®). Our in vivo experiments showed that bupivacaine eluting micro-textured and porous UHMWPE is safe and effective to prevent prosthetic joint infection and reduce pain post- joint surgery.

In conclusion, drug-eluting devices with effective, sustained delivery with the necessary mechanical strength for a fully load bearing and articulating joint implant are no longer elusive. The materials developed in this thesis (VPE, RVPE, and Bupi-PE) are promising candidates for further human clinical trial for treatment of acute PJI, chronic PJI, and infection prophylaxis + pain management, respectively.

References

1. Ayers DC, F.P., *Joint Replacement Registries in the United States: A New Paradigm*. Journal Bone Joint Surg Am, 2014. **96**(18): p. 1567-1569.
2. AOA, *2015 Annual Report on National Joint Replacement Registry*. 2015: p. Fig KT29.
3. Kurtz S, L.E., Watson H, Schmier, J, Parvizi, J. , *Economic burden of periprosthetic joint infection in the United States*. J Arthroplasty, 2012. **27**(8): p. 61-65.
4. Bernd Kubista, R.U.H., Christina M. Wood, Douglas R. Osmon, Arlen D. Hanssen, and David G. Lewallen, *Reinfection after two-stage revision for periprosthetic infection of total knee arthroplasty*. Int Orthop, 2012. **36**(1): p. 65-71.
5. Lentino, J., *Prosthetic joint infections: bane of orthopedists, challenge for infectious disease specialists*. Clin Infect Dis, 2003. **36**(9): p. 1157-1161.
6. Hiroyuki Segawa, D.T.T., Richard F. Kyle, Douglas A. Becker, Ramon B. Gustilo, *Infection After Total Knee Arthroplasty. A Retrospective Study of the Treatment of Eighty-One Infections*. J Bone Joint Surg Am, 1999. **81**(1): p. 1434-1445.
7. Meyer F, W.J., Best S, Cameron R, Rushton N, Brooks R, *Effects of lactic acid and glycolic acid on human osteoblasts: a way to understand PLGA involvement in PLGA/calcium phosphate composite failure*. J Orthop Res., 2012. **30**(6): p. 864-871.
8. Surdam JW, L.D., Baynes NT, Arce BR, *The use of exparel (liposomal bupivacaine) to manage postoperative pain in unilateral total knee arthroplasty patients*. J Arthroplasty, 2015. **30**(2): p. 325-329.
9. Jochen Jung, N.V.S., Jens Kelm , Eduard Schmitt , Konstantinos Anagnostakos, *Complications after spacer implantation in the treatment of hip joint infections*. International Journal of Medical Sciences, 2009. **6**(5): p. 265-273.
10. Kyekyoon Kim, D.W.P., *Microspheres for Drug Delivery, in BioMEMS and Bioemdicinal Nanotechnology*. 2006, Springer. p. 19-50.
11. Baena JC, W.J., Peng Z, *Wear Performance of UHMWPE and Reinforced UHMWPE Composites in Arthroplasty Applications: A Review*. Lubricants, 2015. **3**: p. 413-436.
12. Jared R H Foran, S.J.F. *Total Knee Replacement*. 2015 [cited 2017 03/11]; Available from: <http://orthoinfo.aaos.org/topic.cfm?topic=a00389>.
13. K. E. Barbour, C.G.H., M. Boring, X. Zhang, H. Lu, J. B. Holt, *Morb Mortal Wkly Rep*, 2013. **62**: p. 869.
14. J. M. Hootman, C.G.H., K. E. Barbour, K. A. Theis, M. A. Boring, *Arthritis & Rheumatology*, 2016. **68**: p. 1582.
15. McMaster, W.C., *Early Development of Total Hip Arthroplasty, in Modern Techniques in Total Hip Arthroplasty: From Primary to Complex*, R. Schwarzkopf, Editor. 2014, Jaypee Brothers Medical Publishers: New Delhi. p. 4.
16. Pablo F Gomez, J.A.M., *A Historical and Economic Perspective on Sir John Charnley, Chas F. Thackray Limited, and the Early Arthroplasty Industry*. Iowa Orthopedic Journal, 2005. **25**: p. 30-37.
17. Welch RB, C.J., *Low-Friction Arthroplasty of the hip in rheumatoid arthritis and ankylosing spondylitis*. Clin Orthop Relat Res, 1970. **7**(72): p. 22-32.

18. Charnley, J., *The Long Term Results of Low Friction Arthroplasty of the Hip Performed as a Primary Intervention*. J Bone Joing Surg Br, 1972. **54**: p. 61-76.
19. SM, K., *The clinical performance of historical and conventional UHMWPE in Hip Replacements*, in *UHMWPE Biomaterials Handbook*, K. SM, Editor. 2016, Elsevier: Waltham. p. 45-55.
20. Y. Liao, R.P., M. A. Wimmer, J. J. Jacobs, A. Fischer and L. D. Marks, *Graphitic Tirbological Layers in Metal-on-Metal Hip Replacements*. Science, 2011. **334**: p. 1687.
21. Skollnick MD, B.R., Peterson LF, Combs Jr JJ, Illstrup DM, *Polycentric total knee arthroplasty. A two-year follow-up study*. J Bone Joing Surg Am, 1976. **58**: p. 743-748.
22. Rand JA, C.M., *Ten-year evaluation of geometric total knee arthroplasty*. Clin Orthop, 1988: p. 168-173.
23. Ranawat CS, R.H., Bryan WJ, *Replacement of the patellofemoral joint with the total condylar knee arthroplasty*. Int Orthop, 1984. **8**: p. 61-65.
24. Collier JP, M.M., Surprenant VA, Surprenant HP, Dauphinais LA, Jensen RE *The Bbiomechanical problems of polyethylene as a bearing surface*. Clin Orthop, 1990. **261**: p. 107-113.
25. FF, B.J., *The LCS Story*, in *LCS mobile bearing knee arthroplasty: 25 years of worldwide experience*, S.J. Hamelynck KJ, Editor. 2002, Springer: Berlin.
26. John Charnley, Z.C., *The nine and ten year results of the low friction arthroplasty of the hip*. Clin ORthop Relat Res, 1973. **95**: p. 9-25.
27. Fehring TK, O.S., Griffin WL, mASon JB, Nadaud M, *Early failures in total knee arthroplasty*. Clin Orthop, 2001. **392**: p. 315-318.
28. Sharkey PF, H.W., Rothman RH, Shastri S, Jacoby SM, *Insall Award Paper: Why are total knee arthroplasties failing today ?* Clin Orthop, 2002. **404**: p. 7-13.
29. Kurtz S, P.J., *The Clinical Perfomrance of Highlt Cross-linked UHMWPE in Hip Replacements*, in *UHMWPE Biomaterials Handbook*, K. S, Editor. 2016, Elsevier: Waltham. p. 57-71.
30. Steven M. Kurtz, P., *The Clinical Performance of UHMWPE in Hip Replacements*, in *UHMWPE Biomaterials Handbook*, P. Steven M. Kurtz, Editor. 2009, Elsevier: Burlington. p. 43-44.
31. Malchau H, H.P., Soderman P, Oden A., *Prognosis of total hip replacement: update and validation of results from the Swedish National Hip Arthroplasty Registry, 1979-1998*, in *67th Annual Meeting of the American Academy of Orthopaedic Surgeons, Scientific Exhibition*. 2000.
32. Steven M. Kurtz, K.O., *Contemporary Total Hip Arthroplasty: Hard-on-Hard Bearings and Highly Crosslinked UHMWPE*, in *UHMWPE Biomaterials Handbook*, P. Steven M. Kurtz, Editor. 2009, Elsevier: Burlington. p. 55-74.
33. Gencur SJ, R.C., Kurtz SM, *Fatigue crack propagation resistance of virgin and highly crosslinked polyethylene, thermally treated ultra-high molecular weight polyethylene*. Biomaterials, 2006. **27**(8): p. 1550-1557.
34. PRT Kuzyk, M.S., S. Sprague, N. Simunovic, M. Bhandari, E.H. Schemitsch, *Cross-linked versus conventional polyethylene for total hip replacement. A meta-analysis of randomised controlled trials*. J Bone Joing Surg Br, 2011. **93-B**(5): p. 593-600.
35. Association, A.O., *2016 Annual Report on National Joint Replacement Registry*. 2016. p. 129-130.
36. Premnath V, H.W., Jasty M, Merrill EW. , *Gamma Sterilization of UHMWPE articular implants: an analysis of the oxidation problem*. Biomaterials, 1996. **17**(18): p. 1741-1753.
37. Muratoglu OK, W.K., Rowell SL, BR Micheli, Malchau H, *Ex vivo stability loss of irradiated and melted ultra-high molecular weight polyethylene*. J. Bone Joint Surg. Am, 2010. **92**: p. 2809-2816.
38. Oral E, G.B., Neils A, Muratoglu OK, *A new mechanism of oxidation in ultrahigh molecular weight polyethylene caused by squalene absorption*. J. Biomed. Mater. Res. B Appl. Biomater., 2012. **100**: p. 742-751.

39. Regis M, B.P., Giorgini L, Fusi S, Dalla Pria P, Costa L, Schmid C, *Correlation between in vivo stresses and oxidation of UHMWPE in total hip arthroplasty*. J. Mater. Sci., 2014. **25**: p. 2185-2192.
40. Bracco P, O.E., *Vitamin E-stabilized UHMWPE for total joint implants: a review*. Clin Orthop Relat Res, 2011. **469**(8): p. 2286-2293.
41. Steven M Kurtz, P.B., Luigi Costa, Ebru Oral, Orhun K. Muratoglu, *Vitamin E-Blended UHMWPE Biomaterials*, in *UHMWPE Biomaterials Handbook*, S.M. Kurtz, Editor. 2016, Elsevier: Burlington. p. 293-306.
42. Mats Salemyr, O.M., Torbjorn Ahl, Henrik Boden, Ghazi Chammout, Andre Stark, Olof Skoldenberg, *Vitamin-E Diffused High Cross-Linked Polyethylene Liner Compared to Standard Liners in Total Hip Arthroplasty. A Randomized, Controlled Trial*. International ORthopaedics, 2015. **39**(8): p. 1499-1505.
43. Ebru Oral, O.K.M., *Highly Cross-Linked UHMWPE Doped with Vitamin E*, in *UHMWPE Biomaterials Handbook*, S.M. Kurtz, Editor. 2016, Elsevier: Burlington. p. 307-325.
44. AOANJRR, *2016 Annual Report on National Joint Replacement Registry*. 2016: Australia. p. 137.
45. AOANJRR, *2016 Annual Report on National Joint Replacement Registry*. 2016. p. 229-231.
46. Singh JA, S.J., Schleck C, Harmsen W, Cofield RH, *Periprosthetic infections after shoulder hemiarthroplasty*. J. Shoulder Elbow Surg, 2012. **21**: p. 1304-1309.
47. van de Sande MA, B.R., Rozing PM, *Infections, complications, and results of shoulder arthroplasty*. Scand J Rheumatol, 2006. **35**: p. 426-434.
48. Voloshin I, S.D., Kakar S, Kaye EK, Morrey BF, *Complications of total elbow replacement: a systematic review*. J. Shoulder Elbow Surg, 2011. **20**: p. 158-168.
49. Achermann Y, V.M., Spormann C, Kolling C, Remschmidt C, Wust J, Simmen B, Trampuz A, *Characteristics and outcome of 27 elbow periprosthetic joint infections: results from a 14-year cohort study of 358 elbow prostheses*. Clin Microbiol Infect, 2011. **17**: p. 432-438.
50. Kurtz SM, L.E., Watson H, Schmier JK, Parvizi J, *Economic burden of periprosthetic joint infection in the United States*. J Arthroplasty, 2012. **27**: p. 61-65.e61.
51. Pulido L, G.E., Joshi A, Purtill JJ, Parvizi J, *Prosthetic Joint Infection: the incidence, timing, and predisposing factors*. Clin Orthop Relat Res, 2010. **466**: p. 1710-1715.
52. Kurtz SM, O.K., Lau E, Bozic KJ, Berry D, Parvizi J, *Prosthetic joint infection risk after TKA in the Medicare population*. Clin Orthop Relat Res, 2010. **468**: p. 52-56.
53. Toulson C, W.-S.S., Hur J, *Treatment of infected total hip arthroplasty with a 2-stage reimplantation protocol: update on "our institution's" experience from 1989 to 2003*. J Arthroplasty, 2009. **24**: p. 1051-1060.
54. Berend KR, L.A.J., Morris MJ, Bergeson AG, Adams JB, Sneller MA, *Two-Stage treatment of hip periprosthetic joint infection is associated with a high rate of infection control but high mortality*. Clin Orthop Relat Res, 2013. **471**(510-518).
55. Kapadia BH, M.M., Issa K, Johnson AJ, Bozic KJ, Mont MA, *The economic impact of periprosthetic infections following total knee arthroplasty at a specialized tertiary-care center*. J Arthroplasty, 2014. **24**(1051-1060).
56. Vanhegan IS, M.A., Jayakumar P, Ul Islam S, Haddad FS, *A financial analysis of revision hip arthroplasty: the economic burden in relation to the national tariff*. J Bone Joint Surg Br, 2012. **94**: p. 619-623.
57. Bhavén H Kapadia, R.A.B., Jacqueline A Daley, Jan Fritz, Anil Bhavé, Michael A Mont, *Periprosthetic Joint Infection*. The Lancet, 2016. **387**(23-29): p. 386-394.
58. Zimmerli W, L.P., Waldvogel PA, *Pathogenesis of foreign body infection. Evidence for a local granulocyte defect*. J Clin Invest, 1984. **73**: p. 1191-1200.

59. Puhto AP, P.T., Niinimäki TT, Leppilähti JI, Syrjäla HP, *Two-stage revision for prosthetic joint infection: outcome and role of reimplantation microbiology in 107 cases*. J Arthroplasty, 2014. **29**(1101-1104).
60. Zimmerli W, W.F., Vaudaux P, Nydegger UE, *Pathogenesis of foreign body infection: description and characteristics of an animal model*. J Infect Dis, 1982. **146**(487-497).
61. Kaplan SS, H.R., Simmons RL, *Defensins impair phagocytic killing by neutrophils in biomaterial-related infection*. Infect Immun, 1999. **67**(1640-1645).
62. Giulieri SG, G.P., Ochsner PE, Zimmerli W, *Management of infection associated with total hip arthroplasty according to a treatment algorithm*. Infection, 2004. **32**: p. 222-228.
63. Tande AJ, P.R., *Prosthetic joint infection*. Clin Microbiol Rev., 2014. **27**(2): p. 302-345.
64. Werner Zimmerli, A.T., Peter E. Ochsner, *Prosthetic-Joint Infections*. NEJM, 2004. **351**: p. 1645-1654.
65. Maderazo EG, J.S., Pasternak H, *Late infections of total joint prostheses: a review and recommendations for prevention*. Clin Orthop, 1988. **229**(131-142).
66. Uckay I, I.A., Emonet S, Tovmirzaeva L, Stern R, Ferry T, ASSal M, Bernard L, Lew D, Hoffmeyer P, *Low incidence of hematogenous seeding to total hip and knee prosthesis in patients with remote infections*. J Infect Dis, 2009. **59**: p. 337-345.
67. Murdoch DR, R.S., Fowler VG, Shah MA, Taylor SL, Morris AJ, Corey GR, *Infection of orthopaedic prosthesis after Staphylococcus aureus bacteremia*. Clin Infect Dis, 2001. **32**: p. 647-649.
68. Sendi P, B.F., Graber P, Zimmerli W, *Periprosthetic joint infection following Staphylococcus aureus bacteremia*. J Infect Dis, 2011. **63**: p. 17-22.
69. Dowsey MM, C.P., *Obese diabetic patients are at substantial risk for deep infection after primary TKA*. Clin Orthop Relat Res, 2009. **467**(1577-1581).
70. Mraovic B, S.D., Jacovides C, Parvizi J, *Perioperative hyperglycemia and postoperative infection after lower limb arthroplasty*. J Diabetes Sci Tech, 2011. **5**: p. 412-418.
71. SH, B., *Identification and preoperative optimization of risk factors to prevent periprosthetic joint infection*. World J Orthop, 2014. **5**(3): p. 362-267.
72. Singh JA, H.T., Ponce BA, Maddox G, Bishop MJ, Richman J, Campagna EJ, Henderson WG, Hawn MT, *Smoking as a risk factor for short-term outcomes following primary total hip and total knee replacement in veterans*. Arthritis Care Res (Hoboken). 2011. **63**: p. 1365-74.
73. Duchman KR, G.Y., Pugely AJ, Martin CT, Noiseux NO, Callaghan JJ, *The Effect of Smoking on Short-Term Complications Following Total Hip and Knee Arthroplasty*. J Bone Joint Surg Am., 2015. **97**(13): p. 1049-1058.
74. Duchman KR, G.Y., Miller BJ, *Prognostic factors for survival in patients with Ewing's sarcoma using the surveillance, epidemiology, and end results (SEER) program database*. Cancer Epidemiol., 2015. **39**(2): p. 189-195.
75. Schrama JC, E.B., Hallan G, Engesaeter LB, Furnes O, Havelin LI, Fevang BT, *Risk of revision for infection in primary total hip and knee arthroplasty in patients with rheumatoid arthritis compared with osteoarthritis: a prospective, population-based study on 108,786 hip and knee joint arthroplasties from the Norwegian Arthroplasty Register*. Arthritis Care Res (Hoboken). 2010. **62**(4): p. 473-479.
76. Hailer NP, G.G., Karrholm J, *Uncemented and cemented primary total hip arthroplasty in the Swedish Hip Arthroplasty Register*. Acta Orthop, 2010. **81**: p. 34-41.
77. Jr, M.J., *Wound healing with diabetes mellitus. Better glucose control for better wound healing in diabetes*. Surg Clin North Am, 1984: p. 769-78.
78. Seneviratne CJ, Y.J., Chang JW, Zhang CF, Samaranayake LP, *Effect of culture media and nutrients on biofilm growth kinetics of laboratory and clinical strains of Enterococcus faecalis*. Arch Oral Biol, 2013. **58**(10): p. 1327-34.

79. Yi PH, F.R., Vann E, et al, *Is potential malnutrition associated with septic failure and acute infection after revision total joint arthroplasty?* . Clin Orthop Relat Res, 2015. **473**: p. 175-182.
80. Devoto G, G.F., Marchello C, *Prealbumin serum concentrations as a useful tool in the assessment of malnutrition in hospitalized patients.* Clin Chem, 2006. **52**: p. 2281-2285.
81. Michael Brian Cross, P.H.Y., Charlotte F Thomas, Jane Garcia, Craig Della Valle, *Evaluation of Malnutrition in Orthopaedic Surgery.* Journal of the American Academy of Orthopaedic Surgeons, 2014. **22**(3): p. 193-199.
82. Greene KA, W.A., Stulberg BN, *Preoperative nutritional status of total joint patients. Relationship to postoperative wound complications.* J Arthroplasty, 1991. **6**: p. 321-325.
83. Bozic KJ, L.E., Kurtz S, Ong K, Berry DJ, *Patient-related risk factors for postoperative mortality and periprosthetic joint infection in medicare patients undergoing TKA.* Clin Orthop Relat Res, 2012. **470**(1): p. 130-137.
84. Malinzak RA, R.M., Berend ME, Meding JB, Olberding EM, Davis KE, *Morbidly obese, diabetic, younger, and unilateral joint arthroplasty patients have elevated total joint arthroplasty infection rates.* J Arthroplasty, 2009. **24**(6 Suppl): p. 84-88.
85. Jämsen E, N.P., Eskelinen A, Huotari K, Kalliovalkama J, Moilanen T, *Obesity, diabetes, and preoperative hyperglycemia as predictors of periprosthetic joint infection: a single-center analysis of 7181 primary hip and knee replacements for osteoarthritis.* J Bone Joint Surg Am, 2012. **94**(14): p. e101.
86. Aleeson Eka, A.F.C., *Patient-related medical risk factors for periprosthetic joint infection of the hip and knee.* Ann Transl Med, 2015. **3**(16): p. 233.
87. Bradley KA, R.A., Sun H, Bryson CL, Bishop MJ, Blough DK, Henderson WG, Maynard C, Hawn MT, Tønnesen H, Hughes G, Beste LA, Harris AH, Hawkins EJ, Houston TK, Kivlahan DR, *Alcohol screening and risk of postoperative complications in male VA patients undergoing major non-cardiac surgery.* J Gen Intern Med, 2011. **26**(2): p. 162-169.
88. Tønnesen H, N.P., Lauritzen JB, Møller AM, *Smoking and alcohol intervention before surgery: evidence for best practice.* Br J Anaesth., 2009. **102**(3): p. 297-306.
89. Bongartz T, H.C., Osmon DR, Reinalda MS, Bamlet WR, Crowson CS, Hanssen AD, Matteson EL, *Incidence and risk factors of prosthetic joint infection after total hip or knee replacement in patients with rheumatoid arthritis.* Arthritis Rheum, 2008. **59**: p. 1713-1720.
90. Peel TN, C.A., Buising KL, Choong PF, *Microbiological aetiology, epidemiology, and clinical profile of prosthetic joint infections: are current antibiotic prophylaxis guidelines effective?* . Antimicrob Agents Chemother, 2012. **56**: p. 2386-2391.
91. Mahmud T, L.M., Naudie DD, Macdonald SJ, McCalden RW, *Assessing the gold standard: a review of 253 two-stage revisions for infected KA.* Clin Orthop Relat Res, 2012. **470**: p. 2730-2736.
92. Piper KE, J.M., Cofield RH, Sperling JW, Sanchez-Sotelo K, Osmon DR, McDowell A, Patric S Steckelberg JM, Mandrekar JN, Fernandez Sampedro M, Patel R, *Microbiologic diagnosis of prosthetic shoulder infection by use of implant sonication.* J Clin Microbiol, 2009. **47**: p. 1878-1884.
93. Sperling JW, K.T., Hanssen AD, Cofield RH, *Infection after shoulder arthroplasty.* Clin Orthop Relat Res, 2001. **382**: p. 206-216.
94. Phillips JE, C.T., Noy M, Elliott TS, Grimer RJ, *The incidence of deep prosthetic infections in a specialist orthopaedic hospital: a 15-year prospective survey.* J Bone Joint Surg Br, 2006. **88**: p. 943-948.
95. Konigsberg BS, V.C., Ting NT, Qiu F, Sporer SM, *Acute hematogenous infection following total hip and knee arthroplasty.* J Arthroplasty, 2014. **29**(3): p. 469-472.
96. Lee J, K.C., Lee JH, Joung M, Moon S, Wi YM, Chung DR, Ha CW, Song JH, Peck KR, *Risk factors for treatment failure in patients with prosthetic joint infection.* J Hosp Infect, 2010. **75**: p. 273-276.

97. Rodriguez D, P.C., Euba G, Cobo J, Garcia-Lechuz J, Palomino J, Riera M, Del Toro MD, Granados A, Ariza X, *Acute hematogeneous prosthetic joint infection: prospective evaluation of medical and surgical management*. Clin Microbiol Infect, 2010. **16**: p. 1789-1795.
98. Chodos MD, J.C., *Hematogeneous infection of a total knee arthroplasty with Klebsiella pneumoniae in association with occult adenocarcinoma of the cecum*. J Arthroplasty, 2009. **24**: p. 158.e9-e13.
99. Mäkelä, K.T., et al., *Failure rate of cemented and uncemented total hip replacements: register study of combined Nordic database of four nations*. BMJ : British Medical Journal, 2014. **348**.
100. AJRR, *Third AJRR Annial Report on Hip and Knee Arthroplasty Data*. 2016.
101. Lass R, G.A., Kubista B, Hirschl A.M., Graninger W, Presterl E, Windhager R, Holinka J, *Bacterial adherence to different components of total hip prosthesis in patients with prosthetic joint infection*. International Orthopedics, 2014. **38(8)**: p. 1597-1602.
102. Holinka J, P.M., Hirschl AM, Graninger W, Windhager R, Presterl E, *Differential bacterial load on components of total knee prosthesis in patients with prosthetic joint infection*. Int J Artif Organs, 2012. **35**: p. 735-741.
103. Costerton JW, S.P., Greenberg EP, *Bacterial biofilms: a common cause of persistent infections*. Science, 1999. **284**: p. 1318-1322.
104. Ceri H, O.M., Stremick C, Read RR, Morck D, Buret A, *Tge Calgary Biofilm Device: new technology for rapid determination of antibiotic susceptibilities of bacterial biofilms*. J Clin Mibrobiol, 1999. **37**: p. 1771-1776.
105. Vuong C, G.C., Somerville GA, Fischer ER, Otto M, *Quorum-sensing control of biofilm factors in Staphylococcus epidermidis*. J Infect Dis, 2003. **188**: p. 706-718.
106. Anderl JN, Z.J., Roe F, Stewart PS, *Role of nutrient limitation and stationary-phase existence in Klebsiella pneumoniae biofilm resistance to ampicillin and ciprofloxacin*. Antimicrob Agents Chemother, 2003. **47**: p. 1251-1256.
107. Jose L. Del Pozo, R.P., *Infection Associated with Prosthetic Joints*. New England Journal of Medicine, 2009. **361**: p. 787-794.
108. del Pozo JL, P.R., *The challenge of treating biofilm-associated bacterial infections*. Clin. Pharmacol. Ther., 2007. **82**: p. 204-209.
109. Høiby N, B.T., Givskov M, Molin S, Ciofu O. , *Antibiotic resistance of bacterial biofilms*. Int J Antimicrob Agents, 2010. **35(4)**: p. 322-332.
110. Zimmerli W, W.A., Blatter M, *Role of Rifampin for Treatment of Orthopedic Implant-Related Staphylococcal Infections*. JAMA, 1998. **279(19)**: p. 1537-1541.
111. Tsaras G, O.D., Mabry T, Lahr B, St Sauveur J, Yawn B, Kurland R, Berbari EF, *Incidence, secualr trends, and outcomes of prosthetic joint infection: a popilation-based study, Olmsted county, Minnesota, 1969-2007*. Infect Control Hosp Epidemiol, 2012. **33**: p. 1207-1212.
112. Lora-Tamayo J, M.O., Iribarren JA, Soriano A, Sanchez-Somolinos M, Baraia-Etxaburu JM, Rico A, Palomino J, Rodriguez-Pardo D, Horcajada JP, Benito N, Bahamonde A, Granados A, del Toro, Cobo J, Riera M, Ramos A, Jover-Saenz A, Ariza J, *A large multicenter study of methicillin-susceptible and methicillin-resistant Staphylococcus aureus prosthetic joint infections managed with implant retention*. Clin Infect Dis, 2013. **56**: p. 182-194.
113. Sendi P, B.F., Graber P, Zimmerli W, *Clinical comparison between exogeneous and hematogeneous periprosthetic joint infections caused by Staphylococcus aureus*. Clin Microb Infect, 2011. **17**: p. 1098-1100.
114. Parvizi J, G.T., Chen AF, *Proceedings of the International Consensus on Periprosthetic Joint Infection*. Bone Joint J, 2013. **95**: p. 1450-1452.

115. Berbari E, M.T., Tsaras G, Spangehl M, Erwin PJ, Murad MH, Steckelberg J, Osmon D, *Inflammatory blood laboratory levels as markers of prosthetic joint infection: a systematic review and meta-analysis*. J Bone Joing Surg Am, 2010. **92**: p. 2102-2109.
116. Austin MS, G.E., Joshi A, Lindsay A, Parvizi J, *A simple, cost-effective screening protocol to rule out periprosthetic infection*. J Arthroplasty, 2008. **23**: p. 65-68.
117. Bottner F, W.A., Winkelman W, Becker K, Erren M, Gotze C, *Interleukin-6, procalcitonin and TNF-alpha: markers of periprosthetic infection following total joint replacement*. J Bone Joing Surg Br, 2007. **89**: p. 94-99.
118. Osmon DR, B.E., Berendt AR, Lew D, Zimmerli W, Steckelberg JM, Rao N, Hanssen A, Wilson WR, *Diagnosis and management of prosthetic joint infection: clinical practice guidelines by the Infectious Diseases Society of America*. Clin Infect Dis, 2013. **56**(1): p. e1-e25.
119. Ghanem E, P.J., Burnett RS, Sharkey PF, Keshavarzi N, Aggarwal A, Barrack RL, *Cell count and differential of aspirated fluid in the diagnosis of infection at the site of total knee arthroplasty*. J Bone Joing Surg Am, 2008. **90**: p. 1637-1643.
120. Trampuz A, H.A., Osmon DR, Mandrekar J, Steckelber JM, Patel R, *Synovial fluid leukocyte count and differential for the diagnosis of prosthetic knee infection*. Am J Med, 2004. **117**: p. 556-562.
121. Zmistowski B, R.C., Huang R, Hozack WJ, Parvizi J, *Periprosthetic joint ifnection diagnosis: a complete understading of white blood cell count and differential*. J Arthroplasty, 2012. **27**: p. 1869-1875.
122. Cipriano CA, B.N., Michael AM, Moric M, Sporer SM, Della Valle CJ, *Serum and synovial fluid analysis for diagnosing chronic periprosthetic joint infection after total hip or knee replacement in patients with rheumatoid arthritis*. Arthritis Rheum, 2012. **59**: p. 1713-1720.
123. Bedair H, T.N., Jacovides C, SAxena A, Moric M, Parvizi J, Della Valle CJ, *The Mark Coventry Award: diagnosis of early postopearative TKA infection using synovial fluid analysis*. Clin Orthop Relat Res, 2011. **469**: p. 34-40.
124. Schinsky MF, D.V.C., Sporer SM, Paprosky WG, *Perioperative joint infection diagnosis: a complete understanding of white blood cell count and differetial*. J Arthroplasty, 2008. **27**: p. 1589-1593.
125. Parvizi J, J.C., ANToci V, Ghanem E, *Diagnosis of periprosthetic joint infection: The utility of a simple yet unappreciated enzyme*. J Bone Joint Surg Am, 2011. **93**: p. 2242-2248.
126. Wetters NG, B.K., Lombardi AV, Morris MJ, Tucker TL, Della Valle CJ, *Leukocyte esterase reagent strips for the rapid diagnosis of periprosthetic joint infection*. J Arthroplasty, 2012. **27**: p. 8-11.
127. Tommaso Bonanzinga, A.Z., Michael Dutsch, Christian Lausmann, Daniel Kendoff, Thorsten Gehrke, *How Reliable is the alpha-defensin immunoassay test for diagnosing periprosthetic joint infection ? A prospective study*. Clin OrthopRelat Res, 2017. **475**(2): p. 408-415.
128. Ali F, W.J., Cooper JR, Kerry RM, Hamer AJ, Norman P, Stockley I, *Accuracy of joint aspiration for the preoperative diagnosis of infection i total hip arthroplasty*. J Arthroplasty, 2006. **21**: p. 221-226.
129. Font-Vizcarra L, G.S., Martinez-Pastor JC, Sierra JM, Soriano A, *Blood culture flasks for culturing synovial fluid in proshthetic joint ifnections*. Clin Orthop Relat Res, 2010. **468**: p. 2238-2243.
130. Roberts P, W.A., McMinn DJ, *Diagnosing infection i hip replacements. The use of fine-needle aspiration and radiometric culture*. J Bone Joing Surg Br, 1992. **74**: p. 265-269.
131. Marin M, G.-L.J., Alonso P, Villaneuva M, Alcal L, Gimeno M, Cercenado E, Sanchez-SOmolinos M, Radice C, Bouza E, *Role of universal 16srRNA gene PCR and sequencing in diagnosis of prosthetic joint infection*. J Clin Microbiol, 2012. **50**: p. 583-589.
132. Trampuz A, P.K., JAcobson MJ, Hanssen AD, Unni KK, Osmon DR, Mandrekar JN, Cockerill FR, Steckelberg JM, Greenleaf JF, Patel R *Sonication of removed hip and knee prostheses for diagnosis of infection*. N Engl J Med, 2007. **357**: p. 654-663.

133. Cazanave C, G.-Q.K., Hanssen AD, Karau MJ, Schmidt SM, Gomez Urena EO, Mandrekar JN, Osmon DR, Lough LE, Pritt BS, Steckelberg JM, Patel R, *Rapid molecular microbiologic diagnosis of prosthetic joint infection*. J Clin Microbiol, 2013. **51**: p. 2280-2287.
134. Vergidis P, G.-Q.K., Sanchez-Sotelo J, Morrey BF, Steinmann SP, Karau MJ, Osmon DR, Mandrekar JN, Steckelberg JM, Patel R, *Implant sonication for the diagnosis of prosthetic elbow infection*. J Shoulder Elbow Surg, 2011. **20**: p. 1275-1281.
135. Bori G, M.-M.E., Garcia S, Mallofre C, Gallart X, Bosch J, Garcia E, Riba J, Mensa J, Soriano A, *Interface membrane is the best sample for histological study to diagnose prosthetic joint infection*. Mod Pathol, 2011. **24**: p. 579-584.
136. Douglas R. Osmon, E.F.B., Anthony R. Berendt, Daniel Lew, Werner Zimmerli, James M. Steckelberg, Nalini Rao, Arlen Hanssen, and Walter R. Wilson *Diagnosis and Management of Prosthetic Joint Infection: Clinical Practice Guidelines by the Infectious Diseases Society of America*. Clin Infect Dis., 2012. **56(1)**: p. e1-e25.
137. Bode LG, K.J., Wetheim HF, *Preventing surgical-site infections in nasal carriers of Staphylococcus aureus*. N Engl J Med, 2010. **362**: p. 9-17.
138. Johnson AJ, K.B., Daley JA, Molina CB, Mont MA, *Chlorhexidine reduces infections in knee arthroplasty*. J Knee Surg, 2013. **26**: p. 213-218.
139. Kapadia BH, J.A., Daley JA, Issa K, Mont MA, *Pre-admission cutaneous chlorhexidine preparation reduces surgical site infections in total hip arthroplasty*. J. Arthroplasty, 2013. **28**: p. 490-493.
140. AlBuhairan B, H.D., Hutchinson A, *Antibiotic prophylaxis for wound infections in total joint arthroplasty: a systematic review*. J Bone Joint Surg Br, 2008. **90**: p. 915-919.
141. Harrop JS, S.J., Ooi YC, Radcliff KE, Vaccaro AR, Wu C, *Contributing factors to surgical site infections*. J Am Acad Orthop Surg, 2012. **20**: p. 94-101.
142. RP, E., *Current concepts for clean air and total joint arthroplasty: laminar airflow and ultraviolet radiation: a systematic review*. Clin Orthop Relat Res, 2011. **469**: p. 945-953.
143. Miner AL, L.E., Katz JN, Fossel AH, Platt R, *Deep infection after total knee replacement: impact of laminar airflow systems and body exhaust suits in the modern operating room*. Infect Control Hosp Epidemiol, 2007. **28**: p. 222-226.
144. Brown NM, C.C., Moric M, Sporer SM, Della Valle CJ, *Dilute betadine lavage before closure for the prevention of acute postoperative deep periprosthetic joint infection*. J Arthroplasty, 2012. **27**: p. 27-30.
145. Espehaug B, E.L., Vollset SE, et al, *Antibiotic prophylaxis in total hip arthroplasty. Review of 10,905 primary cemented total hip replacements reported to the Norwegian arthroplasty register, 1987 to 1995*. J Bone Joint Surg Br, 1997. **79**: p. 590-595.
146. Engesaeter LB, L.S., Espehaug B *Antibiotic prophylaxis in total hip arthroplasty: effects of antibiotic prophylaxis systemically and in bone cement on the revision rate of 22170 primary hip replacements followed 0-14 years in the Norwegian Arthroplasty Register*. Acta Orthop Scand, 2003. **74**: p. 644-651.
147. Bratzler DW, D.E., Olsen KM, American Society of Health-System Pharmacists, Infectious Disease Society of America, Surgical Infection Society, Society for Healthcare Epidemiology of America, *Clinical practice guidelines for antimicrobial prophylaxis in surgery*. Am J Health Syst Pharm, 2013. **70**: p. 195-283.
148. Hooper GJ, R.A., Frampton C, Wyatt MC, *Does the use of laminar flow and space suits reduce early deep infection after total hip and knee replacement?: the ten-year results of the New Zealand Joint Registry*. J Bone Joint Surg Br, 2011. **93**: p. 85-90.
149. Gastmeier P, B.A., Brandt C, *Influence of laminar airflow on prosthetic joint infections: a systematic review*. J Hosp Infect, 2012. **81**: p. 73-78.

150. Diaz-Ledezma C, H.C., Parvizi J, *Success after treatment of periprosthetic joint infection: a Delphi-based international multidisciplinary consensus*. Clin Orthop Relat Res, 2013. **471**: p. 2374-2382.
151. Koyonos L, Z.B., Della Valle CJ, Parvizi J, *Infection control rate of irrigation and debridement for periprosthetic joint infection*. Clin Orthop Relat Res, 2011. **469**: p. 3043-3048.
152. Byren O, B.P., Atkins BL, Angus B, Masters S, McLardy-Smith P, Gundle R, Berendt A, *One hundred and twelve infected arthroplasties treated with 'DAIR' (debridement, antibiotics and implant retention): antibiotic duration and outcome*. J Antimicrob Chemother, 2009. **63**: p. 1264-1271.
153. Marculescu CE, B.E., Hanssen AD, Steckelberg JM, Harmsen SW, Mandrekar JN, Osmon DR, *Outcome of prosthetic joint infections treated with debridement and retention of components*. Clin Infect Dis, 2006. **42**: p. 471-478.
154. Brandt CM, S.W., Duffy MC, Hanssen AD, Steckelberg JM, Ilstrup DM, Osmon DR, *Staphylococcus aureus prosthetic joint infection treated with debridement and prosthesis retention*. Clin Infect Dis, 1997. **24**: p. 914-919.
155. El Helou OC, B.E., Lahr BD, Eckel-Passow JE, Razonable RR, Sia IG, Virk A, Walker RC, Steckelberg JM, Wilson WR, Hanssen AD, Osmon DR, *Efficacy and safety of rifampin containing regimen for staphylococcal prosthetic joint infections treated with debridement and retention*. Eur J Clin Microbiol Infect Dis, 2010. **29**: p. 961-967.
156. Azzam KA, S.M., Ghanem E, Austin MS, Purtill JJ, Parvizi J, *Irrigation and debridement in the management of prosthetic joint infection: traditional indications revisited*. J Arthroplasty, 2010. **25**: p. 1022-1027.
157. Senneville E, J.D., Legout L, Valette M, Dezeque H, Beltrand E, Rosele B, d'Escrivan T, Loiez C, Caillaux M, Yazdanpanah Y, Maynou C, Migaud H, *Outcome and predictors of treatment failure in total hip/knee prosthetic joint infections due to Staphylococcus aureus prosthetic joint infections*. Clin Orthop Relat Res, 2011. **461**: p. 48-53.
158. Vlichez F, M.-P.J., Garcia-Ramiro S, Bori G, Macule F, Sierra J, Font L, Mensa J, Soriano A, *Outcome and predictors of treatment failure in early post-surgical prosthetic joint infections due to Staphylococcus aureus treated with debridement*. Clin Microbiol Infect, 2011. **17**: p. 439-444.
159. Leone S, B.S., Monforte A, Mordente G, Petrosillo N, Signore A, Venditti M, Viale P, Nicastrì E, Lauria FN, Carosi G, Moroni M, Ippolito G, GISIG Working Group on Prosthetic Joint Infections, *Consensus document on controversial issues in the diagnosis and treatment of prosthetic joint infections*. Int J Infect Dis, 2010. **14**(Suppl 4): p. S67-S77.
160. Silva M, T.R., Schmalzried TP, *Results of direct exchange or debridement of the infected total knee arthroplasty*. Clin Orthop Relat Res, 2002. **404**: p. 125-131.
161. Barberan J, A.L., Carroquino G, Gimenez MJ, Sanchez B, Martinez D, Prieto J, *Conservative treatment of staphylococcal prosthetic joint infections in elderly patients*. Am J Med, 2006. **119**: p. 993.e7-993.10.
162. Soriano A, G.S., Bori G, Almela M, Gallart X, Macule F, Sierra J, Martinez JA, Suso S, Mensa J, *Treatment of acute post-surgical infection of joint arthroplasty*. Clin Microbiol Infect, 2006. **12**: p. 930-933.
163. Bradbury T, F.T., Taunton M, Hanssen A, Azzam K, Parvizi J, Odum SM, *The fate of acute methicillin-resistant Staphylococcus aureus periprosthetic knee infections treated by open debridement and retention of components*. J Arthroplasty, 2009. **24**: p. 101-104.
164. Siddiqui MM, L.N., Ab Rahman S, Chin PL, Chia SL, Yeo SJ, *Two-year outcome of early deep MRSA infections after primary total knee arthroplasty: a joint registry review*. J Arthroplasty, 2013. **24**: p. 101-104.

165. Jaen N, M.-P.J., Munoz-Mahamud E, Garcia-RAmro S, Bosch J, Mensa J, Soriano A, *Long-term outcome of acute prosthetic joint infections due to gram-negative bacilli treated with retention of prosthesis*. Rev Esp Quimioter, 2012. **2**: p. 194-198.
166. Romano CI, M.G., Logoluso N, Romano D, *Value of debridement and irrigation for the treatment of peri-prosthetic infections. A systematic review*. Hip Int, 2012. **22**(Suppl 8): p. S19-S24.
167. Cobo J, M.L., Euba G, Rodriguez D, Garcia-Lechuz JM, Riera M, Falgueras L, Palomino J, Benito N, del Toro MD, Pigrau C, Ariza J, *Early prosthetic joint infection: outcomes with debridement and implant retention followed by antibiotic therapy*. Clin Microbiol Infect, 2011. **17**: p. 1632-1637.
168. Westberg M, G.B., Snorrason F, *Early prosthetic joint infections treated with debridement and implant retention" 38 primary hip arthroplasties prospectively recoded and followed for median 4 years*. Acta Orthop, 2012. **83**: p. 227-232.
169. Engesaeter LB, D.H., Schrama JC, Hallan G, Lie SA, *Surgical procedures in the treatment of 784 infected THA reported to the Norwegian Arthroplasty Register*. Acta Orthop, 2011. **82**: p. 530-537.
170. Odum SM, G.T., Lombardi AV, Zmistowski BM, Brown NM, Luna JT, Fehring KA, Hansen EN, *Irrigation and debridement for periprosthetic infections: does the organism matter ?* J Arthroplasty, 2011. **26**: p. 114-118.
171. Sukeik M, P.S., haddad FS, *Aggressive early debridement for treatment of acutely infected cemented total hip arthroplasty*. Clin Orthop Relat Res, 2012. **470**: p. 3164-3170.
172. Choong PF, D.M., Carr D, Daffy J, Stanley P, *Risk factors associated with acute hip prosthetic joint infections and outcome of treatment with a rifampin based regimen*. Acta Orthop, 2007. **78**: p. 755-765.
173. Mont MA, W.B., Banerjee C, Pacheco IH, Hungerford DS, *Multiple irrigation, debridement, and retention of components in infected total knee arthroplasty*. J Arthroplasty, 1997. **12**: p. 426-433.
174. Berdal JE, S.I., Mowinckel P, Gulbrandsen P, Bjornholt JV, *Use of rifampicin and ciprofloxacin combination therapy after surgical debridement in the treatment of early manifestation prosthetic joint infections*. Clin Microbiol Infect, 2005. **11**: p. 843-845.
175. Klouche S, L.P., Zeller V, Lhotellier L, Graff W, Leclerc P, Mamoudy P, Sariali E, *Infected total hip arthroplasty revision: one- or two-stage procedure ?* Orthop Traumatol Surg Res, 2012. **98**: p. 144-150.
176. Ure KJ, A.H., Nasser S, Schmalzried TP, *Direct-exchange arthroplasty for the treatment of infection after total hip replacement. An average ten-year follow-up*. J Bone Joint Surg Am, 1998. **80**: p. 961-968.
177. Buechel FF, F.F., D'Alessio J, *Primary exchange revision arthroplasty for infected total knee replacement: a long-term study*. Am J Orthop, 2004. **33**: p. 190-198.
178. Raut VV, S.P., Wroblewski BM, *One-stage revision of total hip arthroplasty for deep infection. Long term followup*. Clin Orthop Relat Res, 1995. **321**: p. 202-207.
179. Raut VV, O.M., ORth MC, Siney PD, Wroblewski BM, *One stage revision arthroplasty of the hip for deep Gram-negative infection*. Int Orthop, 1996. **20**: p. 12-14.
180. Raut VV, S.P., Wroblewski BM, *One-stage revision of ifnected total hip replacements with discharging sinuses*. J Bone Joint Surg Br, 1994. **76**: p. 721-724.
181. Rudelli S, U.D., Honda E, Lima AL, *One-stage revision of infected total hip arthroplasty with bone graft*. J Arthroplasty, 2008. **23**: p. 1165-1177.
182. Bucholz HW, E.R., Engelbrecht E, Lodenkamper H, Rottger J, Siegel A, *Management of deep infection of total hip replacement*. J Bone Joint Surg Br, 1981. **63**: p. 342-353.
183. Callaghan JJ, K.R., Johnston RC, *One-stage revision surgery of the infected hip. A minimum 10-year followup study*. Clin Orthop Relat Res, 1999. **369**: p. 139-143.

184. Hope PG, K.K., Norman P, Elson RA, *Deep infection of cemented total hip arthroplasties caused by coagulase-negative staphylococci*. J Bone Joint Surg Br, 1989. **71**: p. 851-855.
185. Lange J, T.A., Thomsen RW, Soballe K, *Chronic infections in hip arthroplasties: comparing risk of reinfection following one-stage and two-revision. A systematic review and meta-analysis*. Clin Epidemiol, 2012. **4**: p. 57-73.
186. Bejon P, B.A., Atkins BL, Green N, Parry H, Masters S, McLardy-Smith P, Gundle R, Byren I, *Two-stage revision for prosthetic joint infection: predictors of outcome and the role of reimplantation microbiology*. J Antimicrob Chemother, 2010. **65**: p. 569-575.
187. Biring GS, K.T., Garbuz DS, Masri BA, Duncan CP, *Two stage revision arthroplasty of the hip for infection using an interim articulated Prostalac hip spacer: a 10- to 15-year follow-up study*. J. Bone Joint Surg. Br, 2009. **91**: p. 1431-1437.
188. Stockley I, M.B., Hoad-Reddick A, Norman P, *The use of two-stage exchange arthroplasty with depot antibiotics in the absence of long-term antibiotic therapy in infected total hip replacement*. J Bone Joint Surg Br, 2008. **90**: p. 145-148.
189. Fleck EE, S.M., Rapuri VR, Beauchamp CP, *An articulating antibiotic spacer controls infection and improves pain and function in a degenerative septic hip*. Clin Orthop Relat Res, 2011. **469**: p. 3055-3064.
190. McKenna PB, O.S.K., Masterson EL, *Two-stage revision of infected hip arthroplasty using a shortened post-operative course of antibiotics*. Arch Orthop Trauma Surg, 2009. **129**: p. 489-494.
191. Kubista B, H.R., Wood CM, Osmon DR, Hanssen AD, Lewalen DG, *Reinfection after two-stage revision for periprosthetic infection of total knee arthroplasty*. Int Orthop, 2012. **36**: p. 65-71.
192. Silvestre A, A.F., Renovell P, Morante E, Lopez R, *Revision of infected total knee arthroplasty: two-stage reimplantation using an antibiotic-impregnated static spacer*. Clin Orthop Surg, 2013. **5**: p. 180-187.
193. Mortazavi SM, V.D., Ho A, Zmistowski B, Parvizi J, *Two-stage exchange arthroplasty for infected total knee arthroplasty: predictors of failure*. Clin Orthop Relat Res, 2011. **469**: p. 3049-3054.
194. Hanssen AD, R.J., Osmon DR, *Treatment of infected total knee arthroplasty with insertion of another prosthesis. The effect of antibiotic impregnated bone cement*. Clin Orthop Relat Res, 1994. **309**: p. 44-45.
195. Goldman RT, S.G., Insall JN, *2-stage reimplantation for infected total knee replacement*. Clin Orthop Relat Res, 1996. **428**: p. 35-39.
196. Haleem AA, B.D., Hanssen AD, *Mid-term to long-term followup of two-stage reimplantation for infected total knee arthroplasty*. Clin Orthop Relat Res, 2004. **428**: p. 35-39.
197. Tice AD, R.S., Dalovisio JR, Bradley JS, Martinelli LP, Graham DR, Gainer RB, Kunkel MJ, Yancey RW, Williams DN, *Practice guidelines for outpatient parenteral antimicrobial therapy. IDSA guidelines*. Clin Infect Dis, 2004. **38**: p. 1651-1672.
198. Alessandro Bistolfi, G.M., Enrica Verne, Alessandro Masse, Davide Deledda, Sara Feraris, Marta Miola, Fabrizio Galetto, Maurizio Crova, *Antibiotic-Loaded Cement in Orthopaedic Surgery: A Review*. ISRN Orthopedics, 2011. **2011: 290851**: p. 1-8.
199. L. Frommelt, K.K., *Properties of bone cement: antibiotic loaded cement*, in *The Well-Cemented Total Hip Arthroplasty, Part II*. 2006, Springer: Berlin, Germany. p. 86-92.
200. CP Scott, P.H., JH Dumbleton, *Effectiveness of bone cement containing tobramycin. An in vitro susceptibility study of 99 organisms found in infected joint arthroplasty*. J Bone Joint Surg Am, 1999. **81**(3): p. 440-443.
201. S Torrado, P.F., G Frutos, *Gentamicin bone cements: characterisation and release (in vitro and in vivo assays)*. Int. J. Pharmaceuticals, 2001. **217**(1-2): p. 57-69.
202. D Neut, H.v.d.B., JR van Horn, HC van der Mei, HJ Busscher, *The effect of mixing on gentamicin release from polymethylmethacrylate bone cements*. Acta Orthop Scand, 2003. **74**(6): p. 670-676.

203. D Cerretani, G.G., P Fornara et al, *The in vitro elution characteristics of vancomycin combined with imipenem-cilastatin in acrylic bone-cements: a pharmacokinetic study*. J Arthroplasty, 2002. **17**(5): p. 619-626.
204. Daniel Soares, P.L., Pedro Barreira, Ricardo Aido, Ricardo Sousa, *Antibiotic-loaded bone cement in total joint arthroplasty*. Acta Orthop Belg, 2015. **81**: p. 184-190.
205. Koo KH, Y.J., Cho SH et al, *Impregnation of vancomycin, gentamicin, and cefotaxime in a cement spacer for two-stage cementless reconstruction in infected total hip arthroplasty*. J Arthroplasty, 2001. **16**: p. 882-892.
206. Hinarejos P, G.P., Leal J, et al, *The use of erythromycin and colistin-loaded cement in total knee arthroplasty does not reduce the incidence of infection: a prospective randomized study in 3000 knees*. J Bone Joint Surg Am, 2013. **95**: p. 769-774.
207. Chang Y, C.W., Hsieh PH, et al, *In vitro activities of daptomycin, vancomycin, and teicoplanin loaded polymethylmethacrylate against methicillin-susceptible, methicillin resistant, and vancomycin-intermediate strains of Staphylococcus aureus*. Antimicrob Agents Chemother, 2011. **55**: p. 5480-5484.
208. Joseph TN, C.A., Di Cesare PE, *Use of antibiotic impregnated cement in total joint arthroplasty*. J Am Acad Orthop Surg, 2003. **11**: p. 38-47.
209. Hanssen AD, S.M., *Practical applications of antibiotic-loaded bone cement for treatment of infected total joint replacements*. Clin Orthop Relat Res, 2004. **427**: p. 79-85.
210. Samuel S, M.B., Veeraraghavan B, et al, *In vitro study of elution kinetics and bio-activity of meropenem-loaded acrylic bone cement*. J Orthop Traumatol, 2012. **13**: p. 131-136.
211. Park SJ, S.E., Seon JK et al, *Comparison of static and mobile antibiotic-impregnated cement spacers for the treatment of infected total knee arthroplasty*. Int Orthop, 2010. **34**: p. 1181-1186.
212. Portugal, E.M.D., *Deactivation of Palacos R Bone Cement with the Addition of Rifampin Antibiotic Powder. An In-Vivo Experience*. Reconstructive Review, 2011: p. 34-36.
213. E. Bertazzoni Minelli, A.B., B. Magnan, P. Bartolozzi, *Release of gentamicin and vancomycin from temporary human hip spacers in two-stage revision of infected arthroplasty*. J Antimicrob Chemother, 2004. **53**(2): p. 329-334.
214. J Gallo, M.K., AV Florschütz, R Novotny, R Pantucek, M Kesselova, *In vitro testing of gentamicin-vancomycin loaded bone cement to prevent prosthetic joint infection*. Biomedical papers of the Medical Faculty of the University Palacky, Olomouc, Czechoslovakia, 2005. **149**(1): p. 153-158.
215. MJ Penner, B.M., CP Duncan, *Elution characteristics of vancomycin and tobramycin combined in acrylic bone cement*. J Arthroplasty, 1996. **11**(8): p. 939-944.
216. A Gonzalez Della Valle, M.B., B Brause, C Harney, EA Salvati, *Effective bactericidal activity of tobramycin and vancomycin eluted from acrylic bone cement*. Acta Orthop Scandinavica, 2001. **72**(3): p. 237-240.
217. G Lewis, S.J., *Estimation of the optimum loading of an antibiotic powder in an acrylic bone cement: gentamicin sulfate in Smart Set HV*. Acta Orthopaedica, 2006. **77**(4): p. 622-627.
218. DJF Moojen, B.H., H Charles Vogely, AJ Verbout, RM Castelein, WJA Dhert, *In vitro release of antibiotics from commercial PMMA beads and articulating hip spacers*. J Arthroplasty, 2008. **23**(8): p. 1152-1156.
219. JGE Hendriks, J.v.H., HC van der Mei, H J Busscher, *Background of antibiotic-loaded bone cement and prosthetic-related infection*. Biomaterials, 2004. **25**(3): p. 546-556.
220. H van de Belt, D.N., W Schenk, JR van Horn, HC van der Mei, HJ Busscher, *Infection of orthopedic implants and the use of antibiotic-loaded bone cements: a review*. Acta Orthopaedica Scandinavica, 2001. **72**(6): p. 557-571.
221. WA Jiranek, A.H., AS Greenwald, *Antibiotic-loaded bone cement for infection prophylaxis in total joint replacement*. J Bone Joint Surg, Series A, 2006. **88**(11): p. 2487-2500.

222. KL Garvin, B.E., EA Salvati, BD Brause, *Palacos gentamicin for the treatment of deep periprosthetic hip infections*. Clin Orthop Relat Res, 1994. **298**: p. 97-105.
223. Emerson RH, J., Muncie M, Tarbox TR, Higgins LL, *Comparison of a static with a mobile spacer in total knee infection*. Clin Orthop Relat Res, 2002. **404**: p. 132-138.
224. Freeman MG, F.T., Odum SM, Fehring K, Griffin WL, Mason JB, *Functional advantage of articulating versus static spacers in 2-stage revision fo total knee arthroplasty infection*. J Arthroplasty, 2007. **22**: p. 1116-1121.
225. Masri BA, D.C., Beauchamp CP, *Long-term elution of antibiotics from bone-cement: an in vivo study using the prosthesis of antibiotic-laoded acrylic cement (PROSTALAC) system*. J Arthroplasty, 1998. **13**: p. 331-338.
226. Sterling GJ, C.S., Potter JHm Koerbin G, Crawford R, *The pharmacokinetics of Simplex-tobramycin bone cement*. J Bone Joing Surg Br, 2003. **85**: p. 646-649.
227. Cui Q, M.W., Shields JS, Rles M, Saleh KJ, *Antibiotic-impregnated cement spacers for the treatment of infection associated with total hip or knee arthroplasty*. J Bone Joint Surg Am, 2007. **89**: p. 871-882.
228. Cabo J, E.G., Saborido A, Gonzalez-Panisello M, Dominguez MA, Agullo JL, Murillo O, Verdaguer R, Ariza J, *Clinical outocme and microbiological findings using antibiotic-loaded spacers intwo-stage revision prosthetic joint infections*. J Infect Dis, 2011. **63**: p. 23-31.
229. Choi HR, F.A., Malchau H, Rubash HE, Kwon YM, *The fate of unplanned retention of prosthetic articulating spacers for infected total hip and total knee arthroplasty*. J Arthroplasty, 2014. **29**(4): p. 690-693.
230. D Neut, H.v.d.B., I Stokroos, JR van Hor, HC van der Mei, HJ Busscher, *Biomaterial-associated infection of gentamicin-loaded PMMA beads in orthopaedic revision surgery*. J Antimicrob Chemother, 2001. **47**(6): p. 885-891.
231. K. Anagnostakos, P.H., D. Pape, D. Kohn, J. Kelm, *Persistence of bacterial growth on antibiotic-loaded beads: is it actually a problem ?* Acta Orthopaedica, 2008. **79**(2): p. 302-307.
232. JGE Hendriks, D.N., J R van Horn, HC van der Mei, HJ Busscher, *Bacteria survival in the interfacial gap in gentamicin-loadded acrylic bone cements*. J Bone Joing Surg Am, 2005. **87**(2): p. 272-276.
233. Kurtz, S.M., *A Primer on UHMWPE*, in *UHMWPE Biomaterials Handbook*, S.M. Kurtz, Editor. 2009, Elsevier: Burlington, MA. p. 1-10.
234. O. K. Muratoglu, C.R.B., D. O. O'Connor et al, *Unified wear model for highly crosslinked ultra-high molecular weight polyethylenes (UHMWPE)*. Biomaterials, 1999. **20**(16): p. 1463-1470.
235. Meenakshi Goyal, N.G., Harleen Kaur, Ashmeet Gera, Kriti Minocha, Prashant Jindal, *Fabrication and characterisation of low density polyethylene (LDPE)/multi walled carbon nanotubes (MWCNTs) nano-composites*. Perspectives in Science, 2016. **8**: p. 403-405.
236. Ebru Oral, B.N.D., Rizwan M Gul, Andrew L Neils, Sanem Kayandan, Orhun K Muratoglu, *Peroxide Cross-Linked UHMWPE Blended with Vitamin E*. J Biomed Mater Res B Appl Biomater, 2016. **00B**: p. 1-11.
237. Jose Antonio Puertolas, S.K., *UHMWPE Matrix Composites*, in *UHMWPE Biomaterials Handbook*, S.M. Kurtz, Editor. 2016, Elsevier: Burlington. p. 369-397.
238. Aleksey Maksimkin, S.K., VV Tcherdyntsev, DI Chukov, AA Stepashkin, *Technologies for Manufacturing Ultrahigh Molecular Weight Polyethylene-Based Porous Structure for Bone Implants*. Biomedical Engineering, 2013. **47**: p. 73-77.
239. Kevin Plumlee, C.J.S., *Development of Porous UHMWPE Morphologies for Fixation of Gel-Based Materials*. Journal of Applied Polymer Science, 2009. **114**(4): p. 2555-2564.
240. Lahiri D, H.F., Thiesse M, Durygin A, Zhang C, Agarwal A, *Nanotribological behaviour of graphene nanoplatelet reinforced ultra high molecular weight polyethylene composites*. Tribol Int, 2014. **70**: p. 165-169.

241. Galetz MC, B.T., Ruckdaschel H, Sandler JKW, Alstadt V, Glatzel U, *Carbon nanofibre-reinforced ultrahigh molecular weight polyethylene for tribological applicaitons*. J Appl Polymer Sci, 2007. **104**: p. 4173-4181.
242. Sui G, Z.W., Ren X, Wang XQ, Yang XP, *Structure, mechanical properties and friction behaviour of UHMWPE/HDPE/carbon nanofibers*. Mater Chem Phys, 2009. **115**: p. 404-412.
243. L Fang, Y.L., P Gao, *Processing of hydroxyapatite reinforced ultrahigh molecular weight polyethylene for biomedical applications*. Biomaterials, 2005. **26**: p. 3471-3478.
244. Ebru Oral, A.M., Orhun Muratoglu, *Vitamin E does not detrimentally affect properties of UHMWPE at high concentrations*. Transactions Fifty-Second Annual Meeting of the Orthopaedic Research Society, Sand Diego, CA, 2007.
245. G. Strobl, W.H., *Raman spectroscopic method for determiing the crystallinity of polyethylene*. J Polym Sci Polym Phys, 1978. **16**: p. 1181-1193.
246. MC Sobieraj, C.R., *Ultra High Molecular Weight Polyethylene: Mechanics, Morphology, and Clinical Behaviour*. J Mech Behav Biomed Mater, 2009. **2**(5): p. 433-443.
247. Surojit Gupta, M.R., Yun Ji, *Synthesis and Tribological Behaviour of Ultra High Molecular Weight Polyethylene (UHMWPE)-Lignin Composites*. Lubricants, 2016. **4**(3): p. 31.
248. Juan C Baena, J.W., Zhongxiao Peng, *Wear performance of UHMWPE and Reinforced UHMWPE Composites in Arthroplasty Applications: A Review*. Lubricants, 2015. **3**: p. 413-436.
249. P Marsac, S.S., I Taylor, *Theoretical and practical approaches for prediction of drug-polymer miscibility and solubility*. Pharm Res, 2006. **23**: p. 2417-2426.
250. Peter A. George, K.Q., Justin J. Cooper-White, *Hierarchical scaffolds via combined macro- and micro-phase separation*. Biomaterials, 2010. **31**: p. 641-647.
251. Bates FS, F.G., *Block copolymer thermodynamics - theory and experiment*. Annual Review of Physical Chemistry, 1990. **41**: p. 525-557.
252. Yiwei Tian, J.B., Elizabeth Meehan, David S. Jones, Shu Li, Gavin P. Andrews, *Construction of Drug-Polymer Thermodynamic Phase Diagrams Using Flory-Huggins Interaction Theory: Identifying the Relevance of Temperature and Drug Weight Fraction to Phase Separation within Solid Dispersions*. Molecular Pharmaceutics, 2013. **20**: p. 236-248.
253. M Rubinstein, R.C., *Polymer Physics*. 2003, New York: Oxford Univeristy Press Inc.
254. Burke, J., *Solubility parameters: theory and application*. Vol. 3. 1984: BCIN.
255. Teja Kitak, A.D., Odon Planisek, Rok Sibanc, Stanko Srcic, *Determination of Solubility Parameters of Ibuprofen and Ibuprofen Lysinate*. Molecules, 2015. **20**: p. 21549-21568.
256. Stern, S.A., *Polymer for gas separations: the next decade*. J Membr Sci, 1994. **94**: p. 1-65.
257. R J Pace, A.D., *Statistical mechanical model for diffusion of simple penetrants in polymers*. J Polym Sci Polym Phys Ed, 1979. **17**: p. 437-451.
258. J S Vrentas, J.L.D., *Diffusion of small molecules in amorphous polymers*. Macromolecules, 1976. **9**: p. 785-790.
259. M R Tant, G.L.W., *An overview of the nonequilibrium behaviour of polymer glasses*. Polym Eng Sci, 1981. **21**(874-895).
260. R E Kesting, A.K.F., *Polymeric gas separation membranses*. 1993, New York: John Wiley & Sons, Inc.
261. Philip L Ritger, N.A.P., *A Simple Equation for Description of Solute Release II. Fickian and Anomalous Release From Swellable Devices*. Journal of Controlled Release, 1987. **5**: p. 37-42.
262. Langer, R., *Polymeric delivery system for controlled drug release*. Chem. Eng. Commun, 1980. **6**: p. 1-48.
263. Richard W. Korsmeyer, R.G., Eric Doelker, Pierre Burri, Nikolaos A Peppas, *Mechanisms of solute release from porous hydrophilic polymers*. International Journal of Pharmaceutics, 1983. **15**: p. 25-35.

264. Byron Bird, W.W.S., Edwin N. Lightfoot, in *Transport Phenomena*. 2006, Wiley: New York. p. 582-590.
265. R Gurny, E.D., NA Peppas, *Modelling of sustained release of water soluble drugs from porous, hydrophobic polymers*. *Biomaterials*, 1982. **3**: p. 27-32.
266. Peppas, P.L.R.N.A., *A Simple Equation For Description of Solute Release I. Fickian and Non-Fickian Release From Non-Swellable Devices in Form of Slabs, Spheres, Cylinders, or Discs*. *Journal of Controlled Release*, 1987. **5**: p. 23-36.
267. Higuchi, T., *Rate of release of medicaments from ointment bases containing drugs in suspensions*. *J. Pharm. Sci.*, 1961. **50**: p. 874-875.
268. J Siepman, N.P., *Modeling of drug release from delivery systems based on hydroxypropyl methylcellulose (HPMC)*. *Advanced Drug Delivery Reviews*, 2001. **48**: p. 139-157.
269. Broadbent SR, H.J., *Percolation processes: I. Crystals and Mazes*. *Mathematical Proceedings of the Cambridge Philosophical Society*, 1957. **53**(3): p. 629-641.
270. YB, Y., *Void Percolation and conduction of overlapping ellipsoids*. *Physical Review E*, 2006. **74**(031112): p. 1-14.
271. YB, Y.a.A.S., *Analytical Approximation of the Percolation Threshold for Overlapping Ellipsoids of Revolution* *Proc. R. Soc. Lond. A*, 2004. **460**: p. 2353-2380.
272. Sastry, A.M., Cheng, X. & Wang, C. W. , *Mechanics of stochastic fibrous networks*. *J. Thermoplast. Compos. Mater.*, 1998. **11**: p. 288-296.
273. Balberg, I.B., N., *Computer study of the percolation threshold in a twodimensional anisotropic system of conducting sticks*. *Phys. Rev. B*, 1983. **28**: p. 3799-3812.
274. Balberg, I.B., N., *Percolation thresholds in the three-dimensional stick system*. *Phys. Rev. Lett.*, 1984. **52**: p. 1465-1468.
275. Metzner, A., *Rheology of Suspensions in Polymeric Liquids*. *J. Rheol*, 1985(739).
276. T. Kitano, T.K., and T. Shirota, *An empirical equation of the relative viscosity of polymer melts filled with various inorganic fillers*. *Rheol. Acta.*, 1981. **20**: p. 207.
277. EJ Garboczi, K.S., JF Douglas, MF Thorpe, *Geometrical Percolation Threshold of Overlapping Ellipsoids*. *Physical Review E*, 1995. **52**(1): p. 819-828.
278. Baker, D.R.G.P.S.S.H.E.S., *Continuum percolation threshold for interpenetrating squares and cubes*. *Physical Review E*, 2002. **66**(4): p. 046136 [5 pages].
279. Hyytiä, E.J.V., P. Lassila and J. Ott *Continuum Percolation Threshold for Permeable Aligned Cylinders and Opportunistic Networking*. *IEEE Communications Letters*, 2012. **16**(7): p. 1064-1067.
280. Y. Pan, G.J.W., , S. A. Meguid, W. S. Bao, Z.-H. Zhu, and A. M. S. Hamouda, *Percolation threshold and electrical conductivity of a two-phase composite containing randomly oriented ellipsoidal inclusions*. *J. Appl. Phys.*, 2011. **110**: p. 123715.
281. Z. Ounaies, C.P., K.E. Wiseb, E.J. Siochi , J.S. Harrison, *Electrical Properties of Single Wall Carbon Nanotube Reinforced Polyimide Composites*. *Composites Science and Technology*, 2003. **63**: p. 1637-1646.
282. Sasha Stankovich, D.A.D., Geoffrey H. B. Dommett, Kevin M. Kohlhaas, Eric J. Zimney, Eric A. Stach, Richard D. Piner, SonBinh T. Nguyen and Rodney S. Ruoff, *Graphene-based composite materials*. *Nature*, 2006. **442**: p. 282-286.
283. Tajarobi F, A.-A.S., Hansen M, Larsson A., *The impact of dose and solubility of additives on the release from HPMC matrix tablets--identifying critical conditions*. *Pharm Res*, 2009. **26**(6): p. 1496-1503.
284. Qing-hai Guoa, S.-r.G., Zhong-min Wang, *Estimation of 5-fluorouracil-loaded ethylene-vinyl acetate stent coating based on percolation thresholds*. *International Journal of Pharmaceutics*, 2007. **333**(1-2): p. 95-102.

285. Kevin Plumlee, C.J.S., *Development of Porous UHMWPE Morphologies for Fixation of Gel-Based Materials*. Journal of Applied Polymer Science, 2009. **114**(4): p. 2555-2563.
286. Shin, M.S.H., J.Y.; Park, S. , *Gemcitabine release behavior of polyurethane matrixes designed for local anti-cancer drug delivery via stent*. J. Drug Deliv., 2012. **22**: p. 301-306.
287. Charlotte L Huang, T.W.S., Effendi Widjaja, Freddy YC Boey, Subbu S Venkatraman and Joachim SC Loo, *The influence of additives in modulating drug delivery and degradation of PLGA thin films*. NPG Asia Materials, 2013. **5**: p. e54.
288. Jaishri Sharma, M.L., Mark Stewart, Kyle Zygula, Yang Lu , Rajat Chauhan, Xingru Yan, Zhanhu Guo, Evan K. Wujcik, and Suying Wei, *Multifunctional Nanofibers towards Active Biomedical Therapeutics*. Polymers, 2015. **7**(2): p. 186-219.
289. Mayura Oak , R.M., Sushant Lakkadwala, Lindsey Lipp and Jagdish Singh *Effect of Molar Mass and Water Solubility of Incorporated Molecules on the Degradation Profile of the Triblock Copolymer Delivery System*. Polymers, 2015. **7**(8): p. 1510-1521.
290. SHIH-JUNG LIU, F.-J.C., CHAO-YING HSIAO, YI-CHUAN KAU, and KUO-SHENG LIU, *Fabrication of Balloon-Expandable Self-Lock Drug-Eluting Polycaprolactone Stents Using Micro-Injection Molding and Spray Coating Techniques*. Annals of Biomedical Engineering, 2010. **38**(10): p. 3185-3194.
291. Hermawan Nagar Rasyid, H.C.v.d.M., Henderik Frijilink, Danielle Neut, *Concepts for increasing gentamicin release from handmade bone cement beads*. Acta Orthop, 2009. **80**(5): p. 508-513.
292. J.W. Powles, R.F.S., and A.M. Lovering, *Gentamicin release from old cement during revision hip arthroplasty*. Journal of Bone and Joint Surgery, 1998. **Series B, vol. 80**(4): p. 607-610.
293. Xu Tongwen, H.B., *Mechanism of sustained drug release in diffusion-controlled polymer matrix-application of percolation theory*. Int. J. Pharmaceutics, 1998. **170**: p. 139-149.
294. Javier Martinez-Moreno, C.M., Virginia Merino, Amparo Nacher, Monica Climente, Matilde Merino-Sanjuan, *Study of the Influence of Bone Cement Type and Mixing Method on the Bioactivity and the Elution Kinetics of Ciprofloxacin*. Journal of Arthroplasty, 2015. **30**(7): p. 1243-1249.
295. Jun-Bing Fan, C.H., Lei Jiang, Shutao Wang, *Nanoporous microspheres: from controllable synthesis to healthcare applications*. J. Materials Chemistry B, 2013. **1**: p. 2222-2235.
296. Mrinal Musbi, j.J., Karunesh Chakote, Westley Hayes, Subrata Saha, *Microhardness of bi-antibiotic-eluting bone cement scaffolds*. Progress in Biomaterials, 2012. **1**: p. 3.
297. Tanay J. Amin, M.J.W.L., MS; Kelly J. Hendricks, MD; and Terence E. Mciff, PhD, *Increasing the Elution of Vancomycin from High-Dose Antibiotic-Loaded Bone Cement: A Novel Preparation Technique*. J Bone Joint Surg Am, 2012. **94**(21): p. 1946-1951.
298. Zongping Xie, X.C., Cunju Zhao, Wenhui Huang, Jianqiang Wang and Changqing Zhang, *Gentamicin-Loaded Borate Bioactive Glass Eradicates Osteomyelitis Due to Escherichia coli in a Rabbit Model*. Antimicrobial Agents and Chemotherapy, 2013. **57**: p. 3293-3298.
299. Matthew H. Pelletier, L.M., Peter J. Smitham, Koji Okamoto, and William R. Walsh, *The Compressive Properties of Bone Cements Containing Large Doses of Antibiotics*. Journal of Arthroplasty, 2009. **23**(3): p. 454-458.
300. Gregson, J.P.W.R.E.W.R.S.J.a.P.A., *Is prolonged systemic antibiotic treatment essential in two-stage revision hip replacement for chronic Gram-positive infection?* J Bone Joint Surg Br, 2009. **91-B**: p. 44-51.
301. Adriana Fulias, G.V., Titus Vlase, Codruta Soica, Alina Heghes, Marius Craina, Alina heghes, Ionut Ledeti, *Comparative kinetic analysis on thermal degradation of some cephalosporins using TG and DSC data*. Chem Cent J, 2013. **7**: p. 70.

302. Tingyue Gu, L.Z., *Partition Coefficients of Some Antibiotics, Peptides and Amino Acids in Liquid-Liquid Partitioning of the Acetonitrile-Water System at Subzero Temperatures*. Chem Eng Comm, 2007. **194**: p. 838-834.
303. Michele M. Schantz, D.E.M., *Determination of Hydrocarbon-Water Partition Coefficients from Chromatographic Data and Based on Solution Thermodynamics and Theory*. Journal of Chromatography, 1987. **391**: p. 35-51.
304. DM Koehnen, C.S., *The Determination of Solubility Parameters of Solvents and Polymers by Means of Correlations with Other Physical Quantities*. Journal of Applied Polymer Science, 1975. **19**: p. 1163-1179.
305. !!! INVALID CITATION !!!
306. Alexander N. Zelikin, C.E., Anne Marie Healy, *Materials and Methods for delivery of biological drugs*. Nature Chemistry, 2016. **8**: p. 997-1007.
307. Peter Ertl, B.R., and Paul Selzer, *Fast Calculation of Molecular Polar Surface Area as a Sum of Fragment-Based Contributions and Its Application to the Prediction of Drug Transport Properties*. J. Med. Chem., 2000. **43**(20): p. 3714-3717.
308. Garry Laverty, M.Y.A., and Brendan F. Gilmore, *The In Vitro Susceptibility of Biofilm Forming Medical Device Related Pathogens to Conventional Antibiotics*. Dataset Papers in Science, 2014. **2014**: p. 1-10.
309. Xijin Hua, L.W., Mazen Al-Hajjar, Zhongmin Jin, Ruth K Wilcox and John Fisher, *Experimental validation of finite element modelling of a modular metal-on-polyethylene total hip replacement*. Proc J Mech E Part H: J Engineering in Medicine, 2014. **228**(7): p. 682-692.
310. Steven M. Kurtz, W.H., R Ray, A Edidin. *Biomechanical analysis of cementing an acetabular liner in a metal shell for revision total hip arthroplasty*. in *47th Annual Meeting, Orthopaedic Research Society*. 2001. San Fransisco, California.
311. Gordon R. Plank, D.M.E.I., Orhun K. Muratoglu, Daniel O. O'Connor, Brian R. Burroughs, and W.H. Harris, *Contact Stress Assessment of Conventional and Highly Crosslinked Ultra High Molecular Weight Polyethylene Acetabular Liners with Finite Element Analysis and Pressure Sensitive Film*. Journal of Biomedical Materials Research Part B: Applied Biomaterials, 2007. **80**(1): p. 1-10.
312. Gauthier C, L.S.a.S.R., *Elastic recovery of a scratch in a polymeric surface: experiments and analysis*. Tribol Int, 2001. **34**: p. 469-479.
313. R., G.C.a.S., *Time and temperature dependence of the scratch properties of poly(methylmethacrylate) surfaces*. J Mater Sci, 2000. **35**: p. 2121-2130.
314. Bartel DL, B.A., Toda MD, Edwards DL, *The effect of conformity and plastic thickness on contact stresses in metalbacked plastic implants*. J Biomech Eng, 1985. **107**: p. 193-199.
315. Gordon R. Plank, D.M.E.I., Orhun K. Muratoglu, Daniel O. O'Connor, Brian R. Burroughs, William H. Harris, *Contact Stress Assessment of COnventional and Highly Crosslinked Ultra High Molecular WEight Polyethylene Acetabular Liners with Finite Element Analysis and Pressure Sensitive Film*. J Biomed MAter Res Part B: Appl Biomater, 2007. **80B**: p. 1-10.
316. S. Petrović Savić, D.A., G. Devedžić, B. Ristić, A. Matic, *Contact Stress Generation on the UHMWPE Tibial Insert*. Tribology in Industry, 2014. **36**(4): p. 354-360.
317. D.J. van den Heever, C.S., P. Erasmus, E. Dillon, *Contact stresses in patient – specific unicompartmental knee replacement*. Clinical Biomechanics, 2011. **26**(2): p. 159-166.
318. T. Villa, F.M., D. Gastaldi, M. Colombo, and R. Pietrabissa., *Contact stresses and fatigue life in a knee prosthesis: comparison between in vitro measurements and computational simulation*. Journal of Biomechanics, 2004. **18**: p. 45-53.
319. Hiromasa Ishikawa, H.F., *Contact Mechanics in the Artificial Knee Joint*, in *Computational Biomechanics*. 1996, Springer. p. 43-66.

320. Jian Q Yao, C.R.B., Xin Lu, Michel P Laurent, Todd S Johnson, Leslie N. Gilbertson, Dale F. Swarts, and Roy D Crowninshield, *Improved Resistance to Wear, Delamination and Posterior Loading Fatigue Damage of Electron Beam Irradiated, Melt-Annealed, Highly Crosslinked UHMWPE Knee Inserts*, in *Crosslinked and Thermally Treated Ultra-high Molecular Weight Polyethylene for Joint Replacements*, R.G. S.M. Kurtz, and J. Martell, Editor. 2003, ASTM International: West Conshohocken.
321. Campbell, F., *Introduction to Composite Materials*, in *Structural Composite Material*. 2010, ASM International. p. 1-5.
322. Guo QH, G.S., Wang ZM, *Estimation of 5-fluorouracil-loaded ethylene-vinyl acetate stent coating based on percolation threshold*. Int. J. Pharmaceutics, 2007. **333**: p. 95-102.
323. Meng Deng, S.W.S., *Properties of self-reinforced ultra-high-molecular-weight polyethylene composites*. Biomaterials, 1997. **18**: p. 645-656.
324. J S Bradley, E.J.E., *Carbon fibre reinforced ultra-high molecular weight polyethylene for medical application*. Engineering in Medicine, 1977. **6**(4): p. 123-124.
325. Wenchao Pang, Z.N., Guomei Chen, Guodong Huang, Huadong Huang, and Yongwu Zhao, *Mechanical and thermal properties of graphene oxide/ultrahigh molecular weight polyethylene nanocomposites*. RSC Adv, 2015. **5**: p. 63063-63072.
326. Min Zhang, P.P., Richard King, Susan P. James, *A novel ultra high molecular weight polyethylene-hyaluronan microcomposite for use in total joint replacements. II. Mechanical and tribological property evaluation*. J Biomed Mater Res A, 2007. **82A**(1): p. 18-26.
327. Joffre, T., Miettinen, A., Wernersson, E., Isaksson, P., & Gamstedt, E., *Effects of defects on the tensile strength of short-fibre composite materials*. Mechanics of Materials, 2014. **75**: p. 125-134.
328. Hull, D., *Fractography: Observing, Measuring and Interpreting Fracture Surface Topography*. . 1999: Cambridge University Press.
329. Greenhalgh, E., *Delamination growth in carbon fibre composite structures*. Compos. Struct., 1993. **23**: p. 165-175.
330. H Nisitani, Y.M., *Stress Intensity Factors of an Elliptical Crack or A Semi-Elliptical Crack Subject to Tension*. International Journal of Fracture, 1974. **10**(3): p. 353.
331. Stephen Spiegelberg, P., *Characterization of Physical, Chemical, and Mechanical Properties of UHMWPE*, in *UHMWPE Biomaterials Handbook*, P. Steven M. Kurtz, Editor. 2008, Elsevier: London. p. 365-367.
332. John P. Collier, D.B.H.C., MChE; Francis E. Kennedy, PhD; John H. Currier, MS; Graham S. Timmins, PhD; Simon K. Jackson, PhD; Robin L. Brewer, BE, *Comparison of Cross-Linked Polyethylene Materials for Orthopaedic Applications*. Clinical Orthopaedics and Related Research, 2003. **414**: p. 289-304.
333. Pruitt, L., *Conventional and Cross-Linked Polyethylene Properties*, in *Total Knee Arthroplasty: A Guide for Better Performance*, M.R. J. Bellmans, J. Victor, Editor. 2004, Springer-Verlag: Heidelberg. p. 353-360.
334. Bartel DI, B.I., Wright TM. , *The effect of conformity, thickness, and material on stresses in ultra-high molecular weight components for total joint replacement*. J Bone Joint Surg Am, 1996. **68A**: p. 1041-1048.
335. Brinda Doshi, J.S.W., Ebru Oral, Orhun K. Muratoglu, *Fatigue Toughness of Irradiated Vitamine E/UHMWPE Blends*. Journal of Orthopaedic Research, 2016. **34**(9): p. 1514-1520.
336. Williams, M.L., *Stress singularities resulting from various boundary conditions in angular corners of plates in extension*. J Applied Mech, 1952. **19**: p. 526-528.
337. Griffith, A.A., *The phenomena of rupture and flow in solids*. Philosophical Transactions, Series A, 1921. **221**: p. 163-198.

338. Anton E. Bowden, E.O., Jorgen Bergstrom, *Computer Modeling and Simulation of UHMWPE*, in *UHMWPE Biomaterials Handbook*, P. Steven M. Kurtz, Editor. 2008, Elsevier: London. p. 519-531.
339. Steven M. Kurtz, P., *A Primer on UHMWPE*, in *UHMWPE Biomaterials Handbook*, P. Steven M. Kurtz, Editor. 2008, Elsevier: London. p. 3.
340. Mansoo Joun, I.C., Jaegun Eom, Mincheol Lee, *Finite element analysis of tensile testing with emphasis on necking*. Computational Materials Science, 2007. **41**: p. 63-69.
341. Y. Murakami, H.M., A. Abyazi, Y. Fukushima, *Defect size dependence on threshold stress intensity for high-strength steel with internal hydrogen*. Fatigue and Fracture of Engineering Materials and Structures, 2013. **36**(9): p. 836-850.
342. Greenhalgh, E., *Delamination growth in carbon-fibre composite structures*. Compos. Struct. , 1993. **23**: p. 165-175.
343. AE Zachariades, K.T., Polym. Eng. Sci., 1986. **26**: p. 658.
344. Wu JJ, B.C., O'Connor JJ, *Mechanical Integrity of Compression-Moulded Ultra-High Molecular Weight Polyethylene: Effects of Varying Process Conditions*. Biomaterials, 2002. **23**: p. 3773-3783.
345. NC Parasnis, K.R., *Analysis of the effect of pressure on compression moulding of UHMWPE*. Journal of Materials Science: Materials in Medicine, 1998. **9**: p. 165-172.
346. Steven M. Kurtz, P., *Packaging and Sterilization of UHMWPE*, in *UHMWPE Biomaterials Handbook: Ultra-High Molecular Weight Polyethylene in Total Joint Replacement and Medical Devices*, P. Steven M. Kurtz, Editor. 2009, Elsevier: London. p. 21-30.
347. Steven M. Kurtz, P., *Highly Crosslinked and Melted UHMWPE*, in *UHMWPE Biomaterials Handbook*, P. Steven M. Kurtz, Editor. 2008, Elsevier: London. p. 197-203.
348. C. Birknishaw, M.B., S. Daly, M. O'Neill, *The effect of gamma radiation on the physical structure and mechanical properties of ultrahigh molecular weight polyethylene*. Journal of Applied Polymer Science, 1989. **38**: p. 1967-1973.
349. Briscoe BJ, S.S., *Wear of Polymers*. Proc Inst Mech Engrs, 2002. **216**(J): p. 401-412.
350. Czichos, H., *Introduction to Friction and Wear*, in *Composite Materials Series 1: Friction and Wear of Polymer Composites*, K. Friederich, Editor. 1986, Elsevier: Amsterdam.
351. Abdelbary A, A.M.N., ElFahham I M and Gommaa A I, *The influence of cyclic loading parameters on the wear of nylon 66*. The 8th International Conference on Production Engineering, Design, and Control, Alexandria, Egypt, 2004.
352. Abdelbary, A., *Polymer Tribology*, in *Wear of Polymers and Composites*, A. Abdelbary, Editor. 2014, Elsevier: London. p. 1-36.
353. VP Bavaresco, C.Z., SM Malmonge, MC Reis, *Viability of pHEMA Hydrogels as Coating in Human Synovial Joint Prosthesis*. Mat Res, 2002. **5**(4): p. 1-10.
354. Juliana Antonino de Souza, L.C.d., Sergio Alvaro de Souza Camargo, *Wear Mechanisms of Dental Composite Restorative Materials by Two Different in-vitro Methods*. Mat Res, 2013. **16**(2): p. 1-10.
355. Clare M Rimnac, S.M.K., *Ionizing radiation and orthopaedic prostheses*. Nuclear Instruments and Methods in Physics Research Section B Beam Interactions with Materials and Atoms, 2005. **236**(1): p. 30-37.
356. Charles Lipson, L.V.C., *Handbook of mechanical wear: wear, fretting, pitting, cavitation, corrosion*. 1961, University of Michigan Press. p. 449.
357. Muraro MA, K.F., Reisdorfer U, da Silva, CH, *The Influence of Contact Stress Distribution and Specific Film Thickness on the Wear of Spur Gears During Pitting Tests*. J. Braz. Soc. Mech. Sci. & Eng., 2011. **XXXIV**(2): p. 135-144.
358. Al-Bukhaiti MA, A.-H.K., Gabbert U, *The Influence of High Contact Stresses and Lubricant Type on The Rolling Contact Fatigue Life and Failure Mode of AISI 52100 Steel Balls*. Emirates Journal for Engineering Research, 2011. **16**(1): p. 9-22.

359. Wakuda, M., Yamauchi, Y., Kanzaki, S., and Yasuda, Y., *Effect of Surface Texturing on Friction Reduction Between Ceramic and Steel Materials Under Lubricated Sliding Contact*. *Wear*, 2003. **254**(3-4): p. 356-363.
360. Lu X, G.E., *The Stribeck Curve: Experimental Results and Theoretical Prediction*. *Journal of Tribology*, 2006. **128**: p. 789-794.
361. Stachowiak GW, B.A., *Hydrodynamic Lubrication*, in *Engineering Tribology*. 2014, Elsevier: Waltham. p. 106-210.
362. Stachowiak GW, B.A., *Elastohydrodynamic Lubrication*, in *Engineering Tribology*. 2014, Elsevier: Boston. p. 293-370.
363. Stachowiak GW, B.A., *Boundary and Extreme Pressure Lubrication*, in *Engineering Tribology*. 2014, Elsevier: Boston.
364. J. Sugimura, T.O.a.Y.Y., *Effects of Transverse Atomic Steps on Bilayer Lubricating Films of Simple Hydrocarbons*. *Tribology Letters*, 2007. **25**: p. 117-131.
365. Strutt), L.R.J.W., *On the Lubricating and Other Properties of Thin Oily Films*. *Phil. Mag. J. Science*, 1918. **35**: p. 157-163.
366. Hyunok Kim, N.K., *Friction and Lubrication*, in *Sheet Metal Forming-Fundamentals*, T.A.a.A. Tekkaya, Editor. 2012, ASM International: Ohio. p. 89-98.
367. A, W., *A unified theory of wear for ultra-high molecular weight polyethylene in multi-directional sliding*. *Wear*, 2001. **248**: p. 38-47.
368. Jalali-Vahid D, J.M., Jin ZM, Dowson D, *Prediction of lubricating film thickness in UHMWPE hip joint replacements*. *Journal of Biomechanics*, 2001. **34**: p. 261-266.
369. Elfick AP, H.R., Pinder IM, Unsworth A, *Surface topography of retrieved PCA acetabular liners: proposal for a novel wear mechanism*. *J. Mater. Sci. Lett.*, 1998. **17**: p. 1085.
370. Delport, H.P.B., S.A.; De Schepper, J.; Bellemans, J. , *A kinematic comparison of fixed- and mobile-bearing knee replacements*. *J. Bone Joint Surg. Br*, 2006. **88**: p. 1016-1021.
371. Williams, J.A., *Wear and wear particles—Some fundamentals*. *Tribol. Int.*, 2005. **38**: p. 863-870.
372. A. Wang, D.C.S., B. Edwards, M. Sokol, A. Essner, V.K. Polineni, C. Stark, J.H. Dumbleton, *Orientation softening in the deformation and wear of ultra-high polyethylene*. *Wear*, 1997. **203/204**: p. 230-241.
373. Wang A, S.C., Dumbleton JH, *Mechanistic and morphological origins of ultra-high molecular weight polyethylene wear debris in total joint replacement prostheses*. *Proc. Inst. Mech. Engrs., Part H: J. Eng. Med*, 1996. **210**(H3): p. 141-155.
374. DF, M., *A History of Research on Surface Texture Effects*. *Wear*, 1969. **13**: p. 381-412.
375. Costa HL, H.I., *Hydrodynamic Lubrication of Textured Steel Surfaces under Reciprocating Slide Conditions*. *Tribology International*, 2007. **40**: p. 1227-1238.
376. Kovalchenko A, A.O., Erdemir A, Fenske G, Etsion I, *The Effect of Laser Texturing of Steel Surfaces and Speed-Load Parameters on the Transition of Lubrication Regime from Boundary to Hydrodynamic*. *Tribology Transactions*, 2004. **47**: p. 299-307.
377. Ryk G, E.I., *Testing Piston Rings with Partial Laser Surface Texturing for Friction REduction*. *Wear*, 2006. **261**: p. 792-796.
378. Etsion I, S.E., *Improving Fuel Efficiency with Laser Surface Textured Piston Rings*. *Tribology International*, 2009. **42**: p. 542-547.
379. Gao, L., Yang, P., Dymond, I., Fisher, J., and Zhongmin, J., *Effect of Surface Texturing on the Elastohydrodynamic Lubrication Analysis of Metalon-Metal Hip Implants*. *Tribol Int*, 2010. **43**(10): p. 1851-1860.
380. Ronen, A., Etsion, I. and Kligerman, Y, *Friction-Reducing Surface Texturing in Reciprocating Automotive Components*. *Tribol. Trans.*, 2001. **44**: p. 359-366.

381. Krupka, I., Svoboda, P., and Hartl, M., *Effect of Surface Topography on Mixed Lubrication Film Formation During Start Up Under Rolling/Sliding Conditions*. Tribol. Int., 2010. **43**(5-6): p. 1035-1042.
382. Krupka, I., Hartl, M., Zimmerman, M., Houska, P., and Jang, S., *Effect of Surface Texturing on Elastohydrodynamically Lubricated Contact Under Transient Speed Conditions*. Tribol Int, 2011. **44**(10): p. 1144-1150.
383. Krupka, I., and Hartl, M., 2007, *The Effect of Surface Texturing on Thin EHD Lubrication Films*. Tribol. Int., 2007. **40**(7): p. 1100-1110.
384. Sudeep U, T.N., Pandey RK, *Performance of Lubricated Rolling/Sliding Concentrated Contacts With Surface Textures: A Review*. Journal of Tribology, 2015. **137**: p. 1-11.
385. Andersson, P., Koskinen, J., Varjus, S., Gerbig, Y., Haefke, H., and Georgiou, S., *Microlubrication Effect by Laser-Textured Steel Surfaces*. Wear, 2007. **262**(3-4): p. 369-379.
386. Wang, X., Liu, W., Zhou, F., and Zhu, D., *Preliminary Investigation of the Effect of Dimple Size on Friction in Line Contacts*. Tribol. Int., 2009. **42**(7): p. 1118-1123.
387. Podgornik, B., Vilhena, M., Sedlacek, M., Rek, Z., and Zun, I., *Effectiveness and Design of Surface Texturing for Different Lubrication Regimes*. Meccanica, 2012. **47**(7): p. 1613-1622.
388. Vilhena, L.M., Sedlacek, M., Podgornik, B., Vizinti, J., Babnik, A., and Mozina, J, *Surface Texturing by Pulsed Nd:YAG Laser*. Tribol. Int., 2009. **42**(10): p. 1496-1504.
389. Ito H, K.K., Yuhta T, Nishimura I, Yasuda K, Matsuno T, *Reduction of polyethylene wear by concave dimples on the frictional surface in artificial hip joints*. J Arthroplasty, 2000. **15**(3): p. 332-338.
390. Chyr A, Q.M., Speltz J, Jacobsen RL, Sanders AP, Raeymaekers B, *A patterned microtexture to reduce friction and increase longevity of prosthetic hip joints*. Wear, 2014. **315**(1-2): p. 51-57.
391. Ishihara K, I.Y., Ebihara S, Shindo Y, Nakabayashi N, *Photoinduced graft polymerization of 2-methacryloyloxyethyl phosphorylcholine on polyethylene membrane surface for obtaining blood cell adhesion resistance*. Colloids and Surfaces B: Biointerfaces, 2000. **18**(3-4): p. 325-335.
392. Leslie DC, W.A., Berthet JB, Valentin TM, Watters AL, Jain A, Kim P, Hatton BD, Nedder A, Donovan K, Super EH, Howell C, Johnson CP, Vu TL, Bolgen DE, Rifai S, Hansen AR, Aizenber M, Super M, Aizenberg J, Ingber DE, *A bioinspired omniphobic surface coating on medical devices prevents thrombosis and biofouling*. Nature Biotech, 2014. **32**(11): p. 1134-1140.
393. Bergmann G, G.F., Rohlmann A., *Hip joint loading during walking and running, measured in two patients*. J Biomech, 1993. **26**(8): p. 969-990.
394. BJ, H., *Film Thickness For Different Regimes of Fluid-Film Lubrication*. NASA Technical Memorandum, 1980. **TM-81550**: p. 1-13.
395. Cohen JM, D.P., *Dosimetry for In Vitro Nanotoxicology: Too Complicated to Consider, Too Important to Ignore*, in *Nanoparticles in the Lung: Environmental Exposure and Drug Delivery*, G.P. Tsuda A, Editor. 2015, CRC Press: Boca Raton. p. 284-285.
396. *Titanium Ti-6Al-4V (Grade 5), Annealed*.
397. *Typical Poisson's Ratios for some Common Materials*. Available from: http://www.engineeringtoolbox.com/poissons-ratio-d_1224.html.
398. Chen J, N.Y., Hoffman AS, *Fracting copolymerization of 2-methacryloyloxyethyl phosphorylcholine (MPC) onto pre-irradiated cellulose films*. J Biomater Sci Polym Ed, 2004. **15**(7): p. 841-849.
399. Parker RJ, K.J., *Elastohydrodynamic Film Thickness Between Rolling Disks With A Synthetic Paraffinic Oilk to 589 K (600 F)*. NASA Technical Note, 1971. **TN D-6411**: p. 1-26.
400. Greene GW, Z.B., Soderman O, Topgaard D, Rata G, Zeng H, Israelachvili JN, *Anisotropic dynamic changes in the pore network structure, fluid diffusion and fluid flow in articular cartilage under compression*. Biomaterials, 2010. **31**(12): p. 3117-3128.

401. Greene GW, Z.B., Soderman O, Topgaard D, Rata G, Zeng H, Israelachvili JN, *Changes in pore morphology and fluid transport in compressed articular cartilage and the implications for joint lubrication*. Biomaterials, 2008. **29**(33): p. 4455-4462.
402. Ebru ORal, O.K.M., *Radiation cross-linking in ultra-high molecular weight polyethylene for orthopaedic applicaitons*. Nucl Instrum Methods Phys Res B, 2007. **265**(1): p. 18-22.
403. Toru Moro, Y.T., Kazuhiko Ishihara, Tomohiro Konno, Yorunibu Takigawa, Tomiharu Matsushita, Ung-il Chung, Kozo Nakamura, Hiroshi Kawaguchi, *Surface grafting of artificial joints with a biocompatible polymer for preventing periprosthetic osteolysis*. Nature Materials, 2004. **3**: p. 829-836.
404. Ishihara, K., *Highly lubricated polymer interfaces for advanced artificial hip joints through biomimetic design*. Polymer Journal, 2015(1-13).
405. Oral E, N.A., Rowell SL, Lozynsky AJ, Muratoglu OK, *Increasing irradiation temperature maximizes vitamin E grafting and wear resistance of ultrahigh molecular weight polyethylene*. J Biomed Mater Res B Appl Biomater, 2013. **101**(3): p. 436-440.
406. Salgado CD, D.S., Cantey JR, Marculescu CE., *Higher Risk of Failure of Methicillin-Resistant Staphylococcus aureus proshthetic joint infection*. Clin Orthop Relat Res, 2007. **461**: p. 48-53.
407. Lamagni, T., *Epidemiology and burden of prosthetic joint infections*. Journal of Antimicrobial Chemotherapy, 2014. **69 Suppl 1**: p. i5-i10.
408. Mittal Y, F.T., Hanssen A, Marculescu C, Odum SM, Osmon D., *Two-stage reimplantation for periprosthetic knee infection involving resistant organisms*. J Bone Joint Surg Am, 2007. **89**: p. 1227-231.
409. Parvizi J, A.K., Ghanem E, Austin M, Rothman R., *Periprosthetic infection due to resistant staphylococci: serious problems on the horizon*. Clin Orthop Relat Res, 2009. **467**: p. 1732-1739.
410. Kilgus DJ, H.D., Strang A, *Results of periprosthetic hip and knee infections caused by resistant bacteria*. Clin Orthop Relat Res, 2002. **404**: p. 116-124.
411. Andor W.J.M. Glaudemans, F.G., Marta Pacilio and Alberto Signore, *Leukocyte and Bacteria Imaging in Prosthetic Joint Infection*. European Cells and Materials, 2013. **25**: p. 61-77.
412. Health, N.Y.S.D.o., *Hospital-Acquired Infections New York State 2011*. September 2012, Department of Health: Albany, NY.
413. Peel, T.N., *Microbiological aetiology, epidemiology, and clinical profile of prosthetic joint infections: are current antibiotic prophylaxis guideline effective ?* Antimicrob Agents Chemoter, 2012. **56**: p. 2386-2391.
414. Jaime Lora-Tamayo, O.M., Jose Antonio Iribarren, et al, *A Large Multicenter Study of Methicillin-Susceptible and Methicillin-Resistant Staphylococcus aureus Prosthetic Joint Infections Managed with Implant Retention*. Clin Infect Dis, 2013. **56**(2): p. 182-194.
415. Bennie Lindeque, Z.H., Andriy Noshchenko, Margaret Cruse, *Infection After Primary Total Hip Arthroplasty*. Orthopedics, 2014. **37**(4): p. 257-265.
416. Andrzej Kaminski, M.C., Thomas Armin Schildhauer, Tobias Fehmer, *Success Rates for Initial Eradication of Peri-prosthetic Knee Infection Treated with a Two-Stage Procedure*. Ortopedia Traumatologia Rehabilitacja, 2014. **16**(1): p. 11-16.
417. V Post, P.W., I Uckay, P Ochsner, W Zimmerli, S Corvec, C Loiez, RG Richards, TF Moriarty, *Phenotypic and genotypic characterisation of Staphylococcus aureus causing musculoskeletal infections*. Int J Med Microbiol, 2014. **304**(5-6): p. 565-576.
418. M Mashfiqul A. Siddiqui, N.N.L., Shaifuzain Ab Rahman, Park Lin Chin, Shi-Lu CHia, Seng Jin Yeo, *Two-Year Outcome of Early Deep MRSA Infections After Primary Total Knee Arthroplasty*. J Arthroplasty, 2013. **28**(1): p. 44-48.

419. Giuliana Carrega, V.B., Giorgio Burastero, Giorgetta Casalino-Finocchio, Guido Grappiolo, Carlo Salomone, Clemente Sandrone, Luisa Santoriello, Giovanni Riccio, *Aetiology of prosthetic joint infections in a tertiary care centre in Italy*. *Le Infezioni in Medicina*, 2008. **4**: p. 204-208.
420. E Moran, S.M., AR Berendt, P McLardy-Smith, I Byren, BL Atkins, *Guiding empirical antibiotic therapy in orthopaedics: The microbiology of prosthetic joint infection managed by debridement, irrigation, and prosthesis retention*. *J Infect Dis*, 2007. **55**(1): p. 1-7.
421. Trampuz A, Z.W., *Prosthetic Joint Infections: Update in Diagnosis and Treatment*. *Swiss Med Wkly*, 2005. **135**(17-18): p. 243-251.
422. David J Schurman, H.P.H., Donald A Nagel, *Antibiotic Penetration of Synovial Fluid in Infected and Normal Knee Joints*. *Clin Orthop Relat Res*, 1978. **136**: p. 304-310.
423. Goldstein EJ, S.B., Lipsky B, *Systemic Antibiotic Therapy for Chronic Osteomyelitis in Adults*. *Clinical Infectious Disease*, 2012. **54**(3): p. 393-407.
424. CE Marculescu, E.B., AD Hanssen, JM Steckelberg, SW Harmsen, JN Mandrekar, DR Osmon, *Outcome of Prosthetic Joint Infections Treated with Debridement and Retention of Components*. *Clin Infect Dis*, 2006. **42**: p. 472-478.
425. Claudia M. Brandt, W.W.S., Mary C. Duffy, Arlen D. Hanssen, James M. Steckelberg, Duane M. Ilstrup, Douglas R. Osmon, *Staphylococcus aureus Prosthetic Joint Infection Treated with Debridement and Prosthesis Retention*. *Clinical Infection*, 1997. **24**(5): p. 914-919.
426. Julia C. Dombrowski, L.G.W., *Clinical failures of appropriately-treated methicillin-resistant Staphylococcus aureus infections*. *Journal of Infection*, 2008. **57**: p. 110-115.
427. Pioletti DP, G.O., Stadelmann VA, Bujoli B, Guicheux J, Zambelli PY, Bouler JM, *Orthopedic Implant Used as Drug Delivery System: Clinical Situation and State of Research*. *Current Drug Delivery*, 2008. **5**: p. 59-63.
428. Duncan CP, M.B., *Antibiotic depots*. *J Bone Joint Surg Br*, 1993. **75**(3): p. 349-350.
429. Duncan CP, M.B., *The role of antibiotic-loaded cement in the treatment of an infection after a hip replacement*. *Instr Course Lec*, 1995. **44**: p. 305-313.
430. Jiri Gallo, M.H., Calin S. Moucha, *Antibacterial Surface Treatment for Orthopaedic Implants*. *Int J Mol Sci*, 2014. **15**(8): p. 13849-13880.
431. Thomas Fuchs, R.S., Gerhard Schmidmaier, Micahel J Raschke, *The use of gentamicin-coated nails in the tibia: preliminary results of a prospective study*. *Arch Orthop Trauma Surg*, 2011. **131**(10): p. 1419-1425.
432. Thomas Fuchs, G.S., Michael J. Raschke, Richard Stange, *Bioactive-coated Implants in Trauma Surgery*. *Eur J Trauma Emerg Surg*, 2008. **34**: p. 60-68.
433. Antoci V Jr, K.S., Jose B, Parvizi J, Zeiger AR, Wickstrom E, Freeman TA, Composto RJ, Ducheyne P, Shapiro IM, Hickok NJ, Adam CS, *Vancomycin covalently bonded to titanium alloy prevents bacterial colonization*. *J Orthop Res.*, 2007. **25**(7): p. 858-866.
434. Radin S, C.J., Ducheyne P, Cuckler JM, *Calcium phosphate ceramic coatings as carriers of vancomycin*. *Biomaterials* 1997. **18**(777).
435. Lin SS, U.S., Liu SJ, Chan EC, Chao EK, Tsai CH, Chen KT, Wei FC, Shih CH, *Development of a biodegradable antibiotic delivery system* *Clin Orthop Relat Res*, 1999. **362**: p. 240-250.
436. Setor K. Kunutsor, M.R.W., Erik Lenguerrand, Ashley W. Blom, Andrew D. Beswick, INFORM team, *Re-Infection Outcomes Following One- And Two-Stage Surgical Revision of Infected Knee Prosthesis: A Systematic Review and Meta-Analysis*. *PLOS One*, 2016. **11**(3): p. e0151537.
437. Szu-Yuan Chen, C.-C.H., Chun-Chieh Chen, Yu-Han Chang, and Pang-Hsin Hsieh, *Two-Stage Revision Arthroplasty for Periprosthetic Hip Infection: Mean Follow-Up of Ten Years*. *BioMed Research International*, 2015: p. 345475.

438. Berend KR, L.A.J., Morris MJ, Bergesson AG, Adams JB, Sneller MA, *Two-stage treatment of hip periprosthetic joint infection is associated with a high rate of infection control but high mortality.* Clin Orthop Relat Res, 2013. **471**(2): p. 510-518.
439. Hanssen AD, T.R., Osmon DR, *Patient outcome with reinfection following reimplantation of the infected total knee arthroplasty.* Clin Orthop Relat Res, 1995. **321**: p. 55-67.
440. Mont MA, W.B., Hungerford DS., *Evaluation of preoperative cultures before second-stage reimplantation of a total knee prosthesis complicated by infection. A comparison-group study.* J Bone Joint Surg Am, 2000. **82-A**: p. 1552-1557.
441. Fenelon GC, V.F.G., Engelbrecht E, *Disarticulation of the hip as a result of failed arthroplasty. A series of 11 cases.* J Bone Joint Surg Br, 1980. **62-B**(4): p. 441-446.
442. KD, K., *Bone Cements: Up-to-Date Comparison of Physical and Chemical Properties of Commercial Materials.* 2000, Berlin: Springer-Verlag.
443. C, L., *The Mechanical Properties of PMMA Bone Cement,* in *The Well-Cemented Total Hip Arthroplasty: Theory and Practice.* 2005, Springer Medizin Verlag: Berlin. p. 60-66.
444. Kei Osano, R.N., Mitsugu Todo, and Makoto Kawasaki, *The Effect of Malrotation of Tibial Component of Total Knee Arthroplasty on Tibial Insert during High Flexion Using a Finite Element Analysis.* The Scientific World Journal, 2014: p. 1-7.
445. Cho C H, M.T., Sawae Y, Sakai N, Miura H, Kawano T and Iwamoto Y., *Elasto-plastic contact analysis of fatigue wear behaviour of UHMWPE tibial components.* Japan J Clin Biomech., 2002. **23**: p. 373-379.
446. Rami K Korhonen, A.K., Yrjö T Konttinen, Seppo S Santavirta and Reijo Lappalainen, *The effect of geometry and abduction angle on the stresses in cemented UHMWPE acetabular cups – finite element simulations and experimental tests.* BioMedical Engineering OnLine, 2005. **4**: p. 32.
447. Aaron J. Tande, R.P., *Prosthetic Joint Infection.* Clinical Microbiology Reviews, 2014. **27**(2): p. 302-345.
448. Parag Garg, R.R., Utpal Bandyopadhyay, Shiv Chouksey, SR Mitra, Samar K Gupta, *Antibiotic-Impregnated Articulating Cement Spacer for Infected Total Knee Arthroplasty.* Indian J Orthop, 2011. **45**(6): p. 535-540.
449. Duey RE, C.A., McQueen DA, Womack JL, Song Z, Steinberger TA, Wooley PH, *Mechanical Properties and Elution Characteristics of Polymethylmethacrylate Bone Cement Impregnated with Antibiotics for Various Surface Area and Volume Constructs.* Iowa Orthop J, 2012. **32**: p. 104-115.
450. Lilikakis A, S.M., *The effect of vancomycin addition to the compression strength of antibiotic-loaded bone cements.* Int Orthop, 2009. **33**(3): p. 815-819.
451. Xie Z, C.X., Zhao C, Huang W, Wang J, Zhang C, *Gentamicin-Loaded Borate Bioactive Glass Eradicates Osteomyelitis Due to Escherichia coli in a Rabbit Model.* Antimicrob Agents Chemother, 2013. **57**(7): p. 3293-3298.
452. Baker A S, G.L.W., *Release of gentamicin from acrylic bone cement.* J Bone Joint Surg Am, 1988. **70**: p. 1551-1557.
453. Picknell B, M.L., Sutherland R, *Antibacterial activity of antibiotics in acrylic bone cement.* J Bone Joint Surg Br, 1977. **59**: p. 302-307.
454. Hoff S F, F.R., Kelly PJ, *The depot administration of penicillin G and gentamicin in acrylic bone cement.* J Bone Joint Surg Am, 1981. **63**: p. 798-804.
455. Chohfi M, L.F., Fouraster J, Minet J, Thomazeau H, Cormier M, *Pharmacokinetics, uses, and limitations of vancomycin-loaded bone cement.* Inter Orthop, 1998. **22**: p. 171-177.
456. Penner MJ, D.C., Masri BA, *The in vitro elution characteristics of antibiotic-loaded CMW and Placos-R bone cement.* J Arthrop 1999. **14**: p. 209-214.

457. Bunetel L, S.A., Cormier M, Percheron E, Langlais F, *Release of gentamicin from acrylic bone cement*. Clin Pharmacokinet, 1989. **17**: p. 291-297.
458. Torholm C, L.L., Kahlmoter G, *Total hip joint arthroplasty with gentamicin-impregnated cement. A clinical study of gentamicin excretion kinetics*. Clin Orthop, 1983. **181**: p. 99-106.
459. E. Bertazzoni Minelli, A.B., B. Magnan and P. Bartolozzi, *Release of gentamicin and vancomycin from temporary human hip spacers in two-stage revision of infected arthroplasty*. Journal of Antimicrobial Chemotherapy, 2004. **53**: p. 329-334.
460. Hilbrand van de Belt, D.N., Willem Schenk, Jim R van Horn, and H.J.B. Henny C van der Mei, *Gentamicin release from polymethylmethacrylate bone cements and Staphylococcus aureus biofilm formation*. ACTA ORTHOPAEDICA SCANDINAVICA, 2000. **71(6)**: p. 625-629.
461. van de Belt H, N.D., Schenk W, et al, *Staphylococcus aureus biofilm formation on different gentamicin-loaded polymethylmethacrylate bone cements*. Biomaterials, 2001. **22**: p. 1607-1611.
462. Neut D, v.d.B.H., van Horn JR, van der Mei HC, Busscher HJ, *Residual gentamicin-release from antibiotic-loaded polymethylmethacrylate beads after 5 years of implantation*. Biomaterials, 2003. **24(10)**: p. 1829-1831.
463. D. Baykal, R.S.S., H. Haider, V. Saikko, T. Ahlroos, S.M. Kurtz, *Advances in tribological testing of artificial joint biomaterials using multidirectional pin-on-disk testers*. Journal of The Mechanical Behavior of Biomedical Materials 2014. **31**: p. 117-134.
464. Lauderdale KJ, M.C., Boles BR, Morcuende J, Horswill AR. , *Biofilm dispersal of community-associated methicillin-resistant Staphylococcus aureus on orthopedic implant materia*. J Orthop Res., 2010. **28(1)**: p. 55-61.
465. Marsha A. Moses, H.B., and Robert Langer, *Advancing the field of drug delivery: Taking aim at cancer*. Cancer Cell, 2003. **4**: p. 337-341.
466. MA McNally, J.F., ACK Lau, M Diefenbeck, M Scarborough, AJ Ramsden, BL Atkins, *Single-stage treatment of chronic osteomyelitis with a new absorbable, gentamicin-loaded, calcium sulphate/hydroxyapatite biocomposite*. Bone Joint J, 2016. **98-B**: p. 1289-1296.
467. Burnett RS, K.M., Hanssen AD, Barrack RL, *Technique and timing of two-stage exchange for infection in TKA*. Clin Orthop Relat Res, 2007. **464**: p. 164-178.
468. Bohner, M., *Designing ceramics for injectable bone graft substitutes*, in *Injectable biomaterials: Science and applications*, B. Vernon, Editor. 2011, Woodhead Publishing: Cambridge. p. 24-39.
469. Neut D, v.d.B.H., Stokroos I, et al, *Biomaterial-associated infection of gentamicin-loaded PMMA beads in orthopaedic revision surgery*. J Antimicrob Chemother, 2001. **47**: p. 885-891.
470. Suzanne Stewart. Stephanie Barr, J.E., Noreen J. Hickok, Irving M. Shapiro, Dean W. Richardson, Javad Parvizi, Thomas P. Schaer, *Vancomycin-Modified Implant Surface Inhibits Biofilm Formation and Supports Bone-Healing in an Infected Osteotomy Model in Sheep*. J. Bone Joint Surg. Am, 2012. **94(15)**: p. 1406-1415.
471. Beatriz Amorena, E.G., marta Monzon, Jose Leiva, Concepcion Oteiza, Marta Perez, Jose-Luis Alabart, Jose Hernandez-Yago, *Antibiotic susceptibility assay for Staphylococcus aureus in biofilms developed in vitro*. Journal of Antimicrobial Chemotherapy, 1999. **44(1)**: p. 43-55.
472. Toshiyuki Sakimura, S.K., Shinji Adachi, Ko Chiba, Akihiko Yonekura, Masato Tomita, Hironobu Koseki, Takashi Miyamoto, Toshiyuki Tsurumoto, Makoto Osaki, *Biofilm-Forming Staphylococcus epidermidis Expressing Vancomycin Resistance Early after Adhesion to a Metal Surface*. BioMed Research International, 2015. **2015(94305)**: p. 1-8.
473. Lluís Font-Vizcarra, M., 1 Sebastián García, MD, PhD, 1 Juan C. Martínez-Pastor, MD, 1 Josep M. Sierra, MD, 2 and Alex Soriano, MD, PhD, *Blood Culture Flasks for Culturing Synovial Fluid in Prosthetic Joint Infections*. Clin Orthop Relat Res, 2010. **468(8)**: p. 2238-2243.

474. Andrea Volpin, M.S., Sulaiman Alazzawi, Fares Sami Haddad, *Aggressive Early Debridement in Treatment of Acute Periprosthetic Joint Infections After Hip and Knee Replacements* The Open Orthopaedics Journal, 2017. **10**: p. 669-678.
475. Southwood RT, R.J., McDonald PJ, Hakendorf PH, Rozenbils MA, *Infection in experimental hip arthroplasties*. J. Bone Joint Surg Br., 1985. **67**: p. 229-231.
476. R. Tresbe, V.P., A. Trampuz, *Treatment of infected retained implants*. Journal Bone Joint Surg Br, 2005. **87-B(2)**: p. 249-256.
477. John E. Cockarell, A.D.H., Douglas R. Osmon, Bernard F. Morrey, *Treatment of Infection with Debridement and Retention of the Components Following Hip Arthroplasty*. J Bone Joint Surg Am, 1998. **80(9)**: p. 1306-1313.
478. Ana Lucia L. Lima, P.R.O., Vladimir C. Carvalho, Eduardo S. Saconi, Henrique B. Cabrita, Marcelo B. Rodrigues, *Periprosthetic Joint iNfections*. Interdisciplinary Perspectives on Infectious Diseases, 2013. **2013(542796)**: p. 1-7.
479. MJ Spangehl, B.M., JX O'Connell, CP Duncan, *Prospective analysis of preoperative and intraoperative investigations for the diagnosis of infection at the sites of two hundred and two revision total hip arthroplasties*. Journal Bone Joint Surg Am, 1999. **81(5)**: p. 672-683.
480. Leo A. Whiteside MD, M.P.P., Tariq A. Nayfeh MD, PhD, Marcel E. Roy PhD, *Methicillin-resistant Staphylococcus aureus in TKA Treated With Revision and Direct Intraarticular Antibiotic Infusion*. Clin Orthop Relat Res, 2011. **469**: p. 26-33.
481. T. Taggart, R.M.K., P. Norman, I. Stockley, *The use of vancomycin-impregnated cement beads in the management of infection of prosthetic joints*. J Bone Joint Surg Br, 2002. **84-B**: p. 70-72.
482. Dunne WM Jr, M.E., Kaplan SL, *Diffusion of rifampin and vancomycin through a Staphylococcus epidermidis biofilm*. Antimicrob Agents Chemother 1993. **37**: p. 2522-2526.
483. Darouiche RO, D.A., Miller AJ, et al. *Vancomycin penetration into biofilm covering infected prostheses and effect on bacteria*. J Infect Dis, 1994. **170**: p. 720-723.
484. Shivani Chopra, K.H., Sanjay Chhiber, *Antibiotic Susceptibility of ica-positive nad ica-negative MRSA in different phases of biofilm growth*. The Journal of Antibiotics, 2014. **68**: p. 15-22.
485. Trampuz A, Z.W., *Prosthetic joint infections: update in diagnosis and treatment*. Swiss Med Wkly, 2005. **135**: p. 243-251.
486. Cédric Jacqueline, J.C., *Impact of bacterial biofilm on the treatment of prosthetic joint infections* J Antimicrob Chemother, 2014. **69**: p. i37-i40.
487. Leite B, G.F., Teixeira P, et al. *In vitro activity of daptomycin, linezolid and rifampicin on Staphylococcus epidermidis biofilms*. Curr Microbiol, 2011. **63**: p. 313-317.
488. Vergidis P, R.M., Euba G, et al, *Treatment with linezolid or vancomycin in combination with rifampin is effective in an animal model of methicillin-resistant Staphylococcus aureus foreign body osteomyelitis*. Antimicrob Agents Chemother, 2011. **55**: p. 1182-1186.
489. Younger AS, D.C., Masri BA, *Treatment of infection associated with segmental bone loss in the proximal part of the femur in two stages with use of an antibiotic-loaded interval prosthesis*. J Bone Joint Surg Am, 1998. **80**: p. 60-69.
490. Kendall RW, M.B., Duncan CP, et al., *Temporary antibiotic loaded acrylic hip replacement: a novel method for management of the infected THA*. Semin Arthroplasty, 1994. **5**: p. 171-177.
491. Ke Liu, J.Z., Yi Jin, Yong-qiang Zhao, *Application of temporarily functional antibiotic-containing bone cement prosthesis in revision hip arthroplasty*. Eur J Orthop Surg Traumatol, 2014. **24**: p. 51-55.
492. Fares S. Haddad, B.A.M., David Campbell, Robert W. McGraw, Christopher P. Beauchamp, Clive P. Duncan, *The PROSTALAC functional spacer in two-stage revision for infected knee replacements*. J Bone Joint Surg Br, 2000. **82-B(6)**: p. 807-813.

493. Angela Scharfenberger, M.C., Guy Lavoie, Greg O'Connor, Edward Masson, Lauren A. Beaupre, *Treatment of an infected total hip replacement with the PROSTALAC system. Part 1: Infection Resolution*. Canadian Journal of Surgery, 2007. **50**(1): p. 24-28.
494. GS Biring, T.K., DS Garbuz, BA Masri, CP Duncan, *Two-stage revision arthroplasty of the hip for infection using an interim articulated Prostalac hip spacer*. J Bone Joing Surg Br, 2009. **91-B**(11): p. 1431-1438.
495. Angela Scharfenberger, M.C., Guy Lavoie, Greg O'Connor, Edward Masson, Lauren A. Beaupre, *Treatment of an infected total hip replacement with the PROSTALAC system*. Can J Surg, 2007. **50**(1): p. 29-34.
496. Morthin, L.L., T, Andrew, D; Vann Praagh, D; Zhang, S; Zhang, X; Alder, J, *Rapid Bactericidal Activity of Daptomycin against Methicillin-Resistant and Methicillin-Susceptible Staphylococcus aureus Peritonitis in Mice as Measured with Bioluminescent Bacteria*. Antimicrob. Agents Chemotherapy, 2007. **51**(5): p. 1787-1794.
497. Quanjun Cui, W.M.M., John S. Shields, Michael Ries and Khaled J. Saleh, *Antibiotic-Impregnated Cement Spacers for the Treatment of Infection Associated with Total Hip or Knee Arthroplasty*. J. Bone Joint Surg. Am, 2007. **89**: p. 871-882.
498. Mellor JA, K.J., Cafferkey M, Keane CT, *Vancomycin toxicity: a prospective study*. J. Antimicrob. Chemother., 1985. **15**(6): p. 773-780.
499. Administration, F.a.D. *Summary of Safety and Probable Benefit (PROSTALAC Hip Temporary Prosthesis System)*. 1997 [cited 2017 01/26/2017]; Available from: http://www.accessdata.fda.gov/cdrh_docs/pdf/H000004b.pdf.
500. Yan Q Xiong, J.W., Jagath L. Kadurugamuwa, Jun Yu, Kevin P. Francis, and Arnold S. Bayer, *Real-Time In Vivo Bioluminescent Imaging for Evaluating the Efficacy of Antibiotics in a Rat Staphylococcus aureus Endocarditis Model*. Antimicrob Agents Chemoter, 2005. **49**(1): p. 380-387.
501. Jagath L. Kadurugamuwa, L.V.S., Jun Yu, Kevin P. Francis, Richard Kimura, Tony Purchio, and Pamela R. Contag, *Rapid Direct Method for Monitoring Antibiotics in a Mouse Model of Bacterial Biofilm Infection*. Antimicrob Agents Chemoter, 2003. **47**(10): p. 3130-3137.
502. Paulo Castaneda, A.M., Gamuchirai Tavaziva, Derek Overstreet, *Biofilm Antimicrobial Susceptibility Increases With Antimicrobial Exposure Time*. Clin Orthop Relat Res, 2016. **474**(7): p. 1659-1664.
503. Paul Stoodley, G.D.E., Parish P. Sedghizadeh, Luanne Hall-Stoodley, Mark E. Baratz, Daniel T. Altman, Nicholas G. Sotereanos, John William Costerton, and Patrick DeMeoe, *Orthopaedic biofilm infections*. Curr Orthop Pract, 2011. **22**(6): p. 558-563.
504. Filos KS, K.L., *Current concepts and practice in postoperative pain management: need for a change?* Eur Surg Res, 1999. **31**: p. 97-107.
505. Follin SL, C.S., *Acute pain management: operative or medical procedures and trauma*. Ann Pharmacother, 1997. **31**: p. 1068-1076.
506. Sriwatanakul K, W.O., Alloza JL, Kelvie W, Weintraub M, Lasagna L, *Analysis of narcotic analgesic usage in the treatment of postoperative pain*. JAMA, 1983. **250**: p. 026-929.
507. Warfield CA, K.C., *Acute pain management. Programs in US hospitals and experiences and attitudes among US adults*. Anesthesiology, 1995. **83**: p. 1090-1094.
508. Apfelbaum JL, C.C., Mehta SS, Gan Tj, *Postoperative pain experience: results from a national survey suggest postoperative pain continues to be undermanaged* Anest Analg, 2003. **97**: p. 534-540.
509. Chung F, R.E., Su J, *Postoperative pain in ambulatory surgery*. Anest Analg, 1997. **85**: p. 808-816.
510. Rawal N, H.J., Nydahl PA, Olofsson I, Gupta A, *Survey of postoperative analgesia following ambulatory surgery*. Acta Anesthesiol Scand, 1997. **41**: p. 1017-1022.

511. Parvizi J, P.M., Gandhi K, Viscusi ER, Rothman RH, *Postoperative pain management techniques in hip and knee arthroplasty*. Instr Course Lect, 2009. **58**: p. 769-779.
512. Maheshwari AV, B.Y., Shekhar L, Ranawat AS, Ranawat CS, *Multimodal pain management after total hip and knee arthroplasty at the Ranawat Orthopaedic Center*. Clin Orthol Relat Res, 2009. **467**: p. 1418-1423.
513. Parvantaneni HK, R.A., Ranawat CS, *The use of local periarticular injections in the management of postoperative pain after total hip and knee replacement: a multimodal approach*. Instr Course Lect, 2007. **56**: p. 125-131.
514. Sinatra RS, T.J., Bustos AM, *Pain management after major orthopaedic surgery: current strategies and new concepts*. J Am Acad Orthop Surg, 2002. **10**: p. 117-129.
515. PN Baker, J.v.d.M., PJ Gregg, *The role of pain and function in determining patient satisfaction after total knee replacement*. J Bone Joint Surg Br, 2007. **89-B(7)**: p. 893-890.
516. Noble PC, C.M., Cook KF, Mathis KB, *The John Insall Award: Patient expectations affect satisfaction with total knee arthroplasty*. Clin Orthol Relat Res, 2006. **452**: p. 35-43.
517. Brokelman RB, v.L.C., Rijnberg WJ, *Patient versus surgeon satisfaction after total hip arthroplasty*. J Bone Joint Surg Br, 2003. **85(4)**: p. 495-498.
518. Park KK, S.K., Chang CB, Kim SJ, Kim TK, *Functional disabilities and issues of concern in female Asian patients before TKA*. Clin Orthol Relat Res, 2007. **461**: p. 143-152.
519. Trousdale RT, M.B., Berry DJ, Becker MW, Hamsen WS, *Patients' concerns prior to undergoing total hip and total knee arthroplasty*. Mayo Clin Proc, 1999. **74(10)**: p. 978-982.
520. Mangano DT, W.M., London MJ, Tubau JF, Rapp JA, *Perioperative myocardial ischemia in patients undergoing noncardiac surgery-II: Incidence and severity during the 1st week after surgery. The Study of Perioperative Ischemia (SPI) Research Group*. J Am Coll Cardiol, 1991. **17(4)**: p. 851-857.
521. DH, W., *A stepwise logistic regression analysis of factors affecting morbidity and mortality J Trauma*, 1990. **30(7)**: p. 799-805.
522. Watwill, M., *Postoperative pain relief and gastrointestinal motility*. Acta Chir Scand Suppl, 1989. **550**: p. 140-145.
523. Krych AJ, H.T., Hebl JR, Pagnano MW, *Contemporary pain management strategies for minimally invasive total knee arthroplasty*. Instr Course Lect, 2010. **59**: p. 99-109.
524. Wheeler M, O.G., Ashburn MA, Lipman AG, *Adverse events associated with postoperative opioid analgesia: a systematic review*. J Pain, 2002. **3(3)**: p. 159-180.
525. Hance Clarke, N.S., Dennis T Ko, Lingsong Yun, DumindaN Wijeyesundera, *Rates and risk factors for prolonged opioid use after major surgery: population based cohort study*. BMJ, 2014. **348**: p. g1251.
526. Alam A, G.T., Zheng H, Mamdani MM, Juurlink DN, Bell CM, *Long-term analgesic use after low-risk surgery: a retrospective cohort study*. Arch Intern Med, 2012. **172(5)**: p. 425-430.
527. Jenna Goesling, S.E.M., Bilal Zaidi, Afton L Hassett, Paul Hilliard, Brian Hallstrom, Daniel J Clauw, Chad M Brummett, *Trends and predictors of opioid use after total knee and total hip arthroplasty*. Pain, 2016. **157(6)**: p. 1259-1265.
528. Franklin PD, K.J., Li WJ, Yang WY, Ayers DC, *Reduction in narcotic use after primary total knee arthroplasty and association with patient pain relief and satisfaction*. J Arthroplasty, 2010. **25**: p. 12-16.
529. Long-Co L Nguyen, D.C.S., Kevin J Bozic, *Preoperative Reduction of Opioid Use Before Total Joint Arthroplasty*. J Arthroplasty, 2016. **31(9)**: p. 282-287.
530. Society, K.K., *Guidelines for the Management of Postoperative Pain after Total Knee Arthroplasty*. Knee Surg Relat Res, 2012. **24(4)**: p. 201-207.

531. Buvanendran A, K.J., Tuman KJ, Lubenow TR, Elmofty D, Moric M, Rosenberg AG, *Effects of perioperative administration of a selective cyclooxygenase 2 inhibitor on pain management and recovery of function after knee replacement: a randomized controlled trial.* JAMA, 2003. **290**(18): p. 2411-2418.
532. Reuben SS, B.S., Maciolek H, Joshi W, Sklar J, *The preemptive analgesic effect of rofecoxib after ambulatory arthroscopic knee surgery.* Anesth Analg, 2002. **94**(1): p. 55-59.
533. Cheville A, C.A., Oster G, McGarry L, Narcessian E, *A randomized trial of controlled-release oxycodone during inpatient rehabilitation following unilateral total knee arthroplasty.* J Bone Joint Surg Am, 2001. **83-A**(4): p. 572-576.
534. Klasen J, H.M., Graf S, Harbach H, Quinzio L, Jurgensen I, Hempelmann G, *Impact on postoperative pain of long-lasting pre-emptive epidural analgesia before total hip replacement: a prospective, randomised, double-blind study.* Anesthesia, 2005. **60**(2): p. 118-123.
535. Ong CK, L.P., Seymour RA, Jenkins BJ, *The efficacy of preemptive analgesia for acute postoperative pain management: a meta-analysis.* Anesth Analg, 2005. **100**(3): p. 757-773.
536. Ringrose NH, C.M., *Femoral nerve block in knee joint surgery.* Am J Sport Med, 1984. **12**(5): p. 398-402.
537. Mallory TH, L.A.J., Fada RA, Dodds KL, Adams JB, *Pain management for total joint arthroplasty: preemptive analgesia.* J Arthroplasty, 2002. **17**: p. 129-133.
538. Hebl JR, K.S., Ali MH, Horlocker TT, Dilger JA, Lennon RL, Williams BA, Hanssen AD, Pagnano MW, *A comprehensive anesthesia protocol that emphasizes peripheral nerve blockade for total knee and total hip arthroplasty.* J Bone Joint Surg Am, 2005. **87**: p. 63-70.
539. PF, W., *The changing role of non-opioid analgesic techniques in the management of postoperative pain.* Anesth Analg, 2005. **101**: p. S5-S22.
540. Christopherson R, B.C., Frank SM, Norris EJ, Meinert CJ, Gottlieb SO, Yates H, Rock P, Parker SD, Perler BA, Williams GM, *Perioperative Ischemia Randomized Anesthesia Trial Study Group. Perioperative morbidity in patients randomized to epidural or general anesthesia for lower extremity vascular surgery. Perioperative ISchemia Randomized Anesthesia Trial Study Group.* Anesthesiology, 1993. **79**: p. 422-434.
541. Throburn J, L.J., Vallance R, *Spinal and general anesthesia in total hip replacement: frequency of deep vein thrombosis.* Br J Anaesth., 1980. **52**: p. 1117-1121.
542. Sharrock NE, H.S., Hargett MJ, Urquhart B, Insall JN, Scuderi G, *Effects of epidural anesthesia on the incidence of deep-vein thrombosis after total knee arthroplasty.* J Bone Joint Surg Am, 1991. **73**: p. 502-506.
543. Indelli PF, G.S., Nielsen K, Vail TP, *Regional anesthesia in hip surgery.* Clin Orthop Relat Res, 2005. **441**: p. 250-255.
544. Sharma S, I.R., Specht LM, Davies-Lepie S, Healy WL, *Complications of femoral nerve block for total knee arthroplasty.* Clin Orthol Relat Res, 2010. **468**: p. 135-140.
545. Capdevila X, B.Y., Biboulet P, Ryckwaert Y, Rubenovitch J, d'Athis F, *Effects of perioperative analgesic technique on the surgical outcome and duration of rehabilitation after major knee surgery.* Anesthesiology, 1999. **91**(1): p. 8-15.
546. Horlocker TT, K.S., Pagnano MW, Hebl JR, *Analgesia for total hip and knee arthroplasty: a multimodal pathway featuring peripheral nerve block.* J Am Acad Orthop Surg, 2006. **14**(3): p. 126-135.
547. Kandasami M, K.A., Sarungi M, Baines J, Scott NB, *Femoral nerve block for total knee replacement-a word of caution.* Knee 2009. **16**: p. 98-100.
548. J, L., *Prolonger motor weakness after femoral nerve block with bupivacaine 0.5 % Anaesthesia,* 1990. **45**: p. 421.
549. LR, M., *Palsy after femoral nerve block.* Anaesthesia, 1988. **43**: p. 509.

550. Parvataneni HK, S.V., Howard H, Cole N, Ranawat AS, Ranawat CS, *Controlling pain after total hip and knee arthroplasty using a multimodal protocol with local periarticular injections: a prospective randomized study.* J Arthroplasty, 2007. **22**: p. 33-38.
551. Busch CA, S.B., Bhandari R, Ganapathy S, MacDonald SJ, Bourne RB, Rorabeck CH, McCalden RW, *Efficacy of periarticular multimodal drug injection in total knee arthroplasty: A randomized trial.* J Bone Joint Surg Am, 2006. **88**(5): p. 959-963.
552. Chelly JE, G.R., Greger J, Al Samsam T, *Regional anesthesia for outpatient orthopedic surgery.* Minerva Anestesiol, 2001. **67**: p. 227-232.
553. Vendittoli PA, M.P., Drolet P, LAvigne M, Fallaha M, Guertin MC, Varin F, *A multimodal analgesia protocol for total knee arthroplasty: A randomized, controlled study.* J Bone Joint Surg Am, 2006. **88**: p. 282-289.
554. Andersen LO, K.B., Husted H, Otte KS, Kehlet H, *Local anesthetics after total knee arthroplasty: intraarticular or extraarticular administration ? A randomized, double-blind, placebo-controlled study.* Acta Orthop, 2008. **79**(6): p. 800-805.
555. Dobrydnjov I, A.C., Olsson C, Shapurova O, Angel K, Bergman S, *Intraarticular vs extraarticular ropivacaine infusion following high-dose infiltration analgesia after total knee arthroplasty: a randomized double-blind study.* Acta Orthop, 2011. **82**(6): p. 692-698.
556. JA, G., *Patient-controlled analgesia.* Anesth Analg, 2005. **101**(S44-S61).
557. PE, M., *Intravenous patient-controlled analgesia: one size does not fit all.* Anesthesiol Clin North America, 2005. **23**(1): p. 109-123.
558. Crawford CH, M.A., *Patient-controlled analgesia for total joint arthroplasty.* Instr Course Lect, 2007. **56**: p. 115-119.
559. NH Badner, R.B., CH Rorabeck, SJ MacDonalds, ARN Doyle, *Intra-articular injection of bupivacaine in knee-replacement operations. Results of use for analgesia and for preemptive blockade.* J Bone Joint Surg Am, 1996. **78**(5): p. 734-738.
560. Shih-Jyun Shen, P.-Y.P., Hsiu-Pin Chen, Jr-Rung Lin, Mel S. Lee, Huang-Ping Yu, *Analgesic Effects of Intra-Articular Bupivacaine/Intravenous Parecoxib Combination Therapy versus Intravenous Parecoxib Monotherapy in Patients Receiving Total Knee Arthroplasty: A Randomized, Double-Blind Trial.* Bio Med Research International, 2015. **2015**(450805): p. 1-5.
561. Mauerhan DR, C.M., Miller JS, Mokris JG, Gregory A, Kiebzak GM, *Intra-Articular morphine and/or bupivacaine in the management of pain after total knee arthroplasty.* J Arthroplasty, 1997. **12**(5): p. 546-552.
562. Dave W. Chen, C.-C.H., Yu-Han Chang, Mel S. Lee, Chee-Jen Chang, Pang-Hsin Hsieh, *Intra-articular bupivacaine reduces postoperative pain and meperidine use after total hip arthroplasty: a randomized, double-blind study.* J Arthroplasty, 2014. **29**(12): p. 2457-2461.
563. Kenneth Bramlett, E.O., Eugene R. Viscusi, Kevin Jones, *A randomized, double-blind, dose-ranging study comparing wound infiltration of DEpoFoam bupivacaine, and extended-release liposomal bupivacaine, to bupivacaine HCl for postsurgical analgesia in total knee arthroplasty.* The Knee, 2012. **19**: p. 530-536.
564. Sakamoto B, K.S., Meidrum R, Harker G, Freese A, *Efficacy of Liposomal Bupivacaine Infiltration on the Management of the Total Knee Arthroplasty* JAMA Surgery, 2017. **142**(1): p. 90-95.
565. Yu S, S.A., Walton S, Bosco J, Iorio R, *Pain Control and Functional Milestones in Total Knee Arthroplasty: Liposomal Bupivacaine versus Femoral Nerve Block.* Clin Orthop Relat Res, 2017. **475**(1): p. 110-117.
566. Preet Mohinder Singh, A.B., Anjan Trikha, Lia Michos, Ashish Sinha, Bawavana Goudra, *Role of Periarticular Liposomal Bupivacaine Infiltration in Patients Undergoing Total Knee Arthroplasty-A Meta-analysis of Comparative Trials.* J Arthroplasty, 2017. **32**: p. 675-688.

567. Stephen W. Yu, A.L.S., Sharon L. Walton, Roy I. Davidovitch, Joseph A. Bosco, Richard Iorio, *Liposomal Bupivacaine as an Adjunct to Postoperative Pain Control in Total Hip Arthroplasty*. J Arthroplasty, 2016. **31**(7): p. 1510-1515.
568. Benjamin G Domb, A.G., Jon E Hammarstedt, Christine E Stake, Kinzie Sharp, John M Redmond, *The effect of liposomal bupivacaine injection during total hip arthroplasty: a controlled cohort study*. BMC Musculoskelet Disord, 2014. **15**: p. 310.
569. Nitin Goyal, J.M., Peter F Sharkey, Javad Parvizi, William J Hozack, Matthew S Austn, *The 2012 Chitranjan Ranawat Award: Intraarticular Analgesia After TKA Reduces Pain: A Randomized, Double-Blinded, Placebo-Controlled, Prospective Study*. Clin Orthop Relat Res, 2013. **471**(1): p. 64-75.
570. Gomez-Cardero P, R.-M.E., *Postoperative Analgesia in TKA: Ropivacaine Continuous Intraarticular Infusion*. Clin Orthop Relat Res 2010. **468**(5): p. 1242-1247.
571. Antoni M, J.J., Noll E, *Postoperative pain control by intra-articular local anesthesia versus femoral nerve block following total knee arthroplasty: impact on discharge*. Orthop Traumatol Surg Res, 2014. **100**(3): p. 313-316.
572. Reinhardt KR, D.S., Umunna BP, Reinhardt GA, Nam D, Alexiades M, Cornell CN, *Intraarticular analgesia versus epidural plus femoral nerve block after TKA: a randomized, double-blind trial*. Clin Orthop Relat Res, 2014. **472**(5): p. 1400-1408.
573. Abdulemir A, M.S., Ulrik H, Johan M, Gunnar F, *Doubtful effect of continuous intraarticular analgesia after total knee arthroplasty, a randomized, double-blind study of 200 patients*. Acta Orthopaedica, 2015. **86**(1): p. 1-5.
574. Lee JS, H.A., Kubus JJ, Makepeace H, Hutton M, Campbell DA Jr, Englesbe MJ, *Local anesthesia: a strategy for reducing surgical site infections*. World J Surg, 2011. **35**(12): p. 2595-2602.
575. Eldor, J., *The Antibacterial and Antifungal Effects of Bupivacaine Wound Analgesia*. Journal of New York School of Regional Anesthesia, 2009. **14**: p. 1-10.
576. Klaus Petz, M.W.-A.-A., Christian Bogdan, Jorg-Elard Otten, *Analysis of the antimicrobial activity of local anaesthetics used for dental analgesia*. Journal of Medical Microbiology, 2008. **57**: p. 88-94.
577. Database, P.C.O.C. *Bupivacaine*. [cited 2017 02/20]; Available from: <https://pubchem.ncbi.nlm.nih.gov/compound/bupivacaine#section=Computed-Properties>.
578. Mather, G.T.T.a.L.E., *Properties, Absorption, and Disposition of Local Anesthetic Agents*, in *Neural Blockade in Clinical Anesthesia and Management of Pain, Volume 494*, P.O.B. Michael J. Cousins, Editor. 1998, Lipincott-Raven: Philadelphia. p. 59-60.
579. Jaymin C. Shah, M.M., *pH-Dependent solubility and dissolution of bupivacaine and its relevance to the formulation of a controlled release system*. J Controlled Release, 1993. **23**: p. 261-270.
580. McCafferty, D.W.a.D., *Local Anesthetics*, in *Percutaneous Local Anaesthesia*, D.W.a.D. McCafferty, Editor. 1993, Ellis Horwood: New York. p. 66.
581. ChemicalBook. *14252-80-3(Bupivacaine hydrochloride) Product Description*. Available from: http://www.chemicalbook.com/ChemicalProductProperty_US_CB1386202.aspx.
582. Columb MO, L.G., *Determination of the minimum local analgesic concentrations of epidural bupivacaine and lidocaine in labor*. Anesth Analg, 1995. **81**(4): p. 833-837.
583. Capogna G, C.D., Fusco P, Lyons G, Columb M, *Relative potencies of bupivacaine and ropivacaine for analgesia in labour*. British Journal of Anesthesia, 1999. **82**(3): p. 371-373.
584. Shaw, A.B. *NDA 22496 Exparel (bupivacaine) liposomal injection*. 2011; Available from: http://www.accessdata.fda.gov/drugsatfda_docs/nda/2011/022496Orig1s000ChemR.pdf.
585. Goyal N, M.J., Sharkey PF, Parvizi J, Hozack WJ, Austin MS. , *The 2012 Chitranjan Ranawat Award: Intraarticular Analgesia After TKA Reduces Pain: A Randomized, Double-blinded, Placebo-controlled, Prospective Study*. Clin Orthop Relat Res, 2013. **471**(1): p. 64-75.

586. Perry, E., *Antimicrobial Prophylaxis in Joint Arthroplasty*. US Pharm, 2012. **37**(11): p. HS-23-HS-26.
587. Subramanian S Parvathy, W.M., *Gait analysis of C57BL/6 mice with complete Freund's adjuvant-induced arthritis using the CatWalk system*. BMC Musculoskelet Disord, 2013. **14**: p. 14.
588. Masocha W, P.S., *Assessment of weight bearing changes and pharmacological antinociception in mice with LPS-induced monoarthritis using the Catwalk gait analysis system*. Life Sci, 2009. **85**(11-12): p. 462-469.
589. Weidenhielm L, S.O., Broström Lk LÅ, *Surgical correction of leg alignment in unilateral knee osteoarthritis reduces the load on the hip and knee joint bilaterally*. Clin Biomech (Bristol, Avon), 1995. **10**(4): p. 217-221.
590. Platto MJ, O.C.P., Hicks JE, Gerber LH, *The relationship of pain and deformity of the rheumatoid foot to gait and an index of functional ambulation*. J Rheumatol, 1991. **18**(1): p. 38-43.
591. Gabriel AF, M.M., Honig WM, Walenkamp GH, Joosten EA, *The CatWalk method: a detailed analysis of behavioral changes after acute inflammatory pain in the rat*. J Neurosci Methods., 2007. **163**(1): p. 9-16.
592. Angeby-Möller K, B.O., Hamers FP, *Using the CatWalk method to assess weight-bearing and pain behaviour in walking rats with ankle joint monoarthritis induced by carrageenan: effects of morphine and rofecoxib*. J Neurosci Methods, 2008. **174**(1): p. 1-9.
593. Ferland CE, L.S., Beaudry F, Vachon P, *Gait analysis and pain response of two rodent models of osteoarthritis*. Pharmacol Biochem Behav, 2011. **97**(3): p. 603-610.